

Materials Horizons: From Nature to Nanomaterials

Jince Thomas
Sabu Thomas
Zakiah Ahmad *Editors*

Crosslinkable Polyethylene Based Blends and Nanocomposites

 Springer

Materials Horizons: From Nature to Nanomaterials

Series Editor

Vijay Kumar Thakur, School of Aerospace, Transport and Manufacturing,
Cranfield University, Cranfield, UK

Materials are an indispensable part of human civilization since the inception of life on earth. With the passage of time, innumerable new materials have been explored as well as developed and the search for new innovative materials continues briskly. Keeping in mind the immense perspectives of various classes of materials, this series aims at providing a comprehensive collection of works across the breadth of materials research at cutting-edge interface of materials science with physics, chemistry, biology and engineering.

This series covers a galaxy of materials ranging from natural materials to nanomaterials. Some of the topics include but not limited to: biological materials, biomimetic materials, ceramics, composites, coatings, functional materials, glasses, inorganic materials, inorganic-organic hybrids, metals, membranes, magnetic materials, manufacturing of materials, nanomaterials, organic materials and pigments to name a few. The series provides most timely and comprehensive information on advanced synthesis, processing, characterization, manufacturing and applications in a broad range of interdisciplinary fields in science, engineering and technology.

This series accepts both authored and edited works, including textbooks, monographs, reference works, and professional books. The books in this series will provide a deep insight into the state-of-art of Materials Horizons and serve students, academic, government and industrial scientists involved in all aspects of materials research.

More information about this series at <http://www.springer.com/series/16122>

Jince Thomas · Sabu Thomas · Zakiah Ahmad
Editors

Crosslinkable Polyethylene Based Blends and Nanocomposites

 Springer

Editors

Jince Thomas
Research and Post Graduate Department
of Chemistry
St. Berchmans College
Changanassery, Kerala, India

Sabu Thomas
International and Inter University Centre
for Nanoscience and Nanotechnology
and School of Energy Materials
Mahatma Gandhi University
Kottayam, Kerala, India

Zakiah Ahmad
Faculty of Civil Engineering
Universiti Teknologi Mara
Shah Alam, Selangor, Malaysia

ISSN 2524-5384

ISSN 2524-5392 (electronic)

Materials Horizons: From Nature to Nanomaterials

ISBN 978-981-16-0485-0

ISBN 978-981-16-0486-7 (eBook)

<https://doi.org/10.1007/978-981-16-0486-7>

© Springer Nature Singapore Pte Ltd. 2021

This work is subject to copyright. All rights are reserved by the Publisher, whether the whole or part of the material is concerned, specifically the rights of translation, reprinting, reuse of illustrations, recitation, broadcasting, reproduction on microfilms or in any other physical way, and transmission or information storage and retrieval, electronic adaptation, computer software, or by similar or dissimilar methodology now known or hereafter developed.

The use of general descriptive names, registered names, trademarks, service marks, etc. in this publication does not imply, even in the absence of a specific statement, that such names are exempt from the relevant protective laws and regulations and therefore free for general use.

The publisher, the authors and the editors are safe to assume that the advice and information in this book are believed to be true and accurate at the date of publication. Neither the publisher nor the authors or the editors give a warranty, expressed or implied, with respect to the material contained herein or for any errors or omissions that may have been made. The publisher remains neutral with regard to jurisdictional claims in published maps and institutional affiliations.

This Springer imprint is published by the registered company Springer Nature Singapore Pte Ltd. The registered company address is: 152 Beach Road, #21-01/04 Gateway East, Singapore 189721, Singapore

Preface

The book titled *Crosslinkable Polyethylene Based Blends and Nanocomposites* outlines the latest technological and scientific research accomplishments in the area of cross-linked polyethylene (XLPE) blends and nanocomposites. Encompassed in the book are presentations of state of art in XLPE blends and nanocomposites, types of nanoparticles used in XLPE blends and nanocomposites, new challenges, and opportunities. Also discussed are the critical issues in XLPE nanocomposites, their general usages and commercial significance. Other topics enclosed are the luminescence studies in XLPE and modified XLPE and their morphological, mechanical, thermal, and flame-retardant properties, XLPE versus conventional materials, theoretical studies on XLPE nanocomposites. As the title specifies the book emphasizes numerous facets of XLPE based blend & nanocomposites and their outputs to the society.

This novel book aids as an up to date record on the vital findings, studies, and creation of XLPE based blend & nanocomposites to power cable insulation field. It is aimed to support as a pioneer reference resource for insulation industry as well as in science fields. The various chapters in this book are contributed by prominent researchers from academe, industry, and government-private research laboratories across the world. This book is a very valuable reference source for university and college faculties, professionals, post-doctoral research fellows, senior graduate students and researchers (from R&D laboratories) who are working in the area of automobiles, energy resources, aviation etc.

Chapter 1 delivers a comprehensive outline and an overview of XLPE based blends and their nanocomposites and introduces the general methods for the fabrication of blends and nanocomposites. Opportunities and the significance on XLPE blends and nanocomposites, and different types of applications are also mentioned on this chapter. Chapter 2 discussed the studies on XLPE nanocomposites and blends. The author explains the preparation and types of nanoparticles used in XLPE matrix. Chapter 3 provides the different techniques used for the incorporation inorganic nanoparticles to XLPE systems. The authors also mentioned the surface modification process of inorganic nanoparticles and their intercalation and exfoliation process.

Chapter 4 focuses the critical issues of XLPE based nanocomposites and blends during the processing and installation time. Chapter 5 presents the common usages of XLPE based nanocomposites and blends systems. In Chap. 6, advanced characterization techniques in XLPE and modified XLPE. In this chapter the authors review the benefit of luminescence studies in XLPE systems. The procedures for the luminescence analysis in XLPE and XLPE compounds and their outcomes are also correlated on this chapter. Morphological and mechanical properties of XLPE based nanocomposites and blends are discussed in Chap. 7. This chapter indicates the dynamic and static mechanical properties of XLPE based nanocomposites and blends. Chapter 8 presents the thermal and flame-retardant properties of XLPE based nanocomposites and blends.

Potential importance of XLPE based nanocomposites and blends are discussed in Chap. 9. Chapter 10 discusses XLPE versus conventional materials in electrical insulation fields. This chapter includes various discussions on evolution of power cable, AC and DC cable insulation techniques. Computational studies on XLPE based nanocomposites and blends are discussed in Chap. 11. Chapter 12 discussed the XLPE based products available in markets and their applications. Research developments and the production of XLPE based nanocomposites and blends discussed in Chap. 13. This chapter analyzes the research papers on XLPE nanocomposites and blends published by academic journals mainly from 2005 to 2020 year in detail. Final Chap. (14) on this book presents the risks and limitations associated with XLPE based nanocomposites and blends. In this chapter risks, challenges, and constraints associated with electrical issues, crosslinking agents, recyclability, surface characteristics, and aging behaviors on XLPE based nanocomposites and blends have been analyzed.

Finally, Thanks to God for the successful accomplishment of this book and the editors would like to convey their sincere appreciation to all the contributors of this book who provided excellent support for the fruitful completion of this endeavor. We appreciate them for their commitment and the genuineness for their contributions to this book. Especially we thanks to Dr. Gilbert Teyssedre, Dr. Notingher Petru, Dr. Mohsen Mohseni, Dr. Harry Orton for the review process of chapters. We would like to acknowledge all the other reviewers who have taken their valuable time to make critical comments on each chapter. We also acknowledge the assistance of Springer Nature Singapore Pte Ltd.

Kottayam, India

Jince Thomas
Sabu Thomas

Contents

1	An Overview of XLPE-Based Blends and Nanocomposites	1
	Jince Thomas, Minu Elizabeth Thomas, and Sabu Thomas	
2	Types of Nanoparticles Used in XLPE Systems	19
	Karakkad P. Sajesha	
3	Different Techniques Used for the Incorporation of Inorganic Nanoparticles in XLPE Matrix	49
	Athulya Pillai and Balasubramanian Kandasubramanian	
4	Critical Issues in XLPE-Based Polymer Nanocomposites and Their Blends	63
	Abdallah Hedir, Omar Lamrous, Issouf Fofana, Ferhat Slimani, and Mustapha Moudoud	
5	General Applications of XLPE Nanocomposites and Blends	85
	Divya Radha, Jisha S. Lal, K. Asha Krishnan, and K. S. Devaky	
6	Advanced Characterization Techniques Based on Luminescence in XLPE and Modified XLPE	99
	Gilbert Teyssèdre, Christian Laurent, and Bo Qiao	
7	XLPE Nanocomposites and Blends: Morphology and Mechanical Properties	159
	K. C. Nimitha, Jiji Abraham, Soney C. George, and Sabu Thomas	
8	Thermal and Flame Retardant Properties of XLPE Nanocomposites and Blends	177
	Jiji Abraham, K. C. Nimitha, Soney C. George, and Sabu Thomas	
9	Potential Applications of XLPE Nanocomposites in the Field of Cable Insulation	197
	R. Jose Varghese, L. Vidya, Tomy Muringayil Joseph, Apparao Gudimalla, G. Harini Bhuvaneshwari, and Sabu Thomas	

10	Electrical Insulation: XLPE Versus Conventional Materials	215
	Petru V. Notingher, Cristina Stancu, and Ilona Pleşa	
11	Theoretical Aspects of XLPE-Based Blends and Nanocomposites	299
	Minu Elizabeth Thomas, Rajamani Vidya, Jince Thomas, and Zakiah Ahmad	
12	XLPE-Based Products Available in the Market and Their Applications	321
	Detlef Wald and Harry Orton	
13	Research Developments in XLPE Nanocomposites and Their Blends: Published Papers, Patents, and Production	353
	Yinghui Han, Zhiwen Xue, Dongtao Liu, Feng Gao, Xiaosong Yang, Wenchao Dong, Junxiu Zhou, Guodong Jiang, Junzhe Lin, Yifei Xia, and Huanhuan Luo	
14	Risks and Limitations Associated with XLPE Nanocomposites and Blends	411
	Navid Mostofi Sarkari, Mohsen Mohseni, and Morteza Ebrahimi	

About the Editors

Jince Thomas received his Master's degree in Polymer Chemistry in 2012 and M.Tech. in Polymer Science and Technology in 2014 from Mahatma Gandhi University (MGU), India. He conducted his doctoral research at MGU in the research group of Prof. Sabu Thomas, the present Vice Chancellor of MGU, and Prof. Bejoy Francis (Ph.D. Guide), Assistant Professor, St. Berchmans College, India. He was a visiting student at the University of Tennessee (Knoxville) in 2014 and a project trainee at the International and Inter University Centre for Nanoscience & Nanotechnology, MGU, during 2015–2016. He worked as a project assistant in an Indo-Malaysian Project during 2016–2017 in collaboration with University Technology Mara, Malaysia. He also worked as a visiting student in Ariel University, Israel. He has contributed to numerous publications, book chapters, and books. His research interest focuses on polymer and polymer nanocomposites.

Prof. Sabu Thomas is currently Vice Chancellor of Mahatma Gandhi University, Kerala, India. Professor Thomas is an outstanding leader with sustained international acclaim for his work in Nanoscience, Polymer Science and Engineering and Green Materials. Professor Thomas has received more than 30 national and international awards. He has published over 1200 peer reviewed research papers, reviews, and book chapters. He has co-edited 150 books, and is an inventor of 15 patents. The H index of Prof. Thomas is 108 and has more than 56,000 citations. Professor Thomas has delivered over 350 plenary/inaugural and invited lectures in national/international meetings over 40 countries. Professor Thomas has supervised 115 Ph.D. programmes and his students occupy leading positions in academia and industry in India and abroad.

Prof. Zakiah Ahmad is the Dean of Faculty of Civil Engineering at Universiti Teknologi Mara. She obtained her Bachelor's and Master's at the Memphis State University (USA), and pursued her Ph.D. in Timber Engineering at the University of Bath, United Kingdom. Professor Ahmad specialises in timber engineering and timber composites, and her other interest includes nano-polymer composites as well

as cement composites. She serves as a consultant, committee member and advisor to numerous public agencies and institutions, and has been appointed as visiting scientist at BRE Research Institute, University of Bath, UK, Centre for Nanoscience and Nanotechnology, School of Chemical Sciences, Mahatma Gandhi University India and Timber Research Institute, Kyoto University Japan. Professor Ahmad has published more than 300 papers in journals and proceedings, and plays an essential role in the Malaysian Standard committees as the Chairman and committee member and as Malaysian delegates/representative for ISO technical committee.

Chapter 1

An Overview of XLPE-Based Blends and Nanocomposites



Jince Thomas, Minu Elizabeth Thomas, and Sabu Thomas

1 Introduction

Cross-linked polyethylene (XLPE) and its nanocomposites/blends have put on a significant interest especially in the area of power cable insulation. Due to high operational temperature of XLPE provide more life span for insulation purposes compare to polyethylene (PE). However, the XLPE cannot prove the efficiency to perform high-voltage power cable with absolute accuracy due to water treeing, partial charge discharges, etc. (discussed in volume 1 of this series). Hence, scientists were constantly searching for a solution not only in XLPE power insulation cables but also in other applications and concluded to the material XLPE/nanocomposites and XLPE blends.

Polymer/nanocomposites are multiphase materials, which consist of a polymer/copolymer (10^{-5} – 10^{-3} mm) bearing nanoparticles/nanofillers (1–50 nm), dispersed in the polymer matrix, appreciably influence several physicochemical properties. In XLPE, the incorporation of nanofillers will enhance its various properties [1]. A schematic representation of XLPE/nanocomposites is indicated in Fig. 1. The major phase is the continuous phase, and the other is dispersed minor phase, which can vary from spheres to fibrils.

J. Thomas

Research and Post Graduate Department of Chemistry, St. Berchmans' College, Changanassery, Kerala, India
e-mail: jincethomas25@gmail.com

J. Thomas · S. Thomas (✉)

International and Inter University Center for Nanoscience and Nanotechnology, and School of Energy Materials, Mahatma Gandhi University, Kerala, India
e-mail: sabuthomas@mgu.ac.in

M. E. Thomas · S. Thomas

School of Chemical Sciences, Mahatma Gandhi University, Kerala, India
e-mail: minuputhen@gmail.com

© Springer Nature Singapore Pte Ltd. 2021

J. Thomas et al. (eds.), *Crosslinkable Polyethylene Based Blends and Nanocomposites*, Materials Horizons: From Nature to Nanomaterials, https://doi.org/10.1007/978-981-16-0486-7_1

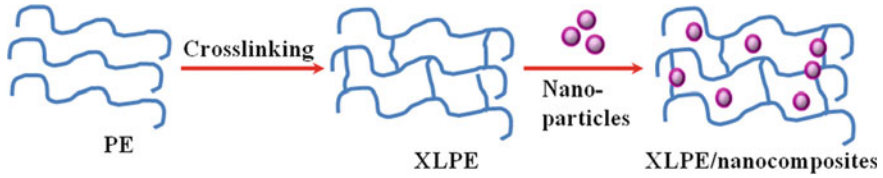


Fig. 1 Schematic representation of PE, XLPE and XLPE/nanocomposites

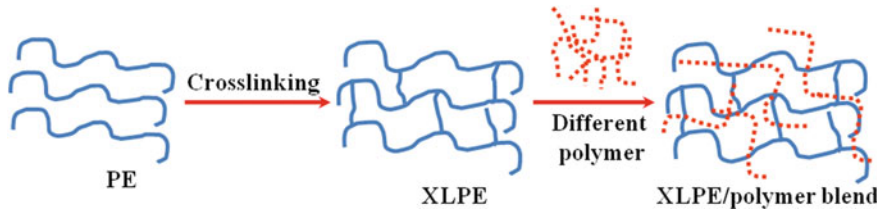


Fig. 2 Schematic representation of PE, XLPE and XLPE/polymer blend

Today, the ongoing research regarding wide variety of nanofillers to XLPE/nanocomposites leads to a promising material for future application. In addition to the incorporation of nanoparticles, XLPE blends (in Fig. 2) also reinforce the physicochemical properties [2]. Polymer blends are mixing of chemically different polymers and/or copolymers with multiphase structures without any chemical bonding.

The tailoring of nanocomposites and blends will lead to a material with desired properties, which can reinforce the defects of XLPE. The structure–property relation of nanocomposites and blends of the XLPE are related with physicochemical properties. Hence, here is the significance of the better understanding of nanofillers and polymer incorporation in XLPE matrix.

2 Importance of Incorporation of Nanoparticles or Other Polymers to XLPE

The incorporation of nanofillers to the XLPE matrix will reinforce the material properties in different aspects. The physicochemical properties of the XLPE/nanocomposites have strongly influenced by the nanofiller–XLPE matrix interactions. These properties extremely vary with the properties of XLPE with the same chemical and morphological compositions. The high aspect ratio of nanofillers is another chief factor of reinforcing efficiency.

Like XLPE/nanocomposites, XLPE blends also reinforced the polymer matrix. These blends show the synergism in all properties of the polymers used for blending. Like nanocomposites, blends also exhibit better performance, making of

unique materials with unique features. The tailoring of nanocomposites and blends to achieve desired properties require excellent control on morphology and stability of phases. As the aspect ratio of nanofillers, the interaction of the inter-phase is the main factor of reinforcing efficiency. Hence, better knowledge of the fillers and its preparation methods are needed for tailoring of XLPE matrix.

3 Effect of Nanoparticles in XLPE Matrix

Generally, additives or fillers are treated in polymeric matrix to improve the physicochemical properties of a polymer. The bulk properties of XLPE/nanocomposites are depended upon geometric nature, particle size and surface features of the filler [1, 3]. Hence, understanding of the various varieties of nanoparticles is essential for the better output in physicochemical properties of bulk. Depending upon the dimension or growth/extension dimension of nanofillers, it is classified into four

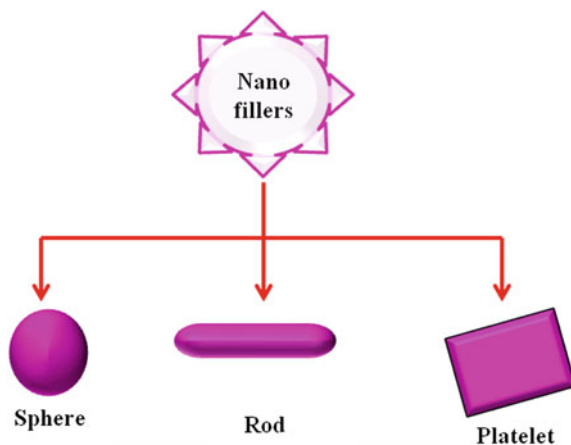
1. Zero-dimensional, e.g., spherical silica
2. One-dimensional, e.g., nanotubes
3. Two-dimensional, e.g., nanofilms
4. Three-dimensional, e.g., graphite

Depending upon the geometry of particles, nanofillers are classified into three (Fig. 3)

1. Sphere
2. Rod
3. Platelets

Sphere-shaped nanoparticles are efficient than the other two, due to the large surface area that make more dispersion in the matrix and have high interaction.

Fig. 3 Classification of nanofillers based on geometry



Depending upon the origin of particles, nanofillers are classified into two (Fig. 4): natural and synthetic.

The preparation of the nanofillers is by two approaches: the top-down approach and the bottom-up method. The schematic representation of the nanofiller preparation approaches is represented in Fig. 5.

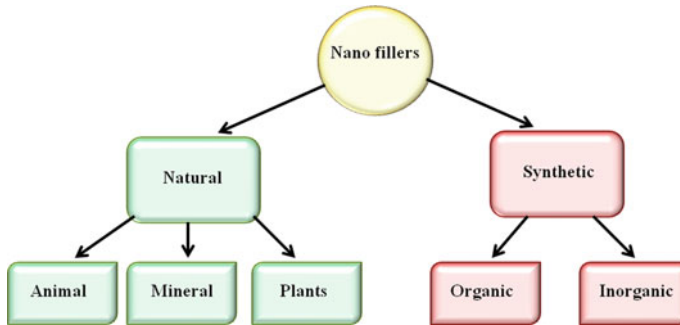


Fig. 4 Classification of nanofillers based on origin

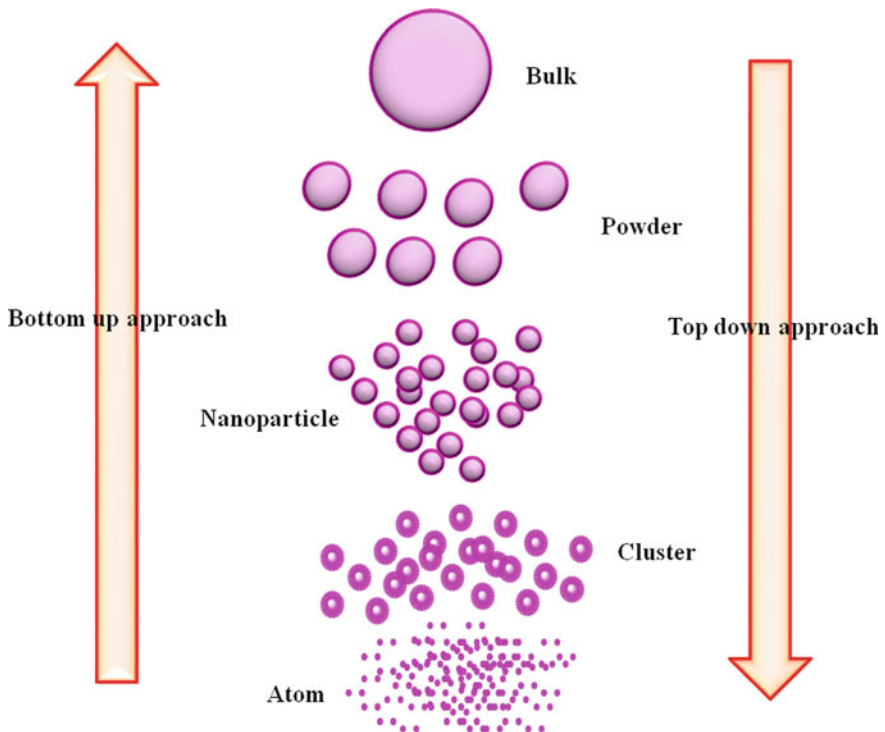


Fig. 5 Schematic representation of the nanofiller preparation approaches

Nanofillers such as Al_2O_3 , carbon black, CaCO_3 , graphite, graphene oxide, MgO , SiO_2 , TiO_2 and ZnO are utilized to boost the physicochemical properties. However, these properties not only depend on the geometry, dispersed state, etc., but also depends on the filler dispersion in the polymer matrix. Hence, the method of preparation of nanocomposites is also taken for account.

Polymer blends are the direct outcome of physical mixing of two polymers to achieve the desirable properties. Polymer blends are classified according to miscibility into two: miscible and immiscible [4]. The schematic representation of the classification of polymer blends is depicted in Fig. 6.

- Miscible blends: Homogeneity is observed at the molecular level. The miscible blend is of two types: homogeneous and heterogeneous.
- Immiscible blends: Poor adhesion with sharp inter-phase and irregular morphology.

Like nanocomposites, other than the property of polymer used for blending, the choice of method for blending is also a factor for all the resultant properties. Hence, the technique of preparation of blends is also figured out.

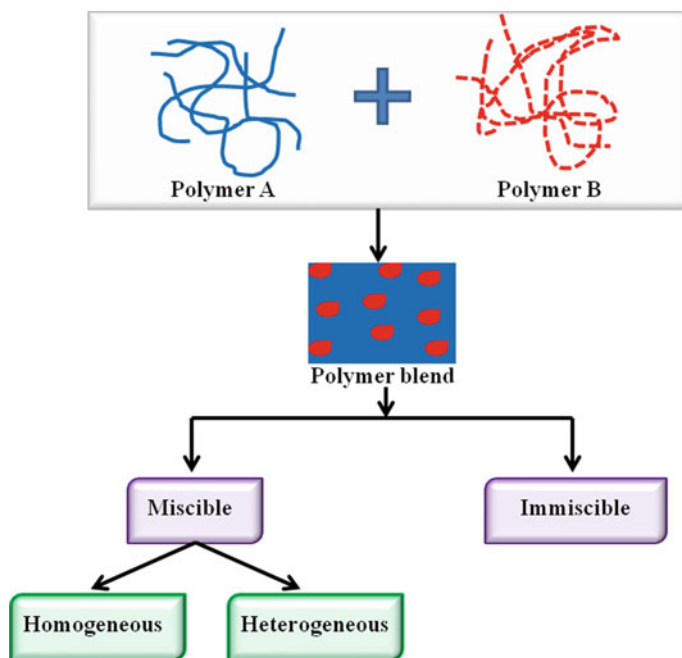


Fig. 6 Classification of polymer blends

4 Methods for the Preparation of Nanocomposites and Blends

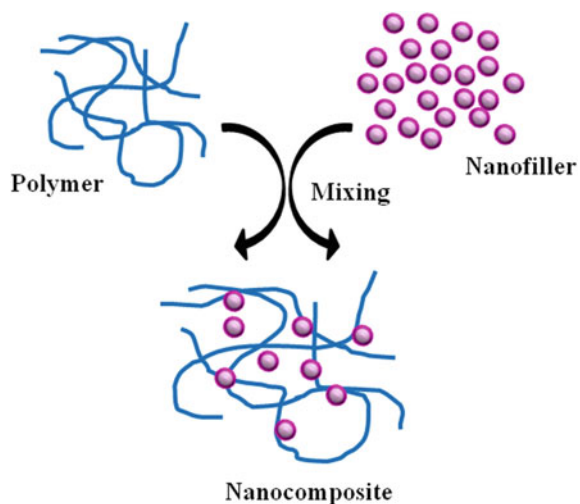
Vigilantly tailored interfaces of the integrated nanofillers and blending polymer help the preparation of nanocomposites or blends with desired properties. The mode of preparation is also a key factor for reinforcement of the properties.

4.1 Preparation of Nanocomposites

The physicochemical properties mainly depend on the method of preparation of XLPE/nanocomposites [1, 5–8]. There are four main means for the successful incorporation of nanofillers into the polymer matrix, they are

1. **Direct mixing:** Direct mixing of polymer and nanofillers is the simplest method. This method can approach in two different ways: melt compounding method and solution-mixing method. In the melt compounding method, both polymer and nanofillers are melted at melting point ‘ T_m ’ or at glass transition temperature ‘ T_g ’ of the polymer. The solution-mixing method is carried out at a polymer solution followed by evaporation of the solvent. Schematic representation of the direct mixing method of nanocomposites preparation is shown in Fig. 7.
2. **In situ intercalative polymerization:** Intercalation is mainly done by exfoliation of layered nanofillers. Intercalation is executed by different methods, direct intercalation from the solution or polymer melts and intercalation of the monomer and then polymerization. Intercalation in solution method corresponds to the exfoliation of layered fillers by the migration of polymer solution

Fig. 7 Schematic representation of direct mixing



followed by evaporation of the solvent. Intercalation of nanofillers and both resultant nanofillers and polymer melts are directly mixed, and the exfoliation of nano-layers is due to shear forces. In situ intercalative polymerization is the polymerization of a monomer, in which layered filler is intercalated in the monomer. Schematic representation of intercalative method of nanocomposites preparation by intercalative method is depicted in Fig. 8.

3. **Sol-gel process:** In the sol-gel method, the assembly of cluster-to-cluster builds the resultant polymer nanocomposites. This method involves two processes colloidal suspension of the fillers forming sols, which are condensed to form interconnected networks called gels. Schematic representation of intercalative method of nanocomposites preparation using sol-gel method is depicted in Fig. 9.
4. **In situ formation of nanofillers in the polymer matrix:** In this method, the nanofillers are incorporated in monomer first followed by polymerized. Here the formation of nanoparticles is by the reduction of its metal ions using UV radiation or tuning the pH. Schematic representation of intercalative method of nanocomposites preparation of in situ formation of nanocomposite is depicted in Fig. 10.

During the preparation of nanocomposites, occasionally nanofillers tend to agglomerate. To improve the dispersion of the nanofillers in polymer matrix, surface modifications of fillers must be carried out. The surface modification of fillers also enhances to build a strong bond between fillers and matrix and dispersion stability of fillers [9]. The different approaches of the surface modification of nanofillers are

1. **Chemical treatment**—Chemical reaction involving the formation of a chemical bond with a bifunctional organic compound in which one functional group is attached to the surface nanofillers and others as an organic shell.

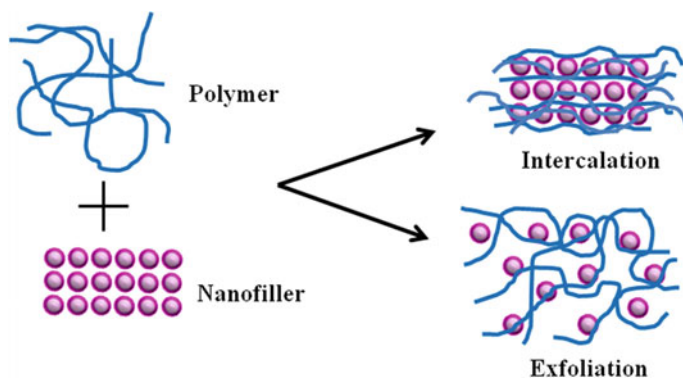


Fig. 8 Schematic representation of intercalative method of nanocomposites preparation

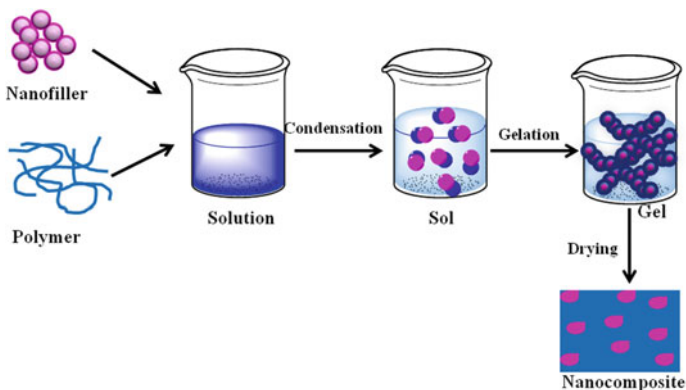


Fig. 9 Schematic representation of the sol-gel method of nanocomposites preparation

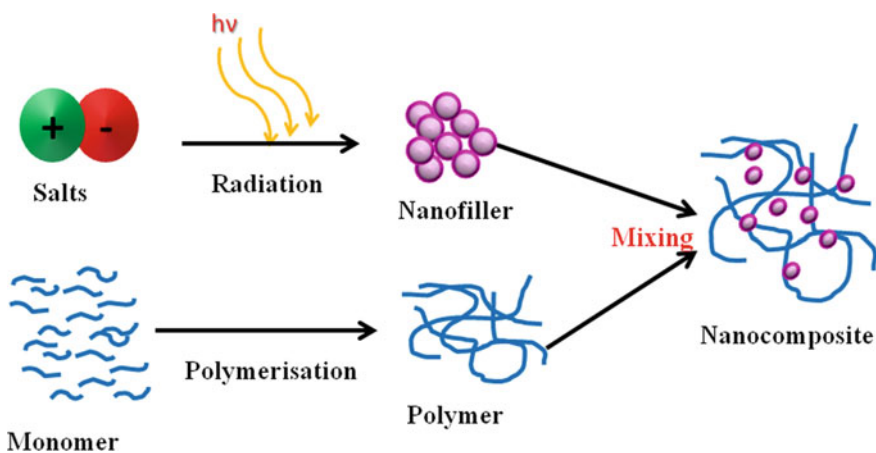


Fig. 10 Schematic representation of in situ polymerization method of nanocomposites preparation

2. **Grafting**—Reaction involves two different forms, grafting onto and grafting from. ‘Grafting onto’ is a direct coupling of nanoparticles with surface reacting center to the polymer with a functional group. In ‘grafting from’, polymerization takes place in the nanofillers surface in which monomer is unable to move on the surface.
3. **Physical adsorption of polymer**—As the name indicates, this method is the adsorption through physical forces of polymer dispersants on the nanofillers surface.

The selection of preparation methods and the modification techniques are depending upon the nature of the nanofillers.

Out of these nanocomposite preparation methods, direct mixing method (with the help of melt mixer) is commonly used for the fabrication of XLPE nanocomposites.

4.2 Preparation of Polymer Blends

The preparation method is a key factor for the tuning of the property of the polymer blends [2]. There are mainly three types of blending methods:

1. **Solution blending:** Polymers with physically incompatible but thermodynamically miscible due to melting viscosity under compounding conditions and degradation may occur under melt processing. In this method, a solvent is chosen in which both polymer miscible and dissolved are separately followed by mixing these thoroughly. After the thorough mixing, the diluents are removed. The schematic representation preparation of blend by melt blending is depicted in Fig. 11.
2. **Latex blending:** In latex blending, the polymers to blend in the suspended micro-phase in the interaction of neighboring spheres are controlled by a suspended medium. However, this method is of high cost and causes environmental hazards. Figure 12 represents the schematic sketch for the preparation of blend by latex blending.
3. **Melt blending:** This method is most acceptable for blending, in which the polymers to be blend are mixed in the molten stage under pressure. Batch mixers or extruders are used for such mixing. The melt blending has many advantages over solution blending and latex blending. Resultant blends do not degrade on temperature during processing. It is cost-effective, and we can expect a good

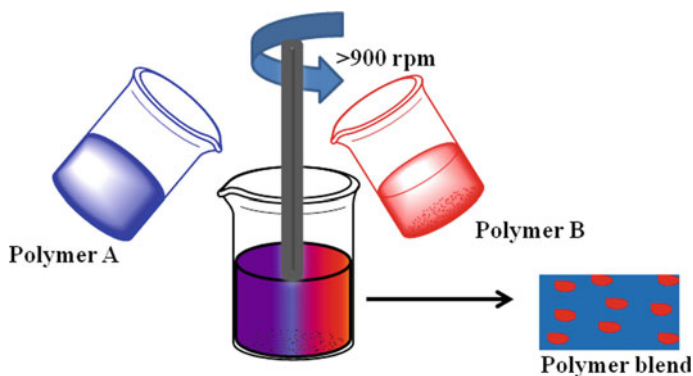


Fig. 11 Schematic representation preparation of blend by solution blending

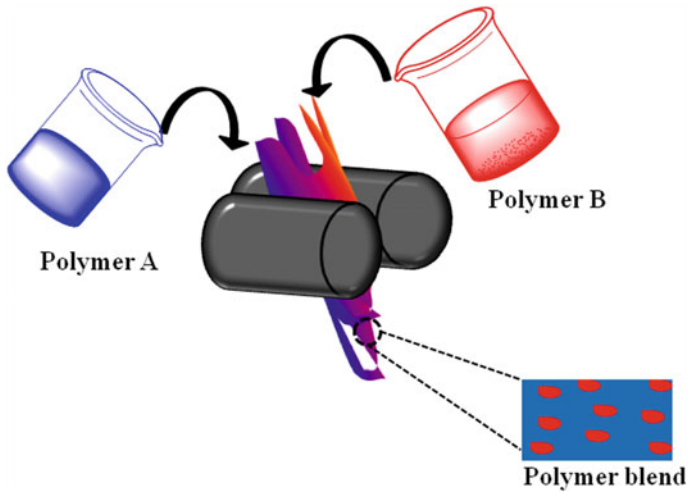


Fig. 12 Schematic representation preparation of blend by latex blending

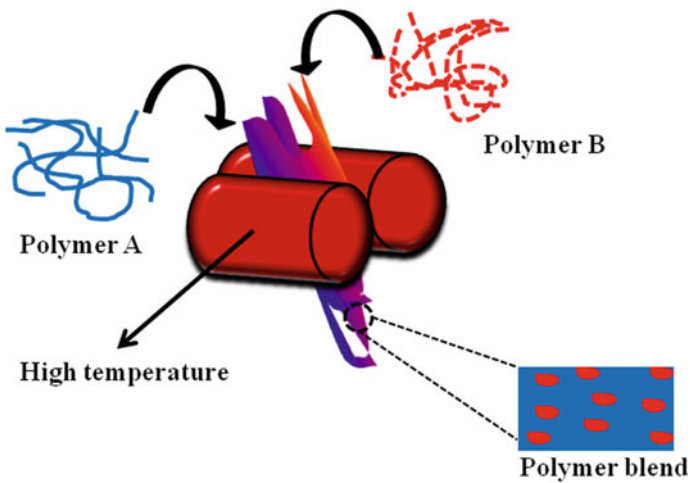


Fig. 13 Schematic representation preparation of blend by melt blending

result in the desired product than from another blending. The schematic representation preparation of blend by melt blending is depicted in Fig. 13.

Out of these techniques, melt blending is the commonly used method for the preparation of XLPE blends.

5 Importance of XLPE/Nanocomposites and Blends in Various Fields of Applications

The major explorations on the benefit of both XLPE/nanocomposites and XLPE/blends are accomplished in the field of power cables insulation. To tune the electrical and mechanical properties of extruded polymers, the loading of nanofillers and property of the fillers are also taken into account.

The introduction of cross-links in PE to make XLPE improves the thermochemical properties, but the proliferation degree of water trees was found to be more rapid in PE compared with XLPE. The impact is caused by the space charge and stress inversion phenomena. However, the space charge accumulation accelerates aging and leads to a breakdown in XLPE insulation cables. However, XLPE/nanocomposites can effectively control the space charge accumulation and stress inversion phenomena. The nanofillers can trap the charges, reduce its mobility and gradually diminish the space charge accumulation. These properties lead to resist the electrical aging in cables. The electrical treeing, water treeing and partial discharges are mostly involved in the mechanism of electrical aging. A detailed study of these terminologies is given below.

Water treeing: It is a process in which dendritic (or looks like branches of a tree) water-filled micro-cavity and unified trenches set off in the presence of moisture [10, 11]. These are at a risk to premature aging that further leads to complete failure of the cable.

Electrical treeing: Some electrical fracture/crack that occurs in the polymeric materials is called electrical treeing. Like water treeing, this electrical treeing looks like branches of tree hence got the name [10].

Partial discharge: Under International Electromechanical Commission (IEC) 60270, partial discharge is described as “a localized electrical discharge or breakdown of a minor section of a solid or fluid electrical insulation system under high-voltage stress and which may or may not occur adjacent to a conductor” [12]. This developed because of the occurrence of voids and cracks in a dielectric material. Partial discharges are of two types: internal and surface partial discharges. Internal partial discharges occur due to the internal defects like voids and cracks in insulations, mostly at boundaries. Surface partial discharges occur due to the presence of contaminants and moisture in the material. Partial discharge is the factor for water treeing and electrical treeing [10, 13].

The presence of nanofillers in XLPE nanocomposites shows evidence of outstanding high-voltage direct current (HVDC) insulations characteristics chiefly improved DC breakdown strength, high volume resistivity, low down the space charge accumulation, increase lifespan, etc.

Nanoparticles can control the breakdown strength of XLPE/nanocomposites by a nucleation agent, build conductivity pathways, scatter the electrons and resist partial discharge. The partial discharge is reduced with nanoparticles by reducing the free volume of the matrix, and the difference in the electrical permittivity of nanoparticles decreases the local electric field. They also resist the growth of electric treeing

by creating an interfacial region between the XLPE matrix and the fillers [14]. Thus, treeing required more time to cover the way. Here discuss some main XLPE/nanoparticles in detail.

The XLPE/silica nanoparticles are mainly used in the cable industry, but the introduction of silica may cause agglomeration. In this point of view, Hui et al. introduced a vinyl silane, functionalized silica nanoparticles [15]. These XLPE-vinyl silane functionalized silica nanocomposites are a good candidate for the resistance of water treeing in the power cables. The space charge performance of XLPE/silica nanocomposites was studied by Zhang et al., unmodified silica in XLPE nanocomposite shows an agglomeration, and hence silica is coupled with agents like titanate and vinylsilane which helps to reduce the agglomeration. Zhang et al. presented an approach for the suppression of space charge in XLPE by XLPE/poly (stearyl methacrylate)-grafted SiO_2 nanocomposite in which poly(stearyl methacrylate) is used to reduce agglomeration. The outcome of these studies leads to a material with improved space charge reduction and enhanced DC breakdown strength [17–22].

Other interesting Si-based nanoparticles are silicon carbide, SiC. Wang et al. studied the dielectric properties, breakdown strength and space charge distribution in XLPE/SiC nanocomposites [23]. However, they do not study the agglomeration of SiC in XLPE matrix. These nanocomposites decrease the chance of the DC breakdown. Tanaka et al. studied that SiC nanoparticles in the matrix create deep traps of electrons and holes around each nanoparticle [21]. Hence, electrical neutralization around each nanoparticle helps to block the charge accumulation, thus protects the material from DC breakdown.

The XLPE/ CaCO_3 nanocomposites are helping to improve the electrical performance of XLPE in HV cables [24]. XLPE/ZnO nanocomposites helps to enhance the dielectric breakdown strength [25]. For XLPE/ TiO_2 , nanocomposite enhances the thermal and chemical stability and reduces space charge accumulation [26]. The XLPE/ SiO_2 and XLPE/ Al_2O_3 nanocomposites have also enhanced the thermochemical stability and mechanical property [16, 27].

Widely explored nanofiller is MgO whose XLPE/MgO nanocomposites are used in HV cables. Wang et al. and Murata et al. studied the effect of it in XLPE and stated that these nanocomposites can reduce the space charge accumulation because of the high volume resistivity [28, 29].

Li et al. studied about the XLPE/montmorillonite nanocomposites using intercalants like octadecyl quaternary ammonium salt, double octadecyl benzyl quaternary ammonium salt, etc., with two alkyl chains [30]. Direct incorporation of these nanofillers leads to a little amount of agglomeration, which is reduced by adding ethylene-vinyl acetate (EVA) as compatibilizers. The strong interfacial interaction of intercalants and XLPE leads to a restriction in the segmental movement of the polymer chain. This restriction in movement of polymer chain decreases the polarization ability of molecules, and hence, reduces the dielectric loss.

Recent studies with carbon nanoparticles also lead to the cable industry, and they also proved the improvements in thermal stability and fire safety properties in

non-polar polymers [31]. Thus, graphene oxide (GO) nanoparticles are also incorporated in the XLPE matrix. Hence, XLPE/GO or XLPE/GO-functionalized with hyperbranched nanocomposites are used as a good candidate for flame retardant materials. Wang et al. done the thermal studies in the XLPE/GO functionalized with hyperbranched N-aminoethyl piperazine and di(acryloyloxyethyl) methyl phosphonate nanocomposites [32, 33], and they found excellent results. Also, the XLPE/carbon black composites can decrease the dielectric constant with frequency [24].

Rather than single nanofillers, hybrid fillers are also used to enhance the mechanical and thermal properties of XLPE. XLPE/alumina/clay nanoscale hybrid [27, 34] and XLPE/SiO₂/TiO₂ hybrid [35] nanocomposites are examples of such improvements in XLPE properties. Thus, XLPE/nanocomposites proved a better improvement in electrical properties in insulation cables than pure XLPE cables.

Like XLPE/nanocomposites, XLPE blends also enhance the electrothermal–chemical–mechanical properties of XLPE matrix. A blend of XLPE with polybutadiene enhances thermal stability [36]. This blend has a wide variety of applications like in electrical conductors as insulation, plumbing pipes and tubing, in articles such as dishwasher impellers, washing machine, floor, gear and bearings needed for high resistance in temperature and being hard at high temperature. XLPE/EVA blend also enhances the mechanical property [37, 38]. There are limited patents specifically for XLPE/nanocomposites or XLPE blends, and some important patents of this category are listed in Table 1.

Table 1 Some important patents in specifically of XLPE/nanocomposites and XLPE/polymer blends

Patent No	Assignee/ Inventors	Filed on	Title	Composite/ blend
US7579397B2	Nelson J K et al.	January 27, 2005	Nanostructured dielectric composite materials	Nano-silica composite
US7884149B2	Nelson J K et al.	July 17, 2009	Nanostructured dielectric composite materials	Nano-silica composite
US9589700B2	Sun, ka Ram	July 31, 2012	Cross-linked polyethylene composition	Nano-MgO composite
US2912410	Quinton P. Cole	January 27, 1956	Process of preparing a cured blend of form stable, cross-linked polyethylene and polybutadiene and compositions thereof	Polybutadiene blend
US2016/ 0208073A1	Paranthaman M P et al.	Jan. 15, 9 2016	Method for producing radiation-resistant polymer composite materials	SiO ₂ composite
US2005/ 0245665A1	Chen C et al.	May 23, 2005	Method of forming nanocomposite material	Silica composite

6 Challenges of XLPE Nanocomposites and Blends

Incorporation of nanoparticles into XLPE matrices will considerably improve the mechanical, electrical and thermal properties, which depend on different issues like processing method, type of nanoparticles, aspect ratio and loading of nanoparticles. Some processing settings or techniques that are superior for one property may be inferior to another. Therefore, the selection of all these criteria needs much experience. In addition, XLPE blend's processing method, loading of polymer etc., are taken into account for tailoring the desired properties. Besides, due to synergism, some desired property will cover up, and adverse properties will uncover if we concentrate on a particular property. This will trim down the quality of polymer; hence, a better understanding of polymers is needed.

Another issue is regarding the health problems of workers during the loading of nanoparticles. Because the very fine size of particle is inhaled easily to lungs, some may cause toxicity through fire. This can cause some respiratory problems because heavy concentrations of nanoparticles are used in industries, but serious issues are not reported yet. However, caution must be taken for these health hazards [39]. The problem can be reduced by the immobilization of nanoparticles.

Concurrently, preparation of specially tailored XLPE/nanocomposites or XLPE/blends of desired properties using the cream of the crop of filler/polymer desires expertise. Even though there are more advantages of these materials in the application of power cables as an insulator, some problems must be solved. One of the main problems is the homogenous dispersion not so practical which will affect the properties of the material too. Besides, the interactions occur in the interfaces, structure–property relationships, the degradation mechanism and defects that lead to aging and so on.

Recycling or reuse of polymer is a great challenge for the researchers. In some studies, pristine XLPE recycling with supercritical fluids is reported [40]. However, the nanocomposites and blends of XLPE are not efficiently used for recycling or reuse. The wide use of these materials leads to environmental pollution; hence, methods for recycling and reuse are very needful.

7 Conclusion

The necessity for better-quality materials has guided us to polymer nanocomposites and polymer blends with the characteristic synergy of two or more materials with different physical and chemical properties. The addition of nanofillers or blending polymers will improve the mechanical properties and electrical properties than the pristine XLPE. Increase in the resistance of water treeing, electrical treeing and partial discharge can offer by the introduction of even low content of nanofillers. Depending upon the compatibilizers, we can tune the lifetime of material.

The structure–property relationship is the key to all the physicochemical properties of both nanocomposites and blends; hence, theoretical studies will incorporate in latter researches for better tuning for desired properties. There are many structural aspects and interactions, its mechanism and the curing ability of these materials which are not much explored even now. Also, the application of these materials is restricted to cable insulation, only very rare cases of other applications are reported. Therefore, more such researches are done on these specially tailored materials to the new endeavors of applications.

References

1. Pleşa I, Noñinger PV, Stancu C et al (2018) Polyethylene nanocomposites for power cable insulations. *Polymers (Basel)* 11. <https://doi.org/10.3390/polym11010024>
2. Stahl PO, Sederel WL (1996) *Polymer blends*
3. Thabet A, Mobarak YA, Bakry M (2011) A review of nano-fillers effects on industrial polymers and their characteristics
4. Utracki LA (2014) *Polyethylenes and their blends*. *Polymer blends handbook*. Springer, Netherlands, pp 1559–1732
5. Thomas SP, Thomas SP, Stephen R et al (2007) *Rubber nanocomposites: preparation, properties and applications* *polymer nanocomposites: preparation properties and*
6. Akram S, Nazir MT, Castellon J et al (2019) Preparation and distinguish dielectric properties of multi-layer nanoparticles-based polyimide films. *Mater Res Express* 6:125092. <https://doi.org/10.1088/2053-1591/ab5c40>
7. Akram S, Castellon J, Agnel S et al (2020) Multilayer polyimide nanocomposite films synthesis process optimization impact on nanoparticles dispersion and their dielectric performance. *J Appl Polym Sci* 49715. <https://doi.org/10.1002/app.49715>
8. Akram S, Castellon J, Agnel S et al (2019) Impact of nanocomposite thin layer on nanoparticles dispersion and their dielectric properties. In: *Annual report—conference on electrical insulation and dielectric phenomena, CEIDP*, pp 336–339. Institute of Electrical and Electronics Engineers Inc.
9. Kochetov R, Korobko AV, Andritsch T et al (2011) Thermal and electrical properties of nanocomposites, including material properties
10. Densley J (2001) Ageing mechanisms and diagnostics for power cables—an overview. *IEEE Electr Insul Mag* 17:14–22. <https://doi.org/10.1109/57.901613>
11. Conlan S, Courtney J, Looby T. Accelerated aging test on multiple XLPE MV cables simultaneously to induce water trees
12. Iec (2000) Iec international 60270 standard high-voltage test techniques-partial discharge measurements Iec international 60270 standard high-voltage test techniques-partial discharge measurements including photocopying and microfilm, without permission in writing f. Iec 60270:2000
13. Raymond W, Illias H, Measurement HM (2015) *Undefined partial discharge classifications: review of recent progress*. Elsevier
14. Thomas J, Joseph B, Jose JP et al (2019) Recent advances in cross-linked polyethylene-based nanocomposites for high voltage engineering applications: a critical review. *Ind Eng Chem Res* 58:20863–20879
15. Hui L, Smith R, Nelson JK, Schadler LS (2009) Electrochemical treeing in XLPE/silica nanocomposites. In: *Annual report—conference on electrical insulation and dielectric phenomena, CEIDP*, pp 511–514

16. Zhang L, Zhou Y, Cui X et al (2014) Space charge behavior of XLPE/SiO₂ nanocomposites with nanoparticle surface modification. In: EIC 2014—Proceedings of the 32nd electrical insulation conference. IEEE Computer Society, pp 402–406
17. Zhang L, Zhou Y, Cui X et al (2014) Effect of nanoparticle surface modification on breakdown and space charge behavior of XLPE/SiO₂ nanocomposites. *IEEE Trans Dielectr Electr Insul* 21:1554–1564. <https://doi.org/10.1109/TDEI.2014.004361>
18. Crine JP (2005) Influence of electro-mechanical stress on electrical properties of dielectric polymers. *IEEE Trans Dielectr Electr Insul* 12:791–800. <https://doi.org/10.1109/TDEI.2005.1511104>
19. Crine JP (2005) On the interpretation of some electrical aging and relaxation phenomena in solid dielectrics. *IEEE Trans Dielectr Electr Insul* 12:1089–1107. <https://doi.org/10.1109/TDEI.2005.1561789>
20. Han B, Wang X, Sun Z et al (2013) Space charge suppression induced by deep traps in polyethylene/zeolite nanocomposite. *Appl Phys Lett* 102:012902. <https://doi.org/10.1063/1.4773918>
21. Tanaka T (2006) Promising characteristics of nanocomposite dielectrics. In: Proceedings of the IEEE international conference on properties and applications of dielectric materials. Institute of Electrical and Electronics Engineers Inc., pp 12–22
22. Zhang L, Khani MM, Krentz TM et al (2017) Suppression of space charge in crosslinked polyethylene filled with poly(stearyl methacrylate)-grafted SiO₂ nanoparticles. *Appl Phys Lett* 110:132903. <https://doi.org/10.1063/1.4979107>
23. Wang Y, Wang C, Testing KX-P (2016) Undefined investigation of the electrical properties of XLPE/SiC nanocomposites. Elsevier
24. Habib MA, Nasart LS, Sharkawy RM (2017) Improvement the electrical performance of cross-linked polyethylene high voltage cables. In: 2016 18th International middle-east power systems conference, MEPCON 2016—proceedings. Institute of Electrical and Electronics Engineers Inc., pp 21–25
25. Kim YM, Cha YK, Lim KJ et al (2012) Electrical insulation evaluation of crosslinked polyethylene nanocomposite blended with ZnO. In: Proceedings of 2012 IEEE international conference on condition monitoring and diagnosis, CMD 2012, pp 1242–1245
26. Jose JP, Mhetar V, Culligan S, Thomas S (2013) Cross linked polyethylene/TiO₂ nanocomposites: morphology, polymer/filler interaction, mechanics and thermal properties. *Sci Adv Mater* 5:385–397. <https://doi.org/10.1166/sam.2013.1469>
27. Jose JP, Thomas S (2014) XLPE based Al₂O₃-clay binary and ternary hybrid nanocomposites: self-assembly of nanoscale hybrid fillers, polymer chain confinement and transport characteristics. *Phys Chem Chem Phys* 16:20190–20201. <https://doi.org/10.1039/c4cp03403a>
28. Nagao M, Watanabe S, Murakami Y et al (2008) Water tree retardation of MgO/LDPE and MgO/XLPE nanocomposites. In: Proceedings of the international symposium on electrical insulating materials, pp 483–486
29. Murata Y, Goshowaki M, Reddy CC et al (2008) Investigation of space charge distribution and volume resistivity of XLPE/MgO nanocomposite material under DC voltage application. In: Proceedings of the international symposium on electrical insulating materials, pp 502–505
30. Li X, Xu M, Zhang K et al (2014) Influence of organic intercalants on the morphology and dielectric properties of XLPE/montmorillonite nanocomposite dielectrics. *IEEE Trans Dielectr Electr Insul* 21:1705–1717. <https://doi.org/10.1109/TDEI.2014.004317>
31. Wang X, Kalali EN, Wan JT, Wang DY (2017) Carbon-family materials for flame retardant polymeric materials. *Prog Polym Sci* 69:22–46
32. Hu W, Zhan J, Wang X et al (2014) Effect of functionalized graphene oxide with hyper-branched flame retardant on flammability and thermal stability of cross-linked polyethylene. *Ind Eng Chem Res* 53:3073–3083. <https://doi.org/10.1021/ie4026743>
33. Tripathi SN, Rao GSS, Mathur AB, Jasra R (2017) Polyolefin/graphene nanocomposites: a review. *RSC Adv* 7:23615–23632

34. Jose JP, Thomas S (2014) Alumina-clay nanoscale hybrid filler assembling in cross-linked polyethylene based nanocomposites: mechanics and thermal properties. In: Physical chemistry chemical physics. Royal Society of Chemistry, pp 14730–14740
35. Jose JP, Ahmad Z, Thomas S (2014) Hybrid nanoparticle-based XLPE/SiO₂/TiO₂ and XLPE/SiO₂ nanocomposites: nanoscale hybrid assembling, mechanics and thermal properties. In: InCIEC 2013, pp 895–902. Springer, Singapore
36. Marcilla A, Garcia-Quesada JC, Hernandez J et al (2005) Study of polyethylene crosslinking with polybutadiene as coagent. *Polym Test* 24:925–931. <https://doi.org/10.1016/j.polymertesting.2005.06.002>
37. Kumara S, Xu X, Hammarström T et al (2020) Electrical characterization of a new crosslinked copolymer blend for DC cable insulation. *Energies* 13. <https://doi.org/10.3390/en13061434>
38. Azizi H, Barzin J, Morshedian J (2007) Silane crosslinking of polyethylene: the effects of EVA, ATH and Sb₂O₃ on properties of the production in continuous grafting of LDPE. *Express Polym Lett* 1:378–384. <https://doi.org/10.3144/expresspolymlett.2007.53>
39. Tanaka T, Imai T (2013) Advances in nanodielectric materials over the past 50 years. *IEEE Electr Insul Mag* 29:10–23. <https://doi.org/10.1109/MEI.2013.6410535>
40. Lee JS, Cho KC, Ku KH et al (2012) Recyclable insulation material based on polyethylene for power cable. In: Proceedings of 2012 IEEE international conference on condition monitoring and diagnosis, CMD 2012, pp 88–90

Chapter 2

Types of Nanoparticles Used in XLPE Systems



Karakkad P. Sajesha

1 Introduction

Polymer composites are a combination of two or more components of different phases that include polymers and fillers. These fillers belong to different geometries like fibrous, irregular flakes, spheres, circular, cubic and plate-like structures, etc., which can be continuous (long fibers) or discontinuous (short fibers, flakes, platelets) in nature [1]. Physically they are rigid materials, immiscible in polymer matrix in molten or solid states giving rise to different morphology. These fillers can be classified as inorganic and organic materials further based on their origin, fillers can be classified as natural and synthetic. The different classification of these fillers with examples has been summarized in Table 1.

The dispersion of fillers is homogeneously in the polymer matrix, in very small concentrations usually less than 10 wt% and when the particles are in the nanometer range, the materials are known as nanocomposites. The formation of interface zone between the polymer and nanoparticles makes the nanocomposite different from microcomposite. Hence, the unique properties of nanocomposites [2] give them the great potential for advanced applications. Various nanoparticles, such as nanoclays like montmorillonite, nano-oxides like TiO_2 , SiO_2 , Al_2O_3 , etc., semiconducting particles like SiC , ZnO , etc., have been widely studied due to their property of improving the performances of different thermoplastic and thermosetting polymers. Thus, the properties of nanocomposites are influenced by the nature of polymer matrix and filler used, their internal properties, size and shape of fillers, the surface functionalization, thickness of the filler surface, and interactions between the polymer matrix and fillers.

Cross-linked polyethylene (XLPE) which is an alternative to polyvinyl chloride (PVC), chlorinated polyvinyl chloride (CPVC), and copper tubing has an extensive

K. P. Sajesha (✉)

School of Chemical Sciences, Mahatma Gandhi University, Kottayam, Kerala 686560, India
e-mail: kp.sajesha@gmail.com

© Springer Nature Singapore Pte Ltd. 2021

J. Thomas et al. (eds.), *Crosslinkable Polyethylene Based Blends and Nanocomposites*, Materials Horizons: From Nature to Nanomaterials,
https://doi.org/10.1007/978-981-16-0486-7_2

Table 1 Classification of fillers and their examples

Classification	Chemical structure	Examples
Natural	Animal	Silk, wool, hair
	Mineral	Asbestos
	Cellulose	Wood, seed, leaf, fruit, grass
Synthetic	Inorganic	Oxides: TiO ₂ , SiO ₂ , Al ₂ O ₃ , ZnO, MgO,
		Hydroxides: Al(OH) ₃ , Mg(OH) ₂
		Metals: Al, Au, Ag, B, Sn, Cu, steel
		Silicates: asbestos, talc, mica, nanoclay, kaolin
		Salts: CaCO ₃ , BaSO ₄ , CaSO ₄ , etc.
		Carbides and nitrides: AlN, BN, SiC
	Organic	Carbon and graphite fibers and flakes, carbon nanotubes, carbon black, graphene, graphene oxide
		Synthetic polymers: polyester, polyamide, polyvinyl alcohol fibers

Adapted from [1]

range of applications due to its specific physical and chemical properties. It has very high enhanced properties when compared with ordinary polyethylene (PE). PE [3] itself is an insulating material due to its excellent dielectric strength, high insulation resistance, and a low dissipation factor. It being a commodity plastic with low cost, easy availability and processing has major application in household items, packaging, and insulation, net ropes, fishing rods, medical applications, etc., and being thermoplastic can be easily reprocessed. The main defect of PE is its limited temperature range. On increasing the temperature, it softens and begins to flow there by losing its critical physical properties. Cross-linking the PE increases the temperature range of the insulation without damaging its electrical properties. Both physical and chemical approaches [4] are followed by the scientific word in cross-linking the polyethylene. Some of the methods of cross-linking are given in Fig. 1.

Almost all types of polyethylene like linear low density polyethylene (LLDPE), low density polyethylene (LDPE), high density polyethylene (HDPE), etc., [5] are cross-linked to improve their properties. Upon cross-linking, the polymer changes from thermoplastic to thermosetting resulting in a polymer matrix which is durable. Also, cross-linking inhibits the flow of melt. XLPE is suitable for high-to-low voltage ranges thus surpassing other insulation materials like PVC, ethylene propylene rubber (EPR), and silicone rubbers. Cross-linking the polyethylene also enhances the chemical and oil resistance at elevated temperatures making it suitable for use as a low smoke zero halogen material, for natural gas and offshore oil applications, chemical transportation, and transportation of sewage and slurries [6]. It is widely used in pipework systems, hydronic radiant heating and cooling systems, domestic water piping, etc. It is a thermoset insulation [7] material for high tension electrical cables. Cross-linking of the polymer increases low-temperature

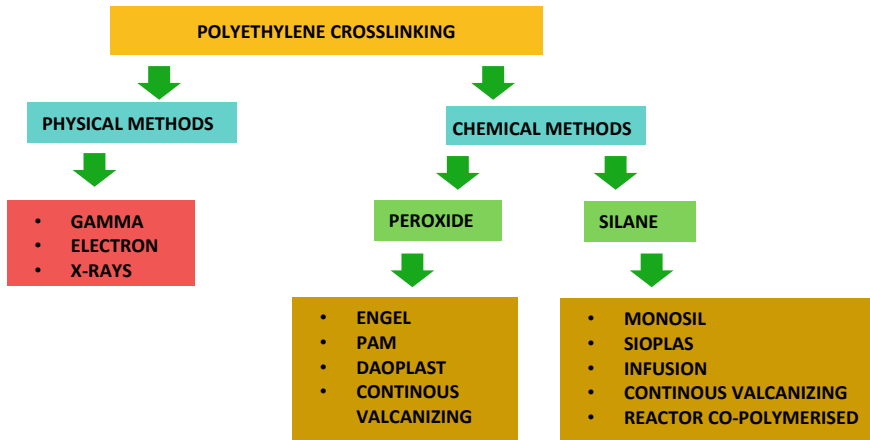


Fig. 1 Different methods for cross-linking polyethylene

impact strength, abrasion resistance, and environmental stress cracking resistance, reducing hardness and rigidity. The mechanical properties of the XLPE like greater tensile strength, elongation and impact resistances make it superior to other insulating materials. Even at very high temperatures, the XLPE insulation will not melt or drip. It is also characterized by the increased flow resistance and better aging property. XLPE also shows improved water tree resistance which is another benefit of XLPE insulating materials used for low voltage (LV) cables and medium voltage (MV) cables over PE insulating materials [8]. Thus, the replacement of LDPE with XLPE [9] increased the thermomechanical properties of insulators in power cables. As a result of cross-linking, the thermal stability and long-lasting operation in service was significantly increased and hence XLPE with the ability to withstand even short circuit for few seconds over 200 °C has a large extent of application. However, the degree of cross-linking varies from application to application. Table 2 gives the variation in the properties of PE upon cross-linking.

In spite of these advantages, XLPE faces certain drawbacks. The accumulation of space charge [10] inside them creates distortion of local electric field, giving acceleration to insulating aging, shortening the lifespan of the cable, etc. The advancement of nanotechnology in recent years has helped the scientific world in improving the properties of polymer through the introduction of nanocomposites [11, 12]. Nanocomposites, the multicomponent system, include a matrix and one or more than one dispersed fillers. They proved that the interface between nanoparticles and polymer matrix provides a great impact on the dielectric properties of the nanocomposite. Figure 2 gives the pathway involved in formation of XLPE nanocomposite from PE.

These nanocomposites find their applications in biomedical, clinical, and electrical fields. For example, in high voltage applications, nanodielectrics [13], etc. These polymer nanocomposites due to their potential benefits as dielectrics are

Table 2 Degree of change in the properties of PE upon cross-linking

Polyethylene properties	Change in properties on cross-linking of polyethylene
Density	No change or slight decrease
Melt index	Decrease
Molecular weight	Significant increase
Tensile strength	No change or slight increase
Elongation at break	Decrease
Impact resistance	Significant improvement
Abrasion resistance	Great improvement
Stress crack resistance	Great improvement
Elastic properties	Great improvement
Environmental stress crack resistance	Increase
Resistance to slow crack growth	Increase
Temperature resistance	Great improvement
Chemical resistance	Significant improvement

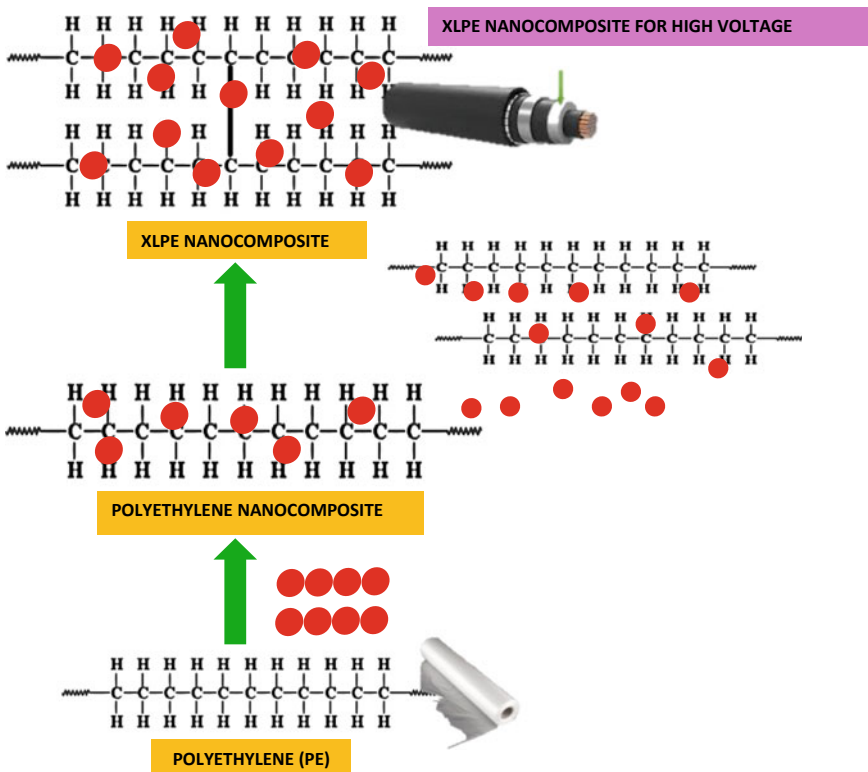


Fig. 2 Schematic representation of the pathway from PE to XLPE nanocomposites

gaining great attention as they have very much improved dielectric strength. The nanosized inclusion benefitted the electrical insulation with low dielectric loss. When there is disturbance in maintaining the applied voltage across the material in a stable manner without excess current flow, electrical breakdown occurs. The best candidate can be the cross-linked polyethylene nanocomposites which can work as an insulator with high breakdown strength resisting the breakdown mechanisms. Along with this, the filler size, material and aspect ratio, surface functionalization, filler grade, host material, type of synthesis, etc., affect the insulating capacity of nanocomposite. XLPE is thus the most widely used insulation polymer at high breakdown voltage. A large number of different nanomaterials of spherical shape have been applied as fillers for the formation of nanocomposites. They include metals like Al, Fe, Au, metal oxides like Al_2O_3 , Fe_3O_4 , ZnO, TiO_2 , semiconductors like PbS and CdS, metalloid oxides like SiO_2 , etc. There are also other types of nanofillers like carbon nanotubes and cellulose whiskers, fillers of the form of sheets such as graphite, layered SiO_2 including montmorillonite, hectorite, saponite, etc. Thus, cross-linked polyethylene nanocomposites with organic/inorganic nanoparticle fillers exhibit enhanced electrical breakdown strength compared to their unfilled or micron filled members and is the newly emerging dielectric materials which over heads the existing ones. The development of insulation cables since 1913 is described in Fig. 3. Some of the important nanoparticles in XLPE nanocomposites are discussed in detail in this chapter.

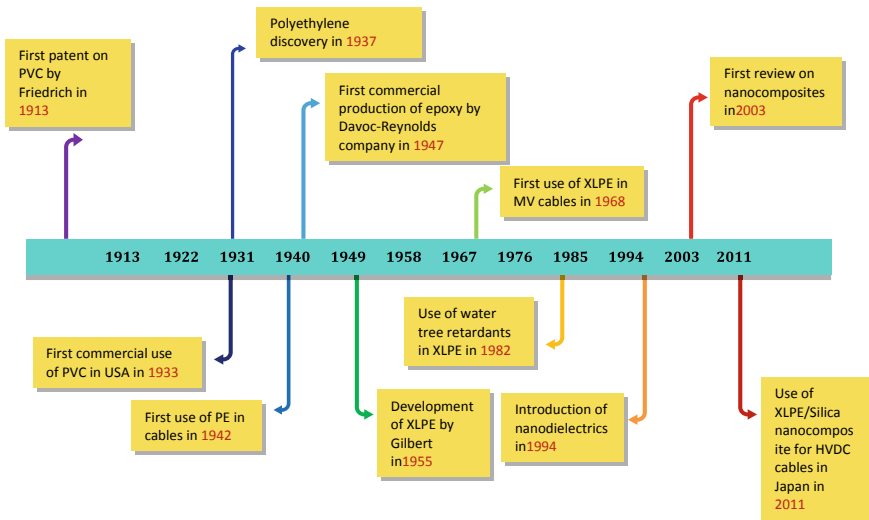


Fig. 3 Development of insulation cables since 1913

2 XLPE Nanocomposites

Nanomaterials have been attaining attraction recently by the researchers in the field of dielectrics and electrical insulation [14]. Nanocomposites are materials in which the polymer matrix is filled with inorganic particles that are nanosize in nature. The XLPE as insulation material for DC cables has been improved by the addition of nanosized inorganic particles [15]. This technology guarantees the improvement in the insulating performance of the polymer. Some of the main applications of XLPE nanocomposites are pictorially represented in Fig. 4. A few of the nanofillers in XLPE are discussed in this chapter which includes SiO_2 , TiO_2 , Al_2O_3 , Clay, MgO , GO, BNNs, etc.

3 SiO_2 Nanoparticles in XLPE Matrix (SiO_2/XLPE Nanocomposite)

A number of experimental studies performed in recent years indicate that the nanoparticles can be used as a promising filler in power cable insulation which suppresses the growth of electrical tree and prevents the degradation of polymer matrix [16–18]. Among the different nanofillers used, SiO_2 has been widely studied with different polymer matrices due to their mild and easy process involved in its preparation. Hence, a lot of efforts have been applied on the investigation of the polymer/ SiO_2 nanocomposites to modify their properties for the special applications. The experimental studies by Tanaka et al. using XLPE and fumed silica (SiO_2) showed that SiO_2 additives in XLPE matrix could be largely applied in the fields of extruded high voltage (HV) and extra high voltage (EHV) cables [19].

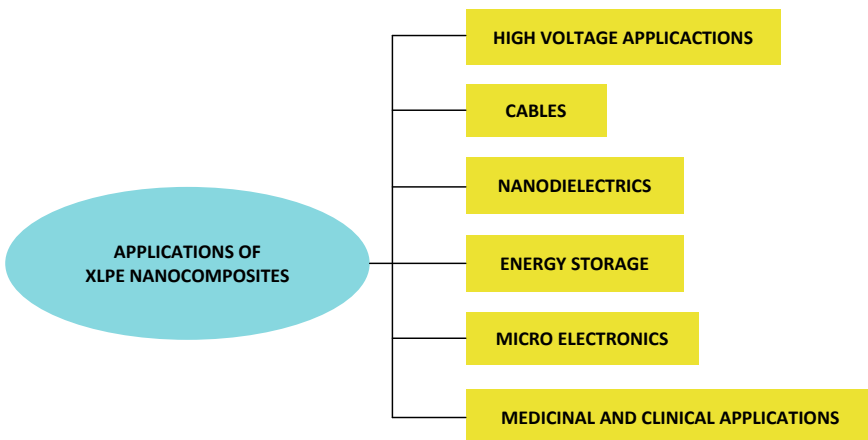


Fig. 4 Applications of XLPE nanocomposites

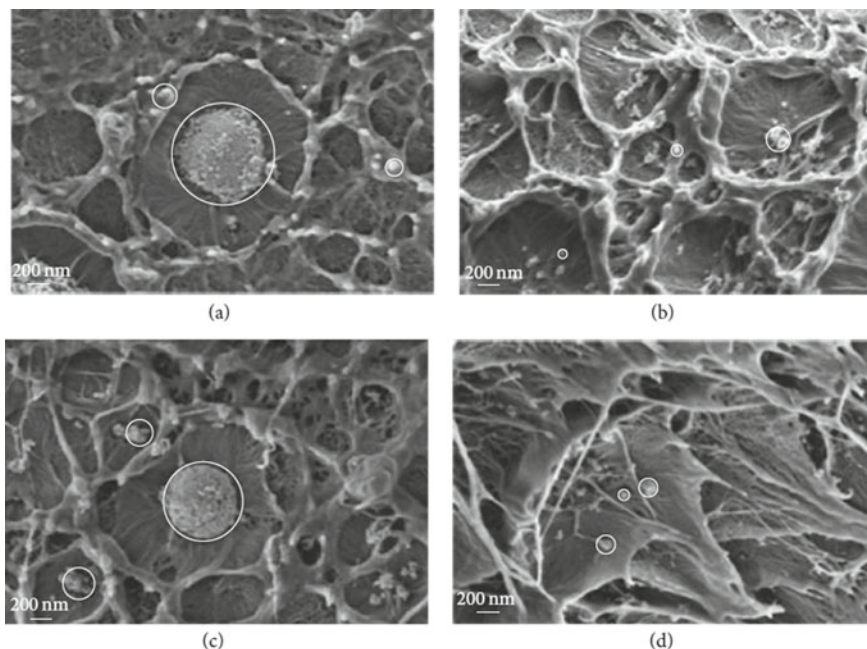


Fig. 5 SEM of TiO_2/XLPE . **a** UN- TiO_2/XLPE (1 wt%), **b** MDOS- TiO_2/XLPE (1 wt%), **c** UN- TiO_2/XLPE (5 wt%), and **d** MDOS TiO_2/XLPE (5 wt%). Adapted from [10]

Unfilled XLPE, XLPE filled with 5% non-functionalized fumed silica nanofiller, and XLPE filled with 5% functionalized fumed silica nanofiller were used for their study. In order to study the distribution of fillers, they used SEM. The unfilled sample of XLPE showed no significant morphological features when examined by SEM and thus compared to the SEM of untreated filler sample it was evident that the filler particles span a wide size approximately 300 nm to 30 μm and are uniformly distributed throughout the material. The SEM micrographs of the morphology of peroxide cross-linked XLPE, XLPE with untreated nanofiller and XLPE with treated nanofiller has also been obtained. DSC measurements gave the melting behavior of the XLPE samples. All melting traces were obtained at a heating rate of 10 K min^{-1} . Here, both of the treated and untreated nanofiller nanocomposites melted at a significantly lower temperature of 102 $^\circ\text{C}$ than the unfilled system of 104 $^\circ\text{C}$. Thus, the nanoparticles reduce the formation of crystalline order due to the presence of nanoparticle interactions with the polymer. Gas chromatography studies showed that cross-linking residues diminishes by the heat treatment at 80 $^\circ\text{C}$ for a week in vacuum, whereas by heat treatment at 60 $^\circ\text{C}$ for a week some might remain. A three-terminal cell system with its gold coated electrodes was used in DC charging measurements. At an electric field of 20 kV/mm a steady-state current was obtained. The DC current density data between unfilled XLPE filled XLPE before and after heat treatment shows that the DC conductivity is decreased with XLPE

filled with 5 wt% silica nanofillers. Heat treatment for 5 days at 80 °C causes much more reduction in DC conductivity, except for unfilled XLPE. Hence, nanofillers act as nucleation items for by-products and contaminants. The space charge measurements were performed by different methods like pulsed electroacoustic (PEA) and thermal step (TSM) method. Small amount of heterocharge existed for filled XLPE and homocharge for unfilled XLPE with thin sample of 85 μm thickness at a field of 50 kV/mm. Montanari (low field) PEA results gave lower space charge accumulation for filled XLPE samples than unfilled one and the lowest value was obtained surface-treated nanofiller XLPE. They also showed the reduction in space charge for filled XLPE on thermal treatment. Tanaka and Ohki (high field) PEA results gave evidence for heterospace charge in unfilled XLPE and homospace charge in filled XLPE. Y. Tanaka (high field) PEA results gave no significant space charge for 1 mm thick samples at the field 30 and 40 kV/mm. Castellon (low field) TSM results showed that filled XLPE accumulates less space charge than unfilled XLPE and functionalized filler filled XLPE exhibited the lowest electric field and double injection occurs here. Thus, in short heterocharge is formed for unfilled XLPE which reduces on addition of nanofiller. Also, shorttime breakdown (BD) strength and impulse BD strength are unaffected by the addition of nanofillers. And partial discharge (PD) resistance is markedly improved by nanofiller addition. As a result of their wide studies, SiO_2/XLPE nanocomposite can be considered as one of the best examples of modified polymer with extensive interface regions and having enhanced synergistic or unique dielectric properties.

Apart from these kinds of studies, there are also studies on functionalization of SiO_2/XLPE nanocomposites that results in modified properties. The use of a titanate coupling agent (TC9) and 3-(methacryloyloxy)propyltrimethoxysilane (KH570) by Zhang et al. to modify the SiO_2 surface showed an improved DC conductivity, dielectric, and space charge properties in XLPE/ SiO_2 nanocomposites [20]. They used XLPE mixed with unmodified SiO_2 nanoparticles (XLPE/UN- SiO_2), XLPE mixed with surface-modified SiO_2 nanoparticles by KH570 coupling agent (XLPE/KH570- SiO_2), and XLPE mixed with surface-modified SiO_2 nanoparticles by TC9 coupling agent (XLPE/TC9- SiO_2) for studies to examine the influence of different nanoparticle surface modifications on interface effects. They could conclude from FESEM that the XLPE/UN- SiO_2 nanocomposites face agglomerate problems whereas XLPE/KH570- SiO_2 and XLPE/TC9- SiO_2 showed a decrease in agglomeration. The FESEM results show the decrease in agglomeration with KH570 coupling agent (both size and number), compared to XLPE/UN- SiO_2 nanocomposites. The agglomerate size of SiO_2 nanoparticles ranged from several ten nm to several hundred nm. Further decrease in the size of agglomerates was reported with TC9 coupling agent. They also concluded the improvement in surface hydrophobicity of SiO_2 nanoparticles upon surface modification and the decrease in DC conductivity in the XLPE/KH570- SiO_2 and XLPE/TC9- SiO_2 nanocomposites. DC polarization current measurements were done using three-terminal cell system at an electric field of 10 kV/mm lasting for 10 min and four temperatures 20, 40, 60, and 80 °C were chosen. However, with rise in temperature, the DC conductivity increases much more slowly than the unmodified nanocomposites. FTIR studies

were also adopted to study the variation on surface modification. The reflection peaks of XLPE/KH570-SiO₂ and XLPE/TC9-SiO₂ nanocomposites are almost similar and larger than XLPE and XLPE/UN-SiO₂ nanocomposite. This was due to surface modification of SiO₂ nanoparticles. Similarly the trap depth and trap density for modified nanocomposite are more than unmodified one. The surface modification of SiO₂/XLPE nanocomposites and their influence on the DC breakdown and space charge have also been studied by Zhang et al. in 2014. They utilized a titanate and vinylsilane coupling agents having non-polar functional groups as the surface modifiers of SiO₂ nanoparticles. They proved that the surface modification of SiO₂ improved the DC breakdown under different temperature and XLPE/VISiO₂ [21, 22] nanocomposite processed highest DC breakdown strength with low dispersibility. They also showed that the introduction of organic surface modification leads to the formation of deeper trap sites which supports the suppress and greater movement of space charges. In 2017, Zheng et al. also reported the making of matrix compatible PSMA(poly(stearyl methacrylate)) brush grafted SiO₂/XLPE nanocomposite that suppresses the space charge and internal field distortion giving a large range of external DC field from -30 to -100 kV/mm at room temperature. They made use of four samples for their study, namely XLPE, UN-SiO₂/XLPE, free-PSMA/XLPE, and PSMA-SiO₂/XLPE. The uniform distribution of the nanoparticle contributed to the increase in the interfacial volume thus improving its efficiency. Space charge distribution under 30 kV/mm was studied using a pulsed electroacoustic method at room temperature. Just after polarization, a decrease in the positive charge on the anode was observed for all samples. After polarization for 30 min in XLPE, net positive charge is distributed across the sample. Approximately 7 C/m³ of positive carriers accumulated in the bulk of UN-SiO₂/XLPE nanocomposites and smaller quantity of positive carriers accumulated in free-PSMA/XLPE composites. On the other hand, no charge was observed in the bulk of PSMA-SiO₂/XLPE nanocomposites even after 60 min. The ability of the nanocomposites in suppressing space charge was done by applying a field of approximately 100 kV/mm. This resulted in forming a positive charge packet in XLPE that slowed down during the 60 min transit across the insulation and a smaller positive charge packet in UN-SiO₂/XLPE nanocomposite that slowly moved a distance of approximately 50 μm. In the case of free-PSMA/XLPE, initially bipolar charge injection and transport were observed which were then followed by the appearance of a negative charge packet that transited and recombined with positive carriers near the anode. Comparison of the charge trapping ability of XLPE and its composites were studied using TSC measurements. The PSMA-SiO₂/XLPE system showed an exponential growth with the temperature in the TSC spectra that reached 12.7 pA at 90 °C due to traps in the interfacial region and an increase in the nanoparticle matrix interfacial volume. Furthermore, the large TSC in the well-dispersed system at higher temperature suggests that the newly introduced chemical defects act as deep trapping sites. Furthermore, the DC breakdown test was carried out with ball-plane electrodes according to International Electrotechnical Commission (IEC) standard 60243-2: 2001 and DC BDS was assessed by the two parameter Weibull distribution. The results showed that the

lowest breakdown strength was found for agglomerated UN-SiO₂/XLPE system and was the relatively well-dispersed system that outperformed free XLPE. Moreover, the addition of free-PSMA chains did enhance the DC BDS. Also, it has been seen that XLPE encountered a severely increasing trend of field distortion due to the charge evolution. When UN-SiO₂ NPs were incorporated into XLPE field, distortion could be improved but the agglomerates could remain as defects and lead to lower breakdown strengths. The free-PSMA/XLPE group showed a better performance than UN-SiO₂/XLPE NCs with regard to the field distortion. The maximum internal field distortion of PSMA-SiO₂/XLPE NCs was only 9.5% under -100 kV/mm and less than 10.6% for DC fields from -30 to -100 kV/mm. This shows that PSMA-SiO₂/XLPE NCs has a tremendous potential for improving HVDC power cable insulation.

The space charge distribution also depends on the nanocomposite thickness. The investigation on thickness dependence and space charge distribution in unfilled XLPE and SiO₂/XLPE nanocomposites were done by Lv et al. [23] and they could see that the SiO₂/XLPE nanocomposites sample with low thickness accumulated larger heterocharge compared to thicker sample.

Surface modification of SiO₂/XLPE nanocomposites has been widely studied by the scientific world as it offers a major application to high-voltage cables. Roy et al. studied the surface modification of SiO₂/XLPE nanocomposite and its electrical applications by modifying the SiO₂ surface using triethoxyvinylsilane (TES), n-(2-aminoethyl)3aminopropyltrimethoxysilane (AEAPS) and hexamethyldisilazane (HMDS) [24]. The DC breakdown field was 1.45, 1.25, and 1.65 times as neat XLPE for XLPE/AEAPSSiO₂, XLPE/HMDSSSiO₂, and XLPE/TESSSiO₂ nanocomposites, respectively. Sharad et al. also studied the surface modification of SiO₂/XLPE nanocomposite by using octylsilane-modified silica nanofillers [25] and studied the partial discharge characteristics of the nanocomposites. Their studies using the differential scanning calorimetry (DSC), thermogravimetric analysis (TGA), Fourier transform infrared (FTIR), and contact angle measurement proved that the addition of nanosilica resulted in changing the melting point, thermal degradation temperature, heat of fusion, bonding structure, and the contact angle of the polymer. Surface modification were also done by Jin Kaihao et al. in 2018 where the SiO₂ was modified with γ -aminopropyltriethoxysilane KH550, γ -(2,3-epoxypropoxy) propyltrimethoxysilane (KH560), and triethoxyvinylsilane (A-151) [26]. They studied the space charge characteristics of nanocomposites using pulse electroacoustic methods (PEA) and obtained beneficial properties in the modified samples.

Apart from the experimental studies, theoretical calculations have also been carried out relating the nanocomposites. These studies mainly focus on the electronic interaction between the SiO₂ fillers and the polymer and also aim in designing the SiO₂ particle with greater efficiency with improved structure. The stabilizing effect of the double layer around the SiO₂ nanocluster in electron trapping has been studied theoretically using the quantum mechanics/molecular dynamics (QM/MD) simulations [27] based on a self-consistent charge density functional tight-binding (SCC-DFTB) method by Han et al. The results of their

calculations for the high ionization potential (IP) and electron affinity (EA) of SiO₂ nanocluster indicate that it is a promising member for reducing electrical treeing.

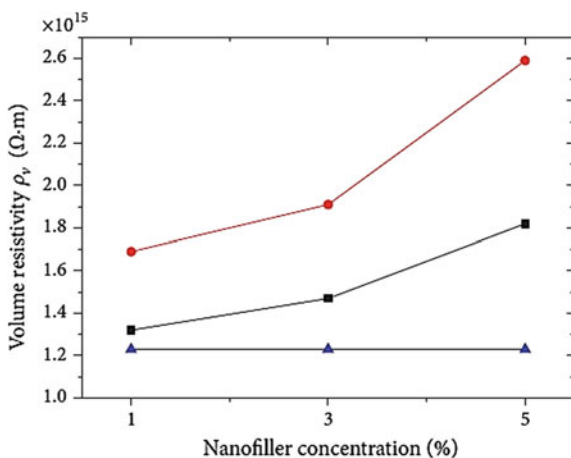
One of the most abundant economic mineral α -SiO₂ known as α -quartz is found to have a wide range of applications beginning from high-frequency devices, cellular and satellite network, quartz crystal microbalance, etc. [28–31]. Different models with the modified surfaces for increasing the rate of reaction developing the adsorption effect have also been proposed. For example, the six-member ring and a triangle-like structured dense model [32, 33], the hydroxylated model giving silanol groups [34], the one with the N or B-doped models [35–38], etc., and these properties of α -SiO₂ affect its interfacial interaction with XLPE thus increasing the performance of SiO₂/XLPE nanocomposites in power cable insulation. Zheng et al. used the computational calculations to study the electrical tree inhibiting mechanism of the SiO₂ fillers with nanosize and various modified surface structures [39]. They used their studies to determine the ability of particles in trapping hot electrons and preventing space charge. They applied the density functional theory (DFT) calculations using the Vienna Ab Initio Simulation Package (VASP) [40–42] with Perdew–Burke–Ernzerhof (PBE) functional [43]. They used the DFT-D2 method to measure the van der Waals interaction and the projected augmented wave (PAW) method [44] to study the interaction between valence electrons and ion cores. They aimed to establish the mechanism involved in improving the anti-aging properties and performance of XLPE by the addition of SiO₂ particles. They analyzed the electrical properties of a series of SiO₂/XLPE nanocomposites on the basis of surface structures, interfacial interaction, H migration activity, and space charge behavior. They concluded the reduction in space charge accumulation and inhibition of electrical treeing on addition of SiO₂ nanosized fillers which increases the power of power cable insulation by trapping hot electrons and limiting the movement of cross-linked polyethylene. They also proved that the incompletely hydroxylated SiO₂ or surfaces with boron doping are not very much effective in insulation cables as they destroy the XLPE chain and also supports the H migration reaction. They showed that the SiO₂ N-doped having a completely hydroxylated surface is the most effective nanocomposite among the different species studied. Their abilities of adsorption to XLPE and transferring charge and the weak chemical activity leads to this efficiency. The studies of Zheng et al. can also lead to the designing of other potential surface-modified SiO₂/XLPE nanocomposites.

A large number of other different studies have been performed in this area focusing on the improvement of the properties of the nanocomposites. These experimental and theoretical studies make SiO₂/XLPE and its surface-modified nanocomposite members a promising material in cables and high-voltage applications.

4 TiO₂ Nanoparticles in XLPE Matrix (TiO₂/XLPE Nanocomposite)

Similar to SiO₂ nanofillers in XLPE, the TiO₂ as nanofillers and their surface modification has also been studied to some extent. The major benefit of titanium dioxide over common nanocomposites is the value of its permittivity constant. The relative permittivity of this material reaches to a level of 100, which is the main reason for attracting many experts in discovering the extraordinary properties of titanium dioxide also called titania. Wang et al. studied the space charge characteristics of the unmodified TiO₂/XLPE [10] nanocomposites and the TiO₂/XLPE modified by dimethyloctylsilane (DMOS) coupling agent where different mass concentrations of coupling agent, 1, 3, and 5 wt% were added in order to determine and modify the properties of TiO₂/XLPE nanocomposite and provide a reasonable explanation of the experimental phenomenon. The experimental techniques like scanning electron microscopy (SEM), volume resistivity testing, and PEA measurements were used for their studies. Interpretation from SEM results showed that the coupling agent DMOS improved the compatibility between TiO₂ nanoparticles and XLPE matrix to some extent and also caused the reduction in agglomeration of TiO₂ nanoparticles compared with unmodified sample. Along with this, the volume resistivity tests were also carried out to analyze the movement of carriers. TiO₂/XLPE nanocomposites had a greater volume resistivity compared to pure XLPE which increased with increasing the filler concentrations. The results of volume resistivity of pure XLPE and TiO₂/XLPE are given in Fig. 6. The PEA method was also used to determine the space charge characteristics of TiO₂/XLPE nanocomposite. They showed that space charge accumulation reduced with increase of TiO₂ nanofiller and also there was an improvement in electric field distribution. The homocharge injection was more predominant in MDOSTiO₂/XLPE than in unmodified one and decreased with increase in filling. The SEM images of TiO₂/

Fig. 6 Volume resistivity of pure-XLPE and TiO₂/XLPE. Adapted from [10]



XLPE, UN-TiO₂/XLPE (1 wt%), MDOS-TiO₂/XLPE (1 wt%), UN-TiO₂/XLPE (5 wt%), and MDOS-TiO₂/XLPE (5 wt%) are shown in Fig. 5.

They showed that MDOS coupling agent improved TiO₂ nanoparticle dispersion and reduced the extent of agglomeration of TiO₂ nanoparticles in XLPE matrix. The order of volume resistivity of three samples is pure XLPE < UN-TiO₂/XLPE < MDOS-TiO₂/XLPE. Their explanation was that MDOS-TiO₂/XLPE nanocomposite had more traps than UN-TiO₂/XLPE, thus capturing more carriers, and the MDOS-TiO₂/XLPE nanocomposite had the largest volume resistivity. From PEA measurements, they showed that TiO₂ nanoparticles largely influenced the space charge accumulation behavior and the DC electric field improved the electric field distribution in TiO₂/XLPE to a large extent.

Wang et al. in 2016 also studied the dielectric properties of TiO₂/XLPE nanocomposites having different mass concentrations of 1, 3, and 5 wt% of TiO₂ [45]. They showed the greater volume resistivity of TiO₂/XLPE nanocomposites compared to XLPE. The TiO₂/XLPE nanocomposites had lower permittivity, low dielectric dissipation, which increased with increase in filling concentrations and decreased with the measured frequency.

Aishwarya S Nair et al. conducted a simulation study to determine the effect of water treeing in XLPE nanocomposites [46]. They showed that common XLPE had a higher electric stress from water treeing and differ from XLPE mixed with titanium dioxide. A two-dimensional single core cable model which was developed using COMSOL MULTIPHYSICS software and electric field distribution was analyzed with the help of finite element method (FEM). The relative permittivity values were changed with respect to the material. Depending on the electric field distribution, water tree was observed. They studied the electrical field distribution and electrical stress experienced in the presence of void, with and without the incorporation of nanoparticles. The duration of the time taken for the initiation of water treeing was found to be prolonged in the presence of nanoparticles. They chose four types of nanofillers namely nanosized titanium, silica, alumina, and nanoclay with XLPE as the base polymer with 2.5 and 15 wt% loading and discarded the higher weight percentage in order to avoid agglomeration. They concluded that the presence of water voids caused more stress on the edges of the water voids due to the high permittivity difference between the XPLE material and water voids. This high stress created a conducting path along the electric field direction resulting in the representation of water tree as a rectangular channel. However, the high electric field path through the insulation led to mechanical damage and insulation breakdown. They showed that the electric field stress inside the nanofiller is lower than that of interface in the presence or absence of water voids. They also added that the nanofillers having high permittivity leads to lower stress when compared to fillers having lower permittivity. Thus, the water treeing process leading to the breakdown of dielectric material was inhibited due to the lower electric stress inside the nanofillers and moves toward maximum stress at the interface points in the nanocomposite material. In the same year, an experimental test was conducted by few researchers; it was found out that the XLPE with titanium dioxide as nanofillers recorded a higher resistivity compared to standard XLPE.

These studies can prove that TiO_2 nanoparticle with XLPE can prove to be a promising member in the nanocomposite material though not as much as SiO_2/XLPE nanocomposite. However, very little studies have been performed relating to TiO_2 with XLPE when compared with SiO_2 with XLPE and hence would require greater attempts of research for a better application of TiO_2 .

5 Organic Montmorillonite Nanoparticles in XLPE Matrix (OMMT/XLPE Nanocomposite)

Montmorillonite (MMT) [47] is a type of layered silicate with two-dimensional nanostructure. Only when it is intercalated with polymer or attains exfoliated dispersion, the composite gives excellent performance. Li et al. investigated the dielectric properties of XLPE/montmorillonite nanocomposites, using two organic intercalants, namely octadecyl quaternary ammonium salt (OMMT1) and double octadecyl benzyl quaternary ammonium salt (OMMT2), each having two long alkyl chains. They also used ethylene vinyl acetate (EVA) that acts as the compatibilizer on this system. The alkane chain part of EVA is compatible with PE/XLPE, and the carboxylic portion of EVA is compatible with OMMT. The organic montmorillonite (OMMT) particles are treated with OMMT1 and OMMT2 and were blended with cross-linked polyethylene to prepare the nanocomposites. XLPE/OMMT composite was obtained by adding a certain proportion of organically modified OMMT1 and OMMT2 into XLPE and was melt blended using a torque rheometer. XLPE/EVA/OMMT composite was obtained by adding the organically modified OMMT1 and OMMT2, polymeric compatibilizer, and the low density polyethylene at a certain proportion for melt blending in the torque rheometer. The specimens under study include XLPE/OMMT1, XLPE/OMMT2, XLPE, XLPE/EVA/OMMT1, and XLPE/EVA/OMMT2. In XLPE/EVA/OMMT1, the interlayer spacing is further enlarged upon the addition of EVA compatibilizer and the layer spacing increases from 3.47 to 3.92 nm.

The variation rate represents the intercalation efficiency. From the morphological studies, they showed the easier intercalation of polyethylene to the OMMT1 layer. The presence of EVA to XLPE/OMMT1 showed a strong interaction at the interface and was free from voids giving excellent nanosized dispersion. However, in the case of OMMT2, the system gave poor intercalation between polyethylene and the OMMT2 layer and no microscale dispersion was observed. The introduction of EVA in XLPE/OMMT2 reduced the agglomeration but not to full extent due to the bulk structure of OMMT2. The dielectric properties of XLPE/OMMT composites were studied using broadband dielectric spectroscopy with a frequency range from 10^{-2} to 10^6 . The dielectric constants of XLPE/OMMT and XLPE/EVA/OMMT nanocomposites were found to decrease with an increase in frequency, and the dielectric constant of the XLPE/EVA/OMMT1 composite was lower than that of XLPE/EVA/OMMT2 due to the melt intercalation of OMMT1 which was well

attained when octadecyl quaternary ammonium salt was used as the intercalant in this system. Hydrogen bonding between the carboxyl parts of EVA was generated by the intercalant present on the surface of the nanocomposite and yields an intense interfacial force. This created difficulty in the turning direction polarization under an applied electric field and thus giving a low polarization rate and dielectric constant. The dielectric loss of neat XLPE remained constant. The accumulation of OMMT2 gave higher loss peak values compared with the accumulation of OMMT1. In the case of OMMT2, two apparent dielectric loss peaks appeared with or without the addition of EVA in the frequency range of 10^2 – 10^5 Hz and in OMMT1 the dielectric loss peak was observed at around 10^4 Hz. The structural difference of two intercalants and their dispersion on the XLPE matrix is the main reason for the difference in the loss peak values of the nanocomposites. The presence of strong interface interaction found between the OMMT layers and XLPE created the controlled segmental movement of the polymer decreasing the molecular polarization ability and thus reducing the dielectric constant and dielectric loss. In XLPE/OMMT nanocomposite, the increase of the melting point system and the broadening of the melting temperature range are closely related to the intercalation efficiency of matrix resin molecules into OMMT. OMMT1 has a greater influence on the melting point and the melting temperature range of the nanocomposites. Thus, OMMT1 has a greater impact on the degree of crystallization and crystalline morphology of the composites than OMMT2. Montmorillonite thus quickens the nucleation in XLPE/OMMT composite. On the other hand, enhanced interfacial interaction and the use of EVA reduce the overall crystallization rate. The use of EVA makes the OMMT and the matrix polymer to be well bounded at the interface. For OMMT1, the PE chains get easily intercalated into the layers and for OMMT2, and the PE was not intercalated and hence the dispersion was only in micron scale. The agglomerated OMMT2 could break away from the PE matrix upon fracture. As the OMMT2 particles are extracted from the matrix, it creates voids. The remaining part of the OMMT2 remains as agglomerate.

Analysis of structure and performance was done with the aid of XRD, DSC, and DMA. These studies show that OMMT are a class of intercalating nanocomposite material with good intercalation. In the rubber state, the system can be completely melted without destroying the interface effect between polymer and nanoparticles that restricts the chain segment movement giving the modulus of elasticity of more than 10^7 MPa. It shows that the addition of OMMT increases the storage modulus of all nanocomposites under a high temperature whose extent depends on the intercalation of polyethylene chain into the montmorillonite. This studies shows that the nanocomposites with good intercalation can improve the storage modulus of XLPE at high temperature.

The dielectric property studies conducted by Li et al. also demonstrate that the addition of OMMT increases the relative dielectric constant of XLPE/OMMT composite. The composites with OMMT1 and OMMT2 are represented by single dielectric loss peak and double dielectric loss peak in the high frequency range, respectively. With increasing temperature, the width of the double peaks increases, the molecular chain segment motion is restricted by the interface interactions, the

distribution of relaxation time widens such that the low-frequency peaks are diffused to a greater extent in the low frequency band. The intercalant of octadecyl quaternary ammonium salt enables a good compatibility between OMMT1 and the matrix resin. The dielectric spectrum displays the single-component dielectric loss peak. Thus, the dielectric constant and dielectric loss of nanocomposite depend on the degree of intercalation in the broadband range. Hence, the higher the degree of intercalation, the lower is the dielectric constant and dielectric loss. And also the dispersion of nanoparticles in matrix resin in the presence of compatibilizer depends on how the compatibilizer matches with the organic intercalants.

Thus, organic intercalants also form an important class of nanocomposites which depends on its performance. Its structure and performance are the keys to design the high-performance polymer nanocomposites.

6 Magnesium Oxide Nanoparticles in XLPE Matrix (MgO/XLPE Nanocomposite)

In addition to SiO_2 , TiO_2 , and montmorillonite particles, MgO particles can also perform its duty as nanomaterial in XLPE nanocomposites. In order to investigate the effect of nano-MgO [48] addition on grounded DC tree in cross-linked polyethylene (XLPE), comparative tree experiments were performed using XLPE and 0.5 wt% MgO/XLPE nanocomposite by periodic prestress-grounding in a needle-plane system by Wang et al. They conducted the space charge measurement using pulsed electroacoustic (PEA) method on both kinds of samples. The MgO/XLPE nanocomposite exhibited higher 50% tree inception voltage in the tree experiment. The results gave more homocharge injection in XLPE which hinders the generation of electrical tree. The MgO/XLPE nanocomposite shows shorter average tree length and width under positive voltages that result in slower tree propagation. Also, the average tree length-width ratio in MgO/XLPE nanocomposite decreases faster with increasing positive voltage. Two kinds of samples were prepared by Wang et al. for their studies, one is pure XLPE, and the other is 0.5 wt% MgO/XLPE nanocomposite. Both the samples were subjected to the grounded DC tree experiments under different polarities at room temperature. The sample placed in a glass container was immersed in pure silicon oil. The ten needles were connected by the copper wire. The DC voltage was provided with a half-wave rectifier. The experiment was done by periodic prestress-grounding, i.e., applying a DC voltage for 3 min and then grounding for 2 s, repeating for 20 times like this. Then the sliced sample was observed under microscope. Under each voltage, one sample with ten needles was tested for each material. Space charge distribution of the samples was measured using a PEA measurement system at room temperature. The upper electrode was set to be a semiconductive material and the lower electrode to be aluminum. The applied electric fields were 10, 20, 30, 40, and 50 kV/mm. The space charge distribution was measured during each electric field applying for

30 min. The ratio between the number of needles with trees and the total number of needles is defined as the tree initiation ratio. And this ratio was found to increase with the increase of voltage, and the tree initiation ratio of MgO/XLPE nanocomposite is lower than XLPE under the same voltage. The 50% tree inception voltage of MgO/XLPE nanocomposite is higher than that of XLPE. They provided relation between the positive voltage and tree initiation ratio, average tree length and average width of the tree. When the DC voltages were negative no obvious change in tree initiation ratio with the increase of voltage was observed. With the increase of voltage, the average tree length increases, and it increases faster under positive voltages. Also, the average tree length under positive voltage is always greater than that under negative voltage. We can also recognize that the average tree length of XLPE is greater than that of MgO/XLPE nanocomposite under the same positive voltage. When the voltage is negative and lower than 29 kV, there is no significant difference in average tree length between the two samples. When it is higher than 29 kV, the average tree length of XLPE is a bit greater than that of MgO/XLPE nanocomposite. With the increase in voltage, the average tree width increases, and the increase is faster under positive voltages. When the voltage is lower than 26 kV, the average tree width of MgO/XLPE nanocomposite under negative voltage is greater than that under positive voltage. When the voltage is higher than 26 kV, the average tree width of both samples under positive voltage is greater than that under negative voltage. When the voltage is positive, the average tree width of XLPE is always greater than that of MgO/XLPE nanocomposite under the same voltage. When the voltage is negative and lower than 32 kV, the average tree width in XLPE is smaller than that in MgO/XLPE nanocomposite. When the negative voltage increases to 35 kV, the average tree width in XLPE is a little bit greater than that in MgO/XLPE nanocomposite. When the voltage is positive, the average tree length–width ratio of both samples decreases with the voltage increasing, indicating that the tree grows not only lengthways, but also laterally. Also, when the voltage is positive, the decrease of average tree length–width ratio of MgO/XLPE nanocomposite is faster than that of XLPE. And when the voltage is lower than 29 kV, the average tree length–width ratio of MgO/XLPE nanocomposite is always greater than that of XLPE. However, when the positive voltage increases to 29 kV, the average tree length–width ratio of XLPE exceeds that of MgO/XLPE nanocomposite. Hence, the lateral branches of electrical tree in MgO/XLPE nanocomposite is very short compared with the lengthways branches when the voltage is low and grow significantly with the voltage increasing. It can be observed that in XLPE, a huge amount of homocharge accumulates near both electrodes. The amount of homocharge increases with the increasing of applied electric field. As for MgO/XLPE nanocomposite, heterocharge is observed near both electrodes and it increases with the increasing of applied electric field. It can be concluded that the homocharge injection is more serious in XLPE than in MgO/XLPE nanocomposite. The heterocharge accumulation in the latter one may due to the dissociation of the impurities introduced by nanoparticles. The result of space charge measurement shows that the homocharge injection is more serious in XLPE than in MgO/XLPE nanocomposite when under

the same voltage. Thus, it can be inferred that when applying a DC voltage during the tree experiment, more homocharge is injected and accumulates around the needle tip in XLPE than in MgO/XLPE nanocomposite. Hence, the local electric strength produced by the injected charge and the electric mechanical energy released by the charge returning at grounding in XLPE is stronger than those in MgO/XLPE nanocomposite. Besides, in MgO/XLPE nanocomposite, the nanoparticles act as traps and hinder the returning of injected charge back to needle tip, which may reduce the release of electric mechanical energy. That explains why it is easier to generate electrical tree in XLPE.

Y Murata et al. investigated the volume resistivity and space charge distribution in XLPE/MgO nanocomposite [49] materials. Investigations were made for both XLPE and XLPE/MgO nanocomposite materials. The results indicate the suitability of XLPE/MgO nanocomposite material for HVDC insulation. The applications of XLPE in AC transmission up to a rated voltage of 500 kV have been well studied but its use in 500 kV DC has not yet been brought to realization. In order for developing this application, Electric Power Development Co., Ltd. and J-Power Systems Corp. jointly studied over several years and developed DC 500 kV XLPE insulated cable in the year 2001. Thus, in order for using the XLPE insulation material for DC cable, inorganic filler was used. The inorganic filler selected was nanosized magnesium oxide (MgO). Four materials, XLPE(C) (conventional XLPE insulation for AC cable), XLPE(C)/MgO (nanocomposite material made by mixing XLPE(C) with nanosized MgO), XLPE(S) (specially manufactured XLPE including lower content of cross-linking by-products such as acetophenone), and XLPE (S)/MgO (nanocomposite material which is made by mixing XLPE(S) with nanosized MgO. This material is excellent for DC application.), were used for their study.

The systems under study for the measurement of volume resistivity and space charge distribution were in the form of hot pressed sheet with a thickness of about 100 μm . The nanosized MgO had an average diameter of about several tens of nm. A three-terminal electrode system was used for the measurement of volume resistivity where the diameter of the main electrode was 65 mm. Applied electric fields were 40, 60, and 80 kV/mm, and measurement temperatures were 30, 60, and 90 $^{\circ}\text{C}$. The volume resistivity was evaluated from the leakage current value noted ten minutes after the DC voltage application. The electric field dependence of volume resistivity is at 90 $^{\circ}\text{C}$, and the temperature dependence of volume resistivity under the electric field is of 80 kV/mm. From the results of electric field dependence of the volume resistivity at a temperature of 90 and 60 and 30 $^{\circ}\text{C}$ and temperature dependence of the volume resistivity at an electric field of 80, 40, and 60 kV/mm, the volume resistivity follows the order XLPE(S)/MgO > XLPE(C)/MgO > XLPE(S) > XLPE(C).

Pulsed electroacoustic (PEA) method has been utilized by Y Murata et al. for the determination of space charge distribution. Ambient temperature was used for the measurement and DC electric field of 150 kV/mm was applied to the specimen during space charge measurement and the duration of the measurement was 60 min. The space charge distribution was at 150 kV/mm. These results when compared

with respective base polymer showed that the MgO nanocomposites have greater volume resistivity. The presence of cross-linking by-products such as acetophenone in XLPE(C) reduces the volume resistivity of XLPE and also the presence of the small amount of by-products in XLPE(S) results in its larger volume resistivity than XLPE(C). XLPE(S) and LDPE have almost nearer value of the volume resistivity. The volume resistivity of XLPE(C)/MgO is lower than that of XLPE(S)/MgO and LDPE/MgO. The volume resistivity of XLPE(S)/MgO is almost the same as that of the LDPE/MgO. This indicates that the by-products (which decreases the volume resistivity) and nanosized MgO (which increases the volume resistivity) act synergistically in insulating material. Thus, the nanosized MgO makes the XLPE(S)/MgO material, excellent for DC application. The results from space charge distribution indicate that nanosized MgO prevents the packet-like charge from appearing in the nanocomposite materials at high electric fields. Of all the materials investigated by Murata et al., the XLPE(S)/MgO can be seen to be excellent for DC application.

7 Silicon Carbide Nanoparticles in XLPE Matrix (SiC/XLPE Nanocomposite)

Apart from inorganic oxide, inorganic carbides also prove to be an important nanoparticle in nanocomposites. Wang et al. investigated the dielectric properties, DC breakdown strength, and space charge distribution of XLPE/SiC nanocomposites [50]. Free additive LDPE was the base polymer, and 1, 3, and 5 wt% SiC nanoparticles were used for the studies. Here, the particle size of SiC was maintained at 40 nm, and DCP was used as the cross-linking agent for this nanocomposite. The SEM images of XLPE and SiC/XLPE is shown in Fig. 7 below. This results shows that SiC nanoparticles were well dispersed effectively in the 1 wt% nanocomposite. The concentration of the 3 wt% nanocomposite showed some amount of agglomerations, where as in the 5 wt% concentration, few separated nanoparticles could be detected, which caused nanoparticle agglomerations.

Wang et al. studied the dielectric properties using a Novocontrol ALPHA-A high-resolution dielectric analyzer in the frequency range of 10^{-1} – 10^6 Hz. The results of dielectric measurements of XLPE and XLPE/SiC nanocomposites are given in figure. With increase in the nanoparticle weight percentage, both the real and imaginary permittivity increases whose high value is due to the Maxwell–Wagner interface polarization and also the Gouy–Chapman layers in the nanocomposites. They used the Weibull probability parameters for analyzing the DC breakdown strength. Table 3 shows the Weibull parameters for XLPE/SiC nanocomposites.

This shows that 1 and 3 wt% XLPE/SiC nanocomposites give a higher-scale parameters compared with neat XLPE. However, in the 5 wt% XLPE/SiC nanocomposites, smaller-scale parameters predominate, and this causes the reduction in DC breakdown strength. This decrease is due to the poor distribution of

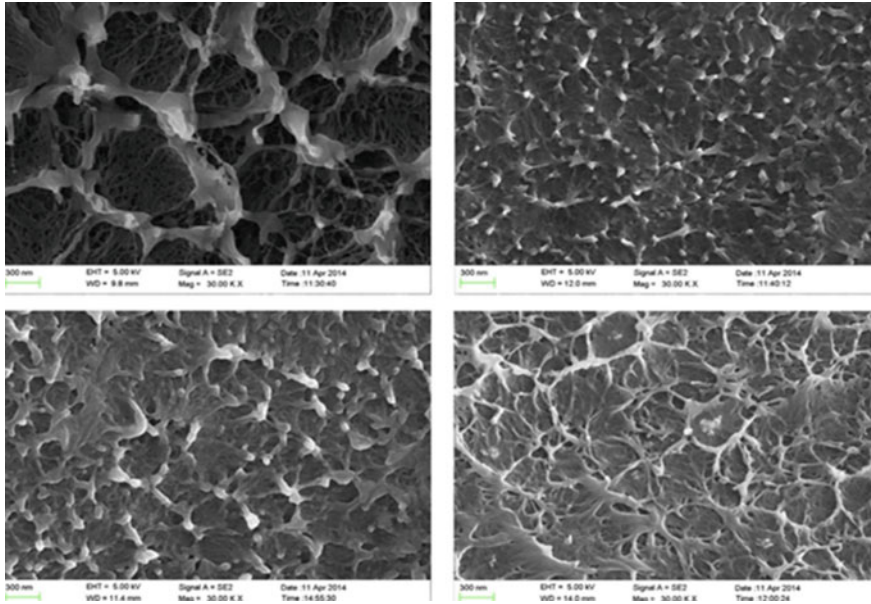


Fig. 7 SEM images of XLPE, 1 wt% XLPE/SiC nanocomposite (right), 3 wt% XLPE/SiC nanocomposite (lower left), 5 wt% XLPE/SiC nanocomposite (lower right). Adapted from [50]

Table 3 Weibull parameters for XLPE/SiC nanocomposites

	XLPE	XLPE/1 wt% SiC	XLPE/3 wt% SiC	XLPE/5 wt% SiC
β	13.08	24.72	15.97	9.71
A	260.67	331.99	297.19	244.71

Adapted from [50]

nanoparticles in the composite. Tanaka et al. gave a multicore model [51] to explain the sharp value of DC breakdown strength which is applicable in space charge behavior. From this model, nanocomposites with lower concentrations of nanoparticles cannot overlap the Gouy–Chapman diffuse layers due to the greater distance between the nanoparticles which also resulted in the better DC breakdown voltage of 1 and 3 wt% sample than 5 wt% sample. In the 5 wt% XLPE/SiC nanocomposite, nanoparticle concentration was high making it difficult to disperse SiC nanoparticles in the polymer matrix. As a result of agglomeration, an overlapping of the Gouy–Chapman diffuse layer was observed. They performed the space charge studies with a pulsed electroacoustic (PEA) method, and the space charge development was confirmed after the 300, 900, and 1800 s of polarization. From the space charge results given in Fig. 8, it has been found that the 1 wt% XLPE/SiC nanocomposite has minimum and 5 wt% XLPE/SiC nanocomposites has the maximum space charge accumulation.

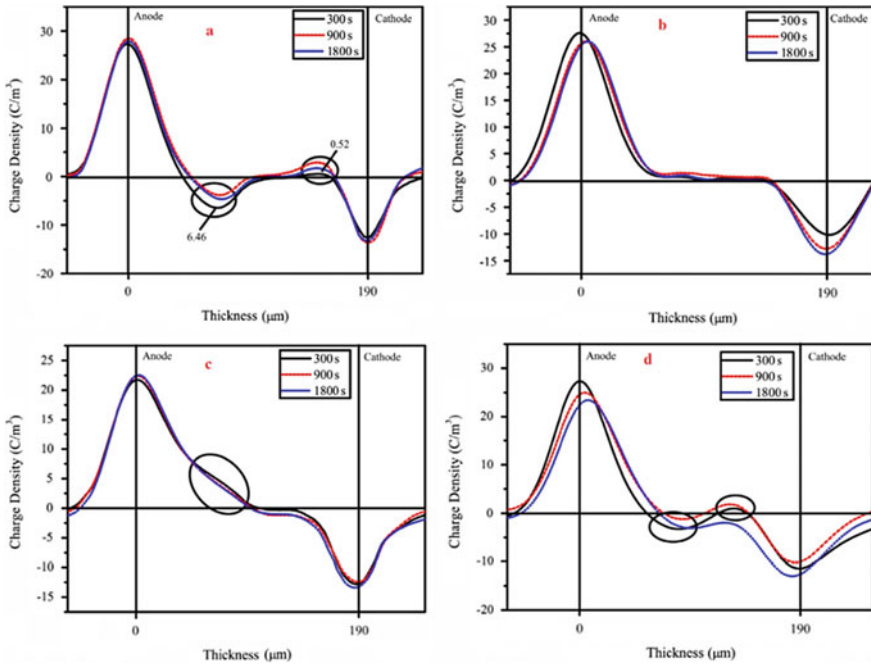


Fig. 8 Space charge behavior of **a** XLPE, **b** 1 wt% XLPE/SiC nanocomposite, **c** 3 wt% XLPE/SiC nanocomposite, and **d** 5 wt% XLPE/SiC nanocomposite. Adapted from [50]

According to Tanaka et al., nanoparticles create deep traps near to the nanoparticle nanocomposite, and each trap could attract a number of electrons and holes. As a result, electrical neutralization occurs when electrons and holes surround a single nanoparticle, preventing charge accumulation in the 1 wt% XLPE/SiC nanocomposite. Also increasing the nanoparticle concentration results in nanoparticle agglomeration affecting the interfacial characteristics between the polymer and nanoparticle. Hence, SiC/XLPE nanocomposite also proves to be an important member of insulation application.

8 XLPE/Clay Nanocomposites

XLPE has proved to be an important insulation material used in nuclear power plant which has been supported by its high melting point, tensile strength, chemical, abrasion, and wear resistance. High voltage, low dielectric loss, resistance to thermal disfigurement, and aging allow them to carry current during different situations like normal conditions, short circuit, emergency, etc., incorporation of clay results on XLPE/clay nanocomposite [52] with unique dielectric properties due to

the multilayered structure of clay. They are a contributing factor to flame retardancy mechanisms.

The XLPE/clay nanocomposites, with different weight composition of nanoparticles up to 5%, were prepared by El Sayed Soliman Said et al. by mixing nanoparticles dispersion in the melted XLPE matrix at a temperature of 120 °C. The nanocomposite material and insulation granules were cooled by water and hot air dried at temperature of 55–65 °C and the obtained materials have been molded at 180 °C in hot press machine for 15 days. Sheets were obtained of thickness 1–2 mm and dimension 20 × 20 cm and pressure 300 Pa. These sheets were divided into two parts in order to study mechanical and electrical characteristics that is dumbbell shape for studying mechanical properties and cubic shape for studying electric properties.

They studied the surface morphology of the nanocomposites using SEM. The SEM of nanocomposite with 1 wt% of nanoclay at different irradiation doses, 50, 100, 300, and 500 KGy as, respectively, showed good mechanical properties. SEM results show that XLPE has a lamellar and spherulitic morphology with an increase in crystallinity and density and hence increases the stiffness and tensile strength of material.

They determined the tensile strength of the nanocomposite of different composition (1%, 2.5%, 4%, and 5%) in the presence and absence of radiation. In the absence of radiation, the tensile strength amounted to (15.69), (21.48), (17.87), (11.06) N/mm², respectively. On the presence of radiation, the tensile strength gradually decreased with increase in the dose of radiation thereby rearranging to cross-linking. This increased the tensile strength for 4 and 5% composition at 100 kGy. Their studies showed that 4% composition gave the best performance of radiation resistance. And 50–300 KGy dose decreases the tensile strength.

They also presented the percentage elongation for different composition. Accordingly the 4% composition had the highest mechanical strength at low doses of radiation. Also, the breakdown strength of nanocomposite increased with incorporation of clay nanoparticles than unfilled one and electrical capacitance and dielectric constant also increased by 20%, for the XLPE/clay nanocomposites at 50 KGy in comparison to pure XLPE. They also presented the comparison of tensile strength, breakdown voltage, and capacitance for neat XLPE and XLPE/clay nanocomposite and showed that the nanocomposite with improved mechanical, electrical, and chemical properties is an ameliorated insulation material for nuclear power plants.

9 XLPE/Al₂O₃ Nanocomposites

The XLPE/ α -Al₂O₃ nanocomposites [53] with its unique qualities have been developed by mechanical blending by Xiangjin Guo et al. and hot press cross-linking where the Al₂O₃ nanosheets were uniformly distributed into a XLPE matrix by the efficient mixing of three constituent namely coated α -Al₂O₃, LDPE,

and dicumyl peroxide (DCP) as cross-linking agent. The presence of Al_2O_3 nanosheets introduced many deep traps that blocked charge injection, reduced charge carrier mobility and conductivity from 3.25×10^{-13} S/m to 1.04×10^{-13} S/m, increased direct current breakdown strength from 220 to 320 kV/mm, and reduced space charge accumulation in XLPE matrix. Further surface modification improved these factors to a larger extent. Al_2O_3 has different crystalline forms with $\alpha\text{-Al}_2\text{O}_3$ showing excellent properties, such as hardness, dimensional stability, good electrical insulation, dielectric constant, and reduced dielectric loss, etc., and the morphological studies were performed using SEM and TEM.

The comparison of DC breakdown strengths of neat XLPE and XLPE/ $\alpha\text{-Al}_2\text{O}_3$ nanocomposites having 0.2, 0.5, 1.0, and 2.0 wt% coated $\alpha\text{-Al}_2\text{O}_3$ is given in Fig. 9. It has been found that in the DC breakdown strength in XLPE/ $\alpha\text{-Al}_2\text{O}_3$ nanocomposites increases with increase in $\alpha\text{-Al}_2\text{O}_3$ percentage.

The space charges distribution of pure XLPE and the XLPE/ $\alpha\text{-Al}_2\text{O}_3$ nanocomposites containing 0.2, 0.5, and 1.0 wt% of $\alpha\text{-Al}_2\text{O}_3$ on the application of a DC voltage of 20 kV/mm is presented in Fig. 10. These space charge studies on neat XLPE and XLPE/ $\alpha\text{-Al}_2\text{O}_3$ nanocomposites using the PEA method show that the presence of $\alpha\text{-Al}_2\text{O}_3$ suppresses the space charge accumulation in the XLPE due to the introduction of number of deep traps in the interface between XLPE matrix and caused by the $\alpha\text{-Al}_2\text{O}_3$. On the application of electric field, such traps capture the electrons or holes injected from the anode or cathode thereby reducing the movement of charge inside the insulation material. As a result of these modified properties, XLPE/ $\alpha\text{-Al}_2\text{O}_3$ nanocomposites may be proved to have important application in the development of materials for HVDC cable insulation.

Yong-Jun Park et al. in 2014 synthesized Al_2O_3 /XLPE nanocomposite using two roll mill [54]. Then the compounds were press-molded at 120 °C for 5 min after

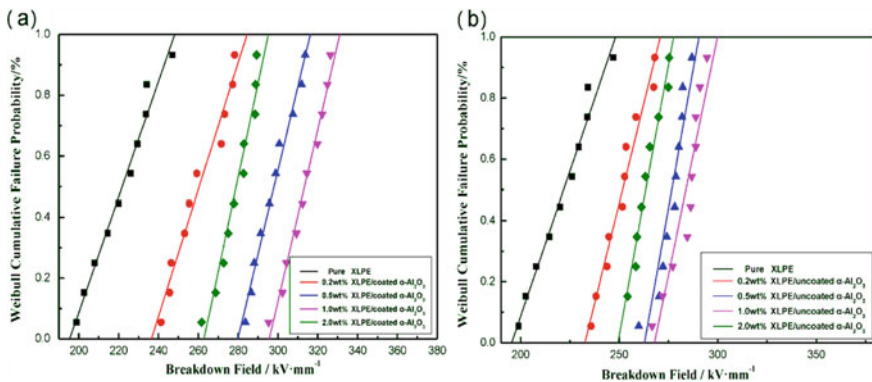


Fig. 9 **a** Weibull plots for comparison of DC breakdown strength of pure XLPE and XLPE/ $\alpha\text{-Al}_2\text{O}_3$ nanocomposites containing 0.2, 0.5, 1.0, and 2.0 wt% coated $\alpha\text{-Al}_2\text{O}_3$ and **b** Weibull plots for comparison of DC breakdown strength of pure XLPE and XLPE/ $\alpha\text{-Al}_2\text{O}_3$ nanocomposites containing 0.2, 0.5, 1.0, and 2.0 wt% uncoated $\alpha\text{-Al}_2\text{O}_3$. Adapted from [53]

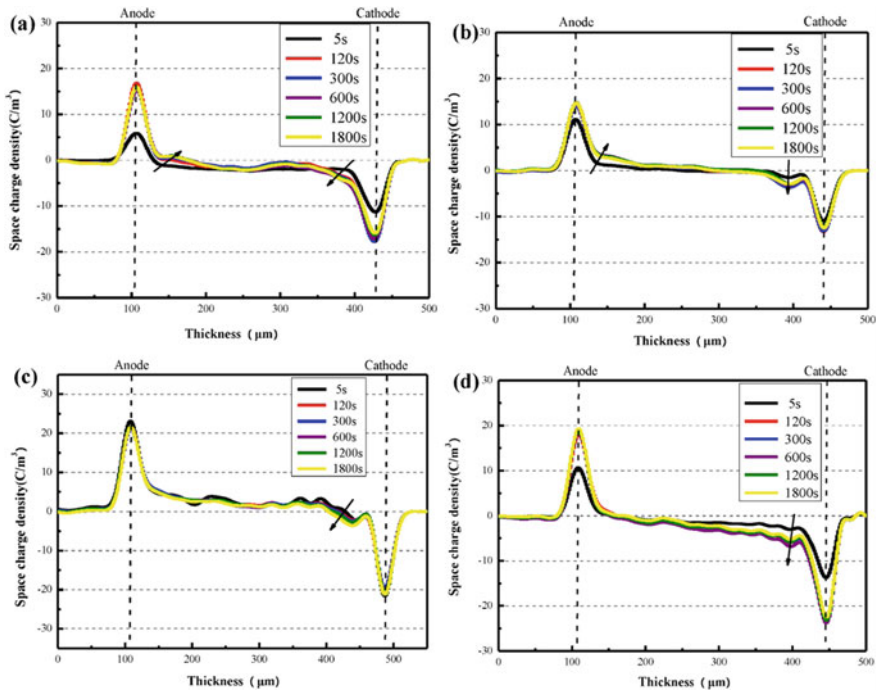


Fig. 10 a The space charge density of pure XLPE varies with the application time of DC voltage (20 kV/mm), b–d the space charge density of the XLPE/ Al_2O_3 nanocomposites containing 0.2, 0.5, and 1.0 wt%— Al_2O_3 varies with the application time of DC voltage (25 kV/mm). Adapted from [53]

that they were cross-linked by hot press at 180 °C for 15 min at a pressure of 10 MPa. It resulted in disk-like structures of 100–120 μm thickness and 100 mm diameter. The resulting samples were then subjected to DC breakdown, DC polarity reversal breakdown, and volume resistivity. The DC breakdown was measured using sphere-to-sphere electrode system at 25 and 90 °C following the IEC60243 standard. The breakdown strength of the systems was studied using Weibull distribution. Their results show that the DC breakdown strength increased with increase in the amount of filler up to 3 phr and the effect of space charge on break down decreased with increase in fillers. They also concluded the increase in volume resistivity with addition if nanofillers and its corresponding decrease with increase in temperature and electric field. Their results were also an additional support to the application of $\text{Al}_2\text{O}_3/\text{XLPE}$ nanocomposite in HVDC insulating materials.

Liang cao et al. presented the conductivity studies of a nano- $\text{Al}_2\text{O}_3/\text{XLPE}$ composite and XLPE filled with polymer from 30 to 90 °C [55]. The current curves of nanocomposites gave similar behavior as ordinary XLPE and different behavior than polymer filled XLPE. Also, the conductivity of polymer filled XLPE was less than nano- $\text{Al}_2\text{O}_3/\text{XLPE}$ composite and ordinary XLPE at temperature lower than

70 °C. These results may be an inspiration for the application of XLPE nanocomposites for HVDC insulations.

10 Other XLPE-Based Nanocomposites

Ahmed Mohammed et al. developed novel nanocomposite as insulation materials for the enhancement of power cables [56]. They focused particularly on thermal conductivity, coefficient of the thermal expansion, and thermal endurance of PVC and XLPE nanocomposites. They result on PVC and XLPE with different nanocomposites like clay, glass beads, and BaTiO₃. Their results proved that glass bead 15 wt% composite has high electric field distribution within insulation due to its low dielectric constant. On the other hand PVC-BaTiO₃ 15 wt% has low electric field distribution due to its high dielectric constant and other composites have electric distribution between these samples. The potential and electric field distribution of the samples were also studied. They inferred that XLPE-Clay 15 wt% nanocomposite showed high electric field distribution and low potential distribution as a result of its reduced dielectric constant and XLPE-Al₂O₃ showed low electric field distribution and high potential distribution as a result of its high dielectric constant. Other members showed electric distribution between these samples. Accordingly addition of nanofillers like clay, BaTiO₃, Al₂O₃ to polymers enhanced their electrical properties and developed their electrostatic field to withstand greater strength. Addition of clay has raised the electric field strength of nanocomposite in comparison to other nano-fillers of fumed silica and Al₂O₃. Hence the composition and type of nanofillers added decides the thickness of the insulating power cables.

Kai Shang Lim et al. in their work reported the effect of nanofillers on the mechanical, physical, dielectric, and thermal properties of XLPE matrix [57]. XLPE having 0.5–2% of ZnO, Al₂O₃, and OMMT nanofillers were prepared by melt mixing with a single screw extruder and then hot press molding. The resulting nanocomposites were subjected to tensile test, water absorption, linear rate of burning, dielectric breakdown strength, thermal stability tests, etc., and the morphological studies were performed using SEM. Their studies showed that the presence of nanofillers increased the tensile strength, elongation at break, Young's modulus, burning rate, dielectric breakdown strength, and decomposition temperature. From their comparison with different nanocomposites, they concluded that Al₂O₃ exhibited the highest properties in comparison to ZnO and OMMT containing nanocomposites. The hydrophilic properties of nanofillers increased the water absorption property with time. However, water absorption increased with time due to the hydrophilic properties of nanofillers.

BX Du et al. investigated the temperature dependence of conductivity and space charge properties of XLPE/graphene oxide (GO) nanocomposites [58]. XLPE samples with varying GO mass fractions of 0, 0.001, 0.01, and 0.1 wt% were prepared. For this the GO prepared by Hummers method with XLPE (mixture of LDPE and dicumyl peroxide) was desiccated for more than 24 h at 80 °C.

Then different concentrations of GO nanoparticles (0, 0.001, 0.01, 0.1 wt%) at 110 °C were blended with XLPE matrix. Finally the resulting was shaped to produce the XLPE/GO nanocomposite of thickness $250 \pm 3 \mu\text{m}$ and maintained in vacuum chamber for 48 h. The related morphological studies were performed using SEM. Using the resulting sample the conductivity, space charge nature and break down strength were analyzed. A three-electrode system was utilized to determine the DC conductivity of the sample. The temperature was maintained between 20 and 150 °C. The space charge studies were conducted using PEA method and the temperature was maintained between 20 and 100 °C DC breakdown strength was conducted using two-copper-ball-electrode system and the power source with a 500 V/s ramping speed was used. They could conclude that the XLPE/GO nanocomposites with GO of 0.01 wt% showed a lower conductivity, space charge accumulation, and higher DC breakdown strength than free XLPE due to the interactions and the deep traps developed by the GO nanoparticles. Also, the temperature dependence of the electrical properties of nanocomposites decreased when appropriate amount of GO was presented. This study also shows that XLPE/GO nanocomposites can also be an important member in HVDC cable insulation.

Guochang Li et al. studied the effect of different concentration of boron nitride nanosheets (BNNSs) on space charge accumulation in XLPE/BNNS nanocomposite [59, 60]. Melt blending method was used to prepare the nanocomposite in an environment of 25 °C and humidity 60 RH%. Finally five different concentrations, 0.1, 0.5, 1, 3, and 5 wt% of BNNS in XLPE were obtained. The results shows a small amount of BNNS (<0.5 wt%) in XLPE matrix that lowers the space charge accumulation due to the formation of deep traps. The increase of BNNS concentration reduces the charge inhibition effect in the system. PEA results show that the accumulated charges increase when the concentration is 1 wt% and for higher concentration the more shallow traps in nanocomposites results in reduced charge accumulation. Hence, these nanocomposites also prove to be better insulation material.

In addition to these nanocomposites, a wide variety of other XLPE nanocomposites has been developed and is also in the course of development to meet the requirements of insulation materials.

11 Conclusion

Apart from these above-mentioned nanoparticles, there are other materials like XLPE/alumina/clay hybrid nanocomposites, Fe_3O_4 , ZnO nanocomposites, semiconductors like PbS- and CdS-based nanocomposites, etc., gaining a great attraction by the scientific world. However, the use of nanocomposite in electrical insulation will increase in the coming days due to its highly encouraging advantages through the addition of small quantities of nanofillers. Also, use of self-healing nanocomposites may acquire the considerable attention in coming days. Furthermore, the interdisciplinary studies in different areas like electrical engineering, computer

science, physics, and chemistry may also accelerate the research to discover new areas of applications. However, the cost reduction and safety issues can also play major roles in its production and implementation.

References

1. Pleša I et al (2016) Properties of polymer composites used in high-voltage applications. *Polymers* 8(5):173
2. Ajayan PM, Schadler LS, Braun PV (2006) Nanocomposite science and technology. John Wiley & Sons
3. Tamboli SM, Mhaske ST, Kale DD (2004) Crosslinked polyethylenes
4. Aljoumaa K, Ajji Z (2016) Mechanical and electrical properties of gamma-irradiated silanecrosslinked polyethylene (Si-XLPE). *J Radioanal Nucl Chem* 307(2):1391–1399
5. Montanari GC et al (2001) Space-charge trapping and conduction in LDPE, HDPE and XLPE. *J Phys D Appl Phys* 34(18):2902
6. Fu M et al (2007) Influence of thermal treatment and residues on space charge accumulation in XLPE for DC power cable application. *IEEE Trans Dielectr Electr Insul* 14(1):53–64
7. Mark JE et al (2005) Inorganic polymers. Oxford University Press on Demand
8. Vahedy V (2006) Polymer insulated high voltage cables. *IEEE Electr Insul Mag* 22(3):13–18
9. Montanari GC et al (2005) From LDPE to XLPE: investigating the change of electrical properties. Part I. Space charge, conduction and lifetime. *IEEE Trans Dielectr Electr Insul* 12(3):438–446
10. Wang Y et al (2016) Effect of nanoparticle surface modification and filling concentration on space charge characteristics in TiO₂/XLPE nanocomposites. *J Nanomater* 2016
11. Lee HWH, Keshavarz M (2004) Nanocomposite materials with engineered properties. U.S. Patent No. 6,710,366, 23 Mar 2004
12. Glatkowski PJ, Arthur DJ (2004) Nanocomposite dielectrics. U.S. Patent No. 6,762,237, 13 Jul 2004
13. Thomas S, Jose JP (2017) 12 Cross-linked polyethylene nanocomposites for dielectric applications. *Advanced composite materials: properties and applications*. Sciendo Migration, pp 527–544
14. Park Y-J et al (2014) Electrical conduction of a XLPE nanocomposite. *J Korean Phys Soc* 65(2):248–252
15. Lewis TJ (1994) Nanometric dielectrics. *IEEE Trans Dielectr Electr Insul* 1(5):812–825
16. Kurnianto R et al (2007) Characterization of tree growth in filled epoxy resin: the effect of filler and moisture contents. *IEEE Trans Dielectr Electr Insul* 14(2):427–435
17. Iizuka T, Tanaka T (2009) Effects of nano silica filler size on treeing breakdown lifetime of epoxy nanocomposites. In: 2009 IEEE 9th international conference on the properties and applications of dielectric materials. IEEE
18. Tanaka T et al (2009) Tree initiation and growth in LDPE/MgO nanocomposites and roles of nano fillers. In: 2009 IEEE conference on electrical insulation and dielectric phenomena. IEEE
19. Tanaka T et al (2011) Dielectric properties of XLPE/SiO₂ nanocomposites based on CIGRE WG D1 24 cooperative test results. *IEEE Trans Dielectr Electr Insul* 18(5):1482–1517
20. Zhang L et al (2014) Effect of nanoparticle surface modification on charge transport characteristics in XLPE/SiO₂ nanocomposites. *IEEE Trans Dielectr Electr Insul* 21(2):424–433
21. Zhang L et al (2014) Effect of nanoparticle surface modification on breakdown and space charge behavior of XLPE/SiO₂ nanocomposites. *IEEE Trans Dielectr Electr Insul* 21(4):1554–1564

22. Zhang L et al (2014) Space charge behavior of XLPE/SiO₂ nanocomposites with nanoparticle surface modification. In: 2014 IEEE electrical insulation conference (EIC). IEEE
23. Lv Z et al (2013) Thickness dependence of space charge in XLPE and its nanocomposites under temperature gradient. In: 2013 IEEE international conference on solid dielectrics (ICSD). IEEE
24. Li S et al (2016) Modelling of dielectric breakdown through charge dynamics for polymer nanocomposites. *IEEE Trans Dielectr Electr Insul* 23(6):3476–3485
25. AshishSharad P, Sathish Kumar K (2017) Application of surface-modified XLPE nanocomposites for electrical insulation-partial discharge and morphological study. *Nanocomposites* 3 (1):30–41
26. Kaihao J et al (2018) Study on dielectric structure and space charge behavior of XLPE/SiO₂ nanocomposites. In: 2018 12th International conference on the properties and applications of dielectric materials (ICPADM). IEEE
27. Han B et al (2016) QM/MD simulations on the role of SiO₂ in polymeric insulation materials. *RSC Adv* 6(1):555–562
28. Balascio JF, Lind T (1997) The growth of piezoelectric alpha quartz crystals. *Curr Opin Solid State Mater Sci* 2(5):588–592
29. De Leeuw NH, Manon Higgins F, Parker SC (1999) Modeling the surface structure and stability of α -quartz. *J Phys Chem B* 103(8):1270–1277
30. Wegener J, Janshoff A, Steinem C (2001) The quartz crystal microbalance as a novel means to study cell-substrate interactions in situ. *Cell Biochem Biophys* 34(1):121–151
31. Ayad MM, Zaki EA, Stejskal J (2007) Determination of the dopant weight fraction in polyaniline films using a quartz-crystal microbalance. *Thin Solid Films* 515(23):8381–8385
32. Rignanese G-M et al (2000) First-principles molecular-dynamics study of the (0001) α —quartz surface. *Phys Rev B* 61(19):13250
33. Koudriachova MV, Beckers JVL, De Leeuw SW (2001) Computer simulation of the quartz surface: a combined ab initio and empirical potential approach. *Comput Mater Sci* 20 (3-4):381–386
34. Del Rosal I et al (2015) Grafting of lanthanide complexes on silica surfaces dehydroxylated at 200 °C: a theoretical investigation. *New J Chem* 39(10):7703–7715
35. Chandrasekhar PS, Komarala VK (2015) Effect of graphene and Au@SiO₂ core–shell nano-composite on photoelectrochemical performance of dye-sensitized solar cells based on N-doped titania nanotubes. *RSC Adv* 5(103):84423–84431
36. Zhao X et al (2011) Investigations on B-doped SiO₂ thermal protective coatings by hybrid sol–gel method. *Thin Solid Films* 519(15):4849–4854
37. Zhang S-S, Zhao Z-Y, Yang P-Z (2015) Analysis of electronic structure and optical properties of N-doped SiO₂ based on DFT calculations. *Modern Phys Lett B* 29(19):1550100
38. Pacchioni G, Vezzoli M, Fanciulli M (2001) Electronic structure of the paramagnetic boron oxygen hole center in B-doped SiO₂. *Phys Rev B* 64(15):155201
39. Zheng X, Liu Y, Wang Y (2018) Electrical tree inhibition by SiO₂/XLPE nanocomposites: insights from first-principles calculations. *J Mol Model* 24(8):200
40. Kresse G, Furthmüller J (1996) Efficient iterative schemes for ab initio total-energy calculations using a plane-wave basis set. *Phys Rev B* 54(16):11169
41. Kresse G, Hafner J (1993) Ab initio molecular dynamics for liquid metals. *Phys Rev B* 47 (1):558
42. Kresse G, Hafner J (1994) Norm-conserving and ultrasoft pseudopotentials for first-row and transition elements. *J Phys: Condens Matter* 6(40):8245
43. Perdew JP, Burke K, Ernzerhof M (1996) Generalized gradient approximation made simple. *Phys Rev Lett* 77(18):3865
44. Blöchl PE, Jepsen O, Andersen OK (1994) Improved tetrahedron method for Brillouin-zone integrations. *Phys Rev B* 49(23):16223
45. Wang Y et al (2016) Study on dielectric properties of TiO₂/XLPE nanocomposites. In: 2016 IEEE international conference on high voltage engineering and application (ICHVE). IEEE

46. Nair AS et al (2016) Influence of nanofillers on resistance to water tree in XLPE nano composite. In: 2016 International conference on circuit, power and computing technologies (ICCPCT). IEEE
47. Li X et al (2014) Influence of organic intercalants on the morphology and dielectric properties of XLPE/montmorillonite nanocomposite dielectrics. *IEEE Trans Dielectr Electr Insul* 21 (4):1705–1717
48. Yani W et al. The effect of nano-MgO addition on grounded DC tree in cross-linked polyethylene
49. Murata Y et al (2008) Investigation of space charge distribution and volume resistivity of XLPE/MgO nanocomposite material under DC voltage application. In: 2008 International symposium on electrical insulating materials (ISEIM 2008). IEEE
50. Wang Y, Wang C, Xiao K (2016) Investigation of the electrical properties of XLPE/SiC nanocomposites. *Polym Testing* 50:145–151
51. Tanaka T, Kozako M, Fuse N, Ohki Y (2005) Proposal of a multicore model for polymer nanocomposite dielectrics. *IEEE Trans Dielectr Electr Insul* 12:669
52. El-kattan WA-E et al (2019) A reduced gamma radiation effects on the electrical insulating cables using XLPE/clay nanocomposites. *J Al-Azhar University Eng Sect* 14(53):1392–1402
53. Guo X et al (2020) Investigation of the space charge and DC breakdown behavior of XLPE/ α -Al₂O₃ nanocomposites. *Materials* 13(6):1333
54. Park Y-J et al (2014) DC conduction and breakdown characteristics of Al₂O₃/cross-linked polyethylene nanocomposites for high voltage direct current transmission cable insulation. *Japanese J Appl Phys* 53(8S3):08NL05
55. Cao L et al (2019) Conductivity of HVDC cable insulation materials: case study between XLPE nanocomposite and polymer filled XLPE. In: 2019 2nd International conference on electrical materials and power equipment (ICEMPE). IEEE
56. Mohamed A, Mobarak Y (2011) Novel nanocomposite insulation materials for the enhancing performance of power cables. In: 21st International conference on electricity distribution, France, Frankfurt
57. Lim KS et al (2019) Properties of nanofillers/crosslinked polyethylene composites for cable insulation. *J Vinyl Addit Technol* 25(S1):E147–E154
58. Du BX et al (2020) Temperature-dependent DC conductivity and space charge distribution of XLPE/GO nanocomposites for HVDC cable insulation. *IEEE Trans Dielectr Electr Insul* 27 (2):418–426
59. Li G et al (2019) Effect of BN nanosheet concentration on space charge characteristics in XLPE/BNNS nanocomposites. *Mater Res Exp* 6(11):115080
60. Li G et al (2020) DC breakdown characteristics of XLPE/BNNS nanocomposites considering BN nanosheet concentration, space charge and temperature. *High Voltage* 5(3):280–286

Chapter 3

Different Techniques Used for the Incorporation of Inorganic Nanoparticles in XLPE Matrix



Athulya Pillai and Balasubramanian Kandasubramanian

1 Introduction

Nanocomposites are materials exhibiting a substantial multiphased component with dimensions in the range of nanometer-scale possessing exceptionally high aspect ratio. When fabricated out of crosslinked polyethylene (XLPE) matrix as inorganic nanocomposites, it received attention in various fields like optoelectronics, electrical insulation, mechanics, catalysis, superconductors, etc. Inorganic nanofillers like TiO_2 , SiO_2 , Al_2O_3 , etc., when incorporated into the XLPE matrix, have shown enhanced properties, and the fundamental characteristics of nanocomposites, in turn, depend on the parameters like geometric shape and particle size, dispersing ability, and surface properties of fillers. The addition of inorganic nanofillers into XLPE matrix tends to increase the mechanical properties of nanocomposites, particularly the tensile strength. Lim et al. performed the tensile strength study of $\text{Al}_2\text{O}_3/\text{XLPE}$ nanocomposite at 1% Al_2O_3 nanoparticle loading [1], alongwith ZnO/XLPE nanocomposites and organoclay/XLPE nanocomposites. The results showed an increasing trend up to 0.5% filler loading after which the trend decreased with a maximum tensile strength of 18.3 MPa for ZnO/XLPE nanocomposites, 17.3 MPa for organoclay/XLPE nanocomposites, and 21.3 MPa for $\text{Al}_2\text{O}_3/\text{XLPE}$ nanocomposites which were 26%, 19%, and 47% greater than that of unloaded XLPE (14.5 MPa), respectively. Out of which, the incorporation of Al_2O_3 in XLPE is more effective than those of ZnO and organoclay nanofillers. Other parameters, like the elongation at break, young's modulus, % water absorption, dielectric

A. Pillai

CIPET: Institute of Plastics Technology (IPT), Udyogamandal, Kochi 68350, India

B. Kandasubramanian (✉)

Nano Surface Texturing Laboratory, Department of Metallurgical and Materials Engineering, Defence Institute of Advanced Technology (DU), Ministry of Defence, Girinagar, Pune, Maharashtra 411025, India
e-mail: meetkbs@gmail.com

© Springer Nature Singapore Pte Ltd. 2021

J. Thomas et al. (eds.), *Crosslinkable Polyethylene Based Blends and Nanocomposites*, Materials Horizons: From Nature to Nanomaterials, https://doi.org/10.1007/978-981-16-0486-7_3

49

breakdown strength, etc., have also shown an increasing trend up to a particular filler concentration [1].

Guo et al. reported preparation of XLPE/ α -Al₂O₃ nanocomposite for DC breakdown and space charge-based applications [2]. They prepared XLPE nanocomposite using molten salt method, with surface-functionalized silane-based coupling agent, followed by blending of coated α -Al₂O₃, LDPE, and dicumyl peroxide. The XLPE nanocomposite was compression molded at a temperature of 356 K and at a 16 MPa pressure. Their results indicated presence of high deep traps, which congested the charge injection, and reduced the charge carrier mobility, thus substantially decreasing the conductivity (from 3.25×10^{-13} to 1.04×10^{-13} S/m). The developed XLPE/ α -Al₂O₃ nanocomposite showed enhanced DC breakdown strength (from 220 to 320 kV/mm) and curbing the space charge buildup in the XLPE matrix [2].

Fabrication of XLPE nanocomposite involves the dispersion of inorganic fillers in the XLPE matrix, which could get agglomerated during processing. The agglomeration of the nanomaterials can be reduced by using processing methods like melt mixing, or by modifying the filler surface or changing the chemical structure of XLPE matrix. Additionally, the incompatibility of inorganic nanoparticles over the polymer matrix can be overcome by different methods of surface modifications including the use of coupling agents by silanization or by grafting, and irradiation technique techniques [3–17].

One of the significant challenges faced during the preparation of XLPE inorganic nanocomposite is the inability of nanoparticles to disperse in the polymer matrix due to its incompatibility with the organic XLPE matrix. Various methods based on coupling agent, grafting, vapor deposition, irradiation, etc., can be employed for enhancing the compatibility of nanoparticles and XLPE matrix to get significant dispersion. The processing of XLPE nanocomposites can be performed using techniques like twin-screw extruder [18], Banbury mixer [19], twin [20], tri-roller [21] mills, etc. (Fig. 1).

In this context, the present chapter discusses various methods used for the functionalization of the inorganic nanomaterials and the following methods used in the preparation of inorganic XLPE nanocomposites.

2 Functionalization and Fabrication Methods of Inorganic XLPE Nanocomposites

2.1 Melt Mixing of XLPE Nanocomposites

XLPE belongs to thermoplastic polymer category, and thus its nanocomposites can be prepared mainly by melt blending technique. Melt blending process is the most extensively utilized method to prepare nanocomposites, especially thermoplastics, and related to other techniques, it is simple, cost-effective, eco-friendly, and

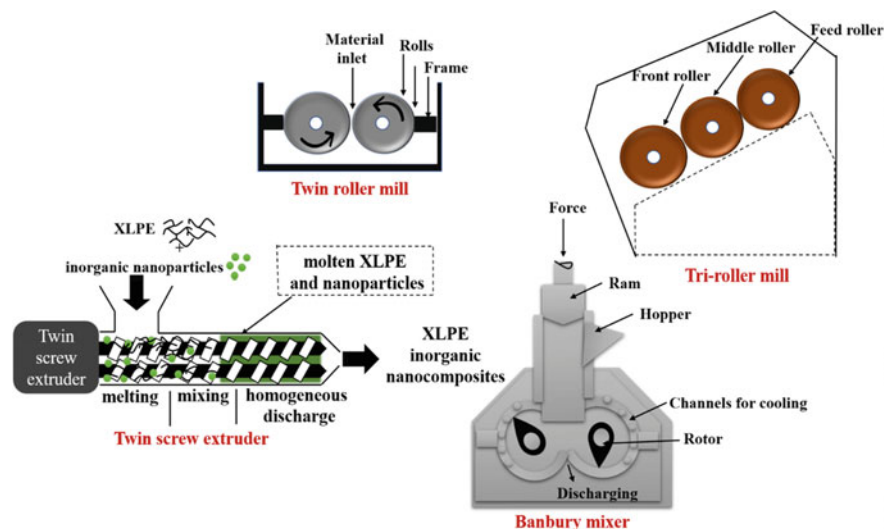


Fig. 1 Twin roller mill, tri-roller mill, twin-screw extruder and Banbury mixer employed for the melt blending of XLPE nanocomposites

commercially favorable [22]. The technique is a high-temperature process carried out at temperatures above melting or glass transitions of polymer requiring high shear mixers or extruders.

Kim et al. reported MgO/XLPE nanocomposites which were prepared under high pressure by mixing LDPE, silane-treated MgO nanoparticles and dicumyl peroxide as a crosslinking agent using compression molding at a temperature of 170 °C for 15 min for attaining complete crosslinking [23]. For XLPE/organoclay nanocomposites, the process helps in exfoliation of clay platelets, control over the distribution and dispersion of clay platelets and their interlayer interactions in the nanocomposite [24]. The high shear forces generated due to the rotational mixing in twin-screw extruder delaminates the clay platelets during melt processing, thereby increasing the inter-gallery space between clay platelets. The effect of dispersion of organically modified montmorillonite (O-MMT) on the dielectric properties was investigated by Zhang et al. who reported the intercalation of O-MMT nanoparticles via melt blending technique that increased the inter-gallery distance of O-MMT with an average value from 2.54 to 3.24 nm [25]. Jose et al. used melt blending for the fabrication of XLPE/Al₂O₃ nanocomposites using dicumyl peroxide curing agent, in Haake mixer conditioned at 160 °C and mixed at the speed of 60 rpm for 12 min [26]. The nanocomposite of TiO₂ and XLPE was prepared by melting TiO₂ and LDPE, followed by blending in an open mixer at 115 °C, whereas the melt blending of TiO₂/LDPE with the crosslinker dicumyl peroxide was carried out in a closed mixer to prevent pre-crosslinking at the same conditions [27].

In another study, Zhang et al. have reported fabrication of XLPE and polypyrrole (PPy)-based composites for DC current electrical applications [28]. The stated that

PPy and low density polyethylene (LDPE) were blended with solution-based method via ultrasonication, and centrifusing followed by crosslinking with dicumyl peroxide under melt mixing at a temperature of 100 °C. They claimed that developed XLPE/PPy composite can decrease the current density of DC electrical conduction and enhance the space charge distribution without affecting the crosslinking and crystalline phase of XLPE [28]. They claimed that addition of nano-PPy (possessing bowl-like structure with 100 nm diameter) exhibiting conductivity in XLPE can possibly create deep traps to arrest space charge carriers and reduce space charge accumulation in the nanocomposites. In a low electric field, the deep traps may capture and toss the charge carriers in the transportation process, and then decrease the current density of conduction. Nevertheless, in a high electric field, the quantity of free electrons amplify due to the breaking of the polaron and the field electron-based emission effect of nano-PPy, thereby decreasing DC breakdown strength of the nanocomposite [28].

2.2 *Surface Modification of Inorganic Nanoparticles*

Surface modification of nanoparticles is the prime method utilized for dispersion in the polymer-based nanocomposites [29–40]. Surface modification of nanoparticles creates organic and non-polar surface functionalities similar to XLPE matrix, thereby increasing the degree of dispersion of nanoparticles and the interfacial surface area of nanocomposites. A study conducted on XLPE/SiO₂ nanocomposites by Zhang et al. found that surface-modified nanoparticles can potentially strengthen DC breakdown at different temperatures as compared to pure XLPE. Further, they reported that unmodified silica/XLPE nanocomposites, and promoted more mobility of space charges than that of unmodified SiO₂ [41, 42]. Similar results were found with TiO₂/XLPE nanocomposites modified with dimethyloctyl silane on the surface charge accumulation and the DC breakdown strength [43]. Trimethoxyoctyl silane (coupling agent)-treated ZnO nanoparticles attach to the surface of XLPE matrix via methoxy (–OCH₃) group, and the octyl group, promoting an enhanced interaction between the filler and the polymer. The nanoparticles in the polymer matrix show the tendency to agglomerate to attain stability by reducing the surface free energy, which occurs by forming hydrogen bonds with the free hydroxyl groups on the surface of nanoparticles. The surface modification of nanoparticles reduces the surface-free energy and prevents the formation of hydrogen bonds on the surface of the nanoparticle, thereby avoiding the agglomeration [41–44].

Some of the chemical surface modification includes surface grafting, which enhances the compatibility of polymer and nanoparticles by forming strong covalent bonds between the surfaces. Maleic anhydride-grafted XLPE matrix has reported improved performance for the electrical cable insulation. Polyethylene treated with the grafting agent maleic anhydride under the presence of UV radiation

by the melt mixing process resulted in its high-voltage application in DC cable materials [45].

Wang et al. used ethyl alcohol solvent for the significant dispersion of TiO_2 nanoparticles and later homogenized in an appropriate instrument followed by the addition of a coupling agent for its surface modification into the solution containing TiO_2 nanoparticles. The solid–liquid part was then separated by centrifugation to obtain nanocomposites, and a comparative study was carried out between modified and unmodified nano- TiO_2 to study its degree of agglomeration. The TiO_2 surface after modification attains a further decrease in its nanoscale dimension with more effective nanoparticle dispersions. The work mainly focused on the effect of incorporation of nano- TiO_2 particles in XLPE for its performance in the space charge accumulation, which is the basis for the insulation performance under DC electric field the inclusion of nano- TiO_2 consequently increased the DC dielectric strength [44].

However, the use of a large amount of solvent for nanoparticle dispersion is not an environmentally benign approach because of the high operating cost, and difficulty in the recovery of solvent makes it an unsafe approach [46].

Schematic representation of the dispersion of nanoparticles in the polymer matrix and the mobility of polymer chains at near and far regions of nanofiller vicinity is shown in Fig. 2 (Table 1).

2.3 Intercalation and Exfoliation of Inorganic Nanoparticles

Intercalation and exfoliation are two critical methods used for dispersion of layered nanomaterials like montmorillonite, layered hydroxides, silicates, organoclays, etc.,

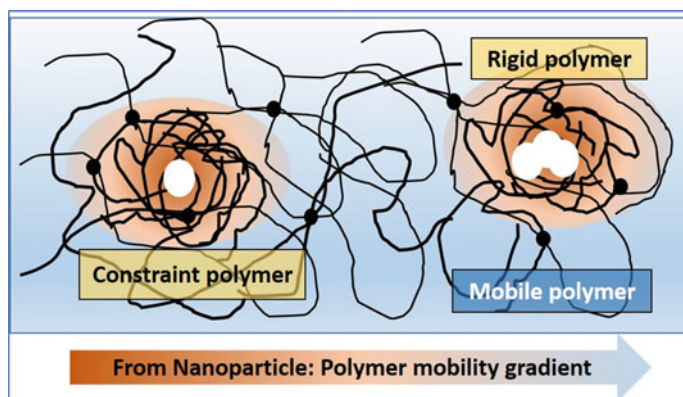


Fig. 2 Typical diagram showing the polymer chain mobility within the polymer nanocomposites Reproduced with permission from Ref. [47]; Copyright 2014, Royal Society of Chemistry

Table 1 Various coupling and grafting agents used in the modification of inorganic nanoparticles in the synthesis of XLPE nanocomposites

Nanocomposites	Coupling/Grafting agent	Ref.
ZnO/XLPE	Trimethoxyoctyl silane	[48]
SiO ₂ /XLPE	Titanate and 3-(Methacryloyloxy) propyltrimethoxysilane	[49]
XLPE/Al(OH) ₃	Silane	[50]
XLPE/silica	Octylsilane	[51]
SiO ₂ /XLPE	poly(stearl methacrylate) (PSMA) brushes	[52]
Montmorillonite/ XLPE	Octadecyl ammonium	[25]
Montmorillonite/ XLPE	Octadecyl quaternary ammonium salt and double octadecyl benzyl quaternary ammonium salt and ethylenevinylacetate(EVA) as compatabiliser	[53]
SiO ₂ /XLPE	Vinyl silane (triethoxy vinyl silane)	[54]

in the polymer matrix [55]. The montmorillonite (MMT) is a widely used class of nanoparticles, which are layered silicates possessing a crystalline structure made of two-dimensional sheets. These are formed by the sandwiching of an octahedral layer of aluminum hydroxide or magnesium hydroxide by two tetrahedral silica layers held by weak van der Waals or dipolar forces of attraction with a layer thickness of 1 nm (Fig. 3). During processing, the polymer chains in the molten state enter into the interlayer space of clay platelets forming intercalate. Since the forces holding the layers of MMT is rather weak so that it is for polymers to intercalate and exfoliate the layers. These layers arrange to form spaces in between them called a gallery or interlayer of organoclay. The cations present within the layers, such as Al³⁺ or Mg²⁺, isomorphically substituted by Mg²⁺ or Li⁺, respectively, developing -ve charges which are counterbalanced by alkali or alkaline earth metal cations located in the gallery space of MMT. The dispersion of MMT particles requires the ion exchange by which the sodium cations get replaced by the ammonium groups of organic amine salts to give organically modified MMT or simply organoclays. The different ways by which organic quaternary ammonium ions get arranged in between the gallery of clay platelets are depicted in Fig. 4. This organic ammonium ions present in the inter-gallery spaces of montmorillonite render them hydrophobic and consequently enhances the polymer-nanoparticle interaction. The ion exchanging of Na⁺ with organic ammonium ion modifies montmorillonite by increasing their inter-layer distances, and the polymers via melt blending or solution blending either intercalates or exfoliates the clay platelets [56]. Li et al. comparatively studied the influence of two different intercalants, namely ion-based salts of octadecyl quaternary ammonium and double octadecyl benzyl quaternary ammonium for the modification of montmorillonite nanoparticles during melt blending of XLPE nanocomposites [53].

When the polymer is incapable of intercalating between the gallery of organoclay, phase-separated composites are obtained as in Fig. 5, whose properties remain the same as conventional micro composites.

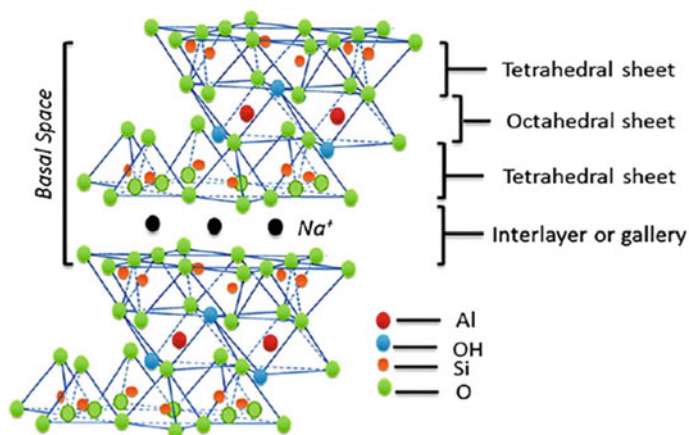


Fig. 3 Structure of Na-montmorillonite (2:1 phyllosilicate form) Reproduced with permission from Ref. [57]; Copyright 2016, American Chemical Society

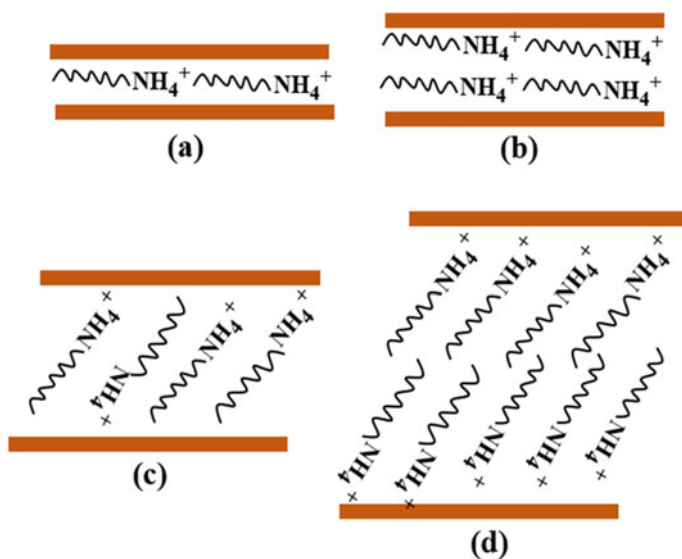


Fig. 4 Alkyl quaternary ammonium ion arrangement in between the gallery of clay platelets **a** lateral monolayer; **b** lateral bilayer; **c** paraffin kind of monolayer; **d** paraffin kind of bilayer

The intercalated-layered nanomaterials like MMT are believed to enhance the dissemination of electric field across the needle tip, which may decrease the electric stress and restrain the water tree expansion in XLPE nanocomposites, which was a report by Li et al. [58]. They reported that the intercalated MMT/XLPE nanocomposites could be prepared by blending polyethylene and MMT at 100 °

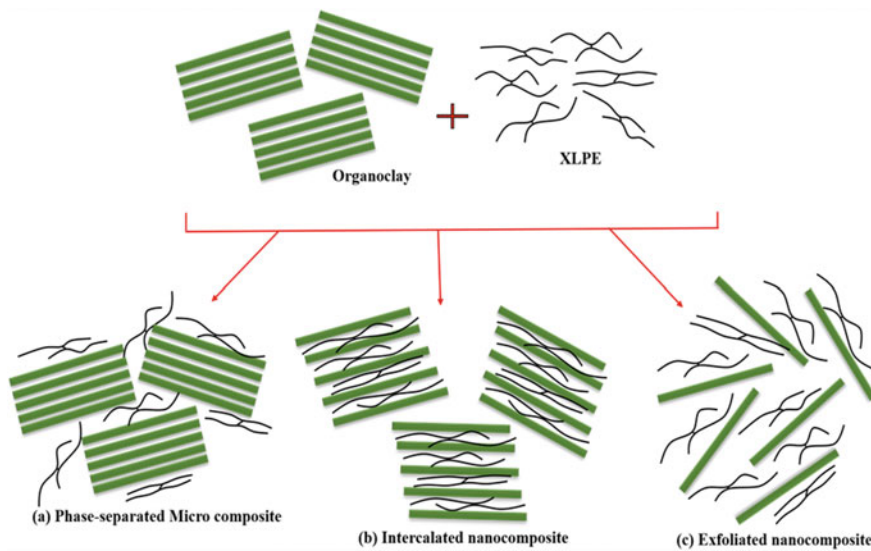


Fig. 5 Schematic representation of composites synthesized by the blending of organoclay and polymer (XLPE) resulting in **a** phase-separated micro composite, **b** intercalated and **c** exfoliated nanocomposite

C, with a screw speed of 40 r/min, in 15 min using Huck Rheometer containing MMT concentration at 20%. Subsequently, prepared masterbatch of 20% MMT was incorporated into XLPE and blended over at 100 °C by the same Rheometer at a concentration of 5, 10, and 15%. The MMT/XLPE nanocomposites with 1, 2, and 3% concentrations were then formulated by mixing masterbatch with XLPE, followed by vulcanization at 150 °C and a pressure 10 MPa for about 30 min [58].

2.4 Irradiation-Based Fabrication of XLPE Nanocomposites

Recently, researchers have been exploring physical functionalization of XLPE using various methods like UV and gamma irradiation.

Zhao et al. reported the fabrication of XLPE nanocomposites using grafting with Maleic Anhydride by applying photon-initiator in the presence of UV irradiation [59]. They utilized 2 wt% of dicumyl peroxide as a crosslinking agent. The polymer in a molten state was bombarded with UV irradiation at a continuous rate via a light-supplied array of UV LED system for 10 s at standard pressure and room temperature in the presence of air. They claimed that space charge properties and dielectric characteristics at higher temperatures had been substantially improved for the developed XLPE nanocomposites [59].

In another work, Fu et al. reported functionalization of silica-based nanomaterials UV irradiation for improving the degree of cross-link and insulation shielding performance of SiO₂ XLPE nanocomposites [60]. They claimed that in UV irradiation, the superior crosslinking reactions of XLPE molecules are aided by the supporting crosslinkers grafted using silica nanoparticles. The reported method helps in enhancing the space charge properties and direct current dielectric breakdown power, contemporaneously utilizing nanodielectric knowhow and functional-group surface variation, the mechanical and dielectric properties XLPE nanocomposites can also be improved [60].

In another study, Liu et al. reported influence of gamma irradiation on the physical properties of the developed XLPE nanocomposite [61]. They performed gamma irradiation for around 2000 h at 100 Gy/h with a temperature of 155 °C and stated that the irradiation speed up the development of polar carbonyls. Further, the complex-permittivity of XLPE nanocomposites was found to increase due to the presence of ample of polar groups generated by oxidation, with a loss of softness [61].

3 Conclusion

XLPE inorganic nanocomposites with wide applications, mostly in the fields of electrical insulation and extruded cables, approaches cost-effective and user-friendly methods of fabrication. Various researchers succeeded in incorporating different nanomaterials in XLPE matrix. The properties of pure XLPE like insulating, environmental stress cracking, and thermal stability can be increased significantly by the addition of inorganic nanofillers, which act as a reinforcing agent and forms a strong and stable network structure in the crosslinked XLPE matrix. The dispersion of such inorganic nanomaterials in XLPE matrix can be achieved by using techniques like melt blending, surface functionalization of nanomaterials, intercalation, and exfoliation of layered nanomaterials, crosslinking agents, grafting, UV, and gamma irradiation. The objective of the present chapter was to discuss the various methods for the incorporation of inorganic nanoparticles into the XLPE matrix. The different techniques for the incorporation of nanoparticles. The present chapter discussed various methods used for the functionalization of the inorganic nanomaterials, and the methods used in the preparation of inorganic XLPE nanocomposites.

Acknowledgements The authors are thankful to Dr. C. P. Ramanarayanan, Vice-Chancellor of DIAT (DU), Pune for the motivation, and support. The first author acknowledges Dr. B. Srinivasulu, Principal Director and Head, CIPET: Institute of Plastic Technology (IPT), Kochi, for the support. The authors are thankful to Mr. Raviprakash MagiSetty, Mr. Prakash Gore, and Mr. Swaroop Gharde for their persistent technical support throughout the review writing. The authors are thankful to all anonymous reviewers and the Editor for improving the quality of the revised manuscript by their valuable suggestions, and comments.

References

1. Lim KS, Mariatti M, Kamarol M, Ghani ABA, Shafi Halim H, Abu Bakar A (2019) Properties of nanofillers/crosslinked polyethylene composites for cable insulation. *J Vinyl Addit Technol* 25:E147–E154. <https://doi.org/10.1002/vnl.21671>
2. Guo X, Xing Z, Zhao S, Cui Y, Li G, Wei Y, Lei Q, Hao C (2020) Investigation of the space charge and DC breakdown behavior of XLPE/ α -Al₂O₃ nanocomposites. *Materials (Basel)* 13:1333. <https://doi.org/10.3390/ma13061333>
3. Liu D, Pourrahimi AM, Pallon LKH, Sánchez CC, Olsson RT, Hedenqvist MS, Fogelström L, Malmström E, Gedde UW (2016) Interactions between a phenolic antioxidant, moisture, peroxide and crosslinking by-products with metal oxide nanoparticles in branched polyethylene. *Polym Degrad Stab* 125:21–32. <https://doi.org/10.1016/j.polymdegradstab.2015.12.014>
4. Kumar V, Kandasubramanian B (2016) Processing and design methodologies for advanced and novel thermal barrier coatings for engineering applications. *Particuology* 27:1–28. <https://doi.org/10.1016/j.partic.2016.01.007>
5. Kumar V, Balasubramanian K (2016) Progress update on failure mechanisms of advanced thermal barrier coatings: a review. *Prog Org Coatings* 90:54–82. <https://doi.org/10.1016/j.porgcoat.2015.09.019>
6. Gudivada G, Kandasubramanian B (2019) Zirconium-doped hybrid composite systems for ultrahigh-temperature oxidation applications: a review. *Ind Eng Chem Res* 58:4711–4731. <https://doi.org/10.1021/acs.iecr.8b05586>
7. Gudivada G, Kandasubramanian B (2020) Polymer—phyllosilicate nanocomposites for high-temperature structural application. *Polym Technol Mater* 59:573–591. <https://doi.org/10.1080/25740881.2019.1669654>
8. Gore PM, Kandasubramanian B (2018) Heterogeneous wettable cotton based superhydrophobic Janus biofabric engineered with PLA/functionalized-organoclay microfibers for efficient oil-water separation. *J Mater Chem A* 6:7457–7479. <https://doi.org/10.1039/c7ta11260b>
9. Gore PM, Balakrishnan S, Kandasubramanian B (2019) Superhydrophobic corrosion inhibition polymer coatings. In: *Superhydrophobic polymer coatings*. Elsevier, pp 223–243
10. Magisetty R, Kumar P, Gore PM, Ganivada M, Shukla A, Kandasubramanian B, Shunmugam R (2019) Electronic properties of poly(1,6-heptadiynes) electrospun fibrous non-woven mat. *Mater Chem Phys* 223:343–352. <https://doi.org/10.1016/j.matchemphys.2018.11.020>
11. Gore PM, Kandasubramanian B (2018) Functionalized aramid fibers and composites for protective applications: a review. *Ind Eng Chem Res* 57:16537–16563. <https://doi.org/10.1021/acs.iecr.8b04903>
12. Gore PM, Purushothaman A, Naebe M, Wang X, Kandasubramanian B (2019) Nanotechnology for oil-water separation. In: Prasad R, Karchiyappan T (eds) *Advanced research in nanosciences for water technology*. Springer Nature Switzerland AG, Cham, pp 299–339
13. Korde JM, Shaikh M, Kandasubramanian B (2018) Bionic prototyping of honeycomb patterned polymer composite and its engineering application. *Polym—Plast Technol Eng*. <https://doi.org/10.1080/03602559.2018.1434667>
14. Deoray N, Kandasubramanian B (2018) Review on three-dimensionally emulated fiber-embedded lactic acid polymer composites: opportunities in engineering sector. *Polym—Plast Technol Eng* 57:860–874. <https://doi.org/10.1080/03602559.2017.1354226>
15. Thakur A, Gharde S, Kandasubramanian B (2019) Electroless nickel fabrication on surface modified magnesium substrates. *Def Technol*. <https://doi.org/10.1016/j.dt.2019.04.006>
16. Thakur K, Kandasubramanian B (2019) Graphene and graphene oxide-based composites for removal of organic pollutants: a review. *J Chem Eng Data* 64:833–867. <https://doi.org/10.1021/acs.jced.8b01057>

17. Kumar V, Singh S, Kandasubramanian B (2017) Thermal ablation and laser shielding characteristics of ionic liquid-microseeded functionalized nanoclay/resorcinol formaldehyde nanocomposites for armor protection. *Polym—Plast Technol Eng* 56:1542–1555. <https://doi.org/10.1080/03602559.2017.1280684>
18. Favis BD, Therrien D (1991) Factors influencing structure formation and phase size in an immiscible polymer blend of polycarbonate and polypropylene prepared by twin-screw extrusion. *Polymer (Guildf)* 32:1474–1481. [https://doi.org/10.1016/0032-3861\(91\)90429-M](https://doi.org/10.1016/0032-3861(91)90429-M)
19. Cheng J-J, Manas-Zloczower I (1989) Hydrodynamic analysis of a banbury mixer 2-D flow simulations for the entire mixing chamber. *Polym Eng Sci* 29:1059–1065. <https://doi.org/10.1002/pen.760291512>
20. Yeh J-M, Chen C-L, Huang C-C, Chang F-C, Chen S-C, Su P-L, Kuo C-C, Hsu J-T, Chen B, Yu Y-H (2006) Effect of organoclay on the thermal stability, mechanical strength, and surface wettability of injection-molded ABS-clay nanocomposite materials prepared by melt intercalation. *J Appl Polym Sci* 99:1576–1582. <https://doi.org/10.1002/app.22329>
21. Zhang BB, Miao MY, Bai J, Yuan GJ, Jia YY, Han ZX, Zhao ZG, Su HQ (2014) Researches on purification and sodium-modification of Ca-bentonite by tri-roller grinder. *Adv Mater Res* 962–965:809–813. <https://doi.org/10.4028/www.scientific.net/AMR.962-965.809>
22. Ercan N, Durmus A, Kaşgöz A (2017) Comparing of melt blending and solution mixing methods on the physical properties of thermoplastic polyurethane/organoclay nanocomposite films. *J Thermoplast Compos Mater* 30:950–970. <https://doi.org/10.1177/0892705715614068>
23. Kim DS, Lee DH, Kim YJ, Nam JH, Ha ST, Lee SH (2013) Investigation of space charge distribution of MgO/XLPE composites depending on particle size of MgO as inorganic filler. *Appl Mech Mater* 481:108–116. <https://doi.org/10.4028/www.scientific.net/AMM.481.108>
24. Rezanejad S, Kokabi M (2007) Shape memory and mechanical properties of cross-linked polyethylene/clay nanocomposites. *Eur Polym J* 43:2856–2865. <https://doi.org/10.1016/j.eurpolymj.2007.04.031>
25. Zhang W, Xu M, Zhang X, Xie D (2013) Study of montmorillonite concentration on dielectric property and dispersion of cross-linked polyethylene/montmorillonite nano-composites. In: 2013 Annual report conference on electrical insulation and dielectric phenomena. IEEE, pp 531–534
26. Jose JP, Abraham J, Maria HJ, Varughese KT, Thomas S (2016) Contact angle studies in XLPE hybrid nanocomposites with inorganic nanofillers. *Macromol Symp* 366:66–78. <https://doi.org/10.1002/masy.201650048>
27. Wang Y, Xiao K, Wang C, Yang L, Wang F (2016) Study on dielectric properties of TiO₂/XLPE nanocomposites. In: 2016 IEEE international conference on high voltage engineering and application (ICHVE). IEEE, pp 1–4
28. Zhang C, Zhang H, Li C, Duan S, Jiang Y, Yang J, Han B, Zhao H (2018) Crosslinked polyethylene/polypyrrole nanocomposites with improved direct current electrical characteristics. *Polym Test* 71:223–230. <https://doi.org/10.1016/j.polymertesting.2018.09.020>
29. Balasubramanian K, Tirumali M, Badhe Y, Mahajan YR (2017) Nano-enabled multifunctional materials for aerospace applications
30. Yadav R, Tirumali M, Wang X, Naebe M, Kandasubramanian B (2019) Polymer composite for antistatic application in aerospace. *Def Technol*. <https://doi.org/10.1016/j.dt.2019.04.008>
31. Yadav R, Naebe M, Wang X, Kandasubramanian B (2017) Structural and thermal stability of polycarbonate decorated fumed silica nanocomposite via thermomechanical analysis and in-situ temperature assisted SAXS. *Sci Rep* 7:7706. <https://doi.org/10.1038/s41598-017-08122-7>
32. Yadav R, Subhash A, Chemmenchery N, Kandasubramanian B (2018) Graphene and graphene oxide for fuel cell technology. *Ind Eng Chem Res* 57:9333–9350. <https://doi.org/10.1021/acs.iecr.8b02326>
33. Yadav R, Naebe M, Wang X, Kandasubramanian B (2016) Temperature Assisted in-situ small angle x-ray scattering analysis of Ph-POSS/PC polymer nanocomposite. *Sci Rep* 6:1–9. <https://doi.org/10.1038/srep29917>

34. Lonkar CM, Kharat DK, Kumar HH, Prasad S, Balasubramanian K (2013) Effect of sintering time on dielectric and piezoelectric properties of lanthanum doped $\text{Pb}(\text{Ni}_{1/3}\text{Sb}_{2/3})\text{-PbZrTiO}_3$ ferroelectric ceramics. *Def Sci J* 63:418–422. <https://doi.org/10.14429/dsj.63.4866>
35. Lonkar CM, Kharat DK, Prasad S, Kandasubramanian B (2015) Synthesis, characterization, and development of PZT-based composition for power harvesting and sensors application. In: *Handbook of nanoceramic and nanocomposite coatings and materials*, pp 551–577. <https://doi.org/10.1016/B978-0-12-799947-0.00025-0>
36. Patil NA, Kandasubramanian B (2020) Biological and mechanical enhancement of zirconium dioxide for medical applications. *Ceram Int* 46:4041–4057. <https://doi.org/10.1016/j.ceramint.2019.10.220>
37. Jimmy J, Kandasubramanian B (2019) Mxene functionalized polymer composites: synthesis and applications. *Eur Polym J* 109367. <https://doi.org/10.1016/j.eurpolymj.2019.109367>
38. Hemanth NR, Kandasubramanian B (2019) Recent advances in 2D MXenes for enhanced cation intercalation in energy harvesting applications: a review. *Chem Eng J* 123678. <https://doi.org/10.1016/j.cej.2019.123678>
39. Panwar SS, Umasankar Patro T, Balasubramanian K, Venkataraman B (2016) High-temperature stability of yttria-stabilized zirconia thermal barrier coating on niobium alloy-C-103. *Bull Mater Sci* 39:321–329. <https://doi.org/10.1007/s12034-015-1140-4>
40. Kandasubramanian B (2016) Generation of micro-porous honeycomb foam of UHMWPE/PHB blend by supercritical CO_2 . *Mater Focus* 5:73–83. <https://doi.org/10.1166/mat.2016.1298>
41. Zhang L, Zhou Y, Cui X, Sha Y, Le TH, Ye Q, Tian J (2014) Effect of nanoparticle surface modification on breakdown and space charge behavior of XLPE/ SiO_2 nanocomposites. *IEEE Trans Dielectr Electr Insul* 21:1554–1564. <https://doi.org/10.1109/TDEI.2014.004361>
42. Zhang L, Zhou Y, Cui X, Zhang Y, Ye Q (2014) Space charge behavior of XLPE/ SiO_2 nanocomposites with nanoparticle surface modification. In: 2014 IEEE electrical insulation conference (EIC). IEEE, pp 402–406
43. Wang Y, Xiao K, Wang C, Yang L, Wang F (2016) Effect of nanoparticle surface modification and filling concentration on space charge characteristics in TiO_2 /XLPE nanocomposites. *J Nanomater* 2016:1–10. <https://doi.org/10.1155/2016/2840410>
44. Wang S, Chen P, Yu S, Zhang P, Li J, Li S (2018) Nanoparticle dispersion and distribution in XLPE and the related DC insulation performance. *IEEE Trans Dielectr Electr Insul* 25:2349–2357. <https://doi.org/10.1109/TDEI.2018.007156>
45. Zhao X-D, Zhao H, Sun W-F (2020) Significantly improved electrical properties of crosslinked polyethylene modified by UV-initiated grafting MAH. *Polymers (Basel)* 12:62. <https://doi.org/10.3390/polym12010062>
46. Zhang M, Li Y, Su Z, Wei G (2015) Recent advances in the synthesis and applications of graphene–polymer nanocomposites. *Polym Chem* 6:6107–6124. <https://doi.org/10.1039/C5PY00777A>
47. Jose JP, Thomas S (2014) Alumina–clay nanoscale hybrid filler assembling in cross-linked polyethylene based nanocomposites: mechanics and thermal properties. *Phys Chem Chem Phys* 16:14730–14740. <https://doi.org/10.1039/C4CP01532K>
48. Jose JP, Chazeau L, Cavailié J-Y, Varughese KT, Thomas S (2014) Nucleation and non isothermal crystallization kinetics in cross-linked polyethylene/zinc oxide nanocomposites. *RSC Adv* 4:31643–31651. <https://doi.org/10.1039/C4RA03731F>
49. Zhang L, Zhou Y, Huang M, Sha Y, Tian J, Ye Q (2014) Effect of nanoparticle surface modification on charge transport characteristics in XLPE/ SiO_2 nanocomposites. *IEEE Trans Dielectr Electr Insul* 21:424–433. <https://doi.org/10.1109/TDEI.2013.004145>
50. Wang S, Chen P, Xiang J, Li J (2017) Study on DC breakdown strength and morphology in XLPE/ $\text{Al}(\text{OH})_3$ nanocomposites. In: 2017 International symposium on electrical insulating materials (ISEIM). IEEE, pp 355–358
51. Ashish Sharad P, Kumar KS (2017) Application of surface-modified XLPE nanocomposites for electrical insulation—partial discharge and morphological study. *Nanocomposites* 3:30–41. <https://doi.org/10.1080/20550324.2017.1325987>

52. Sharad PA, Kumar KS (2017) Application of surface modified XLPE nanocomposites for electrical insulation of high voltage cables—partial discharge study. *Energy Procedia* 117:260–267. <https://doi.org/10.1016/j.egypro.2017.05.130>
53. Li X, Xu M, Zhang K, Xie D, Cao X, Liu X (2014) Influence of organic intercalants on the morphology and dielectric properties of XLPE/montmorillonite nanocomposite dielectrics. *IEEE Trans Dielectr Electr Insul* 21:1705–1717. <https://doi.org/10.1109/TDEI.2014.004317>
54. Reed CW (2010) Functionalization of nanocomposite dielectrics. In: 2010 IEEE international symposium on electrical insulation. IEEE, pp 1–4
55. Kavitha D, Balachandran M (2019) XLPE—layered silicate nanocomposites for high voltage insulation applications: dielectric characteristics, treeing behaviour and mechanical properties. *IET Sci Meas Technol* 13:1019–1025. <https://doi.org/10.1049/iet-smt.2018.5417>
56. Alexandre M, Dubois P (2000) Polymer-layered silicate nanocomposites: preparation, properties and uses of a new class of materials. *Mater Sci Eng R Rep* 28:1–63. [https://doi.org/10.1016/S0927-796X\(00\)00012-7](https://doi.org/10.1016/S0927-796X(00)00012-7)
57. Nuruzzaman M, Rahman MM, Liu Y, Naidu R (2016) Nanoencapsulation, nano-guard for pesticides: a new window for safe application. *J Agric Food Chem* 64:1447–1483. <https://doi.org/10.1021/acs.jafc.5b05214>
58. Li X, Liu X, Xu M, Xie D, Cao X, Wang X, Liu H (2012) Influence of compatibilizers on the water-tree property of Montmorillonite/Cross-linked polyethylene nanocomposites. In: 2012 IEEE 10th international conference on the properties and applications of dielectric materials. IEEE, Bangalore, India, pp 1–4
59. Zhao H, Xi C, Zhao X-D, Sun W-F (2020) Elevated-temperature space charge characteristics and trapping mechanism of cross-linked polyethylene modified by UV-initiated grafting MAH. *Molecules* 25:3973. <https://doi.org/10.3390/molecules25173973>
60. Fu Y-W, Zhang Y-Q, Sun W-F, Wang X (2020) Functionalization of silica nanoparticles to improve crosslinking degree, insulation performance and space charge characteristics of UV-initiated XLPE. *Molecules* 25:3794. <https://doi.org/10.3390/molecules25173794>
61. Liu Z, Miyazaki Y, Hirai N, Ohki Y (2020) Comparison of the effects of heat and gamma irradiation on the degradation of cross-linked polyethylene. *IEEE J Trans Electr Electron Eng* 15:24–29. <https://doi.org/10.1002/tee.23023>

Chapter 4

Critical Issues in XLPE-Based Polymer Nanocomposites and Their Blends



Abdallah Hedir, Omar Lamrous, Issouf Fofana, Ferhat Slimani,
and Mustapha Moudoud

List of Abbreviations

XLPE	Cross-linked polyethylene
MV	Medium voltage
HV	High voltage
DC	Direct current
MMT	Montmorillonite
PEA	Pulsed-electro-acoustic
PE	Polyethylene
DCP	Dicumyl peroxide
CNTs	Carbon nanotubes
PVC	Polyvinyl chloride
EPR	Ethylene propylene rubber
EVA	Ethylene-vinyl acetate
EPDM	Ethylene propylene diene monomer
HVDC	High voltage direct current
PD	Partial discharge

A. Hedir (✉) · F. Slimani · M. Moudoud
Laboratoire des Technologies Avancées en Génie Electrique (LATAGE), Université
Mouloud Mammeri de Tizi-Ouzou, BP 17, RP 15000 Tizi-Ouzou, Algeria
e-mail: abdallah.hedir@ummto.dz

O. Lamrous
Laboratoire de Physique et Chimie Quantique (LPCQ), Université Mouloud Mammeri de
Tizi-Ouzou, BP 17, RP 15000 Tizi-Ouzou, Algeria

I. Fofana
University of Québec in Chicoutimi, 555, Boulevard de l'Université, G7H 2B1, Chicoutimi,
QC, Canada

1 Introduction

Nowadays, cross-linked polyethylene (XLPE) is widely used as power cables insulation. It has progressively replaced other polyethylene in the manufacture of medium (MV) and high voltage (HV) cables thanks to its outstanding electrical [1] and thermal properties compared to original polyethylene (LDPE) [2].

In service conditions, XLPE insulating material with regard to all polymers can undergo disastrous degradations, affecting directly its reliability and lifetime [3, 4]. The degradation rate generally depends on the ambient conditions such as solar irradiation, temperature, moisture, pollution, and the presence of oxygen in the air. According to the results reported in the literature, over time, the operating conditions lead to the irreversible degradation of the XLPE properties. The mechanism responsible for this phenomenon is known as *aging*, which bring together all the stresses to which the insulation is subjected.

Aging causes critical effects, which can manifest themselves in failures such as loss of electrical, mechanical, and physical properties [5].

Due to the constantly increasing demand for energy, and new stresses induced by renewable energy sources and electric vehicles in the networks, it has become essential to find new solutions to improve the efficiency of the equipment connected to the electrical grid. In this context, the research of high-performance cable insulation material is still a need for engineering applications.

Recently, the development of nanotechnologies has significantly boosted the use of XLPE as an insulating material. On this basis, it is shown that the XLPE nanocomposites exhibit improved electrical properties, such as high dielectric strength, space charges suppression, high resistance to the partial discharges, low conductivity, and dielectric losses. A number of studies have proven that nano-MgO and nano-SiO₂ can effectively improve the ability of polyethylene to inhibit space charge [6–8], thus reducing its electrical conductivity and increasing its DC breakdown strength. Gao et al. [9] also shown that the XLPE nanocomposite fabricated with montmorillonite (MMT) treated by chemical method can effectively inhibit space charge accumulation. Li et al. [10] evidenced that the addition of nano-Al₂O₃ fillers is a good approach to improve once-lowered breakdown strength and the partial discharges resistance to protect the power cable. Similarly, Ding and Varlow investigated treeing phenomena in epoxy-ZnO nanocomposites and found that the addition of a small amount (0.5 to 1 wt%) of zinc oxide particles in the epoxy insulation could extend the treeing time to breakdown [11]. Wang et al. [12] explored the dielectric characteristics of the interface between SiC and XLPE using the pulsed-electro-acoustic (PEA) technique. They found that the best activity of electrical tree inhibition is realized when the concentration of nanocomposite is 1 wt%.

Nevertheless, the performances of the operational XLPE nanocomposite cables are affected by several parameters, some of which are related to the choice and preparation of a nanofiller, aging or the damage exponent due among other reasons, to the space charges accumulation and treeing [13]. This shows that despite having better insulating properties, the XLPE nanocomposite may not offer longer service

life, which poses a challenge to the cable manufacturing industry. Therefore, a better understanding of the issues and fundamental mechanisms in XLPE-based nanocomposites engineering will lead to a successful deployment of the operational XLPE nanocomposite cables.

This contribution provides a review of the major critical issues of XLPE-based nanocomposites and is organized as follows: Sect. 2 discusses the use of XLPE as insulation of power cables. The nanofillers in power cable technology are enumerated in Sect. 3. Section 4 addresses the need of XLPE-based nanocomposite. The critical issues in XLPE-based nanocomposite are exposed in Sect. 5. Finally, Sect. 6 draws the main conclusion.

2 Power Cables Insulation Based on XLPE

Polymer materials are increasingly used for insulation in electric distribution systems [14]. Actually, traditional insulating materials such as impregnated paper have been replaced by synthetic insulators, especially polyethylene [15]. Polyethylene (PE) is a semi-crystalline polymer with good mechanical properties, good heat stability, and high dielectric properties [16]. In addition, PE is known for being one of the cheapest and easiest to use polymers. For all these reasons, polyethylenes are often used as electrical insulation for MV and HV cables [17].

Low-density polyethylene (LDPE), despite having good insulating characteristics, has several disadvantages, in particular, a low glass transition temperature which, limits the service temperature to 75 °C [16]. This problem could be overcome by PE cross-linking which increases the operating and the maximum short circuit temperatures between 90 °C and 250 °C, respectively [16]. Consequently, more power may be transmitted by a cable insulated with cross-linked polyethylene compared to a cable of the same size, insulated with basic PE (LDPE). This results from the fact that the temperature is proportional to the intensity of the current or to the quantity of charge, which crosses the cable. Generally, the cross-linking of PE aims to preserve the desired properties at high temperature and to produce a non-melting and more durable polymer matrix. In addition, cross-linking changes the thermoplastic PE into thermoset XLPE, allowing improving its mechanical and electrical properties [18].

Reason why, XLPE is widely used as insulation. It has gradually replaced other polyethylenes in the manufacture of MV and HV cables owing to its excellent electrical [1] and thermal properties compared to basic polyethylene (LDPE) [2]. In the 1960s, it was used as insulation for 3 to 6 kV distribution cables [19]. Actually, it is used as an insulator for very high voltage cables ranging from 275 to 500 kV [20].

XLPE may be prepared by various methods outlined hereafter.

Reticulation by Radiation

Cross-linking of LDPE by irradiation was developed in the 1950s using (γ) rays generated by sources of cobalt 60 [21]. A. Charlesby compared the effects of the radiation of an atomic cell, γ rays, and X-rays, and he demonstrated that all these sources of energy are capable of causing the LDPE to cross-link [22]. A year later, Lawton et al. shown that LDPE could be cross-linked with the energy of electron beams (i.e., β rays) and its degree of cross-linking is proportional to the irradiation dose absorbed per unit of mass. As an indication, the dose necessary to cross-link the PE is approximately 20–30 Mrad (1 Mrad = 10 kJ/ kg) [22].

Reticulation by Silane

Silane cross-linking is the most recent method, initially introduced by Dow Corning [23]. It uses organofunctional unsaturated silanes, vinyltrimethoxysilane, in general. Cross-linking with silane is carried out in three steps [23]: The silane is grafted onto the polyethylene chain using a small amount of peroxide as an initiating agent. Then the silane groups are hydrolyzed, and finally, the condensation of these groups under the form $-\text{Si}-\text{O}-\text{Si}-$ connecting the polyethylene molecules is produced.

Reticulation by Peroxide

Historically, W. L. Alderson using inorganic peroxides introduced the cross-linking of PE with a peroxide in 1945 [22]. After a few months, P. S. Pinkney and R. H. Wiley revealed other organic peroxides as benzoyl to cross-link LDPE [22]. In 1955, F. M. Precopio and A. R. Gilbert implemented new peroxides, among which, dicumyl peroxide (DCP) [24]. Cross-linking by peroxide consists in linking the chains of molecules by radial bonds (bridging of the molecular chains) and in transforming them into a three-dimensional network which makes it possible to avoid the sliding of all the molecular chains with respect to each other [25].

3 Nanofillers

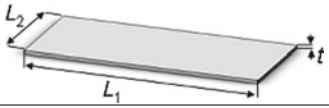
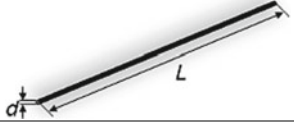

3.1 Definitions

Nanocharges are particles having at least one of their dimensions less than 100 nm. They are classified according to their geometric dimensions (Table 1), namely nanoplatelet, nanofiber, and nanoparticle, corresponding to one, two, and three dimensions, respectively.

One-Nanoscale Dimension

In this category, one of the dimensions is of the order of a nanometer; these fillers have a plane form, with lateral dimensions ranging from a few tens to many hundred nanometers and a form factor (length/width) at least equal to 25. These fillers lamellar can be natural (montmorillonite) and synthetic clays (laponite) as

Table 1 Geometrical shape and typical dimensions of more representative nanoparticles

Shape	Number of dimensions on the nanoscale	Example
	1 $t = 0.1\text{--}100\text{ nm}$ $L_1, L_2 > 100\text{ nm}$	Nanoclays Graphene
	2 $d = 0.1\text{--}100\text{ nm}$ $L > 100\text{ nm}$	Carbon nanotubes Halloysite nanotubes Cellulose nanocrystals
	3 $d = 0.1\text{--}100\text{ nm}$	Fullerene Ceramic nanoparticles (SiO ₂ , Al ₂ O ₃ , TiO ₂) Metal nanoparticles (Ag, Fe)

Reproduced from [27], Copyright (2017), with permission from Elsevier

well as transition metal phosphates (zirconium phosphate). Clays are generally used at rates of less than 10% by mass due to the significant increase in viscosity with the rate of the high filler.

Two-Nanoscale dimension

The two dimensions of the nanofiller approximately of nanometer range and the third is much larger ($>100\text{ nm}$), thus forming a fibrillar structure such as carbon nanotubes or cellulose whiskeys. The form factor (length/diameter) is at least 100. Such nanofillers lead to materials with exceptional properties, in particular in terms of stiffness.

Three-Nanoscale Dimension

The three dimensions of the nanocharge are of the order of a nanometer, and they are isodimensional nanoparticles, for example, spherical made of silica as reported in [26]. To improve the highly anisotropic mechanical and barrier properties of polymers, nanofillers of lamellar structures are preferred. On the other hand, a fibrillar structure will rather favor mechanical rigidity. Due to their very small size, certain spherical nanofillers increase the rigidity of the composite while retaining the transparency of the matrix.

3.2 Nano-Clays

The types of clay structures and minerals are shown in Fig. 1. Silicates or layered clays fall into the class of hybrid organic–inorganic nanocomposites [28, 29]. Historically, clay was believed to consist of small inorganic particles. The most

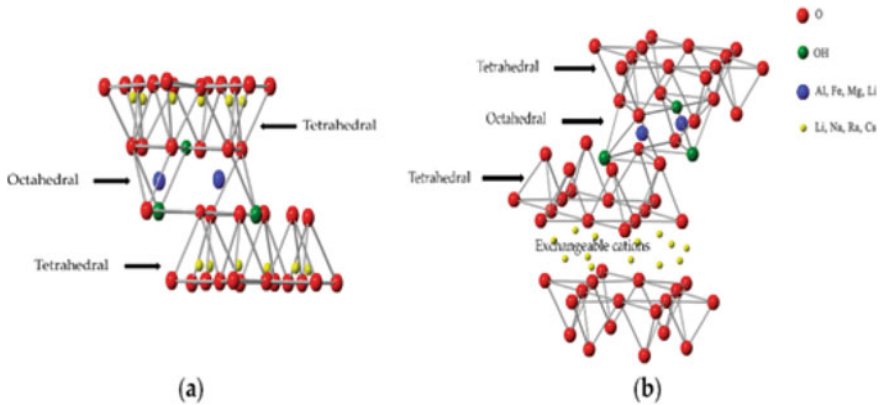


Fig. 1 Clay structure of clay minerals **a** Type 1:1; **b** Type 2:1. Reproduced from [30], Copyright (2017), with permission from Elsevier

investigated clay in the research industry is montmorillonite (MMT) [18]. Because of its structure and chemical composition, it is the one that has the most reinforcing ability. Part of the smectite family, this aluminum silicate, is composed of an octahedral layer of aluminum oxide inserted between two tetrahedral layers of silica (SiO_2). Its 2:1 reticular structure allows the network to be extensible by the absorption of water between its crystals and allows a large number of cation exchanges.

3.3 Carbon Nanotubes

Carbon nanotubes (CNTs) were discovered in 1960 by Roger Bacon and then characterized in 1991 by Sumio Iijima [31]. They are often arranged in two types as follows:

- Monolayer carbon nanotubes, consisting of a graphene plane wound on itself and closed at its ends by two half fullerenes with a diameter between 1 and 2 nm (Fig. 2).
- Multi-walled carbon nanotubes, where several planes of graphene as shown in Fig. 2, are wound concentrically, the ends of the tubes having a more complex structure with a diameter between 4 and 150 nm. In particular, the double layer carbon nanotubes consist of two concentric planes of graphene with a diameter ranging between 2 and 4 nm.

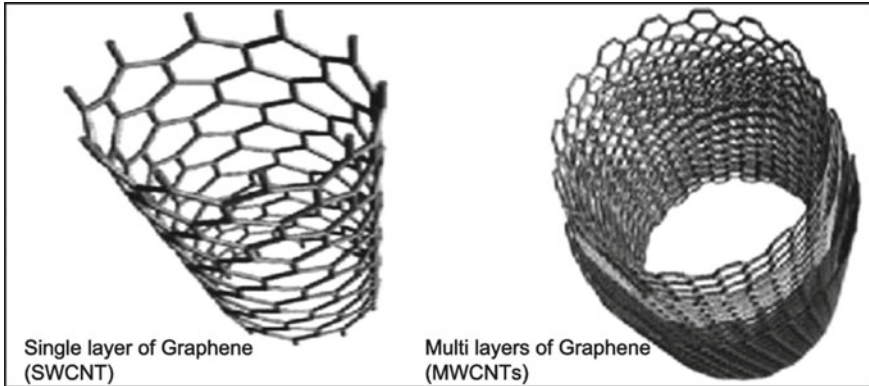


Fig. 2 Two types of carbon nanotubes. Reproduced from [32], Copyright (2017), with permission from Elsevier

3.4 Inorganic Nanoparticles

These nanoparticles have a diameter ≤ 100 nm; they are made from inorganic particles, which allow improving the composite materials' properties. Thus, to develop polymer/inorganic nanocomposites type, different kinds of nanoparticles are used:

- Metal nanoparticles of (Al, Fe, Au, Ag, etc.);
- Metal oxide nanoparticles (ZnO, Al₂O₃, CaCO₃, TiO₂, etc.);
- Non-metallic nanoparticles.

Obviously, the thermal, mechanical, electrical properties, and therefore, the application assigned to nanocomposites are correlated with the selection of nanoparticles [31]. Furthermore, it is worth mentioning here that nano α -Al₂O₃ (Fig. 3) are selected as fillers for polymers due to their particular chemical and physical properties, such as, excellent resistance to heat, high specific resistance, and good resistance to oxidation.

3.5 Silica Nanoparticles

Silica or silicon dioxide is very widespread in nature. It represents more than 70% of the mass of the earth's crust. It is an inorganic polymer of general formula SiO₂ or (SiO₂, xH₂O), consisting of an assembly of molecules of silicic acid Si(OH)₄ condensed in tetrahedral geometry. It is abundantly present in its natural state in minerals, such as quartz, in plants such as bamboo and rice or marine organisms, for example, sponges and diatoms. It has also been shown that soluble silica, even in trace amounts, is involved in the development of mammals. It can be of natural or synthetic origin and amorphous or crystalline (Fig. 4).

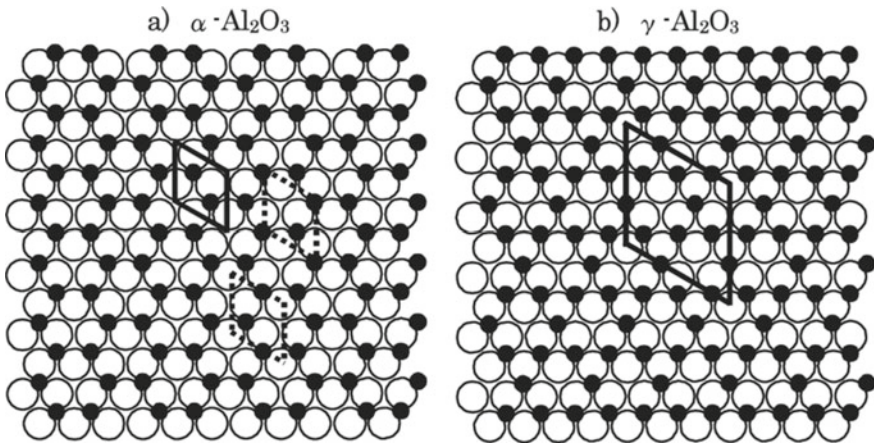
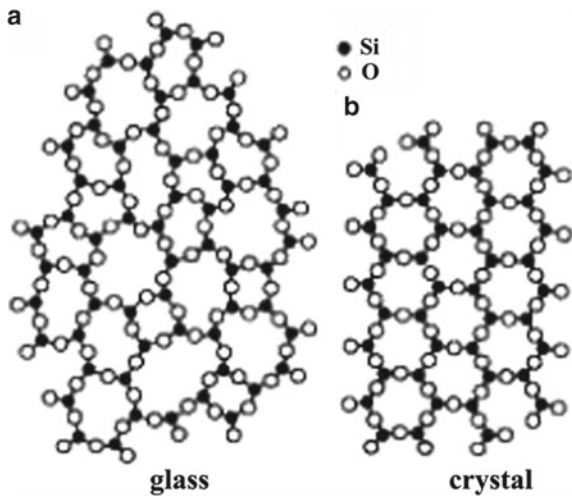


Fig. 3 Model structures of α - Al_2O_3 (0001) and γ - Al_2O_3 (111). Rhombuses in the structures show the unit cells [33]

Fig. 4 Schematic of structure of SiO_2 **a** glass and **b** crystal [34]



4 Need of XLPE Nanocomposites

The prime application of electrical cable is to carry power and signals over relatively long distances without compromising its performance, availability, and security. For these reasons, the power cables must withstand all stresses to which they can be subjected during service conditions. A typical high voltage cable contains several layers with various functions. The schematic representation of a simple high voltage cable is shown in Fig. 5. Different layers, viz (1) Conductor, (2) Strand shield, (3) main insulation, (4) Insulation shield, (5) Metallic shield (6) PVC cable jacket, are shown in the figure.

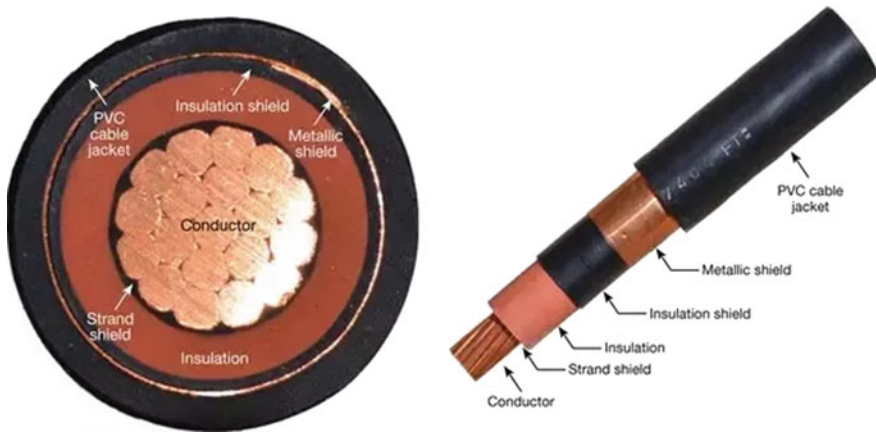


Fig. 5 Schematic diagram of a typical high voltage

Since insulation is a key element in medium and high voltage manufacturing, insulating materials are receiving the widespread attention of the electrical cable industry. The most commonly used materials are polyethylenes. There are also polyvinyl chloride (PVC) or rubber (EPR, EVA, or EPDM) insulations. The insulation material must have, in addition to dielectric specifications (resistivity and high dielectric strength, dielectric permittivity and low dielectric losses), good characteristics related to its use in the cable (insensitivity to shocks, vibrations and chemical attacks, resistance to fire, and resistance to aging). Nowadays, cross-linked polyethylene (XLPE) becomes the preferred insulation material due to its advantages of low cost and good reliability [35]. The application of extruded XLPE cables for HVDC power transmission has extensively increased in the recent years, and in the operational projects, 320 kV is the highest voltage level till now [36]. Despite, their excellent properties, polymers depict many problems when used as power cables insulation, XLPE insulated cables, similar to all polymers, can undergo several degradations under service conditions [3]. The major problems encountered by XLPE-based electrical cables are space charges accumulation, water trees, electrical trees, PD, etc., inside insulation [37].

With the rapid development of the energy industry, better performance and greater reliability of the insulation material for power cables are required for engineering applications [38]. In recent years, polymer nanocomposites as dielectric materials have attained considerable attention [39]. The inclusion of nanofiller to insulation material leads to marginal improvement in its dielectric, electrical, thermal properties, etc. [40–42].

There are various methods for maintaining the insulation performance of the XLPE polymer subject to the conditions of service. For example, it has been widely demonstrated that the addition of nanofillers in the XLPE improves its dielectric

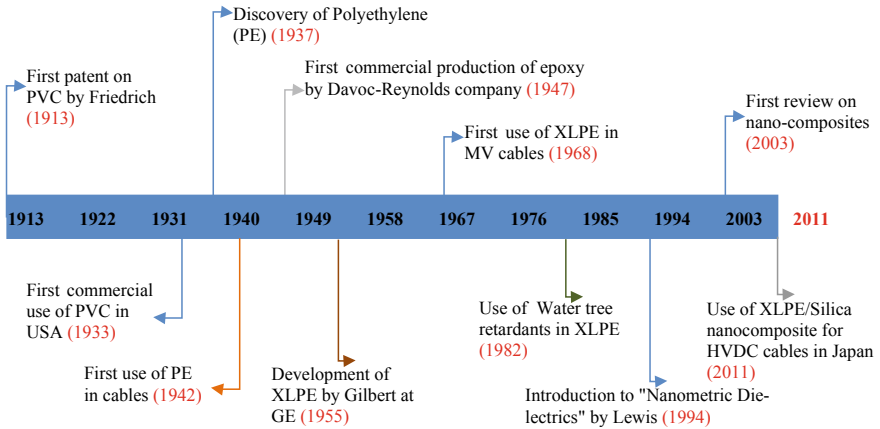


Fig. 6 Major developments in the field of electrical insulation [45]

properties while reducing the space charge [37]. This approach allowed to boost the commercial manufacturing and the commissioning of XLPE nanocomposite cables [43, 44]. These cables experienced a growing development as illustrated in Fig. 6.

5 Critical Issues in XLPE Polymer-Based Nanocomposites

It is well known that nanocomposite-based XLPE improves the major problems of XLPE insulated cables, such as partial discharges and the accumulation of space charges. As opposed to this, the use of nanofillers has certain disadvantages, which tend to slow down the deployment of the XLPE nanocomposite functioning of cables [46, 47]. In what follows, the fundamental shortcomings of nanocomposites-based XLPE insulation are exposed.

5.1 Water Absorption by Nanofillers

The absorption of humidity/moisture linked to the environment of the material cause changes in the thermophysical, mechanical, and chemical characteristics of the polymer matrix by plasticization and hydrolysis [48]. In the case of XLPE-based polymer nanocomposites, the moisture diffusion process is very complex, and it depends on the type and amount of filler of the nanoparticle. Hui et al. [49] in the study of the electrochemical tree structure in XLPE/silica nanocomposites have shown that the gain in humidity increases significantly with the charge of particles (Fig. 7). This is in agreement with the results obtained by other authors in the case of moisture resorption of epoxy [50].

Fig. 7 Moisture ingress at 100% rh RT [49]

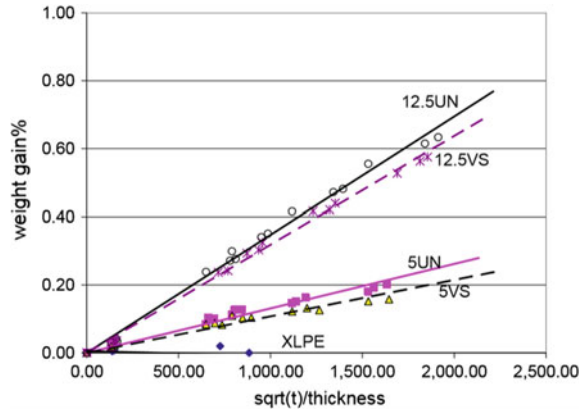
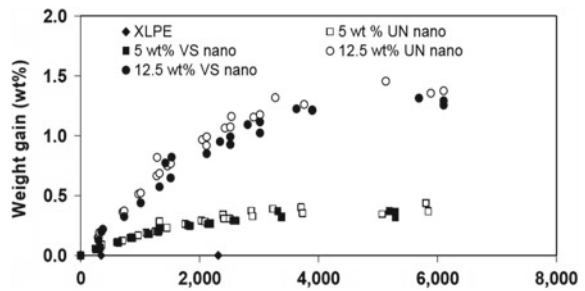


Fig. 8 Moisture uptake by XLPE and XLPE/silica nanocomposites at 50 °C with a relative humidity of 100% [51]



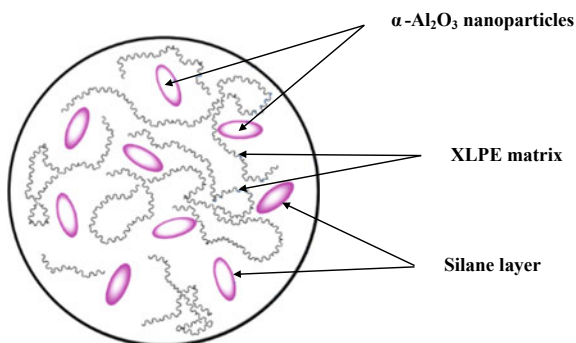
It is shown in another study of the moisture absorption profile of five materials conditioned at 50 °C and 100% RH for 9 months, that the XLPE/silica nanocomposite sites absorb more moisture than that of the XLPE polymer base (Fig. 8) [51]. The absorption of water is due to the introduction of charges known to alter the small processes of molecular diffusion [52, 53]. One of the reasons for the abnormal behavior of composites is the immobilization of penetrating molecules on the surface of hydrophilic charges [54, 55].

5.2 Compatibility Problem: Polymer Matrix/Nanoparticle

One of the major problems faced by polymers-based nanocomposites is the incompatibility between fillers and polymer matrix and the strong tendency to aggregation of nanoparticles. Thereby, to produce a homogenous polymer nanocomposite, a good compatibility between the components is crucial, irrespective of the preparation method of the polymer nanocomposite [56].

Although the importance of the size of the filler in determining the global properties (electrical, mechanical, and thermal) is undeniable [57], the chemistry of

Fig. 9 Schematic diagram of dispersion of nanoparticles in matrix [60]

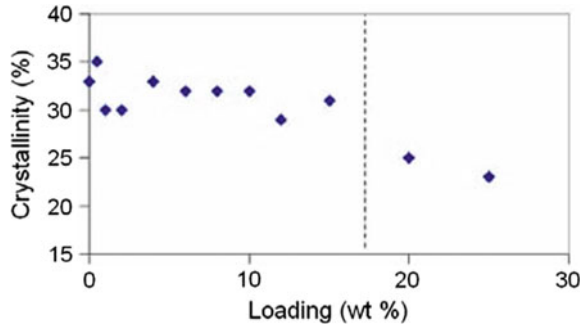


the particle surface is also critical. The addition of molecules that are more or less compatible with the matrix and, with a polar or non-polar nature, will affect the breakdown strength. In addition, the changes in morphology due to incorporation of nanoparticles, particularly for semi-crystalline polymers are of crucial importance [58, 59]. A silane coupling agent can affectively enhance the compatibility of the nanoparticle and polymer matrix; it can react with hydroxyl groups on the surface of nanoparticles, thus coating the surface of nanoparticles with a silane layer. This can prevent the agglomeration of nanoparticles and improve the dispersion of nanoparticles in the polymer matrix [60] (Fig. 9).

5.3 Morphological Changes

The crystallinity of a polymer refers to the degree as to which there are regions where the polymer chains are aligned with one another [61]. The degree of crystallinity is an inherent characteristic of each polymer, but it can be affected or controlled by certain processes such as polymerization or thermo-oxidation. In XLPE-based nanocomposites, the impact of nanofillers on crystallinity is still unclear. Therefore, it should be pointed out that as reported in the literature, there is no conclusion on the change of crystallinity in cross-linked polyethylene-based nanocomposites [62]. The crystallinity may increase, decrease or does not change after the introduction of nanoparticles, which is related to the choice of materials and the preparation process [63, 64]. Smith [65] showed that the addition of fumed silica has been found to alter the crystallinity of XLPE. As such, Fig. 10 shows that the addition of fumed silica at low loadings induces an increase in crystallinity. In this case, the particles form fractal agglomerates. This morphology leads to increased particle/particle interactions relative to individual spherical particles. Due to these interactions, the viscosity increases rapidly with particle addition and consequently induces an increase of crystallinity.

Fig. 10 First heat DSC curves for vinylsilane treated silica nanocomposites [65]



Sharad et al. [37] showed that nanofiller addition leads to the decrease in the surface energy which causes secondary or incomplete crystallization. The secondary crystallization intervenes in the amorphous phase of the material. Inflections formed due to secondary or incomplete crystallization can be seen in Fig. 11. The secondary crystallization induces changes in the mechanical characteristics. Since the chains are denser in the crystalline state, there is also a shrinkage. Dastjerdi et al. [66] studied the morphological changes of calcium carbonate-based nanocomposites of cross-linked high density polyethylene and showed that addition of NCCs decreases the apparent enthalpy of fusion (ΔH_m) of the material which leads to reduction of crystal domains and subsequently the reduction of the melting temperature (Fig. 12).

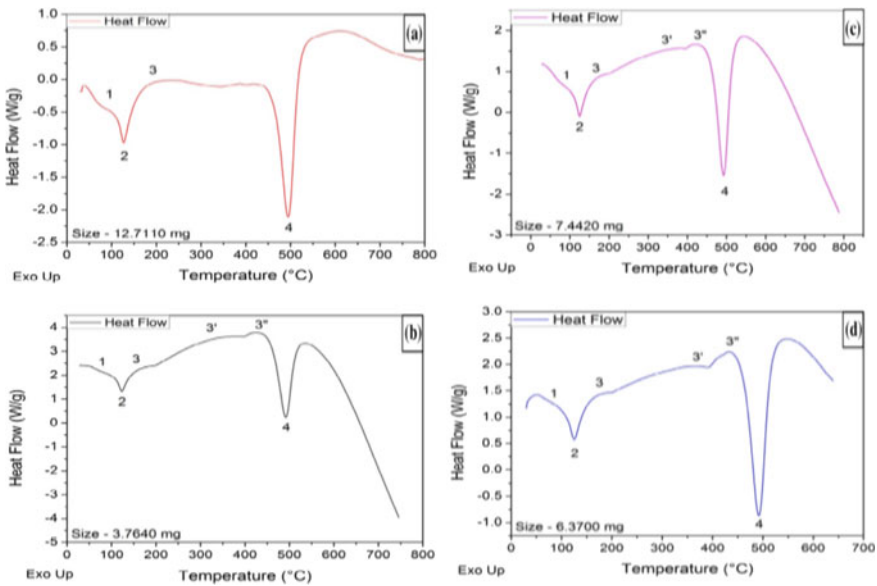


Fig. 11 Differential scanning calorimetry (DSC) of **a** virgin XLPE, **b** nano 1 wt% unmodified, **c** nano 1 wt% agglomerated, **d** nano 1 wt% Octylsilane modified [37]

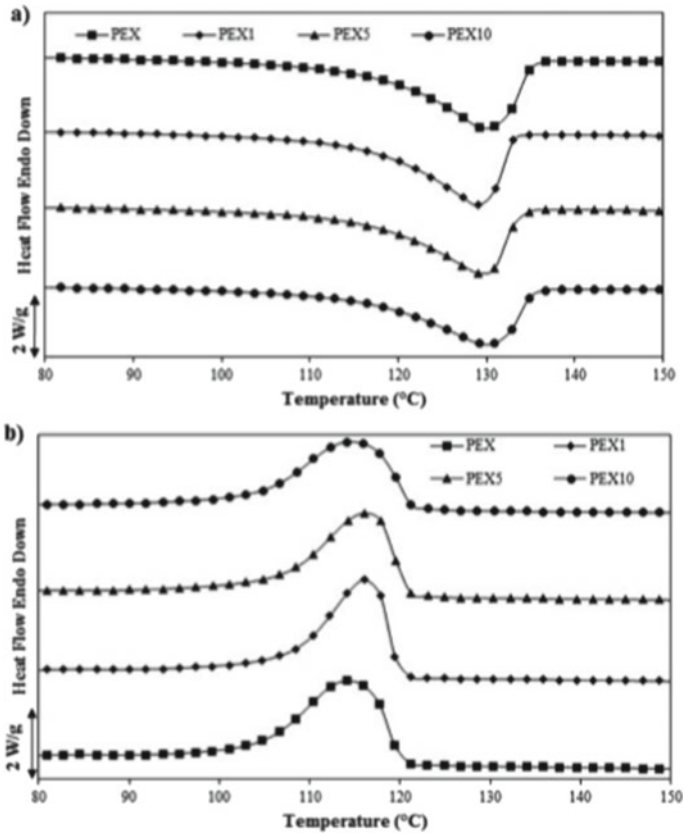


Fig. 12 DSC **a** heating and **b** cooling scans for PEX (XLPE) and nanocomposites [66]

5.4 Aggregation and Agglomeration

The aggregation/agglomeration of nanoparticles reduces the potential enhancement of mechanical properties in nanocomposites, due to the restriction of interfacial area [67, 68]. The big nanoparticles induce small interfacial area which attenuates the role of nanoparticles in nanocomposites. Consequently, although the high contents of nanoparticles in nanocomposites strengthen the accumulation, the aggregation/agglomeration of nanoparticles generally occur in polymer nanocomposites at different filler concentrations which decrease the interfacial area and weaken the mechanical characteristics. Sharad et al. [37] have investigated the problem of agglomeration in XLPE/silica nanocomposites. It was reported from SEM analysis as shown in Fig. 13 that during the preparation process of XLPE/silica, the nano-fillers cannot be dispersed in homogenous manner.

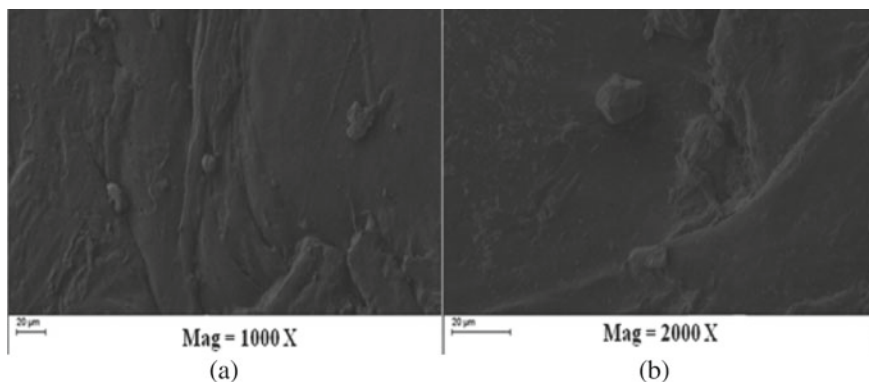


Fig. 13 SEM images of **a** XLPE/silica nano 2 wt% agglomerated nanocomposites, **b** XLPE/silica nano 3 wt% agglomerated nanocomposites [37]

In order to obtain a better dispersion, XLPE/ silica nanocomposites is treated with Octylsilane, which is used due to its smaller size (7–14 nm), hydrophobicity and high specific surface area ($150 \text{ m}^2/\text{g}$). Octylsilane acts as a chemical adhesion between polymer matrix and nanosilica. Commonly, silane coupling agent tries to separate nanoparticles from each other by acting as compatibilizer between nanoparticle surface and polymer matrix which eventually leads to homogenous dispersion of nanofiller [69, 70]. Figure 14a, b shows that the better (or ideal) dispersion of nanoparticles is achieved. In this case, Octylsilane acts as a coupling agent between polymer matrix and silica nanoparticles. Hereafter, the nanocomposites prepared using this method are referred as Octylsilane-modified nanocomposites.

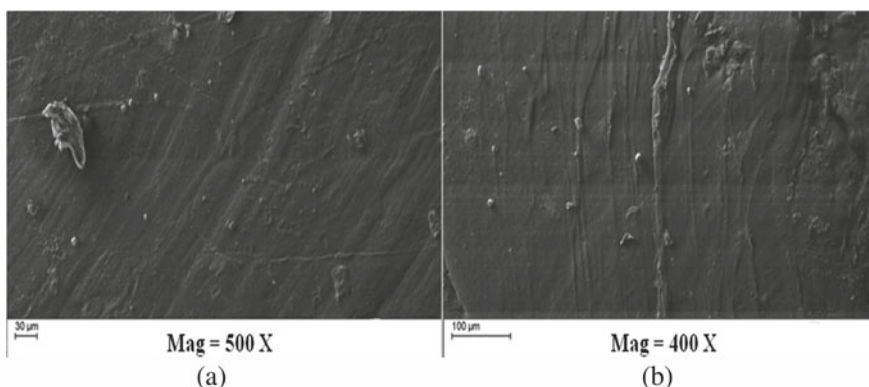


Fig. 14 SEM images of **a** XLPE/silica nano 2 wt% Octylsilane-modified nanocomposites, **b** XLPE/silica nano 3 wt% Octylsilane-modified nanocomposites [37]

In order to clarify the disadvantages of agglomeration in XLPE nanocomposites, partial discharge (PD) characteristics of cross-linked polyethylene for unmodified, agglomerated, and Octylsilane-modified silica nanocomposites were investigated in this study.

The obtained results reveal that agglomerated XLPE nanocomposites present a highest PD activity, lowest discharge inception voltage and breakdown voltage compared to XLPE Octylsilane-modified silica nanocomposites. This behavior can be assigned to the fact that the surface-modified nanocomposites have low optimal content of nanofiller toward PD characteristic. These results are shown in Figs. 15 and 16.

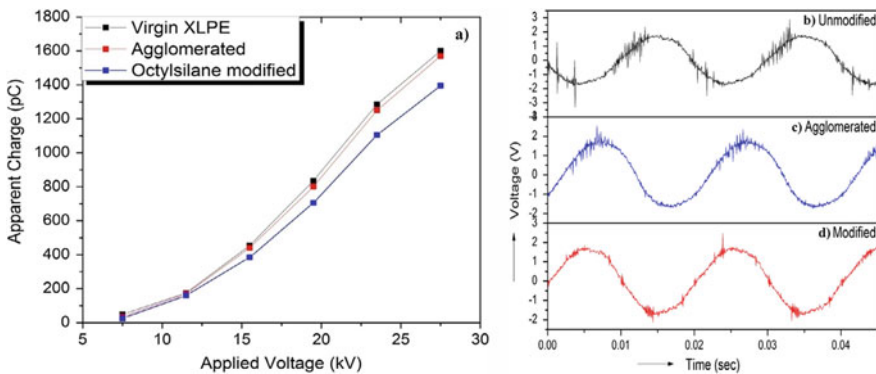


Fig. 15 a PD characteristics of agglomerated and Octylsilane surface-modified XLPE/silica nanocomposites for nano 2 wt%, PD pulses appearing at 15.5 kV in **b** unmodified, **c** agglomerated, **d** Octylsilane surface-modified XLPE/Silica nanocomposite for nano 2 wt% [37]

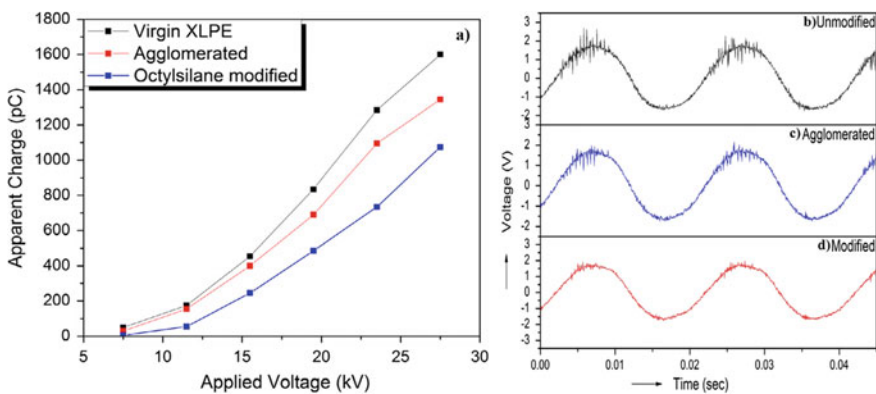


Fig. 16 a PD characteristics of agglomerated and Octylsilane Surface-surface-modified XLPE/silica nanocomposites for nano 2 wt%, PD pulses appearing at 15.5 kV in **b** unmodified, **c** agglomerated, **d** Octylsilane surface-modified XLPE/Silica nanocomposite for nano 3 wt% [37]

It can be summarized from these investigations that agglomeration in XLPE nanocomposites negatively affects the PD performances. It has been also reported that structural changes in XLPE due to addition of nanofiller mainly occur in amorphous phase. Also, Octylsilane-modified silica nanofillers addition to XLPE lead to decrease in surface energy which causes secondary or incomplete crystallization.

5.5 Partial Discharge Quantity and Erosion

The common manifestation of electrical tracking on the surface of XLPE insulation will be the decrease in the insulation strength with concomitant breakdown and damage of the cable [71–73]. Fairus et al. [71] investigated the surface tracking behavior such as total discharge quantity, and area of the tracking path and erosion in XLPE filled with untreated ZnO nanofiller.

The nanocomposite samples were manufactured into various ZnO nanofiller concentration (1–4 wt%). As can be seen from Fig. 17, unfilled XLPE (0% wt) composite displays smaller total discharge quantity (4.04 C) compared with XLPE filled with 1–4 wt% untreated ZnO nanofiller for which the total discharge are gradually increased from 6.73 to 10.42 C. It can be concluded that XLPE containing untreated ZnO nanofiller (1–4 wt%) has imparted a bad performance in delaying the period of time to track compared to unfilled XLPE composite because of the higher level of total discharge quantity.

Figure 18 shows the area of tracking path and erosion result of unfilled XLPE and XLPE containing untreated ZnO nanofiller (1–4 wt%).

As can be seen from Fig. 3, the area of the tracking path and erosion for unfilled XLPE (0% wt) are smaller than XLPE containing untreated ZnO nanofiller

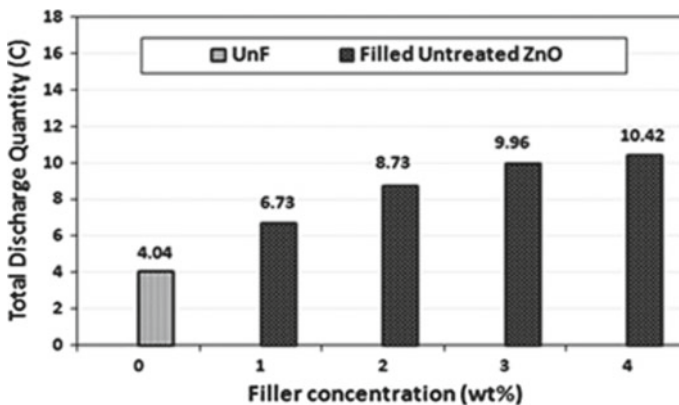


Fig. 17 Total discharge quantity at various concentrations of untreated ZnO nanofiller in XLPE. Reproduced from [71], Copyright (2019), with permission from Springer

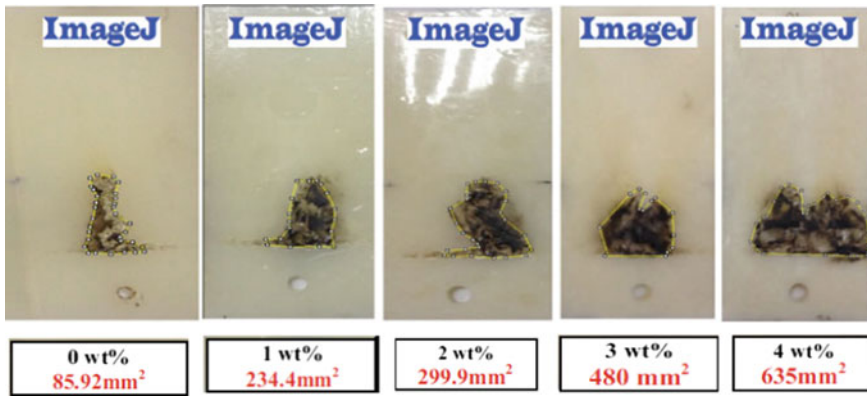


Fig. 18 Photographs of image J measurement on tracking path and erosion area of unfilled and untreated ZnO nanofiller (1–4 wt%) in XLPE. Reproduced from [71], Copyright (2019), with permission from Springer

(1–4 wt%) for which the area increased from 234.44 mm² (1 wt%) to 635.03 mm² (4 wt%). The increases of nanofiller concentrations in XLPE composites have weakened the mechanical strength of the material, as a consequence of, dry band arcing (DBA) occurrences on the material which affect the large surface area of tracking path and erosion.

6 Conclusion

The development of more efficient, less costly, and environmentally friendly materials remains one of the concerns of the cable manufacturing industry for the transport of electrical energy and engineering signals. In this context, the interest of polymer composites in the field of electrical insulation has been highlighted in this chapter. Based on the literature, various methods of manufacturing XLPE cables intended for the transport of medium and high voltage electrical energy have been reviewed. Various aspects of the nanofillers introduced into polymers to improve their electrical, thermal, and mechanical have also been recalled. In this regard, studies on the effects of the nature, dimensions, shape, diffusion, and concentration of nanoparticles were listed. In view of previous studies, it appears that the practical application and commercial production of XPLE nanocomposites for electrical insulation are still being improved. Thanks to nanotechnology experts, inter-disciplinary teams in the fields of electrical engineering, physics, and chemistry are joining forces to optimize the performance of these insulation materials. Obviously, the use of small amounts of nanocharges in XPLE cables will increase due to their very interesting benefits. However, as discussed in this chapter, the overcoming of certain critical problems related to the absorption of water by

nanofillers, the compatibility between the polymer matrix and the nanoparticle, morphological changes, aggregation and agglomeration, amount of partial discharge, and erosion will also play a major role in the optimization of the efficiency of XLPE-based polymer nanocomposites and their blends.

What the Future Holds?

Cross-linked polyethylene (XLPE) is widely used as an insulator in cables due to its dielectric properties and its improved thermomechanical stability. Past experiences with polyethylene cables and foreign impurities in XLPE cables have caused many tree problems. For this reason, ultra-pure insulation for cables is used today. In addition, this material is not easily recycled, raising questions about its long-term durability. In recent years, environmental concerns have become strong components to take into account when selecting insulation. Traditional thermoplastics such as polyethylene and polypropylene are currently widely recycled, which would eventually allow suitable replacement for XLPE in cables in the medium and long term. Polypropylene (PP) has good dielectric properties, almost unaffected by environmental humidity and frequency. PP also has excellent resistance to chemical degradation and heat which can make it usable for a long time under high voltage. However, (1) PP has low flexibility, (2) spherulites develop easily and the insulation resistance on the surface of the spherulite is much lower, and (3) its degradation is clearly favored by contact with copper.

Different nanocomposites based on a polypropylene (PP) matrix are being developed. The stereo-regular syndiotactic polypropylene (s-PP) with a metallocene catalyst has very interesting properties. It has potentially sufficient flexibility, mechanical properties equivalent to those of XLPE, low dielectric losses, and higher electrical breaking strength [74]. In addition, due to its high melting point, it can be used at higher temperatures than XLPE. Nanotechnology is poised to play an important role in this technology development.

Acknowledgements The authors thank the Algerian Ministry of Higher Education and Scientific Research for supporting this work through the project PRFU A01L07UN150120180005.

References

1. Gulmine JV, Akcelrud L (2006) *Eur Polym J* 42:553
2. Bouanga CV, Couderc H, Fréchette MF, Savoie S, Malucelli G, Camino G, Castellon J, Banet L, Toureille A (2012) *IEEE Trans Dielectr Electr Insul* 19:1269
3. Hedir A, Moudoud M, Lamrous O, Rondot S, Jbara O, Dony P (2020) *J Appl Polym Sci* 137
4. Hedir A, Jbara O, Moudoud M, Slimani F, Rondot S, Bellabas F (2019) *Proceedings 2018 3rd international conference on electrical sciences and technologies in Maghreb CISTEM 2018*. Institute of Electrical and Electronics Engineers Inc
5. Aglan H, Calhoun M, Allie L (2008) *J Appl Polym Sci* 108:558
6. Xu M, Zhao H, Ji C, Yang J, Zhang W (2012) *Gaodianya Jishu/High Volt Eng* 38:684
7. Tanaka T, Montanari GC, Mülhaupt R (2004) *IEEE Trans Dielectr Electr Insul*, pp 763–784

8. Chen, DMX, Wang X, Wu K, Peng ZR, Cheng YH, Tu (2011) *Trans China Electrotech Soc* 12:13
9. Junguo G, Jinmei Z, Quanquan J, Jiayin L, Mingyan Z, Xiaohong Z (2008) *Proceedings international symposium on electrical insulation materials*, pp 597–600
10. Li Z, Okamoto K, Ohki Y, Tanaka T (2010) *IEEE Trans Dielectr Electr Insul* 17:653
11. Ding HZ, Varlow BR (2004) *Annual report—conference on electrical insulation and dielectric phenomena, CEIDP*, pp 332–335
12. Wang Y, Wang C, Xiao K (2016) *Polym Test* 50:145
13. Paramane A, Chen X, Dai C, Guan H, Yu L, Tanaka Y (2020) *Polym Compos* 41:1936
14. Hedir A, Bechouche A, Moudoud M, Teguar M, Lamrous O, Rondot S (2020) *Turkish J Electr Eng Comput Sci* 28:1763
15. Ying L, Xiaolong C (2014) *IEEE Trans Dielectr Electr Insul* 21:1540
16. Nóbrega AM, Martinez MLB, De Queiroz AAA (2014) *J Mater Eng Perform* 23:723
17. Cao L, Grzybowski S (2015) *IEEE Trans Dielectr Electr Insul* 22:2809
18. Aljoumaa K, Ajji Z (2017) *J Radioanal Nucl Chem* 311:15
19. Kim C, Jin Z, Huang X, Jiang P, Ke Q (2007) *Polym Degrad Stab* 92:537
20. Boukezzi L, Boubakeur A (2013) *IEEE Trans Dielectr Electr Insul* 20:2125
21. Elvira M, Tiemblo P, Gómez-Elvira JM (2004) *Polym Degrad Stab* 83:509
22. Corrales T, Catalina F, Peinado C, Allen NS, Fontan E (2002) *J Photochem Photobiol A Chem* 147:213
23. Gubanski SM, Montanari GC, Motori A (1994) *Conference record of the IEEE international symposium on electrical insulation. IEEE*, pp 54–57
24. Rabello MS, White JR (1997) *Polym Degrad Stab* 56:55
25. Kobayashi K, Nakayama S, Niwa T (1994) *Proceedings of 5th international conference on properties and applications of dielectric materials. IEEE*, pp 678–681
26. Hu H, Onyebuoke L, Abatan A (2010) *J Miner Mater Charact Eng* 09:275
27. Rallini M, Kenny JM (2017) *Modification of polymer properties. Elsevier Inc.*, pp 47–86
28. Giannelis EP (1998) *Appl Organomet Chem* 12:675
29. Zou H, Wu S, Shen J (2008) *Chem Rev* 108:3893
30. Jlassi K, Krupa I, Chehimi MM (2017) *Overview: clay preparation, properties, modification. In: Clay-polymer nanocomposites. Elsevier Inc.*, pp 1–28
31. Kurahatti RV, Surendranathan AO, Kori SA, Singh N, Kumar AVR, Srivastava S (2010) *Def Sci J* 60:551
32. Parveen S, Kumar A, Husain S, Husain M (2017) *Phys B Condens Matter* 505:1
33. Yoshitake M, Bera S, Yamauchi Y, Song W (2003) *Hyomen Kagaku* 24:438
34. Cao C, Bin Li Z, Wang XL, Zhao XB, Han WQ (2014) *Front Energy Res* 2:25
35. Al-Arainy AA, Malik NH, Qureshi MI, Al-Saati MN (2007) *IEEE Trans Power Deliv* 22:744
36. Cao L, Zhong L, Li Y, Gao J, Chen G, Li W, Li W, Zhang C (2019) *ICEMPE 2019—2nd International conference on electrical materials and power equipment, proceedings. Institute of Electrical and Electronics Engineers Inc.*, pp 349–352
37. Ashish Sharad P, Kumar KS (2017) *Nanocomposites* 3:30
38. Youyuan Wang FW, Xiao K, Wang C, Yang L (2016) *J Nanomater* 2016:1
39. Thomas J, Joseph B, Jose JP, Maria HJ, Main P, Ali Rahman A, Francis B, Ahmad Z, Thomas S (2019) *Ind Eng Chem Res* 58:20863
40. Bafekrpour E, Thomas S, Jose JP (2017) *Advanced composite materials: properties and applications. De Gruyter Open*
41. Iyer G, Gorur RS, Richert R, Krivda A, Schmidt LE (2011) *IEEE Trans Dielectr Electr Insul* 18:659
42. Reddy CC, Ramu TS (2008) *IEEE Trans Dielectr Electr Insul* 15:221
43. Murata Y, Sakamaki M, Abe K, Inoue Y, Mashio S, Kashiyama S, Matsunaga O, Igi T, Watanabe M, Asai S, Katakai S (2013) *Development of high voltage DC-XLPE cable system*
44. Lee SB, Kim YH, Jung EH, Hong SP, Cho DS, Kim SY, Son SH, Lee IH (2018) *Proceedings of IEEE international conference on properties and applications of dielectric material. Institute of Electrical and Electronics Engineers Inc.*, pp 393–399

45. Paramane AS, Kumar KS (2016) *Trans Electr Electron Mater* 17:239
46. Li Z, Du B (2018) *IEEE Electr Insul Mag* 34:30
47. Montanari GC, Seri P, Lei X, Ye H, Zhuang Q, Morshuis P, Stevens G, Vaughan A (2018) *IEEE Electr Insul Mag* 34:24
48. de Brito MKT, dos Santos WRG, de B. Correia BR, de Queiroz RA, de S. Tavares FV, de O. Neto GL, de Lima AGB (2019) *Polymers (Basel)* 11
49. Hui L, Smith R, Nelson JK, Schadler LS (2009) Annual report—conference on electrical insulation and dielectric phenomena, CEIDP, pp 511–514
50. Zou C, Fothergill JC, Rowe SW (2008) *IEEE Trans Dielectr Electr Insul* 15:106
51. L. Hui, L. Schadler, Keith Nelson J (2013) *IEEE Trans Dielectr Electr Insul* 20:641
52. Zou C, Fu M, Fothergill JC, Rowe SW (2006) Annual report—conference on electrical insulation and dielectric phenomena, CEIDP, pp 321–324
53. Drozdov AD, de Christiansen JC, Gupta RK, Shah AP (2003) *J Polym Sci Part B Polym Phys* 41:476
54. Zou C, Fothergill JC, Rowe SW (2007) 2007 International conference solid dielectric ICSD, pp 389–392
55. Fukuda A, Mitsui H, Inou Y, Goto K (1997) Proceedings of IEEE international conference on properties and applications of dielectric materials. IEEE, pp 58–61
56. Amin M, Ali M, Amin M, Ali M (2015) *Polymer Nanocomposites for High Voltage Outdoor Insulation Applications*
57. Fothergill JC, Nelson JK, Fu M (n.d.) 17th Annual meeting IEEE lasers and electro-optics society, LEOS. IEEE, pp 406–409
58. Ma D, Akpalu YA, Li Y, Siegel RW, Schadler LS (2005) *J Polym Sci Part B: Polym Phys* 43:488
59. Malec D, Truong VH, Essolbi R, Hoang TG (1998) *IEEE Trans Dielectr Electr Insul* 5:301
60. Guo X, Xing Z, Zhao S, Cui Y, Li G, Wei Y, Lei Q, Hao C (2020) *Materials (Basel)* 13:1
61. Crawford CB, Quinn B (2017) *Microplastic pollutants*. Elsevier, pp 57–100
62. Wang S, Chen P, Yu S, Zhang P, Li J, Li S (2018) *IEEE Trans Dielectr Electr Insul* 25:2349
63. Jose JP, Chazeau L, Cavallé JY, Varughese KT, Thomas S (2014) *RSC Adv* 4:31643
64. Tanaka T, Bulinski A, Castellon J, Fréchette M, Gubanski S, Kindersberger J, Montanari GC, Nagao M, Morshuis P, Tanaka Y, Péliou S, Vaughan A, Ohki Y, Reed CW, Sutton S, Han SJ (2011) *IEEE Trans Dielectr Electr Insul*:1484–1517
65. Smith RC (2009) Mechanistic electrical behavior of crosslinked polyethylene/silica nanocomposites. Rensselaer Polytechnic Institute
66. Dastjerdi J, Motlagh EN, Garmabi H (2017) *Polym Compos* 38:E402
67. Chen J, Yu Y, Chen J, Li H, Ji J, Liu D (2015) *Appl Clay Sci* 115:230
68. Khan A, Shamsi MH, Choi TS (2009) *Comput Mater Sci* 45:257
69. Geng Y, Liu MY, Li J, Shi XM, Kim JK (2008) *Compos Part A Appl Sci Manuf* 39:1876
70. Shokoohi S, Arefazar A, Khosrokhavar R (2008) *J Reinf Plast Compos* 27:473
71. Fairus M, Hafiz M, Mansor NS, Ishak D, Mariatti M, Halim HSA, Basri ABA, Kamarol M (2019) *Lecture notes in electrical engineering*. Springer Verlag, pp 269–275
72. Chen XG, Gu L, He XR, Liao HY (2012) ICHVE 2012—International conference on high voltage engineering and application, pp 51–54
73. Du BX, Zhu XH, Gu L, Liu HJ (2011) *IEEE Trans Dielectr Electr Insul* 18:176
74. Dang B, He J, Hu J, Zhou Y (2015) *J Nanomater* 16:439

Chapter 5

General Applications of XLPE Nanocomposites and Blends



Divya Radha, Jisha S. Lal, K. Asha Krishnan, and K. S. Devaky

List of Abbreviations

AC	Alternating current
DC	Direct current
DBS	Dielectric breakdown strength
BN	Boron nitride
EB	Electrical breakdown
EPDM	Ethylene propylene diene rubber
EPR	Ethylene propylene rubber
EVA	Ethyl vinyl acetate
FDA	Food and drug administration
HPTE	High-performance thermoplastic elastomer
HV	High voltage
HVDC	High voltage direct current applications
LDPE	Low density polyethylene
LLDPE	Linear low density polyethylene
MH	Magnesium hydroxides
MV	Medium voltage
PEX	Crosslinked polyethylene
POS	Polyhedral oligomeric silane
SMPs	Smart shape polymers
UHMWPE	Ultra high molecular weight polyethylene
XLPE	Crosslinked polyethylene

D. Radha (✉) · J. S. Lal · K. S. Devaky
School of Chemical Sciences, Mahatma Gandhi University, Kottayam, Kerala, India
e-mail: aquaregiazone@gmail.com

K. Asha Krishnan
International and Inter University Centre for Nanoscience and Nanotechnology,
Kottayam, Kerala, India

1 Introduction

Polymer blending is used to develop highly advanced and sophisticated materials from commonly available polymers and thereby modifying their various physical and chemical properties. Those blends possess an excellent combination of properties of their pristine polymers. Polyethylene (PE) was the most suitable insulation material in the cable production during the earlier times due to its low permittivity and high electrical break down strength. However, the major drawbacks of PE were the limitation of the maximum operating temperature around 70 °C and addition of antioxidants for avoiding the deterioration of the polymer-based insulation [1]. Taking into consideration of all these matters, a new solution was put forth by the crosslinking of PE yielding XLPE. Crosslinking can improve various properties of the polymers like high performance at a reasonable rate, reuse of plastic scrap, generation of a unique material for the desired applications, long shelf life, extending the performance of expensive resins [2]. A surplus of applications of these materials are being explored in various areas like electronic applications, cable insulations, shock absorbers, foam packaging, thermal insulation and sports goods.

Addition of nanofillers to the crosslinked polyethylene yields nanocomposites which improve its electrical, mechanical, physical and thermal properties. Introduction of nanofillers aids to provide the characteristics of finite size effect, quantum effect, high ratio of surface to volume and specific high strength at minimum the cost [3]. The most commonly added nanofillers are metal oxides, graphene and cellulose, glass, and carbon nanotube and carbon fibres.

This chapter put forth the role of crosslinked polyethylene nanocomposites and blends in various areas of research like dielectrical applications, packaging, insulations, moulding applications and medical fields.

2 Applications of Crosslinked Polyethylene Blends

XLPE blends own a variety of properties like corrosion resistance, thermal stability, abrasion resistance, chemical stability, durability which aids these to be applied in various areas of applications

- Cable and wire insulations
- Orthopaedic applications
- Shape memory effects.

2.1 Crosslinked Polyethylene Blends in Orthopaedic Applications

Generally, crosslinking of polyethylene was done by chemical and irradiation methods. Chemical crosslinking is generally done using peroxide or silane, whereas irradiation methods make use of ionizing radiations like gamma and electron beam radiation for crosslinking [4]. Due to no FDA approval chemically crosslinked polyethylene would have to confirm its safety before it is used in the medical implants. Hence, the orthopaedic applications make use of irradiation crosslinked polyethylene [5]. Orthopaedic manufacturers use this crosslinked polyethylene as substitutes for pristine polyethylene. Such blends are substituted for being employed in orthopaedic applications like artificial knee and hip joints replacement polyethylene as it causes the osteolysis. Crosslinked polyethylene blends are widely used due to their wear and tear resistance. Though the modification of the parent polymer using crosslinking can reduce the mechanical properties needed for the knee joints, electron beam irradiated XLPE can improve the oxidation resistance and mechanical properties like toughness, elongation at break and so on [6].

Oxidative degradation of the XLPE can be inhibited by the addition of antioxidants before the consolidation and crosslinking via irradiation. The additions of these antioxidants can maintain the original morphology, more resistant to fatigue and thereby making oxidation resistant [7].

A number of studies have investigated the use of antioxidant vitamin E as a stabilizer for the oxidation in XLPE [8]. Vitamin E a radical scavenger not only inhibits the oxidation but also enhances the efficiency of crosslinking. Therefore, a balance between the concentration of vitamin E, tocopherol and radiation dose should be maintained so as to produce wear and oxidation-resistant polymer. The diffusion of vitamin E into the polymer after the radiation crosslinking does not reduce the crosslinking efficiency but make the polymer oxidation resistant. Homogenization is a mandatory requirement to make the concentration of antioxidants uniform throughout the implants [9].

It is also reported that the crosslinked polyethylene prepared using irradiation methods become more wear-resistant than the uncrosslinked polyethylene which makes it a wonderful candidate for the orthopaedic applications [10]. The reports show that the combination of ceramics like alumina with UHMWPE shows an excellent wear and tear resistance in the applications of knee, hip, ankle joint simulators [11]. Although UHMWPE is proved to be an excellent wear-resistant material, it is not so, some sort of wear debris are found to present over the surface which gets occluded over the bone and induces the osteolysis as time passes by and results in dangerous biological reactions [12].

Radiation crosslinked polyethylene with high mechanical strength, wear resistance, oxidation stability is an unavoidable requirement for the lifelong performance of a joint. Reports regarding the use of crosslinked polyethylene blends based on the natural polyphenols like gallic acid and dodecyl gallate are available. The antioxidants like these polyphenols enhance the oxidative stability, thereby

increasing the lifespan of implants [13]. These blends are found superior when compared to the vitamin E blended XLPE. The tensile strength, wear-resistant and impact properties of polyphenol-based materials are far better than the unblended polyethylene entities making them as a potential candidate for the joint implant applications.

Recently, X-rays proved to be an excellent radiation method for the crosslinking of polyethylene due to its greater penetration rate as well as a low rate of dosage as compared to the gamma and electron beam radiation. Vitamin E blended UHMWPE highly crosslinked by X-ray radiation has an improved wear resistance, thereby making this blend a material of choice for the total hip arthroplasty. X-ray radiation at high temperature greatly enhanced the crosslinking and oxidation resistance of the blend. The blend retained the mechanical properties, oxidative stability, improved wear resistance which is very much pivotal in reducing the rate of osteolysis [14].

2.2 Crosslinked Polyethylene Blends in Cable and Wire Insulations

In the field of MV, HV cables, cable jackets and semiconducting layers, extruded polymers are being commonly used due to low raw material and processing costs along with high reliability and adequate material performance, polyethylene (PE) and crosslinked polyethylene (XLPE) are widely applied in cable and wire applications [15, 16]. Excellent crosslinking efficiency of polyolefin like polyethylene can improve the physical properties of the parent analogues. Polyethylene suffers the defects like low-temperature degradation, low retention of mechanical properties at high temperature, high flammability and poor compatibility with fillers. As we all know the blending of crosslinked polymers with various substances like metal hydroxides, olefins can alter the physical, mechanical, flame retardancy, electrical properties. The cables used in various industries, power plants, restaurants, vehicle, constructions must satisfy with the electrical and mechanical standards as per the material characteristics and specifications like flame retardancy, less toxicity and low density. Hence, a necessity of halogen-free solutions for crosslinked thermoplastic elastomers is common. It is reported that addition of metal hydroxides like aluminium trihydrate and magnesium hydroxide to the XLPE/ethyl vinyl acetate (EVA) blends can improve the flammability, mechanical, thermal and electrical properties for using them in cable and wire applications [17]. XLPE/EVA/magnesium hydroxide (MH) blends exhibits greater flame retardancy, excellent mechanical properties for wire and cable applications. These blends have greater melt flow index values making them more flow resistant and the stronger physical adhesion and hydrogen bonds present between the metal hydroxide and XLPE/EVA blends assure that these does not get elongated even at higher temperature. These blended polymers are found as tough blend polymers as they

possess high EB values. Studies show that MH/XLPE/EVA blends shows high flame retardancy than AH blends. This is due to the fact that MH has a greater endothermic decomposition temperature than aluminium hydroxide. Hence, aluminium blends start to decompose even at 100–180 °C. This makes MH/XLPE/EVA blends as better flame retardants, which is a mandatory requirement for the cable and wire insulation applications [17].

Montmorillonite, a silicate more precisely belonging to the phyllosilicate mineral is a hydrated sodium calcium aluminium magnesium silicate hydroxide. Addition of these montmorillonite to the XLPE/EVA blends filled with inorganic hydrated flame retardants such as aluminium hydroxide, magnesium hydroxide and synthetic hydromagnesite improves the thermal and flame requirements [18]. This is due to a barrier effect resulted from the dispersion of the nanoclay that limits the diffusion of oxygen and decomposition of products. The presence of montmorillonite enhances the flame retardancy of these blends by forming a protective layer of char leading to increase of the stability of the ceramic residue formed [19].

Blends of polyethylene and ethyl vinyl acetate containing flame retardants ammonium polyphosphate crosslinked by the ionizing radiations and chemical like dicumylperoxide (DCP) with excellent mechanical and thermal properties were used for wire and cable applications [20]. XLPE/EVA blends though has lower tensile strength had much higher elongation at break and prove to be a better oxidation-resistant material [21].

LDPE/Polyamide/Ethylene acrylic acid blends crosslinked with electron beam radiation are employed for cable sheathing applications due to its improved heat resistance and improved barrier properties against permeation of fuel and mineral oil [22]. XLPE/POE/DCP blends can also be used for the wire and cable insulation applications. Reports suggested that addition of DCP and POE greatly enhances the crosslinking of polyethylene, toughness and similar to that of an elastomer. Exhibiting an excellent dielectric properties and a high dissipation factor is a major break through the blends. All the aforementioned properties together make these blends an excellent tool for the insulation applications.

2.2.1 Drawbacks

Modern sophisticated high voltage cable industries prefer XLPE as the insulation materials due to the great advantages possessed by the XLPE blends like excellent dielectric properties, thermo mechanical properties and low dielectric loss and enhanced thermomechanical performance at high temperature due to the cross-linked macromolecular networks. One of the greatest disadvantages regarding the XLPE blends is that the crosslinking process yields the formation of thermosetting materials, thereby making the materials non-recyclable. Nowadays, recyclability of the materials is something demanded in all aspects as it affects the human as well as the environment [23]. Hence, urgency occurs regarding the development of recyclable insulation materials. Studies are being conducted on low density polyethylene (LDPE) and their blends for the application of insulation purpose.

Even though they are recyclable, they cannot be used in HVDC applications due to their poor electrical properties in the presence of high voltage. Studies reported that for a material to be an excellent insulation material for the purpose of using in HVDC application it must possess electrical resistivity in the working range of electrical field and temperatures, better DC breakdown performance, less sensitive to electrical ageing and space charge behaviour.

Hence, considering all these disadvantages of crosslinked poly ethylene and their blends researches are being conducting to explore innovative substitutes for XLPE blends for using in HVDC cable insulation applications. One such example is that, poly propylene. Even though traditional polypropylene is not a good candidate for the insulation applications [24] due to its stiffness and brittleness, their modifications can make good results [25]. Apart from all these properties, the traditional polypropylene is eminent for its recyclability, having high melting point and its excellence in electrical properties.

2.3 Crosslinked Polyethylene Blends in Foam Industries

A wide variety of inherent properties like lightweight, non-toxicity, buoyancy, cushion performance, shock absorption, thermal insulation, low water absorption and chemical resistance make the polyolefin foams an unavoidable substitutes in automotive, construction and building, marine, packaging, medical, sport markets [26]. Blending generally modifies the properties of the crosslinked polyethylene foams. Crosslinked LDPE foam is blended using Ethyl vinyl acetate in order to extend its range of properties. Blending with the ethyl vinyl acetate decreased the static and dynamic modulus and thermal stability, whereas it increased the instantaneous recovery, loss factor and thermal expansion at low temperature. This blended foam has more flexibility, a lower thermal conductivity, higher storage factor, a lower storage and static modulus. All these attributes helped these foams to be used in packaging, automotive applications and so on [27]

2.4 Shape Memory Polymers (SMPS) Based on Crosslinked Polyethylene Blends

Shape memory polymers are an emerging class of active polymers having dual shape capability. They can alter their shape from one form to another. They belong to a group of actively moving polymers. They are smart polymeric materials having the ability to return from a temporary shape to their original shape induced by an external stimulus [28] like a change in temperature [29], light [30]. XLPE blends are being exploited as smart shape polymers in markets.

Irradiation crosslinked polyethylene/polypropylene blends exhibit a well-defined shape memory effects. These blend exhibits triple shape memory effects which can be used as potential biomedical devices and actuators [31]. Blends of crosslinked polyethylene with natural *Eucommia Ulmoide* gum also exhibits wonderful shape memory behaviour [32, 33]. The study proved that the shape memory behaviour of these blends depend on the crystalline regions and crosslinked network of these blends. Water proof and thermoactive shape memory active membranes obtained from the crosslinked LLDPE polycylooctocene blends were excellently used for the textile applications [34].

3 Applications of XLPE Nanocomposites

Since the introduction of XLPE in 1960s, XLPE is being widely explored due to the inherent properties like excellent mechanical strength, flexibility, low cost, chemical resistance and easy processing. However, the application of XLPE in underground and overhead transmission cables is limited due to space charge accumulation and water treeing which decreases its life time. In order to modify this defect nanofillers are added to improve the thermal and DC breakdown strength, mitigate the space charge, and increase the electrical conductivity and to reduce the water and electrical treeing [35]. All these make the XLPE nanocomposites a favourable material for the wire and cable applications. In the manufacture of many cable insulations, the introduction of PE-based nanocomposites for power cables insulation is an alternative solution. Nanocomposites have to fulfil several requirements for commercial use involving improved thermomechanical and electrical properties and sustainable economic, environmental characteristics. For AC cables and their joints, the polymeric materials must show certain properties such as low electrical conductivity, tailor-made permittivity and low loss factor, high dielectric breakdown strength, partial discharge resistance, absence of electric and electrochemical treeing, stability at higher operating temperatures and so forth. In the case of HVDC, the insulating materials must face two additional essential requirements: (i) low variations in electrical conductivity with varying temperature and electric field intensity and (ii) low space charge accumulation [36, 37].

Yong Jun park and his co-workers reported the features of crosslinked XLPE/ Al_2O_3 nanocomposite in terms of DC conduction and breakdown and their application in HVDC transmission cable insulations. They studied the DC insulation properties of the nanocomposites and found that the addition of the aluminium oxide nanofillers improved the DC breakdown strength and volume resistivity of the XLPE. The increase of DC breakdown strength could be explained by the fact that the addition of fillers induced the mechanism of electronic breakdown and the increase in volume resistivity by the electronic hopping mechanism [38].

Tanaka et al. reported that the XLPE/ SiO_2 nanocomposites augur well for applications for insulating extruded power cables. They found that the presence of the nanofiller, silica greatly enhances the dielectric properties by improving the

partial discharge resistance, melting point, voltage endurance and reducing the dielectric loss [39].

Study on the partial discharge features of agglomerated, modified and unmodified XLPE/silica nanocomposites shows that the octyl silane modified composite has excellent partial discharge features compared to the unmodified and agglomerated due to the excellent alignment of the octyl silane modified fibrils with the XLPE chains. The excellence in partial discharge features of these composites aids them in the market of insulations [40].

Zhanga and his co-workers designed the synthesis of XLPE/polypyrrole nanocomposites for the application in cable industries. It is reported that the concentration of polypyrrole has an impact on its electrical characteristics. The composite shows an improvement in DC electrical conduction, space charge distribution upon the addition of the polypyrrole. Besides doping with polypyrrole does not affect the crosslinking of the polyethylene [41].

The investigation on the space charge attributes of XLPE/organic montmorillonite nanocomposites indicates that 0.5%-1% content of montmorillonite in the composite decreases the space charge and increases the trap depth parameter. This supports the application of this composite in electrical insulating materials.

Boron nitride nanosheets XLPE nanocomposites are proved to be excellent dielectric materials due to the improved DC breakdown strength than that of XLPE. On increasing temperature, it is found that the breakdown strength of the aforementioned nanocomposite found to decrease, whereas it has a better performance at room temperature [42].

Water trees are three-dimensional plumes like structure formed in XLPEs commonly used in underground applications due to the improper manufacturing and moisture exposure. Water tree formation ultimately results in the breakdown of cable and can be reduced by the addition of nanofillers. Nanocomposites are resistant to the formation of water tree due to the reality that the high interface/volume ratio and the resulting scattering in interfacial region [43]. The studies reported that the addition of 1 wt% of Al_2O_3 nanofiller in XLPE impedes the formation of water tree in XLPE [44]. MgO nanofillers have a strong tendency to inhibit the water tree formation in XLPE. As the content of MgO nanofillers increases, rate of water tree growth decreases [45]. XLPE/silane nanocomposites are reported to be potential candidates for cable and wire insulation applications due to the decrease in water treeing, decrease in AC breakdown strength.

The thermal conductivity of cable insulation can be improved by the introduction of nanoparticles into PE, namely in reducing their thermal ageing. For example, in the case of LDPE and polyhedral oligomeric silsesquioxanes (POS) nanocomposites, an increase in thermal conductivity was achieved, whereas the dielectric rigidity remained unaltered and the discharge resistance increased [46]. In addition, the introduction of boron nitride (BN) particles into LDPE resulted in an increase of the thermal conductivity [47].

The XLPE nanocomposites have an excellent progress in electrical properties due to the presence of nanoparticles. Based on literature surveys, it is known that the nanoparticles are good candidate for DC and AC cables, insulations and

semiconductor screen applications. Some nanoparticles like SiO_2 and different types of nanoclay are used for both AC and DC cable applications. The presence of silica nanoparticles to the polymer effectively enhanced the AC and DC breakdown voltage by 15% compared to virgin polymers. Hence, SiO_2 -based XLPE nanocomposites are used for medium and low voltage cables [48]. SiC-based XLPE nanocomposites are perfect for DC cable insulation and alumina/silicate/nanoclay-based nanocomposites are efficient for low voltage insulation applications [49].

It is reported that the addition of SiO_2 , Al_2O_3 and TiO_2 nanoparticles into the matrix of XLPE improved the thermal and chemical stability and mechanical strength [50]. MgO-based nanocomposites are reported to be used for DC cable applications [48], whereas carbon black-based nanocomposites for semiconductor screen applications [51].

Though a series of XLPE-based nanocomposites with electrical and thermal properties are superior to the unfilled PE polymer, the introduction of these new materials into the market of power cables requires the extensive testing to validate both the space charge trapping properties and the long-term life performance, in order to define suitable levels for the design field and reach cost-effectiveness [52].

It is also reported that the XLPE nanocomposites exhibits shape memory effects. XLPE/nanocalcium carbonate nanocomposites is reported to show the shape memory properties. shape memory effects are being exploited in medical fields, wirings. Crosslinked polyethylene/clay nanocomposites augurs well for its application in actuators due to its reported shape memory effects.

XLPE nanocomposites are widely used in piping applications. Carbon nanotubes reinforced crosslinked high density polyethylene pipes were used for geothermal application. For geothermal application, high polymer thermal conductivity and comprehensive thermal decomposition were required. From the studies, it is proved that the addition of multi-walled carbon nanotubes has great effect on thermal properties like thermal conductivities, thermal diffusivity and heat capacity of PEX [53]

Some of the important patents for the applications of XLPE blends and nanocomposites are enlisted in Table 1.

4 Conclusions

The amelioration in the field of polymer science led to the development of a large number of multifunctional materials. Among those materials, crosslinked polyethylene-based blends and their nanocomposites have attracted much attention due to their inherent thermal, mechanical and electrical properties. For the past few years, a tremendous progress is obtained in the field of blends and nanocomposites with high potential that can be employed in various research applications.

This chapter discusses applications of crosslinked polyethylene-based blends and nanocomposites. These materials are used in various applications like in cable

Table 1 Important patents for the applications of XLPE blends and nanocomposites

Patent No	Assignee/inventors	Filed on	Title
EP 1176161	Nexans Fr	July 24, 2000	Manufacture of electric wires insulated with crosslinked polyethylene blends with ethylene acrylate ester copolymer
JP 63160109	Fuji kura Ltd, Japan	December 24, 1986	Electric power cable insulated with crosslinked polyethylene blends
CN 109102929	Anhui Yangzi Cable Co, Ltd, People republic of china	December 28, 2018	Oxidation resistant electric cable and its production thereof
WO 2020088333	Jiang Su Dewei Advanced material Co Ltd, People Republic of China	October 24, 2019	Silane-Xlpe insulation material used for heating cable preparation method thereof and applications thereof
CN 106633303	Xi'an Jiaotong University, People Republic of China; China Electric Power Research Institute	December 21, 2016	Nanocomposite crosslinked polyethylene insulating material of high DC breakdown field strength and preparation method thereof

wire and insulation materials, biocompatible orthopaedic applications, piping and foam industries. They also augur well for the applications as smart shape polymers.

References

1. Hampton RN (2008) Some of the considerations for materials operating under high-voltage, direct current stresses. *IEEE Electr Insul Mag* 24:5–13
2. Fortman DJ, Brutman JP, De Hoe GX, Snyder RL, Dichtel WR, Hillmyer MA (2018) Approaches to sustainable and continually recyclable cross-linked polymers. *ACS Sustain Chem Eng* 6(9):11145–11159
3. Müller K, Bugnicourt E, Latorre M, Jorda M, Echegoyen Sanz Y, Lagaron JM, Miesbauer O, Bianchin A, Hankin S, Bölz U, Pérez G (2017) Review on the processing and properties of polymer nanocomposites and nanocoatings and their applications in the packaging, automotive and solar energy fields. *Nanomaterials* 7(4):74
4. Tamboli SM, Mhaske ST, Kale DD (2004) Crosslinked polyethylene
5. Del Prever EMB, Bistolfi A, Bracco P, Costa L (2009) UHMWPE for arthroplasty: past or future? *J Orthop Traumatol* 10(1):1–8
6. Muratoglu OK, Bragdon CR, O'Connor DO, Jasty M, Harris WH (2001) A novel method of cross-linking ultra-high-molecular-weight polyethylene to improve wear, reduce oxidation, and retain mechanical properties: recipient of the 1999 HAP paul award. *J Arthroplasty* 16(2):149–160
7. Turner A, Okubo Y, Teramura S, Niwa Y, Ibaraki K, Kawasaki T et al (2014) The antioxidant and non-antioxidant contributions of vitamin E in vitamin E blended ultra-high molecular weight polyethylene for total knee replacement. *J Mech Behav Biomed Mater* 31:21–30

8. Takahashi Y, Yamamoto K, Pezzotti G (2015) Effects of vitamin E blending on plastic deformation mechanisms of highly crosslinked ultrahigh molecular weight polyethylene (HXL-UHMWPE) in total hip arthroplasty. *Acta Materialia Inc*, 1742–7061
9. Shibata N, Tomita N (2005) The anti-oxidative properties of alpha-tocopherol in gamma-irradiated UHMWPE with respect to fatigue and oxidation resistance. *Biomaterials* 26:5755–5762
10. Shen FW (2007) Ultrahigh-molecular-weight polyethylene (UHMWPE) in joint replacement
11. Oonishi H, Kim SC, Oonishi H Jr, Masuda S, Kyomoto M, Ueno M (2008) Clinical applications of ceramic-polyethylene combinations in joint replacement, Bio ceramics and their clinical applications. In: Woodhead publishing series in biomaterials, pp 699–717
12. Collier JP, Currier BH, Kennedy FE, Currier JH, Timmins GS, Jackson SK, Brewer RL (2003) Comparison of cross-linked polyethylene materials for orthopaedic applications. *Clin Orthop Relat Res* 1976–2007(414):289–304
13. Fu J, Shen J, Gao G, Xu Y, Hou R, Cong Y, Chenga Y (2013) Natural polyphenol-stabilised highly, crosslinked UHMWPE with high mechanical properties and low wear for joint implants. *J Mater Chem B* 1:4727–4735
14. Mulliez MA, Fritz B, Holderied M, Schilling C, Grupp TM (2020) In vitro wear performance of X-ray cross-linked vitamin E blended polyethylene. *Biotribology* 21:100115
15. Hanley TL, Burford RP, Fleming RJ, Barber KW (2003) A general review of polymeric insulation for use in HVDC cables. *IEEE Electr Insul Mag* 19:13–24
16. Hanley TL, Burford RP, Fleming RJ, Barber KW (2003) A general review of polymeric insulation for use in HVDC cables. *IEEE Electr Insul Mag* 19(1):14–24
17. Sabet M, Hassan A, Ratnam CT (2012) Polymer degradation and stability, electron beam irradiation of low density polyethylene/ethylene vinyl acetate filled with metal hydroxides for wire and cable applications. *Polym Degrad Stab* 97:1432–1437
18. Haurie L, Fernández A, Velasco JC, Lopez C, Espiell F (2007) Thermal stability and flame retardancy of LDPE/EVA blends filled with synthetic hydromagnesite/aluminum hydroxide/montmorillonite and magnesium hydroxide/aluminiumhydroxide/montmorillonite mixtures. *Polym Degrad Stab* 92:1082–1087
19. Laia H, Ana IF, Jose IV, Josep M, Jose ML, Ferran E (2006) Synthetic hydromagnesite as flame retardant. Evaluation of the flame behaviour in a polyethylene matrix. *Polym Degrad Stab* 91:989–994
20. Basfar AA, Mosnáček J, Shukri TM, Bahattab MA, Noireaux P, Courdreuse A (2008) Mechanical and thermal properties of blends of low-density polyethylene and ethylene vinyl acetate crosslinked by both dicumyl peroxide and ionizing radiation for wire and cable applications 107:642–649
21. Mohammed A, Bahattab J, Ahmed AB (2010) Cross-linked poly(ethylene vinylacetate) (EVA)/low density polyethylene (LDPE)/metal hydroxides composites for wire and cable applications. *Polym Bull* 2010(64):569–580
22. Kang DAI Electron-beam radiation cross linkable and compatibilized PA11/PA12/LDPE blends with good barrier properties and improved heat resistance for cable sheathing application
23. Hosier IL, Vaughan AS, Swingler SG (2011) An investigation of the potential of polypropylene and its blends for use in recyclable high voltage cable insulation systems. *J Mater Sci* 46(11):4058–4070
24. Yoshino K, Demura T, Kawahigashi M, Miyashita Y, Kurahashiand K, Matsuda Y (2004) The application of novel polypropylene to the insulation of electric power cable. *Electr Eng Jpn* 146(1):872–879
25. Green CD, Vaughan AS, Stevens GC, Pye A, Sutton SJ, Geussens T, Fairhurst MJ (2015) Thermoplastic cable insulation comprising a blend of isotactic polypropylene and a propylene-ethylene copolymer. *IEEE Trans Dielectr Electr Insul* 22:639–648
26. Rodríguez-Pérez MA (2005) Crosslinked polyolefin foams: production, structure, properties, and applications. In: Crosslinking in materials science. Springer, Berlin, Heidelberg, pp 97–126

27. Rodríguez-Pérez MA, Duijsens A, De Saja JA (1998) Effect of addition of EVA on the technical properties of extruded foam profiles of low-density polyethylene/EVA blends. *J Appl Polym Sci* 68(8):1237–1244
28. Hager MD, Bode S, Weber C, Schubert US (2015) Shape memory polymers: past, present and future developments. *Prog Polym Sci* 49:3–33
29. Kashif M, Chang YW (2015) Triple-shape memory effects of modified semi crystalline ethylene–propylene–diene rubber/poly (caprolactone) blends. *Eur Polym J* 70:306–316
30. Wu L, Jin C, Sun X (2011) Light-induced shape memory effect of multiblock polyester urethanes containing biodegradable segments and pendant cinnamide groups. *Bio macromolecules* 12:235–241
31. Zhao J, Chen M, Wang X, Zhao X, Wang Z, Dang ZM, Ma L, Hu GH, Chen F (2013) Triple shape memory effects of cross-linked polyethylene/polypropylene blends with cocontinuous architecture. *ACS Appl Mater Interfaces* 5(12):5550–5556
32. Xia Lin, Chen Shuai, Wenxin Fu, Qiu Guixue (2019) Shape memory behaviour of natural eucommia ulmoides gum and low-density polyethylene blends with two response temperatures. *Polymers* 11:580
33. Xia L, Chen S, Fu W, Qiu G (2019) Shape memory behavior of natural Eucommia ulmoides gum and low-density polyethylene blends with two response temperatures. *Polymers* 11 (4):580
34. Reizabal A, Laza JM, Cuevas JM, León LM, Vilas-Vilela JL (2019) PCO-LLDPE thermoresponsive shape memory blends. Towards a new generation of breathable and waterproof smart membranes. *Eur Polymer J* 119:469–476
35. Thomas J, Joseph B, Jose JP, Maria HJ, Main P, Ali Rahman A, Francis B, Ahmad Z, Thomas S (2019) Recent advances in cross-linked polyethylene-based nanocomposites for high voltage engineering applications: a critical review. *Ind Eng Chem Res* 58(46):20863–20879
36. Zhou Y, Peng S, Hu J, He J (2017) Polymeric insulation materials for HVDC cables: development, challenges and future perspective. *IEEE Trans Dielectr Electr Insul* 24:1308–1318
37. Li Z, Du B (2018) Polymeric insulation for high-voltage DC extruded cables: challenges and development directions. *IEEE Electr Insul Mag* 34:30–43
38. Park YJ, Kwon JH, Sim JY, Hwang JN, Seo CW, Kim JH, Lim KJ (2014) DC conduction and breakdown characteristics of Al₂O₃/cross-linked polyethylene nanocomposites for high voltage direct current transmission cable insulation. *Jpn J Appl Phys* 53
39. Tanaka T, Bulinski A, Castellon J, Frechette M, Gubanski S, Kindersberger J, Montanari GC, Nagao M, Morshuis P, Tanaka Y, Péliou S, Vaughan A, Ohki Y, Reed CW, Sutton S, Han SJ (2011) Dielectric properties of XLPE/SiO₂ nanocomposites based on CIGRE WG D1.24 cooperative test results. *IEEE Trans Dielectr Electr Insul* 18(5)
40. Ashish Sharad P, Kumar KS (2017) Application of surface-modified XLPE nanocomposites for electrical insulation partial discharge and morphological study. *Nanocomposites* 3(1): 30–41
41. Zhanga C, Zhanga H, Lia C, Duana S, Jiangb Y, Yanga J, Hana B (2018) Hong Zhaoa Crosslinked polyethylene/polypyrrole nanocomposites with improved direct current electrical characteristics. *Polym Testing* 71:223–230
42. Li G, Zhou X, Li X, Wei Y, Hao C, Li S, Lei Q (2020) DC breakdown characteristics of XLPE/BNNS nanocomposites considering BN Nano sheet concentration, space charge and temperature. *Emerg Mater High Energy Appl* 5:280–286
43. Hui L, Smith R, Nelson JK, Schadler LS (2009) Electrochemical treeing in XLPE/silica nanocomposites. In: 2009 Annual report conference on electrical insulation and dielectric phenomena
44. Wahab A, Mansor NS, Ishak D, Kamarol M, Mariatti M, Ghani ABA, Halim HS (2017) Investigation of water tree characteristic in XLPE nanocomposites for medium voltage cable application. In: 2017 International conference on high voltage engineering and power system, 2–5, Oct 2017, Bali, Indonesia

45. Nagao M, Watanabe S, Murakami Y, Murata Y, Sekiguchi Y, Goshowaki M (2008) Water tree retardation of MgO/LDPE and MgO/XLPE nanocomposites. In: Proceedings of 2008 international symposium on electrical insulating materials, 7–11 Sept, 2008, Yokkaichi, Mie, Japan
46. Guo M, Fr chet M,  ric D, Demarquette NR, Daigle JC (2017) Polyethylene/polyhedral oligomeric silsesquioxanes composites: electrical insulation for high voltage power cables. *IEEE Trans Dielectr Electr Insul* 24:798–807
47. Du BX, Kong XX, Cui B, Li J (2017) Improved capacity of buried HVDC cable with high thermal conductivity LDPE/BN insulation. *IEEE Trans Dielectr Electr Insul* 24:2667–2676
48. Paramane AS, Kumar KS (2016) A review on nanocomposite based electrical insulations. *Trans Electr Electron Mater* 17(5):239
49. Aigbodion VS, Achiv FM, Agunsoye OJ, Isah LA (2016) Evaluation of the electrical porcelain properties of alumina-silicate nano-clay. *J Chin Adv Mater Soc* 4(2):99–109
50. Contreras JE, Rodriguez EA, Taha-Tijerina J (2017) Nanotechnology applications for electrical transformers—a review. *Electr Power Syst Res* 143:573–584
51. Li W, Yan HD, Zhou Y, Zhang C, Chen X (2017) Supersmooth semiconductive shielding materials use for XLPE HVDC cables. In: 2017 1st International conference on electrical materials and power equipment (ICEMPE). IEEE, pp 447–451
52. Montanari GC, Seri P, Lei X, Ye H, Zhuang Q, Morshuis P, Stevens G, Vaughan A (2018) Next generation polymeric high voltage direct current cables—a quantum leap needed? *IEEE Electr Insul Mag* 34:24–31
53. Roumeli E, Markoulis A, Kyratsi T, Bikiaris D, Chrissafis K (2014) Carbon nanotube-reinforced crosslinked polyethylene pipes for geothermal applications: From synthesis to decomposition using analytical pyrolysis–GC/MS and thermogravimetric analysis. *Polym Degrad Stab* 100:42–53

Chapter 6

Advanced Characterization Techniques Based on Luminescence in XLPE and Modified XLPE



Gilbert Teyssède, Christian Laurent, and Bo Qiao

1 Introduction

Cross-linked polyethylene (XLPE) is used for several decades now as insulation in high-voltage buried or submarine power transmission cables, i.e. rated above 60 kV [1]. The major advantages of XLPE over the competitive technology based on traditional oil-impregnated paper insulation are lower dielectric losses, less complicated installation procedure and maintenance and no risk of leakage implying improved respect for environment. The technical risks of XLPE-insulated high-voltage cables could be a lack of knowledge of the degradation withstanding ability of the insulation. Today's hot topics are more related to the extension of its application to HVDC energy transport. Significant progresses have been achieved in adapting the material formulation to the new challenges brought by the form of stress to be supported. Space charge processes and conduction processes are two properties that had to be seriously addressed for ensuring the reliability of cables under high-voltage direct current stresses. These issues have been addressed in a number of recent reviews, and we will not go into more details here [2, 3].

G. Teyssède (✉) · C. Laurent

Laboratory on Plasma and Energy Conversion - Laplace, University of Toulouse, and CNRS,
Toulouse 31062, France

e-mail: gilbert.teyssedre@laplace.univ-tlse.fr

C. Laurent

e-mail: christian.laurent@laplace.univ-tlse.fr

B. Qiao

Key Laboratory of Luminescence and Optical Information, Ministry of Education Institute of
Optoelectronics Technology, Beijing Jiaotong University, Beijing 100044, P. R. China

e-mail: boqiao@bjtu.edu.cn

© Springer Nature Singapore Pte Ltd. 2021

J. Thomas et al. (eds.), *Crosslinkable Polyethylene Based Blends and Nanocomposites*, Materials Horizons: From Nature to Nanomaterials,
https://doi.org/10.1007/978-981-16-0486-7_6

Failure in transmission has always important consequences related to the time for energy outage and repairing costs. While some failures may arise from isolated events as natural disasters or human mistakes with digging for example, the repetition of middle term failure due to intrinsic weakness of the cable under continuous application of nominal stress is really a catastrophic aspect. In this perspective, the aim of the European project named ARTEMIS [4] was to investigate degradation processes and derive diagnostic properties for ageing evaluation and modelling of high-voltage XLPE-insulated cables. The progresses in producing ever safer cables have been achieved with improving extrusion processes in cables as well as cleanliness of rough materials used in HV cable production.

XLPE has therefore some high-end niches in which high-quality materials must be produced. Materials quality in the cable industry is naturally being assessed with electrical characterization as impedance spectroscopy, conductivity measurements, breakdown measurements, space charge measurements, etc., on one hand, mechanical properties and thermal stability on the other hand. XLPE became at the top of cable insulation materials firstly because of its excellent thermo-mechanical properties [5]. The improvement of thermo-mechanical properties was achieved with compounding materials: peroxide cross-linking and protection against oxidation by introducing antioxidants is the way it is generally achieved. Because of this compounding, XLPE is a material containing, besides defects in the main chain, by-products, being volatile or not, and small amounts of residues. In turn, these moieties impart most of the differences in electrical properties compared to low-density polyethylene for example. There has been a need for characterization techniques capable of making the link between chemicals on the one hand and their impact on the behaviour of electrical charges in the insulation on the other hand. Indeed, depending on excitation means, different relaxation mechanisms can be at play such as the relaxation of optically excited groups, the recombination of charges of opposite polarity coexisting in the same region or energy relaxation following hot carrier processes (impact excitation or ionization).

Luminescence techniques have appeared as original characterization tools in this perspective, the reason why we have dedicated one chapter on its principles and results in this book. Depending on the excitation means, luminescence features may provide information related to chemicals or to the interaction between electrical charges and groups acting as deep traps. These techniques can therefore be considered as at the frontier between physico-chemical and electrical characterization tools.

Before going into the details, let us mention a few specificities of luminescence methods when applied to materials such as XLPE:

- Ideally, polyethylene does not contain unsaturations in its main chain, and then no luminescence should be detected in the UV-Vis domain. Then, the response necessarily comes from additives, residues, defects, ageing by-products, etc.,

being dispersed into the material. Both extrinsic (additives, cross-linking by-products) and intrinsic (oxidized groups, insaturations) chromophores are potentially emitting groups in XLPE materials.

- Luminescence can be very sensitive in the presence of optically active moieties. However, moieties can be present without being luminescent. Therefore, it cannot pretend to cover all the possible defects.
- In a solid material, many energy exchange phenomena can be at play, the response of a molecule can be dependent on its environment and therefore identifying the luminescence bands is not as straightforward as it can be for infrared spectroscopy for example.

In the next section, we first present the general aspects of luminescence phenomena, particularly in the case of organic solids. In Sect. 3, we present the kind of XLPE materials that have been considered in luminescence experiments, how it was processed, and we describe the methods that were implemented.

Then, the results are presented in two main sections related to luminescence from compounds and to ageing and degradation aspects viewed from the luminescence standpoint.

2 Luminescence from Materials

2.1 Definitions

Luminescence is the light emitted by a substance when the excitation is not due to heat, by opposition to incandescence. The excited states responsible for material luminescence can be produced by different excitation sources [6], among them: photon absorption (photoluminescence PL) [7], chemical reactions (chemiluminescence CHL) [8], recombining charges (recombination-induced luminescence RIL) [9, 10], electric field application (electroluminescence EL) [11, 12], electron-beam irradiation (cathodoluminescence CL or electron-beam-induced luminescence EBIL) [13–15], temperature (thermoluminescence TL) [16–18], etc. PL, CHL, RIL, EL, EBIL and TL refer to the source of excitation itself which can generate a series of elementary excitations contributing to the luminescence. As example, photon absorption can raise excited states of atoms/molecules but also can ionize them. The luminescence will result from relaxation of neutral excited states and from charge recombination in case of ionization. Another example is thermoluminescence where the thermal energy is used to detrapp electrical charges, the luminescence being due to subsequent charge recombination. The generic term used to name a form of luminescence does not imply a single elementary process. Common luminescence mechanisms typical in polymeric materials are given in Table 1.

Table 1 Overview of common luminescence types in insulating polymers

Luminescence type	Promotion of excited state
Photoluminescence PL	Absorption of photon (mild UV)
Chemiluminescence CHL	Chemical reaction (typical: oxidation of polyolefins)
Recombination-induced luminescence RIL	Recombination between trapped carriers (no kinetic energy)
Electroluminescence EL	Mixture of excitation processes induced by electric field
Cathodoluminescence CL or Electron-beam-induced luminescence EBIL	Hot electron impact and processes induced by irradiation
Plasma-induced luminescence PIL	Luminescence following excitation of the surface by a plasma discharge
Thermoluminescence TL	Luminescence in a temperature ramp following excitation of the surface by a ionizing radiation or other way of depositing charges

2.2 Absorption and Emission Phenomena in Organic Molecules

2.2.1 Absorption

The absorption of UV–Vis radiations in organic molecules are restricted to functional groups called chromophores that have valence electrons of weak energy. Under excitation conditions, electrons located on the orbitals σ (simple covalence bonds), π (multiple covalence bonds) and n (lone electron pair) will be promoted to anti-bonding orbital (excited state) π^* or σ^* . Transitions $\sigma \rightarrow \sigma^*$ and $\pi \rightarrow \pi^*$ have a strong energy, whereas transitions $n \rightarrow \sigma^*$ and $n \rightarrow \pi^*$ have a weak energy. n electrons do not form bonds, and they do not have anti-bonding orbitals [19, 20]. The possible electronic transitions upon mild UV absorption are schematically represented in Fig. 1.

(a) $\sigma \rightarrow \sigma^*$ transitions

One electron located on simple covalent bond is excited to the corresponding anti-bonding orbital. The energy gap between the two states is strong. As example, methane which has only C–H bonds can only stand $\sigma \rightarrow \sigma^*$ transitions corresponding to a maximum in absorption at 125 nm which cannot be observed in classical UV spectroscopy (200–300 nm).

(b) $n \rightarrow \sigma^*$ transitions

Compounds containing atoms with lone electron pairs (oxygen, nitrogen) are able of such transitions of lower energy. They can be promoted by photons of wavelength between 150 and 250 nm.

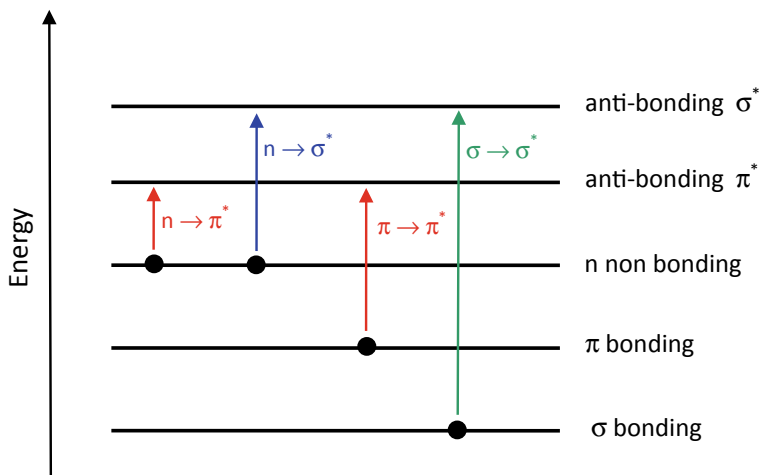


Fig. 1 Possible electronic transitions in organic molecules in the UV-Vis spectrum

(c) $n \rightarrow \pi^*$ and $\pi \rightarrow \pi^*$ transitions

Optical spectroscopy of most organic compounds is based on the electronic transitions from n or π state to the excited state π^* . The presence of unsaturated groups in the molecule is therefore needed to provide π electrons. One can quote a strong transition $\pi \rightarrow \pi^*$ in the far UV for the molecules containing $C = C$ groups. In contrast, $n \rightarrow \pi^*$ transitions have a weak intensity but classical in carbonyls spectroscopy.

2.2.2 Emission

The electronic state of most organic molecules can be separated in singlet (S) and triplet states (T). Difference between these two types is based on spin coupling—see Fig. 2. In singlet state, two electrons of the same energy state have a coupled spin (anti-parallel spin), whereas in triplet state, they have a parallel spin [19].

The energy conversion in a molecule can be approached with reference to the Jablonski representation (Fig. 3) [20].

(d) **Energy absorption (transition 1 in Fig. 3)**

The molecule absorbs some energy raising an electron from the ground state to an excited state with vibrational and rotational components.

(e) **Energy relaxation (transitions 2, 5 and 6 in Fig. 3)**

The molecule can relax following radiative and non-radiative pathways.

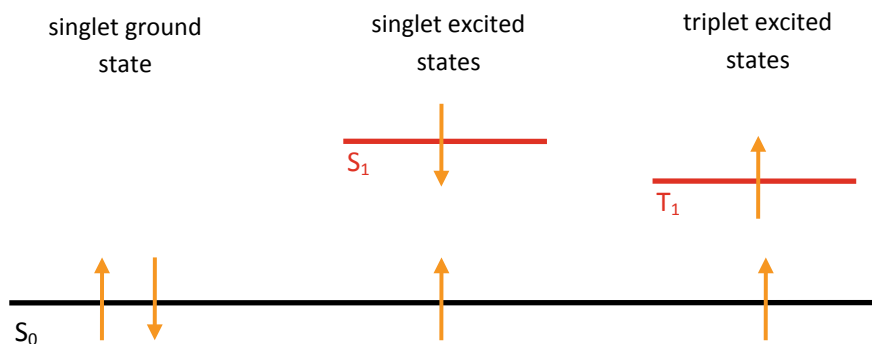


Fig. 2 Spin coupling in ground and excited states defining singlet and triplet excitons

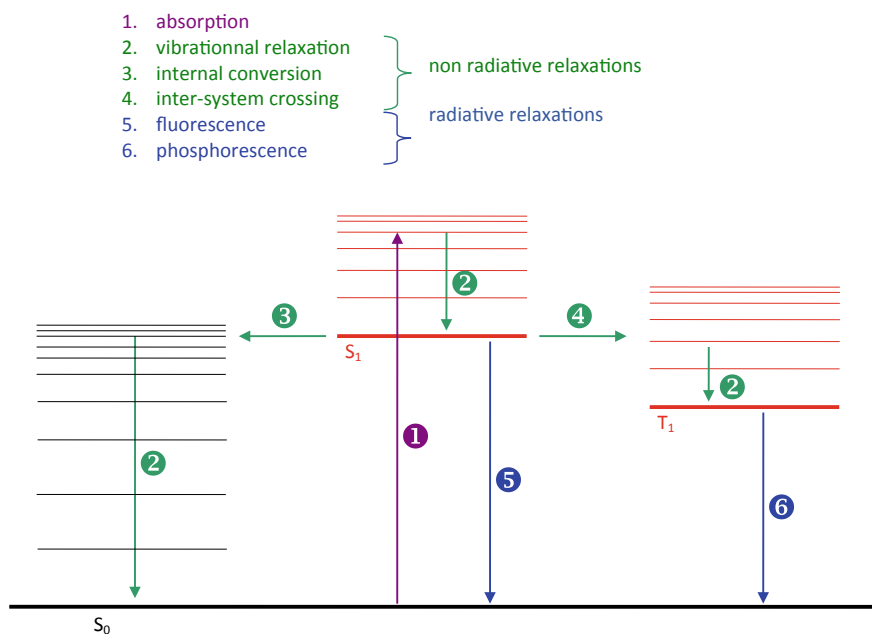


Fig. 3 Absorption, fluorescence and phosphorescence spectra of a small organic molecule and the corresponding energy state diagram with radiative and non-radiative transitions in a Jablonski representation

In non-radiative relaxation, the energy is dissipated by internal conversion (transitions 2) through collision with other atoms/molecules or by intersystem crossing (transition 4). In the latter, the electron spin is reversed, and the molecule lies in a lower energy triplet state.

In radiative relaxation, the excited electron loses its energy going from the first excited state to the ground state. This can happen from the first excited singlet state (fluorescence) or from the first excited triplet state (phosphorescence). The lifetime of a triplet state is much longer (up to several s) than the one of a singlet state (order of ns) because it is a spin-forbidden transition. Moreover, non-radiative transfers compete with radiative relaxation from a triplet state in such a way that phosphorescence is usually observed only at low temperature which hinders inhibition by another atom/molecule.

2.3 Luminescence from Polymers

The emission of light by a substance following an optical excitation is called photoluminescence which is a common spectroscopic technique in the field of materials even if its interpretation is not straightforward in the case of polymers [6]. Two kinds of polymers have to be distinguished depending on the chromophores they contain. In the first kind, the chromophores are not belonging to the monomer unit and can be bonded (unsaturation of the hydrocarbon chain) or not (impurities or residues of cross-linking in XLPE) to the macromolecular chain. In the second kind, chromophores are present in the monomer units (as in PET or PEN). This distinction is important as the interpretation of the emission spectra will not be as straightforward in the first type when compared to the second type.

Both emission and excitation spectra are usually recorded in photoluminescence spectroscopy. If the former is straightforward, the latter is less common: the frequency of the excitation light is varied, and the luminescence is monitored at the typical emission frequency of the material being studied.

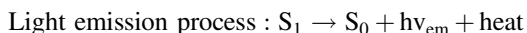
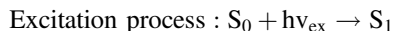
2.3.1 Photoluminescence

In photoluminescence, the emitted light has a lower energy and therefore longer wavelength than the excitation light. The time between absorption and emission may vary from femtoseconds to milliseconds or even to minutes or hours under special circumstances. The relative short and relative long time between absorption and emission lead to fluorescence and phosphorescence, respectively.

There is another peculiarity of polymer photoluminescence, which is due to the existence of interaction between neighbour molecules. The emitting species can be different from the excited ones, and excited states can be formed upon the interaction of several atoms (excimers and exciplexes). Quenching processes are also of particular importance.

(a) Fluorescence

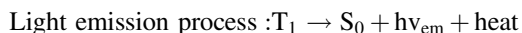
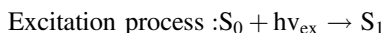
Fluorescence occurs when an orbital electron of a molecule, atom or nanostructure releases back to its ground state keeping the same parity. The relaxation is fast (order on ns).



Here, $h\nu$ is photon energy with h (Planck's constant) and ν (frequency of the light). State S_0 is the ground state while state S_1 is its first excited singlet state.

(b) Phosphorescence

Phosphorescence occurs when an orbital electron of a molecule, atom or nanostructure releases back to its ground state after spin reversal. The relaxation is much longer/fluorescence and order of ms to some s. Hence, phosphorescent materials can 'store' absorbed energy for a certain time.

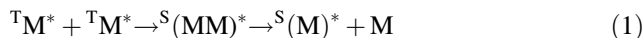


Here, $h\nu$, S_0 , S_1 and heat mean the same as above, while T_1 is a triplet state.

During the phosphorescence process, the material is excited to higher energy states, then undergoes an intersystem crossing into energy state of higher spin multiplicity, usually triplet states, $S_1 \rightarrow T_1$, as seen in Fig. 3. The transition $T_1 \rightarrow S_0$ is normally a spin-forbidden transition, which is why the lifetime of triplet states (phosphorescence) is longer than that of singlet states (fluorescence).

(c) Excimers and exciplexes

In the excited state, energy transfer between monomeric units of a single chain, or between units of different chains, gives birth to specific excitation called excimers and exciplexes. In the former case, an excited state of a chromophore is coupled to a ground state of another identical chromophore. Experimentally, this gives birth to a broader emission band, without apparent structure, with a weaker energy than the single chromophore emission. Another form of complex is the exciplexes, which results from the coupling between an excited molecule and a different molecule in its ground state. These complexes can be at the origin of delayed fluorescence when two excited molecules are in a triplet state. In this case, a complex can be formed between the two molecules M with subsequent relaxation to a singlet excited state and a ground state according to:



In certain circumstances, the fluorescence is delayed in time far beyond its natural lifetime.

(d) Inhibition (quenching)

This is an important phenomenon where a species can interact with an excited state inhibiting thereby the luminescence. Quenchers are usually heavy atoms or paramagnetic molecules. A current process is the quenching of the luminescence of a molecule M by an oxygen molecule (triplet ground state), according to:



2.3.2 Luminescence Due to Charge Recombination

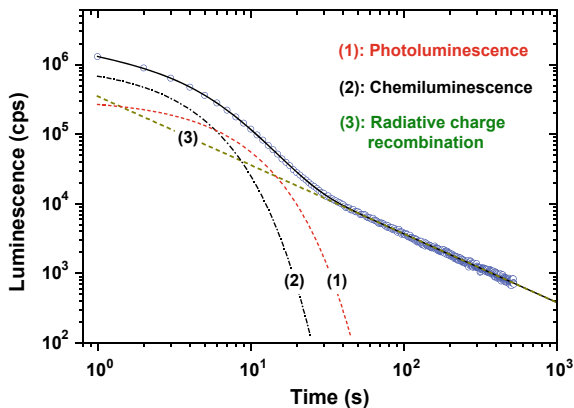
The luminescence induced by charge recombination (RIL) is the light emitted by the material after its irradiation by an ionizing source (x-rays, γ -rays, electron beam, plasma source, etc.) [16, 18, 21–27]. The phenomenon of RIL is general and can be unravelled in most of the polymeric materials [10, 27]. During the irradiation, or a short time after (typically <1 s), different mechanisms can contribute to the emission like direct excitation of the molecules without ionization, or immediate recombination between electrons (or anions) and holes (or cations). Recombination-induced luminescence dominates afterwards where the thermal fluctuations (isothermal luminescence) control the detrapping of charges and subsequent recombination with the recombining centres. Thermoluminescence is due to the same effect of charge detrapping and recombination due to the thermal energy provided to the polymer during heating.

In Sect. 4 of the present chapter, we will intensively use the emission spectra in charge recombination-induced luminescence to infer the nature of recombining centres in XLPE. The recombination regime is obtained in plasma-induced luminescence, or PIL, where a polymer film is put in contact with a cold plasma [25]. Some details of the analysis are given below.

(a) Charge recombination regime after contact with a cold plasma: isothermoluminescence

Here we illustrate the phenomenon by taking the example of luminescence analysis in XLPE films after contact with a cold plasma of helium at low pressure [7]. Further information on the techniques is given in Sect. 3.2.3. A typical example of the kinetic of the luminescence is shown in Fig. 4 where the overall signal is fitted to three different luminescence components: the first one is due to the photoluminescence of the PE sample excited by the UV of the discharge, with time constant corresponding to the lifetime of triplet states; the second one is due to

Fig. 4 Kinetic of isotherm luminescence of XLPE after contact with a cold plasma and its contributing phenomena. Adapted from [7]



chemiluminescence—see Sect. 2.3.3 [8], and the third one is due to charge recombination with a typical kinetic, giving a total light decay in time of the form:

$$I(t) = I_{01} \exp\left(-\frac{t}{\tau_1}\right) + I_{02} \exp\left(-\frac{t}{\tau_2}\right) + I_{03}(1 + \alpha t)^{-m} \quad (3)$$

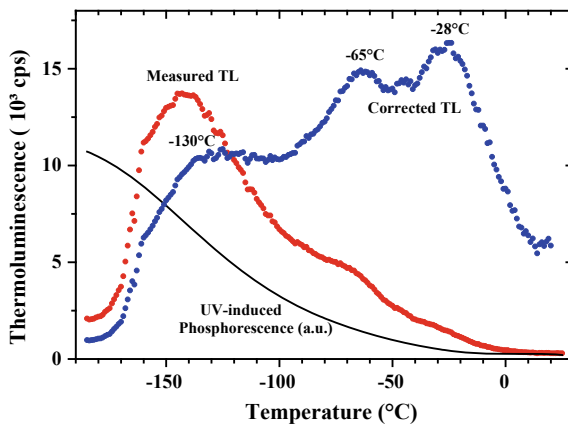
where I is the luminescence amplitude, I_{0i} are pre-exponential factors, t is the time elapsed from the end of the plasma treatment, α and m are adjustable coefficients, and τ_i are time constants. The order of magnitude of α is 0.1 s^{-1} and $m \approx 1$. In the example shown in Fig. 4, α is large; hence, the last term is of the form $I_3 t^{-m}$.

The reciprocal time dependence of the light amplitude can be assigned to electron tunnelling to positively charged luminescence centres [26, 28–30]. Such kinetic analysis allows to define a time window where recombination is the sole contribution and therefore to isolate the emission spectrum of the process.

(b) Charge recombination regime after contact with a cold plasma: thermoluminescence

Figure 5 shows the thermoluminescence (TL) curve recorded for cross-linked polyethylene after the end of an isotherm luminescence record while heating at a linear rate of about $5 \text{ }^\circ\text{C}/\text{min}$. The curve in blue was obtained after correction from the temperature dependence of the main emission derived from temperature-dependent photoluminescence experiments [7]. Two transition regions appear at about -120 and $-60 \text{ }^\circ\text{C}$. It is tempting to associate these with the γ and β relaxations of polyethylene which occur in the respective temperature regions according to dynamical mechanical analysis [31]. Overall, the luminescence is due to charge detrapping following recombination. The emission spectrum is the same as in isothermal RIL experiments.

Fig. 5 Thermoluminescence curve obtained after excitation of cross-linked polyethylene by a plasma discharge. The luminescence is corrected from the temperature dependence of the main emission at about 450 nm in photoluminescence experiments [7]



2.3.3 Other Forms of Luminescence

(a) Chemiluminescence

Chemiluminescence is the light emitted during a chemical reaction. It is a well-known phenomenon in polyolefins where oxidation reactions lead to the formation of C = O bonds. The light is generated during the last step of chemical reaction from C = O* to C = O with a typical signature at 415 nm [32]. Chemiluminescence has been deeply investigated in our group along thermal degradation of polyolefins, both through the kinetics of the integral emission and its spectrum that changes as a function of the reaction [25, 27, 32–37].

(b) Cathodoluminescence (or electron-beam-induced luminescence)

Cathodoluminescence is the light emission following excitation of the matter by an electron beam [38]. Exposure of a solid to an electron beam with several keV in energy induces a number of processes in the specimen, which lead to the formation of secondary and backscattered electrons and generate also characteristic radiation and X-ray and Auger electrons. The secondary electrons generate electron–holes pairs which can recombine directly or be trapped and further released to excite the luminescence by recombination. It is noteworthy that the energy of excitation considerably exceeds the band gap width of any material. The excitation of luminescent centres can occur not only via direct excitation, but also as a result of radiative and non-radiative transitions from higher lying energy states. As a consequence, CL spectra often demonstrate a larger amount of emission bands than other luminescence spectra.

(c) Electroluminescence

Electroluminescence is the light emitted by a material put under electric stress. It is a well-known process in any media. It was firstly reported in 1963 [39] in organic semiconductors and exploited as organic light emitting devices. On the other hand,

electroluminescence in insulating polymers was firstly reported in 1967 [40]. In these large band gap materials, the excitation mechanisms can be related to the kinetic energy of the charges, or their potential energy. In the former case, injected charges of a few electron volts kinetic energy can impact and excite some centres. In the latter, recombining charges can be the source of the light. Mechanisms involved in EL of insulating materials are still under debate [41], and complex phenomena are involved as will be seen in Sect. 5.

2.3.4 Correlation Between Luminescence and Analytical Techniques

As a general analytical method for polymers, luminescence spectroscopy suffers from the same problem as UV–visible absorption spectroscopy: the level of information obtained is coarse because of the close similarity in energy of the electronic transitions and their vibronic progressions, in which substituent effects are either absent or not resolved. The technique has been particularly powerful, however, in detecting trace amounts of oxidation products [42].

Different reasons make it not as a classical analytical method for characterizing solid polymers. First, luminescence techniques can be very sensitive on compounds having high yield and can be relatively insensitive for non-luminescent dyes. So it makes a first difference with other methods like infrared spectroscopy in which any molecule in principle provides absorption. Second, luminescence suffers from a lack of database of reference spectra for given chemical groups, mainly because the signature may depend on the environment of the molecule. It is therefore not easy to precisely identify chemical groups based only on their luminescence properties. Thirdly, in solid state notably, it is extremely delicate to pretend being quantitative, because of the many de-excitation and transfer routes that can be followed by excited states.

Though luminescence in solids is not developed as an ordinary physico-chemical characterization technique, several works tentatively established correlations between luminescence, particularly chemiluminescence and other analytical techniques [43]. Techniques such as electron spin (or paramagnetic) resonance—ESR or EPR [44] or FTIR emission [45]—are interesting as they provide signal linked to active groups during reactions. Rychly et al. have published works in favour for decomposition of hydroperoxides as being responsible for the light emission during oxidation of polypropylene [46]. However, the correlation is not necessarily straightforward. For example, Blakey and George [45] demonstrated through FTIR emission that the chemiluminescence intensity was proportional to the accumulation of carbonyl species formed during oxidation, rather than the rate of oxidation, which is predicted from classical chemiluminescence mechanisms associated with auto-oxidation. Kron et al. correlated the amount of peroxide contained in polypropylene, as determined by iodometry, and the amount of light being detected under thermoluminescence curve in inert atmosphere [47]. A good correlation between ESR and CL as peroxy radical detectors has been found under mechanical stress, though the level of information in the reaction is not the same [48].

All of these works are based on integral light and do not use the spectral distribution of the light for bringing understanding. For a qualitative comparison of information brought by FTIR and photoluminescence, one may consider Fig. 6 with phosphorescence spectra of benzophenone (a) [49] compared to that of XLPE grafted with a benzophenone derivative (b) [10]. Carbonyl derivatives have intense phosphorescence from their $^3(n \rightarrow \pi^*)$ states. Phosphorescence spectra of most aromatic carbonyl compounds show a common feature as regards their vibrational structure. The vibronic structure observed in the spectra corresponds to relaxation to vibronic levels of the ground level. The vibronic structure of acetophenone phosphorescence emission was perfectly resolved at 4 K, and the strongest bands have been identified as harmonics of the ν (C = O) Raman band at 1684 cm^{-1} [50]. At 100 K, the energy difference between structured peaks is less due to overlapping of several vibronic states [7]. Because of this broadening introduced by vibrational levels, broad bands are obtained and identification of emitting groups is not direct.

Besides, luminescence may have extraordinary and unique features as with electroluminescence, which as we shall see in the following provides signatures of degradation products being formed, in quantities that are not detectable with other methods specially when it is mixed with a great number of other chemicals in low concentration. In (electrical) ageing, we must admit that there are no detectable new chemicals being formed (cf. ARTEMIS project [4]), due to field application, whereas EL could be detected. We also showed that chemicals being quinoline derivatives, that have been proved to diffuse from semiconducting screens in

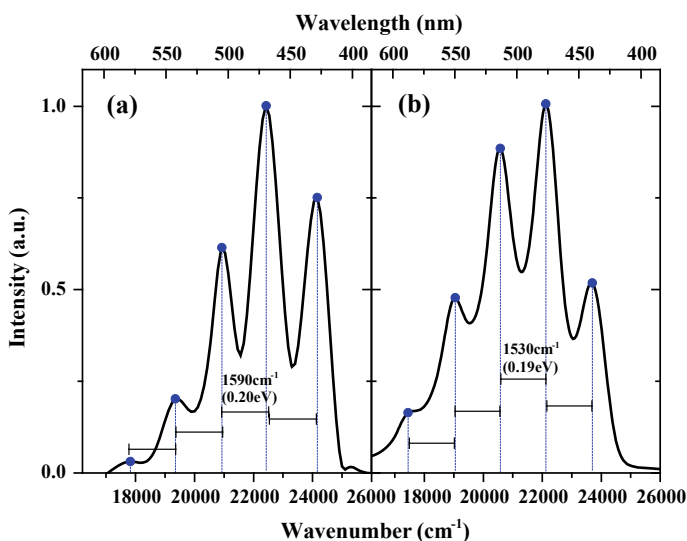


Fig. 6 Phosphorescence spectra of benzophenone (a) in ethanol [49] and of XLPE grafted with benzophenone protonoxy (b) [10]. The averaged vibronic structure is of 1590 cm^{-1} in (a) and 1530 cm^{-1} in (b)

medium voltage cables, were not detected by any other analytical method applied in the same project on the same samples.

3 Implementation of Luminescence Measurements

3.1 Materials

As state above, hydrocarbons made of aliphatic bonds do not emit light in the visible domain. For being emissive, unsaturation must be present. A first family of defects is those existing in low-density polyethylene as depicted in Fig. 7. Jacques and Poller [51] investigated model compounds of these defects by photoluminescence, and this study guided the interpretation of fluorescence from LDPE.

A second set of defects is that provided by additives (antioxidant) and residues due to the cross-linking process. Examples are given in Fig. 8 in the case of dicumyl peroxide chemically cross-linked PE. Compared to in-chain defects presented above, residues do not have chemical bonds to the PE chains and can therefore migrate and be expelled from the polymer. Therefore, particular care has to be taken about sample handling and storage as the amount of by-products evolves in time. In some cases, outgassing of the sample at 60 °C is achieved to force by-products expelling and probe a ‘dried’ material. We will show that there can be traces of by-product detected in the luminescence response.

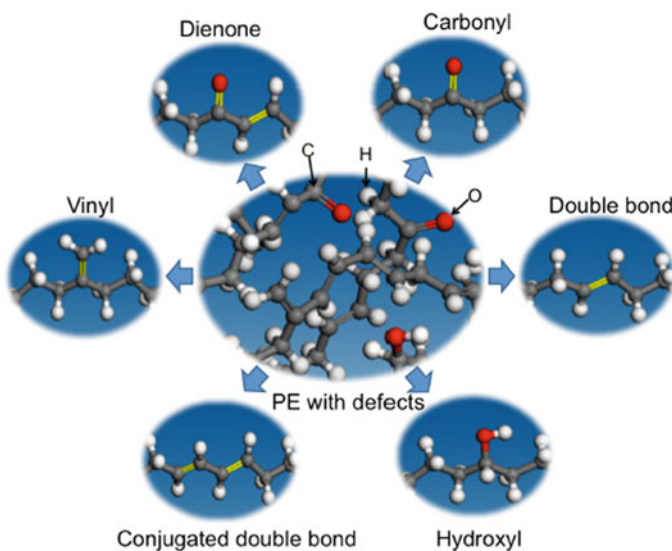


Fig. 7 Six typical chromophore structures that may occur in the carbon chain of polyethylene: carbonyl, dienone, hydroxyl, double bond, conjugated double bond and vinyl. Taken from [52]

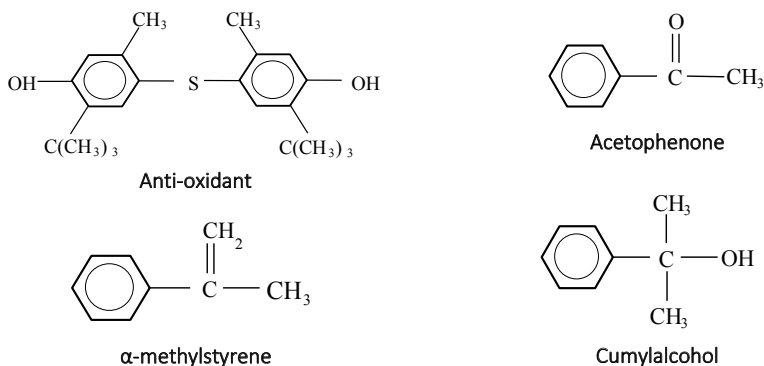


Fig. 8 Chemical structure of possible additives and residues of DCP-chemically cross-linked PE [53]

3.1.1 Standard XLPE

All of the luminescence methods applied to polymers can be applied to materials in film form. An advantage of film with respect to powder or pellets is that the excitation and the amount of probed material are well controlled. Results presented herein were obtained on two kinds of samples.

- (1) Pressmoulding and peroxide cross-linking in a single run—Like for cable production, pellets containing expected amounts of peroxide and of antioxidants, of the order of 1 wt% each, are first moulded under pressure at temperature slightly above the melting point, and then the temperature is increased to 190 °C to perform the cross-linking. The sample is then progressively cooled down to room temperature. Caution along this process is with moulding material: to make unmoulding easy, a protective polymer film is laid onto the mould. However, it was shown that when using PET as protecting film, specific luminescence signatures could be produced. The second caution is about the release of by-products: to control this amount, the cooling and the environment of samples should be kept the same. The sample thickness of typically 100 μm is a good balance. Making thinner films with repeatable and homogenous thickness can be problematic. Making thicker films means higher voltage needs to be applied when carrying out recombination-induced luminescence or electroluminescence experiments.
- (2) The second way of making films is by peeling from high-voltage cables. Provided high-quality knife can be used, films of good surface quality can be produced. In the frame of the Artemis project performed on aged cables, such peelings were produced within the 15-mm-thick insulation: continuous rolls of 8 cm width, about 15 m in length and 150 μm in thickness were analysed with different electrical and non-electrical methods, including luminescence [4]. An advantage was that the rolls reflected the position of samples along the cable

radius. Also, compared to pressmoulded samples, peeled samples tend to retain better the by-products. An important result was obtained in this study of photoluminescence spectra versus position along the radius of the cable. It concerns the diffusion of antioxidant from the semiconducting screens of the cable into the insulation. This was reported in a pair of papers and further commented later on [54, 55].

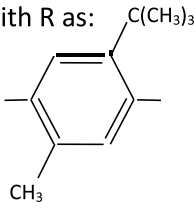
3.1.2 Models of XLPE Compounds

On the one hand, XLPE is a rich material in terms of residues compared to thermoplastic materials. On the other hand, there is a lack of tabulated data on spectral features of potential chemicals involved in luminescence. To isolate these signatures, selected compounds were incorporated into LDPE. It concerns the main cross-linking by-products, acetophenone, cumyl alcohol and alpha-methylstyrene, an antioxidant (4, 4'-thiobis (2-terbutyl-5-methylphenol), AO-), and some of its known derivatives once it has reacted with oxygen [56, 57] as presented in Table 2. The results about this study will be commented in Sect. 4. The way samples were realized is by mixing 0.1 wt% of the products with LDPE and pressmoulding the pellets at 130 °C [56].

3.1.3 Grafted XLPE

The last set of samples investigated was XLPE with grafted groups on it [10]. The project participated in the general objective to develop anti-treeing compounds, often called voltage arresters, for XLPE insulation. These aromatic groups, styrene and benzophenone derivative notably, cf. Figure 9 are supposed to easily catch the energy provided by hot carriers and prevent material ionization. The modification process is patented [58]. We shall see that groups can be strongly luminescent.

Table 2 Chemical formula of the antioxidant 4, 4'-thiobis (2-terbutyl-5-methylphenol) and its reaction products

AO:	$\text{OH}-\text{R}-\bar{\text{S}}-\text{R}-\text{OH}$	with R as: 
AO _{R1} :	$\text{OH}-\text{R}-\bar{\text{S}}\text{O}-\text{R}-\text{OH}$	
AO _{R2} :	$\text{OH}-\text{R}-\text{SO}_2-\text{R}-\text{OH}$	
AO _{R3} :	$[-\text{R}-\bar{\text{S}}-\text{R}-\text{O}-]_n$	

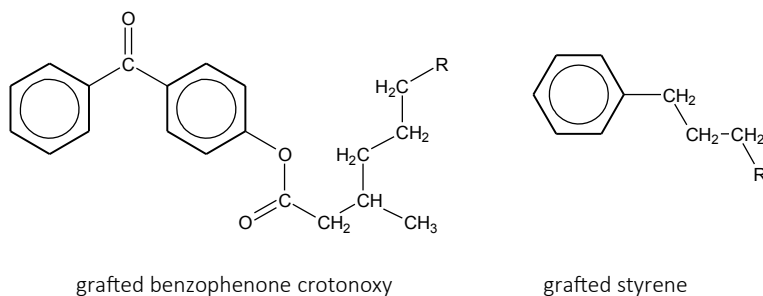


Fig. 9 Chemical structures of grafted groups on XLPE [10]

3.2 Multi-purpose Luminescence Set-up

The available luminescence commercial systems are mainly for PL detection, which cannot meet the requirement of luminescence measurement of insulating polymers. In addition, commercial apparatuses tend to be dedicated to probe liquid solutions more than solid and they often do not apply to large samples. Collecting light from a large surface can be a solution when working with low intensity luminescence signal. For all of these reasons, we have developed a multi-purpose chamber for light detection.

3.2.1 Outlook of the Characterization System

The chamber that has been developed is depicted in Fig. 10. A specificity of the installed system is to detect faint light intensity and to be efficient, for photoluminescence excitation, in the UV region (from 220 nm and on) when commercial spectrofluorimeters operate beyond 280 nm. The system contains five main elements:

- (1) excitation source system (electric field, electron beams, photons and plasma);
- (2) optical detecting system (PM system and CCD camera system);
- (3) optical path controlling system;
- (4) temperature controlling system;
- (5) pumping system.

The excitation source system and the testing system are two core parts for luminescence measurements, while the other systems are auxiliary components. The testing system also contains three parts according to the optical axes:

- Optical axis N°1 for photoluminescence excitation;
- Optical axis N°2 with a cooled photomultiplier (PM) working in photon counting mode for integral light detection;

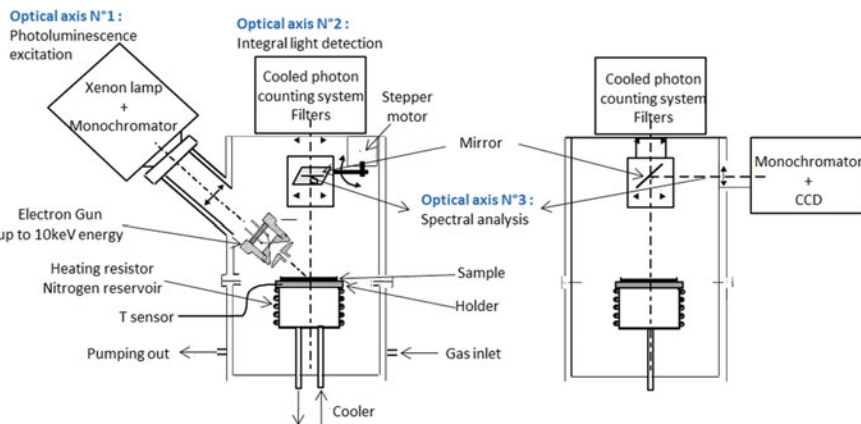


Fig. 10 Experimental set-up used for multi-purpose luminescence detection

- Optical axis N°3 for a grating dispersive system (4.5 nm in resolution) coupled to a liquid nitrogen-cooled charge-coupled device (CCD) camera for spectral analyses which covers the wavelength range from 230 to 840 nm.

The mechanical environment is a light proof dark chamber connected to a turbo-molecular double pumps system to achieve high vacuum, up to 10^{-7} mbar. High vacuum is used in electroluminescence measurements in order to avoid gaseous discharges during measurements. Samples can be placed on the holder which contact to a heating resistor, a reservoir that can receive liquid nitrogen or a thermostated liquid and a temperature sensor, to control the temperature from liquid nitrogen temperature up to ≈ 150 °C (in atmosphere only). The multi-purpose chamber is designed to accommodate different kinds of luminescence excitation as described below. Some key parts of the set-up will be introduced below.

3.2.2 Detection Systems

The photomultiplier (PM), type of Hamamatsu R943-02, is used to count photons emitted by the material. It allows recording resolved luminescence in time. It operates at a controlled temperature of -30 °C by a Peltier cooling system. This temperature has the effect of reducing the thermal emission of electrons from the photocathode, which implies extremely low noise (a few counts per second). The spectral response of the photocathode of the photomultiplier is from 210 to 900 nm; it is relatively flat in the wavelength range from 300 to 900 nm.

The signal transmitted by the PM is pre-amplified and then passes through a set of amplifier/discriminator and is finally transferred to a computer via a card of 'fast' acquisition pulse counter from ORTEC. The integration time (dwell time) is

variable from microseconds to several minutes. We use the PM signal recording for lifetime estimation in photoluminescence, or integral light variation as a function of time or stress for example for field threshold estimation in electroluminescence.

The CCD camera (charge-coupled device) from Princeton Instruments (LN/CCD-1100-PB) works at a controlled temperature of $-110\text{ }^{\circ}\text{C}$. This camera is associated with an imaging spectrograph (type: Jobin Yvon CP200) which ranges at 200 lines/mm. It covers a spectral range between 190 and 820 nm. The sensitive part of the camera has a resolution of 1100×330 pixels, each covering an area of $24 \times 24\text{ }\mu\text{m}^2$, summing information over the 330 rows. The spectral resolution is 4.5 nanometres. The CCD camera works either in spectral detection mode or in imaging mode. The output of the dispersive system extends over the length of the detector at 1100 pixels, i.e. a point per 0.573 nm. The spectrometer is calibrated periodically using known emission lines of a Xenon lamp.

All the optical coupling is achieved using quartz lenses and mirrors. Band pass filters, 2.5" in diameter can be interposed along axis 2 for realizing light detection in given wavelength range. Also, such filters can be put along axis 3: it was used for example to make imaging of the EL emission from the surface of samples with filtering in selected wavelength ranges [59].

3.2.3 Luminescence Techniques According to Excitation Means

(a) Optical excitation: Photoluminescence

During photoluminescence (PL) measurement, the samples mounted into the chamber were excited by a Xenon source coupled to an irradiation monochromator. The excitation beam is with an angle of 40° in respect to the vertical axis. In this way, the specular reflexion from the excitation beam does not enter the light collecting system. The Xenon lamp has a power of 150 W from Jobin Yvon. It is coupled to an excitation monochromator (double-pass monochromator HD10UV from Jobin Yvon with 1200 lines/mm grating). The excitation wavelength varies from 220 to 700 nm and is set manually. The bandwidth of the irradiation window can be adjusted from 0.2 to 4 nm using slits. Coupling between the sample, the excitation source and CCD camera was achieved by optical path through the quartz lenses window of the chamber. PL measurements are performed at $\approx -130\text{ }^{\circ}\text{C}$ especially for phosphorescence and at room temperature especially for fluorescence. Prior to testing samples in photoluminescence measurements at low temperature, the chamber is evacuated and filled in with helium at atmospheric pressure. The phosphorescence spectra can be isolated by synchronizing the light excitation switch off of the shutter placed in front of the irradiation source and the exposure to the CCD camera. In this way, fluorescence, which has a very short lifetime, and the excitation beam are not present in the obtained spectra.

There is a high-pass filter at 300 nm in front of the CCD camera in order to cut off the excitation light of wavelength shorter than 300 nm, which is particularly useful for samples as XLPE where most of the excitation wavelengths are in the

range 220–300 nm. The emission spectrum is integrated under different times by the CCD camera; typically 10–20 s integration proves enough to have a good resolution when realizing photoluminescence spectra.

Phosphorescence lifetimes can be estimated using the photomultiplier, by synchronizing excitation shutter switch off and start of pass trigger in the counting board of the PM. Lifetimes down to microseconds can be detected in this way.

(b) Electric field excitation: Electroluminescence

During electroluminescence (EL) measurement, the sample arranged as seen in Fig. 11 was installed in the chamber and put under high vacuum. Samples are provided with semi-transparent electrodes of gold, 30 nm in thickness or of ITO (Indium Tin oxide). The electrode diameter is typically 50 mm. The two electrodes, HV ring electrode (inner diameter 30 mm) and ground flat electrode (diameter 40 mm), are connected to the high voltage and ground, respectively. The ring electrode allows the light emission analyses from the centre of the sample.

Most of the measurements are carried out under secondary vacuum to avoid discharges in the environment of the sample and characterize luminescence only from the solid. Light detection is carried out by two systems—PM and CCD as explained above. The integration time with the CCD for EL spectra acquisition is usually longer than for PL, of several minutes, due to a much lower light intensity compared to PL.

Direct current (DC) or alternating current (AC) stresses are applied to the dielectric in film form. The DC stress is applied using 35 kV power supply from Fug, Germany. DC current is measured simultaneously using a Keithley 617 programmable electrometer. The AC power supply consists of a high-voltage amplifier ($\times 2000$, up to 20 kV voltage amplifier from Trek, USA) controlled by a function generator. The phase of AC voltage can be synchronized with the counting board of the PM for achieving the phase-resolved EL of the materials.

(c) Electron-beam excitation: Cathodoluminescence

During cathodoluminescence (CL) measurement, we use a home-designed electron-beam gun mounted into the chamber, cf. Figure 10, providing electrons of up to 10 keV in energy. The filament is at high voltage and the anode at the ground. The distance between the electron gun and the sample on the holder is about 40 mm. The axis of the gun is at 50° to the normal of the sample plane rendering possible light detection along the normal to the samples. The beam current is about 0.5 μA . Experiments were also carried out under a vacuum better

Fig. 11 Configuration of EL measurement

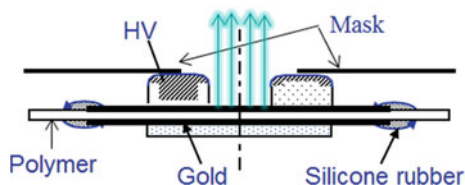
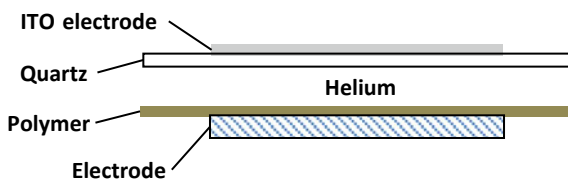


Fig. 12 Configuration for recombination-induced luminescence measurement



than 10^{-6} mbar, at ambient temperature. Emission spectra and light intensity were recorded for different electron-beam energies and for different radiation time with the same beam energy.

(d) Plasma silent discharge for recombination-induced luminescence

In order to charge the surface of the sample, we produce a silent discharge obtained between two plane parallel electrodes, as shown Fig. 12. The sample is deposited on the lower one, and the upper one is made of quartz in such a way that the discharge is initiated between the two dielectrics. The plasma gap of 5 mm is powered at a frequency of 5.5 kHz under a voltage of about 1.5 kV rms.

The sample is contacted with a reservoir in which liquid nitrogen circulates: experiments are achieved at low temperature to increase luminescence yield. The discharge is produced in helium at atmospheric pressure. Before introducing the helium, the chamber is pumped down to 10^{-5} Pa. An electronic circuit controls the interaction time of the plasma with the surface. It adjusts the delay between the end of plasma generation and the beginning of measurement. In this way, the luminescence of the polymer surface can be analysed in situ through the upper transparent electrode. For our purpose, we deal with short plasma interaction times (≈ 5 s) for which it has been shown that the surface modification is mild. The relaxation of the surface is quite slow, and the luminescence can be detected during more than 30 min after plasma interaction at low temperature and for about 5 min at room temperature. As shown previously, photon counting is achieved with the photomultiplier and spectra are acquired with the CCD in different time intervals after the discharge switch off.

Thermoluminescence can be achieved while heating up the sample after isothermal light decay measurements.

4 Luminescence in XLPE and XLPE Compounds

As previously underlined, chemically cross-linked (vs. irradiation cross-linked) XLPE is a complex material. Based on cross-linkable LDPE (a special PE in which the number of $C = C$ is controlled for providing sites for cross-linking), it has all the complexity of the base LDPE (unsaturations, oxidized species, etc., belonging to the chain and antioxidant agent as additive to protect the base material from oxidation, plus other additives likely) plus the ones due to the cross-linking process itself, i.e. it contains by-products of cross-linking agent which can be formed as isolated molecules (i.e. non-bonded to the main chain) or be strongly bonded to the

chain. In addition, by-products of the antioxidant are found as species bonded or not bonded to the macromolecular network. All these chemical species can potentially trap electrical charges and therefore are potential candidates as recombination centres for carriers of opposite polarity. Investigation on the luminescence properties of different formulations gives information about the active trapping sites.

4.1 Base Line for Luminescence Properties: LDPE Base Resin Versus XLPE

4.1.1 LDPE Base Resin

Figure 13 shows the luminescence features resulting from PL and RIL experiments on LDPE base resin. A commercial peroxide cross-linkable LDPE base resin was used. As it constitutes the baseline for the overall study and to improve the control on its purity, LDPE powder has been treated in a solution of ethanol before being processed under film form. The objective was to remove extractable impurities due to pollution from the ambient. No antioxidant was used during the moulding procedure so as to get the simplest possible reference. The thickness of the film was 150 μm . The fluorescence of the reference LDPE sample peaks at 335 nm for short excitation wavelengths (210–245 nm). For longer excitation wavelengths, two bands at 360 and 378 nm appear as shown in the emission spectrum in Fig. 13. These bands are best resolved for an excitation wavelength of 250 nm. At low temperature, a strong phosphorescence emission exceeding the fluorescence yield is detected. The spectrum is broad, structureless, with a maximum peaking at around 458 nm. Note that the fluorescence band is visible at low temperature as a wing in the short wavelength domain. The spectral shape and band positions are consistent with data in the literature [6, 60]. Polyolefins usually fluoresce at about 330–340 nm.

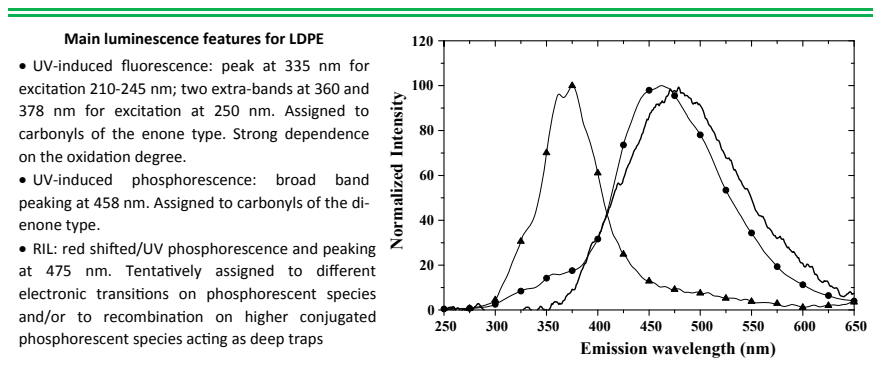
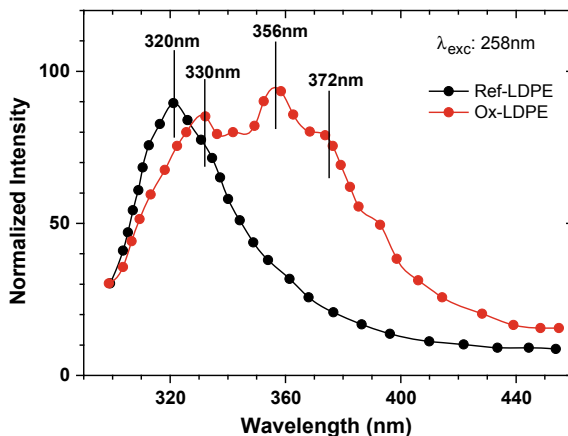


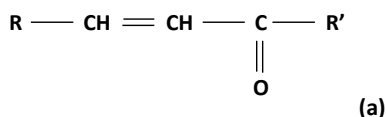
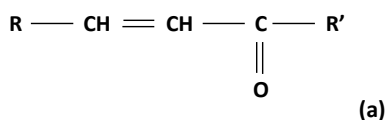
Fig. 13 Luminescence features in LDPE base resin tested in film form. Photoluminescence: (\blacktriangle) at RT; (\bullet): at low temperature. $\lambda_{\text{exc}} = 250$ nm. RIL spectrum (—) [53]

Fig. 14 Fluorescence from LDPE: Reference versus oxidized, with an excitation wavelength of 258 nm. Adapted from [60]



With increasing oxidation degree, extra bands in the region 360–380 nm have been reported [60]; see Fig. 14. As the reference material was antioxidant-free, it is not unexpected that oxidation took place in the specific sample under study.

Phosphorescence at around 450 nm is also a classical feature for such material. So, following data from the literature, the luminescence of LDPE base resin is related to the presence of carbonyls and unsaturated carbonyls of the enone type in the case of fluorescence [51, 61] and of the dienone type for phosphorescence [6, 61], for which the structure is given below:



The RIL spectrum is clearly in the phosphorescence domain. It is shifted towards long wavelengths relatively to the UV-induced phosphorescence spectrum and the maximum intensity is found at around 475 nm. This shift may have two origins: either it corresponds to the involvement of different chromophores, such as longer polyenone sequences, or it results from the excitation of different energy levels of the same chromophore. Carbonyl compounds exhibit both (n, π^*) and (π, π^*) states, and as (n, π^*) states are the lowest lying triplets in enone compounds they would be preferentially involved upon charge recombination [9]. Note that they have the lowest ionization potential of the molecule.

4.1.2 XLPE and Thermally Treated XLPE

Two high-voltage cables insulated by XLPE were produced specially for the Artemis project [4]. The insulation thickness was 14 mm. Samples cut from the insulation of these cables are referenced A and B. Another cable with 27-mm-thick XLPE insulation has been introduced in the project for validating the present approach, since it was available in both the unaged and aged forms. Samples from this reference cable are labelled C.

(a) Sample handling

Measurements were performed on rolls cut from the cables, having width 80 mm and mean thickness 150 μm [54]. In order to minimize effects of diffusion of low molecular weight species from the screen, samples corresponding to the region 2–4 mm from the inner screen of the cable were analysed. More details on the effect of sample handling and cutting procedures on the measurements are given elsewhere [4]. A further problem that was considered is the preconditioning of the specimens before any measurement, in order to have reproducible results. It is clear that not all cross-linking by-products will exit the cable during ageing and thus could contribute to degradation processes. On the other hand, it is necessary to prepare samples whose properties change little with storage time. Therefore, a preconditioning procedure in which the samples were placed in an oven for 48 h at 50 °C in order to expel cross-linking by-products has been adopted. No by-products were detected after such treatment using either high-performance liquid chromatography (HPLC) or infrared spectroscopy (FTIR) [4]. As the luminescence features of these by-products are of interest, we have compared results obtained on specimens before and after preconditioning.

(b) Fluorescence

Figure 15a shows the principal features of the emission spectra obtained from preconditioned samples. Figure 15b shows the corresponding excitation spectra monitored at the peak wavelength of the components identified in the emission spectra, for preconditioned and non-preconditioned samples. The fluorescence excitation spectra—i.e. the emitted light intensity monitored at a given emission wavelength while scanning the excitation wavelength—have been corrected for the wavelength dependence of the excitation power. However, the region 220–230 nm is probably overestimated. Therefore, these spectra should be considered only for comparison of the relative emission yield of the different materials. The effect of preconditioning is shown on the excitation spectra for cable A, which is known as the material containing the highest content of volatile species, due to extrusion conditions. At least three emission bands have been identified as follows:

- an emission at 340 nm, which is best resolved when exciting at short wavelength (230 nm, see Fig. 15a). The relative intensity of this band is weaker in samples B and C which contain less volatile species. Therefore, it might be

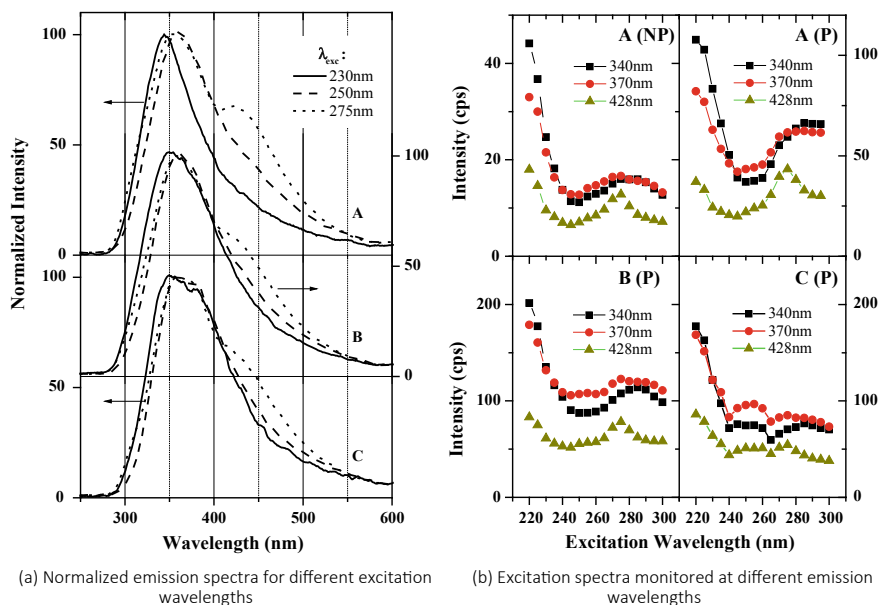


Fig. 15 Photoluminescence at 20 °C from XLPE samples peeled from different cables (A, B, C) from Artemis project. P = preconditioned (thermally treated); NP = not preconditioned. Adapted from [7]

characteristic of volatile groups. However, we did not detect any clear effect of preconditioning on the strength of the band.

- an emission in the range 360–375 nm, with excitation band at about 280–290 nm. Preconditioning strengthens this band. As emissions peaking at 340 and 360–375 nm are close lying and relatively broad, the related excitation spectra cannot be easily distinguished. In sample C, a component at around 380 nm appears distinctly (see Fig. 15a). It is also detected as a shoulder for the other two cables, especially for the spectrum under excitation at 250 nm. Considering the excitation spectra, this component corresponds to a peak at 250 nm in the excitation spectrum of sample C which is not seen for the other samples. The growing of this band is possibly in relation to the fact that cable C was stored for a long time after cable production.
- an emission at around 425 nm with excitation peak at 275 nm. The fluorescence of low-density polyethylene is comparatively simpler (see Fig. 13). Hence, this emission is clearly a characteristic of cross-linked polyethylenes. It seems not to be related to volatile species since preconditioning enhances it. In case of XLPE, the emission is strengthened by a factor of about 3 after preconditioning. We observed that it still increased in a sample previously treated at 50 °C for 2 days and kept at this temperature for one extra day. One would expect a decrease of the emission rather than an increase since volatile products, which are candidate as emitters, are removed at higher temperature. However, the increase of the

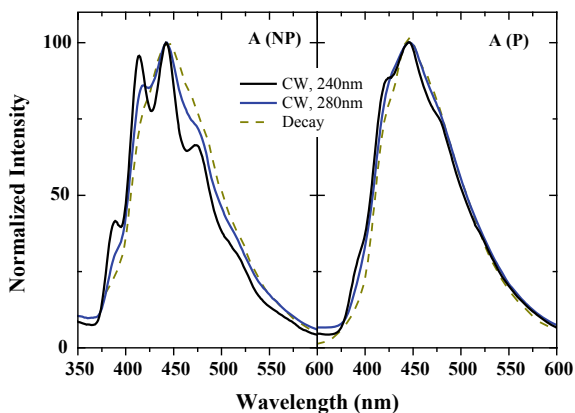
emission does not necessarily mean that more emitting species are produced. It could result from removal of either strongly absorbing species which do not emit and/or from efficient quenching (energy transfer) of the excitation of the emitting groups by non-emitting species. In the first situation, one would expect a different UV–Vis transmission spectrum after thermal treatment. In the second case, the change of shape of the excitation spectrum would be indicative of different quenching efficiency and/or difference in the volatility of emitting species. In any case, fluorescence measurements can be indicative of the quantity of remaining by-products.

(c) Phosphorescence

The emission spectra obtained at $-130\text{ }^{\circ}\text{C}$ are shown in Fig. 16. Results for as-received and preconditioned samples A are compared. These spectra are representative of what was obtained on the other materials. The excitation spectra (not shown) exhibit two maxima, at about 240–250 nm and 280 nm for all the samples. They differ markedly from the excitation spectrum of fluorescence, which means that phosphorescing species are different from fluorescing species. A strongly structured emission, significantly dependent on the excitation wavelength, was obtained for the as-received material. This structure is best resolved when exciting at 240 nm. Several maxima are found at 388, 415, 443, 476 and 515 nm.

These results show that at least two kinds of species contribute to the phosphorescence emission. They have distinct excitation spectra with maxima estimated at around 240 nm and 280 nm. As for fluorescence (see Fig. 15b), preconditioning of sample A increased the emission by a factor ≈ 2 . After preconditioning, the spectrum did not evolve greatly when changing the excitation wavelength. Upon excitation at 240 nm, the structure described above was also detected. The spectrum obtained along the phosphorescence decay is also represented on Fig. 16. Our present understanding of these phosphorescence spectra is that at least two kinds of

Fig. 16 Phosphorescence spectra obtained at low temperature on as-received (NP) and preconditioned (P) sample A. The spectra during the decay were obtained with an integration time of 1 s. CW = continuous wave excitation. Adapted from [7]



species contribute to the emission: acetophenone and an unspecified one. There is no doubt that the structured emission is related to acetophenone. The position in wavelength of the bands is in good agreement with the literature data as will be seen later.

(d) RIL spectra

Figure 17 compares the RIL spectra obtained for the different materials that have been tested. Except for preconditioned sample A, the spectra for the different materials are approximately the same. Structures can be distinguished at about 420, 450 and 475 nm. Though these spectra are broader than those presented in Fig. 16, they exhibit the same components.

(e) Luminescence spectra obtained on other kinds of XLPE samples

The results presented above have been obtained on slices taken from the insulation of power cables. Here we report on results on thin films, either after a thermal treatment (Fig. 18), or cross-linked from different base resins (Fig. 19).

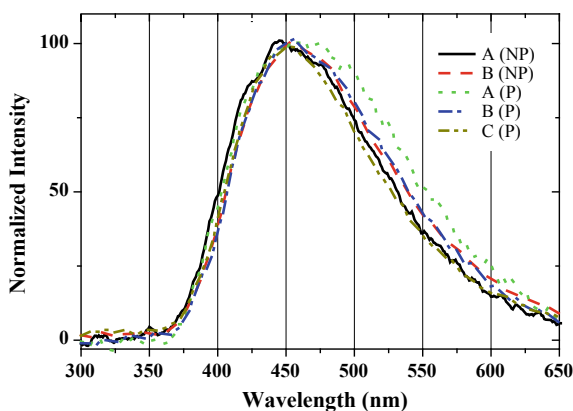
The signature at 428 nm in fluorescence emission is confirmed. Being not due to volatiles species, it should be in relation with strongly bonded species.

There is superposition of the UV phosphorescence and RIL spectra, as previously reported. The centres responsible for deep trapping in XLPE are not those identified in LDPE, and they are strongly bonded to the hydrocarbon chain.

4.1.3 Overall: LDPE Versus XLPE

On the way of understanding XLPE intrinsic recombining centres, we have compared LDPE and XLPE photoluminescence/RIL spectra. If the origin of the LDPE luminescence properties is relatively well understood, this is contrary to the case of XLPE which exhibits specific properties. If the importance of by-products of the

Fig. 17 RIL spectra of the different materials tested. NP and P stand for not preconditioned and preconditioned, respectively. Adapted from [7]



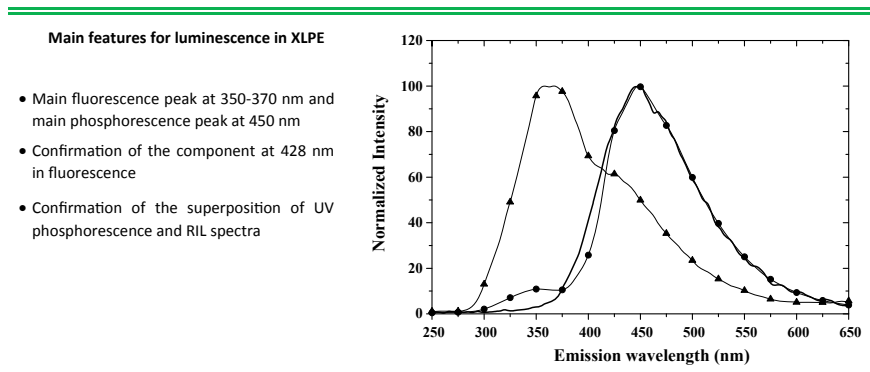


Fig. 18 Luminescence spectra from XLPE under film form (by-products expelled). Photoluminescence: (▲) at RT; (●): at low temperature. $\lambda_{exc} = 270$ nm. RIL spectrum (—) [53]

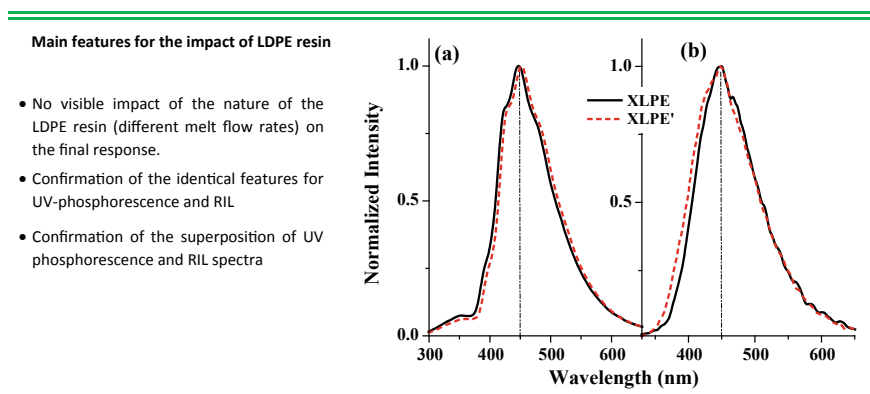


Fig. 19 Luminescence features of XLPE (solid line) and XLPE' (dashed line) at low temperature (-110 °C). **a** normalized phosphorescence spectra for excitation at 250 nm; **b** normalized RIL spectra. From [57]

cross-linking reactions is well described as revealed by differences between spectra of treated and non-treated films, the UV photoluminescence and the RIL spectra on treated films are identical but specific to the XLPE. This demonstrates the recombining centres are strongly bonded to the hydrocarbon chains. Their origin cannot be linked with differences in the cross-linkable base resin as the spectra obtained on two XLPEs with different base resins are identical. Identification of their origin needs model materials to be synthesized and tested. This is the object of the following section.

4.2 *Model Compounds for Interpretation of XLPE Deep Trapping Sites*

4.2.1 **Luminescence Signature of Model Compounds: By-Products of Cross-Linking Reaction**

Figure 20 shows a summary of PL and RIL data obtained with soaking LDPE with the three main by-products of cross-linking [53].

(a) **LDPE plus acetophenone**

The luminescence spectra of LDPE samples soaked into acetophenone with about 1% as final concentration are presented in Fig. 20a. The fluorescence exhibits the same features as in LDPE with about the same emission yield. Depending on the excitation conditions, emission is found at 335 nm or in the range 360–380 nm. As the only similarity between these two samples is the base resin, it is straightforward to conclude that the fluorescence is due to the base resin itself. The fact that acetophenone does not contribute to fluorescence is in accordance with the literature which points out that acetophenone is only a phosphorescent dye with no fluorescence [62]. The phosphorescence spectrum exhibits a structured emission with bands at 390, 418, 445 and 480 nm upon excitation between 240 and 250 nm. The shape of the spectrum is the typical signature of acetophenone emission [50, 63], along with the short phosphorescence lifetime which does not exceed 10 ms. This structure arises from relaxation of the triplet states involving ground state vibrations of the chromophore, and the difference in energy between the bands is related to the ν (C = O) vibration band. The recombination spectrum does not fit the phosphorescence spectrum and, in particular, it does not display the typical signature of acetophenone within LDPE. However, the RIL spectrum is stretched towards the short wavelengths relative to that of LDPE. The strengthening of the emission in the region 380–450 nm probably arises from a contribution of the acetophenone. Then, acetophenone probably acts as a recombination centre, in addition of the LDPE recombination centres.

(b) **LDPE plus cumylalcohol**

The fluorescence spectrum of the cumylalcohol-containing sample (Fig. 20b) presents two peaks at 318 and 329 nm correlated with two maxima in the excitation spectra at 225 and 255 nm, respectively. These features are unique in the set of materials studied. The fluorescence component is most probably due to the cumylalcohol itself, and the fluorescence of the base resin is overwhelmed.

The phosphorescence spectrum clearly shows a structure with peaks at 438, 465 and 491 nm when the excitation wavelength is at about 260–270 nm. It is noteworthy that the excitation spectrum is the same as for fluorescence. This structure is therefore assigned to the phosphorescence of cumylalcohol. The RIL spectrum clearly fits with the cumylalcohol phosphorescence spectrum though the structures are smoother. Therefore, cumylalcohol acts as an efficient recombination centre.

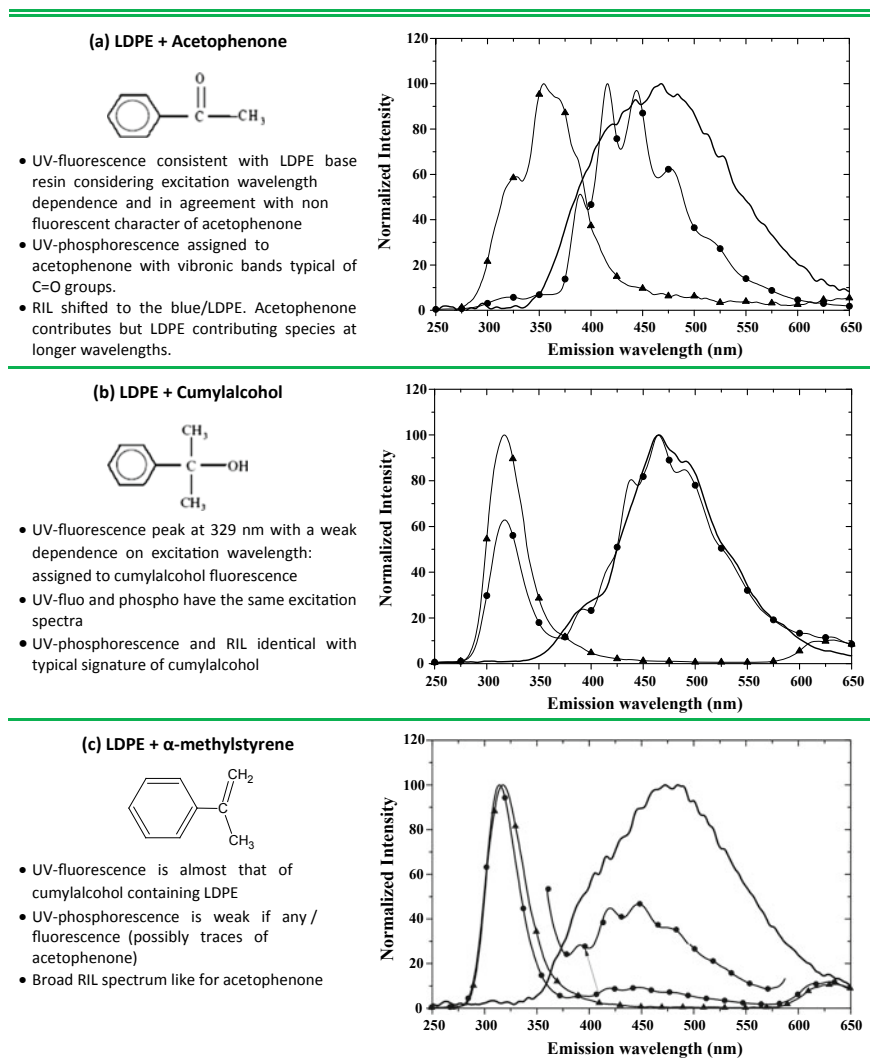


Fig. 20 Luminescence spectra from LDPE samples dipped at $\approx 1\%$ w./w. into by-products. (a) acetophenone, PL: $\lambda_{\text{exc}} = 250$ nm; (b) cumylalcohol, $\lambda_{\text{exc}} = 270$ nm; and (c) α -methylstyrene $\lambda_{\text{exc}} = 240$ nm. Photoluminescence: (▲) at RT; (●): at low temperature. RIL spectrum (—) [53]

(c) LDPE plus alpha-methylstyrene

The fluorescence spectra of 1% containing alpha-methylstyrene LDPE look like cumylalcohol-containing LDPE. There are two maxima at 317 and 325 nm, correlated with maxima in the excitation spectra at 220 nm and 250–255 nm, respectively. The possible slight difference in emission/excitation wavelengths at

peak maximum relatively to cumylalcohol could be due to the presence of OH group in the latter that shifts the emission peak towards longer wavelength [6]. Phosphorescence is weak if any. The free rotation of the phenyl group around C–C bond (which is constrained in the case of cumylalcohol due to the electronegative oxygen atom) could be accounted for.

4.2.2 Luminescence Signature of XLPE Model Compounds with Grafted Species

We consider here two kinds of grafted species onto XLPE. Both are aromatic groups. The difference with the previous case is that those molecules cannot be diffused and be released from the material after processing. The corresponding PL and RIL spectra are shown in Fig. 21.

(a) XLPE plus grafted benzophenone

The photoluminescence spectrum at room temperature is constituted of a weak fluorescence peaking at about 340 nm and a broadband with maximum at 450 nm and some structures at both sides as shown in Fig. 21a. By comparison with the spectrum obtained at 80 K, it is clear that this broadband corresponds to phosphorescence of the material. The emission in this wavelength range is increased by a factor of about 15 upon cooling. A strongly structured emission with bands at 422, 451, 487, 526, 570 and 624 nm appears in the low-temperature spectrum. This structure is consistent with the one reported for the phosphorescence of benzophenone [62]. The only difference is a red shift by about 7 nm of the phosphorescence with respect to that of benzophenone, which is attributable to the fact that a benzophenone derivative is grafted on to the XLPE matrix. It is worth noting that the spectrum does not evolve to a great extent when the excitation wavelength is changed and that the phosphorescence lifetime is very short (some ms). The RIL spectrum matches very well with the phosphorescence structure, the only difference being some broadening of the bands. The recombination process is assumed to be entirely controlled by the species with a characteristic spectrum identified as the phosphorescence spectrum. From the integral light decay signal, it was observed that the radiative charge recombination contribution dominates the decay of the PIL in a large time range ($t > 8$ s). The grafted species therefore acts as a very efficient trapping centre.

(b) XLPE plus grafted styrene

We carried out PL measurements on a 1% grafted styrene and 5% grafted styrene XLPE (same spectral features for a given excitation wavelength, same excitation maxima). The only important difference is in the photoluminescence yield which is about twice for the sample with 1% styrene that is to say the luminescence is not a linear function of the phenyl chromophore concentration. This behaviour is well known and can be due to non-radiative de-excitation routes (intramolecular

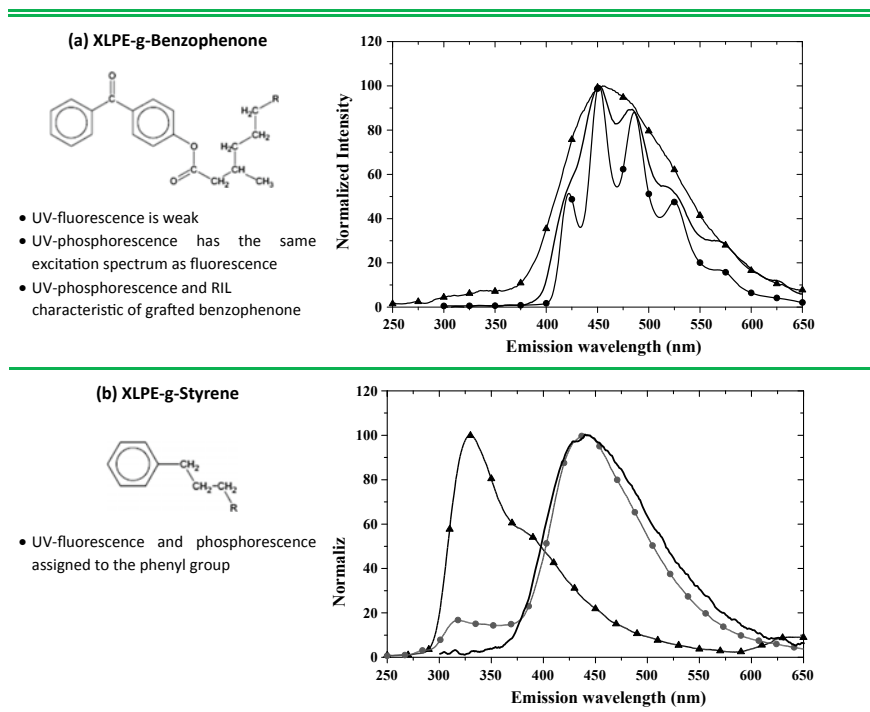
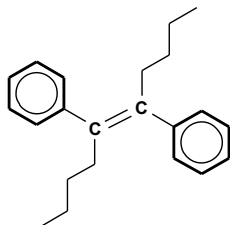


Fig. 21 Luminescence spectra from XLPE with grafted molecules. (a) benzophenone derivative, PL: $\lambda_{\text{exc}} = 270$ nm; (b) styrene, $\lambda_{\text{exc}} = 280$ nm. Photoluminescence: (\blacktriangle) at RT; (\bullet): at low temperature. RIL spectrum (—) Adapted from [10]

quenching) which are open when nearby chromophores are able to interact. This is likely to happen when the grafted styrene concentration is increased from 1 to 5%. As shown in Fig. 21b, the emission peaking at 325 nm (RT) has an excitation maximum between 250 and 260 nm which fits the absorption peak of benzene ring in hexane solution, leading us to assign it to the fluorescence of the π orbital system of the phenyl group [63, 64]. This is further supported by considering the fluorescence emission of polystyrene that is reported between 310 and 330 nm, depending on the commercial source and purity of the polymer [6]. It is tempting to associate the 440 nm emission observed at LT to the phosphorescence emission of the phenyl ring. However, phosphorescence has not the same excitation spectrum as fluorescence, which indicates that the two emissions could have a different origin. Polystyrene phosphorescence has been reported in the same energy domain and assigned to acetophenone-type terminal groups [6]. On another hand, the phosphorescence spectrum of Fig. 20b is not strongly structured contrary to what is observed in the case of acetophenone-type emission, and the general shape is not the same. We therefore attributed the phosphorescence peak to the presence of the phenyl groups. XLPEsty (with 5% or 1% grafting) exhibits also a fluorescence

emission at wavelengths 335, 355 and 390 nm on excitation with light of wavelengths larger than 300 nm. This emission has already been reported as an 'anomalous' fluorescence in polystyrene [65] and has been assigned to the presence of trans-stilbene linkages of the form given below:



Confirmation of the involvement of phenyl groups in fluorescence will be given in the next section.

4.2.3 Luminescence Signature of Model Compounds with Antioxidant and Its Derivatives

(a) LDPE base resin plus antioxidant

The samples used refer to LDPE containing 0.2% of an antioxidant (Santonox). The PL and RIL spectra are shown in Fig. 22a. Relative to LDPE, the fluorescence spectra have in common the band at 335 nm. This band is strengthened for short excitation wavelengths for both materials. However, when a longer excitation wavelength is used (in the range 250–260 nm), another emission is found at 354 nm, being lower in magnitude than the emission at 360 nm found in LDPE. The fluorescence intensity is much weaker, and therefore it seems that the antioxidant by itself does not add a significant extra-fluorescence contribution. The differences are attributed to the protecting action of the antioxidant. Considering that the long wavelength part of the fluorescence spectrum is related to oxidation, the shape of the spectrum may be explained by prevention of oxidation by the antioxidant.

The phosphorescence spectrum is relatively broad and structureless as observed in LDPE. However, it is significantly blue-shifted, compared to LDPE, with a maximum peaking at 444 nm. The long wavelength part of this phosphorescence spectrum is probably broadened by the response of the species emitting in LDPE. So, it can be inferred that the antioxidant phosphoresces with a maximum of emission at around 440 nm which rather favourably compare to the 430 nm reported in the literature [6], bearing in mind that the chemical composition of such a product is really complex. The RIL spectrum is again clearly in the phosphorescence domain. It is also markedly different from the one obtained in LDPE. As

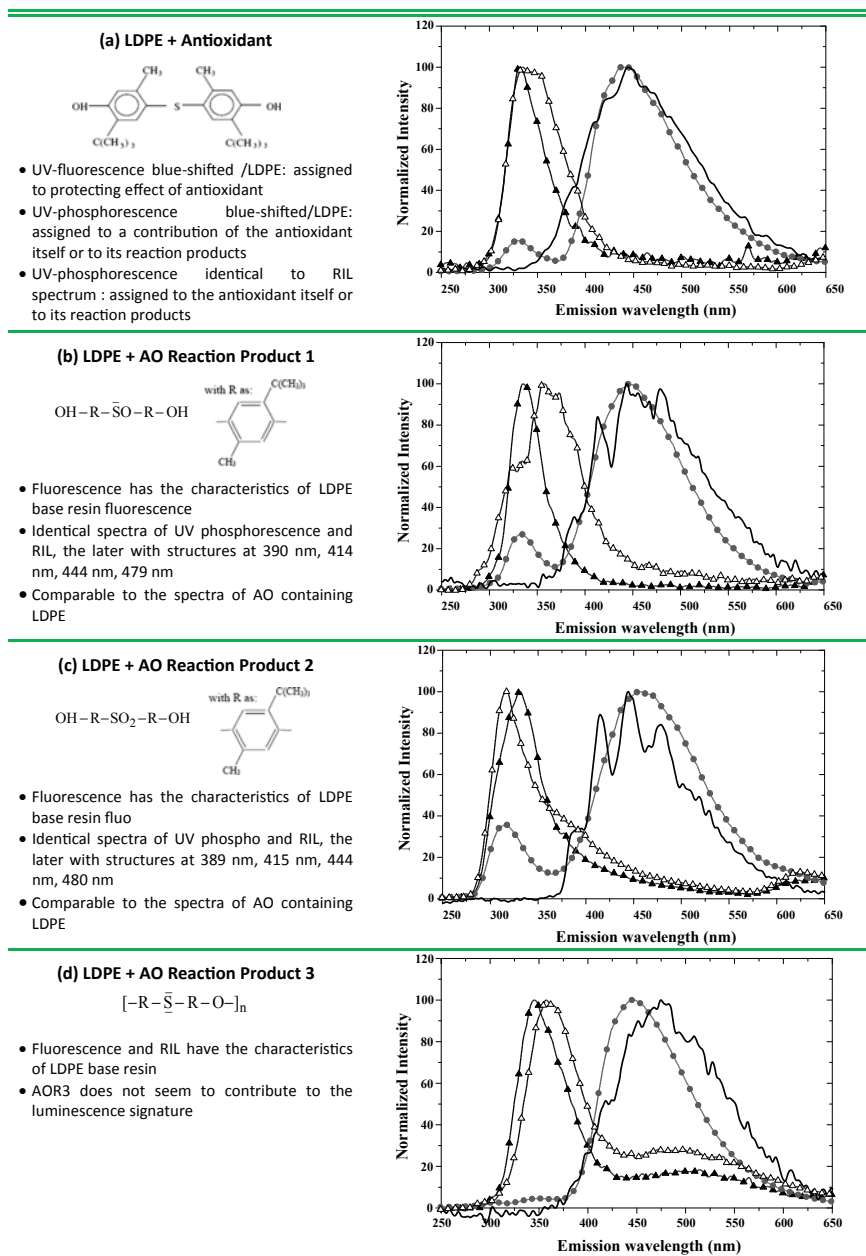


Fig. 22 Luminescence spectra of LDPE with antioxidant and its reaction products. PL: (\blacktriangle) $\lambda_{\text{exc}} = 230$ nm; (Δ) $\lambda_{\text{exc}} = 255$ nm at RT; (\bullet): $\lambda_{\text{exc}} = 225$ nm at low temperature. RIL spectrum (—)

this RIL spectrum fits well to the phosphorescence spectrum, it can be concluded that the antioxidant and/or its by-products are efficient recombination centres.

(b) LDPE base resin plus reaction products of the antioxidant

Another important potential source of chemical traps is provided by the reaction products of the antioxidant, i.e. molecular groups created by reaction of AO with oxidative agents such as peroxide and oxygen, thus preventing polyethylene oxidation, mainly during the cross-linking process. The reaction products of the antioxidant (4, 4'-thiobis (2-tertbutyl-5-methylphenol), AO-) can be classified into three categories labelled as AOR1 and AOR2, corresponding, respectively, to 1 and 2 oxidation levels of the sulphide function, and AOR3 consisting of an oligomer form of the phenolic function, the respective chemical formula being given in Sect. 3.1.2 and recalled in Fig. 22. They were incorporated into LDPE base resin at a level of 0.1% per weight, and then films of typically 130 μm thickness were produced by pressmoulding at 130 $^{\circ}\text{C}$ (thermoplastic materials) or 180 $^{\circ}\text{C}$ (cross-linkable materials).

RIL and photoluminescence spectra of LDPE-AO and related reaction products are clearly different from the one of LDPE. This means that the emissions in the model materials are characteristic of these additives. The structure found in the RIL spectrum of LDPE AO is clearly revealed in two of the model compounds of AO reaction: LDPE-AOR1 and LDPE-AOR2. Both exhibit emission bands peaked at 390, 415, 445, 478 and 510 nm. Such structured RIL spectra have been observed so far only in one instance, with a benzophenone derivative grafted on the LDPE chain (see above). Occurrence of a structured emission in phosphorescence spectra corresponds to relaxation of triplet states involving ground state vibrations of the chromophore. An example of this is luminescence from centres involving carbonyl groups, giving bands equally spaced in energy by the ν ($\text{C}=\text{O}$) vibration energy and enhanced structuration when (n, π^*) states are involved [50, 66]. Out of the four AO and AO derivatives containing samples, the two materials exhibiting the strongest structure in the RIL spectrum are those being oxidized to 1 or 2 degrees that are those containing $\text{S}=\text{O}$ or $\text{O}=\text{S}=\text{O}$ groups. It can then be speculated that the structure is related to these groups. The structure is however less clear when considering photoluminescence spectra. This might be because both (n, π^*) and (π, π^*) states coexist, due to the oxygen doublet, and that charges recombination involve preferably (n, π^*) states, giving rise to a structure, whereas photoluminescence involves preferably (π, π^*) states, giving rise to more diffuse spectra.

The important output of this study is that the typical UV phosphorescence and RIL spectra of XLPE have been reproduced in materials containing AO reactions products (AOR1 and AOR2). Spectra of LDPE-AO exhibit a weaker structure, whereas the phosphorescence emission of the antioxidant itself is normally structureless and has peak at 430 nm [6]. It is however likely that part of the AO has reacted during film processing, and this could be the reason for observing discernable structures. The explanation is supported by the fact that the photoluminescence yield in AOR1 and AOR2 is much stronger than for the other materials

and thus AO reaction products can be detected, even if in low quantity. Finally, AOR3, the oligomer form of the AO, exhibits structureless photoluminescence and RIL spectra with comparable features with LDPE. AOR3 does not seem to participate to the response of XLPE, contrary to AO, AOR1 and AOR2.

4.3 Investigating Cable XLPE Insulation with Screen Diffusing Species

As example of the application of photoluminescence technique for investigating XLPE properties, we discussed here below the differences that exist when dealing with XLPE or XLPE coextruded with its semiconductor screens as they exist in power cables. In the latter case, diffusing species from the semiconductor screens are detected depending on the ageing conditions of the cable.

Samples were peeled from two 90 kV HVAC cables produced by the cable manufacturers within the ARTEMIS project [67]. The major difference between the cables is the design of the cross-linking manufacturing systems at the two cable producers. Both the cable construction and the polymeric materials used are the same. Cables will be referenced to as A and B, depending on the manufacturer. The cables have an insulation thickness of 14 mm. The insulating material is a XLPE while the semiconducting (SC) material (1.2–1.5 mm in thickness) is a carbon black-doped ethylene butyl acrylate copolymer [68]. Both materials contain antioxidants for thermal stabilization and peroxide for cross-linking. The cross-linking is accomplished by heating the cable core materials up to at least 180 °C in a pressurized tube. Long sections of cables were aged in dry conditions for time up to 10,000 h, voltages up to 325 kV (corresponding to a field of 31.2 kV/mm at the inner semiconducting layer) and temperatures of 20 or 90 °C. The complete list of ageing conditions, 23 in total, is given in [67]. Peelings were cut from the cables using a lathe equipped with a specially designed knife to get optimum surface smoothness. They have a nominal width of 8 mm and a thickness of 150 µm. One full roll for each ageing condition was tested by PL. The length of insulation within each roll was approximately 14.5 m. Except when otherwise stated, no thermal preconditioning was applied to the samples prior to the PL measurements reported here. Photoluminescence measurements were carried out at 21 positions along the roll length and the measurement points being tightened next to the inner and outer semiconducting screens.

4.3.1 Influence of Storage Duration of XLPE Slices in the Presence of SC

The first section of the cables was taken just after cable production. It was processed into a roll, the two ends of it being made of semiconducting material (about 1 m long each). A section of that roll, corresponding to the region 2–3 mm from the

inner SC of the cable, was cut for the purpose of carrying out PL and other measurements, as shown in Fig. 23. The two parts were then stored separately in plastic bags in laboratory room conditions.

Figure 23 compares the PL spectra obtained short after roll production on the isolated sample taken at 3 mm from the inner SC to those obtained 1 year after storage of the roll, at various positions along the roll. Here and in the following results, the position '0' corresponds to XLPE at the edge of the SC. Clear differences are observed between these spectra: a band is detected with peak at about 400 nm except for the isolated sample which exhibits the previously reported characteristics of XLPE. The intensity of the band is all the stronger that the sample is taken close to either the inner or the outer SC. Initially, it was thought that diffusion of volatiles from the screen to the insulation had occurred during the 1 year roll storage. Hence, from then on, a minimum amount of SC was let attached to the ends of the rolls being produced and all PL measurements have been carried out short after roll distribution.

4.3.2 Fluorescence and Phosphorescence Versus Cable Radius in Unaged and Aged Samples

Figure 24 shows the variation of the shape of the spectra along the cable radius along with the intensity monitored at two characteristic positions (335 and 400 nm). A new roll of reference (i.e. unaged) cable A was used for that purpose. We observe that, despite cautions taken between roll production and characterization, the

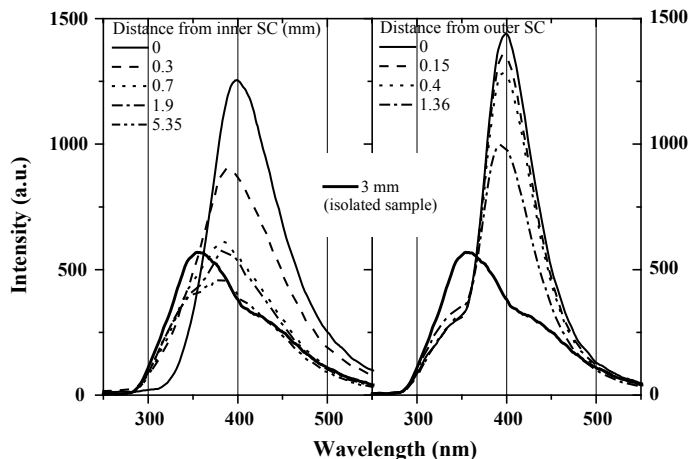


Fig. 23 Bold line: PL spectrum obtained short after cable A production; sample taken at 3 mm from the inner screen. Thin lines: spectra obtained after 1 year of storage of the roll with the semiconducting screen; sample position as indicated in the caption. Excitation wavelength = 275 nm. From [55]

emission at 400 nm is detected within almost all the bulk of the insulation. In Fig. 24a, it is clearly seen that the ratio $I_{400\text{nm}}/I_{335\text{nm}}$ is the stronger close to the SCs. Also, the profile is clearly sharper close to the inner SC: this is a general feature of the results obtained in these measurements. For spectra taken in the range 1–6 mm, the emission is dominated by features usually detected in XLPE (bands at 425 nm and in the range 350–375 nm, see Fig. 23). After thermoelectric ageing (Fig. 24b), the emission at 400 nm dominates at any position in the dielectric. The profile for the emission at 400 nm becomes more flat, and again this is a general feature observed in these experiments.

A further proof of specific PL signatures close to the SC is given by photoluminescence measurements realized at low temperature, which bring information on phosphorescence processes. Figure 25 shows the spectrum obtained close to the inner SC, under continuous wave (CW) excitation at 250 nm, and the spectrum obtained just after excitation shutter switch off (decay spectrum). They are compared to the spectrum obtained on the isolated sample (see Fig. 23) for the same cable roll at 3 mm from the inner SC. The emission in the bulk is dominated by the response of acetophenone with bands at 388, 415, 443, 476 and 510 nm. We can see that spectrum (1), obtained under CW excitation, is a convolution of spectra (2) and (3). Consistently with what has been previously shown, the phosphorescence lifetime of acetophenone is extremely short (order of some ms), and its contribution is not detected in the decay spectrum (2). Several decay spectra were recorded consecutively in the timescale of several seconds, and no evolution was detected. This decay spectrum, which differs markedly from that obtained in bulk XLPE, exhibits clearly four bands at 461, 492, 522 and 567 nm. It is supposed that

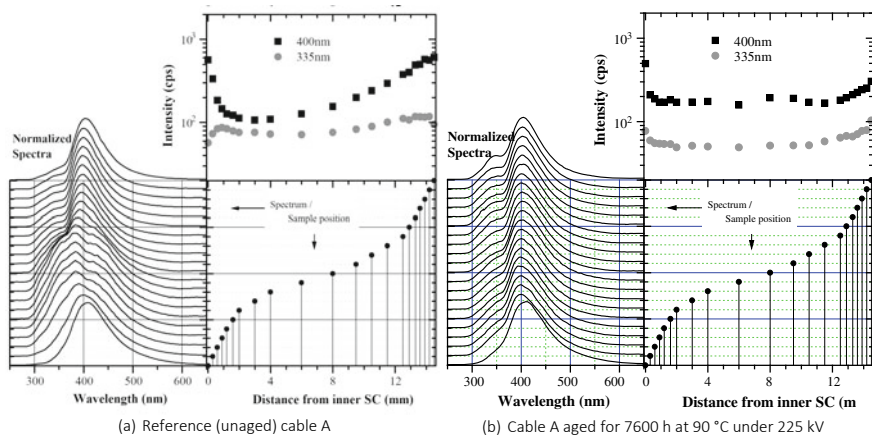


Fig. 24 Spectra obtained along the radius of the insulation of reference and aged cable A. Excitation wavelength = 275 nm. Spectra were normalized to the intensity at emission maximum. The upper-right figure shows the intensity (given in counts per second) monitored at 335 and 400 nm. The position of spectra along the roll is given in the lower-right figure. From [55]

Fig. 25 Normalized photoluminescence spectra of samples taken from cable

A. Excitation

wavelength = 250 nm.

(1) Sample close to inner SC,

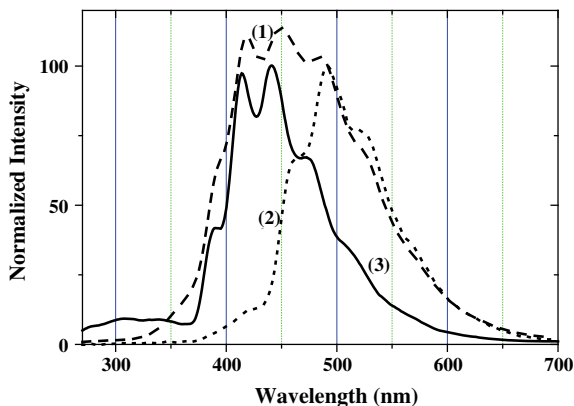
CW excitation; (2) same as

(1)—decay spectrum;

(3) isolated sample, taken at

3 mm from inner SC, CW

excitation

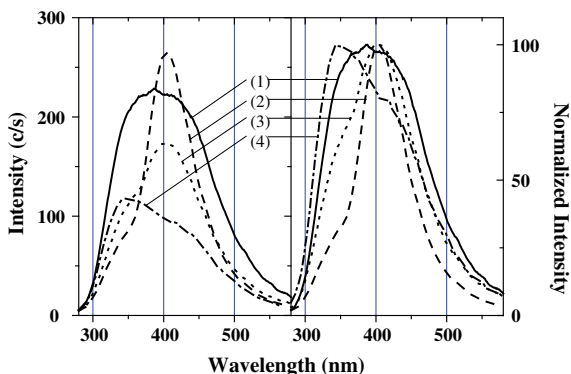


the same species as that which fluoresces at 400 nm is at the origin of this phosphorescence process since these emissions are enhanced in the region adjacent to the SCs.

4.3.3 Identification of Photoluminescence Contributions

Semiconducting screens are quite complex materials providing various candidates as diffusing molecules among which ionic impurities are associated with the carbon black, acrylate oligomers pertaining to the matrix, antioxidant and cross-linking by-products. For the cable samples under investigation, diffusion of acrylate groups in the insulation has been reported using infrared spectroscopy, with a concentration profile evolving with electro-thermal ageing [67, 68]. However, the structured nature of emission spectra (Fig. 25) and their wavelength range are more relevant to phenyl (as is the case for acetophenone) or naphthalene-containing groups. In addition, the concentration profiles of acrylate groups remain sharp close to the semiconductors, even after extensive thermal ageing. So the strategy adopted for unravelling the nature of the new emission was to test different combinations of XLPE/SC interfaces. This was achieved by manufacturing samples constituted of a 500 μm thick layer of XLPE cross-linked altogether with a 500 μm -thick layer of SC of different formulations: the latter was taken either in its full formulation, without antioxidant or without cross-linking agent. The respective photoluminescence spectra appear in Fig. 26. The 400 nm emission is clearly present when the SC contains the antioxidant and clearly lacking when no antioxidant is introduced. In addition, the emission appears stronger when peroxide is not introduced, i.e. when the SC is not cross-linked, which might result from a more favourable condition for diffusion when the SC is a pure thermoplastic. In conclusion, these results clearly show that AO from the semiconducting screens is most probably at the origin of the new features observed in XLPE insulation when coextruded as a cable with the semiconducting material. As to the evolution of the shape of the profile

Fig. 26 Photoluminescence spectra of laboratory-compounded samples. (1): XLPE; (2): XLPE/SC without peroxide; (3) XLPE/SC full formulation; (4): XLPE/SC without AO. In all cases, the full formulation of XLPE was used. Excitation wavelength = 275 nm. Normalized spectra to the right



during thermoelectric ageing, it is difficult to decide if diffusion from the SCs is an ongoing process, or if it results just from a redistribution of the species once cables have been produced. Luminescence techniques in general have the advantage of being very sensitive to low concentrations of luminescent species; they have the drawback of being delicate to implement for quantification purpose, due to the complex energy exchange processes that may happen, as is probably the case in the complex materials investigated here.

5 Diagnosis, Degradation and Ageing Processes

5.1 Electroluminescence from LDPE and XLPE

5.1.1 Rationale for EL Measurements

In the field of electrical insulation, understanding the physical/chemical processes at play during electric ageing and defining transport regimes in which these mechanisms start to be critical is a prime goal to prevent degradation and to develop new formulations or new materials with improved properties. It is thought that a way to define these critical regimes is to investigate under which conditions (in terms of stress parameters) light is generated in the material by excitation with an electric field [52, 53, 69].

This can happen through impact excitation/ionization involving hot carriers or upon bipolar charge recombination [70]. Although structural and chemical changes induced by hot electrons have often been evoked in electrical ageing [71, 72], a clear evidence of their existence in polymeric insulation is still lacking. The other excitation mechanism of EL is encountered when bipolar charge domains spatially interact, leading eventually to radiative charge recombination.

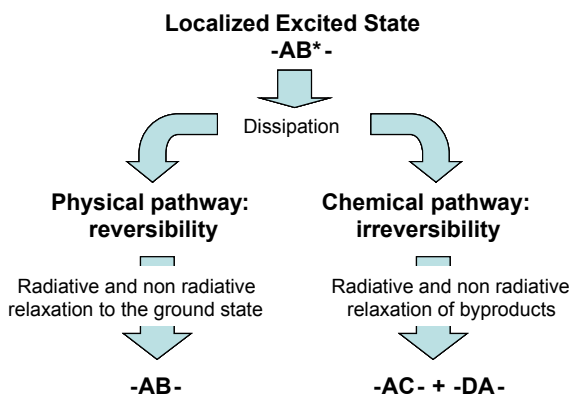
The question of charge interaction with materials goes with questioning about the way excess energy is dissipated into the materials and whether the dissipative

pathways have some irreversible routes. Luminescence naturally reflects the optical route of relaxing energy, besides the phonons route and thermal energy release. The excess energy dissipated in this way—called electroluminescence (EL)—is analysed in multiple ways as it couples the information on the electrical side (charge, current, field) to molecular features (emission spectra). Once excited states have been formed by impact or recombination, they can decay radiatively because the energy of the electronic excitation is of the order of a few electron volts, i.e. in the range of the visible wavelengths. One can further distinguish between two main classes, i.e. physical versus chemical relaxation pathways; see Fig. 27. The balance between these two mechanisms will determine the relationship between EL emission and electrical degradation.

Along the physical pathway, a molecule AB is excited in a non-dissociative state AB^* and returns to its ground state by a purely reversible effect. The relaxation can occur through a number of radiative (fluorescence and/or phosphorescence) or non-radiative (heat dissipation, quenching) processes. The probability of these different pathways is determined by the nature of the excited molecule, its environment and other experimental parameters such as the temperature and the presence of gas able to act as reaction partner. The transfer of the excitation to an oxygen molecule, which is able to induce further reactions, is obviously important for ageing. Energy transfer can be very efficient in polymers, and thus, the luminescence spectrum is not always related to the species initially excited. If EL resulted only from physical processes, it would be a way to probe the excitation rate, but its spectral shape would not give any direct information on ageing.

Along the chemical pathway, the excited group dissociates into molecular fragments that can be very reactive and lead to excited states of neutral or charged species. If chemical processes were involved in EL, specific features of the EL spectrum would be expected with possible signatures of degradation products providing a way to measure the dissociation rate, i.e. the ageing rate.

Fig. 27 Schematic representation of the ageing reactions, A = repeat unit of the chain, B = chain defect, C and D = new chemical functions



5.1.2 Field Regimes of Light Emission—AC Versus DC EL

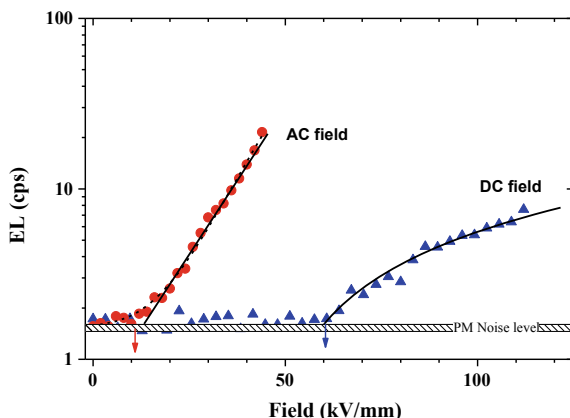
Figure 28 shows EL vs field characteristics obtained for XLPE samples either under 50 Hz AC or DC stress. The presence of by-products of cross-linking reaction led to time-dependent characteristics if the materials were not stabilized before being tested. Samples were consequently thermally treated at 50 °C for 48 h. Semi-transparent gold layers were subsequently deposited by cold sputtering on both sides of the films.

For AC characteristics [73], we have used a short wavelength pass filter with a cut-off wavelength of 600 nm enabling to get rid of emissions in the red region of the spectrum and which appears as a response of gold electrodes [74]. The characteristic was tentatively fitted following a Schottky-type dependence of EL vs field and the result is represented as a dashed line:

$$EL \propto \exp(\alpha\sqrt{E}) \quad (4)$$

The AC field threshold is found at about 10 kV/mm (rms value). In case of DC stress [57], the field threshold is much larger, about 60 kV/mm. Increasing the field up to 120 or 150 kV/mm still gives a very small signal in case of polyethylene materials. Under AC, higher signal can be obtained, with levels of several 100 s of counts per second, which makes it possible recording spectra of the emitted light. For these reasons, EL spectra shown in the following were obtained with AC stress. The reason for having more light intensity under AC arises from alternate injection of charges at one electrode and subsequent recombination. For DC stress, charges need to move through the insulation with carriers of opposite polarity generated at the opposite electrode. Modelling and analysis of the EL phase pattern and space charge measurements indicated that very probably the gross of recombination

Fig. 28 Electroluminescence versus field characteristics obtained from pressmoulded films of typically 150 μm thickness. In red: 50 Hz AC stress (rms field). The dashed line is a fit to a Schottky-type law. In blue: DC stress. The line is a fit to linear dependence of EL versus field above a threshold. Cps stand for photomultiplier counts per second. Data taken from [57, 73]



processes occur in a region of less than 1 μm away from the electrodes while for DC stress space charge measurements show the existence of positive and negative charges in the bulk of the insulation with the possibility of charge recombination.

5.1.3 Electroluminescence Spectra

Comparing spectra obtained in different materials can be a way to improve our understanding of related excited groups. Figure 29 compares the EL spectra obtained on LDPE and XLPE, and for one or the other, the effect of outgassing, of changing electrode material or of film thickness. The results in the ensemble show no great difference from one sample to the other: looking at a glance, the main peak in the spectra is found at about 570 nm, and a clear shoulder appears at about 450 nm, plus a discernible band at 510 nm.

In detail, regarding the effect of electrode material, we have shown that there are two contributions in the EL spectrum under AC stress: one related to the investigated material and the other, in the red region, that has been interpreted as the relaxation of surface plasmon in the metallic electrode [74, 75]. We do not discuss these effects here as they are beyond the scope of this book. After correction for this contribution, we can deduce that the spectra are roughly the same, i.e. qualitatively they do not depend on the electrode metal.

The spectra obtained markedly differ from those presented previously, being photoluminescence or RIL spectra. First fluorescence is not detected at all, neither in LDPE nor XLPE. The emission in the range 430–460 nm could be related to phosphorescence of the material (even though it is not detected at room temperature

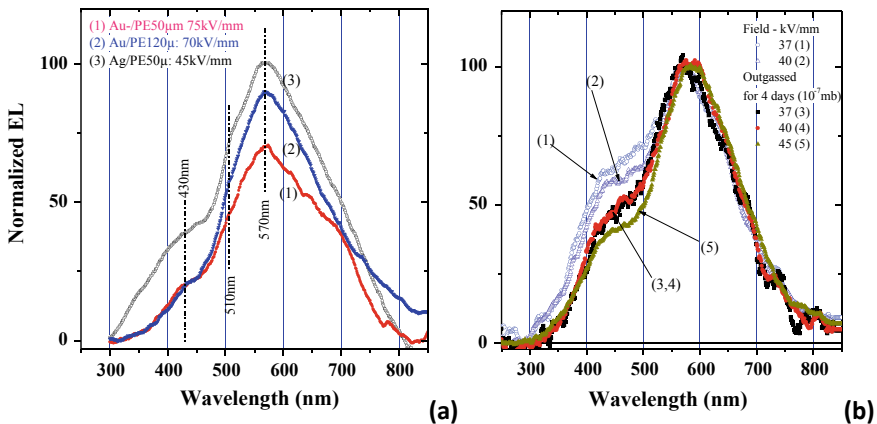


Fig. 29 Electroluminescence spectra of LDPE (a) and XLPE (b) obtained in various conditions. **a** Effect of metal electrode, film thickness and electric field on the EL spectrum of LDPE. See [74]. **b** EL from XLPE from cable peelings, 150 μm thick and Au metallization. The effect of outgassing of peelings not initially thermally treated is put forward

in PL). Under long treatment of XLPE under vacuum this contribution should grow if it corresponds to phosphorescence contribution (due to a decrease of the oxygen concentration inside the film), which is not the case. Instead, as will be seen later on, this emission is related to chemiluminescence of PE that is consistent with a decrease of its contribution with outgassing. Considering other materials like poly(ethylene naphthalate) or epoxies for example, we have always found EL from insulation in the long wavelength range compared to the photoluminescence spectra. This makes a strong distinction compared to the EL in organic semiconductors where both singlet and triplet states relaxations are found. It seems therefore that in the EL of insulating polymers mostly lowest lying exciting states, i.e. triplet states are excited. The shoulder at 510 nm may have relation to the RIL spectrum too. What is noticeable is the remarkable similarity of the spectra for XLPE and LDPE, as if the signatures were not influenced by the presence of by-products and more characteristic of the main polymeric chain defects.

The main band in the spectrum with a peak at 570 nm is not characteristic of the photophysical properties of LDPE or XLPE. As discussed in the following, a hypothesis is that it reflects modification of the materials under the field through the emission from new chemicals formed in the excited state.

5.2 *Cathodoluminescence as a Prototype Source for Interpreting EL Spectra*

A real challenge in the results presented above is the identification of the origin of the main band in EL. With the different ways of exciting the material, PL, including PL of oxidized PE, PIL, and chemiluminescence during thermal oxidation, never such emission was revealed. Only with e-beam excitation was it reproduced [15, 76, 77]. It led us to consider electron beam as a prototype source for understanding the EL mechanisms with a much more yield than can be provided under electric field.

5.2.1 **The CL Spectra from Polyolefins**

Figure 30 shows the cathodoluminescence spectra obtained on LDPE and on XLPE by changing the electron-beam energy from 2 to 10 keV. With this energy, the penetration depth of electrons is less than 1 μm . The experiments were achieved with the same beam current; only the energy of the electrons was changed. The amplitude of the peaks is grossly proportional to the energy deposited by incident electrons. In the timescale of the measurements, of the order of 10 s at each energy level, we did not observe significant evolution of the spectrum. The EL spectrum obtained under AC stress is added for comparison.

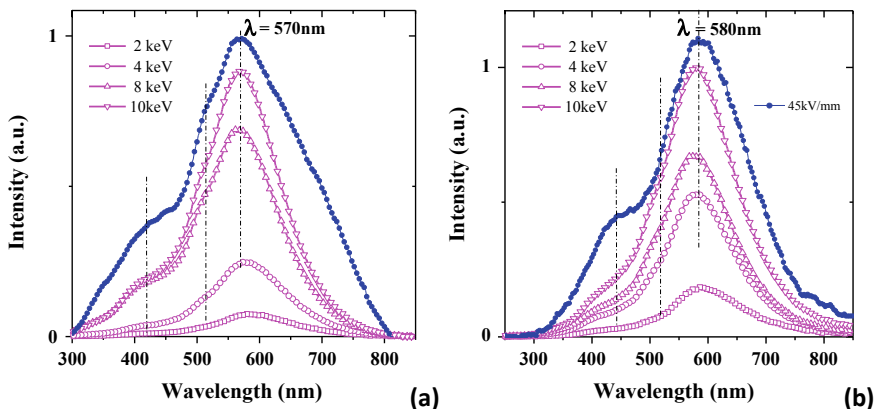


Fig. 30 Cathodoluminescence spectra of **a** LDPE and **b** XLPE under different e-beam energy. EL spectra given for comparison, for AC fields of 75 kV/mm (LDPE) and 45 kV/mm (XLPE) [76]

Two main observations can be made. The first one is that the EL and CL spectra show obvious similarities, much more than any of the spectra shown in the previous sections. Grossly, there are three main bands located at ≈ 420 nm, at 510 nm as a shoulder and at 570 nm (main band). The shoulder found at 700 nm in the EL spectrum of LDPE is more probably related to the treatment done in removing the red component—surface plasmon related—in the EL spectrum [74]. The three main processes are interpreted as a superposition of chemiluminescence from the material, a contribution from charge recombination and a main band associated to the formation of by-products under the effect of energy deposition. The spectra are analysed in more details in the next section.

The second feature is the similarity between the results obtained for LDPE and XLPE response, and this is consistent with the comparison of the EL features. So again, while residues, some of them aromatics, drive the photophysical properties of XLPE, it is apparently the main chain of the polymer that drives the luminescence response under electron irradiation.

The similarity between EL and CL spectra leads to the conclusion that EL involves material degradation, like it has already been reported in case of poly(ethylene naphthalate) [78]. The signatures of charge recombination and chemiluminescence seen in the EL spectra of polyethylenes support the existence of these mechanisms under electrical stress. They can be a direct consequence of hot electron impact with the creation of reactive species (which could further react with oxygen molecules dissolved in the amorphous fraction of the polymer) and the generation of secondary electrons (which would then be trapped and be available to recombine with trapped holes at low to moderate field). The extra spectral features revealed in CL, which provide a full understanding of the EL spectrum, are likely linked with a specific pathway bound to electronic impact. The use of a 10 keV electron-beam energy could appear too far from the energy of hot electrons in

polymers (<10 eV) to be typical. However, one has to keep in mind that interaction between electron beam and matter leads first to a decrease of energy of the individual electrons by X-ray emission (Bremsstrahlung) before they efficiently start their interaction with valence electrons and localized centres in the gap. It follows a set of possible excitation mechanisms among which are impact ionization at moderate kinetic energy (order of 15 eV), impact excitation (10 eV), quasi-elastic scattering with phonons (energy <10 eV) and finally electron trapping at thermal energy [79]. All these events are those that are thought to be important under electric field.

5.2.2 The CL Spectrum Decomposition into Different Processes

Results discussed above show that EL and CL from polyethylenes have rather generic signatures, not obviously dependent on the type of PE. The finding was further substantiated by considering CL and EL in bi-oriented polypropylene (BOPP), which is another polyolefin. The same generic features were obtained, which led us to decompose each spectrum (CL or EL) into a sum of 'elementary' contributions, represented by spectra discussed in the previous section [75].

The obtained results are summarized in Fig. 31. The reference bands for fluorescence and RIL do not need to be further commented as they have already been described before. For chemiluminescence, we refer to chemiluminescence spectra obtained along thermal oxidation at the earliest stages of the process as measured during the oxidation of polypropylene [8]. This contribution was already used to interpret the different contributions in plasma-induced luminescence experiments [27]. Note that for PIL, there was an evolution of the spectra during the decay time. Here in case of polyolefins the CL spectrum did not evolve significantly when changing the irradiation energy or during the irradiation time though the intensity dropped in a matter of minutes during irradiation. Therefore, the change in spectrum shape could not guide the interpretation of the processes. For EL, in the same way it is not easy to reveal relative changes in contributions in the case of polyolefins. For PEN, there were indeed significant field effects in spectrum shape [80].

In CL, the kinetic energy of electrons is a powerful source of excitation. The main part of the energy of the electron is spent during deceleration on the production of secondary electrons and plasmons with energy of 20–30 eV. Secondary electrons that do not leave the sample in turn generate electron–hole pairs. Thus, the main fraction of the electronic energy (up to 90%) is spent on the creation of electron–hole pairs [81]. It is important to note that, upon excitation of luminescence by an electron beam, the energy of excitation considerably exceeds the band gap width of the material. Therefore, excitation of luminescent centres does not result only from direct excitation but also as a result of radiative and non-radiative transitions from higher lying energy states. The main primary mechanism of luminescence excitation will be impact excitation on the molecules of the polymer. The energy exchange during the impact may give rise to excitonic states that will

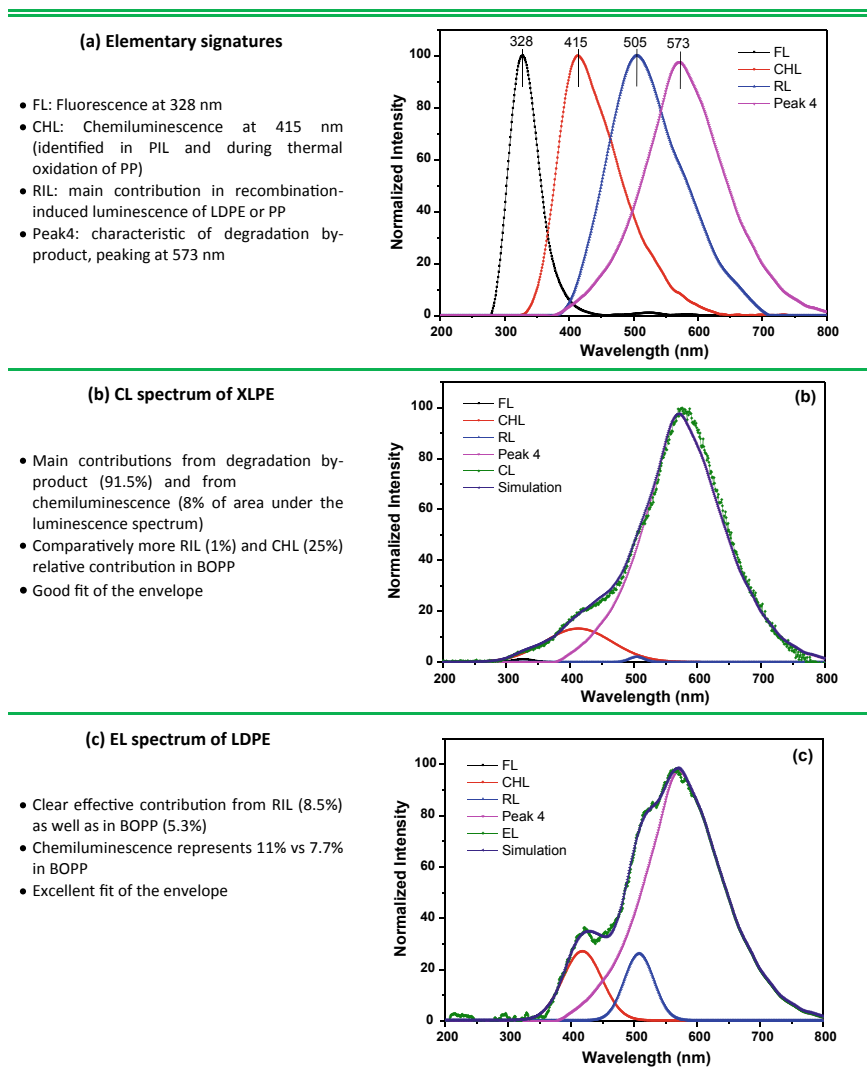


Fig. 31 Decomposition of EL and CL spectra of PE into elementary contributions and examples of application. **a** CL in XLPE (5 keV energy) and **b** EL in LDPE (ac field 45 kV/mm). Adapted from [75]

further relax to their ground state (generating fluorescence and/or phosphorescence emission) or be brought into dissociative states. The formation of new chemical species upon degradation is therefore inherent to CL. Alternatively, transient excitonic states may react with oxygen molecules dissolved in the polymer, particularly in the case of a triplet exciton taking into account the triplet ground state of oxygen molecule. It follows the possibility to emit light through

chemiluminescence. Impact ionization will be a source of positive charges, and there is the possibility of charge recombination generating light. In recombination processes, the emitting species will be those able to act as recombination centres, i.e. those providing deep traps for electric charges. In polyolefins, these centres are conjugated CC bonds bound to CO species. Owing to the chemical degradation of the material under the electron beam, all these recombination processes can occur on by-products leading to new components in the spectra. CL experiments provide therefore a full set of excitation channels.

In EL, the source of excitation is much less efficient and is still the topic of debates in large band gap materials [41]. Hot electrons processes and charge recombination are the main potential sources of excitation, depending on the electric stress. In case of hot electron processes [72] and although the kinetic energies are far apart from that in CL experiments (a few eV in EL vs. a few keV in CL), there is still the possibility for impact processes, with or without ionization. Impinging electrons with kinetic energies of a few eV do not have the energy required for impact ionization (15 eV) [82] but they can excite species among which the natural chromophores that will relax through fluorescence and phosphorescence emission, or be stabilized to form transient ions (negative attachment) able to subsequently dissociate into molecular fragments [83]. Recombination between charges of opposite polarity being injected at cathode and anode also provides the conditions for EL in polyolefins [41]. It has to be realized that recombination opens the way to chemiluminescence as well through the excitonic states created by the recombination process itself that can react with dissolved oxygen. Because a chemical pathway is open through reactive excited species, recombination can further affect newly formed chemical groups.

The main component in the emission in CL and EL has not been identified. We think it is a signature of material degradation either through the formation of by-products under an excited form or through their excitation upon charge recombination. Indeed, the fate of excitons formed upon recombination of electron/hole pairs has been investigated in PE using density functional calculations and ab initio molecular dynamics simulations. Two situations were investigated where excitons are self-trapped along a chain [84, 85] or trapped at chemical defects [86]. The relaxation can occur following different pathways depending on the case. When the exciton is trapped on a chemical defect, the relaxation pathway depends of the nature of the chemical defect leading to trapping of the charges, non-radiative recombination or homolytic bond breaking. This is of course the latter process that is relevant for damage. When the exciton is self-trapped along a chain, CH bonds breaking is promoted according to a recent calculation [86]. With the opening of a chemical route, by-products could be produced in the excited state and be responsible for emission in a wavelength range that is not typical of the initial chemistry of the polymer. The main peak in electroluminescence could reveal such degradation process.

5.3 Ageing Diagnosis

Besides online light detection under application of the stress as presented above, luminescence can be used as post-ageing diagnosis method like any other physico-chemical analysis, with its own specificities as the strong dependence of the sensibility upon the nature of molecular groups. In general, the trends are not an increase of luminescence, as could be expected with the formation of new groups. Rather, the luminescence yield decreases with ageing and the shape of the spectrum exhibits modification like broadening and shift to long wavelength. This is typically the case during thermal oxidation of polyolefins.

5.3.1 EL Yield of Aged Materials

A series of experiments has been achieved concerning EL-field characteristics of aged XLPE. Mary et al. showed that upon prestressing of materials under DC stress, the phase patterns under AC stress are considerably modified [87]. This is a consequence of space charge build-up of the material that can be viewed as (possibly reversible) ageing.

In the frame of the Artemis project, cable insulation slices were characterized using EL, through EL-field characteristics under AC and DC. The trend was an increase in the field threshold with ageing (mostly thermal ageing), along with a decrease in the slope of the characteristic. Figure 32 shows an example of EL-field characteristics under DC stress. The cables had a 1600 mm² copper conductor and a 26.6-mm-thick XLPE insulation. One of them was aged at different levels of field and temperature (maximum test field = 27.5 kV/mm, withstood for 1 year, maximum temperature 95 °C). The field threshold is significantly shifted to higher value. This was correlated with space charge measurements showing that the recombination domain in aged cable is forming at a higher field than in unaged, due to a smaller penetration depth of positive space charges. These changes were explained by an increase in density and energy distribution of trapping centres [88]. The photoluminescence yield was halved after ageing.

5.3.2 PL from Thermally Degraded Materials

Still within the Artemis project, the photoluminescence was used to monitor the changes in material property with ageing time. Already some results have been shown in Sect. 4.3.2. The diffusion of antioxidant from the semiconductor to the insulation has been followed by luminescence. AO diffusion was not the only process at play. Cable yellowing was detected, and this was correlated with the appearance of extra band in photoluminescence spectra [54, 55]. The analysis of the PL data revealed quite complex shape of PL spectra, with several overlapping processes. As each contributing band is usually broad, monitoring the intensity of

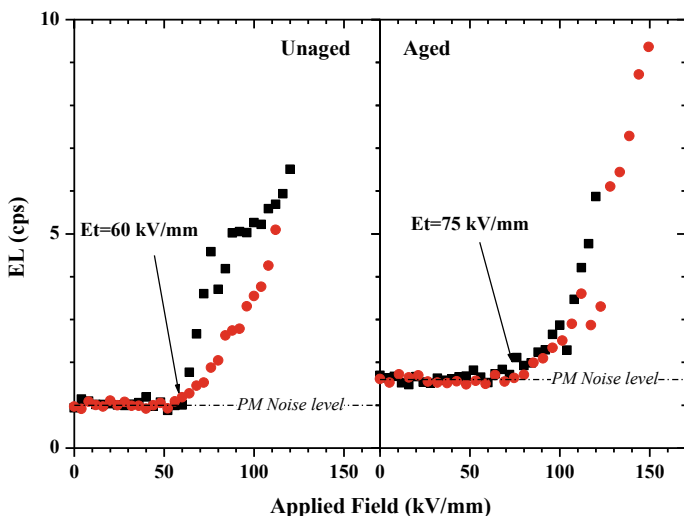


Fig. 32 EL-field characteristics from XLPE peelings taken from reference and aged cable in Artemis project. Ageing condition: 95 °C, max ac field 27.5 kV/mm, 1 year [88]

the emission related to one mechanism is not possible since significant overlap of the bands occurs. In order to provide a systematic evaluation of photoluminescence spectra versus position in the roll, ageing conditions and excitation wavelength, a set of elementary spectra was isolated. The identification of those isolated bands took into account the fact that XLPE was produced with two different companies with different cross-linking process which gave significant differences in PL signatures. The identified bands, their characteristics and significance are given in Table 3. The fluorescence bands are sorted out in three groups:

Table 3 List of fluorescence signatures isolated in cable insulation with the corresponding attribution. The area of the bands is given for spectra normalized to 1 at peak intensity

Label-Peak wavelength (nm)	Area of the band (nm)	Attribution
XL-440	87.1	Bulk XLPE emission
XL-370	87.0	Bulk XLPE emission
XL-330	44.8	Bulk XLPE emission
SC-400	100.2	AO from SC
SC-410	90.6	AO from SC + ageing?
SC-340	45.2	AO from SC
Y-540	175.5	Thermal ageing

- (i) those related to XLPE, with emission maxima at 330, 370 and 440 nm. The details of these bands depend notably on the excitation wavelength.
- (ii) those associated with the antioxidant of the SC screens: the main band is at 400 nm; it may shift to 410 nm after thermal ageing. Finally, a small fluorescence band at 340 nm is found in some cases, with higher amplitude close to semicons.
- (iii) the last emission, at 540 nm is detected after significant thermal ageing; it appears correlated with the yellowing of the cables. The spectrum is very broad with a width at half maximum of about 200 nm while that of the XLPE-related fluorescence is less than 100 nm. This broadness reflects probably the disorder introduced in the related chemicals.

Some results obtained after fitting are plotted in Fig. 33. The contributions to the spectra for the three groups of processes, XL for bulk XLPE, SC for diffusing species from screen and Y for yellowing were used and summed up. We consider here specifically the behaviour of the AO-related band (labelled SC) and yellowing (Y) band in one type of cable (B). As electric field ageing effects are of second order compared to thermal ageing, we indicated in the caption only the ageing times at 90 °C for this set.

The profiles presented in Fig. 33a for the SC-related band differ significantly from those shown in Fig. 24a. The reason is with the cable processing conditions which were different between the two cables, revealing that the chemical disorder in XLPE structure remains process dependent. Without thermal ageing (rolls B0 to B2), the relative contribution of the yellow band is perfectly reproducible from one roll to another (though it was not so clear for cable A). After thermal ageing, the profile becomes more flat and the intensity in the middle of the sample grossly

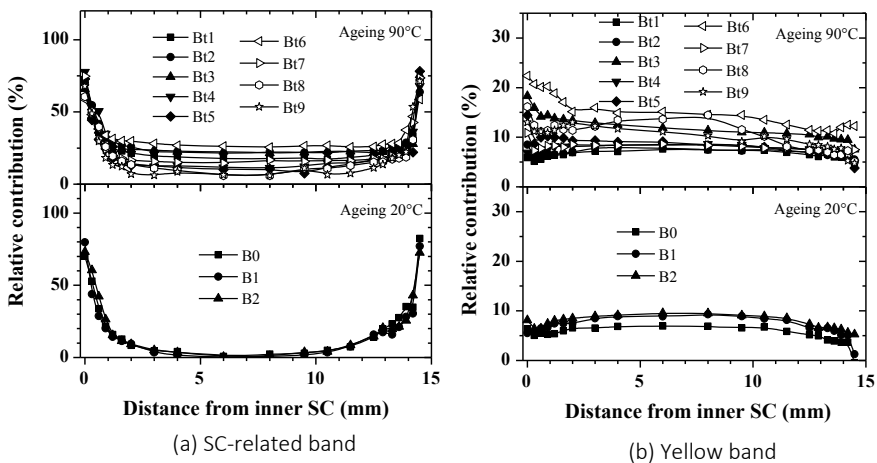


Fig. 33 Relative contribution of the SC-related and yellow bands to the total PL spectrum area versus insulation radius for cables B. Ageing times at 90 °C: Bt5: 3000 h, Bt1, 2, and 4: 5000 h; Bt9: 6000 h; Bt7: 7800 h; Bt3 and 6: 10,000 h; Bt8: 15,000 h

increases with ageing time. Concerning the band related to yellowing, Fig. 33b, a maximum contribution is found close to the inner semicon, where the ageing temperature was at maximum. In consequence, the profile is no more symmetrical.

UV-Vis absorption spectra were correlated with PL measurements. A broad absorption appears in the region 350–450 nm, strong close to the inner SC and decreasing in intensity with the distance from the inner SC. It appeared related to a thermal effect during ageing since the temperature is the higher at the core of the cable and decreases when going towards the outer SC. It was suspected that the photoluminescence emission at 540 nm and the broad absorption in the range 350–450 nm are associated with the same kind of species formed by thermal oxidation. The apparent yellowing would be mainly due to the absorption. As to the nature of reacting groups, one has to consider the involvement of AO-related species that have diffused from SC to the insulation bulk during cable production. As antioxidant agent, such species are prone to reaction with oxygen during thermal ageing, leading potentially to the absorption responsible for the yellowing. Further support to the interpretation was brought by comparing the behaviour of cables A and B and by considering the profiles of the diffusion and yellow bands [55].

5.3.3 Contact Sensitization

As final example of application of luminescence to probe defects into polyethylene, we present the case of LDPE films processed using different cover layers during pressmoulding [89]. As a base insulation material, we used a non-stabilized low-density polyethylene from ExxonMobil™, which is designed for medium/high-voltage insulation, and which can be peroxide cross-linked. The samples were processed by pressmoulding at 140 °C, in films of 200–250 μm thickness and using aluminium film (Al), polyimide (PI) or polyethylene terephthalate (PET) cover layers. Surprisingly, very different PL spectra were obtained depending on the kind of pressmoulding films used in the process, despite the fact that the processing temperature was moderate.

Figure 34a shows the PL spectra obtained on various materials, for an excitation wavelength of 280 nm (the emission spectrum appeared dependent on the excitation wavelength). The bands at 300 and 340 nm are consistent with previous reports on PL from LDPE, the main band being assigned to enone $\text{C}=\text{C}-\text{CO}-$ groups [9]. The shoulder at 390 nm is not so commonly observed in fluorescence of PE. In fact, considering the films made with PET cover layer, one can deduce that this emission is strengthened and its position is consistent with that detected in the PET film itself. The emission at 390 nm in PET was ascribed to a ground state dimer emission [90].

FTIR spectra shown in Fig. 34b feature three main absorption bands changing depending on the type of cover film used. Bands at 1722, 1263 and 1100 cm^{-1} appear for the sample processed with PET. They are ascribed, respectively, to $\text{C}=\text{O}$ and $\text{C}-\text{O}$ stretching vibrations and to cyclic ether vibrations. The band at

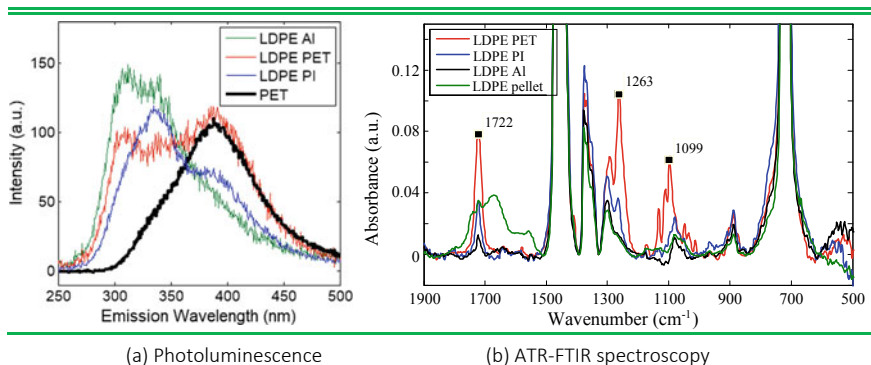


Fig. 34 **a** PL emission spectra for LDPE processed with Al, PET or PI cover layers compared to PET film (intensity was divided by a factor 5 for the PET film). Excitation wavelength: 280 nm. **b** FTIR spectra of LDPE pellets and of films processed using different cover layers. ATR mode with internal reflection angle of 45°

1645 cm⁻¹ (in the pellets) ascribed to C = C groups, which disappears after processing, is presumably some kind of process stabilizer.

Both the PL and FTIR data reveal a specific response of the material processed with PET cover layer. The signatures might be interpreted in terms of oxidation of the material due to the contact with the PET cover layer (e.g. formation of carbonyl groups). This would be consistent with the fact that some of the signatures are detectable in LDPE processed with or without PET, the difference being that the magnitude is higher when contact with PET is made. A second possibility is the diffusion of low molecular weight molecules from the PET to the LDPE during the thermal processing. As PET contains carbonyl groups in the repeat unit, the response of both pre-oxidized groups and of diffusing groups would be combined.

The interpretation given to the extra signatures was therefore to diffusion of oxidized groups—presumably decomposition products or oligomer chains from PET into the LDPE sub-surface. Substantial differences in space charge [91] and conductivity [92] were reported for LDPE exposed to PET moulding layers; the diffusion is one of the possibilities for such differences. Oxidized groups may act on interface properties through different ways: changing the surface potential, acting as trapping sites for charges, or they may ultimately lead to dipole-induced effects.

6 Conclusions

By using luminescence techniques, we have been able to show that the by-products of cross-linking reactions may act as deep traps in XLPE. This provides an explanation for the dependence of the space charge distribution on the thermal treatment of the samples that has been reported in the literature [93]. These

chemicals are not the only trapping centres in XLPE as denoted by the emission spectrum of this last material. Antioxidant and its reaction products have been shown to be very active species for stabilizing electric charges. Example has been given where diffusing species from the semicon screens give their contribution to the photoluminescence emission. A careful treatment of the emission spectra with the help of spectra obtained on model compounds allow to de-convolute the complex response obtained on XLPE.

Examples have been given where luminescence techniques can be useful to tackle the question of the ageing mechanisms and ageing diagnosis. The interpretation of electroluminescence spectra of PE-related materials has only been possible with the help of database related to the emission of model material compounds under different excitation sources, among them cathodoluminescence with its characteristic emission spectrum that maps those of PE-related compounds. This has been fundamental in establishing the relationship between electroluminescence and ageing.

The application of luminescence experiments to derive the nature of the recombination centres may suffer from some limitations. First, the light that is analysed may not be emitted directly by the recombination centre, but through energy transfer to an efficient emitter. This would prevent a direct correlation between the emission spectrum and the recombination centre. However, this study has shown that the RIL spectra are indeed linked to the chemicals introduced into the material. This drawback would not therefore be as drastic as is often postulated. Second, different chemicals can give emissions in a narrow range of wavelengths thereby rendering critical the assignment of a particular spectrum to a given species. Moreover, the spectrum can become intractable when dealing with technical materials containing different kinds of recombination centres. This is why knowledge of the optical signature of different additives is of great help.

Finally, the approach is limited to recombination centres that are optically active. This item is difficult to address since the emission yield as probed by photoluminescence as for example is not necessarily the same as in RIL. The requisite condition is that the centres must have a finite probability of emitting light when interacting with electrical charges. In photoluminescence, the probability of creating a triplet state depends on the rate of intersystem crossing from singlet states. It can be very low, especially when the difference in energy between the singlet and triplet states is large. Conversely, the probability of creating a triplet excited state in a charge recombination event is theoretically three times as large as the probability of creating a singlet excited state [94]. This means that species known to be non-phosphorescing may be so because of excitation limitations under UV irradiation, and they may behave in a completely different way regarding emission yield excited by electrical charges. Clearly, there are not so many alternative principles for measuring luminescence that are able to bring direct information on the interaction between electrical charges and chemicals within insulators. This technique can be useful when used in conjunction with different sources of luminescence excitation to check the possible role of additives or impurities in space charge accumulation phenomena and to probe ageing mechanisms.

References

1. Teyssedre G, Laurent C (2013) Advances in high-field insulating polymeric materials over the past 50 years. *IEEE Trans Electr Insul Mag* 29(5):26–36
2. Chen G, Hao M, Xu ZQ, Vaughan A, Cao JZ, Wang HT (2015) Review of high voltage direct current cables. *J Power Energy Syst* 1:9–21
3. Zhou Y, Peng S, Hu J, He J (2017) Polymeric insulation materials for HVDC cables: development, challenges and future perspective. *IEEE Trans Dielectr Electr Insul* 24:1308–1318
4. Fothergill JC, Montanari GC, Stevens GC, Laurent C, Teyssedre G, Dissado LA, Nilsson UH (2003) Electrical, microstructural, physical and chemical characterization of HV XLPE cable peelings for an electrical aging diagnostic data base. *IEEE Trans Dielectr Electr Insul* 10:514–527
5. Blodgett RB, Fisher RG (1963) Insulations and jackets for cross-linked polyethylene cables. *IEEE Trans Power Apparatus Syst* 82:971–980
6. Zlatkevich L (ed) (1989) *Luminescence technique in solid state polymer research*. Marcel Dekker
7. Teyssedre G, Tardieu G, Laurent C (2002) Characterisation of crosslinked polyethylene materials by luminescence techniques. *J Mater Sci* 37:1599–1609
8. Tiemblo P, Gomez-Elvira JM, Teyssedre G, Massines F, Laurent C (1999) Chemiluminescence spectral evolution along the thermal oxidation of isotactic polypropylene. *Polym Degrad Stab* 65:113–121
9. Teyssedre G, Cisse L, Laurent C, Massines F, Tiemblo P (1998) Spectral analysis of optical emission due to isothermal charge recombination in polyolefins. *IEEE Trans Dielectr Electr Insul* 5:527–535
10. Teyssedre G, Laurent C, Perego G, Montanari GC (2009) Charge recombination induced luminescence of chemically modified cross-linked polyethylene materials. *IEEE Trans Dielectr Electr Insul* 16:232–240
11. Shimizu N, Katsukawa H, Miyauchi M, Kosaki M, Horii K (1979) The space charge behavior and luminescence phenomena in polymers at 77 K. *IEEE Trans Electr Insul EI-14:256–263*
12. Lebey T, Laurent C (1990) Charge injection and electroluminescence as a prelude to dielectric breakdown. *J Appl Phys* 68:275–282
13. Yamamoto H, Mikami M, Nakamura S (2003) Nonlinear cathodoluminescence from insulators. *J Lumin* 102–103:782–784
14. Brillson LJ (2012) Applications of depth-resolved cathodoluminescence spectroscopy. *J Phys D Appl Phys* 45:183001
15. Teyssedre G, Franceschi JL, Laurent C (2007) Cathodo- and electro-luminescence spectra in insulating polymers: a parallel approach for inferring electrical ageing mechanisms. In: *Proceedings of the Conference of Electrical Insulation and Dielectric Phenomena (CEIDP)*, Vancouver, Canada, pp 824–827
16. Hagekyriakou J, Fleming RJ (1982) Determination of the kinetic order of thermoluminescence in the presence of a distribution of electron trap activation energies. *J Phys D Appl Phys* 15:163–176
17. Markiewicz A, Balbachas DV, Fleming RJ (1991) Simultaneous thermally stimulated luminescence and depolarization current in low density polyethylene. *J Therm Anal* 37:1137–1152
18. George T, Randle KJ (1975) The isothermal luminescence and thermoluminescence of gamma-irradiated polyethylene at 77 K. *J Phys D Appl Phys* 8:1585–1594
19. Becker RS (1970) *Theory and interpretation of fluorescence and phosphorescence*. Wiley
20. Ranby B, Rabek JF (1975) *Photodegradation, photo-oxidation and photostabilization of polymers: principles and applications*. Wiley
21. Delbecq CJ, Toyozawa Y, Yuster P (1974) Tunneling recombination of trapped electrons and holes in KCl:AgCl and KCl:TlCl. *Phys Rev B* 9:4497–4505

22. Butlers P, Tale I, Pospisil J, Nespurek S (1988) Self-trapping of charge carriers in polymers: a comparative study of poly(p-phenylene) and poly(n-vinylcarbazole). *Prog Coll Polym Sci* 78:93–96
23. Cordier P, Delouis JF, Kieffer F, Lapersonne C, Rigaut J (1974) Etude cinétique de la luminescence différée isotherme d'un verre organique après impulsion d'électrons accélérés. *C R Hebd Acad Sci C* 279:589–591
24. Charlesby A, Owen GP (1976) Luminescence enhancement in irradiated polyethylene. *Int J Radiat Phys Chem* 8:343–347
25. Massines F, Tiemblo P, Teyssède G, Laurent C (1997) On the nature of the luminescence emitted by a polypropylene film after interaction with a cold plasma at low temperature. *J Appl Phys* 81:937–943
26. Hama Y, Kimura Y, Tsumura M, Omi N (1980) Studies of the recombination of cation-electron pairs by long-range tunneling, as studied by ITL measurement in irradiated polymers. *Chem Phys* 53:115–122
27. Tiemblo P, Gomez-Elvira JM, Teyssède G, Massines F, Laurent C (1999) Effect of a cold helium plasma at $-180\text{ }^{\circ}\text{C}$ on polyolefin films—II: the chemiluminescence component. *Polym Degrad Stab* 64:67–73
28. Hagston WE (1975) Interpretation of electrophotoluminescence in terms of electron tunneling. *J Phys C: Solid State Phys* 9:647–661
29. Jonscher AK, de Polignac A (1984) The time dependence of luminescence in solids. *J Phys C: Solid State Phys* 17:6493–6519
30. Huntley DJ (2003) An explanation of the power-law decay of luminescence. *J Phys: Condensed Matter* 18:1359–1365
31. Balbachas DV, Fleming RJ (1992) Thermally simulated conductivity and luminescence in cross-linked polyethylene. In: *Proceedings of the IEEE Conference of Electrical Insulation and Dielectric Phenomena (CEIDP)*, Victoria, Canada, pp 93–98
32. Tiemblo P, Gomez-Elvira JM, Teyssède G, Laurent C (2000) Degradative luminescent processes in atactic polypropylene II: chemiluminescence after a cold He plasma attack at $-180\text{ }^{\circ}\text{C}$. *Polym Degrad Stab* 68:353–362
33. Tiemblo P, Gomez-Elvira JM, Teyssède G, Massines F, Laurent C (1998) Correlation between polypropylene microstructure, cold plasma interaction and subsequent luminescent emission. *Polym Int* 46:33–41
34. Tiemblo P, Gomez-Elvira JM, Teyssède G, Massines F, Laurent C (1999) Effect of a cold helium plasma at $-180\text{ }^{\circ}\text{C}$ on polyolefin films—I: plasma induced luminescence features of polyethylene and polypropylene. *Polym Degrad Stab* 64:59–66
35. Duran M, Massines F, Teyssède G, Laurent C (2001) Luminescence of plasma-treated polymer surfaces at ambient temperature. *Surf Coat Technol* 142:743–747
36. Jonsson J, Ranby B, Mary D, Massines F, Laurent C, Mayoux C (1995) An interpretation of electroluminescence of polyolefins based on the similarity between electro- and plasma-induced luminescence spectra. In: *Proceedings IEEE International Conference Solid Dielectric (ICSD)*, pp 701–705
37. Alison JM, Champion JV, Dodd SJ, Stevens GC (1995) Dynamic bipolar charge recombination model for electroluminescence in polymer-based insulation during electrical tree initiation. *J Phys D Appl Phys* 28:1693–1701
38. Zamoryanskaya MV, Trofimov AN (2013) Cathodoluminescence of radiative centers in wide-bandgap materials. *Opt Spectrosc* 115:79–85
39. Pope M, Kallmann HP, Magnante P (1963) Electroluminescence in organic crystals. *J Chem Phys* 38:2042–2043
40. Hartman WA, Armstrong HL (1967) Electroluminescence in organic polymers. *J Appl Phys* 38:2393–2395
41. Laurent C, Teyssède G, Le Roy S, Baudoin F (2013) Charge dynamics and its energetic features in polymeric materials. *IEEE Trans Dielectr Electr Insul* 20:357–381
42. George GA (1985) Characterization of solid polymers by luminescence techniques. *Pure Appl Chem* 57:945–954

43. Jacobson K, Eriksson P, Reitberger T, Stenberg B (2004) Chemiluminescence as a tool for polyolefin oxidation studies. *Adv Polym Sci* 169:151–176
44. Naveed KR, Wang L, Yu H, Ullah RS, Haroon M, Fahad S, Li J, Elshaarani T, Khana RU, Nazira A (2018) Recent progress in the electron paramagnetic resonance study of polymers. *Polym Chem* 9:3306–3335
45. Blakey I, George GA (2001) Simultaneous FTIR emission spectroscopy and chemiluminescence of oxidizing polypropylene: evidence for alternate chemiluminescence mechanisms. *Macromolecules* 34:1873–1880
46. Rychly JJ, Matisova-Rychla L, Tiemblo P, Gomez-Elvira J (2001) The effect of physical parameters of isotactic polypropylene on its oxidisability measured by chemiluminescence method: contribution to the spreading phenomenon. *Polym Degrad Stab* 71:253–260
47. Kron A, Stenberg B, Reitberger T, Billingham NC (1996) Chemiluminescence from oxidation of polypropylene: correlation with peroxide concentration. *Polym Degrad Stab* 53:119
48. Kron A, Reitberger T, Stenberg B (1997) Luminescence from γ - and β -irradiated HDPE and LLDPE. *Polym Int* 42:131–137
49. Owen EJ (ed) (1968) *Luminescence in chemistry*. Princeton, New Jersey
50. Koyanagi M, Zwarich RJ, Goodman L (1972) Phosphorescence spectrum of acetophenone: an example of pseudo-Jahn-Teller distortion. *J Chem Phys* 56:3044–3060
51. Jacques PPL, Poller RC (1993) Fluorescence of polyolefins-2: use of model compounds to identify fluorescent species in thermally degraded polymers. *Eur Polym J* 29:83–89
52. Chen L, Huan TD, Wang C, Ramprasad R (2015) Unraveling the luminescence signatures of chemical defects in polyethylene. *J Chem Phys* 143:124907
53. Tardieu G, Teyssedre G, Laurent C (2002) Role of additives as recombination centres in polyethylene materials as probed by luminescence techniques. *J Phys D Appl Phys* 35:40–47
54. Teyssedre G, Laurent C (2009) Semi-quantitative analysis of photoluminescence in thermoelectrically aged cables: I-Identification of optical signatures. *IEEE Trans Dielectr Electr Insul* 16:1180–1188
55. Teyssedre G, Laurent C, Montanari GC (2009) Semi-quantitative analysis of photoluminescence in thermoelectrically aged cables: II-analysis of a population of cables. *IEEE Trans Dielectr Electr Insul* 16:1189–1198
56. Teyssedre G, Laurent C, Campus A, Nilsson UH, Montanari GC (2003) Antioxidant and its reaction products as charge trapping centres in crosslinked polyethylene. In: *Proceedings of the IEEE International Conference on Electrical Insulation and Dielectric Phenomena (CEIDP)*, Albuquerque, USA, pp 96–99
57. Teyssedre G, Montanari GC, Laurent C, Campus A, Nilsson UH (2005) From LDPE to XLPE: investigating the change of electrical properties—Part 2: Luminescence. *IEEE Trans Dielectr Electr Insul* 12:447–454
58. Peruzzotti F, Martinotto L, Del Brenna M (2004) Cable, in particular for transport or distribution of electrical energy and insulating composition, US Patent 6696154
59. Teyssedre G, Tardieu G, Mary D, Laurent C (2001) AC and DC electroluminescence in insulating polymers and implication for electrical ageing. *J Phys D Appl Phys* 34:2220–2229
60. Laurent C, Massines F, Mayoux C, Ryder DM, Olliff C (1995) Comparison between photo- and electro-induced luminescence spectra of polyethylene. In: *Proceedings of the IEEE International Conference on Electrical Insulation and Dielectric Phenomena (CEIDP)*, Virginia Beach, USA, pp 95–96
61. Allen NS, Homer J, McKellar JE (1977) Origin and role of the luminescent species in the photo-oxidation of commercial polypropylene. *J Appl Polym Sci* 21:2261–2267
62. Bowen EJ (1968) *Luminescence in chemistry*. Van Nostrand, Toronto
63. Becker RS (ed) (1968) *Theory and interpretation of fluorescence and phosphorescence*. Wiley, New York
64. Williams I, Fleming DH (1973) *Spectroscopic methods in organic chemistry*. McGraw Hill, London
65. Klopffer W (1975) Luminescent groups in very weakly degraded polystyrene. *Eur Polym J* 11:203–208

66. Lamola AA (1967) Lowest π - π^* triplet state of acetophenone. *J Chem Phys* 47:4810–4816
67. Laurent C, Campus A et al (2003) Evaluation and modelling of thermoelectric ageing of XLPE insulated power cables: the ARTEMIS outcome. In: Proceedings of the 6th International Conference on Insulated Power Cables, JiCable, Versailles, pp 525–533
68. Herman H, Thomas J, Stevens G (2004) Spectroscopic and chemometrics analysis of cable condition in the Artemis program. In: Proceedings of the IEEE International Conference Solid Dielectrics (ICSD), Toulouse, France, pp 623–627
69. Le Roy S, Teyssède G, Laurent C (2005) Charge transport and dissipative processes in insulating polymers: experiments and model. *IEEE Trans Dielectr Electr Insul* 12:644–654
70. Pankove JI (ed) (1977) *Electroluminescence*. Springer, New York
71. Sanche L (1993) Electronic aging and related electron interactions in thin-film dielectrics. *IEEE Trans Electr Insul* 28:789–819
72. Zeller HR, Pflugner P, Bernasconi J (1984) High-mobility states and dielectric breakdown in polymeric dielectrics. *IEEE Trans Electr Insul* 19:200–204
73. Laurent C, Teyssède G, Montanari GC (2004) Time-resolved space charge and electroluminescence measurements in polyethylene under AC stress. *IEEE Trans Dielectr Electr Insul* 11:554–560
74. Teyssède G, Cisse L, Mary D, Laurent C (1999) Identification of the components of the electroluminescence spectrum of PE excited in uniform fields. *IEEE Trans Dielectr Electr Insul* 6:11–19
75. Qiao B, Laurent C, Teyssède G (2016) Electroluminescence and cathodoluminescence from polyethylene and polypropylene films: spectra reconstruction from elementary components and underlying mechanisms. *J Appl Phys* 119:024103
76. Teyssède G, Laurent C (2008) Evidence of hot electron-induced chemical degradation in electroluminescence spectra of polyethylene. *J Appl Phys* 103:046107
77. Qiao B, Laurent C, Teyssède G (2014) Evidence of exciton formation in thin polypropylene films under AC and DC fields and relationship to electrical degradation. In: Proceedings of the International Symposium on Electrical Insulating Materials (ISEIM), Niigata City, Japan, pp 81–84
78. Laurent C, Teyssède G (2003) Hot electron and partial-discharge induced aging of polymers. *Nucl Instr Meth Phys Res B* 208:442–447
79. Sanche L (1997) Nanoscopic aspects of electronic aging in dielectrics. *IEEE Trans Dielectr Electr Insul* 4:507–543
80. Teyssède G, Mary D, Augé JL, Laurent C (1999) Dependence of electroluminescence intensity and spectral distribution on ageing time in polyethylene naphthalate as modelled by space charge—modified internal field. *J Phys D Appl Phys* 32:2296–2305
81. Goldstein J, Newbury D, Joy D, Lyman C, Echlin P, Sawyer L, Michael J (2003) *Scanning electron microscopy and X ray microanalysis*. Kluwer Academic/Plenum Publishers, New York
82. Allen JW (1991) Impact processes in electroluminescence. *J Lumin* 48:18–22
83. Sanche L (1992) Dissociative attachment and surface reactions induced by low-energy electrons. *J Vac Sci Technol, B* 10:196–200
84. Ceresoli D, Righi MC, Tosatti E, Scandolo S, Santoro G, Serra S (2005) Exciton self-trapping in bulk polyethylene. *J Phys: Condens Mat* 17:4621
85. Bealing CR, Ramprasad R (2013) An atomistic description of the high-field degradation of dielectric polyethylene. *J Chem Phys* 139:1749043
86. Ceresoli D, Tosatti E, Scandolo S, Santoro G, Serra S (2004) Trapping of excitons at chemical defects in polyethylene. *J Chem Phys* 121:6478–6484
87. Mary D, Malec D (2001) Electroluminescence measurements to detect accumulated charge at the electrode-insulator interface. *IEEE Trans Dielectr Electr Insul* 8:771–775
88. See A, Fothergill JC, Dissado LA, Stevens GC, Montanari GC, Laurent C, Teyssède G (2001) Evaluation of the onset of space charge and electroluminescence as a marker for cross-linked polyethylene ageing. In: 4th International Conference on Electric Charges in non-Conductive Materials (CSC), Tours, France, pp 185–188

89. Gullo F, Villeneuve-Faure C, Le Roy S, Laurent C, Teyssedre G, Christen T, Hillborg H (2017) Impact of press-molding process on chemical, structural, and dielectric properties of insulating polymers. In: Proceedings of the 8th International Symposium on Electrical Insulating Materials (ISEIM), Toyohashi City, Japan, pp 69–72
90. Teyssedre G, Menegotto J, Laurent C (2001) Temperature dependence of the photoluminescence in Poly(ethylene terephthalate). *Polymer* 42:8207–8216
91. Li Y, Takada T (1992) Space charge distribution in multi-ply LDPE. In: Proceedings of the Conference Electrical Insulation and Dielectric Phenomena (CEIDP), Victoria, Canada, pp 397–402
92. Ghorbani H, Abid F, Edin H, Saltzer M (2016) Effect of heat-treatment and sample preparation on physical properties of XLPE DC cable insulation material. *IEEE Trans Dielectr Electr Insul* 23:2508–2516
93. Ohki Y, Hirai N, Kobayashi K, Minami R, Okashita M, Maeno T (2000) Effects of byproducts of crosslinking agent on space charge formation in polyethylene—comparison between acetophenone and α -methylstyrene. In: Proceedings of the IEEE Conference on Electrical Insulation and Dielectric Phenomena (CEIDP), Victoria, Canada, pp 535–538
94. Kalinowski J (1997) Chap 1. In: Miyata S, Nalwa HR (ed) *Organic electroluminescent materials and devices*. Gordon and Breach, New York

Chapter 7

XLPE Nanocomposites and Blends: Morphology and Mechanical Properties



K. C. Nimitha, Jiji Abraham, Soney C. George, and Sabu Thomas

1 Cross-Linked Polyethylene and XLPE Polymer Nanocomposites: Introduction

Polyethylene is being considered as a unique polymer in the whole plastic industry and it has numerous applications. Low-density polyethylene (LDPE) has tremendous electrical insulating properties, and therefore it has been using as a good insulator for the last 60 years. However, it has some demerits too. It always requires a low upper service temperature which makes it unsuitable for several applications like in hot water pipes. Several modifications have been done to improve the properties and the better strategy is the replacement of LDPE by cross-linked polyethylene (XLPE). XLPE has superior heat deformation characteristics [1].

Applications of cross-linked polyethylene include heat shrinkable products, chemical resistant seals, means for thermal insulation and food stuff packaging. It has a wide range to tolerate thermal shocks and electric loading. XLPE requires only a small thickness for insulation. These reasons make it as a suitable material for cable jacketing industry [2].

From 1994, various studies have been carried out on nanodielectrics. The interface zone generated by two different materials (nanomaterials and the polymer) will increase when the filler particles are in the nanometer scale. Nanotechnology provides an easy way to tune the properties of a composite by developing the

K. C. Nimitha · J. Abraham (✉)
Vimala College (Autonomous), Thrissur 680009, Kerala, India
e-mail: jijiabraham02@gmail.com

S. C. George
Centre for Nanoscience and Nanotechnology, Amal Jyothi College of Engineering,
Kottayam, Kerala, India

S. Thomas
International and Inter University Centre for Nanoscience and Nanotechnology,
Mahatma Gandhi University, Kottayam 686560, Kerala, India

structure and distribution of the filler in the polymer matrix [3]. Polymer composites containing nanosized fillers can drastically improve the electrical, mechanical and thermal properties without changing its compositions [4]. Polymer-based nanocomposite dielectrics have gained wide attention due to its unique structure and excellent performance. This is due to the nature of the interfacial region between the polymer and nanoparticles. L. Zhang used modified nano-SiO₂ and introduced into XLPE polymer and found that it shows good improvement in the conductance of DC current. It also increases the trap density and reduces charge injection. When the nanoparticles disperse in the matrix of polymer, it forms very strong interfacial forces with the matrix and improves the performance of composites like breakdown strength and field strength conductivity, etc. [5].

2 Processing of XLPE Polymer Nanocomposites

Polyethylene (PE) can be cross-linked to get cross-linked polyethylene using several methods. Methods can be classified as chemical and physical. Chemical methods include azo, peroxide and silane methods. Radiation is an example for physical method [2].

Nanomaterials can be incorporated into the polymer matrix by chemical or mechanical means. Homogeneous dispersion of nanoparticles in the polymer matrix is one of the major challenges faced during the fabrication of such materials. The nanofillers will always have the tendency to get agglomerated, thereby diminishing the properties of the same. This can be achieved by chemical methods, modified of nanofillers. Common methods for the fabrication of polymer—nanocomposites are given below:

- Direct mixing of polymer and nanofillers.
- Sol–Gel method.
- Intercalation method.
- In situ polymerization.

Direct mixing is a top-down approach and it is based on the breakdown of associated nanofillers during mixing process. In sol–gel method, solid nanoparticles are dispersed in the monomer solution and then polymerization process is carried out in the sol formed followed by hydrolysis. Intercalation is a top-down approach and it requires surface modification of nanofillers for the homogeneous dispersion. Melt intercalation is one of the most common methods used widely now. It involves mixing of fillers into the matrix at molten temperature. Melt blending is a similar process and involves the melting of polymer to form highly viscous solution followed by the addition of the nanofillers. The shape can be attained by methods like injection molding, compression molding, etc. In situ polymerization involves the swelling of the nanofillers in monomer solution and the polymer is seeped further. The other important methods are melt compounding and solvent method. In solvent

method, nanofillers and polymer are dissolved in a solvent and mixed. The resulting nanocomposites are obtained by removing the solvent by evaporation or solvent coagulation method [6]. Preparation of XLPE nanocomposites with different nanofillers is discussed below.

Preparation of XLPE/Silica Nanocomposites

XLPE/silica nanocomposites are prepared by twin screw extruder and injection molding methods. Here, granules of polyethylene are mixed with unmodified silica nanoparticles at a temperature of 120 °C for 10–15 min. Dicumyl peroxide (DCP) is used as cross-linking agent. The formed particles are termed as unmodified nanocomposites on which further surface modifications can be made. Schematic representation of preparation method for XLPE/SiO₂ nanocomposite can be given in Fig. 1.

Morphological studies show that nanofillers are not getting dispersed uniformly in the composites. This will clearly indicate the importance of surface modification on nanoparticles. Use of octylsilane modified silica nanoparticles enables higher interactions at the interface of nanofiller and polymer matrix. Octylsilane acts as a chemical adhesion between nanosilica and polymer matrix [7]. The melting of XLPE and nanocomposite is carried out in a torque rheometer. The samples were preheated for 3 min on plate vulcanizing press at 175 °C and 15 MPa [8]. XLPE/SiC nanocomposites can also be prepared in a similar way. Here, nanoparticles are uncoated silicon carbide (SiC) with particle size of 40 nm. Nanoparticles are dried in vacuum drier at 190 °C to avoid moisture. Then, SiC nanoparticles are mixed with PE in twin screw extruder. The mixing process lasts up to 20 min in this case. Here also, DCP is used as cross-linking agent. The samples are prepared then using plate curing machine and degassed in vacuum drier to remove residues [9].

Preparation of XLPE/TiO₂ Nanocomposites

For the preparation of XLPE/TiO₂ nanocomposites, rutile TiO₂ nanoparticles were selected as filler with diameter approximately 20–25 nm, and the dicumyl peroxide (DCP) was used as cross-linking agent. TiO₂/PE mixture was prepared by melting blend method in an opened type mixer at 115 °C. DCP is added and mixed in a

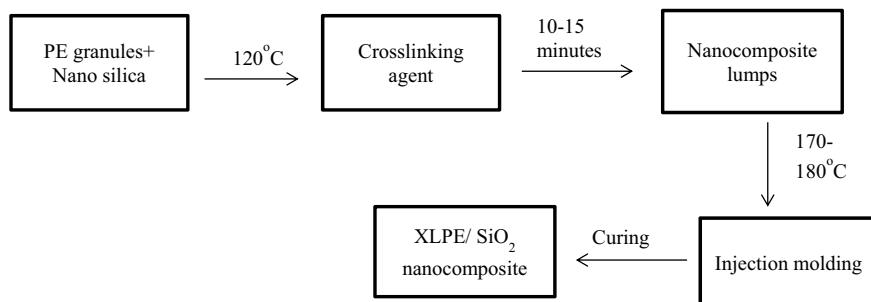


Fig. 1 Schematic diagram showing the preparation of XLPE/SiO₂ nanocomposite

Fig. 2 XLPE thin film samples [10]



close type mixture so as to avoid pre-cross-linking. Film samples are made out of it using a flat vulcanizing machine at 180 °C, 15 MPa. Prepared film samples are placed in a vacuum oven to eliminate the residual matter [10]. The film samples are shown in Fig. 2.

In solution mixing method, cross-linkable polyethylene pellets were used as the matrix resin, which contained dicumyl peroxide (DCP) and antioxidants. The average size of nano-TiO₂ particle is taken approximately as 40 nm. TiO₂ particles are vacuum dried before surface modification. The nanoparticles were then mixed in a suitable solvent like ethyl alcohol. It is then dispersed using a homogenization instrument. A suitable coupling agent is added into TiO₂/ethyl alcohol solution mixture in a beaker and ultrasonicated for 15 min at 60 °C. The obtained mixture is centrifuged for separation of solid and liquid. In order to remove ethyl alcohol, samples are dried in an oven. A torque rheometer was used to disperse the nanoparticles into the cross-linkable polyethylene pellets uniformly. The films were prepared by hot pressing at 140 °C for 20 min with a pressure of 10 MPa. Cross-linking by-products are removed by heating in vacuum oven [11].

Preparation of XLPE/ZnO Nanocomposites

XLPE/ZnO nanocomposites can also be prepared using melt mixing method. DCP is acting as the cross-linking agent and an antioxidant is also added during the preparation. The mixing is carried out in a mixture. The nanocomposites prepared are compression molded. High pressure should be applied, otherwise, escaped methane will form pores in the films [12].

Preparation of XLPE/MgO Nanocomposites

MgO nanocomposites can also be prepared by melt mixing method. Here, the coupling agent, (3-aminopropyl) triethoxysilane can be taken to modify the nanoparticles. Film samples can be obtained by using compression molding at the

temperature of 140 °C under the pressure of about 15 MPa. Then, the films are cooled. Films are then annealed in the vacuum oven to eliminate the residues [13]. Similarly, XLPE nanocomposites with different nanofillers can be prepared in this way.

3 Morphology of XLPE Nanocomposites

Studies show that the tendency of agglomeration of the nanofillers on XLPE can be controlled by the surface modification of nanofillers using suitable agents.

Morphology of XLPE/SiO₂ Nanocomposites

From the morphological study of XLPE SiO₂ nanocomposites, it is evident that XLPE pure crystals are spherulitic in nature and the size of particles is not uniform. Addition of surface-modified SiO₂ makes a difference. Here, SiO₂ acts as a nucleating agent for XLPE. This further causes a significant reduction in the particle size. Aminopropyl triethoxysilane (KH550), γ -(2, 3-epoxypropoxy) propyltrimethoxysilane (KH560) and triethoxyvinylsilane (A-151) are taken as surface modifiers here. With the addition of KH560, particle size is found to be smallest and the distribution is more uniform in this case. This causes a tremendous increase in the surface area of the materials and extends ways to several applications [8].

Morphology of XLPE/TiO₂ Nanocomposites

Figure 3 shows scanning electron microscopy (SEM) images of XLPE/TiO₂ nanocomposites. Here, dimethyloctylsilane (MDOS) is used as the surface modifier and it is added in different concentrations (1 and 5 wt%) to the nanofillers in order to study the effect of surface modifier on the filler.

It is seen that the dispersion of TiO₂ nanofillers is uniform in unmodified sample. But there is an unwanted agglomeration that occurs, and there for the particle size exceeds up to 400–600 nm. But on addition of MDOS, particle radius sharply decreased to 25–200 nm. Here, the chances of agglomeration are controlled by the reduction of free hydroxyl groups by the MDOS on the surface of TiO₂. Functional groups on MDOS replace the hydroxyl groups on TiO₂ and the dispersion of TiO₂ on XLPE is improved [10]. Similar trend is also observed in the case of XLPE/TiO₂ nanocomposites where KH560 is used as the coupling agent. From the SEM images of XLPE/TiO₂ and XLPE/TiO₂-KH560 nanocomposites in which composition of TiO₂ is 0.1 wt% at high magnification, it is clear that uniform dispersion of nanofillers on XLPE in presence of a coupling agent like KH-560 [11].

Morphology of XLPE/ZnO Nanocomposites

Transmission electron microscopy (TEM) images also provide a vivid picture about the dispersion of nanofillers in the composites. Figure 4 shows TEM images of XLPE/ZnO nanocomposites in which the filler is taken in different compositions 2, 5 and 10 wt%.

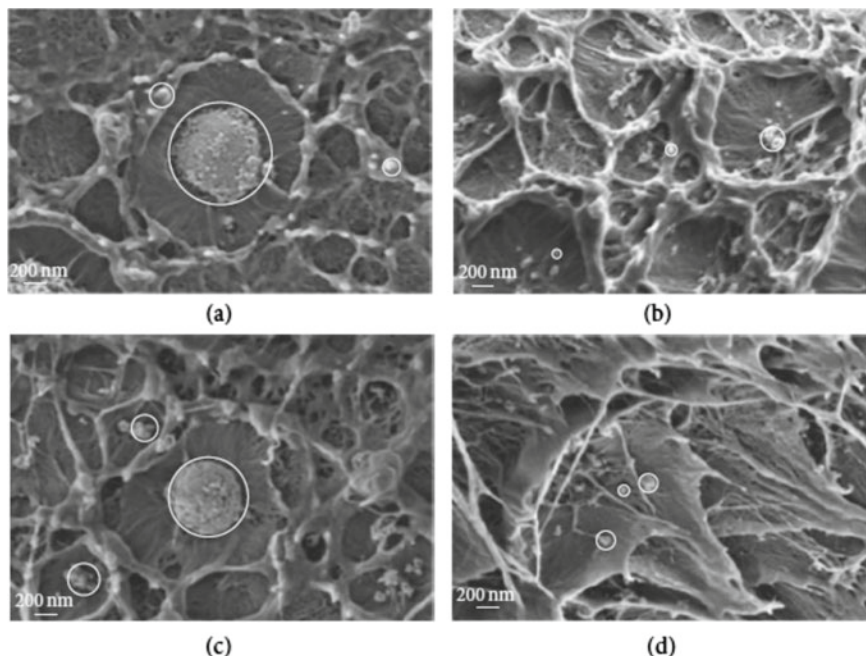


Fig. 3 SEM of TiO_2/XLPE . **a** UN- TiO_2/XLPE (1 wt%), **b** MDOS- TiO_2/XLPE (1 wt%), **c** UN- TiO_2/XLPE (5 wt%), and **d** MDOSTiO₂/XLPE (5 wt%) [10]

It is seen that as the concentration of filler increases, chances of agglomeration are also found to be increased. This observation says the importance of surface modification of the filler materials. ZnO is a typical inorganic material and XLPE is an organic material and therefore they need an interface to connect them. Presence of an alkyl group on the nanoparticles acts as a bridge between the filler and the polymer and this will enhance the nucleating ability of ZnO-like nanofillers on XLPE like polymers. TEM analysis thus gives a clear picture on the crystallization kinetics of nanoparticles on XLPE matrix [12].

Transmission electron microscopy images of XLPE nanocomposites with different nanofillers of same concentration are compared in Fig. 5. XLPE/ Al_2O_3 , XLPE/ TiO_2 and XLPE/clay nanocomposites show better dispersion. In XLPE/ SiO_2 nanocomposite, nanoparticle aggregation is more and large agglomerates are found. The reason for the better dispersion of nanofillers in XLPE matrix is the organic link on the surface [14].

Morphology of XLPE/Barium Titanate (BaTiO_3) Nanocomposites

Surface morphology of XLPE and XLPE/ BaTiO_3 nanocomposite can also be studied using SEM. Pure XLPE is characterized by a dark matrix in which barium titanate is dispersed uniformly which is observed as small bright domains.

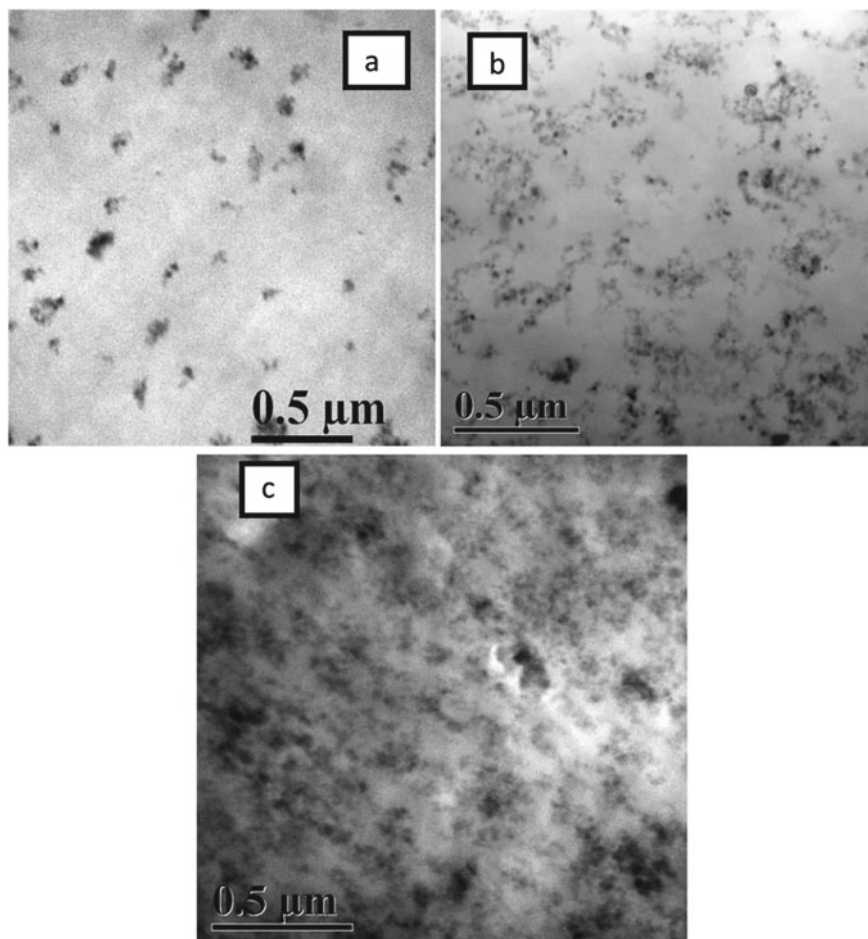


Fig. 4 Transmission electron micrographs of **a** XLPE/2 wt% ZnO nanocomposite, **b** XLPE/5 wt% ZnO nanocomposite and **c** XLPE/10 wt% ZnO nanocomposite [12]

Here also, well-dispersed nanoparticles are observed for low concentration nanofillers. A tear is observed on the surface when the filler is taken in a higher concentration which is shown in Fig. 8d [15].

Morphology of XLPE/Aluminum Hydroxide ($\text{Al}(\text{OH})_3$) Nanocomposites

XLPE consists of well-ordered crystalline lamellar ribbons to form spherulites. It is generally having diameters more than 10 μm. Addition of nanosized $\text{Al}(\text{OH})_3$ has a slight influence on crystallinity and a great influence on spherulite size. It is due to the nucleation process. Here, hexadecyltrimethoxysilane is used as the coupling agent. The chemical and physical nature of modified nano- $\text{Al}(\text{OH})_3$ enables it to act

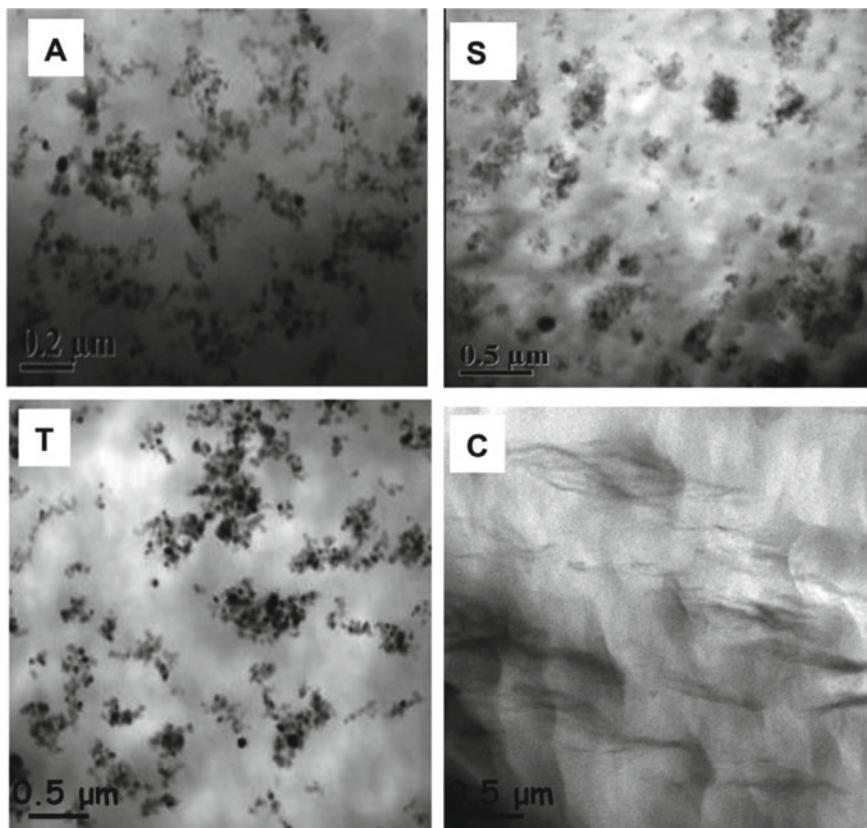


Fig. 5 TEM images of XLPE with Al_2O_3 (A), SiO_2 (S), TiO_2 (T) and clay nanocomposites at 5 wt% filler concentration [14]

as a nucleating center. It increases the number and reduces the size of spherulites [16]. Similar trend is also observed for XLPE/other nanocomposites. The specimens were quenched in liquid nitrogen, and the section was sprayed with gold before observing the samples under microscope [17]. BNNSs can be observed clearly, and they are dispersed uniformly in the polymer matrix. For high concentration, the quantity of BNNSs upsurges considerably and there do not have noticeable agglomeration phenomenon. Further, the element analysis of BN nanosheets labeled with the black arrow was carried out by the Phenom SEM. It can be seen that nitrogen can be observed about 34.57 wt%, while boron is not apparent, only 8.97 wt%, this may be because boron and carbon are adjacent to each other in the periodic table, and the device cannot identify them.

4 Mechanical Properties

Polymers are considered to be viscoelastic materials having intermediate properties between viscous liquids and elastic solids. Practical applications as well as strength and durability of polymeric materials can be amended by the introduction of a wide variety of nanosized fillers. The reinforcing behavior in polymer nanocomposites is explained by several mechanisms. Among these one is based on the establishment of hydrodynamic (volumetric) interaction between filler and polymer chains rather than filler agglomeration or percolation [18]. Area of this interfacial region can be upgraded either by increasing the surface area of filler or by its surface modification. In contrary to above finding, Dorigato et al. demonstrated primary nanoparticle aggregation is the important parameter responsible for reinforcement effect rather than the filler polymer interaction at the interface [19]. Formation of three-dimensional filler network is another possible mechanism for reinforcement. According to Perez-Aparicio, the reinforcement mechanism is based on the filler–matrix interaction at filler surface and this macromolecular chain adsorption results in increased amount of immobilized macromolecular chains at the vicinity of fillers (an increased density of trapped entanglements). The mechanical stiffening of interphase region because of the presence of immobilized macromolecular chains is considered as further reinforcing component of the system.

4.1 Stress–Strain Behavior

The tensile modulus (measure of stiffness) and yield strength (measure of onset of viscoelastic deformation) of materials are important selection parameters determining final applications. Figure 6 shows the stress–strain behavior of neat XLPE and nanocomposites. All the samples show a linear elastic behavior followed by an inelastic plastic deformation. It can be seen that all the composites exhibit higher stress values than the unfilled systems over the entire range of strain. The tensile strength of the nanocomposites shows higher values compared to the neat XLPE. The hybrid nanocomposite of Al_2O_3 :clay = 1:1 shows the highest yield strength. The presence of clay platelets reduces the aggregation tendency of alumina nanoparticles, and due to the difference in surface characteristics between nanoparticles, it is dispersed properly. Such synergistic interactions result in a unique microstructural development which explains the very high increase in yield strength and Young's modulus value [20] (Fig. 6).

Stress–strain behavior of XLPE/ Al_2O_3 -clay hybrid nanocomposites above melting temperature is used to get an idea about network structure of the system. Total network density has contribution both from chemical cross-links and physical networks. Nanoreinforcement can contribute toward both chemical cross-links and physical networks by immobilized polymer fractions. Here, the ternary hybrid system, i.e., XLPE contains two fillers (Al_2O_3 :clay = 1:1) showed better

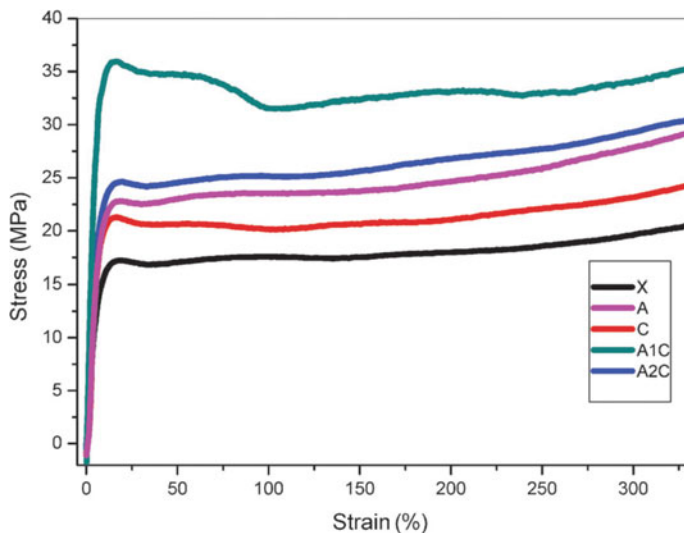


Fig. 6 Stress–strain behavior of XLPE (X), XLPE/Al₂O₃ (A), XLPE/clay (C), XLPE/Al₂O₃: clay = 1: 1 (A1C), XLPE/Al₂O₃: clay = 2: 1 (A2C) [20]

performance than binary systems. This is due to the synergism between the fillers. As the concentration of alumina, doubled modulus value decreased due to the self-aggregation of alumina over the interaction between alumina and clay [21]. XLPE nanocomposites exhibited superior network density that the neat XLPE polymer. When a nanoparticle is incorporated into polymer matrix, three regions are generated. Polymer interacts with forms a rigid phase. The second region consists of polymer chains strongly bound to the rigid phase. The loose region (third region) is a zone loosely coupled to the second region. It has a different chain structure and mobility and free volume compared to the polymer [22]. A hypothetical model indicating the rigid amorphous fraction is given in Fig. 7.

Polyethylene is cross-linked using various types of cross-linking agents' better physical properties. There are three methods for preparing cross-linked PE industrially: cross-linking with radiation, cross-linking with peroxide and cross-linking with water. Cross-linking with water is achieved by grafting with silane, followed by hydrolysis to Si–OH groups and subsequently condensation to form Si–O–Si bonds. Kuan et al. investigated the effects of varied cross-linking time on the mechanical properties of the cross-linked polyethylenes. Mechanical properties especially tensile strength, flexural strength, flexural modulus, and notched Izod impact strength of water cross-linked LDPE was increased with increasing cross-linking time [23]. The influence of gamma irradiation on the mechanical properties of linear low-density polyethylenes (LLDPE) has been investigated. Radiation cross-linked polyethylene cross-linked by radiation belongs to the economically most efficacious products of radiation chemistry research. Cross-linking with gamma irradiation is the widest used technique [24]. The mechanical

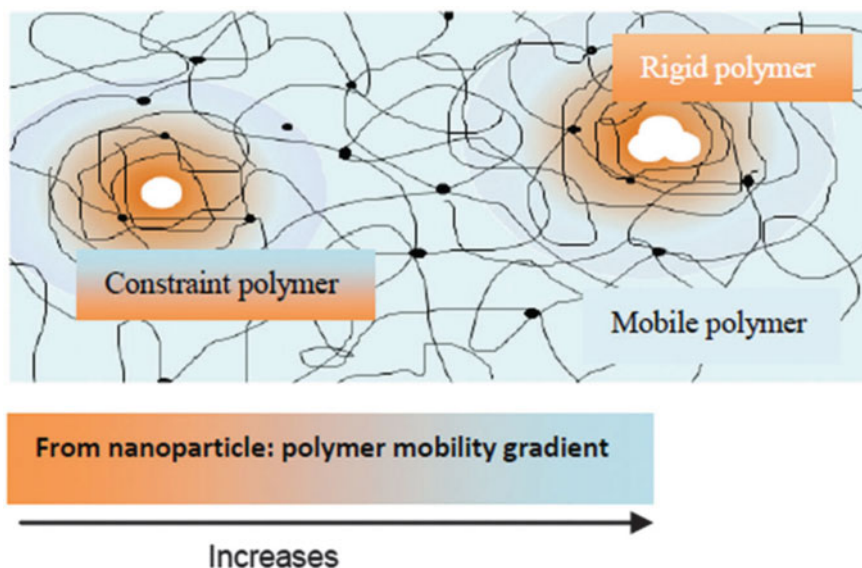


Fig. 7 Schematic representation of polymer chain dynamics in nanocomposites [20]

properties of uncross-linked and cross-linked LLDPE are summarized in Table 1. Young's modulus increase with an increase in radiation dose and this is due to the increase in crystallinity after radiation. The cross-linking does not have a significant influence on the yield stress. Elongation at yield, elongation at break and stress at break strongly depend on the radiation dose [25]. Khonakdar et al. made an investigation of chemical cross-linking effect on properties of high-density polyethylene. It is observed that at any specific temperature, the elongation at break, yield strength and tensile strength at break are generally diminished with augmented peroxide content. Table 1 illustrates the effect of temperature and peroxide content on the tensile properties of cross-linked high-density polyethylene. At room temperature, both physical cross-links (crystalline ties) and chemical cross-links are observed between polymeric chains. As the number of chemical cross-links increases, which are stronger than the physical cross-links, the restriction executed on elongational behavior of the polymer upsurges. As a result, mechanical characteristics of polymer improved with increase in cross-linking agent. With increase in temperature, the physical cross-links are weakened as a result of disappearance of the crystallites. So, there is reduction in the mechanical performance [26]. Azizi et al. studied the effect of alumina trihydrate (ATH) and antimony trioxide (Sb_2O_3) in the mechanical characteristics of uncross-linked and silane cross-linked low-density polyethylene. Table 1 displays the tensile strength and elongation at break of neat LDPE (sample A), XLPE (sample D), LDPE-ATH (sample B), XLPE-ATH (sample E), LDPE- Sb_2O_3 (sample C) and XLPE- Sb_2O_3 (sample F). Addition of ATH and Sb_2O_3 decreases the tensile strength and

Table 1 Effect of ATH and Sb₂O₃ on tensile properties of XLPE [27]

Sample	Elongation at break (%)	Tensile strength (N/mm ²)	Sb ₂ O ₃ (phr)	ATH (phr)
A	576	12.2	0	0
B	23	8.4	0	30
C	48	10.5	30	0
D	395	14.5	0	0
E	22	11.7	0	30
F	30	12.7	30	0
G	23	11.7	15	15

elongation at break. This is possibly due to poor interactions between the polymer chains and the filler. In contrast, with cross-linking of LDPE, tensile strength improves (samples E, F, G, B, C) [27].

Roumeli et al. introduced some micromechanical modeling to predict the enhanced mechanical properties of multi-walled carbon nanotubes reinforced cross-linked high-density polyethylene [28]. A significant improvement of mechanical properties was found for all nanocomposites. There was a major turning point of the elastic and deformation behavior of these composites as a consequence of filler content. A modern three-phase approach accounting for the matrix, aggregated and finely dispersed filler states adequately define the experimental data below the turning point, while for higher concentrations, a standard two-phase model is selected to describe the nanocomposites' elastic behavior. This behavioral change can be accredited to the contribution of two competitive mechanisms governing the introduction of MWCNTs in cross-linked polyethylene a tendency to improve the mechanical properties of cross-linked polyethylene by load transfer and an effort to form bundles that decrease the progressive effect on these properties. Evidence of both these competitive mechanisms was found by micro-Raman spectroscopy and SEM observations of the failure surfaces.

4.2 Dynamic Mechanical Properties

4.2.1 Storage Modulus and Loss Modulus

Jose et al. studied dynamic mechanical properties of alumina–clay nanoscale hybrid filler-based cross-linked polyethylene nanocomposites. Storage modulus and loss modulus of XLPE and nanocomposites as a function of temperature are given in Fig. 8. Nanocomposites exhibit high storage modulus value than neat polymer due to the reinforcing effect of fillers. When the temperature is lower than -100 °C, the storage modulus decreases rapidly, and then it decreases gently at the temperature range lower than -50 °C. In a temperature range of -50 °C to 25 °C, the storage

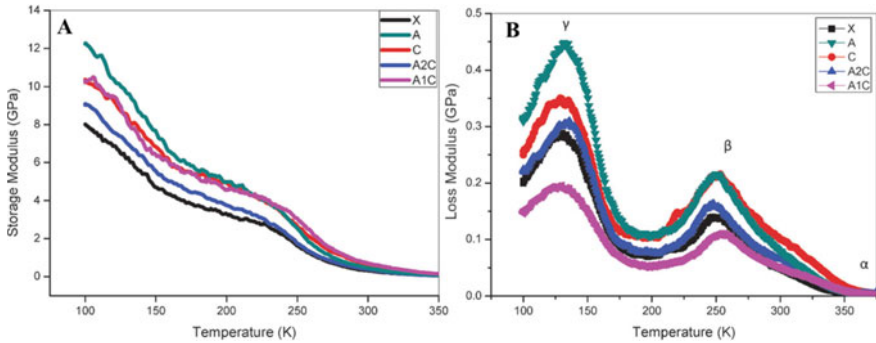


Fig. 8 **a** Storage modulus XLPE and nanocomposites as a function of temperature, **b** loss modulus of XLPE and nanocomposites as a function of temperature. XLPE–Al₂O₃–clay hybrid ternary composites of Al₂O₃ and clay in 1:1 and 2:1 composition [20]

modulus decreases quickly with a rise in temperature, and then it decreases slightly. At high temperature, molecular chain motion is enhanced and thus there is a reduction in storage modulus values. The α , β and γ transitions could be identified using a loss modulus versus temperature curve: γ at -120 °C, glass transition, β at 0 °C, side chain movement, α at 80 °C, orientation motion in crystals. Loss modulus values of nanocomposites are higher than neat polymer and this is because of the excessive heat generation within the polymer composite system [19].

4.2.2 Estimation of Effectiveness of Filler (Coefficient ‘ β_f ’)

$$\beta_f = \frac{\left(\frac{E'_g}{E'_r}\right)_{\text{Composite}}}{\left(\frac{E'_g}{E'_r}\right)_{\text{Pure}}} \tag{1}$$

where E'_g and E'_r are the storage modulus values in the glassy and rubbery regions, respectively. The low value of β_f shows the better effectiveness of the nanofiller. The lower the value of the constant β_f , the higher the effectiveness of the filler. The values of ‘ β_f ’ obtained for different composites are given in Table 2. The effectiveness of the filler is highest for Al₂O₃:clay = 1:1. Maximum stress transfers between the matrix and the filler and takes place for this composition. The superior properties obtained for tensile strength and Young’s modulus can be correlated to this result.

4.2.3 Estimation of Constrained Region

For linear viscoelastic behavior, the energy loss fraction of the polymer nanocomposite W is related to $\tan\delta$ by the following equation

Table 2 Storage modulus at 100 K, 300 K and the coefficient ' β_f ' for neat XLPE and nanocomposites [19]

Sample	Storage modulus at 100 K (GPa)	Storage modulus at 300 K (GPa)	Coefficient ' β_f '
X	8	0.3	–
A	12.2	0.5	0.76
C	10.4	0.6	0.65
A1C	10.4	0.7	0.55
A2C	9	0.4	0.84

$$W = \frac{\pi \tan \delta}{\pi \tan \delta + 1} \quad (2)$$

The energy loss fraction W at the $\tan \delta$ peak is given by the following equation

$$W = \frac{(1 - C_v)W_0}{1 - C_0} \quad (3)$$

where C_v is the volume fraction of the constrained region ($1 - C_v$) is the fraction of the amorphous region and W_0 and C_0 represent the energy fraction loss and volume fraction of the constrained region for pure XLPE, respectively. From the estimated constrained region, it is clear that filler-filler networks and reinforcing effects lead to the formation of an efficient constrained region. Hybrid fillers make the polymer chains less mobile as compared with single filler.

4.2.4 Dissipation Factor

Deviation in the dissipation factor (ratio of loss modulus to storage modulus) as a function of temperature with different nanocomposites is plotted in Fig. 9. It can be seen that the height of the $\tan \delta$ peak (glass transition) declines with the incorporation of nanoreinforcement. This indicates that the mobilization of polymer chains was constrained due to the incorporation of a nanoreinforcement. Reduced chain movement due to the physical and chemical adsorption of the polymer chain segments on the filler surface causes a height reduction of the $\tan \delta$ peak during dynamic mechanical deformation. A decrease in the $\tan \delta$ peak proves minimum heat build-up as a result of lesser damping characteristics for the compounds containing nanofillers.

Haddou et al. studied the mechanical relaxation modes of bamboo flour (BF)-reinforced XLPE composites. Dynamic mechanical analysis demonstrates that the addition of BF increases the glassy modulus due to van der Waals interactions (Fig. 10). This result is augmented in XLPE/BF due to polar interactions generated by the coupling agent. The amount of 5 mass% of coupling agent corresponds to an optimum of viscoelasticity. Above this critical content, the storage modulus reduces

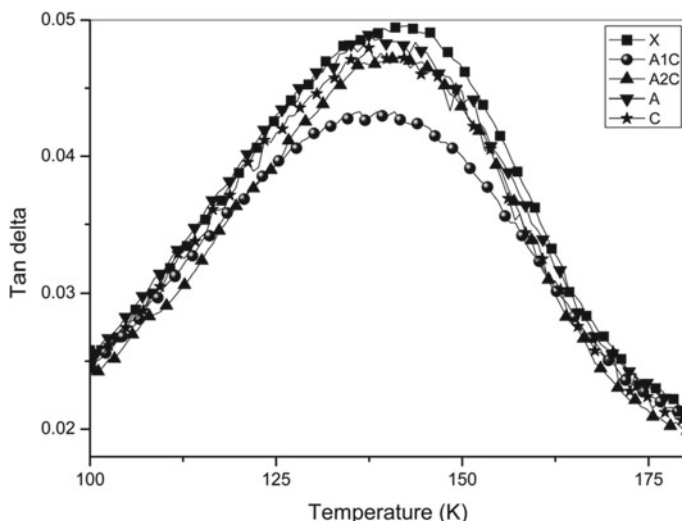


Fig. 9 $\tan\delta$ values of XLPE and nanocomposites [21]

because of the bad interphase created. The inelastic relaxation modes of XLPE/BF composites are located at the same temperatures than for the XLPE matrix showing the absence of plasticization independently from the coupling agent content. The γ relaxation located at -120 °C relates to the viscoelastic energy loss related to the glass transition of the amorphous phase free from chemical defects. It exhibits, around -80 °C, a shoulder peak which corresponds to bamboo flour within the amorphous XLPE phase. The α_c mode, situated around 40 °C, has been associated with the mobility in the interfacial regions. In XLPE, this molecular mobility is located at the periphery of crystallites. Since its magnitude of the α_c mode is higher in all XLPE/BF composites, the mobility at the periphery of BF is also involved [29].

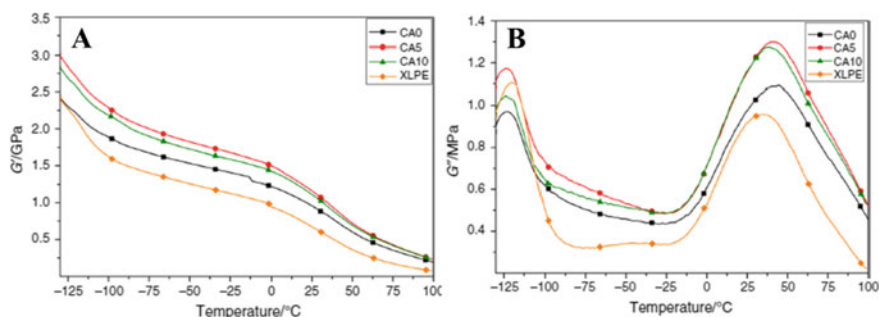


Fig. 10 **a** Storage modulus G' for XLPE and XLPE/BF composites, **b** loss modulus G'' for XLPE and XLPE/BF composites [29]

5 Conclusion

We have reviewed mechanical and morphological characteristics of XLPE-based nanocomposites and blends. Several methods have been introduced to fabricate nanocomposites. Among these melt mixing is the most adopted one. Static mechanical behavior is illustrated by studying the stress–strain behavior using tensile testing. Dynamic mechanical analysis done to know about the viscoelastic behavior of prepared nanocomposites. From DMA analysis, we got information about effectiveness of filler (coefficient ' β_f '), amount of constrained region and dissipation factor.

References

1. Nilsson S, Hjertberg T, Smedberg A (2010) Structural effects on thermal properties and morphology in XLPE. *Eur Polymer J* 46:1759–1769
2. Morshedian J, Hoseinpour PM (2009) Polyethylene cross-linking by two-step silane method: a review. *Iran Polym J* 18(2):103–128
3. Zhong S-L, Dang Z-M, Zhou W-Y, Cai H-W (2018) Past and future on nanodielectrics. *IET Nanodielectr* 1(1):41–47
4. Mansor NS, Ishak D, Mariatti M, Halim HSA, Basri ABA, Kamarol M (2017) Investigation on electrical treeing characteristics of XLPE containing ZnO nano-filler. In: *Proceedings of ISEIM 2017 Conference*
5. Oonghel O, Xiu Feng L, Jin S, Peijie Y, Youfu C (2017) The influence of surface modifier on structural morphology and dielectric property of XLPE/SiO₂ nanocomposites. In: *1st International Conference on Electrical Materials and Power Equipment*. Xi'an, China
6. Tanahashi M (2010) Development of fabrication methods of filler/polymer nanocomposites: with focus on simple melt-compounding-based approach without surface modification of nanofillers. *Materials* 3:1593–1619
7. Sharad PA, Sathish Kumar K (2017) Application of surfacemodified XLPE nanocomposites for electrical insulation—partial discharge and morphological study. *Nanocomposites* 3 (1):30–41. <https://doi.org/10.1080/20550324.2017.1325987>
8. Kaihao J, Donghe D, Richang X, Xiaoqui Wang, Peijie Y, Xiu Feng L (2018) Study on dielectric structure and space charge behavior of XLPE/SiO₂ nanocomposites. In: *12th IEEE International Conference on the Properties and Applications of Dielectric Materials*. Xi'an, China
9. Wang Y, Wang C (2015) Effect of nanoparticles on space charge behavior of XLPE/SiC nanocomposites. In: *2015 Annual Report Conference on Electrical Insulation and Dielectric Phenomena*
10. Wang Y, Xiao K, Wang C, Yang L, Wang F (2016) Effect of nanoparticle surface modification and filling concentration on space charge characteristics in TiO₂/XLPE nanocomposites. Hindawi Publishing Corporation. *J Nanomater* 2016(Article ID 2840410):10pp. <http://dx.doi.org/10.1155/2016/2840410>
11. Wang S, Chen P, Yu S, Zhang P, Li J, Li S (2018) Nanoparticle dispersion and distribution in XLPE and the related DC insulation performance. *IEEE Trans Dielectr Electr Insul* 25(6):Dec
12. Jose JP, Chazeau L, Cavaille JY, Varughese KT, Thomas S (2014) Nucleation and nonisothermal crystallization kinetics in cross-linked polyethylene/zinc oxide nanocomposites. *RSC Adv* 4:31643

13. Peng S, He J, Hu J, Huang X, Jiang P (2015) Influence of functionalized MgO nanoparticles on electrical properties of polyethylene nanocomposites. *IEEE Trans Dielectr Electr Insul* 22 (3):June
14. Jose JP, Abraham J, Maria HJ, Varughese KT, Thomas S (2016) Contact angle studies in XLPE hybrid nanocomposites with inorganic nanofillers. *Macromol Symp* 366:66–78
15. Madani L, Belkhat S, Berrag A, Nemdili S (2015) Investigation of dielectric behavior of water and thermally aged of XLPE/BaTiO₃ composites in the low-frequency range. *Int J Mod Phys B* 29(27):1550186, 23pp
16. Wang S, Chen P, Xiang J, Li J (2017) Study on DC breakdown strength and morphology in XLPE/Al(OH)₃ nanocomposites. In: *Proceedings of ISEIM 2017 Conference*
17. Li G, Zhou X, Wei Y, Hao C, Lei Q (2019) Effect of BN nanosheet concentration on space charge characteristics in XLPE/BNNS nanocomposites. *Mater Res Express* 6:115080
18. Heinrich G, Klüppel M, Vilgis TA (2002) Reinforcement of elastomers. *Curr Opin Solid State Mater Sci* 6(3):195–203
19. Dorigato A, Dzenis Y, Pegoretti A (2013) Filler aggregation as a reinforcement mechanism in polymer nanocomposites. *Mech Mater* 61:79–90
20. Jose JP, Thomas S (2014) Alumina–clay nanoscale hybrid filler assembling in cross-linked polyethylene based nanocomposites: mechanics and thermal properties. *Phys Chem Chem Phys* 16:14730
21. Jose JP, Thomas S (2014) XLPE based Al₂O₃–clay binary and ternary hybrid nanocomposites: self-assembly of nanoscale hybrid fillers, polymer chain confinement and transport characteristics. *Phys Chem Chem Phys* 16:20190
22. Abraham J, Thomas J, Kalarikkal N, George SC, Thomas S (2018) Static and dynamic mechanical characteristics of ionic liquid modified MWCNT-SBR composites: theoretical perspectives for the nanoscale reinforcement mechanism. *J Phys Chem B* 122:1525–1536
23. Kuan H-C, Kuan J-F, Ma C-CM, Huang J-M (2005) Thermal and mechanical properties of silane-grafted water crosslinked polyethylene. *J Appl Polym Sci* 96:2383–2391
24. Narkis M, Raiter I, Shkolnik S, Siegman A, Eyerer P (1987) *J Macromol Sci Phys B* 26:37
25. Krupa I, Luyt AS (2001) Thermal and mechanical properties of LLDPE cross-linked with gamma radiation. *Polym Degrad Stab* 71:361–366
26. Khonakdara HA, Morshedian J, Wagenknecht U, Jafari SH (2003) An investigation of chemical crosslinking effect on properties of high-density polyethylene. *Polymer* 44:4301–4309
27. Azizi H, Barzin J, Morshedian J (2007) Silane crosslinking of polyethylene: the effects of EVA, ATH and Sb₂O₃ on properties of the production in continuous grafting of LDPE. *eXPRESS Polym Lett* 1(6):378–384
28. Roumeli E, Pavlidou E, Bikiaris D, Chrissafis K (2014) Microscopic observation and micromechanical modeling to predict the enhanced mechanical properties of multi-walled carbon nanotubes reinforced crosslinked high density polyethylene. *Carbon* 67:475–487
29. Haddou G, Dandurand J, Dantras E, Maiduc H, Thai H, Giang NV, Trung TH, Pontains P, Lacabanne C (2016) Mechanical and thermal behaviour of bamboo flour-reinforced XLPE composites. *J Therm Anal Calorim* 124:701–708

Chapter 8

Thermal and Flame Retardant Properties of XLPE Nanocomposites and Blends



Jiji Abraham, K. C. Nimitha, Soney C. George, and Sabu Thomas

1 XLPE Nanocomposites and Blends

Polymer matrix composites with suitable inorganic nanofillers have been receiving much attention recently because of their novel characteristic properties such as extraordinary mechanical properties, tremendous thermal resistance and good chemical reagent inertness. Incorporation of nanosized fillers into the polymer matrix uniformly enhances the properties of polymeric materials which include optical, electrical and magnetic properties. The nanocomposites are potential candidates for catalysts, contact lenses, gas separation membranes and bio-active implants [1].

Similarly, polymer blends have also gained great attraction since they play an vital role in the modern polymer industry due to the development of novel materials and also for practical recycling. The properties of blends can be modified by changing the ratio and types of polymers that are getting mixed. But sometimes, polymer blends tend to form aggregates and separate out due to the unfavorable enthalpy of mixing and it will adversely affects the mechanical properties. So, it always requires enhancement in the interface properties of polymer blends. One of the most efficient ways to do this is the addition of copolymers. Copolymers should be compatible with both the phases, thereby providing good interfacial interaction. An example for this strategy is the copolymer incorporated polyamide/

J. Abraham (✉) · K. C. Nimitha
Vimala College (Autonomous), Thrissur 680009, Kerala, India
e-mail: jijiabraham02@gmail.com

S. C. George
Centre for Nanoscience and Nanotechnology, Amal Jyothi College of Engineering,
Kottayam, Kerala, India

S. Thomas
International and Inter University Centre for Nanoscience and Nanotechnology,
Mahatma Gandhi University, Kottayam 686560, Kerala, India

polyphenylene oxide (PA/PPO) blend. This method faces some challenges also. Major drawback is the effect of copolymers on the strength of blends which makes them soft. Sometimes, the addition of a copolymer adversely affects the mechanical properties. Cost of production is another challenge faced. Other methods are also available for the processing of polymer blends which shows tremendous characteristic features [2]. The chapter focuses on the flame retardant and thermal properties of XLPE nanocomposites and blends.

2 Thermal Properties

Properties of composites and blends are highly temperature dependent. There are transition properties like flexibility and brittleness which depend upon the melting temperature (T_m) and the glass transition temperature (T_g). Thermal behavior of composites and blends depend upon the additives, fillers, etc., and thus these are not intrinsic properties as well.

2.1 Heat Capacity

Specific heat or heat capacity is the amount of heat per unit mass that is required to raise the temperature by 1 °C. It is very much essential in thermodynamic analysis and involves both first and second law of thermodynamics. Heat capacity per unit mass can be expressed as

$$C = \frac{\delta q}{\delta T} \quad (1)$$

where δq is the heat absorbed by the system and δT is the infinitesimal temperature change occurred during the process [3]. It is an important factor that determines the processing of materials. At normal temperatures, amorphous materials are having a heat capacity in the range 0.9–1.6 J/g K. Heat capacities of semicrystalline materials are in the range 0.9–2.3 J/g K. Specific heat of materials is measured using the ASTM C351 standard test [4].

2.2 Thermal Stability

Thermal stability of polymer is the capacity to resist the action of heat. Thermally stable materials have the ability to sustain their properties like strength, toughness or elasticity at a particular temperature. Thermogravimetric analysis (TGA) is used to check the thermal stability of polymers. Molecular weight and chemical structure

of polymers are the two factors which affect its thermal stability. Aromatic structure and C–C backbones help to increase the thermal stability of polymeric materials. Generally, polymers are having low thermal stability and it thus limits the applications also. Organic polymers decompose at temperatures from 150 to 300 °C. So it will definitely affect the processing of polymers. Decomposition of polymer chains depends on heating rate, heating temperature and the chemical modifications take place on polymers. The degradation of polymer can be initiated by heat and by oxidation reactions. The degradation highly depends on the chemical structure of polymer. Generally, groups like C–O and end groups like –OH decreases the thermal stability of polymer. Polymers having bonds like Si–O, C–X and Si–N contributes to higher thermal stability. So modifications are required to enhance the thermal stability of polymers. Incorporation of nanofillers to polymers is one of the efficient methods to improve the thermal stability of polymers. Surface-modified nanofillers incorporated polymer matrix can show good thermal stability [5].

2.3 Thermal Expansion

Thermal expansion is the tendency of a material to vary the volume when temperature gets changed. When a substance is heated, particles are free to move and thus intermolecular distances are increased. The expansion rate of material is expressed in terms of thermal expansion coefficient. It is a very important structural designing parameter and it depends on the size, thermal shock resistance and stress distribution of materials [6]. Two components of thermal expansion coefficient are linear expansion coefficient and volume expansion coefficient. Linear expansion coefficient is the ratio of degree of linear expansion to the change in temperature. It is designated as α_L and is given by,

$$\alpha_L = \left(\frac{\partial L}{\partial T} \right) \cdot \left(\frac{p}{L} \right) \quad (2)$$

Volume expansion coefficient is the ratio of volume expansion to the change in temperature. It is designated as β and is given by,

$$\beta = \left(\frac{\partial V}{\partial T} \right) \cdot \left(\frac{p}{V} \right) \quad (3)$$

Coefficient of thermal expansion can be quantitatively analyzed using thermo-mechanical analysis (TMA) and dilatometers can also be used for the same. Dilatometers can be used for the analysis of materials with low α_L values [7]. Thermal expansion coefficients of polymers are generally positive and are termed as hot expansion and cold shrinkage. Materials with negative coefficient of thermal expansion are termed as hot shrinkage and cold expansion. This is because when the temperature varies, the amplitude of interacting particle changes

Table 1 Linear thermal expansion coefficient of materials ($10^{-6}/\text{K}$) [6]

Material	α
Quartz glass	0.5
Aluminum	25
Copper	15
Iron	12
SiC	3.5
Polyethylene	120
Polypropylene	100
Polystyrene	80
Polytetrafluoroethylene (PTFE)	140
Rubber	250

asymmetrically. If this change influences on the interacting particle's outer side, then such materials undergo hot expansion and cold shrinkage. If the change experiences on the internal side, then materials show hot shrinkage and cold expansion. Table 1 shows the values of linear thermal expansion coefficients of some materials [6].

2.4 Thermal Conductivity

Process of conduction of heat from one part to another of an object is termed as heat conduction. Concept of thermal conductivity is put forward by Joseph Fourier from France in 1822. He gave a very important expression for thermal conductivity [8]. It is the rate of transmission of heat through a material of unit area of cross section and a unit thickness for a unit change in temperature. It can be represented as 'k'.

$$k = \frac{\Delta Q}{\Delta t} \cdot \frac{1}{A} \cdot \frac{x}{\Delta T} \quad (4)$$

where $\Delta Q/\Delta t$ is the rate of heat flow, A is the area of cross section, x is the thickness and ΔT is temperature difference. The unit of thermal conductivity is $\text{Wm}^{-1}\text{K}^{-1}$. Thermal conductivity can be considered as a transport property since it involves the energy transfer in a solid or fluid. Energy transport in solids is due to the movement of electrons and lattice vibration [7]. Thermal conductivity for different materials varies as a function of temperature, and even for the same materials, thermal properties varies with density.

The thermal diffusivity β defines the rate of temperature change and is associated with the heat transmission. It is a combination of thermal conduction change and temperature change. Higher the value of β , lesser the temperature change at the different areas of matter, and thus the temperature of the material tends to be

uniform. Thermal conductivity can be measured in two ways, they are steady and dynamic measurements. A steady measurement is otherwise called static measurement. Here, the thermal conductivity is measured by checking the values of temperature gradient and heat flux. The method for the measurement is termed as in-flow method. This is further divided into comparison method and direct method.

In dynamic measurement, the rate of change in temperature is measured over different time periods. Here, the thermal conductivity is derived finally from the specific heat capacity of the material. The method for the dynamic measurement is termed as flashing method. Here, a laser thermal conductance meter is used as the measuring device. A solid Nd laser is used as the heat source. Thermocouple is employed as a temperature sensor. Dynamic measurements are fast and simple compared to steady-state method. It is also applicable for the manufacture of refractory materials. However, high requirements and large potential for heat loss exist as challenges [8]. Table 2 gives the values for thermal conductivity for some materials. From the table, it is found that the thermal conductivity of diamond is pretty good.

Thermal conductivity of polymers is much small and is close to that of air. Porous polymer has got a much smaller thermal conductivity. This property enables polymers to act as a perfect heat insulating material. Solid polymers are having a narrow range of thermal properties. Thermal conductivity of crystalline polymers is much greater than the amorphous polymers. Thermal conductivity of polymers increases with the increase in chain length and this is due to the fact that ease of heat flow is higher in the molecular chain than across the molecules. Thermal conductivity of some polymers increases, but for some others, adverse trend is observed. Thermal conductivity of porous polymers is extremely low. Porous polymer's thermal conductivity is exceptionally small. Thermal conductivity further decreases with density. Thermal conductivity of polymer also depends on the moisture content, sample size and temperature of testing. If the moisture content increases, thermal conductivity also increases. This is due to the temperature gradient produced due to the presence of substances of different temperature in close vicinity. The water content is responsible for the thermal conductivity. Thermal conductivities (k) of some polymers are given in Table 3.

Table 2 Thermal conductivity of some materials (W/(mK) [6]

Material	k
Diamond	600
Graphite	355
SiC (single crystalline)	100
Silver	425
Copper	400
Aluminum	220

Table 3 Thermal physical properties of selected polymers (W/(mK)) [6]

Polymer	k
Polymethyl methacrylate (PMMA)	0.19
Polyvinyl chloride (PVC)	0.16
Low-density polyethylene (LDPE)	0.35
High-density polyethylene (HDPE)	0.44
Natural rubber	0.18
Polypropylene (PP)	0.24
Polytetrafluoroethylene (PTFE)	0.27

3 Thermal Characterization of Nanocomposites and Blends

Thermal analysis is a sequence of procedures that offer physical property measurement as a function of temperature, time and other variables. There are several methods to characterize different thermal properties of materials which include thermogravimetry (TGA), thermomechanical analysis (TMA), differential scanning calorimetry (DSC), etc. DSC and TGA coupled with infrared spectroscopy are excellent starting points for characterization of new or unknown materials. Thermal analysis techniques give an insight into the thermal properties of polymer materials. Thermal analysis has a vital role in investigating a broad range of materials properties.

3.1 Thermogravimetry (TG)

Thermogravimetric analysis (TGA) is an analytical technique in which mass of sample is measured as a function of temperature or time. Material is heated in two ways. In dynamic measurement, the sample is heated at constant heating rate and in isothermal measurements sample is heated in an environment of constant temperature. The selection of temperature is based on the nature of information required. Atmosphere of TGA analysis plays an important role. Results obtained are represented by a TGA curve in which mass or percentage mass is plotted against temperature and/or time. An alternative representation involves the use of first derivative of TGA curve with respect to temperature and/or time. This is known as differential thermogravimetric (DTG) curve. Here, the rate at which the mass changes is represented. Mass loss or gain in sample can occur in several ways which include evaporation of volatile components, oxidative decomposition of organic substances, oxidation of metals, thermal decomposition of components, uptake or loss of water in a humidity controlled experiment, etc. These process can produce steps in TGA curve [9]. Honda in 1915 developed initial TG instrument in which heating rate is gradually reduced from an initial stage during weight loss.

Modern TGA regulates the quantity and frequency of the weight variation of the samples against temperature and time in a controlled atmosphere. TGA found applications in the determination of thermal stability, oxidative stabilities and compositions of the sample materials [10]. TGA has wide range of applications in polymers. Properties of polymers which have applications in electronic, pharmaceutical, food and petroleum industries can be determined by TGA method [11].

TG instrument consists of four different components, they are balance, furnace, temperature programmer and recorder. A balance beam deviates from its mean position as the weight variations occur. In a null type of balance, deviation of the balance beam is detected by a sensor. A restoring force is then applied to restore the position of the beam. These beam deflections are then get converted into a suitable weight using different techniques. There are several factors that determine the accuracy and precision of TG analysis. Source, purity and the particle size of the sample, capacity of the sample holder, material by which crucible is made, and the atmosphere in which the TG measurements are carried out will determine the accuracy and precision of measurements. Platinum crucible is generally used in TG measurements. Similarly, an inert or oxidative atmosphere is generally demanded [11].

Thermal stability of polymers can be determined using thermogravimetry. The decomposition curves on TG define the characteristics and identification of the polymer. It is found that the polymers with suitable nanofillers have numerous applications in several fields. TGA can be employed to measure the amount of filler within a polymer. When the polymer with the filler is positioned on the balance and heated inside of a furnace all organic matter will burn away and filler content remain intact. TGA offers a fraction of mass that remain after the process. Another important application of TGA is the determination of composition of polymer blends. TGA-FTIR (Fourier infrared spectroscopy) can be employed for compositional analysis. TGA can be also used for the quantitative measurement of low level of volatile matter present in the sample. Existence of moisture can be determined by this way which paves way for the application of samples in pharmaceutical sector [12]. TGA can combine with differential scanning calorimetry (DSC) to carry out the determination of thermal characteristics of materials and is having wide range of applications.

3.2 Thermomechanical Analysis

The deformation of solid materials can be done by temperature variations. These variations can be done using various heat sources with different intensity and spatial distribution and it also depends on the diffusivity of the material [13]. Thermomechanical analysis (TMA) is another important technique to analyze the thermal characteristics of materials. TMA measures the variation in the dimensions of the material with change in temperature. TMA can be treated as a sensitive micrometer. Generally, TMA measures the change in free volume of a polymer

material. TMA characterization provides valuable information about the structure and composition of materials. It can be used to find the thermal expansion coefficient, glass transition temperature and melting temperate of materials.

Glass transition temperature (T_g) is an important property of a thermosetting polymer. At glass transition temperature, rigid glass softens and becomes a rubber like mass. Glass transition temperature makes an interconnection between the rigid and soft, flexible state of polymer. Below T_g , mobility of molecules of polymer is limited due to the insufficient energy and therefore they remain as rigid entities. Above T_g , molecules have got enough energy to move. Above glass transition temperature, the chemical crosslinks inhibit the thermosetting polymer from flowing and thus they become rubbery in nature. Even after softening, the polymers are generally tend to gain its original shape. Glass transition temperature has several important applications. For example, if we want to use a polymer as a flexible material, then T_g symbolizes a lower bound on its performing temperature [14].

Thermomechanical analysis can be effectively used to determine the glass transition temperature of materials. An advantage of these methods is that all these properties can be finding out by a single experiment. Here, changes in dimensions are measured as a function of temperature and/or time under a nonoscillatory load. Viscous and elastic properties of materials like polymers can be efficiently find out using this method. Figure 1 gives a schematic diagram of TMA analysis.

Usually, TMA measurements are carried out in an inert atmosphere, and for that, gases like argon, nitrogen and carbon monoxide are continuously purging into the system. Here, the sample is placed in a chamber. Thermocouple is used to control the temperature. Sample can be taken in a large amount, and therefore the heating and cooling rates are kept low. Dimensional changes occurring in the sample is transmitted through a push rod to the sensor. Usually, a highly precise inductive transducer is used as a sensor. The displacement of pushrod accompanied by the dimensional change is then converted to digital form and is recorded by a computer.

Fig. 1 Schematic representation of a thermomechanical analyzer. LVDT, linear variable displacement transducer [15]

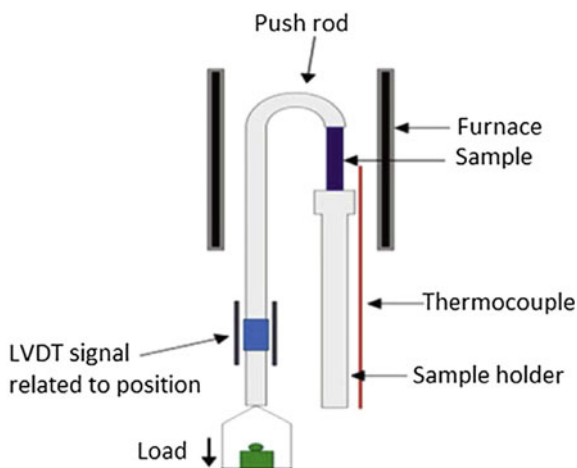
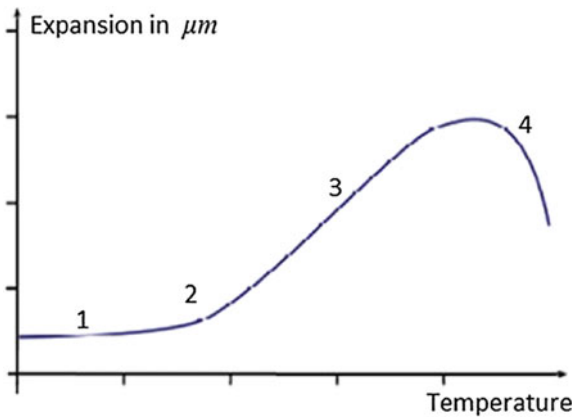


Fig. 2 Typical thermomechanical analysis curve [15]



It will produce a graph in which dimensional change is plotted against time or temperature. Figure 2 represents a typical thermomechanical analysis curve.

Different stages are numbered as 1, 2, 3 and 4 represent the expansion of material below glass transition temperature, 2 gives the range of glass transition temperature, 3 represents expansion above glass transition temperature and 4 is the region at which plastic deformation occurs. Other important application of TMA analysis is the determination of thermal expansion coefficient. It is also a good method for the analysis of anisotropy of crystals. Phase transformation temperature in alloys can also be analyzed by TMA measurements. Sintering in ceramics is a major cause of shrinkage in them. Extent of sintering in ceramics can be determined by TMA [15].

3.3 *Differential Scanning Calorimetry (DSC)*

DSC is an important technique for investigating the thermal properties of polymers or in other words the response of polymers toward heating. Like TMA, DSC can also be used to explore the melting of a polymer, i.e., the glass transition temperature. DSC instrument is composed of a measurement chamber and computer. There are two pans in the measurement chamber. These two pans are heated. Material is placed in one pan and it is investigated. Empty pan is taken as reference. Computer regulates the temperature and monitors the temperature. Rate of temperature rise or fall for a definite amount of heat will be different for two pans. When sample release heat through some process, the DSC plot shows an increase in the heat flow and is called exothermic. In endothermic reaction, sample absorbs heat and DSC plot shows a decrease. While considering the principle behind DSC, we have to consider some important terms related to it [16].

3.3.1 Temperature Gradient

It is the unequal dispersal of heat energy inside the material and it depends on the heating rate, sample's thermal diffusivity, sample holder and sample size. Usually, sample holders with great thermal diffusivity are favored. Temperature gradient can be varied according to heating rate and sample size. Temperature gradient increases with increase in the heating rate and sample thickness.

3.3.2 Thermal Lag

Thermal lag should maintain as minimum in DSC measurements. It is defined as the temperature difference between sample and sensor. It arises due to thermal resistance which is the capability of the material to delay the heat flow.

3.3.3 Lag Time

It is the time required to reach steady state after a DSC run has started. So it is otherwise called time to steady state. It becomes important once steady state is attained.

3.3.4 Heating Rate and Cooling Rate

Heating rate expresses the extent of heating of the sample and the unit is ($^{\circ}\text{C}/\text{min}$). By knowing the heating rate, time can be saved in DSC runs. Fast heating rates can lead to low temperature resolution due to large temperature gradient and this will lead to high thermal lag which is not desirable.

Cooling rate is another important parameter. In polymers, change in cooling rate will drastically change the material properties. Glass transition temperature and crystallization temperature are largely affected by changes in cooling rate. At fast cooling, polymers directly become glassy in nature without crystallization.

Sample should take as accurate weight. Accuracy should be at least $\pm 0.2\%$. DSC cells should be constantly purged with inert gases like nitrogen. Heating pans in DSC are generally made out of extra pure metals like Al, Pt, Au, Ag and Cu [17]. Figure 3 represents the heat flow rate and temperature profile for polyether ether ketone. (PEEK).

From the value of heat flow rate, scan rate and sample mass, heat capacity of the polymer can be calculated. Figure 4 represents the heat capacity of the polymer which is obtained from the calculations. From the graph, Tg and crystalline nature of the polymers can be determined [18].

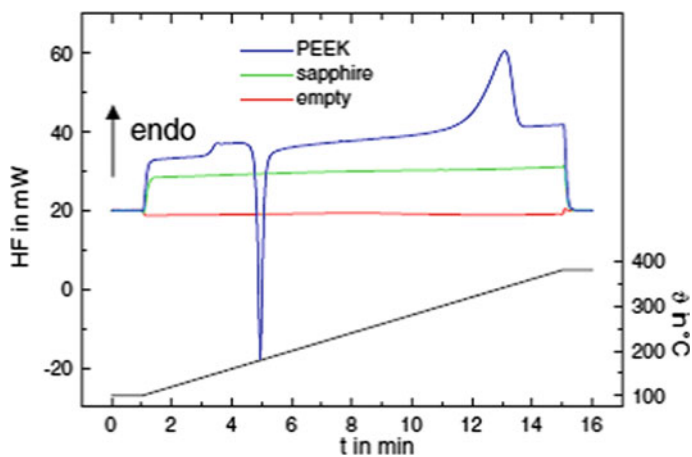


Fig. 3 Temperature profile and measured heat flow rate for empty pans, sapphire calibration standard (31.3 mg) and initially amorphous polyether ether ketone (PEEK) (29 mg). Heating rate of $\beta = 20 \text{ Kmin}^{-1}$ [18]

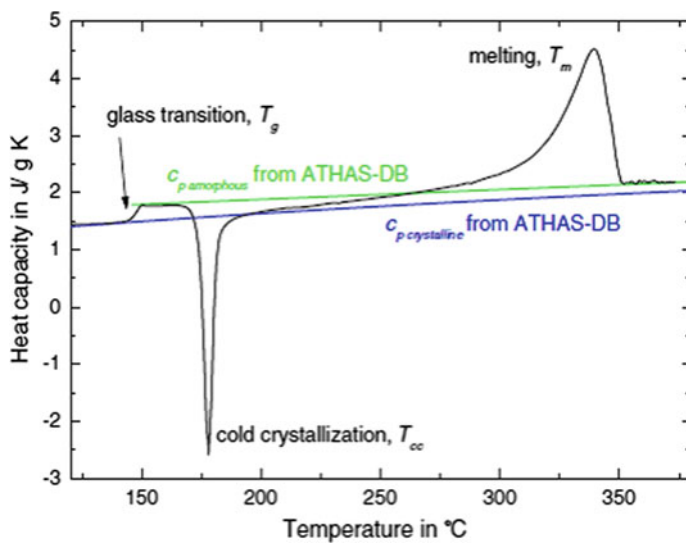


Fig. 4 Specific heat capacity versus temperature for an initially amorphous PEEK polymer [18]

4 Thermal Properties of XLPE Nanocomposites and Blends

4.1 Thermal Stability

Zhang et al. studied the influence of grafting matrix-compatible polymer brushes onto spherical colloidal SiO₂ nanoparticles (NP) to get an even NP dispersal. Reversible addition-fragmentation transfer (RAFT) polymerization was implemented to make poly(stearl methacrylate) (PSMA) brushes on SiO₂ NPs surface. Here, the polymer grafted spherical SiO₂-based XLPE nanocomposite has better thermal stability. This is due to the comparatively homogeneous dispersion of small aggregates (less than 100 nm), which intern resulted in augmented interfacial adhesion [19].

Thermal characteristics of nanoscale alumina–clay hybrid filler reinforcement in cross-linked polyethylene proved that supreme thermal stability has been attained by incorporating 5 wt% nano-Al₂O₃, trailed by alumina clay hybrid system and clay alone. The high thermal characteristics effect Al₂O₃/XLPE nanocomposites are because of the augmented thermal properties of Al₂O₃ nanoparticles and the increased transmission of thermal energy from the polymer phase to the reinforced phase through the better interface. Thermal stability of ternary hybrid systems is lower than binary systems because of the presence of lengthy organic chain on the clay platelets which are thermally less stable [20]. Sharad et al. explored the morphology and electrical insulation partial discharge applications of surface-modified XLPE nanocomposites. The addition of nanoreinforcement to polymeric material improves dielectric, electrical and thermal properties. However, the agglomeration of nanofillers adversely affects reliability and application of polymer nanocomposites. Surface modification of nanofillers enhances the interaction between minor phase and major phase which augments the dispersal of nanoreinforcement.

Structural deviations in XLPE by the integration of fillers mostly happen in amorphous part. Nanofiller addition leads to decline in surface energy which causes secondary or incomplete crystallization. The rise in melting point by the addition of nanofillers is observed [21]. This is because of the upsurge in crystal thickness and crystallization. Nanofiller incorporation to polymer matrix quickens the process of lamellar thickness inside polymer which upsurges heat of fusion. Variation in thermal degradation temperature of polymer with the incorporation of nanosilica can be obviously observed. Here, surface alteration aids to attain improved thermal stability than agglomerated and unmodified nanocomposites. Chemical changes in nanosilica after surface modification is responsible for the better performance. Reactive groups (Si–O) present on the surface-modified silica co-operate with the polymer matrix which leads to improvement in thermal stability [22].

4.2 Crystallinity

Effect of bamboo flour (BF) on XLPE crystallinity is explored by differential scanning calorimetry technique. The degree of crystallinity for XLPE was found out by the equation given below

$$\chi_c = \frac{\Delta H_m}{\Delta H_\infty} * 100\% \quad (5)$$

χ_c represents the crystallinity ratio, ΔH_m is the melting enthalpy measured and ΔH_∞ is the theoretical melting enthalpy of 100% crystalline polyethylene and it is 290 J/g [23]. Melting temperature of composites is greater than that of neat XLPE. Bamboo flour contains cellulose and this cellulose is a better thermal insulator than XLPE. Bamboo flour has no substantial effect on the crystallinity of XLPE and it is evident in Fig. 5 [24].

Jose et al. examined the non-isothermal crystallization kinetics of cross-linked system (XLPE) contains nano-ZnO to analyze the crystallization characteristics of the system [25]. The protocol of the experiment is given in Fig. 6. All experiments were accomplished in the standard DSC mode. Crystallization parameters were assessed from the cooling curves (Fig. 6).

The Flynn–Wall–Ozawa method and Avrami analysis have been taken to define the non-isothermal crystallization kinetics of prepared polymer composites. At low temperature, polymer chains are less mobile so more time is required for the polymer chain to organize into crystallites. Thus, the degree of crystallite perfection is also diminished with faster cooling rates. Here, the favorable role of nanoparticles is to partially compensate the opposing result of fast cooling. Normally, fillers in polymer matrix act as nucleating agents to improve crystallization below the percolation threshold and as a limitation to delay crystallization above the percolation concentration. In XLPE/ZnO nanocomposite systems, ZnO always accelerate the

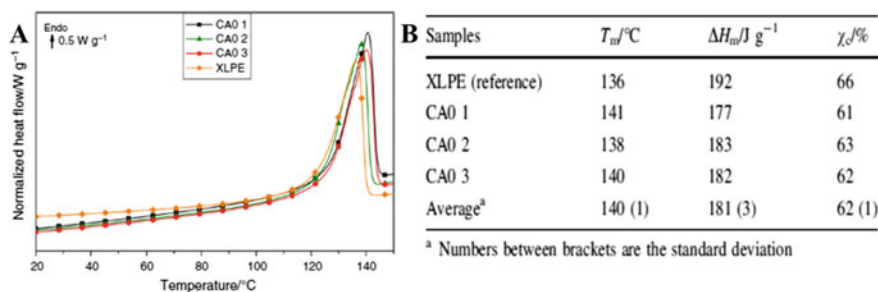


Fig. 5 (a) Differential scanning calorimetric curve of XLPE and CA0 composites, (b) the thermal properties of bulk XLPE and CA0 composites [24]

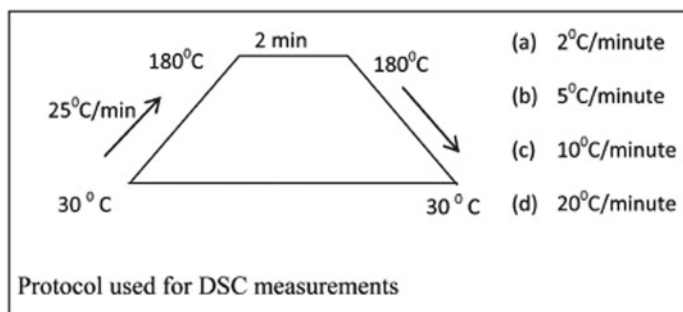


Fig. 6 Experimental procedure for DSC measurements [25]

crystallization. There are two types of activation energies for any crystal growth process, i.e., the activation energy for nucleation and activation energy for growth. Since these two processes are separated by very low energy barrier, both are condensed into a single energy barrier. Crystallization activation energy of XLPE and nanocomposites was determined using Flynn–Wall–Ozawa approach. XLPE has high E_a value compared with its nanocomposites which refers the reduction in energy barrier for crystallization in presence of fillers. In the presence of ZnO, E_a value decreases thus the molecular chains of polyethylene easier to crystallize and hence there is an upsurge in rate of crystallization. The decrease in E_a could be due to the fact that this energy is the sum of two components: one term corresponding to the nucleation and the other to the growth. When crystallization progresses, the energy required for nucleation can progressively disappear and then E_a can decrease (Fig. 7).

Antioxidant characteristics of XLPE nanocomposites on dynamic and steady temperature are measured by conducting oxidative induction temperature (OITm) and oxidative induction time (OITs) test measurements using DSC (Fig. 8) [26]. OITm values of nanocomposites (XLPE–GO) are lower in comparison with pure XLPE. It is found that oxygen molecules can be absorbed on nanomaterial's surface [27]. Many radicals can be formed on the surface of GO by the interaction between oxygen molecules and hydroxyl or carboxyl groups on the surface of GO. These radicals quicken the thermal oxidation reaction which leads to the decline in the OITm value. But the incorporation of functionalized graphene oxide (FGO) into the XLPE matrix displays a progressive influence on the OITm value.

XLPE–FGO nanocomposites displayed prolonged antioxidative times than that of pure XLPE as observed from the results of OITs display. OITm value and OITs are different because measuring OITm is in a rapid heating process condition, which cannot lead to the degradation of the hydroxyl and carboxyl groups on GO surface. As in the OITs measurement, the temperature is sustained for a comparative extended time, decomposing the hydroxyl and carboxyl groups of GO, and conserving the capacity of graphene to capture oxygen. In the case of the XLPE–FGO, because of the higher thermal stability and the capability of cross-linked with matrix

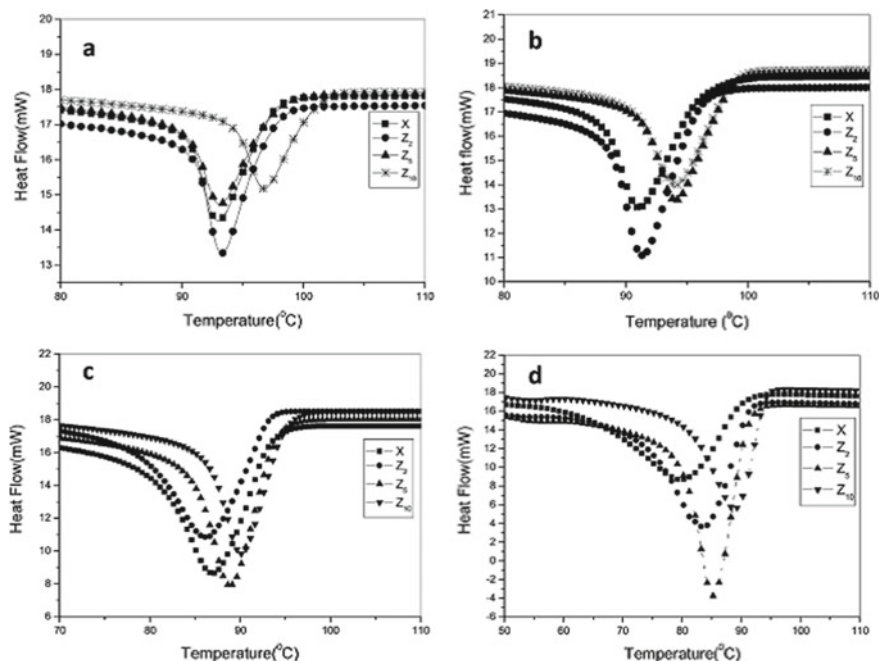


Fig. 7 Non-isothermal crystallization patterns (exothermic curves) of XLPE and nanocomposites at cooling rates 2 °C min⁻¹ (a), 5 °C min⁻¹ (b), 10 °C min⁻¹ (c), and 20 °C min⁻¹ (d) [25]

of FGO to enhance the property of captive oxygen, the OITs of XLPE–FGO is longer than that of the XLPE–GO. Therefore, incorporating FGO into XLPE displays greater antioxidation property over GO.

4.3 Flame Retardant Properties of XLPE Nanocomposites and Blends

Flammability behaviors of polymer composites are measured by cone calorimeter. Limited oxygen index (LOI) tests are widely accepted to evaluate the efficiency of fire performance. The heat release rate (HRR) and total heat release (THR) versus time curves of the XLPE nanocomposites are displayed in Fig. 9. It can be noticed that pure XLPE burns very rapidly after ignition, with the heat release rate (HRR) and total heat release (THR) values of 1741 kW/m² and 103.1 MJ/m², respectively. Balance of physical barrier and heat conduction effects of the GO is effective in the reduction of HRR of pure XLPE [28]. But in the case of XLPE–FGO nanocomposites, the heat release rate decreases apparently, compared to the pure XLPE. The HRR value is reduced by 10.2%, 27.9% and 28.9% for XLPE

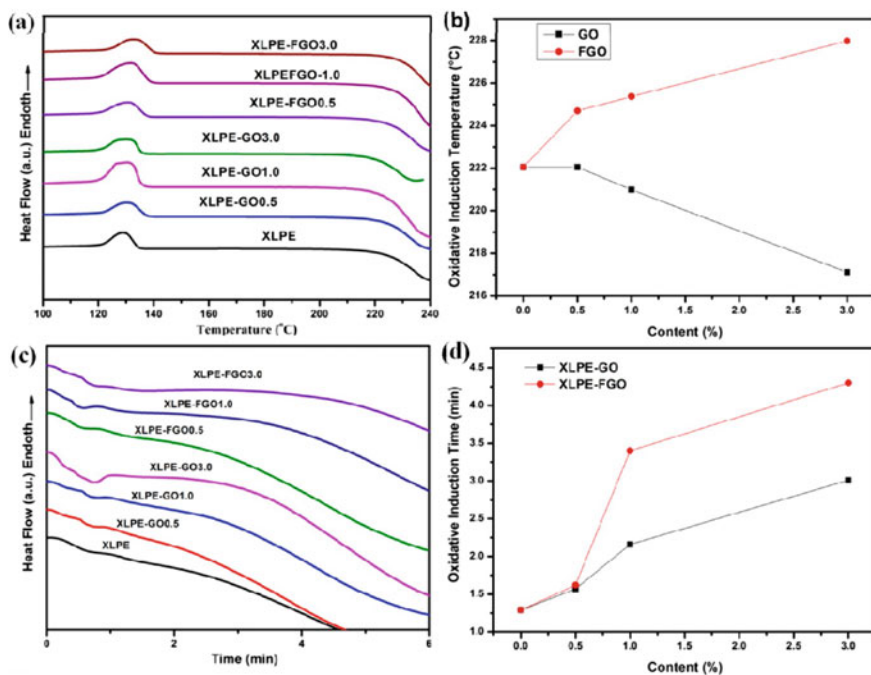


Fig. 8 OITm curves (a) and the OITm data (b), OITs curves (c) and the OITs data (d) of XLPE, XLPE-GO and FGO nanocomposites [26]

-FGO -0.5, -1.0 and -3.0, respectively; signifying that functionalized graphene oxide is more effective in augmenting the flame retardancy of polymers. The functionalized GO with hyper-branched flame retardant stimulates the char formation of GO, enhances the physical barrier effect and decreases the heat conduction effect of GO.

4.4 Thermal Conductivity

Poostforush et al. investigated the thermal conductivity of cross-linked polyethylene composites containing hexagonal boron nitride (hBN) and aluminum nitride (AlN) fillers [29]. Variation of thermal conductivity of PEX/AlN/PT180 and PEX/AlN/PT371 at a total filler content of 60 vol.% is shown in Fig. 10. The thermal conductivity of PEX/AlN (60 vol.%) was 4.23 W/mK which is much higher than PEX/AlN (40 vol.%) with 1.63 W/mK. This increase may be attributed to the more formation of thermal conductive paths at higher AlN concentrations. The thermal conductivity of PEX/AlN was higher than that of PEX/hBN composites at 60 vol.% of filler content in the through-plane direction. The large

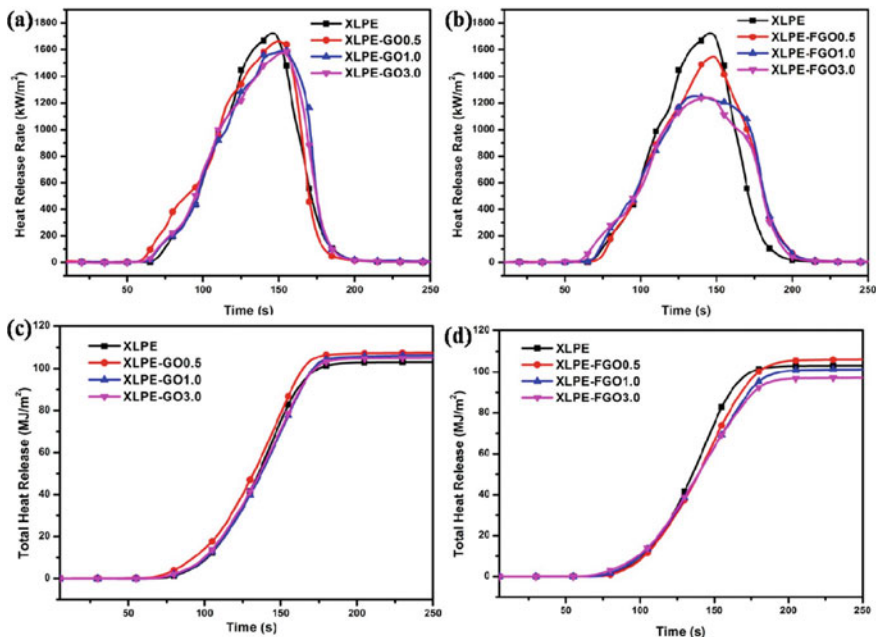


Fig. 9 HRR and THR curves of XLPE, XLPE-GO and FGO nanocomposites [26]

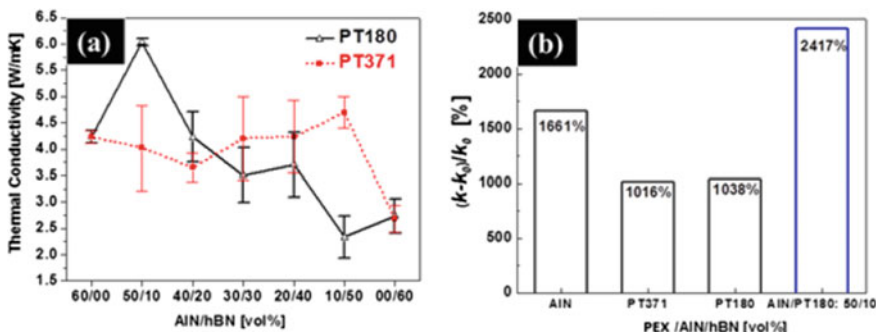


Fig. 10 Thermal conductivity and thermal conductivity enhancement of PEX/AIN/hBN [29]

difference in thermal conductivity of BN crystal in basal plane (300 W/mK) and in through-plane direction (3 W/mK) [24] could be a reason. Due to the large difference in thermal conductivity of BN in basal and thickness direction, it is needed to align the hBN flakes in random direction to enhance the through-plane thermal conductivity. The addition AIN polygonal particles with isotropic thermal conductivity (70–180 W/mK) into polymer matrix.

5 Conclusion

Properties of composites and blends are highly temperature dependent. There are transition properties like flexibility and brittleness which depend upon the glass transition temperature (T_g) and melting temperature (T_m). There are other thermal properties which are key factors for the applications of such materials. Thermal behavior of composites and blends depend upon the additives, fillers, etc., and thus these are not intrinsic properties as well.

References

1. Tanahashi M (2010) Development of Fabrication Methods of Filler/Polymer Nanocomposites: With Focus on Simple Melt-Compounding- Based Approach without Surface Modification of Nanofillers. *Materials* 3:1593–1619
2. Cao Y, Zhang J, Feng J, Peiyi W (2011) Compatibilization of Immiscible Polymer Blends Using Graphene Oxide Sheets. *Am Chem Soc* 5(7):5920–5927
3. Standard Handbook of Petroleum and Natural Gas Engineering, <http://dx.doi.org/10.1016/B978-0-12-383846-9.00002-3> Copyright © 2016 Elsevier Inc. All rights reserved
4. Speight JG, CD&W Inc., Laramie WY Assessing fuels for gasification: analytical and quality control techniques for coal Gasification for Synthetic Fuel Production. <http://dx.doi.org/10.1016/B978-0-85709-802-3.00008-4> Copyright © 2015 Elsevier Ltd. All rights reserved
5. Klaudia KM, Pielichowska K Thermal Decomposition of Polymer Nanocomposites With Functionalized Nanoparticles, <https://doi.org/10.1016/B978-0-12-814064-2.00013-5>
6. Wang R-M, Zheng S-R, Zheng Y-P (2011) Other properties of polymer composites. *Polymer Matrix Composites and Technology*, 513–548. <https://doi.org/10.1533/9780857092229.3.513>
7. Ratna D (2012) Thermal properties of thermosets, Woodhead Publishing Limited
8. Liu PS, Chen G F (2014) Characterization Methods. *Porous Materials*, 493–532. <https://doi.org/10.1016/b978-0-12-407788-1.00010-1>
9. Bottom R (nd) Thermogravimetric Analysis. Principles and Applications of Thermal Analysis, 87–118. <https://doi.org/10.1002/9780470697702.ch3>
10. Abraham J, Mohammed AP, Ajith Kumar MP, George SC, Thomas S (2018) Thermoanalytical Techniques of Nanomaterials. In: *Characterization of Nanomaterials*, pp 213–236. Woodhead Publishing
11. Ng, HM, Saidi NM, Omar FS, Ramesh K, Ramesh S, Bashir S (2018) Thermogravimetric Analysis of Polymers. *Encyclopedia of Polymer Science and Technology*, 1–29. <https://doi.org/10.1002/0471440264.pst667>
12. Gerhardt H (2009) Moisture effects on solid dosage forms—formulation. *GXP Compliance* 13:58–66
13. Chrysochoos A (2012) Thermomechanical Analysis of the Cyclic Behavior of Materials. *Procedia IUTAM* 4:15–26
14. Hale A (2002) Thermosets. *Handbook of Thermal Analysis and Calorimetry*, 295–354. [https://doi.org/10.1016/s1573-4374\(02\)80012-7](https://doi.org/10.1016/s1573-4374(02)80012-7)
15. James J (2017) Thermomechanical Analysis and Its Applications. In: *Thermal and Rheological Measurement Techniques for Nanomaterials Characterization*, pp 159–171. Elsevier
16. Instrumental techniques for the characterization of nanoparticles, Cintil Jose Chirayil, Jiji Abraham, Soney C George, Sabu Thomas, *Thermal and Rheological Measurement*

- Techniques for Nanomaterials Characterization, ISBN: 9780323461399, publisher: Elsevier, Volume 3
17. Menczel JD, Prime RB (Eds) (2009) Thermal Analysis of Polymers. <https://doi.org/10.1002/9780470423837>
 18. Schick C (2009) Differential scanning calorimetry (DSC) of semicrystalline polymers. *Anal and Bioanalytical Chem* 395(6):1589–1611. <https://doi.org/10.1007/s00216-009-3169-y>
 19. Zhang L, Khani MM, Krentz TM, Huang Y, Zhou Y, Benicewicz BC, Keith Nelson JC, Schadler LS (2017) Suppression of space charge in crosslinked polyethylene filled with poly(stearyl methacrylate)-grafted SiO₂ nanoparticles. *Appl Phys Lett* 110. <https://doi.org/10.1063/1.4979107>
 20. Jose JP, Thomas S Alumina–clay nanoscale hybrid filler assembling in cross-linked polyethylene based nanocomposites: mechanics and thermal properties. <https://doi.org/10.1039/c4cp01532k>
 21. Sharad PA, Sathish Kumar K Application of surface-modified XLPE nanocomposites for electrical insulation-partial discharge and morphological study. <https://doi.org/10.1080/20550324.2017.1325987>
 22. Choudhury AK, Ong BC, Soddemann M (2010) Effect of various nanofillers on thermal stability and degradation kinetics of polymer nanocomposites. *J Nanosci Nanotechnol* 10:5056–5071
 23. Ke QQ, Huang XY, Wei P, Wang GL, Jiang PK (2007) Thermal, mechanical, and dielectric behaviors of crosslinked linear low density polyethylene/polyolefin elastomers blends. *J Appl Polym Sci* 104:1920–1927
 24. Haddou G, Dandurand J, Dantras E, Maiduc H, Thai H (2016) Nguyen Vu Giang, Tran Huu Trung, Philippe Pontains, Colette Lacabanne Mechanical and thermal behaviour of bamboo flour-reinforced XLPE composites. *J Therm Anal Calorim* 124:701–708
 25. Jose JP, Chazeau L, Cavaille JY, Varughese KT, Thomas S (2014) Nucleation and nonisothermal crystallization kinetics in cross-linked polyethylene/zinc oxide nanocomposites. *RSC Adv* 4:31643
 26. Hu W, Zhan J, Wang X, Hong N, Wang B, Song L, Stec AA, Richard Hull T, Wang J, Hu Y (2014) Effect of Functionalized Graphene Oxide with Hyper-Branched Flame Retardant on Flammability and Thermal Stability of Cross-Linked Polyethylene. *Ind Eng Chem Res* 53:3073–3083
 27. Gorrasi G, Sorrentino A (2013) Photo-oxidative stabilization of carbon nanotubes on polylactic acid. *Polym Degrad Stab* 98:963–971
 28. Bao CL, Song L, Xing WY, Yuan BH, Wilkie CA, Huang JL, Guo YQ, Hu Y (2012) Preparation of graphene by pressurized oxidation and multiplex reduction and its polymer nanocomposites by masterbatch-based melt blending. *J Mater Chem* 22:6088–6096
 29. Poostforush M, Azizi H, Ghasemi I (2017) Thermal conductivity of cross-linked polyethylene composites contained nitride based ceramics. *Bulgarian Chemical Communications* 49 (Special Issue J): 273–280

Chapter 9

Potential Applications of XLPE Nanocomposites in the Field of Cable Insulation



R. Jose Varghese, L. Vidya, Tomy Muringayil Joseph, Apparao Gudimalla, G. Harini Bhuvaneshwari, and Sabu Thomas

1 Introduction

Cables and insulated wires are used in a wide range of products. Typical applications include power wires, communication cables, equipment wiring, automotive wiring, signal and control cables, and construction cables [1]. In the basic form, the system can be isolated by a conducting material surrounded by a dielectric layer, but in the case of optical dielectric conductor cables, the optical signal must be confined to the fiber core with a jacket that reflects the optical signal. Papers used in telegraph wires were known to be one of the earliest insulating materials reported in 1795 [2]. Since the nineteenth century, telegraph cables have been embedded in grooved wooden rails covered with strips of wood. Later, the development of vulcanized natural rubber occurs for applications like arc lighting [3]. In 1950s, polyethylene was introduced into distribution cables and subsequent transmission cables [4]. Applications of extruded synthetic insulation materials continue to grow,

R. Jose Varghese (✉) · A. Gudimalla · S. Thomas
International and Inter University Center for Nanoscience and Nanotechnology,
Mahatma Gandhi University, Kottayam, Kerala, India
e-mail: josv3209@gmail.com

L. Vidya
School of Pure and Applied Physics, Mahatma Gandhi University, Kottayam, Kerala, India

T. M. Joseph
Polymers Technology Department, Chemical Faculty, Gdansk University of Technology,
80-233 Gdansk, Poland

A. Gudimalla
Jožef Stefan International Postgraduate School, Jamova Cesta 39, 1000 Ljubljana, Slovenia

G. Harini Bhuvaneshwari
CAS Key Laboratory of Design and Assembly of Functional Nanostructures, Fujian Key
Laboratory of Nanomaterials, Fujian Institute of Research on the Structure of Matter,
Chinese Academy of Sciences, Fuzhou, Fujian 350002, People's Republic of China

© Springer Nature Singapore Pte Ltd. 2021

J. Thomas et al. (eds.), *Crosslinkable Polyethylene Based Blends and Nanocomposites*, Materials Horizons: From Nature to Nanomaterials,
https://doi.org/10.1007/978-981-16-0486-7_9

and improvements in materials offer greater incentives for their use [5]. Examples of these extruded materials are

Polyvinyl chloride (PVC),

Polyethylene (PE),

Ethylene-propylene elastomers (EPM and EPDM).

Initially, PVC and PE were unable to access in high voltage applications. However, for low voltage applications, the use of PE and PVC without cross-linking provided a cost-effective insulating material. Polyethylene (PE) is one of the commonly used plastic, mainly for packaging. Polyethylene is Polyethylene s a thermoplastic polymer composed of long hydrocarbon chains with different chain lengths (C_2H_4) nH_2 . High-density polyethylene generally has a melting point in the range of $T = 120\text{--}130\text{ }^\circ\text{C}$, and low-density polyethylene has a melting point of about $105\text{--}115\text{ }^\circ\text{C}$. Also, it exhibits good chemical resistance. They are highly resistant to both strong acids and bases, and too mild oxidants and reducing agents. Polyethylene (in addition to cross-linked polyethylene) can be dissolved in aromatic hydrocarbons or chlorinated solvents at high temperatures. Polyethylene is a homopolymer or copolymer in which ethylene is the main constituent of the monomer. It is one of the versatile polymers which offers high performance compared to other polymers. PE is a semi-crystalline polymer which possesses low-to-moderate strength and immense toughness. On raising the crystallinity, the properties such as stiffness, elastic limit, mechanical and thermal properties also increase. At low temperatures, PE exhibits excellent strength. PE is relatively inexpensive and exhibits excellent strength at low temperature. PE is highly resistant to both solvents and acids [6].

Low-density polyethylene (LDPE) is manufactured under high pressure and it possesses a long chain branch. This particularly affects the rheological behavior of the alloy. Recovery of flexible alloys increases with the number of long-chain branches. Samples of polyethylene with the same average molecular weight under high split load deviate further from Newton's behavior and have better accessibility. Highly branched, high molecular weight polymers generally cause gel formation and reduce the optical properties of the film. LDPE can be produced by free-radical polymerization. Due to the high degree of branching in LDPE proves, chain do not pack well in the crystal structure, which leads to low-density properties ($0.9100, 940\text{ g/cm}^3$). The intermolecular forces are small due to low instantaneous dipole-dipole interactions. As a conclusion of the above properties, LDPE shows low strength and high ductility [7]. The high degree of branching with long chains provides molten LDPE with unique and desirable flow properties. Its applications include both rigid containers and plastic films such as plastic bags, pipes and films.

The cross-linking process of polyethylene, resulting in high-density cross-linked polyethylene (XHDPE) or cross-linked low-density polyethylene (XLPE), extends the use of PE, increases the operating limit at high temperature, and results in good mechanical properties. It could be due to the creation of 3D structures. This structure improves the tensile strength and thermal stability of the polymer and also

improves hardness and chemical resistance. PE cross-linking is activated in three different ways:

- Radiation
- Addition of peroxide or addition of silane.

The addition of silane, which was patented by Dow Corning in the late 1960s, did not change the crystallinity of the base polymer observed by Venkatraman and Kleiner, and also made the material more flexible by cross-linking (Si-O-Si) instead of making the process more difficult [8]. This is especially interesting because it guarantees each Si atom has three active sites, which allows it to attach to six network bridges up to six polymer chains. However, optimization of production conditions is useful for better performance when mechanical, chemical and thermal resistances are required. Currently, cross-linked polyethylene is used in various industries, such as the cable and wire industries, hot water pipes, steam-proof food packaging. Along with these, most studies on XLPE are based on, cross-linking low-density polyethylene (LDPE) with peroxide or silane.

Due to high operating temperature, performance and well-controlled extrusion technology cross-linked polyethylene (XLPE) plays a major role by replacing oil paper insulated systems and in high voltage AC cables. The polyethylene (PE) is the base matrix and can be cross-linked by peroxide. Cross-linking is considered necessary, but the low-density PE (LDPE) exhibits a more significant melting at the temperature of about 100 °C, leads a loss in its mechanical stability [(9)]. On the contrary, linear high-density PE (HDPE) shows a high melting point and achieve a higher operating temperature. XLPE is now widely used in the field of HV cable insulation. Today, one of the most commonly used cross-linking methods was a radical reaction with an organic peroxide. But the by-products remaining from the cross-linking process announce some degradation in electrical properties which creates space charge accumulation. To reduce these byproducts, XLPE insulation cables need degassing process.

2 Insulation Materials

2.1 *Natural Rubber (NR)*

NR will act as effective thermostable insulating material when they are compounded and cured properly. A variety of inorganic/organic materials has been used as fillers, anti-degradants, plasticizers, vulcanizing agents to improve the dielectric properties of the NR. Traditionally, up to 25 kV of natural rubber has been used for insulation. Later, it can be replaced by saturated hydrocarbons. These materials exhibit good resistance and constant electrical behavior [10].

2.2 *Styrene Butadiene Rubber (SBR)*

It is a copolymer of butadiene and styrene and styrene butadiene rubber is commonly used in applications like low voltages. The electrical properties mainly depend on the ratio of particulate filler, the morphology of the particles and the method of processing and forming and possible interactions between the conductive and the nonconductive phases [11].

2.3 *Butyl Rubber*

The processing of butyl rubber is similar to the NR with the complex procedure and the final properties are comparable to the NR. The temperature tolerance of butyl rubber is 85 °C and for the NR is 60 °C. Used for sulfur vulcanization, because it is a copolymer of isobutylene and isoprene. Due to its saturated Skelton, butyl rubber offers betterment over natural rubber. So, a modified version of natural rubber is used in both insulation and lining applications [12].

The polymeric insulating materials, listed as

- Thermoplastics,
- Cross-linked elastomers,
- Thermoplastic elastomers.

2.4 *Other Polymeric Materials*

For a long time, polymeric insulation materials have been used with great success in underground power transmission of extruded high voltage alternating current (HVAC) cables. Later, in the 1950s, prime 110 kV extruded polymeric HVAC cable came into the field, and then polymer insulation materials have been extensively recycled in HVAC cables. Japan was the first one who use the prime 500 kV extruded HVAC cable. The outgrowth of high voltage direct current (HVDC) cables is far behind the HVAC cable. The aftereffect of extruded polymeric HVDC cable is not that too long but it shows large advances in power transmission better the HVAC cables, which includes, extruded polymeric HVDC cable shows lower transmission loss compared to HVAC cables, avoids the oil leaks appeared to be one of the most environmental hazards, also it has low maintenance cost compared to OF and MIND cables. Along with this, the advancement of polymeric HVDC cables also contributes to modern power transmission [3].

3 Properties of Nanocomposites for Cable Insulation

An improvement in insulation performance is expected when nanocomposites are used in place of the traditional microcomposite due to the enhanced area of interface between filler and the polymer system. Electrical properties which play a significant role in cable insulation are discussed below.

3.1 Conductivity

Conductivity, the ability of materials to conduct electrical current is greatly influenced when nanofillers are incorporated into the base matrix. Yan et al. studied the effect of incorporation on carbon black in XLPE on electrical conductivity and showed that the dependence of conductivity on DC electric field was slow to increase up to 20 kV/mm above which nonlinear characteristics were observed. The effect of temperature was not much pronounced up to 90 °C. The inclusion of carbon black proved to inhibit space charge accumulation and at the same time reduces electric field distortion thereby improving the conductivity of the prepared composites [13]. The effect of modified and unmodified silica nanoparticles in XLDPE was studied by Zang et al. which showed an increase in values with temperature [14]. Similar studies were conducted for magnesium oxide incorporated cross-linked low-density polyethylene (XLDPE) [15] and TiO₂ nanoparticle filled XLDPE matrix [16].

3.2 Permittivity

The main property in dielectric parameters is the relative permittivity and the effect of the addition of nanoparticles to XLDPE on dielectric properties has been studied in detail. Various factors affect the dielectric properties such as temperature, moisture, frequency along with material properties. It has been shown that the addition of nanosilica particles in XLDPE improves the dielectric properties [17, 18]. However, the effect of humidity on such nanocomposites at different frequencies must be investigated to select the material for industrial purposes. In such a study, it was observed that as the incorporation of silica nanoparticles increases the moisture absorption of the composite, a reduced breakdown strength and increased loss was observed [19].

3.3 *Electric Treeing and Water Treeing*

Electrical treeing is a pre-breakdown in insulation systems and a primary cause for failure leading to damage of systems especially in high voltage insulations [20]. Stress points such as protrusions, contaminants initiate the development of these channels which thereafter grows through continuous partial discharge activity within the medium [21]. The addition of nanofillers is found to suppress the electrical treeing of polymer nanocomposites for high voltage applications [22]. Addition of zinc oxide and aluminum oxide nanofillers in XLPE has proved to inhibit the electrical treeing in the nanocomposites up to 1% concentration, beyond which the addition of fillers propagates the tree growth. Similarly, the addition of SiO₂ nanoparticles inhibited the electrical tree growth [23].

Water trees are plume-like structures consisting of water-filled cavities developing from point of stress which can initiate electrical treeing leading to electrical breakdown [24]. The study of XLPE nanocomposites containing ZnO and Al₂O₃ and SiO₂ nanoparticles proved to improve the water treeing characteristics of the composites [25]. In a similar study, the addition of Montmorillonite clay particles in the composite is found to suppress the water treeing behavior due to the layered structure formed by the addition of nanoparticle [26].

4 **Future Breakthrough of HVDC Cables**

There are three types of HVDC cables which includes

1. Mass impregnated (MI)
2. Self-contained fluid filled (SCFF)
3. Cross-linked polyethylene

Reliable, cost-effective and environmentally responsible power grid by extruded polymeric cables is preferred as a mean for electric energy transportation. From the use of HVAC and HVDC cable networks will be able to raise their operating voltage levels which can withstand the resulting increase in electric stress. XLPE matrix with fewer impurities is preferred. For the advancement of direct current (DC) applications, General Electric Global Research Center developed a new insulation material, which uses nanoclay particles to support ethylene propylene rubber (EPR) insulation results N-EPR [27]. When compared to XLPE insulation, N-EPR exhibits space charge propagation. Because of the structural pattern of N-EPR insulation, it is possible to limit the electrical enhancement. In addition to these, N-EPR provides higher power density and neglects the lengthy and costly degassing needed for XLPE insulation. Cross-linked polyethylene (XLPE) is widely applied for the cable insulation due to its very good dielectric properties, processing feasibility, desirable chemical properties and ecofriendly. These properties help in the transmission of electricity and the distribution of electric energy

[28]. Also, the high resistance to thermal shocks and tuneable thickness makes it a suitable candidate for the cable industry. These properties were utilized for the application of XLPE in underground electric cables. In addition to the advantages associated with XLPE, it is also capable of absorbing high loadings of fillers (e.g., carbon black, silica) compared to uncross-linked polyethylene which becomes brittle on the incorporation of fillers. The addition of NPs to insulation material results in a marginal improvement in its dielectric, electrical, thermal properties. The reason is that by the formation of cross-links, the particles are bonded and trapped within the polymer matrix [29]. As a result, levels of filler that are disadvantageous and make the polymer brittle would impart reinforcement in XLPE [30]. By cross-linking of polyethylene, there can be an improvement in properties (Table 1) which can be applied in cable installation, heat-resistant food packaging (up to 200 °C), foams for thermal insulation, and chemical-resistant seals.

5 Current Perspective

The space charge, trapping and detrapping of electrons followed by the release of energy can lead to partial discharge and aging of insulation materials. Dielectrics made up of nanocomposites have been extensively reported and shown to have many desirable properties under DC field. Properties such as space charge and DC breakdown strength can be improved. The most common nanofillers that have been reported are MgO, SiO₂, Al₂O₃ and TiO₂. The mechanism behind the improvement in dielectric properties is believed to be charge trap characteristics modified by nanofillers [34]. The interface developed in nanocomposites between polymer matrix and nanoparticles can be the main reason for the improvement of electrical

Table 1 Cross-linking of polyethylene and its change in properties [30–33]

S. no	Property of polyethylene	After cross-linking of polyethylene
1	Melt index	Decrease
2	Density	No changes/decrease
3	Molecular weight	Significantly increased
4	Tensile strength	No changes/slightly increase
5	Elongation-at-break	Decrease
6	Impact resistance	Significantly improved
7	Abrasion resistance	Greatly improved
8	Stress crack resistance	Greatly improved
9	Elastic properties	Greatly improved
10	Environmental stress crack resistance	Increase
11	Resistance to slow crack growth	Increase
12	Temperature resistance	Greatly improved
13	Chemical resistance	Significantly increased

properties. The dispersion of nanoparticles in semi-crystalline polymers is important and not explored much. If there is no good dispersion of nanoparticle in polymer matrix, there will be agglomeration. Distances between adjacent spherulites are so small that agglomeration of the introduced nanoparticles may act as passages between spherulites in the amorphous area.

Etching method can be used to treat the nanoparticle incorporated polyethylene. Proper surface modification by desirable coupling agent can improve the dispersion of nanoparticle, spherulite structure and can prevent the overlap between interaction zones. Commercial (AC grade) XLPE and its nanocomposite are also tested to use it for DC application. The incorporation of nanofiller (e.g., nanosilica) is reported to be improved its breakdown strength on the DC step test [35].

SiC nanoparticles are reported to suppress the space charge accumulation at a concentration of 1 wt%. Further increase in concentration inhibited the effect of NPs on the space charge accumulation [36]. In the low concentration of NPs, there will be a large distance between NPs. According to previous reports on MgO XLPE composites, they reported deep traps which were surrounding MgO nanoparticles in nanocomposites which attracted charges to MgO NPs. An NP which is surrounded by electrons or holes can be considered as electrically neutral [37].

Moisture combined with electrical stress is another factor which affects the aging of the insulation material. This process can affect the partial discharge on the material followed by disintegration. There can occur a significant reduction in flash voltage when the water is combined with impurities on the insulation surface. The major factors that affect the characteristics of insulation materials are conductivity of the droplets, insulation surface roughness and the moisture droplet arrangement. As the conductivity of the moisture content is increased, there is a decrease in flashover voltage as shown in [38].

The nanocomposites made by MgO/XLPE (0.5 wt%) reported having higher flashover results compared to PE. This explains that the NP addition improves the flash overvoltage. This is due to the hindering of movement of surface charges by NPs [38]. The ratio of NPs to the polymer matrix depends on the type of NPs. As discussed earlier above the optimum concentration the property of insulating material can deteriorate. Surface modification of insulation material can improve the adhesion between nanofillers and polymer matrix which in turn improves the dispersion of NPs. This, in turn, will have a great improvement in breakdown strength (AC/DC), electrical and water tree resistance, permittivity and dielectric loss.

Figure 1 shows the SEM images of XLPE/silica composite that represents that nanofillers are not dispersed inhomogeneous manner. Some of the samples in each wt% show agglomeration (Fig. 1a and b). Figure 1c and d shows that the nanoparticle is better dispersed in the polymer matrix. The octylsilane-modified XLPE can promote chemical adhesion between NPs and polymer matrix. It is essential to understand the role of nanofillers in the hindrance of partial discharge (PD). From Fig. 2a, we can see that unmodified nanofillers are not well dispersed. This can cause a decrease in PD frequency of encounter with NPs (Fig. 2 denoted by black color line). This, in turn, can affect the lifetime of insulation material.

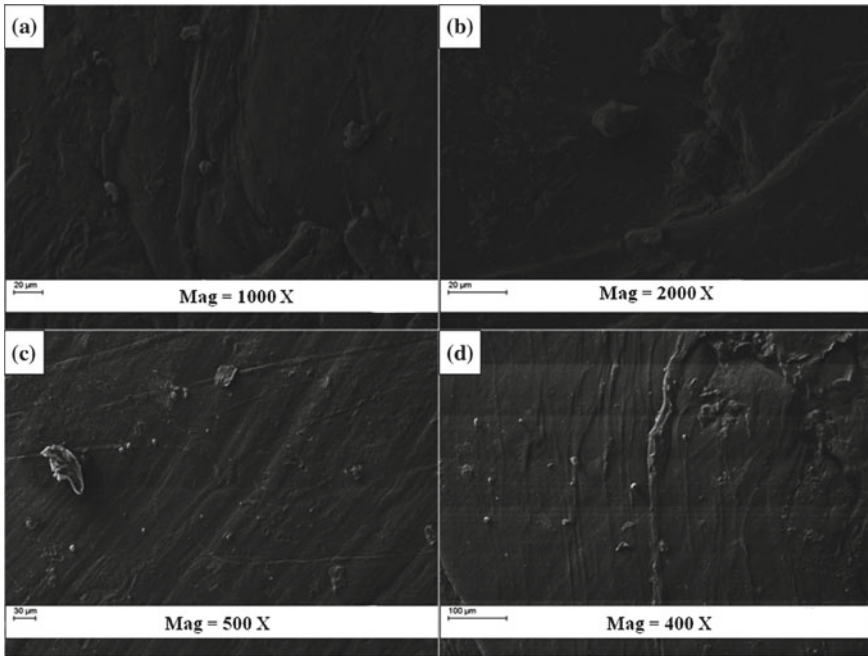


Fig. 1 SEM images of (a) XLPE/silica nano 2 wt% agglomerated nanocomposite, (b) XLPE/silica nano 3 wt% agglomerated nanocomposite, (c) XLPE/silica nano 2 wt% Octylsilane-modified nanocomposite, (d) XLPE/silica nano 3 wt% Octylsilane-modified nanocomposites (39)

Agglomeration of NPs leads to the segregation of nanofillers at several points. Hence, there will be easy propagation of PD to ground electrode in unmodified samples as shown in Fig. 2b. Formation of the electrical tree will lead to the degradation of XLPE matrix. Previous reports have shown an improvement in electrical treeing resistance of another polymer matrix (e.g., epoxy resin, polyethylene) with the loading of NPs [40–42]. Mansor et al. [43] studied the influence of ZnO and Al₂O₃ NPs on electrical treeing properties of XLPE matrix. When 1 wt % of ZnO and Al₂O₃ NPs was added, there was improvement insulation which might be due to the inhibition of the rapid growth of the electrical tree with a tree inception voltage (TIV) of 10.3 and 11.6%.

The modification of the polymer surface using a coupling agent can improve the dispersion and the distribution of NPs as shown in Fig. 2c. This can delay the propagation of PD and improves the lifetime of insulation material. The change in morphology of the final nanocomposite is also important to determine the final property of the material. NPs addition can lead to the decrease in surface energy or degradation of polymer which can cause secondary or incomplete crystallization.

Like PD, water tree phenomenon, first discovered in 1969, is another factor which reduces the lifetime of XLPE cables [44, 45]. The water tree problem was widely researched between 1980 and 1990. The reasons for the development of

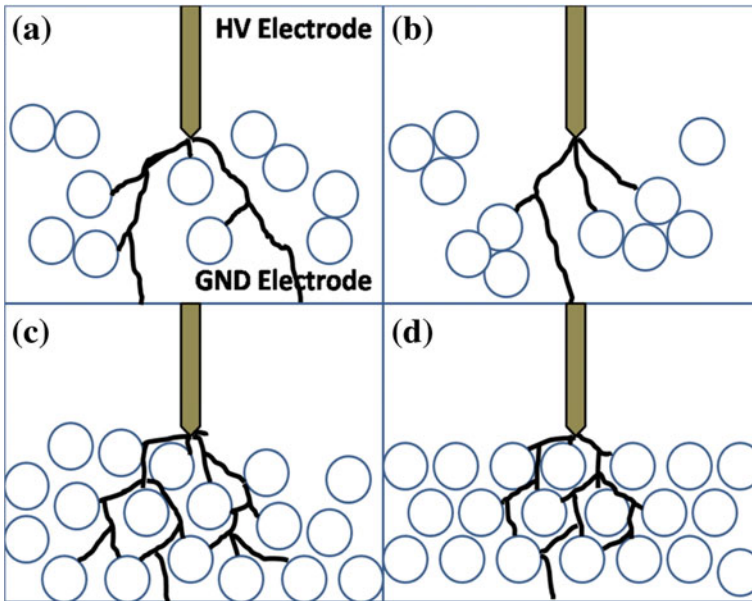


Fig. 2 schematic representation of propagation of partial discharge (PD) in (a) unmodified, (b) agglomerated (c) surface-modified, (d) ideally dispersed XLPE nanocomposite [39]

water tree are cable crosslink process by steam curing, extrusion of screens, semiconductors and insulations processes, and the cables lying in wetlands. The water tree is reported to be in the shape of microscopic scale voids which is connected to nanoscale and is like dendritic patterns discussed before (Fig. 3) [46]. Water trees are visualized as the presence of voids, contaminants which results in the formation of defects and lead to a powerful alternating electric field [47]. These deformations decrease the breakdown voltage and the impulse strength of the cable. The electrical tree is observed as the last stage of water tree growth before electrical breakdown. Because of the creation of an electric tree, the power cable is reported to fail in 15 days [48]. Phenylmethyldimethoxysilane (PMDMS) and titanium tetraisopropoxide catalyst (TTIP) were also studied in MV cables to resist this phenomenon [48].

Shirazi et al. [48] studied the use of phenylmethyldimethoxysilane (PMDMS), trimethylmethoxysilane (TMMS), ferrocene and sodiumdodecylsulfate with titanium tetraisopropoxide (TTIP) and α -alumina nanofiller for the reduction of water treeing behavior. They reported that the alumina nanofiller-improved the dielectric characteristics of degraded XLPE. During the addition of NPs, the process of lamellar thickness can also get accelerates which in turn can increase the heat of diffusion. The rearrangement of lamellae during the addition of NPs can be easily characterized using the DSC curves as shown in Fig. 4. By using a wire-plane test object for evaluating material resistance to electrical treeing, a relatively large

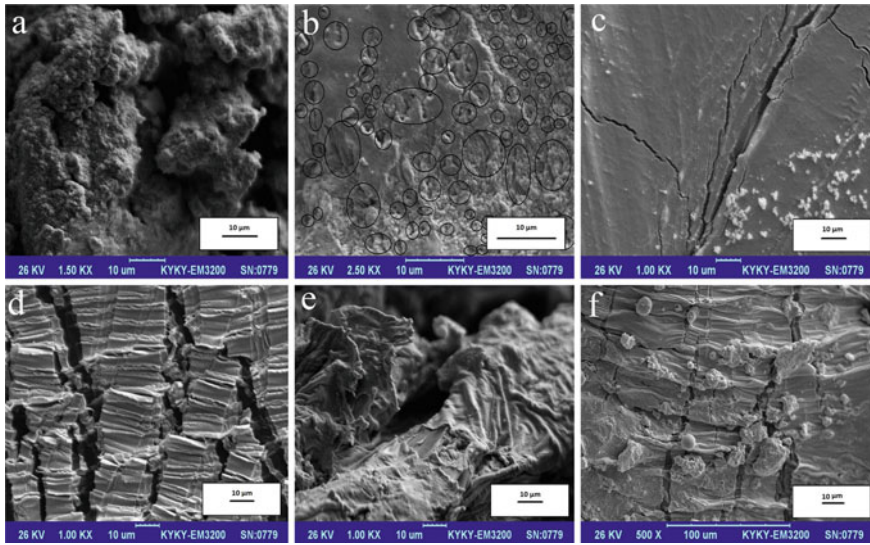


Fig. 3 Microstructure image of aged cable insulation and semiconductor material. (a) Water tree micro-voids. (b) Water tree aged area. (c) Cracks on aged insulation surface. (d) Electrical breakdown channels in the aged insulation. (e) Close-up view of aged inner semiconductor material. (f) Aged area of inner semiconductor material (48)

volume of the material is stressed, presumably also in its weakest points, and the growth of electric trees is not forced to one specific location like in the needle electrode objects. It thus provides an opportunity to better explore the influence of material structure and constituency on electrical tree inception. Several promising stabilizers of benzil-, thioxanthone-, fullerene- and melamine-types have also been tested and characterized. Majority of them exhibit a positive impact on the resistance to electrical treeing in cross-linked polyethylene, ranging from 20% up to well above 100% of the increased tree initiation field. It was found through correlating these test results with molecular modeling of electronic properties of the stabilizers that the electron affinity of stabilizing molecules generally correlates well with their stabilizing efficiency. This indicates that electron scavenging is here the dominant mechanism. Also, the addition of nanofillers to polyethylene-based materials yields a similar, though not equally strong effect nanocomposites at a filler content of 3 wt %. It appears, when considering our investigations and available literature data, that the effect is not related to the chemical nature of the nanofiller but rather to the formation of polymer-particle interfacial layer that provides deeper charge trapping sites and reduced long range molecular mobility.

Simulation studies were also carried out to analyze the electrical and mechanical properties of XLPE nanocomposites using different NPs [49, 50]. Nanoclay is widely applied for the production of nanocomposites. They have a multilayer structure with nanometer thickness with excellent electrical properties [51, 52]. The nanocomposites with clay exhibit good shielding of polymer matrices from heat and

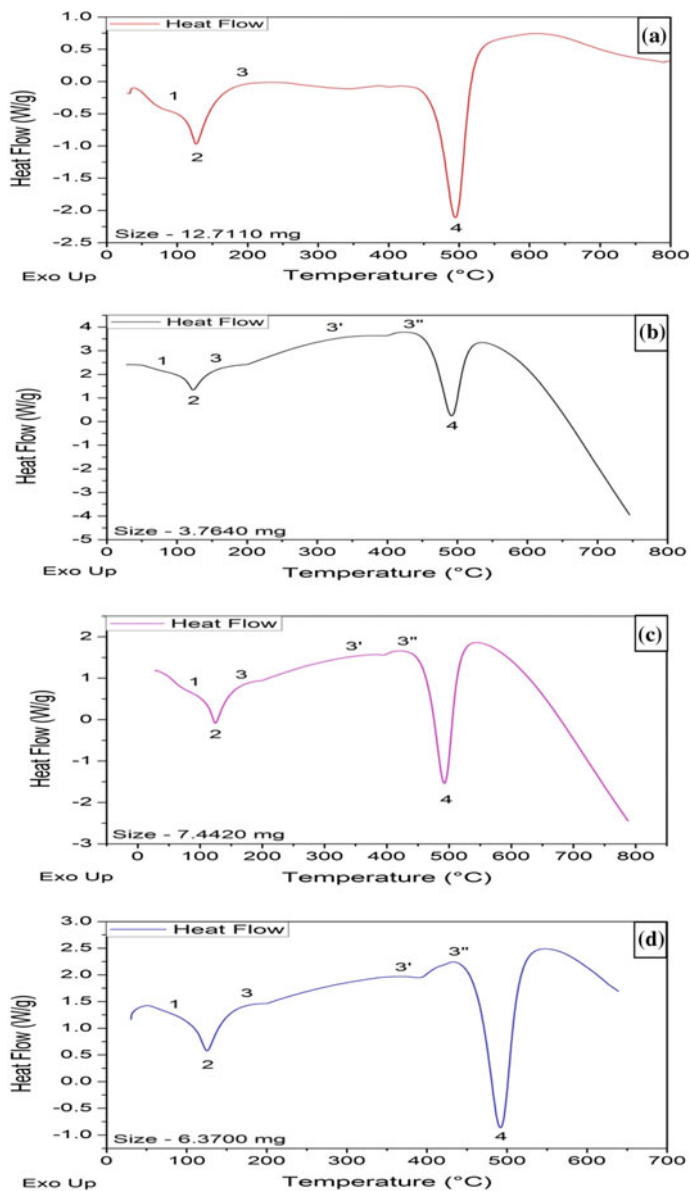


Fig. 4 Differential scanning calorimetry (DSC) of (a) Virgin XLPE, (b) nano 1 wt% unmodified, (c) nano 1 wt% agglomerated, (d) nano 1 wt% Octylsilane modified [39]

Table 2 Other studies on the XLPE-based nanocomposite

Material	Filler content	DC breakdown strength	Thermal activation energy	Space charge	Other significant result	References
XLPE/Al ₂ O ₃	10 wt%		0.99 eV			[57]
XLPE/MgO	3 wt%			75% suppression		[58]
XLPE/SiO ₂	2 wt%	increased			Temperature dependent conductivity	[59]
XLPE/BN	0.1 wt%			Suppressed space charge		[60]
XLPE/ZnO	2 wt%				1 wt% and 2 wt % improved the TIV	[61]
XLPE/SiO ₂	1.5 wt%				improve the tree growth resistance of the polymer	[62]

mass transfer due to its char structure with exfoliated silicate layers [53, 54] which also helps in flame retardancy mechanisms.

Said et al. [55] studied the clay XLPE composites with a different ratio. 1% clay composition exhibited a 14% increase in electrical properties, 20% higher of electrical capacitance and dielectric constant compared to pure XLPE. This structure material could, therefore, be used dominantly for nuclear power plant. Furthermore, the high voltage and low dielectric loss of XLPE cables insulation are one of the related important advantages. The higher of both resistance to thermal disfigurement and aging feature of the XLPE cable, permit it to carry large current under normal (90 °C), emergency (130 °C) or short circuit (250 °C) conditions [56].

Earlier reports have shown that the incorporation of nanoparticles (e.g., MgO, and SiO₂) which improved the electrical properties and reduced the space charge accumulation in the PE-based matrix [6, 7]. However, the high content of the nanoparticles had a negative impact on the PE matrix due to the introduction of impurities and defects [8] (Table 2).

6 Conclusion and Future Outlook

The addition of nanofillers to cross-linked polyethylene has gained attention in the high voltage research field toward the improvement of insulation materials since the beginning of the last century. The current need for research is the development of systems suitable for direct current–long distance transmissions. Such high-end application material needs to have good physical strength, degradation performance, and high insulation integrity while being available at an economic

economical cost. Many of the disadvantages of using PE-based cables have been covered by the introduction of XLPE-based nanocomposites. However, many questions are yet to be answered. The proper dispersion of the nanofillers needs to be ensured to obtain the enhanced properties, also the detailed mechanism of action of such composites needs to be studied. Hence, proper selection of the nanofiller, process and design are highly essential in order to extend the life of high voltage equipment and also to reduce the maintained cost.

References

1. Rizk FAM, Trinhhigh GN (2014) High voltage engineering. High Voltage Engineering
2. Kram SL, Lukas C, Ross L, Beach MW, Beulich I, Davis JW, et al (2016) Polystyrene foam insulation: Implementation of alternate sustainable flame retardant. In: Annual Technical Conference—ANTEC, Conference Proceedings
3. Mok KL, Eng AH (2018) Characterisation of crosslinks in vulcanised rubbers: From simple to advanced techniques. *Malaysian J Chem*
4. Ronca S. (2017) Polyethylene. In: Brydson's *Plastics Materials: 8th Edition*
5. Mazzanti G, Marzinotto M (2013) Extruded cables for high-voltage direct-current transmission: Advances in research and development. *Extruded Cables for High-Voltage Direct-Current Transmission: Advances in Research and Development*
6. Kasirajan S, Nkouajio M (2012) Polyethylene and biodegradable mulches for agricultural applications: A review. *Agronomy for Sustainable Development*
7. Elhrari W (2018) The Influence of LDPE Content on the Mechanical Properties of HDPE/LDPE Blends. *Res Dev Mater Sci*
8. Venkatraman S, Kleiner L (1989) Properties of three types of crosslinked polyethylene. *Adv Polym Technol*
9. Jin H, Gonzalez-Gutierrez J, Oblak P, Zupančič B, Emri I (2012) The effect of extensive mechanical recycling on the properties of low density polyethylene. *Polym Degrad Stab*
10. Tangjuank S (2011) Thermal insulation and physical properties of particleboards from pineapple leaves. *Int J Phys Sci*
11. Mohanraj GT, Chaki TK, Chakraborty A, Khastgir D (2007) Measurement of AC conductivity and dielectric properties of flexible conductive styrene-butadiene rubber-carbon black composites. *J Appl Polym Sci*
12. Waddell WH, Tsou AH (2015) Butyl rubbers. In: *Rubber Compounding: Chemistry and Applications, Second Edition*
13. Yan Z, Han B, Zhao H, Yang J, Li C (2014) Space charge and conductivity characteristics of CB/XLPE nanocomposites. In: *Proceedings of the International Symposium on Electrical Insulating Materials*
14. Zhang L, Zhou Y, Huang M, Sha Y, Tian J, Ye Q (2014) Effect of nanoparticle surface modification on charge transport characteristics in XLPE/SiO₂ nanocomposites. *IEEE Trans Dielectr Electr Insul*
15. Kim DS, Lee DH, Kim YJ, Nam JH, Ha ST, Lee SH (2014) Investigation of space charge distribution of MgO/XLPE composites depending on particle size of MgO as inorganic filler. In: *Applied Mechanics and Materials*
16. Wang Y, Xiao K, Wang C, Yang L, Wang F (2016) Study on dielectric properties of TiO₂/XLPE nanocomposites. In: *ICHVE 2016—2016 IEEE International Conference on High Voltage Engineering and Application*
17. Roy M, Nelson JK, MacCrone RK, Schadler LS, Reed CW, Keefe R, et al (2005) Polymer nanocomposite dielectrics - The role of the interface. *IEEE Trans Dielectr Electr Insul*

18. Tanaka T, Bulinski A, Castellon J, Fréchet M, Gubanski S, Kindersberger J, et al (2011) Dielectric properties of XLPE/SiO₂ nanocomposites based on CIGRE WG D1.24 cooperative test results. In: IEEE Transactions on Dielectrics and Electrical Insulation
19. Hui L, Schadler L, J Keith Nelson (2013) The influence of moisture on the electrical properties of crosslinked polyethylene/silica nanocomposites. IEEE Trans Dielectr Electr Insul
20. Chen X, Xu Y, Cao X, Gubanski SM (2015) Electrical treeing behavior at high temperature in XLPE cable insulation samples. IEEE Trans Dielectr Electr Insul
21. Xiangrong Chen, Mantsch AR, Libin Hu, Gubanski SM, Blennow J, Olsson C-O (2014) Electrical treeing behavior of DC and thermally aged polyethylenes utilizing wire-plane electrode geometries. IEEE Trans Dielectr Electr Insul
22. Kurnianto R, Murakami Y, Hozumi N, Nagao M (2007) Characterization of tree growth in filled epoxy resin: The effect of filler and moisture contents. IEEE Trans Dielectr Electr Insul
23. Zheng X, Liu Y, Wang Y (2018) Electrical tree inhibition by SiO₂/XLPE nanocomposites: insights from first-principles calculations. J Mol Model
24. Acedo M, Radu I, Frutos F, Filippini JC, Notinger P (2001) Water treeing in underground power cables: Modelling of the trees and calculation of the electric field perturbation. J Electrostat
25. Hui L, Smith R, Nelson JK, Schadler LS (2009) Electrochemical treeing in XLPE/silica nanocomposites. In: Annual Report—Conference on Electrical Insulation and Dielectric Phenomena, CEIDP
26. Li X, Xu M, Xin L, Xie D, Cao X (2011) Study of montmorillonite on morphology and water treeing behavior in crosslinking polyethylene. In: Proceedings of the International Symposium on Electrical Insulating Materials
27. Sellick RL, Sullivan JS, Chen Q, Calebrese C (2017) Future improvements to HVDC cables through new cable insulation materials. In: IET Conference Publications
28. Montanari GC, Mazzanti G, Palmieri F, Motori A, Perego G, Serra S (2001) Space-charge trapping and conduction in LDPE, HDPE and XLPE. J Phys D Appl Phys
29. Williams PA, Brown CM, Tsukamoto R, Clarke IC (2010) Polyethylene wear debris produced in a knee simulator model: Effect of crosslinking and counterface material. J Biomed Mater Res—Part B Appl Biomater. 2010
30. Morshedian J, Hoseinpour PM (2009) Polyethylene cross-linking by two-step silane method: A review. Iranian Polymer Journal (English Edition)
31. Ghasemi I, Morshedian J (2003) The effect of co-agent on the peroxide crosslinking of LDPE. Iran Polym J (English Ed)
32. Suzuki A, Sugimura T, Kunugi T (2001) Thermal fractionation and crystallization enhancement of silane-grafted water-crosslinked low-density polyethylene. J Appl Polym Sci
33. Tamboli SM, Mhaske ST, Kale DD (2004) Crosslinked polyethylene. Indian J Chem Technol
34. Wang S, Chen P, Yu S, Zhang P, Li J, Li S (2018) Nanoparticle dispersion and distribution in XLPE and the related DC insulation performance. IEEE Trans Dielectr Electr Insul
35. Lei W, Wu K, Wang Y, Cheng Y, Zheng X, Dlsado LA, et al (2017) Are nano-composites really better DC insulators? A study using silica nanoparticles in XLPE. IEEE Trans Dielectr Electr Insul
36. Wang Y, Wang C (2015) Effect of nanoparticles on space charge behavior of XLPE/SiC nanocomposites. In: Annual Report—Conference on Electrical Insulation and Dielectric Phenomena, CEIDP
37. Murata Y, Goshowaki M, Reddy CC, Sekiguchi Y, Hishinuma N, Hayase Y, et al (2008) Investigation of space charge distribution and volume resistivity of XLPE/MgO nanocomposite material under DC voltage application. In: Proceedings of the International Symposium on Electrical Insulating Materials
38. Charalambous C, Danikas M, Yin Y, Vordos N, Nolan J, Mitropoulos A (2016) Study of the Behavior of Water Droplets Under the Influence of a Uniform Electric Field on Conventional Polyethylene and on Crosslinked Polyethylene (XLPE) with MgO Nanoparticles Samples. Eng Technol Appl Sci Res 7(1):1323–1328

39. Ashish Sharad P, Kumar KS (2017) Application of surface-modified XLPE nanocomposites for electrical insulation—partial discharge and morphological study. *Nanocomposites*
40. Alapati S, Thomas MJ (2010) Electrical treeing in polyethylene: Effect of nano fillers on tree inception and growth. In: 2010 International Conference on High Voltage Engineering and Application, ICHVE 2010
41. Mohanty A, Srivastava VK (2013) Dielectric breakdown performance of alumina/epoxy resin nanocomposites under high voltage application. *Mater Des*
42. Fairus M, Mansor NS, Hafiz M, Kamarol M, Mariatti M (2015) Investigation on dielectric strength of alumina nanofiller with SiR/EPDM composites for HV insulator. In: Proceedings of the IEEE International Conference on Properties and Applications of Dielectric Materials
43. Mansor NS, Wahab JA, Fairus M, Ishak D, Mariatti M, Kamarol M, et al (2017) Influence of ZnO and Al₂O₃ nanofillers on electrical treeing in XLPE insulation. In: International Conference on High Voltage Engineering and Power Systems, ICHVEPS 2017—Proceeding
44. Zhou K, Tao X, Wang X, Zhao W, Tao W (2015) Insight into the new role of titanium isopropoxide catalyst on rejuvenation for water tree aged cables. *IEEE Trans Dielectr Electr Insul*
45. Boggs S, Xu J (2001) Water treeing—filled versus unfilled cable insulation. *IEEE Electr Insul Mag*
46. Abderrazzaq MH (2005) Development of water tree structure in polyester resin. *IEEE Trans Dielectr Electr Insul*
47. Wen Shu E, Stagi WR, Derezes JG, Chatterton WJ (2014) Lightning protection for aged cable systems—Problems with water trees. In: Proceedings of the IEEE Power Engineering Society Transmission and Distribution Conference
48. Merati Shirazi AH, Hosseini SMH (2019) Comparing the Performance of γ -Alumina Nanofiller and Titanium Tetraisopropoxide Catalyst in the Rejuvenation of Water Tree Degraded XLPE Cables. *J Electron Mater*
49. Jayakrishnan A, Kavitha D, Arthi A, Nagarajan N, Balachandran M (2016) Simulation of electric field distribution in nanodielectrics based on XLPE. In: *Materials Today: Proceedings*
50. Gopalakrishnan CN, Kavitha D, Kathiravan N (2015) Theoretical investigation on electric field in XLPE nanocomposite using finite element method. *Int J Appl Eng Res*
51. Henk PO, Kortsens TW, Kwarts T (1999) Increasing the electrical discharge endurance of acid anhydride cured DGEBA epoxy resin by dispersion of nanoparticle silica. *High Perform Polym*
52. Kaynak C, Ibibikan E (2014) Contribution of nanoclays to the flame retardancy of polyethylene-based cable insulation materials with aluminum hydroxide and zinc borate. *J Fire Sci*
53. Nelson JK (2010) Dielectric polymer nanocomposites. *Dielectric Polymer Nanocomposites*
54. Lee BC, Yoo JS, Ogay V, Kim KW, Dobberstein H, Soh KS, et al (2007) Electron microscopic study of novel threadlike structures on the surfaces of mammalian organs. *Microsc Res Tech*
55. El-kattan W, Ezz-eldin M, A. Said E-S, Othman ES (2019) A reduced gamma radiation effects on the electrical insulating cables using XLPE/clay nanocomposites. *J Al-Azhar Univ Eng Sect*
56. Nelson JK (2007) Overview of nanodielectrics: Insulating materials of the future. In (2007) *Electrical Insulation Conference and Electrical Manufacturing Expo. EEIC 2007*
57. Cao L, Zhong L, Li Y, Gao J, Chen G, Li W, et al (2019) Conductivity of HVDC Cable Insulation Materials: Case Study between XLPE Nanocomposite and Polymer Filled XLPE. In: *ICEMPE 2019—2nd International Conference on Electrical Materials and Power Equipment, Proceedings*
58. Ramani AN, Ariffin AM, Rahman MSA, Ghani ABA, Baharin KA (2018) Observation of Space Charge Formation in XLPE/MgO Nanocomposite. *J Adv Res Mater Sci*
59. Donghe D, Xiufeng L, Jin S, Peijie Y, Youfu C (2017) The influence of surface modifier on structural morphology and dielectric property of XLPE/SiO₂ Nanocomposites. In: *ICEMPE 2017—1st International Conference on Electrical Materials and Power Equipment*

60. Xiang J, Wang S, Chen P, Li J (2018) Space charge characteristics in XLPE/BN nanocomposites at different temperatures. In: Proceedings of the IEEE International Conference on Properties and Applications of Dielectric Materials
61. Mansor NS, Ishak D, Mariatti M, Halim HSA, Basri ABA, Kamarol M (2017) Investigation on electrical treeing characteristics of XLPE containing ZnO nano-filler. In: Proceedings of the International Symposium on Electrical Insulating Materials
62. Nazar NSM, Mansor NS, Muhamad NA, Kamarol M, Mariatti M, Mohamed AI (2018) Electrical Tree Propagation in XLPE Containing Untreated and Treated Silica Nanofiller. In: 2018 Condition Monitoring and Diagnosis, CMD 2018—Proceedings

Chapter 10

Electrical Insulation: XLPE Versus Conventional Materials



Petru V. Noșingher, Cristina Stancu, and Ilona Pleșa

1 Introduction

An electrical insulation system (or simply, electrical insulation) represents, by definition, the electrical insulating materials or the assembly of electrical insulating materials that are in direct contact with the conductive parts of an electrical equipment (electric machine, transformer, circuit breaker, contactor, power cable, insulator, etc.) [1]. The electrical function consists in reducing (or, ideally, canceling) the component of the electrical current that flows from one conductor to an adjacent one or from the conductors to the metallic parts of the electrical equipment (magnetic cores, enclosures, etc.) through the environment (air, earth, etc.). The thermal function consists in ensuring the easiest transmission of the heat developed in conductors (Joule losses), magnetic cores (losses through hysteresis and Eddy currents) and in themselves (dielectric losses) to the cooling environment (forced cooling system (with air, hydrogen, etc.) or natural (air)). The mechanical function consists in ensuring a mechanical fixing of the conductors (in the magnetic cores, in the electrical installations) and/or to protect them against mechanical stresses (static or dynamic) of the electromagnetic field, etc.

The diversification of the constructive forms regarding the electrical equipment and the fields of use alongside the increase of the electrical, thermal and mechanical

P. V. Noșingher (✉)

University Politehnica of Bucharest, Splaiul Independentei 313, 060042 Bucharest, Romania

e-mail: petrunot@elmat.pub.ro

C. Stancu · I. Pleșa

Polymer Competence Center Leoben GmbH (PCCL), Roseggerstrasse 12, Leoben 8700, Austria

e-mail: cstancu@elmat.pub.ro

I. Pleșa

e-mail: ilona.plesa@pccl.at

© Springer Nature Singapore Pte Ltd. 2021

J. Thomas et al. (eds.), *Crosslinkable Polyethylene Based Blends and Nanocomposites*, Materials Horizons: From Nature to Nanomaterials, https://doi.org/10.1007/978-981-16-0486-7_10

stresses on the insulation systems have required the performance of systematic investigations on the structure and properties of the insulating materials related to:

- (a) more accurate rating of insulation systems (use of insulation at maximum permissible stresses, in order to reduce the costs of the electrical equipment);
- (b) taking into account the new operating conditions of the insulation systems (high humidity and/or intense radiation environments, low operating temperatures [cryogenics, superconductivity]);
- (c) obtaining materials with higher dielectric strength and operating temperature (for reducing the insulation systems size);
- (d) obtaining insulating materials that require technological processes with low energy consumption;
- (e) obtaining insulating materials with special properties (required in various applications);
- (f) reduction of the pollution produced by the insulating materials disposal in the environment (within the process of production or exploitation);
- (g) producing biodegradable electrical insulating materials;
- (h) increasing the lifetime of the insulation systems.

The construction and structure of the insulation systems are related to the types of equipment they are part of (electric machine, transformer, power energy cable, etc.), substance (copper, aluminum, etc.) and geometric shapes of the conducting paths (round, square, rectangular, etc.), their character (organic, inorganic, etc.) and the physical state (gas, liquid, solid) of the used electrical insulating materials, etc.

Due to the fact that cross-linked polyethylene (XLPE) is mainly used for the insulation of medium, high, and very high voltage power cables [2], this chapter presents information on XLPE and other materials' properties used in the manufacture of power cables and an analysis regarding their application in present and future.

2 Power Cables

A *power cable* is an electrical cable (one or more wires running side by side or bundled), respectively, an assembly of one or more electrical conductors (usually held together with an overall sheath) used for the transmission of electrical energy (power). Power cables may be installed as permanent wiring in buildings, underground, overhead, or exposed.

Besides some technical and aesthetic considerations, the overhead lines arise some safety hazards to lineworkers themselves, firefighters and public. Therefore, underground lines increasingly replace the overhead line structures. Hence, this chapter will be related only to underground power cables, simply called *power cables*.

Power cables consist of three major components, namely conductors, insulation, and protective jacket, while the construction and the material are settled by three main factors:

- (a) working voltage, defining the nature and the thickness of the insulation;
- (b) current-carrying capacity, defining the cross-sectional size of the conductors;
- (c) environmental conditions (temperature, water, chemical or sunlight exposure, and mechanical impact) defining the properties of the outer cable jacket [3].

The first cable insulations were manufactured in the early 1880 s for voltages up to 10 kV based on gutta-percha, natural vulcanized rubber, rosin oil, castor oil, vax, jute, hemp, cotton, black asphalt, oil-impregnated -paper, etc. [2]. For higher voltages (over 35 kV), cables were performed with pressurized-oil, low-viscosity-oil-impregnated-paper (after 1928) and with solid dielectrics (after 1950). For high voltages (275–500 kV) and powers (10 GVA), compressed SF₆ gas power transmission cables were performed (after 1974). In the case of very large capacity power transmission (over 10 GVA), superconducting cables were proposed (see Fig. 1) [4]. Currently, for the transport and distribution of electricity (beside airlines) are used Oil-Impregnated Paper Power, Oil-Pressurized Power Transmission, Solid-Dielectric Extruded Power Transmission, Solid Extruded Dielectric Power Distribution, Underwater (Submarine), Compressed SF₆ Gas Power Transmission, and Superconducting Power Transmission Cables.

Oil-Impregnated Paper Power Cables are, in general, three-phase cables with a nominal voltage of 15–35 kV (but can reach up to 69 kV) (see Fig. 2) [4]. The limitation of these cables for medium voltages is due to the high level of partial discharges that occur at high voltages within the insulation cavities (formed during the manufacturing process or during the load cycling in service). In the case of *Oil-Pressurized Power Transmission Cables*, the effect of the cavities was eliminated by the introduction of a low-viscosity-oil-impregnated-paper insulating system and, therefore, the operating voltages could be increased up to 750 kV. In this case, the cavities formation is practically avoided by maintaining a pressure slightly above

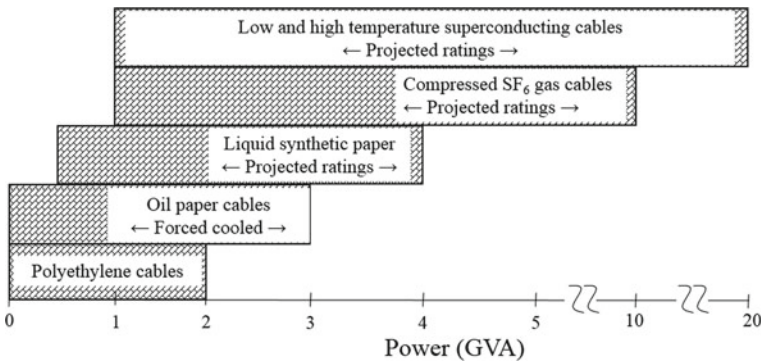


Fig. 1 Ratings of power transmission cables (Redrawn and adapted figure from reference [4])

atmospheric condition of the insulating oil. Starting with 1980, the paper (Kraft) was replaced by polypropylene-laminated-paper (PPLP) as insulation in cables (with lower dielectric constant and losses and higher breakdown strength; see Fig. 3 and Table 1), while branched dodecyl benzene used as an impregnating liquid, reached operating voltages of 750–800 kV [5, 6].

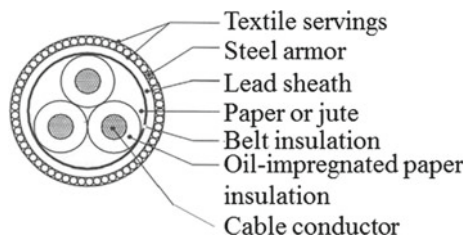
Even though the reliable long-term performance of the oil-paper transmission cables has been proven over years (some cables working even after 60–70 years), however, from environmental (elimination of oil leaks) and maintenance (elimination of hydraulic oil reservoir tank systems, highly skilled personnel for operation, maintenance and repair [8]) considerations, these cables were (after 1950) extensively replaced by *Solid-Dielectric Extruded Power Transmission Cables*. Initially, the insulation was performed from thermoplastic-type low-density linear polyethylene (LDPE) (up to 225 kV; see Fig. 4), and from thermosetting-type solid extruded XLPE (up to 800 kV; see Fig. 5) after 1975 [9].

The problems that arise in these cables during operation are, in particular, the thermo-oxidative degradation of the insulation and the appearance of cavities (with or without water) inside them (which facilitate the development of partial discharges and electric and water trees) (see Fig. 6, [1]). In addition to LDPE and XLPE, butyl rubber, low-density high-molecular-weight polyethylene (HMWPE), tree-retardant XLPE (TR-XLPE) (see Fig. 7a), and ethylene propylene rubber (EPR) are also used (see Fig. 7b). In general, the constructions of other thermoplastic and thermosetting insulated transmission and distribution power cables (medium, high, and very high voltage) are similar to those shown in Fig. 7c [9].

In general, extruded HVDC cables offer significant advantages over traditional paper insulated cable types: a higher conductor temperature, a more compact cable for the same power rating, lighter moisture barriers (resulting in a lighter cable), and an easier way of joining the extruded cables, which requires less skills and avoids the significant long-term environmental hazards associated with oil leaks.

Submarine cables are used for crossing water sectors to interconnect systems (between an island and adjacent shoreline) and may be self-contained oil-filled type (for short distances transmission), high-viscosity oil-impregnated paper (for long distances) or solid extruded dielectric type (XLPE) (see Fig. 8, [12]). *Superconducting cables* are using as insulation cellulose paper, polypropylene or polyethylene paper/tape, and extruded XLPE (Fig. 9, [4]). *Gas-insulated transmission lines* (GITL) are in use for system voltages up to 765 kV. A single-phase

Fig. 2 Cross section of three-conductor belted-type oil-impregnated paper power cable (Redrawn and adapted figure from reference [4])



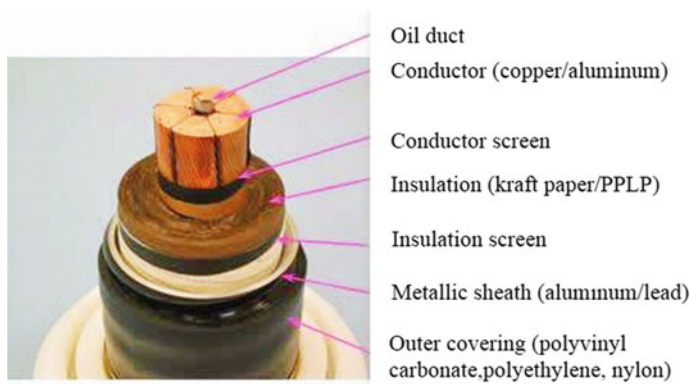


Fig. 3 Extra-high voltage oil-filled cable 110-500 kV (Redrawn figure from reference [7])

Table 1 Electrical characteristics of Polypropylene Paper Composite Tapes (PPP) and Kraft Paper (KP) tapes impregnated with branched dodecyl benzene [5]

Tape	PPP	KP
Thickness (μ)	170	200
Dielectric constant (-)	2.58	3.4
Dissipation factor at 20 kV/mm and 80 °C (-)	5.3×10^{-4}	2.0×10^{-3}
Breakdown strength (MV/m)	150	80
Impulse breakdown strength (MV/m)	256	150

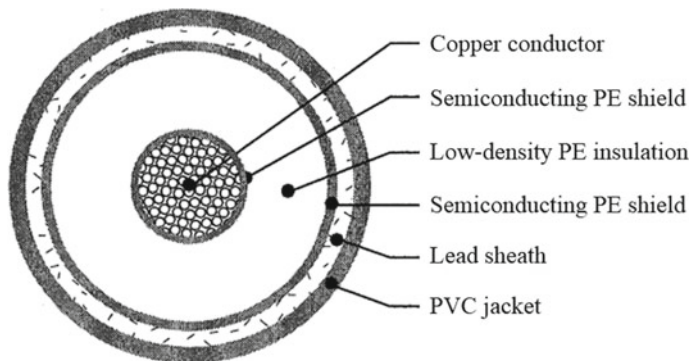


Fig. 4 Cross section of 225 kV LDPE transmission cable (Redrawn and adapted figure from reference [4])

consists of two coaxial cylinders (the inner being the load current conductor and the outer being the grounded pressure vessel that contain gas), which are maintained coaxial by means of the solid-dielectric spacers. These cables present very small

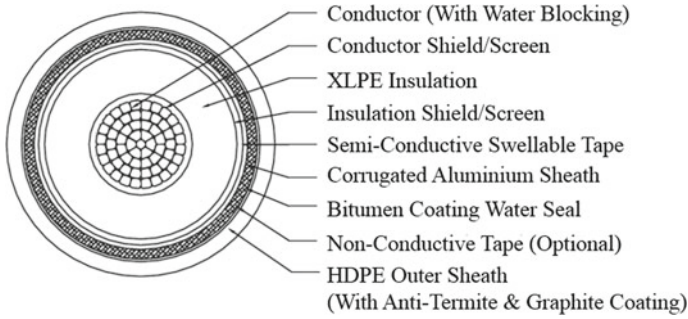
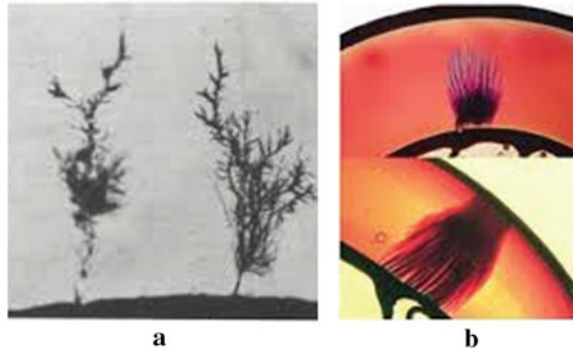


Fig. 5 Cross section of 132 kV XLPE-insulated and HDPE sheathed cable (Redrawn figure from reference [9])

Fig. 6 Electrical (a) and water (b) trees within XLPE insulation [1]



dielectric losses, both in gas (SF_6 for pressures up to 3.5 bars at 20 °C) and in spacers (performed by epoxy resins filled with silica or alumina) [4].

3 Insulating Materials for Power Cables

Electrical insulating materials (or simply insulators) are substances with the electrical conductivity sufficiently low to separate two conductive parts with different electrical potentials. Their electrical resistivity ρ is between 10^6 and 10^{18} Ωm , and the real part of the relative complex permittivity ϵ'_r (or dielectric constant ϵ_r) between 1 and 16. Solid insulators show widths of the forbidden band Fermi w_F between 5 and 8 eV [13].

Considering the very large number, as well as the fast development of the insulators' production (especially in the last 20 years) with increasingly diversified properties and applications, the accomplishment of a complete classification of the

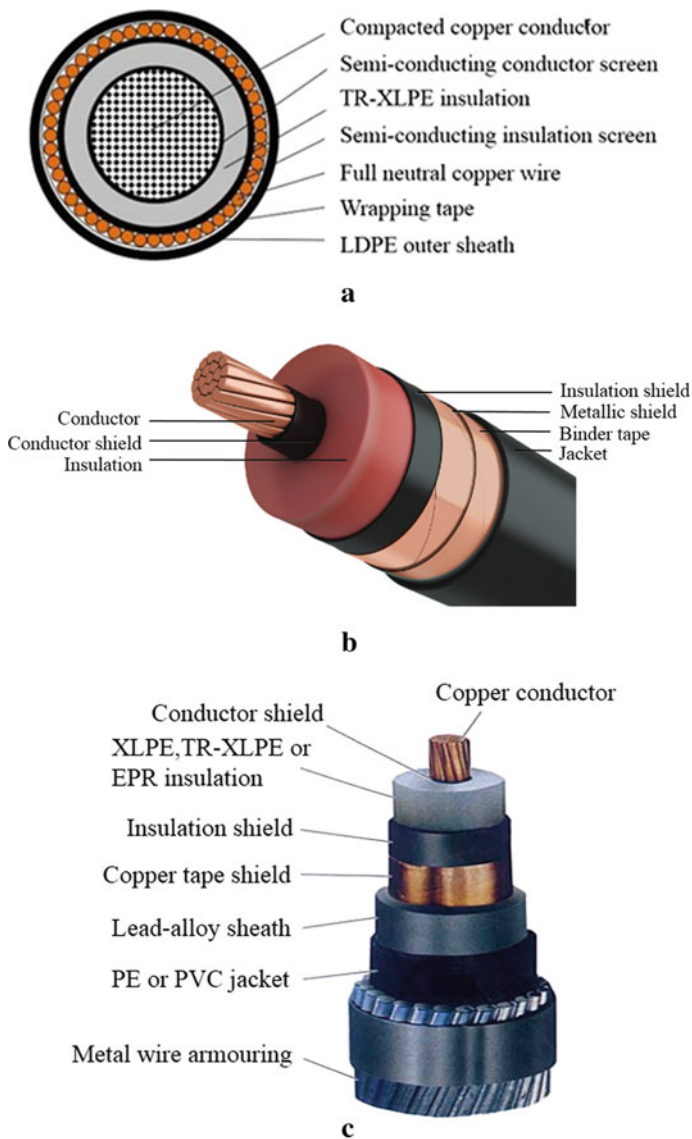


Fig. 7 **a** High voltage cable insulated with TR-XLPE [10]; **b** medium-voltage (35 kV) shielded power cable insulated with EPR [11]; **c** solid extruded dielectric power cable [9]

electrical insulating materials, including all the elements characteristic for their behavior in service is extremely difficult. For this reason, several types of classifications appeared (each with advantages and disadvantages) as follows by:

Fig. 8 Cross-sectional configuration of the bipolar 250-kV DC-XLPE submarine cable within the Hokkaido–Honshu HVDC link (Redrawn and adapted figure from reference [12])

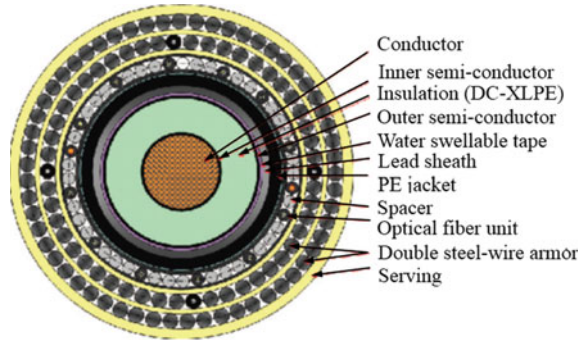
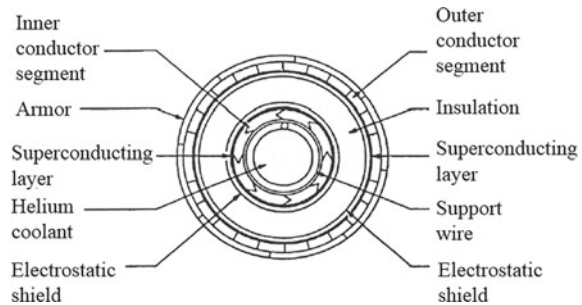


Fig. 9 Cross section of superconducting coaxial cable (Redrawn and adapted figure from reference [4])



- (a) thermal stability (materials were divided into seven classes of insulation, starting with rubber and cellulose products, and ending with inorganic materials),
- (b) chemical composition (organic, transient, inorganic),
- (c) behavior under thermal stresses (thermoplastics and thermosets),
- (d) main component of the final material (mica, synthetic resins, varnishes, etc.),
- (e) usage domain (notch insulation, between layers, impregnation, and coating materials),
- (f) certain practical considerations (defined by the Encyclopedia of electrical insulating materials), etc.

As the electrical insulation is subjected during the operation to multiple simultaneous stresses, it is recommended that the insulators themselves to be characterized by *performance indices*. These values depend, both on the final state of the materials, and on their behavior under the action of temperature, electric field, mechanical stress, radiation, water, etc. [1].

The characteristics of power energy cables are essentially determined by those of the conductive and electrical insulating materials used in their construction. The electrical insulating materials must satisfy the following main conditions:

- (a) increased dielectric strength and resistivity;
- (b) reduced loss factor, dielectric constant, and space charge accumulation;
- (c) high resistance to partial discharges, electric and water trees;
- (d) high thermal conductivity and stability;
- (e) high stretching, tensile strength, and compression resistance;
- (f) high resistance to environmental action (solvents, acids, bases, oxygen, etc.);
- (g) reduced pollution and increased biodegradability.

The general properties of some materials used as insulation of power cables are presented below.

3.1 Oils

Although for a long time, only mineral oils with a certain content of aromatic and naphthenic hydrocarbons have been used as insulation of Oil-Impregnated Paper and Oil-Pressurized Power cables, currently synthetic oils replace them. In the case of pipe-type cable applications polybutene liquids (with a viscosity of 10.6–11.1 cSt, at 99 °C) are used and for the self-contained hollow-core cables, alkyl benzenes are in current use [4].

A predominant role in the use of an oil for power cables insulation is referred to the values of its viscosity at the paper impregnation temperature, due to the fact that during the manufacturing process of the cable, the oil determines the impregnation rate, and at the operating temperature, the viscosity influences the oil speed in the cable insulating system. Moreover, when the cable charge disappears and the oil cools down, its viscosity must be low enough, so that it does not leak out of the paper and produces cavities where partial discharges can develop. The flash point of the oil provides the value of the limit beyond which the oil cannot be heated to avoid the fire hazard of the more volatile emitted vapors. The pour point of the oil is a useful quantity that indicates the lower value of temperature at which partial wax separation within the oil will occur. Furthermore, at lower ambient temperatures, the pour point defines the temperature limit at which no free movement will occur within the cable [4].

The performance of a cable oil in service is determined by the level where it forms sludge and excessive acidity compounds in the presence of oxygen. To reduce the corrosivity of oils, they must be free of sulfur and inorganic chlorides and sulfates, caused by direct contamination or incorrect refining.

Mineral oils (based on crude oil) used for impregnating Kraft paper are composed of aromatic $C_{4n+2}H_{2n+4}$ (12%), naphthenic C_nH_{2n} (38%), and paraffinic C_nH_{2n+2} (50%) hydrocarbons (see Fig. 10). The lengths and structures of the oil molecules are much diversified. One possible molecular arrangement is being the one shown in Fig. 11 [4]. The properties of oils depend on the hydrocarbon contents, as well as on the operating conditions (temperature, oxygen, water, etc.). Aromatic hydrocarbons lead to the increase of dielectric losses of oils, but they are

necessary to decrease the gas production in oils under the action of the electrical stress. Naphthenic hydrocarbons are very stable with a low freezing point, whereas paraffinic ones have a high freezing point, which increase the viscosity of oils [13].

The dielectric constant of cable oils is in the order of 2.2 at room temperature (see Table 2) and decreases with temperature (due to the decreased density [14]). The dissipation factor $\tan\delta$ is less than 10^{-4} and increases with temperature (due to the increased ionic conductivity) [13–15]. It should be emphasized that the magnitude of dielectric losses in oil-impregnated paper are determined, essentially by the impregnated paper instead of impregnating liquid [16–18], as can be observed as well in Figs. 12 and 13 [14, 19].

Polybutene oils have become increasingly popular for use in pipe-type oil-filled cables, both as higher viscosity impregnates and as pipe filling oils, due to their lower costs and electrical and physical properties comparable to those of cable-type mineral oils (see Table 3) [4]. They are obtained by olefins polymerization and contain very long molecules with isobutene as the base unit, characterized by methyl group side chains and molecular weights between 300 and 1350 [20].

The molecular structure of *alkyl benzenes* intended for cable oil applications is a branched one and has the chemical formula $C_6H_5CHR^1R^2$, where $R^1 = C_nH_{2n+1}$, and $R^2 = C_mH_{2m+1}$, where m, n are integers $m \geq 0, n \geq 1$ (typically 10–16). The

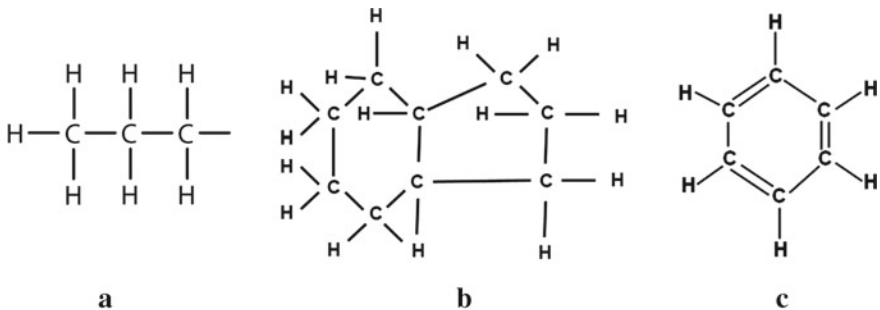


Fig. 10 Molecular constituents of mineral cable insulating oil: **a** paraffinic hydrocarbon; **b** naphthenic hydrocarbon; **c** aromatic hydrocarbon

Fig. 11 Possible molecular structure in mineral cable oil [4]

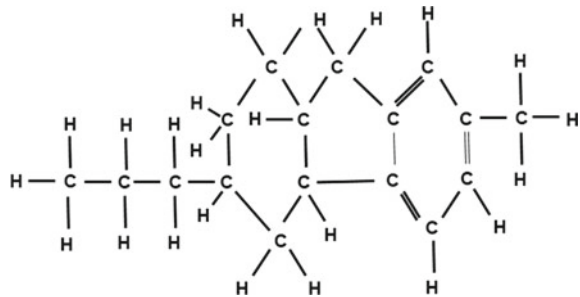
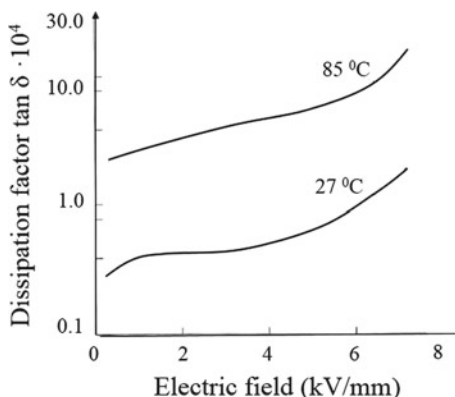


Table 2 Physical and electrical properties of cable oils

Property	Pipe cable oil	Heavy cable oil	Polybutene cable liquid	Self-contained cable oil	Dodecyl benzene
Viscosity (cSt)—at 37.8 °C	170	490	—	7.29	6.0
—at 100 °C	10	21	10.6	1.91	4.5
Flash point (°C)	196.1	243.3	154	130	130
Acidity(mgKOH/g)	0	0	0.01	0.05	0.02
Pour point (°C)	-26.1	-17.8	-34.0	-50.0	-45.0
Density (g/cm ³)	0.928	0.926	0.862	0.883	0.871
Thermal conductivity (W/m °C)	0.125	0.125	—	0.126	0.581
Dielectric strength (kV/mm)	>12	>12	—	>12	>12
Dielectric constant at 60 Hz, 25 °C	2.15	2.23	2.17	2.30	2.20
Dissipation factor at 60 Hz	0.001	0.001	0.0005	0.001	0.0011
Volume resistivity at 100 °C (Ωm)	2×10^{11} (100 °C)	7×10^{11} (100 °C)	1×10^{12} (25 °C)	5×10^{11} (25 °C)	2×10^{11} (25 °C)

Adapted table from reference [4]

Fig. 12 Variation of the dissipation factor with the electric field for mineral oil used in self-contained oil-filled cables (Redrawn and adapted figure from reference [14])



values of n determine the lengths of the molecular chains and, respectively, the average molecular weight (approx. 320 for the self-contained hollow-core cables [4]). The addition of alkyl benzenes to mineral oils greatly reduces the gas production and improves the properties of mineral oil during its exploitation. For pipe-type cables, it is recommended to use polybutene-alkyl benzenes mixtures, with good physical and electrical properties (see Table 4).

Fig. 13 Variation of the dissipation factor with the electric field for mineral oil-Kraft paper insulating system used in self-contained oil-filled cables (Redrawn and adapted figure from reference [19])

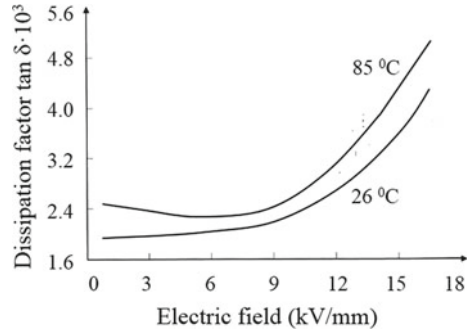


Table 3 Physical and electrical properties of polybutene oils manufactured by costen oil and chemical company [4]

Property	OSH oil	06SH oil	015sh oil	30SH oil
Average molecular weight	340	450	570	1350
Viscosity (SUS*) —at 38 °C	110	575	3440	115,000
—at 99 °C	41	63	158	3070
Flash point (°C)	132	154	160	232
Pour point (°C)	-51	-40	-23	4.4
Acidity (mgKOH/g)	0.01	0.01	0.01	0.01
Water content (ppm)	15	15	15	15
Dissipation factor (60 Hz, 100 °C)	0.0003	0.0003	0.0002	0.0002
Dielectric constant (1 MHz, 25 °C)	2.14	2.16	2.17	2.24
Dielectric strength at 80 °C (kV/mm)	>14	>14	>14	>14
Volume resistivity at 100 °C (Ωm)	8×10^{12}	1×10^{13}	1.2×10^{13}	1.5×10^{13}

SUS*—Saybolt universal seconds

Table 4 Physical and electrical properties of alkyl benzenes (A) and alkyl benzene polybutene mixture (B) [4]

Property	A	B
Average molecular weight	120	380
Viscosity (SUS*) —at 38 °C	100	500
—at 99 °C	38	59
Flash point (°C)	177	177
Pour point (°C)	-50	-20
Acidity (mgKOH/g)	0.02	0.02
Water content (ppm)	25	25
Dissipation factor (60 Hz, 100 °C)	0.0002	0.0002
Dielectric constant (1 MHz, 100 °C)	2.10	—
Dielectric strength at 25 °C (kV/mm)	50	40
Volume resistivity at 100 °C (Ωm)	1×10^{13}	5×10^{12}

SUS*—Saybolt universal seconds

3.2 Papers

Papers used for power cables insulation are composed of cellulose fibers felted together to form mechanically strong sheets (see Fig. 14). These papers are obtained by Kraft process (also known as Kraft pulping or sulfate process), a process by which the conversion of wood into wood pulp (i.e., the main component of paper) is performed.

The Kraft process entails treatment of wood chips with a hot mixture of water, sodium hydroxide (NaOH) and sodium sulfide (Na₂S), which breaks the bonds that link lignin, hemicellulose, and cellulose [21]. The cellulose paper used for common electrical insulation contains ca. 90% cellulose, 6–7% lignin and the rest, up to 100% consists mainly of pentosans [22, 23]. The cellulose molecules (C₁₂H₂₀O₁₀) of which the cellulose fibers are composed consist of a series of glucose repeating units (see Fig. 15) [24]. Cellulose molecules contain carboxyl groups (–COOH), which determine cellulose to behave as a weak acid with an ionization constant of about 2×10^{-14} . These groups are responsible to some extent for ionic conduction and dielectric losses in cellulose paper at lower frequencies. Cellulose paper contains pores with sizes between 10 and 100 Å. Its fibers form a complex interwoven channel system, allowing significant ions displacement (of smaller dimensions), which leads to increased dielectric losses [18]. If the paper temperature reaches 200 °C, the chemical bonds are easily broken and the structure of the paper breaks

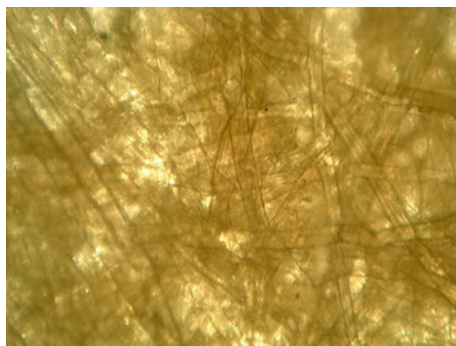


Fig. 14 Structure of the cellulose chains inside Kraft paper [21]

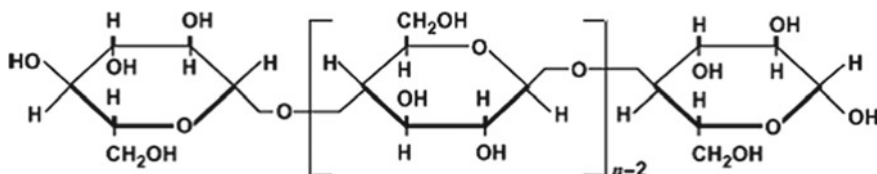


Fig. 15 Molecular structure of cellulose [24]

down gradually to $\text{H}_2\text{O} + \text{CO}_2 + \text{CO}$ [4], the degree of polymerization decreases and the mechanical properties are reduced.

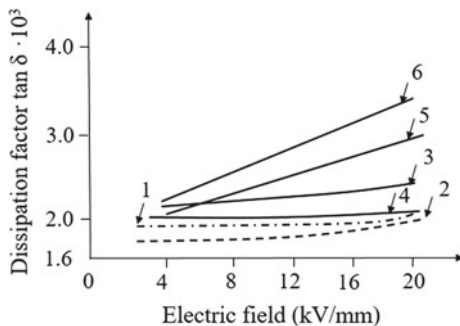
The paper absorbs moisture from the surrounding air (up to 12% under normal conditions) and therefore must be dried in vacuum before impregnation (the water content being reduced to 0.5–1%). The dry paper shows, at the industrial frequency, a relative permittivity of approx. 2.2 (due to the presence of air or vacuum in the pores) and a loss factor of 0.002 [4]. Dried and impregnated with electrical insulating liquids, Kraft papers show high dielectric strength and low losses, necessary properties for AC and DC cables. In addition, Kraft papers have other useful properties, such as lightness, flexibility, compatibility with insulating liquid impregnates and can be manufactured with different values of density, surface friction, mechanical strength, and thickness (0.05–0.2 mm). Since the density of unimpregnated paper is usually 0.75 g/cm^3 and that of cellulose is 1.54 g/cm^3 , it results that Kraft paper is very porous and the oil-impregnated-paper insulation contains one half of oil impregnant by volume. The mechanical strength is 760 bars in the longitudinal direction and 350 bars in the transversal direction [4]. The separation in time of cellulose fibers from paper causes a reduction in the mechanical properties of the paper. On the other hand, another inherent and common defect of Kraft paper is the formation of wrinkles, which causes creases. As the oil tends to fill in the wrinkles in pressurized cables, partial discharges may occur in the oil-impregnated insulation.

Higher density paper tapes contain more water, which results in higher dielectric losses. On the other hand, these bands are less porous and thereby show a higher tensile strength and dielectric constant. To reduce the ions content (and thus the electrical conductivity and dielectric losses), the papers are washed in deionized water. The increased porosity and the existence of pinholes cause a worsening of oil-paper impregnated systems characteristics. Thus, pinholes lead to reduced breakdown voltage values and the increased porosity cause an increase in dielectric losses (due to the increased ion mobility in impregnated paper).

The relative permittivity of oil-impregnated paper is about 3.6 and decreases relatively slow with temperature increasing. The impregnated paper shows high values of dielectric constant due to the high values of the cellulose fibers themselves (6–10). The dissipation factor ($\tan\delta$) of the oil-paper system is approx. 0.002 and increases with temperature (due to the intensification of ionic conduction) [13, 17, 19]. The relatively high values of $\tan\delta$ prevent the use of oil-paper system for cables with nominal voltage higher than 750 kV. The dielectric strength of normal oil-impregnated paper is 40–50 kV/mm for frequencies of 50–60 Hz and 100–200 kV/mm for impulse voltages [4].

The dielectric strength increases with the increase of paper's density, but in the same time, the values of $\tan\delta$ increase, too. The $\tan\delta$ values of the impregnated paper depend not only on the characteristics of the paper, but also on the characteristics of the impregnating oil, temperature, intensity of the electric field, etc. Figure 16 shows the variation curves of the dissipation factor with the electric field intensity and temperature for cables impregnated with a mixture of 06SH and 015SH (Table 3) and an equivalent mixture of mineral pipe cable filling and

Fig. 16 Variation of the dissipation factor with the electric field and temperature for polybutene impregnated paper (1, 25 °C), (2, 85 °C), and (3, 105 °C) and pipe filling and impregnating mineral oils (4, 25 °C), (5, 85 °C), and (6, 105 °C) (Redrawn and adapted from reference [4])



impregnating oils [4]. It can be observed that for 85 and 105 °C, the losses in the mineral oil samples exceed those in the polybutene samples.

3.3 Natural Rubber

Natural rubber is an elastomer which, under tensile stress, will stretch to twice its normal length and return to its initial length after the removal of stress. It has the chemical formula $(C_5H_8)_n$ (see Fig. 17) similar to that of gutta-percha (a trans isomer of natural rubber). Both materials were used in the earlier days for cable construction (up to 25 kV). In order to improve its mechanical, thermal, and environmental (under the action of water) properties, the natural rubber is vulcanized with sulfur (see Table 5). The introduction of sulfur, carbon black, antioxidants, etc., generally, produces a deterioration of dielectric characteristics as follows: the permittivity and the dielectric losses increase (see Fig. 18), whereas the dielectric strength and volume resistivity decrease.

Fig. 17 Molecular structure of natural rubber *cis*-(C_5H_8)_n

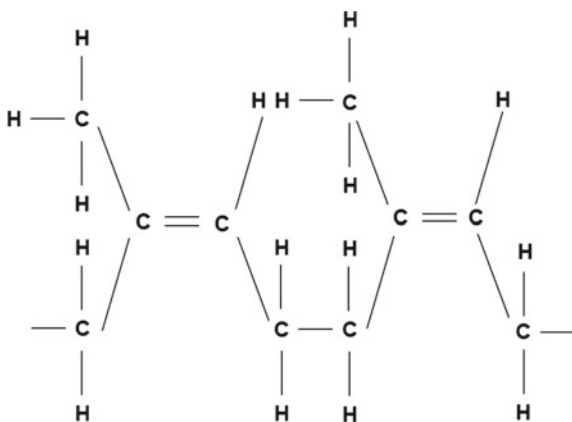


Table 5 Electrical and physical properties of elastomers [25, 26]

Property	Butyl rubber	EPR	EPDM	Neoprene	Natural rubber	Silicone rubber
Volume resistivity (Ωm)	10^{15}	10^{13} – 10^{15}	10^{13} – 10^{15}	10^9	10^{13} – 10^{15}	10^9 – 10^{15}
Dielectric strength (kV/mm)	35	35–41	41	6–35	–	4–26
Dielectric constant at 1 kHz	3.1–3.4	3.17–3.34	3.0–3.5	9.0	2.3–3.0	3.0–3.5
Dissipation factor at 60 Hz	0.0030	0.0066–0.0079	0.004	0.030	0.0023–0.0030	0.001–0.010
Tensile strength, gum (MPa)	17.24–20.68	3.45	1.38	26.68–27.58	17.24–20.68	2.76
Tensile strength, loaded stock (MPa)	17.24–20.68	5.52–20.68	5.52–24.13	20.68–24.13	24.13–31.08	4.14–12.42
Elongation, gum (%)	750–950	200	200	800–900	750–850	200–800
Shore A hardness	15–75	30–90	30–90	20–95	20–100	30–80
Specific gravity, gum	0.91	0.86	0.86	1.23–1.25	0.92–0.96	0.97
Low-temperature brittle point ($^{\circ}\text{C}$)	–60	–51 to –73	–51 to –73	–40 to –57	–62	–68 to –129
Continuous temperature limit ($^{\circ}\text{C}$)	150	150–175	150–175	107	150	260
Processability	G	G	G	G	G	F to E
Resistance to: Oxidation	G to E	E	E	E	E	E
Ozone	E	E	E	E	E	E
Tear	G	F to G	F to G	G	VG	F to G
Abrasion	G	G to E	G to E	E	E	P to G
Radiation	P	–	–	P	F	F to E
Concentrated acids	E	E	E	G	F to G	E
Dilute acids	E	E	E	E	F to G	E
Alkalies	VP	VG	VG	G	F to G	P to G
Aliphatic hydrocarbons	P	P	P	G	P	P
Aromatic hydrocarbons	P	P	P	F	P	P
Chlorinated hydrocarbons	P	P	P	VP	VP	VP
Oil and gasoline	VP	P	P	G	VP	P to G
Animal and vegetable oils	E	G to E	G to E	G	P	E
Water absorption (swelling)	E	E	E	G	E	E
Sunlight aging	VP	E	E	VG	P	E
Heat aging (100 $^{\circ}\text{C}$)	G	E	E	G	G	E
Flame	P	P	P	G	P	F to E

E excellent, *VG* very good, *G* good, *F* fair, *P* poor, *VP* very poor

Natural rubber is used as insulation for flexible electrical pipes, cables for indoor installations, etc., at low voltages and in environments without mineral oil, oxygenated or halogenated solvents, etc.

3.4 *Butyl Rubber*

Butyl rubber (see Fig. 19) is a synthetic product made by co-polymerization of isobutylene ($C[CH_3]_2=CH_2$) (95–99%) and a small amount of isoprene ($CH_2=C[CH_3]-CH=CH_2$) (1–5%) at very low temperatures, in the presence of aluminum chloride. During the polymerization process, sulfur is used as crosslink agent. Butyl rubber has a good resistance to environment, partial discharges, ultraviolet radiation, oils, tearing, aging at elevated temperatures and good electrical properties (see Table 5).

3.5 *Ethylene Propylene Rubber*

Ethylene propylene rubber (EPR) and cross-linked polyethylene (XLPE) are typical thermosetting insulation compounds. Ethylene propylene rubber is an elastomer synthesized from ethylene and propylene with a ratio of 1:1. The molecular structure is presented in Fig. 20, where x and y are the repeating units and take values between 2000 and 3000. The average molecular weights of the EPR used in cables extend from 150,000 to 250,000. Some manufacturers polymerize a diene monomer with ethylene and propylene to form a terpolymer named ethylene propylene diene monomer rubber EPDM (the incorporation of diene allows the curing with sulfur) [27].

The EPR polymer chain formed is not flat, as shown in Fig. 20, but rather three-dimensional with hydrogen atoms and methyl groups from propylene arranged along a zigzag chain of carbon atoms extending above and below the plane. The arrangement of ethylene and propylene molecules is random so that the resulting polymer structure is neither alternating nor very blocky. Statistics regarding ethylene/propylene monomer feed ratio, selectivity of the Ziegler–Natta catalyst, and the polymerization conditions determine the blockiness of EPR and whether it is completely amorphous or contains some crystalline content (due to the ethylene groups that tend to form organized repeated segments, if the ethylene content reaches 60%) [27]. Nevertheless, by increasing crystallinity, the processability is reduced, thus the flexibility of the cable becomes poorer and the hardness of the extruded cable is augmented [4].

When greater hardness is required, the EPR compound can be blended with polyethylene (PE) or polypropylene (PP) to achieve improved physical properties. Mechanical properties include resistance to compression, cutting, impact, tearing and abrasion. Although EPR does not offer a good resistance to oils, it is resistant to

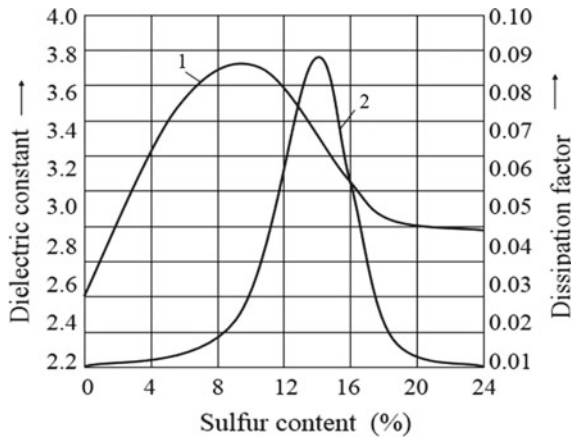


Fig. 18 Variation of relative permittivity (1) and dissipation factor (2) of natural rubber with sulfur content (Reprinted, with permission, from author [13])

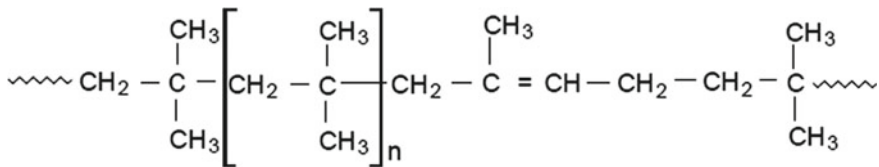
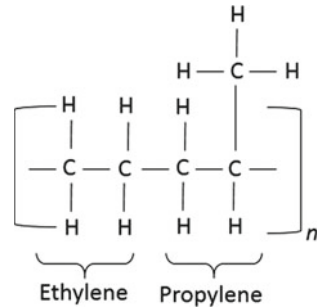


Fig. 19 Molecular structure of the butyl rubber

Fig. 20 Molecular structure of EPR



a wide range of other chemicals including many acids, alkalis, and organic solvents. It is also highly resistant to moisture.

Amorphous EPR insulated power cables are expected to be more stable under high-temperature conditions than crystalline XLPE-insulated cables. The properties of amorphous EPRs are slightly affected by temperature ranging from -30 to 150 °C. The properties of crystalline XLPE deteriorate as temperature exceeds the melting point (around 100 °C) in the crystalline regions. Probably reinforced

amorphous EPR insulated cables are expected to be more stable in wet locations than unfilled XLPE-insulated cables. They do not fail as a result of the formation of water trees as primary mechanism, since the bonds between fillers and polymer are stronger than the forces responsible for water trees formed in XLPE cables in service. The reinforcing effect of fillers in EPR makes questionable any extrapolation from high stress treeing studies of unreinforced PE, XLPE, or EP polymers. A water impermeable metallic sheath, which act against corrosion, mechanical damage, fatigue, cracks, etc., should protect the insulation in order to operate as long as possible in wet locations. Any other insulation will eventually fail to continued exposure at water and electrical stress.

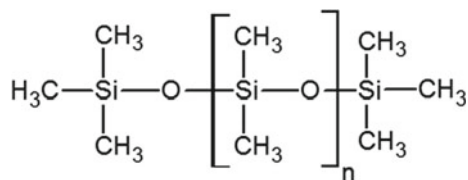
Unlike XLPE, EPR is a compound where the rubber resin (about 50%, [26]) is mixed with other additives (normally eight or more additives) to improve the mechanical and electrical properties. Typical ingredients of an EPR compound may be ethylene propylene rubber (EPR), inorganic mineral fillers, antioxidants/stabilizers, flame retardants (for low-voltage insulation materials), curing catalysts/coagents, and metal oxides including lead oxide. Both EPM and EPDM have outstanding resistance to ozone and oxygen, excellent weathering and heat resistance, low-temperature flexibility, and excellent electrical properties. Weatherability can be achieved without antioxidants or antiozonates. EPR is suitable for continuous service up to 150 °C with excursions up to 175 °C or higher. Chemical resistance to polar materials, such as acids, alkalis, oxygenated solvents, water, and steam, is excellent. Resistance to nonpolar hydrocarbon solvents, such as toluene and gasoline, is poor. The low specific gravity for EPR of 0.86 g/cc can result in reduced costs for final products [27].

Key insulation users are low- and medium-voltage power cable, control and instrument, automotive ignition and motor lead wire, mining cable, etc. [28]. Furthermore, EPR insulation is suitable for many higher voltage applications and while its dielectric properties are not as good as those of XLPE, it does have some important advantages over XLPE including extra flexibility, reduced thermal expansion, and low sensitivity to water treeing [28].

3.6 *Silicon Rubber*

Silicon rubber is an organic-inorganic elastomer obtained by polymerization of organic siloxanes [13]. The number of dimethyl-siloxanes n (see Fig. 21) determines the length and properties of silicone rubber. Cross-linking (vulcanization) of silicone rubber is carried out by the use of different peroxides such as benzoyl peroxide or dichlororobenzoyl peroxide or by gamma or electron radiation. For the improvement of certain properties (mechanical, etc.), different fillers such as silica, calcium carbonates, titanium, iron oxides are introduced in the silicone rubber [29]. They show good dielectric properties (see Table 5), low water absorption, good resistance to partial discharges and can be used as insulations that operate from very low temperatures (−85 °C) to very high temperatures (260 °C).

Fig. 21 Chemical structure of silicone rubber



3.7 Polyethylene

Polyethylene (PE) is obtained by polymerization of ethylene (C_2H_4) (see Fig. 22a), at high pressure (1000–3000 atm and 200–250 °C) resulting in a low-density material (LDPE) or at low pressures (up to 60 atm) resulting in a high-density material (HDPE) (see Table 6). It has symmetrical and linear molecules, and hence, it is nonpolar and thermoplastic. LDPE has a partially crystalline structure and reduced mechanical properties, mainly, due to the presence of $-\text{CH}_3$ radicals, which blocks the ordering of macromolecules (see Fig. 22b). HDPE (low pressure HDPE) has a high degree of crystallinity (up to 93%), which gives it higher hardness, softening temperature, and an improved behavior at lower temperatures (up to -40 °C) than LDPE. In general, the degree of crystallinity influences both physical and electrical properties (such as treeing resistance).

The free radicals generated in LDPE from peroxide at elevated temperatures may induce the ethylene molecules to add linearly, in a normal way, to each other or alternatively, causing a short growth of the side chains of the polymer. The appearance of numerous side chains of various lengths gives to polyethylene a low density. The existence of side chains is also due to the addition of certain amounts of butene (C_4H_8), hexene (C_6H_{12}), or octene (C_8H_{16}) (see Fig. 23). In the case of HDPE, the addition of butene, hexene, or octene leads to an increase in both, the number of side branches and the crystallinity [13]. The presence of such side branches is a reason for variations in a number of important physical properties

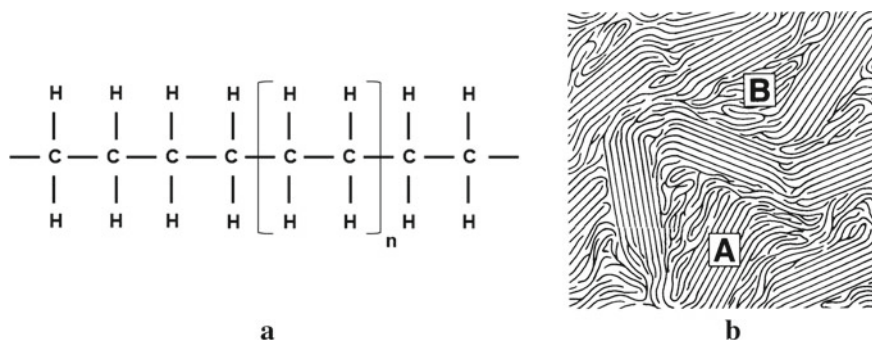


Fig. 22 **a** Molecular structure of polyethylene; **b** crystalline (A) and amorphous (B) zones in polyethylene [30]

Table 6 Electrical and physical properties of polyethylenes [31]

Property	Low-density PE	High-density PE	XLPE
Volume resistivity (Ωm)	$>10^{14}$	$>10^{13}$	$>10^{13}$
Dielectric strength (kV/mm)	18–28	18–20	22
Dielectric constant at 60 Hz	2.3	2.3	2.3
Dissipation factor at 60 Hz	0.0002	0.0002	0.0003
Density (g/cm^3)	0.910–0.925	0.941–0.965	0.92
Elongation (%)	20–650	15–700	550
Tensile strength (MPa)	9.65–13.10	17.93–31.03	16.55
Modulus of elasticity (MPa)	117–242	552–1035	790
Thermal conductivity ($\text{W}/\text{m } ^\circ\text{C}$)	0.335	0.461–0.502	0.24–0.32
Heat distortion temperature ($^\circ\text{C}$)	41–50	49–66	54–107
Operating temperature ($^\circ\text{C}$)	70 (90)*	80 (120)*	90 (130)*
Water absorption (%)	<0.02	<0.01	0.02–0.035

()*—for short duration

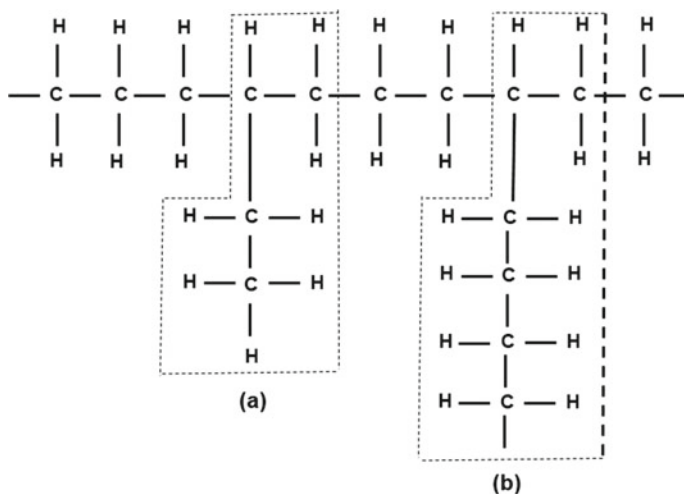


Fig. 23 Polyethylene molecular chain with side branch of butene (a) and hexene (b)

(such as density, hardness, flexibility, and melt viscosity), which delimit polyethylene resins. Chain branches also become points in the molecular network where oxidation may take place [30].

In order to insulate cables, especially LDPE is used. The operating temperature of LDPE may not exceed 80 $^\circ\text{C}$ continuously and 90 $^\circ\text{C}$ for a short time. LDPE shows [13]:

- (a) excellent resistance (no attack/no chemical reaction) to dilute and concentrated acids, alcohols, bases, and esters;
- (b) good resistance (minor attack/very low chemical reactivity) to aldehydes, ketones, and vegetable oils;
- (c) limited resistance (moderate attack/significant chemical reaction, suitable for short-term use only) to aliphatic and aromatic hydrocarbons, mineral oils, and oxidizing agents;
- (d) poor resistance (not recommended for use) with halogenated hydrocarbons.

The disadvantages of polyethylene include high thermal expansion, poor weathering resistance subject to stress cracking, difficult to bond, flammable, poor temperature capability, low strength/stiffness, etc.

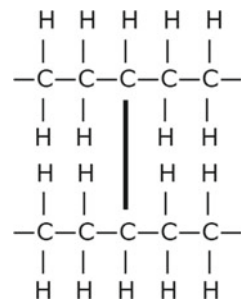
During the operation of cables, under the action of the electric field, polyethylene is degraded due to the partial discharges, the electric and water trees. Against these phenomena, different additives are added [2].

3.8 Cross-Linked Polyethylene

The cross-linking process causes polyethylene a change from a thermoplastic to a thermosetting material with an important improvement in both physical and electrical properties (see Table 6) [2]. Therefore, XLPE (see Fig. 24) is used, both for the insulation of low- and medium-voltage power cables, as well as for those of high and very high voltage. The cross-linking agent is usually dicumyl peroxide, which is decomposed and the acetophenone is formed. The presence of acetophenone in XLPE cables insulation leads to a delay (attenuation) of electrical phenomena [32] and water treeing [33].

The insulation of XLPE power cables that are steam cured present a considerable amount of moisture, which remains in or diffuses out of the insulation. Both cases facilitate the development of water trees. The use of dry curing process has the effect of reducing the concentration of microvoids and, therefore, a reduction in the

Fig. 24 Molecular structure of XLPE



speed of water trees development. However, even in this case, the operation of cables in a moisture environment leads to the initiation and development of water trees [34].

Due to the fact that XLPE is a thermosetting material, it maintains its mechanical properties even at temperatures where linear polyethylenes (LDPE or HDPE) melt, lose shape, and flow. XLPE has good properties at low temperatures and shows increased resistance to ozone and partial discharges (as compared to linear PE) and good impact, abrasion and environmental stress cracking resistance characteristics. As power cables with XLPE insulation can operate at conductor temperatures of 90 °C (e.g., LDPE insulated cable operates at 75 °C), and as the conductor temperature is proportional to the amount of current sent through the cable, it turns out that more power can be sent through an XLPE cable than through a non-cross-linked cable of the same size. Under short-circuit conditions, XLPE insulation withstands for one second to a conductor temperature of up to 250 °C, compared to PVC cable, which supports for one second a conductor temperature of up to 160 °C. XLPE cable possesses higher overloading capacity under emergency conditions. It also can withstand vibration and has up to 100 times more moisture resistance capacity compared to PVC.

Another characteristic of XLPEs is their capability to employ higher filler loadings without significant deterioration of physical properties. Cross-linking forms bonds around a filler and their incorporation into the polymer matrix reduce its effect on the compound [30]. On the other hand, by using a cross-linkable resin base, flame retardant, mineral filler, or carbon black can be disposed in higher concentrations by maintaining physical properties at acceptable levels. This enables the development of highly flame retardant, abrasion resistant, or semiconductive wire compounds [30].

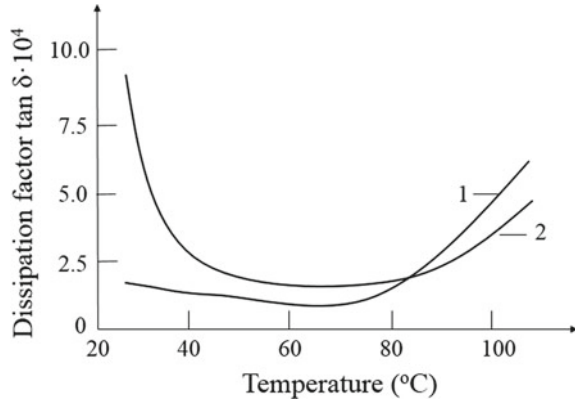
By using certain nano-fillers (e.g., MgO [6]), we can be obtained XLPEs used in DC (DC-XLPE) with high volume resistivity, low space charge accumulation, long DC lifetime, and high DC breakdown strength than the usual XLPE used in AC (AC-XLPE) [35].

3.9 Tree-Retardant XLPE

The use of tree-retardant XLPE (TR-XLPE) for power cables insulation has led to increase initiation times and development rate of water trees. Among the first inhibitors of water, trees were used dodecanol ($\text{CH}_{12}\text{CH}_2\text{OH}$) and ethylene vinyl acetate (EVA), but their effectiveness decreased over time [4]. In 1983, Union Carbide proposed a tree-inhibiting compound with a strong polar character, which resulted in a greater reduction of development rate and water tree concentrations [36]. Definitely, the introduction of a polar additive in XLPE causes an increase in dielectric losses, but smaller than those in EPR compounds.

The variation of dissipation factor ($\tan\delta$) with temperature for the insulation (aged and unaged) of a 20 kV cable is shown in Fig. 25 [37]. It was found that at

Fig. 25 Variation of the temperature dissipation factor within the insulation of a 20 kV cable from XLPE with polar tree-retardant, before (1) and after aging (2) (Redrawn and adapted figure from reference [37])

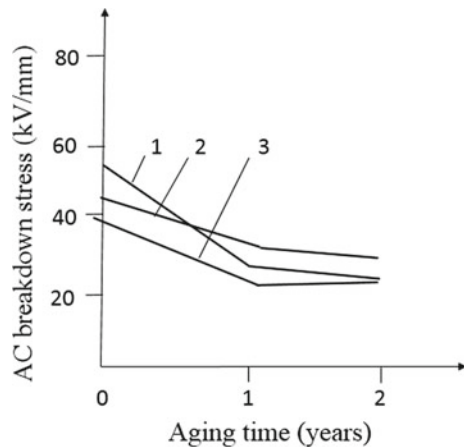


lower temperatures, $\tan \delta$ has lower values for the unaged insulation than for the aged ones, due to the reduction of the molecular dipoles orientation caused by some residual products (peroxides), which are eliminated in the aged insulation. The increase of $\tan \delta$ values, for higher temperatures, in XLPE by the addition of tree-retardant is due to the reduction of effective charge trap depths and to the introduction of mobile ion constituents, whose mobility is intensified at higher temperatures (thermal agitation [13]).

The addition of a polar tree retardant to XLPE diminishes greatly the number and size of bow-tie water trees, when state-of-the-art semiconducting shields are employed. However, the effect on vented-type water trees is essentially insignificant [36, 37]. On the other hand, the use of tree-retardant leads to the reduction of dielectric strength of XLPE cable insulations (see Fig. 26). In general, TR-XLPE is used for the insulation of high and very high voltage power cables.

The worldwide tendency in using HVDC transmission lines makes the demand for better insulation materials increasingly greater and urgent. Many manufactures

Fig. 26 Variation of AC breakdown stress with aging time (30 kV, 50 Hz) for an XLPE 20 kV cable insulation: 1 Conventional XLPE cable; 2 XLPE with tree-retardant and conventional semiconducting shields; 3 XLPE with tree-retardant and higher purity carbon semiconducting shields (Redrawn and adapted figure from reference [37])



have developed XLPE materials that are more adapted to DC power cables insulation, such as the super-clean XLPE (lower concentration of impurities) and XLPE-based nanocomposites [38].

3.9.1 Polyvinyl Chloride

Polyvinyl chloride (PVC) is obtained by polymerization of vinyl chloride (see Fig. 27), in the form of hard PVC without plasticizers or soft PVC with plasticizers (e.g., phthalic, phosphoric, citric acid esters, etc.). Being a polar material, it has lower dielectric characteristics than polyethylene and dependent—as well as mechanical ones—on the plasticizer content (see Figs. 28 and 29). It performs better than natural rubber, both on the action of ozone and mineral oil. However, it has low thermal stability (70 °C) and its properties are inferior to those of polyethylene (see Tables 7 and 8) and vary greatly with frequency and temperature (see Figs. 30 and 31).

Due to low corona resistance, PVC is used to insulate conductors and power cables of low and medium voltages, respectively, between 1 and 20 kV. It is clean to handle and is reasonably resistant to oils and other chemicals. As in DC, it ages very quickly (i.e., due to the electrolysis of salts from the additives), and at high frequencies, it presents high dielectric losses ($\tan\delta = 0.015\text{--}0.3$), and PVC is used only in AC fields of industrial frequencies. PVC has high resistance to abrasion and fire although the wires may burn when exposed to fire and can cease to burn when the source of fire has been eliminated. Nevertheless, when PVC burns, it emits dense smoke and corrosive hydrogen chloride gas. In addition, certain types of PVC can be used for applications where the cables may be exposed to high or low temperatures (including arctic-grade PVC for extreme low conditions), or where protection against UV light is required to avoid degradation [40]. PVC is often used for electrical cable jacketing due to its excellent electrical insulating properties and dielectric constant.

3.10 Polypropylene

Polypropylene (PP) is a thermoplastic resin obtained by polymerization of propylene as a monomer (see Fig. 32, [41]), and depending on its methyl group position

Fig. 27 Chemical structure of polyvinyl chloride

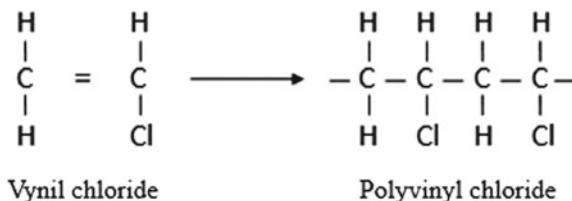


Fig. 28 Variation of relative permittivity (1) and volume resistivity (2) with plasticizer content for PVC (Reprinted, with permission, from author [13])

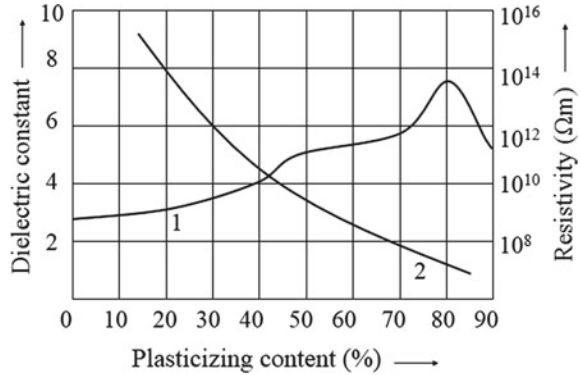


Fig. 29 Variation of tensile strength (1) and relative elongation at break (2) with plasticizer content for PVC (Reprinted, with permission, from author [13])

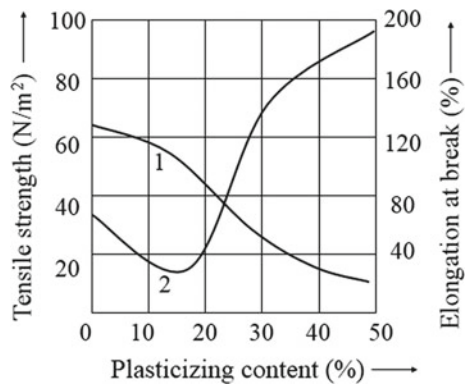


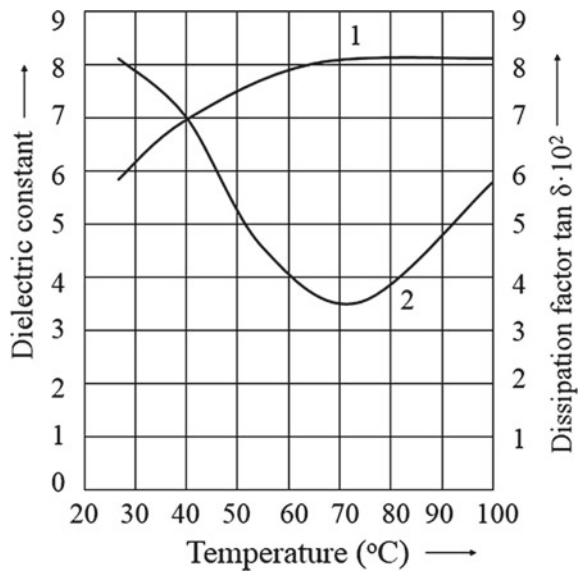
Table 7 Physical properties of polyvinyl chloride (PVC) [13, 39]

Property	Rigid PVC	Flexible PVC
Density (g/cm ³)	1.3–1.45	1.1–1.35
Thermal conductivity (W/(m°C))	0.14–0.28	0.14–0.17
Yield strength (MPa)	310–560	2.14–4.14
Young’s modulus (GPa)	3.4	0.05
Tensile strength (MPa)	50	11
Compression strength (MPa)	66	
Coefficient of thermal expansion (linear) (10 ⁶ mm/mm °C)	50	190
Volume resistivity (Ω m)	10 ¹⁶	10 ¹² –10 ¹⁵
Surface resistivity (Ω)	10 ¹³ –10 ¹⁴	10 ¹¹ –10 ¹²

Table 8 Characteristics of polyethylene (XLPE) and polyvinyl chloride (PVC) insulation

Feature	Insulation	
	XLPE	PVC
Temperature range (°C)	-55 to +100	-10 to +60
Cold Bend	Excellent	Good
Moisture resistance	Excellent	Good
Chemical resistance	Excellent	Good
Abrasion resistance	Excellent	Good
Cut-through resistance	Excellent	Good
Elongation resistance	Excellent	Good
Rodent resistance	Poor	Poor

Fig. 30 Variation of relative permittivity (1) and dissipation factor (2) with temperature for PVC (Reprinted, with permission, from author [13])



on one side of the polymer backbone, it may be isotactic polypropylene (iPP), syndiotactic polypropylene (sPP), and atactic polypropylene (aPP) [41, 42].

Polyethylene (PE) and polypropylene (PP) are bulk commodity polymers, comparably priced and both have an intrinsically nonpolar molecular structure. However, several significant differences exist, such as

- (a) the melting temperature of isotactic polypropylene (iPP) is much higher than that of XLPE;
- (b) the morphology of iPP is based on a number of different crystal structures (notably α , β , and γ);
- (c) iPP tends to form particularly large spherulites and the material is intrinsically clean;

Fig. 31 Variation of volume resistivity with temperature for PVC plasticized with dioctylphthalate (1) or tricresylphosphate (2) (Reprinted, with permission, from author [13])

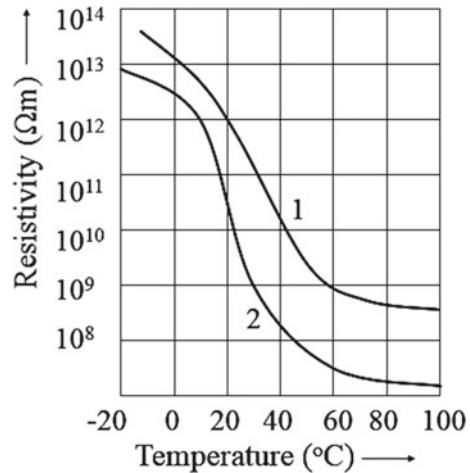
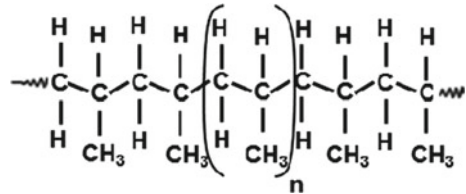


Fig. 32 Molecular structure of isotactic polypropylene



- (d) large spherulites mean that interspherulitic regions are particularly weak;
- (e) synthesis methods of PP do not produce branched molecular structures similar to LDPE.

PP is one of the lightest polymers (with a density of 0.9–0.91 g/cm³; see Table 9) with good chemical resistance to acids, alcohols, bases, aldehydes, esters, aliphatic hydrocarbons, ketones. It maintains its mechanical and electrical properties at elevated temperatures, in humid conditions and submerged in water is non-toxic. It is, however, a highly flammable material, and it is sensitive to microbial attacks, such as bacteria and mold. The melting point of PP can reach more than 150 °C, about 40–50% higher than that of PE, and the long-term working temperature can reach 90 °C.

PP is a nonpolar material with high dielectric breakdown (even over 300 kV/mm [44]), high volume resistivity (up to 10¹⁶ Ωm), and less space charge accumulation. PP hardly absorbs water, so its insulation properties are less affected by the ambient humidity. In addition, PP materials have high mechanical strength without cross-linking treatment and can be recycled and used in line as environmentally friendly cable insulations. However, PP has some disadvantages, such as high

Table 9 Properties of polypropylene [41, 43]

Property	Value
Density (g/cm ³)	0.9–0.91 g/cm ³
Glass transition temperature (°C)	–10
Transparency (%)	85–90
Dielectric constant	2.3
Dielectric strength (kV/mm)	20–28
Dissipation factor	$(3–5) \times 10^{-4}$
Volume resistivity (Ωm)	$(1.6–1.8) \times 10^{14}$
Thermal conductivity (W/mK)	0.15–0.21
Coefficient of linear thermal expansion (1/°C)	$(6–17) \times 10^{-5}$
Melting point (°C)	160–165
Elongation at break (%)	150–600%
Flexural modulus (GPa)	1.2–1.6
Young modulus (GPa)	1.1–1.6
Strength at break (tensile) (MPa)	20–40
Strength at yield (tensile) (MPa)	35–40
Max continuous service temperature (°C)	100–130
Min continuous service temperature (°C)	–20 to –10 °C
Gamma radiation resistance	Poor
UV light resistance	Fair

brittleness at low-temperature, poor aging resistance, and low thermal conductivity, which assess certain limitations on the application of DC cable insulation.

Due to the high values of dielectric strength at high or low temperatures (see Table 10), PP films are used as dielectrics for capacitors [42] or superconducting cables insulation [45]. The insulation of superconducting cables is made of polypropylene sheets (PPLP) or Kraft paper, the resistivity of which did not change with the increase in number of layers [46].

It should be noted that PP has shown great potential as a recyclable HVDC cable insulation material. However, PP has the disadvantages of poor low-temperature impact performance and low thermal conductivity, as well as the problem of space charge accumulation and polymer aging in Dc field. Therefore, PP needs to be modified in order to meet the electrical, thermal, and mechanical properties of the cable insulation material under the complex working conditions of DC high voltage [42].

Table 10 Dielectric strength values of XLPE and sPP [42]

Temperature (°C)		25	90	110
Breakdown strength (kV/mm)	XLPE	135	115	–
	sPP	180	132	112

There is much interest in the development of XLPE replacement materials that are both recyclable (i.e., thermoplastic) and capable of high-temperature operation. Thermally, PP is the ideal choice, although its stiffness and low electrical breakdown strength make a challenging materials design problem [47].

3.11 Polytetrafluoroethylene (PTFE)

Polytetrafluoroethylene (PTFE) is a synthetic fluoropolymer obtained by the polymerization of tetrafluoroethylene (F_2C-CF_2), with a similar structure to PE (see Fig. 33) [48]. PTFE is nonpolar, has good dielectric properties, and does not burn. Due to the high values of bonding energy between carbon (C) and fluorine (F) atoms, PTFE has high thermal stability (250 °C). Microgaps (cavities) where partial discharges can develop appear in PTFE in the case of significant temperature variations due to the large coefficient of linear expansion. Therefore, PTFE is not used in intense electric fields. PTFE is used for the manufacture of insulation systems that operate at higher temperatures (over 180 °C), in humid environments or in highly corrosive atmospheres, as insulation of conductors and high-frequency cables, etc.

The performance of PTFE thermal conductivity over a wide range of temperature is excellent compare to other polymers. The thermal stability is due to the linear high crystalline arrangement of C-F atoms, which give a high value of the melting point (342 °C). PTFE has good mechanical properties, especially if it contains nano-fillers (aluminum oxides, copper, silicon dioxide) [49]. Naturally, PTFE is non-reactive and insoluble due to the strongly bonded C-F atoms. Common reagents such as hydrofluoric, hydrochloric, and chlorosulfonic acids do not affect PTFE. Even above the transition temperature (327 °C), PTFE is insoluble in organic solvents such as hydrocarbons, chlorinated hydrocarbons, or ester and phenol. This is due to the very fewer interaction forces between fluorocarbon and other molecules [49].

PTFE is a thermoplastic polymer (white solid at room temperature) with a density of about 2.2 kg/cm³ (see Table 11). It maintains high strength, toughness, and self-lubrication at low temperatures (5 K) and good flexibility at temperatures above 194 K [48].

PTFE insulation has several advantages, such as excellent thermal stability (from -65 to +260 °C); inert to practically all chemicals (even at elevated temperatures);

Fig. 33 Chemical structure of polytetrafluoroethylene (PTFE)



Table 11 Properties of polytetrafluoroethylene (PTFE) [48]

Property	Value
Density (kg/cm ³)	2.2
Glass temperature (°C)	114.85
Melting point (°C)	326.85
Thermal expansion (K ⁻¹)	(112–125) × 10 ⁻⁶
Thermal diffusivity (mm ² /s)	0.124
Young's modulus (GPa)	0.5
Yield strength (MPa)	23
Bulk resistivity (Ωm)	10 ¹⁶
Dielectric constant (60 Hz)	2.1
Dissipation factor (60 Hz)	<2 × 10 ⁻⁴
Dielectric strength (MV/m)	60

lowest dielectric constant and dissipation factor (see Table 11); excellent flex life, good mechanical strength, excellent resistance to ultra-radiation and stress cracking, good resistance to fungus and mold growth, smaller in size, more flexible, lighter in weight and higher reliability, fire and flame proof, non-contamination, non-toxic, and bio-compatible [50].

4 Synthetic Solid–Liquid Insulations

As cellulose paper–oil insulation system has high dielectric losses, it cannot be used as insulation for cables of voltages over 750 kV. As a result, research has been carried out to obtain low-loss synthetic tapes, chemically compatible with impregnating liquids and with lifetimes at least as long as those of cellulose papers.

The first synthetic solid–liquid insulations were those made of polycarbonate tapes (with $\tan\delta = 0.0025$) in conjunction with mineral oils and silicone liquids (see Table 12) [51]. For a voltage stress of 18 kV/mm, a polycarbonate–mineral oil insulation has a loss factor of 0.003 at room temperature and 0.0022 at 85 °C. If the mineral oil is replaced with a silicone one, $\tan\delta$ values of 0.0015 are obtained at 25 °C and 0.001 at 85 °C, respectively [52]. Using hydrogenated polybutene with 5% tri-isopropylbenzene as impregnated for polycarbonate tapes, a $\tan\delta$ value of 0.00078 was obtained at room temperature [53]. On the other hand, the use of fluorocarbon polymers in conjunction with polybutene fluids has reduced the loss factor of solid–liquid insulation to 0.0003 [54].

Tests were also performed on insulations based on synthetic paper comprising polyester fibers and porous polycarbonate phase impregnated with dodecyl benzene. It has been found that dielectric properties of the insulation are satisfactory ($\tan\delta = 0.0005$ at 80 °C), but the level of partial discharges is too high [55].

Numerous researches have been carried out to characterize the insulations based on laminated polypropylene paper (PPP) and their properties (both unimpregnated

Table 12 Properties of solid–liquid insulating systems [4]

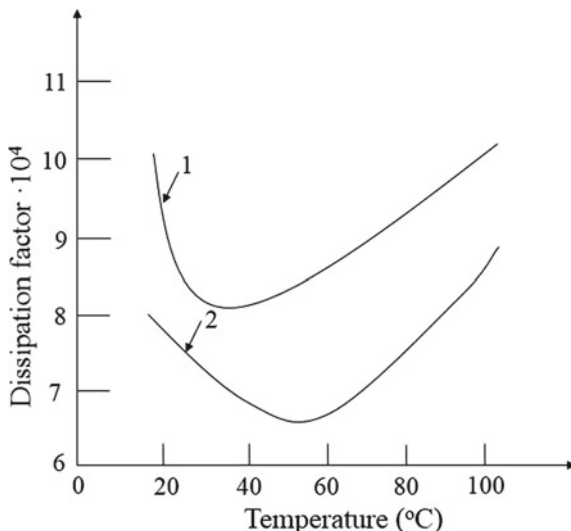
Solid tape	Impregnating liquid	Voltage stress (kV/mm)	Tanδ at operating temperature
Kraft paper	Mineral oil	18	0.0057, 85 °C
Kraft paper	Silicone liquid	18	0.0031, 85 °C
High-loss polycarbonate	Mineral oil	18	0.0022, 85 °C
High-loss polycarbonate	Silicone liquid	18	0.0010, 85 °C
Fluorocarbon	Polybutene liquid	18	0.0030, 100 °C
Polyolefin synthetic paper	Polybutene liquid	12	0.0003, 80 °C
Polyester-polycarbonate	Dodecyl benzene	10	0.0005, 80 °C
Spun-bonded polyethylene fiber	Liquid nitrogen	20	<0.00001, 70 K
Kraft paper-polypropilene-Kraft paper (PPP)	Dodecyl benzene	20	0.00096, 100 °C

and impregnated with dodecyl benzene) have been remarkable (see Table 13). It was concluded that an insulated cable with PPP could operate at 70% higher stresses than those insulated with Kraft paper [4].

Table 13 Physical and electrical properties of PPP tape of thickness *g* (unimpregnated (UIM) and impregnated with dodecyl benzene) (IM) [56]

Property	<i>g</i> = 125 μm	<i>g</i> = 155 μm
Polypropylene to total PPP	0.42	0.42
Dissipation factor for:		
– UIM	0.00098	0.00093
– IM at 100 °C	0.00099	0.00096
Dielectric constant for:		
– UIM	2.8	2.8
– IM	2.82	2.82
AC Breakdown stress (kV/mm)	129.8	128.2
Impuls breakdown (kV/mm)	225.2	217.8
Density (g/cm ³)	0.89	0.89
Tensile strength (N/mm ²)		
– Longitudinal	110	145
– Transverse	58	79
Elongation (%)		
– Longitudinal	3.3	3.4
– Transverse	9.9	10.4

Fig. 34 Variation of dissipation factor with for PPP impregnated (24 h at 100 °C) with dodecyl benzene, before (1) and after impregnation (2)



The impregnation of PP bands with dodecyl benzene is done at 100 °C for 24 h. Following this process, it results in a considerable reduction of loss factor (see Fig. 34) [56]. The variation of the loss factor with temperature highlights the importance of ionic conductivity in dielectric losses: PP bands form barriers against ions movement between adjacent layers, and the charges accumulated at the interfaces between layers generate small, but detectable interfacial polarization losses [4].

A model of insulated cable with PE fiber tapes impregnated with liquid nitrogen and helium was tested under cryogenic conditions [57]. For an electric field of approx. 20 kV/mm, a $\tan\delta$ value of less than 10^{-5} was obtained. Although the losses are much reduced, the use of this insulation system is disadvantageous due to the very high initial costs (for cooling equipment) [58, 59].

5 Gas–Solid Spacer Insulating Systems

Gas-insulated cables have been constructed using compressed sulfur hexafluoride gas (SF₆) and conductors fixed by epoxy or PE spacers. SF₆ has the breakdown strength values of 2.3 times greater than dry nitrogen. It is non-toxic and non-inflammable and can be used for cables up to 500 kV. Under the action of PDs and SF₆ electric arc, it decomposes chemically, resulting in toxic gases that degrade the adjacent insulation and can affect the environment, if leaks occur. In gas-filled cables, it is very important to match the coefficient of thermal expansion of the epoxy spacers to that of the conductor (Cu, Al), in order to avoid stress cracking or separation of the epoxy resin from the metal, respectively the occurrence of PDs [60].

Table 14 Properties of epoxy resins [61]

Property	Unfilled	Silica filled
Volume resistivity (Ωm)	10^{10} – 10^{15}	10^{11} – 10^{14}
Dielectric strength (kV/mm)	16–22	16–22
Dielectric constant at 60 Hz	3.5–5	3.2–4.5
Dissipation factor at 60 Hz	0.002–0.050	0.008–0.03
Specific gravity	1.11–1.14	1.6–2.0
Modulus of elasticity (GN/m^2)	2.1–2.4	2.1–2.4
Elongation (%)	3–6	1–3
Flexural strength (MN/m^2)	89–144	55–97
Compressive strength (MN/m^2)	103–144	103–276
Heat distortion temperature at 1.8 MN/m^2 ($^{\circ}\text{C}$)	46–288	71–288
Thermal conductivity ($\text{W}/^{\circ}\text{C m}$)	0.1672–0.209	0.418–0.836
Thermal expansion (10^{-6} $\text{m/m } ^{\circ}\text{C}$)	45–65	20–40
Water absorption (%)	0.08–0.15	0.04–0.10

In this regard, inorganic fillers such as silica are used, which leads to an important increase of the thermal conductivity and to the reduction of volume resistivity, relative permittivity, coefficient of thermal expansion, and water absorption (see Table 14).

6 XLPE Versus Conventional Materials

The use of XLPE or other electrical materials for insulation and coating of power cables depends on their thermo-electrical stresses, environment stresses, level of safety in operation required by the user, and, of course, costs of the cables (to the manufacturer) and their maintenance costs (to the user). From all accounts, apart from the separation function of the conductors with opposite electrical potentials (for which they must satisfy certain mechanical, thermal, chemical and electrical requirements), the insulation must support the two conductors and to maintain their separation. Moreover, the insulation must often withstand rough handling and abuse during installation, as well as thermal overloading during its service life. In different works, the characteristics of polyethylene (PE), filled PE, cross-linked polyethylene (XLPE), polypropylene (PP) ethylene propylene rubber (EPR), ethylene propylene diene monomer (EPDM), silicone rubber (SR), polytetrafluoroethylene (PTFE), etc., were analyzed. There are many good, solid dielectrics available today, and each has a unique combination of properties [62].

As it will be seen below, some of the electrical insulating materials have one or more properties superior to all the others, properties that recommend them for certain applications.

6.1 Electrical Properties

The choice of a certain material for electrical equipment insulation is based primarily on the electrical properties of the materials, namely the electrical conductivity and permittivity, dielectric losses, dielectric strength, and accumulation of the space charge. In numerous papers, the values and variations with different factors (temperature, intensity, and frequency of the electric field, etc.) of these parameters are analyzed for XLPE, PE, PP, EPR, EPDM, SC, and PTFE. A comparative analysis of the general properties of XLPE and EPR is presented in [62].

6.1.1 Electrical Conductivity

The electrical conductivity σ is the main parameter that characterizes an electrical insulating material (and, therefore, the behavior of the insulation in operation) and is determined with different empirical relations [63–68], such as

$$\sigma(E, T) = A \exp\left(-\frac{E_a}{kT}\right) \frac{\sinh((aT + b) \ln E)}{E^\alpha} \quad (1)$$

where E_a is the activation energy, A , a , b , and α —material constants, k —Boltzmann constant, T —the temperature, and E —the applied electric field (reported, dimensionless). In the case of XLPE, it is considered $\alpha = 1$ [63], and in the case of EPR, $\alpha = 0.21$ – 0.23 [68].

The electrical resistivity values of the insulation materials used in electrical engineering determined by DC or AC measurements must be as low and less dependent on the intensity of the electric field and operating temperature of the insulation, as the values of resistive currents and dielectric losses to be as small as possible. In numerous papers, the values of LDPE, XLPE, EPR, silicone rubber resistivity are determined under standard conditions and are presented and analyzed as variations with different stress factors (temperature, electric field, etc.).

Figures 35, 36, 37 and 38 show the variations of DC electrical conductivity (σ) with the intensity of the electric field and temperature for XLPE and EPR. It was found that the values of σ are lower for XLPE insulation than for EPR, but increase with temperature and electric field intensity for both materials [69]. On the other hand, the variations of σ with temperature and electric field are lower for XLPE than for EPR. This could be due, among other things, to lower values of the impurity concentrations [70] and activation energy ($E_a = 0.88$ eV [63]) of XLPE compare to EPR ($E_a = 0.55$ eV [68]). The AC conductivity values vary with the frequency and are lower in XLPE samples than in EPR samples (see Fig. 39).

It should be noted that the least significant loss in a power cable is due to the insulation resistance (respectively, electrical conduction in insulation). The annual cost of this loss is only a few cents per 300 m, a small fraction of the costs incurred due to other internal cable losses [71]. Insulated Cable Engineers Association

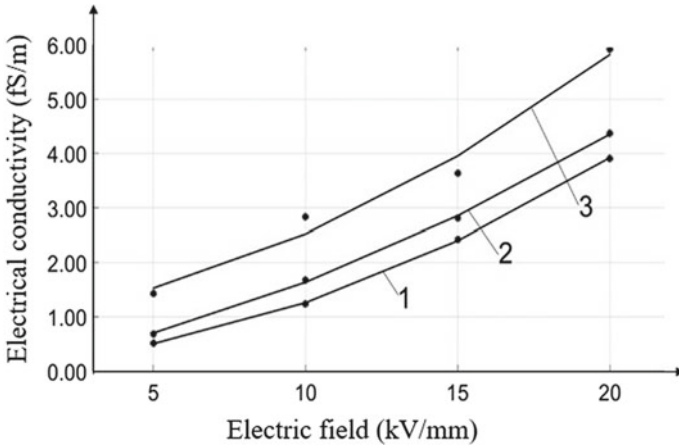


Fig. 35 Variation of DC electrical conductivity of XLPE with the electric field, at $T = 30\text{ }^{\circ}\text{C}$ (1), $50\text{ }^{\circ}\text{C}$ (2) and $70\text{ }^{\circ}\text{C}$ (3) (Reprinted, with permission, from author [63])

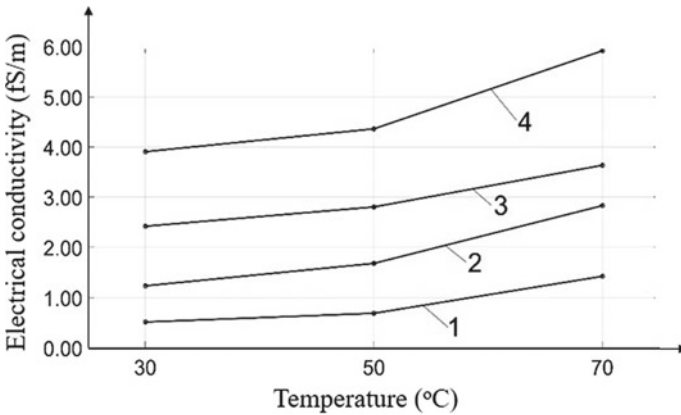


Fig. 36 Variation of DC electrical conductivity of XLPE with temperature, at $E = 5\text{ kV/mm}$ (1), 10 kV/mm (2), 15 kV/mm (3) and 20 kV/mm (4) (Reprinted, with permission, from author [63])

(ICEA) recommends values of the insulation resistance not less than 500–10,000 MΩ for a conductor length of 300 m, in the case of low-voltage insulations, and not less than 20,000 MΩ for medium-voltage insulations. For cables with XLPE pure unfilled insulations, the resistance values can exceed 100 GΩ for 300 m [71].

The introduction of nano-fillers in XLPE leads to important changes in the values of the electrical conductivity (respectively, of the resistivity). Thus in the paper [35], it is shown that by adding nano-fillers in PE, an insulating material was obtained for the DC cables with the electrical resistivity of approx. 100 times higher than that for AC cables (AC-XLPE).

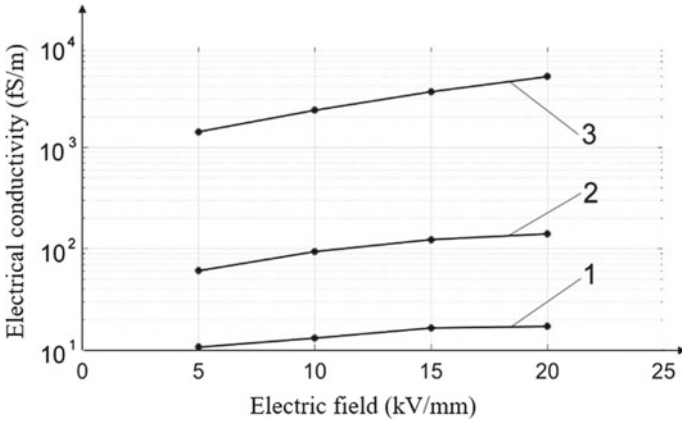


Fig. 37 Variation of DC electrical conductivity of EPR with electric field, for $T = 30\text{ }^{\circ}\text{C}$ (1), $50\text{ }^{\circ}\text{C}$ (2) and $70\text{ }^{\circ}\text{C}$ (3) (Reprinted, with permission, from author [68])

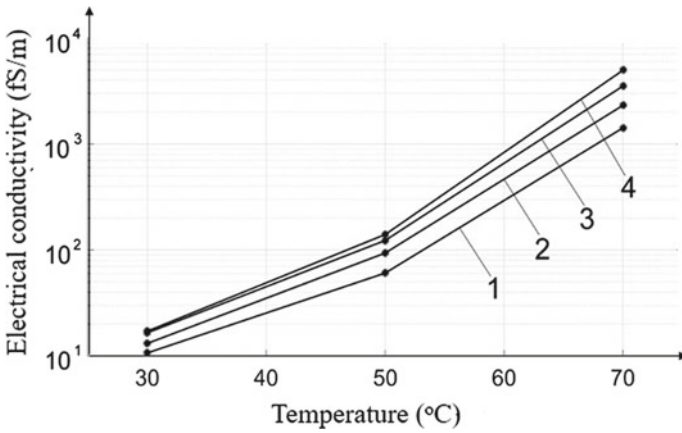


Fig. 38 Variation of DC electrical conductivity of EPR with temperature, for $E = 5\text{ kV/mm}$ (1), 10 kV/mm (2), 15 kV/mm (3) and 20 kV/mm (4) (Reprinted, with permission, from author [68])

6.1.2 Electrical Permittivity

Electrical permittivity is the second main characterization parameter of the insulating materials used in electrical engineering, after the electrical conductivity. The permittivity is a complex parameter ϵ_c and is determined in harmonic electric fields of frequency f (respectively, pulsation $\omega = 2\pi f$), as follows:

$$\epsilon_c = \epsilon' - j\epsilon'' \tag{2}$$

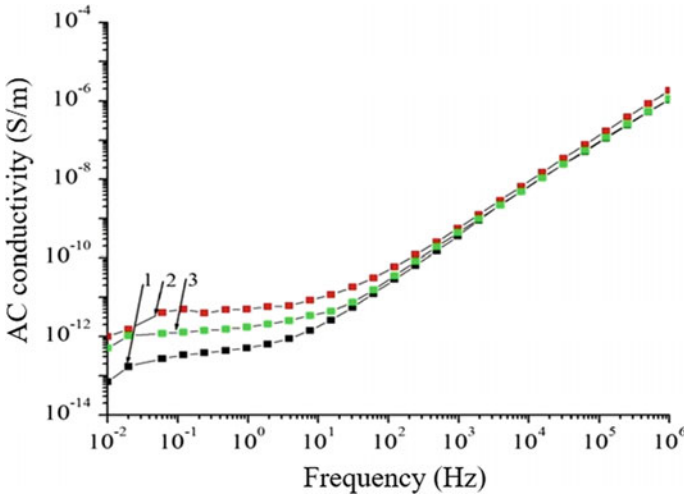


Fig. 39 Variation of the AC electrical conductivity with frequency f , for samples from XLPE (1), EPR (2) and XLPE/EPR (3) ($T = 30\text{ }^{\circ}\text{C}$) (Reprinted, with permission, from author [68])

where the real part of the complex permittivity ϵ' characterizes the temporary electrical polarization of the material, and the coefficient of the imaginary part ϵ'' —the dielectric losses (by electric polarization) [13].

The parameter $\epsilon_r' = \epsilon'/\epsilon_0$ is called relative permittivity or dielectric constant and is noted, simply, ϵ_r . The values of the dielectric constant must be as small as possible, so that the values of the capacitance and of the electric capacitance currents in insulations to be as low as possible. The values of the dielectric constant depend on the material nature and on the characteristics of the stresses (electric field, temperature, radiation, etc.) to which it is subjected in operation.

Thus, in the report [72] it is shown that the decrease of the electric field frequency to small values (of mHz order) determines an increase of the ϵ_r values (see Figs. 40, 41 and 42). Thus, ϵ_r values of the XLPE, for any temperature and frequency, are lower than for EPR and EPDM. On the other hand, the increase in temperature leads to an increase in the ϵ_r values, but these increases are more important in the case of EPR (see Fig. 41) than in the cases of XLPE (see Fig. 40) and EPDM (see Fig. 42).

The experimental tests on XLPE and EPR flat samples with a thickness of 1.14 mm [73] showed that ϵ_r values are influenced by the electric field. Thus, when the electric field increases from 17.3 to 19.15 MV/m, ϵ_r values increase from 2.338 to 2.358 for XLPE samples and decrease from 2.72 to 2.52 for EPR samples. The increase of temperature leads to the reduction of the dielectric constant values of the cable insulations, both for XLPE and EPR (see Fig. 43).

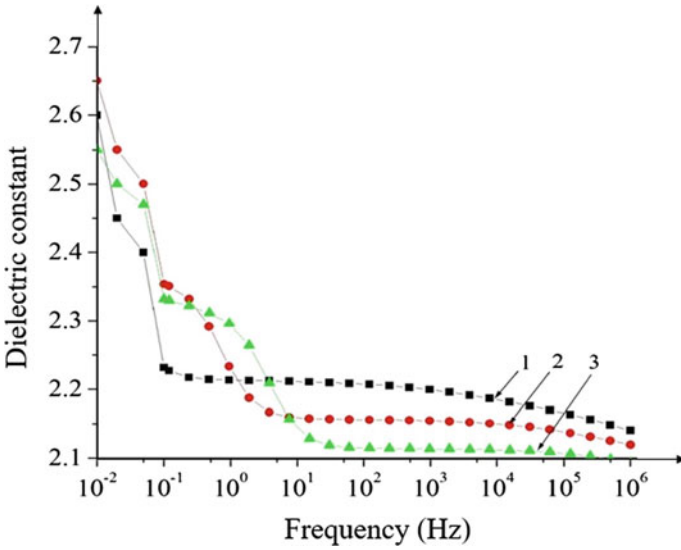


Fig. 40 Variation of the dielectric constant with the frequency for XLPE samples, at 30 °C (1), 60 °C (2), and 80 °C (3) (Reprinted, with permission, from author [72])

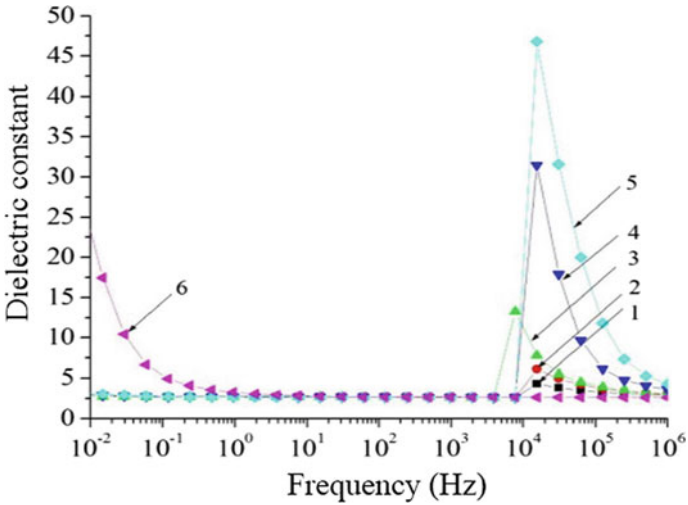


Fig. 41 Variation of the dielectric constant with the frequency for EPR samples, at 30 °C (1), 40 °C, (2), 50 °C (3), 60 °C (4), 70 °C (5), and 80 °C (6) (Reprinted, with permission, from author [72])

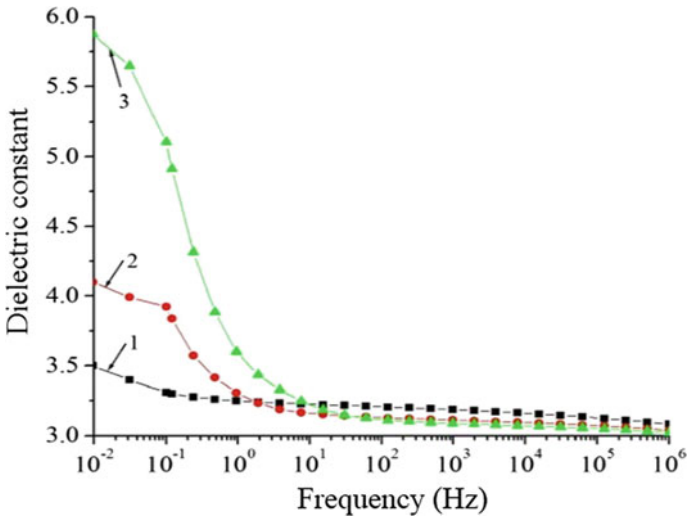


Fig. 42 Variation of the dielectric constant with the frequency for EPDM samples, at 30 °C (1), 60 °C (2), and 80 °C (3) (Reprinted, with permission, from author [72])

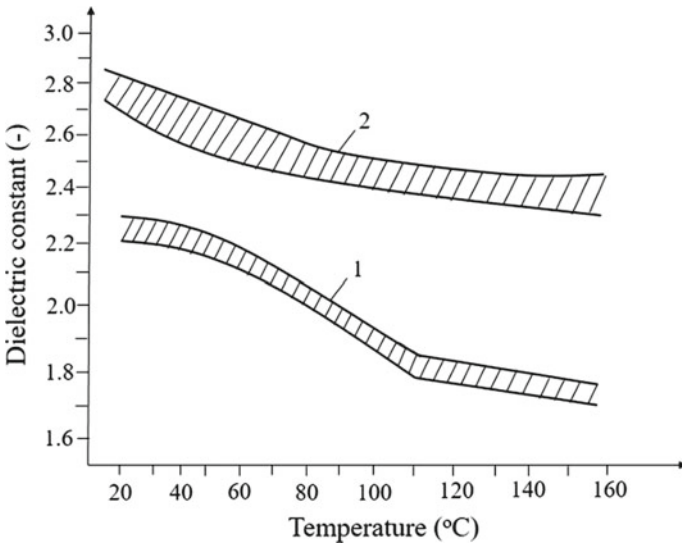


Fig. 43 Variation of the dielectric constant with the temperature for XLPE (1) and EPR (2) samples (Reprinted, with permission, from [62])

6.1.3 Loss Factor

The loss factor (dissipation factor) $\tan\delta$ is defined as the ratio between the coefficient of the imaginary part of the complex permittivity ε'' and its real part ε' , respectively:

$$\tan\delta = \frac{\varepsilon''}{\varepsilon'} + \frac{\sigma}{\omega\varepsilon'} \quad (3)$$

where $\omega = 2\pi f$ and $\tan\delta$ characterizes the total losses produced in the electrical insulating material by polarization and electrical conduction [13].

In general, for the electrical equipment insulation systems, insulating materials with the lowest $\tan\delta$ values are used. These values depend not only on the chemical nature and on physical structure of the material, but also on the intensity and frequency of the stresses to which they are subjected in operation.

As shown in Figs. 44, 45 and 46, XLPE presents the lowest $\tan\delta$ values for any value of electric field frequency and temperature. On the other hand, for all the other studied materials, the values of $\tan\delta$ are higher in the case of very low frequencies (mHz) and have peaks for different values of the frequency (depending on the nature of the material). For these values, the losses within insulations are maximum. The increase of the temperature from 30 to 80 °C leads to an increase in $\tan\delta$ values for all materials, but these variations are much higher for EPR and EPDM than for XLPE. It should be emphasized that if temperature rises, its $\tan\delta$ values decrease in the case of very low and high frequencies and increase in the case of industrial frequencies (5–500 Hz) (see Figs. 44–46).

The loss factor increases with the intensification of the electric field, the increase being lower in the case of XLPE (where the electrical conductivity is lower) and more important in the case of EPR and Kraft paper impregnated with mineral oil (see Fig. 47).

The experimental tests on XLPE and EPR flat samples with a thickness of 1.14 mm [73] showed that $\tan\delta$ values are influenced by the electric field intensity. Thus, when the electric field intensity increases from 17.3 to 19.15 MV/m, $\tan\delta$ values increase from 0.00018 to 0.000258 for XLPE samples and decrease from 0.09 to 0.07 for EPR samples.

The variations of loss factor with temperature for EPR and XLPE insulations are shown in Fig. 48. It was found that, in the case of EPR, its $\tan\delta$ values increase continuously with temperature. Whereas, in the case of XLPE, $\tan\delta$ decreases up to 75 °C, after which it starts to increase (but remain lower than for EPR). A major disadvantage of EPR over XLPE establishes the important variations of dissipation factor from one cable length to another. For instance, for the lengths of 150 kV EPR cable, its $\tan\delta$ values can vary (at 20 °C) between 0.0027 and 0.004 [26]. In general, $\tan\delta$ values of XLPE cables are at least 20 times lower than that of EPR

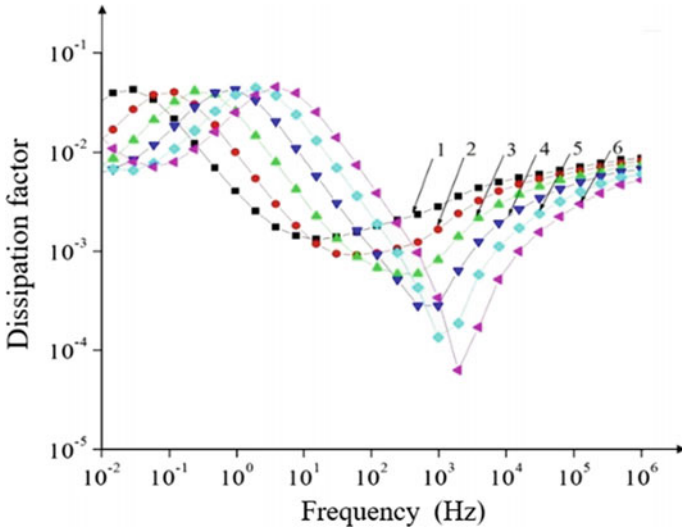


Fig. 44 Variation of the dissipation factor with the frequency for XLPE samples, at 30 °C (1), 40 °C, (2), 50 °C (3), 60 °C (4), 70 °C (5), and 80 °C (6) (Reprinted, with permission, from author [72])

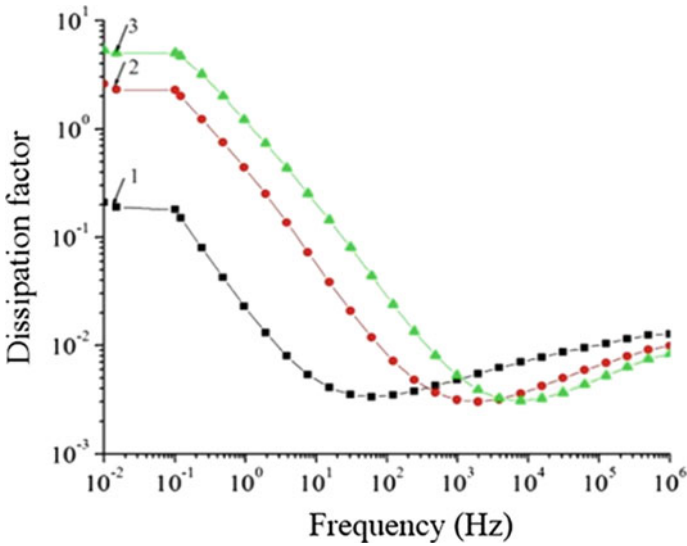


Fig. 45 Variation of the dissipation factor with the frequency for EPR samples, la 30 °C (1), 60 °C (2), and 80 °C (3) (Reprinted, with permission, from author [72])

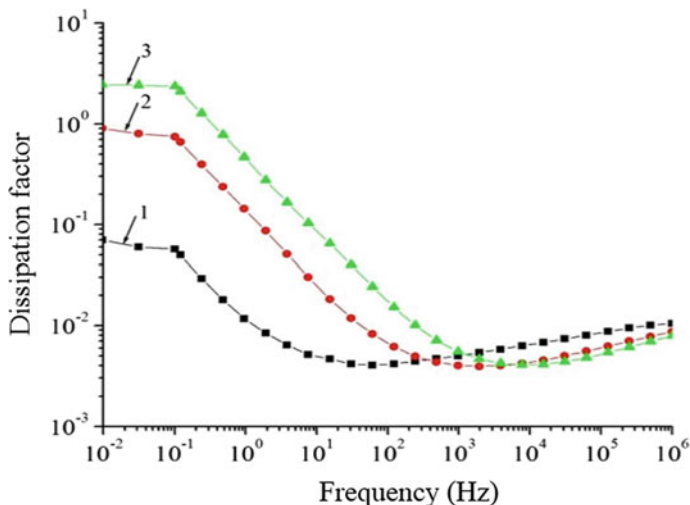
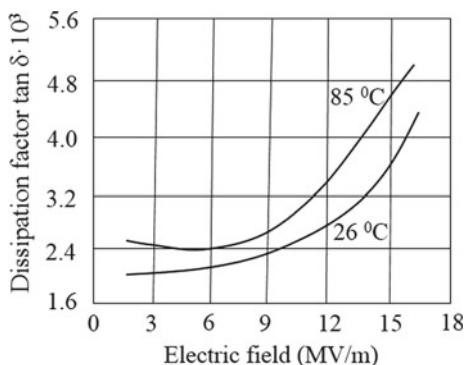


Fig. 46 Variation of the dissipation factor with the frequency for EPDM samples, at 30 °C (1), 60 °C (2), and 80 °C (3) (Reprinted, with permission, from author [72])

Fig. 47 Variation of the dissipation factor with the electric field intensity for Kraft paper cable impregnated with low-viscosity mineral oil [20]



cables. Thus, with XLPE cables, the energy savings per year can be in the order of 15 MWh/cct-km for a 69 kV system, 52 MWh/cct-km for a 138 kV system and 127 MWh/cct-km for a 230 kV system (cct = three-phase circuit kilometer length).

In conclusion, it can be said that very pure insulations such as PE and XLPE exhibit very low $\tan \delta$ values. TR-XLPE has a slightly higher $\tan \delta$ than XLPE, while materials as EPR and PVC have still higher $\tan \delta$ values. However, both EPR and TR-XLPE have acceptably low values for medium-voltage applications.

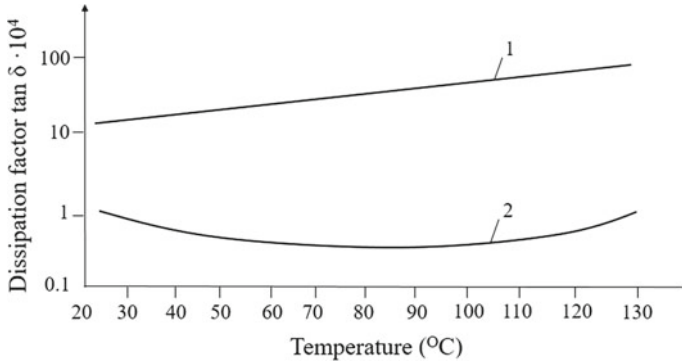


Fig. 48 Variations of the dissipation factor with temperature for insulation from EPR (1) and XLPE (2) [26]

6.1.4 Breakdown Strength

Dielectric strength E_{bd} is determined in harmonic electric fields, on standard samples and with plane, cylindrical or spherical electrodes and represents the ratio between the breakdown voltage of the sample V_{bd} and the distance between the electrodes d [74, 75]:

$$E_{bd} = \frac{V_{bd}}{d} \quad (4)$$

The electrical insulating materials used in electrical engineering must have E_{bd} values as high and less variable as possible with the operating stresses (e.g., temperature, mechanical stresses, environment, etc.). Evermore, the dielectric breakdown strength of oil-paper (ca. 40 kV/mm) and solid-dielectric extruded polymer insulation (ca. 70 kV/mm) is well above their normal accepted operating stress values (5–20 kV/mm).

The variations of dielectric strength with temperature of filled XLPE and EPR are shown in Fig. 49 [4]. It was found that for values below 100 °C, E_{bd} values are higher for XLPE than those for EPR and for temperatures above 100 °C, E_{bd} takes higher values for EPR. Similar results are presented in [62], where it is shown that the breakdown strength of XLPE exceeds that of EPR by 50% for temperature values up to 90 °C (see Fig. 50).

On the other hand, if cables are immersed in water for more than 2 months, those with XLPE insulation will continue to have a higher value of the breakdown voltage than those with EPR insulation (see Fig. 51) [62, 76].

In the paper [47], the dielectric breakdown behavior of electric mini-cables insulated with PP and XLPE was studied. The authors used two sets of PP- and XLPE-based mini-cables, with a length of 6 m and an insulation thickness of about 4 mm. The samples were subjected to a stepped DC test, and the failure voltage was

Fig. 49 Variation of breakdown strength with temperature for filled XLPE (33%) (1) and EPR (38%) (2) [4]

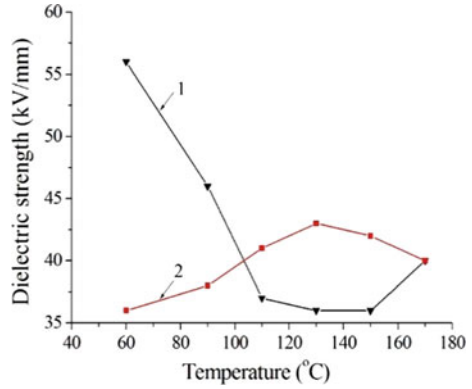


Fig. 50 Dependence of breakdown strength on temperature for XLPE (1) and EPR (2) (Reprinted, with permission, from [62])

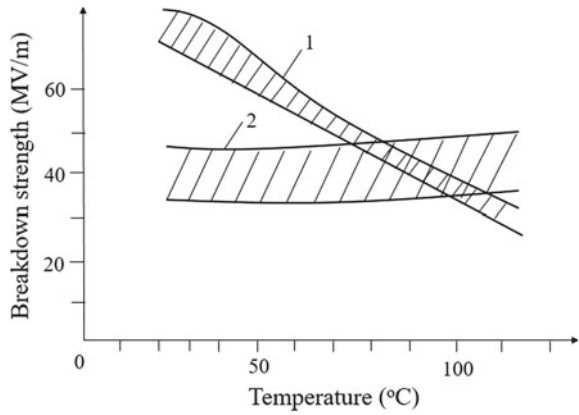
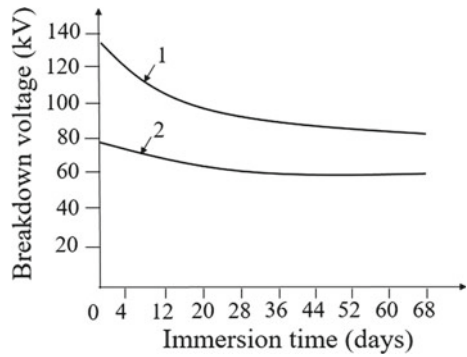


Fig. 51 Variation of AC breakdown voltage with aging duration (water at 70 °C) for 11 kV XLPE (1) and EPR (2) cables [76]



noted. In the case of XLPE-insulated cables, it was found that all samples breakdown around 200 kV, whereas in the case of samples insulated with PP, the values of the breakdown strength exceeded 400 kV. In the paper [35], it was shown that

the addition of nanoparticles in XLPE leads to an increase of dielectric strength of about 2.2 times, as a result of deep-traps produced by nano-fillers.

6.1.5 Impulse Strength

The same variations were found for breakdown strength impulses in the studies [4, 62]. Thus, as can be seen in Fig. 52, for temperatures below 90 °C, XLPE is superior to EPR.

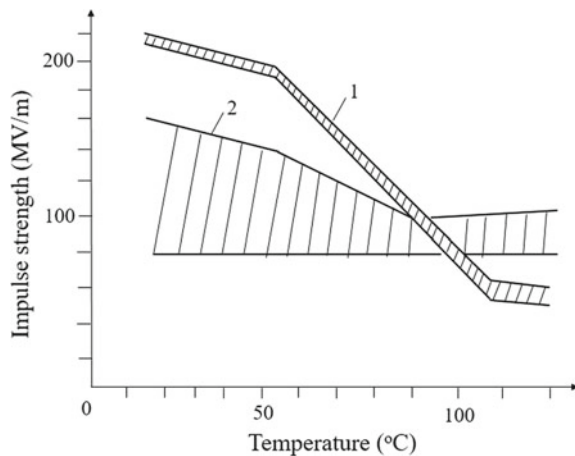
6.1.6 Space Charge Accumulation

Space charge consists of electrons, holes, and ions and is generally understood (as shown in [2]) as:

- (a) a separation of free charge in the volume or interface of their insulation components due to carriers generated in the technological processes,
- (b) a space charge injection on the electrodes,
- (c) the field-assisted thermal ionization of impurities from the insulation,
- (d) the insulation degradation under the action of (electrical, thermal, mechanical, etc.) stresses during operation and the electric and/or water trees development [77].

The presence of space charge in insulations leads to the local intensification of the electric field and, consequently, to the intensification of the degradation processes and to the reduction of the insulations' lifetime. Therefore, especially in the case of DC cables of very high voltages (up to 800 kV), new materials and technological processes that will lead to the reduction of the space charge in insulations are requested [78]. For instance, in the case of XLPE, various additives are

Fig. 52 Dependence on temperature of impulse strength for XLPE (1) and EPR (2) (Reprinted, with permission, from [62])



introduced (e.g., 2,4-Diphenyl-4-methyl-pentene-1, dissolving oxygen, etc.), which prevents the formation of space charge or enables its dissipation.

In numerous studies, the information regarding the values and the distribution of the space charge in insulations based on PE, XLPE, EPR, etc., is presented. The electric stress conditions that can generate space charge in polymeric insulation (going from DC to power electronic repetitive impulses), the effect of space charge promoting acceleration of aging processes and bringing to early failure of electrical apparatus, the influence of space charge on degradation mechanisms, such as electron avalanche and partial discharges are discussed in [79]. It is shown that the space charge accumulated in a polymer under an applied voltage is a cause of aging due to the relevant local field enhancement and associated electromechanical energy storage, whose main effect of lowering the free energy barrier is exceeded and degradation can occur. In the paper [80], the factors that determine the formation and accumulation of space charge are analyzed in detail. Electronic charge injection (with the formation of homo- and heterocharges), field-assisted thermal ionization of impurities (with the formation of ions and molions), spatially inhomogeneous electric polarization (which produces an apparent volume space charge) and the charge generated by steady DC current coupled with a spatially varying ratio of permittivity and conductivity are discussed.

The variations of space charge volume density ρ_v in plane samples based on LDPE and HDPE are shown in [81] (see Fig. 53). It has been found that ρ_v has higher values in LDPE than in HDPE samples. In the paper [82], space charge accumulation profiles were compared for LDPE, LDPE plus antioxidant (LDPE—AO) and XLPE, with consideration of thermal treatment effects in LDPE and XLPE. Significant variations (decreases) of accumulated space charge and apparent mobility have been remarked going from LDPE to LDPE-AO and XLPE which may be associated with the formation of deeper trap levels (or an increase of their density) [83]. As can be seen in Fig. 54, the space charge density accumulated in XLPE samples has lower values than those from LDPE and LDPE-AO, especially for electric field values higher than 5 MV/m.

Fig. 53 Charge build up with unaged HDPE (Reprinted, with permission, from [81])

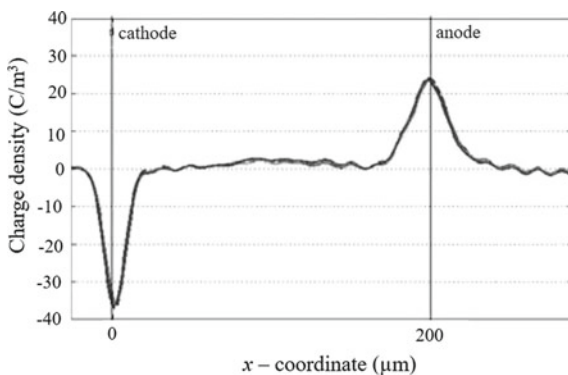
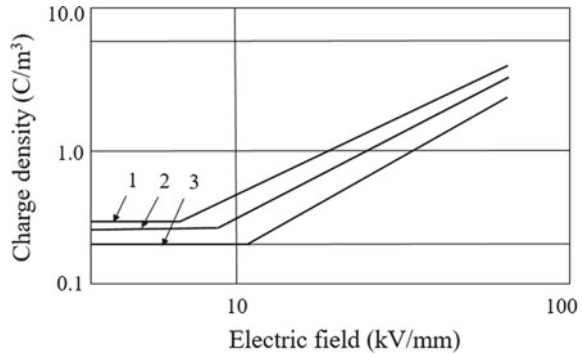


Fig. 54 Variation of the charge density with the electric field for LDPE (1), LDPE-AO (2), and XLPE (3) (Redrawn and adapted figure from reference [82])



In the case of cables insulation with water trees, the average volume density of the space charge increases [84–88]. This increase depends on the number and size of the trees and is higher in LDPE than in XLPE and, especially, in TR-XLPE. Using the step method, in the study [89], the charge accumulation and the remaining field in cross-linked polyethylene (XLPE), very low-density polyethylene (VLDPE), isotactic polypropylene (PPiso), and a polyethylene/polypropylene copolymer (PPCop) samples were determined. It was found that the amount of charge accumulated under AC conditions might reach a maximum value at a given temperature, while the highest space charge was found in polyolefins with the lowest crystallinity ratio (see Table 15).

Space charge measurements in power cables insulation showed that no space charges have been found in either Kraft paper nor PPLP insulation (which denotes a very safe insulation for operating HVDC superconducting cables) [90].

To achieve space charge reduction, the insulation produced should not be heated above 230 °C for periods less than 10 min. This suppresses the production of polar by-products, such as acetophenone and cumyl alcohol [91]. Other methods of reducing the space charge in XLPE are based on the introduction of polar groups bonded to XLPE (e.g., dissolving oxygen gas in the LDPE during the extrusion process), addition of organic (glycerol fatty acid ester) and inorganic additives (TiO₂, BaTiO₃, I, MgO, etc.), carbon black, grafting of PE with maleic anhydride, etc. [92]. While the inclusions of surface modified MgO, TiO₂, ZnO, and Al₂O₃ nanoparticles can suppress space charge accumulation in nanocomposites, the inhibition effect depends on the type of nanoparticles. Nanocomposites based on PP

Table 15 Values of the remaining field for some polyolefin after ac conditioning during 14 days under an rms field of 40 kV/mm [89]

Material	VLPPE	PPCop	XLPE	Ppiso
Crystallinity (%)	10	40	42	55
Remaining field (MV/m)	9.73	3.42	1.78	0.96

with MgO, TiO₂, and Al₂O₃ show the most desirable space charge suppression for a lower content of nanoparticles (under 3 phr) [93]. This result is consistent with the results obtained on MgO/LDPE, MgO/XLPE, TiO₂/LDPE, and Al₂O₃/LDPE nanocomposites [84, 94, 95].

6.1.7 Repetitive Lightning and Switching Impulses

The application of repetitive lightning impulse overvoltages is one of these factors that lead to the aging of polymer insulations [81]. The effect of switching impulses was clearly identified due to the long time of switching impulses and space charge accumulation into the bulk of samples [96]. Repetitive lightning impulse overvoltages may also lead to the acceleration of aging processes of insulating materials [97, 98].

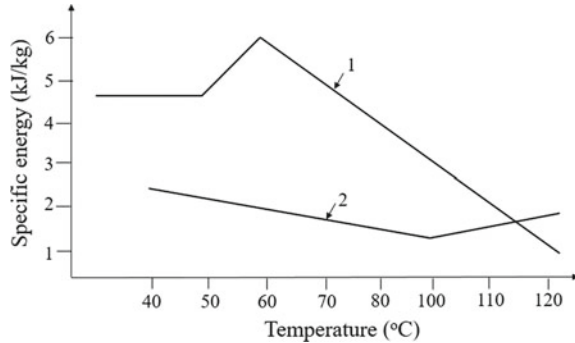
In the work [81], the lightning aging processes of two high voltage insulation materials, namely HDPE and LDPE, were analyzed. The authors used samples with a Rogowski profile and thickness of 200 μm (coated with gold), to which lightning pulses with a front/tail time of 1.2/40 μs and a peak electric field of 85 kV/mm were applied. Both positive and negative lightning impulses (3000 or 6000) were investigated. The authors measured breakdown strength and found that repetitive lightning impulses can reduce the breakdown strength of HDPE, but do not affect LDPE. There was almost no difference between the effects of positive and negative impulses. Concerning the space charge, HDPE becomes lossier and space charge builds up more effectively after aging, while LDPE is largely unaltered.

A study regarding the aging of high voltage EPR and XLPE cables under applied switching impulses is presented in [96]. For tests, 15 kV cable samples were used and were subjected to 4500 switching impulses with a magnitude of 100 kV. Apparent space charge corresponding to PDs and AC breakdown voltage V_{bd} were chosen as parameters to evaluate the status of cables. The results showed that the apparent charge magnitudes for XLPE cables are significantly higher than EPR cables. On the other hand, with the increase in number of impulses, the apparent charge magnitudes have a strong downward trend for XLPE cables opposed to a slight downward trend for EPR cables. For lower values of the impulses number N (up to 1000), the breakdown voltage increases, both for XLPE and EPR, while for $N > 5000$, V_{bd} decreases significant in the case of XLPE (from 130 to 90 kV).

6.1.8 Partial Discharges Resistance

Partial discharges (PDs) deteriorate the insulation (through combination of chemical, mechanical, thermal, and radiative processes), but it does not cause immediate failure or breakdown. If PDs continue to occur for long time, they lead to complete failure of the insulation [99]. There are two necessary conditions for initiation of PDs within a cavity, respectively, the electrical field must be larger than certain critical value E_c and free electrons must be available to start the electron avalanche

Fig. 55 Dependence of partial discharge resistance on temperature for XLPE (1) and EPR (2) (Reprinted, with permission, from [62])



[2]. It has been found that PDs result in gaseous by-products (CO_2 , CO , CH_4 , H_2 , and H_2O) [100, 101], and liquid droplets (mixtures of simple organic compounds, such as formic, acetic, and carboxylic acids) [100, 102], in association with solids, such as oxalic acid crystals [100, 103] (see Fig. 55) [2].

An analysis of the products nature that arise as a result of PDs action on the cavity walls of XLPE cable insulation is presented by Gamez-Garcia et al. in [104] and [100]. The authors subjected XLPE foils (of 160 μm in thickness) to PDs action and analyzed the resulting chemical compounds. It was shown that under PDs action, both gaseous products (CO , CO_2 , H_2O) and liquids and solids result. The liquid and solid products have been found to result from the synthesis reactions taking place in the vapor phase across the interelectrode gap-space. Acetophenone, which evaporates from the XLPE surface after the cross-linking, plays an important role in the formation of other observed degradation products. Benzoic acid, benzamide, toluene, and other aromatic compounds result from corona-chemical reactions of this volatile compound during the degradation process [2].

Figure 55 shows the variation of the energy required to erode or decompose (by PDs) one kg of material (XLPE and EPR) under test as a function of temperature. It can be observed that for temperature values lower than 110 $^\circ\text{C}$, the energy required for XLPE degradation has higher values than for EPR, respectively, that XLPE has a PD resistance higher than EPR.

In general, the apparent charge associated with PDs takes higher values in EPR insulations of the cables, than in XLPE, under the same conditions (humidity, temperature, mechanical stresses, etc.) and for the same aging times [105]. On the other hand, the manufacture of XLPE nanocomposites with inorganic fillers or linear low-density polyethylene (LLDPE)/natural rubber (NR) blends with 4 phr nano-sized montmorillonite filler causes a reduction in the level of PDs [106].

6.1.9 Electrical Treeing Resistance

Electrical trees (ETs) are initiated by the high divergent AC field of a stress enhancing geometrical feature, such as a point or wire electrode (see Fig. 56), or by

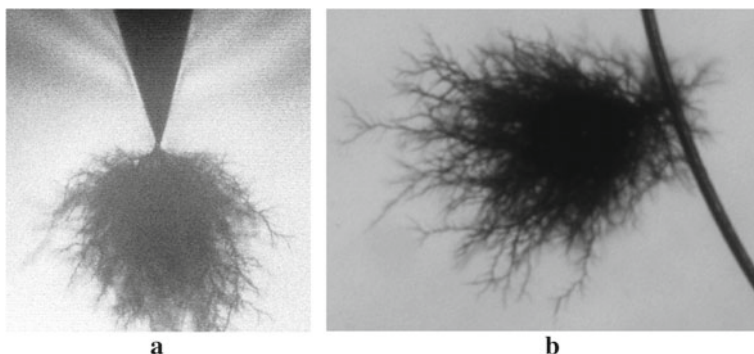


Fig. 56 Electrical trees produced in XLPE with needle (a) and wire (b) electrodes [109]

partial discharges taking place in a gas-filled cavity [107]. In addition, ETs may be produced during a short circuit or polarity reversal of DC fields.

ETs are very fine channel networks (including gases at high pressures) initiated near insulation and/or electrodes defects, which are developing in the insulation during the operation of the electrical equipment. ETs represent one of the main causes of damage and failure in electrical power cable insulation [2]. Propagation of ETs in solid insulation can bridge the electrode gap, leading to the breakdown of the insulation.

The ETs channels are formed by the local destruction of the material under the synergetic action of the electric field, PDs (from the voids and channels) [108], heat and mechanical stresses produced by the electric field and gases from the channels (resulted from the material decomposition). The ETs initiated near the electrodes are called vented trees, and they are developed from the electrode to the 'inside' of the material. In contrast, the ones generated inside the insulation (near voids, metal inclusions, etc.) have a structure of channels developed along the electric field lines on both sides of the defect (electric field concentrator) and they are called bow-tie trees [2].

ETs inception is firmly associated with the injection of charge into the polymer [110] either by a high field electrode or by gas discharges in a cavity [13, 107]. The formation of a discharging tubule (channel) is due to the impact excitation of molecular species by hot electrons (electrons with sufficient kinetic energy to initiate a route to chemical degradation [110]) or by chemical bonds breaking through ultraviolet (UV) radiation emitted during charge recombination [111]. It follows, therefore, that the initiation times and the development speeds of the ETs depend both on the characteristics of the electric field (size, frequency, etc.) and on the chemical structure and nature of the insulation. The higher the bonding energy values corresponding to the constituent elements of the molecules, the less expected the rupture of the bonds and the initiation and development of the ETs are more difficult.

ETs were highlighted in all types of cable insulations, respectively, in LDPE, HDPE, XLPE [2, 110, 112–114], EPR [110, 115], EPDM [108], etc. However, there is no systematic comparative study regarding the development of ETs in polymers. Different polycyclic compounds can be used to reduce the development speeds of ETs in XLPE [116]. The effect of polycyclic compound is related to the temperature. With the temperature increase, the suppression effect to ET growth of polycyclic compounds decreases. If the trees developed in XLPE are of bush tree or branch-pine tree types, those developed in PP have the form of branch tree (see Fig. 57) [42]. On the other hand, in the XLPE insulation, the lifetime of the ETs initiation is higher and the development rate is faster than in PP insulation.

In order to increase the resistance of XLPE to electrical treeing, lately, the use of new stabilizers, respectively, benzyl-, thioxanthone- fullerene-, and melamine-types, has been studied [109]. They were found to cause an increase in resistance toward electrical treeing in the range between twenty up to well above one hundred percent.

6.1.10 Water Treeing Resistance

There is no organic material impermeable to moisture, but the only commonly used high polymer less permeable than PE is PVC (SARAN). At 23 °C, the concentration of water absorbed by XLPE is 350 ppm (0.035%) in boards and 850 ppm in cables insulation [62]. EPR absorbs about 1% moisture by weight after two weeks immersion in water at 80 °C. When removing from water, EPR was observed to dry out much more rapidly than it had been infused with moisture. In general, the water absorption in XLPE and TR-XLPE insulation is much slower than in EPR (see Fig. 58) [105].

Higher water permeability of cables insulation facilitates the formation of water trees. Water treeing is generally observed as a dendritic pattern of water-filled

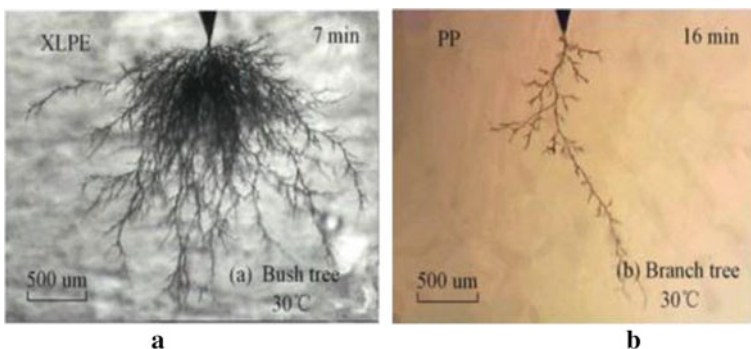
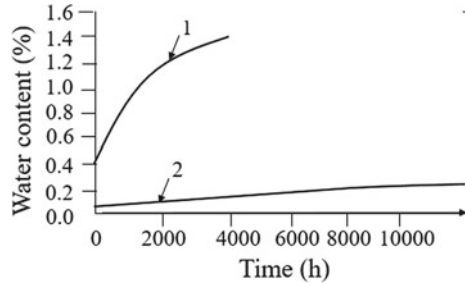


Fig. 57 Electrical trees in XLPE (a) and PP (b) (Redrawn and adapted figure from references [11] and [42])

Fig. 58 Variation in time of water content in EPR (1) and TR-XLPE (2) cable insulation (Redrawn and adapted from reference [105])



microcavities in the polymer connected by oxidized ‘tracks’ (about 10 nm wide) and is described as a self-propagating pattern of electro-oxidation. Self-propagation results from the electro-oxidation of hydrophobic polymer to a more hydrophilic state, which causes condensation of moisture from the surrounding hydrophobic polymer region. Such self-propagation (water treeing) is likely to occur in any polymer that can be oxidized to a substantially more hydrophilic state [117].

As for most organic polymers, PE and XLPE meet all the requirements for water treeing (i.e., they are hydrophobic and can be oxidized to a substantially more hydrophilic state). However, PE is normally very ‘clean,’ with a very low ion concentration. Thus, the water in PE cable, normally dielectric, shows a too low conductivity to create the chemical potential necessary for water treeing. However, the chemical potential will increase with any increase in water conductivity, so that the ionic impurity at the dielectric–semiconductor interface can increase the chemical potential (at about 1 eV) and cause a water tree.

Tests performed on cable insulation samples aged for eight months at three times rated voltage showed relatively large density and a lower length of water trees in unfilled XLPE compared to filled XLPE and EPR (see Table 16). On the other hand, EPR insulation has the lowest density and highest average length of bow-tie trees. In unfilled XLPE, each ‘bow’ is relatively spherical in nature, in contrast to ‘bows’ in EPR, which are longer and narrower (see Fig. 59).

In the case of vented trees (VTs), the values of trees density are much lower in all insulations (see Table 17), but as in the case of bow-tie trees, they are higher in XLPE than EPR. On the other hand, the lengths of the VTs are longer in XLPE than EPR.

Initiation sites of bow-tie trees in XLPE are associated with cavities, particle agglomerates, and flaws such as cracks. These trees are initiated relatively easy, but

Table 16 Bow-tie trees (BT) in XLPE, filled XLPE and EPR cable insulation [117]

Material	BT density (mm^{-3})	BT length (μm)	Water absorption (ppm)
XLPE	>28	90	17
Filled XLPE	4	180	260
Filled EPR	0.3	390	470

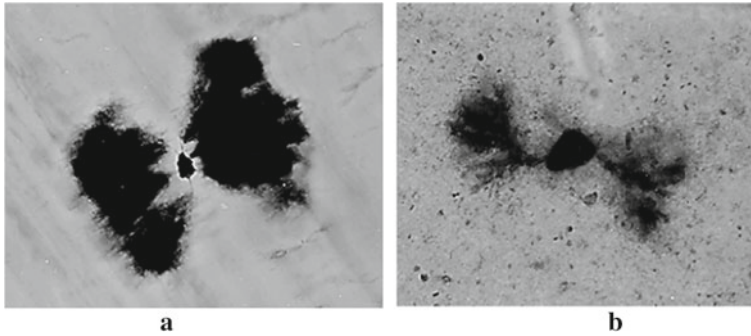


Fig. 59 Bow-tie trees in XLPE (a) and filled EPR (b) (Redrawn and adapted figure from reference [117])

Table 17 Vented trees (VT) in XLPE, filled XLPE and EPR cable insulation [117]

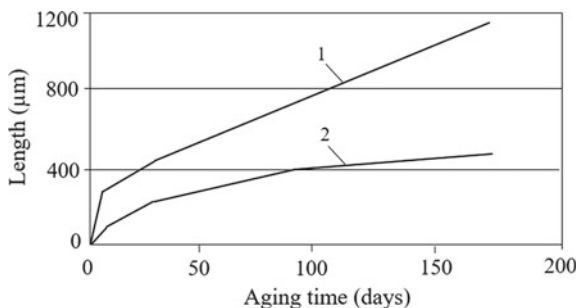
Material	VT density (mm^{-3})	VT length (μm)
XLPE	0.3	60
Filled XLPE	0.2	120
Filled EPR	0.01	45

they are growing slowly [117]. In EPR, initiation sites are somehow associated with catalytic impurities such as iron oxides and vanadium compounds (catalyst residue).

Bow-tie trees are easily initiated and have a high density in steam cured XLPE as a result of the high cavity content and segregation of ionic impurities into such cavities. In newer dry-cured XLPE cables, bow-tie trees density is much lower as a result of the much lower density of cavities in the insulation. In EPR, and due to a lower degree in filled XLPE, bow-tie trees are difficult to initiate, but once initiated appears to grow quite aggressively. The difficulty in initiating bow-tie and VTs in EPR is probably the result of three factors: significant reduced hydrophobicity of EPR relative to unfilled XLPE (see Table 16), higher ionic content of EPR and presence of catalytic ions (vanadium, iron), which reduce the activation energy required for electro-oxidation. In general, the observed treeing patterns are similar to those formed in PE and XLPE insulation [118].

In the case of filled XLPE, the moisture absorption is less than for EPR so that the hydrophobicity is higher in EPR and lower in XLPE. As a result, in terms of the resistance to water treeing, filled XLPE lies between unfilled XLPE and EPR. Filled XLPE and EPR cable insulations have an inherent water tree resistance. The water tree resistance of EPR insulations is caused by the reduced hydrophobicity (which reduces the tendency of water to condense from the bulk dielectric into electro-oxidized regions) and, possibly, relatively high ionic content (which may tend to render any liquid water in the dielectric to conductive that cause water tree growth).

Fig. 60 Variation of tree lengths with the development aging time in XLPE (1) and TR-XLPE (2) (Redrawn and adapted figure from reference [119])



The additives employed to make XLPE insulation water tree resistant, increase its water absorption (i.e., make the polymer less hydrophobic). As it is well known, TR-XLPE insulation does not stop water trees growth, but prevents water trees growth (i.e., the number and size of water trees are reduced) (see Fig. 60), and their forms are changing (see Fig. 61) [119]. The reduction in number of water trees is probably the result of greatly improved cleanliness of modern semicons and reduced hydrophobicity of TR-XLPE. Certain types of TR-XLPE contain a dispersion of hydrophilic molecular clusters in the hydrophobic matrix. The hydrophilic clusters ‘stop’ water tree channels (when a water tree channel ‘hits’ a tree-retardant cluster, it stops propagating—the hydrophilic cluster impedes condensation of water in any electro-oxidized region near it, so that the water tree cannot propagate).

To increase the resistance of cable insulation to water treeing, a blend of PE with ethylene alkyl acrylate copolymer, named ‘copolymer XLPE’ is used. In [120], it is shown that after an aging time of 365 days in water and electric field, the dielectric strength of copolymer XLPE insulations was approx. 40 kV/mm, compared to 35 kV/mm as shown by XLPE-insulated cables, and much lower than TR-XLPE cables insulation (approx. 60 kV/mm).

6.1.11 Tracking Resistance

Tracking deterioration is caused by the carbon formed on the surface of materials, which is precipitated due to the heat from the discharge started locally across a dry band. The surface is carbonized by the heat energy of the discharge and the carbonized conduction path finally forms over the short-circuited path [121]. Therefore, the use of materials with highest tracking resistance is important for the safety and reliability of electrical equipment. For tracking resistance determination, the procedures presented in IEC Publication 587 [122] and IEC Publication 112 [123] can be used. In general, the voltage that will cause failure with the application of 50 drops of electrolyte, respectively, CTI indicator [122], is determined. In [124],

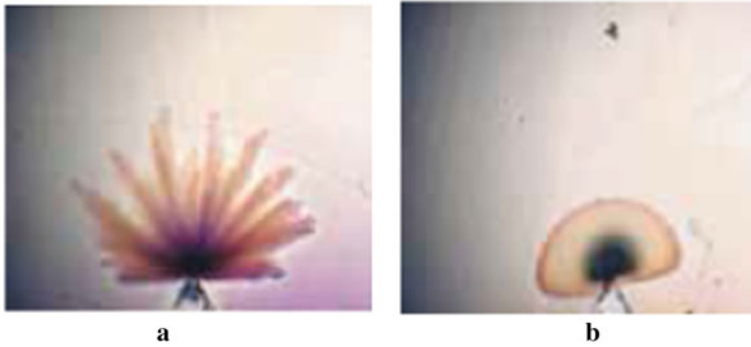


Fig. 61 Water trees in XLPE (a) and TR-XLPE (b) [119]

Table 18 Time to tracking breakdown (h) [124]

Polymer	Filler	Virgin	Acid rain 120 days
Epoxy resin	Al(OH) ₃	>6	>6
PTFE	–	>6	>6
XLPE	Al(OH) ₃	>6	2.20
Silicone rubber	Al(OH) ₃	1.95	0.42
EPR	Al(OH) ₃	0.17	0.32

the results of tests carried out on polymer samples without fillers and with aluminum rehydrate filling, without and with artificial acid rain, at a voltage of 4.5 kV (see Table 18) are presented. It was found that the durations of breakdown appearance due to the tracking phenomenon are much longer in XLPE than silicone rubber and EPR.

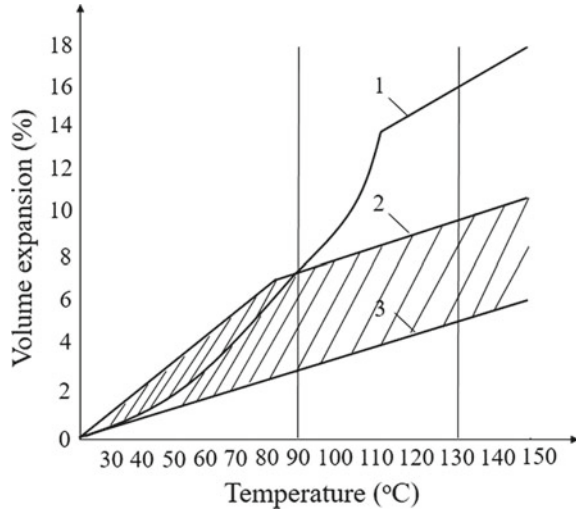
6.2 Thermal Properties

The most important thermal properties of organic high polymers used as electrical insulations on flexible power cables are thermal expansion, thermal conductivity, and thermal stability (see Table 19). Fundamental and analytical investigations of these properties have been published [62, 125] and can be used to provide background and understanding.

Table 19 Properties of cable insulations from polyethylene (PE), cross-linked polyethylene (XLPE) and polyvinyl chloride (PVC) [126]

Insulation	Specific gravity (-)	Tensile yield strength (MPa)	Tensile modulus (GPa)	Coefficient of linear expansion (m/m °C)	Thermal conductivity (W/m °C)	Specific heat (J/kg °C)	Temperature limit (°C)
PE	0.95	22.1	0.827	162	0.462	2303	70
XLPE	0.94	19.3	0.858	162	0.462	2303	90
PVC	1.4	55.2	2.830	54	0.159	1047	65

Fig. 62 Variations of relative (thermal) volume expansion with the temperature for XLPE (1) and EPR semi-crystalline (2) and EPR amorphous (Reprinted, with permission, from [62])



6.2.1 Thermal Expansion

During thermal cycling of a cable, the conductive layers over the conductor and insulation will expand and shrink as the temperature varies. The change in expansion characteristics exhibited by XLPE, particularly in the temperature range near the transition point (see Fig. 62) can lead to increase in dimensions at overload conditions, which cause great pressure on the insulation shield, either extruded or metallic. As a result, splits or cavities may occur between the insulation and the insulation shield.

The thermal expansion is a major issue when a HV cable operates above 90 °C. Over the full operation of a cable from low to high temperatures, thermal expansion differences of up to 20 times may occur. This is caused by differences in thermal expansion coefficient of the metals from conductors, screens and shields (copper, aluminum, lead), which load the main insulation over the full operational temperature range. This does not mean significant changes in the molecular conformation, but the molecules move further apart from another. As an example, typical XLPE used in cable insulations expands with about 15% when going from room temperature to 105 °C, while copper or aluminum expands less than 3% in the same temperature range. The resulting pressure may affect the dielectric properties and can cause damage to the sheath and joints [127].

At any point of physical discontinuity along a cable, such as splices, terminals, grounds, and clamps, the higher expansion of XLPE appears when it is subjected to high thermal cycles that may cause distortion, material migrations, and voids. Shrinking of the insulation can also occur when the end of the cable is cut prior to termination and the longitudinal stresses freezed in the insulation are relaxed. This has proven to be a major problem associated with highly crystalline materials used in cable insulations, since molded terminations may no longer fit properly.

Differences in thermal expansion characteristics between XLPE and EPR can also be a contributing factor in failures that occur at the junction of two types of insulation, which are normally in contact in cable joints [128].

Many electrical failures, which have been experienced in joints and splices, are caused by this incompatibility in expansion characteristics. Consequently, the values of thermal expansion coefficients of the insulation components should be as close as possible to each other, as well as those of the semiconductor layers or conductors that are in contact. All the organic materials expand much more than metals and minerals when their temperature increases in from 0 to 200 °C range. PE and XLPE expand more than mineral-filled EPR or EPDM. This is because homopolymers are partially crystalline and have melting temperatures around 115 °C, also because the fillers have relatively negligible expansion in this range.

The work [62] showed that, starting with the solid phase, as thermal energy is supplied to crystalline regions by heating, molecular motion increases till PE crystallites are disrupted and the ordered molecular segments add to the amorphous fraction. The result of this effect is shown in Fig. 62, curve 1.

The long concave upward portion of XLPE curve results from the fact that crystalline regions, called crystallites, have lattice energies or stabilities proportional to their sizes. Hence, small crystallites have low stability and their lattice energies are exceeded by the thermal energy of the molecules, which decompose them at low temperature. As temperature increases, crystallites of larger and larger size are melted, causing an increase of the rate of expansion until the largest is melted. After this point, called thermodynamic melting point (MP), the material is completely amorphous.

Thermal expansion increases with further temperature then continues at a constant rate characteristic of the molecular structure. From 20 to 90 °C, EPR expands between 3.5 and 6.5%, while XLPE expands with 6 or 7%. That is a small difference, particularly for the new, higher voltage, partially crystalline EPRs that lie at the top of EPR range. The literature contains many data on PE thermal expansion [62], but rather on filled compounds of EPR or EPDM. XLPE and PE expand more than mineral-filled EPR or EPDM. This is because homopolymers are partially crystalline and have the melting temperature around 115 °C, and also because the fillers have relatively negligible expansion in this range.

6.2.2 Thermal Conductivity

Thermal conductivity (λ) of the cable's insulation controls how rapidly the heat generated by conductor and dielectric losses can be transferred to the surroundings. Thus, it is a major factor with the nature of surroundings, in determining the cable ampacity [62]. In order to eliminate the losses as efficiently as possible, insulations must have the highest thermal conductivity. Figures 63 and 64 present comparing data of the thermal conductivities of XLPE, PE, EPDM, and EPR over a wide temperature range.

Fig. 63 Variation of thermal conductivity with temperature for semi-crystalline EPR (1), amorphous EPR (2) and XLPE (Reprinted, with permission, from [62])

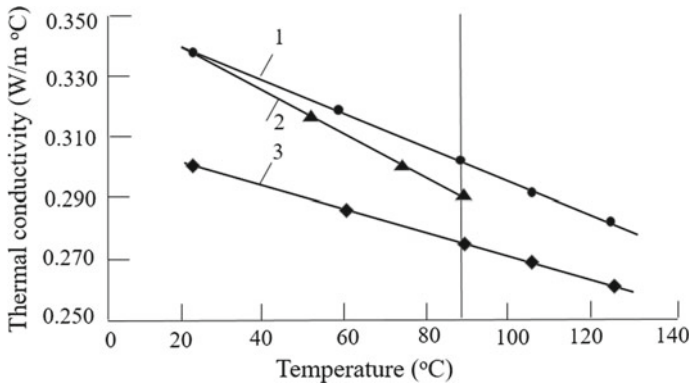
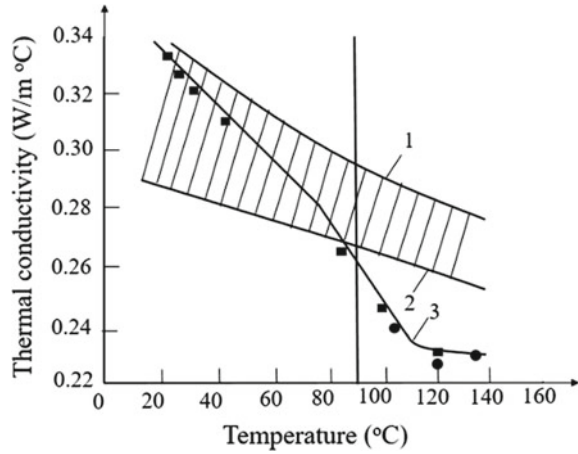


Fig. 64 Variation of thermal conductivity with temperature for XLPE (1), PE (2) and EPDM (Reprinted, with permission, from [62])

If in Fig. 63, the variation of an XLPE-type conductivity for temperatures higher than 90 °C shows a sharp decrease, in Fig. 64 its variation is linear and in agreement with the results presented in several works [62, 129, 130]. On the other hand, for temperatures below 90 °C, there are no significant differences between the values of thermal conductivity of XLPE, PE, and EPDM, only the values for EPDM being slightly lower. It should be noted that the values of λ are higher for EPR than for XLPE. For example, at 90 °C, $\lambda = 0.268\text{--}0.272$ W/m °C for EPR and $\lambda = 0.226$ W/m °C for XLPE [128].

Tests performed on samples based on EPR with different filler concentrations and TR-XLPE [131] showed that commercially available EPR and TR-XLPE cable dielectrics have typically about the same thermal conductivity although the thermal

conductivity of TR-XLPE above the melting point of crystallites drops below that of EPR dielectrics.

6.2.3 Thermal Stability

Thermal stability of XLPE and EPR has been evaluated in the laboratory in an inert nitrogen atmosphere at temperatures up to 427 °C on other copolymers of ethylene [132], to determine their suit ability for high-temperature and dry nitrogen curing. It was observed that degradation started at 360 °C for a cross-linked EPR formulation and at 375 °C for XLPE.

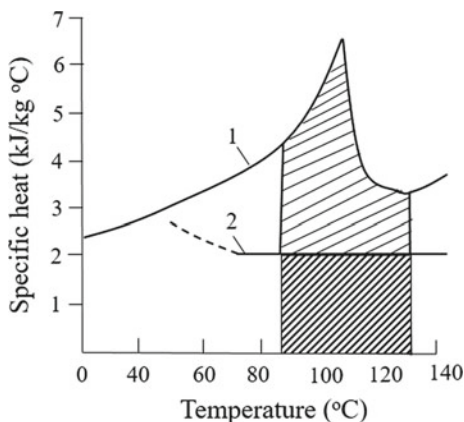
In isothermal studies, the initial degradation rates for XLPE and EPR at 260 °C were 0 and 0.013% wt. loss per minute. At 315 °C, the rates were 0.013 and 0.121, respectively, while at 370 °C, the rates were 0.186 and 0.200. These low rates indicate that thermal stability of EPR, as XLPE, should be satisfactory for the curing process in pure nitrogen. Other thermal analysis studies carried on in air showed that temperatures at which rapid oxidation started were 160 °C for EPR and 230 °C for XLPE [62].

6.2.4 Effect of Melting

However, a cable operates at its maximum permissible continuous temperature of the conductor, at 90 °C, which is suddenly overloaded by a substantial amount. Thus, the conductor temperature will rise and the insulation temperature will follow. Under these conditions, EPR insulation will reach an overload temperature of 130 °C faster than XLPE, because XLPE must be completely melted before its temperature to exceed about 115 °C (as shown in Fig. 65).

Figure 65 shows that the areas below the two curves, between 90 and 130 °C, give the amount of heat required to cause that temperature increase. For EPR, it is

Fig. 65 Variation of specific heat with temperature for XLPE (1) and EPR (2) (Reprinted, with permission, from [62])



about 7.369 MJ/kg, while for XLPE is about cca. 2.5 times higher, respectively 18.42 MJ/kg. As a result, the time required for XLPE heated from 90 to 130 °C is approx. 2.5 times higher than for EPR heating. Obviously, when the overload disappears, the cable cools down, but the cooling is done much faster in EPR insulation than in XLPE insulation.

6.2.5 Working Temperature

The values of working temperature (T_w) of an insulation depend, first on the chemical nature of its components, and also on the physical structure and their stresses. In Table 20, it is observed that the highest values of T_w were showed by silicone rubber insulation, followed by those of XLPE and EPR.

6.2.6 Mechanical Properties

In general, the mechanical properties of XLPE are better than those of thermoplastic PE, respectively, XLPE, which has deformation at a lower temperature (see Fig. 66), a higher resistance to tensile strength (see Fig. 67), lower elongation at break (see Table 21), etc. [133]. In addition, the mechanical properties of XLPE are superior to those of EPR [62].

Table 20 Operating temperature values for insulating and sheathing materials

Material	Max. cond. temp. for continuous operation (°C)	Max.cond.temp. for short circuit (°C)	Min. working temperature (°C)
Natural Rubber	60	200	-55
Ethylene Propylene Rubber (EPR)	90	250	-50
Polychloroprene (PCP)	70	200	-40
Chlorosulphonated Polyethylene (CSP)	90	200	-35
Silicone rubber	150/180	350	-55
XLPE	90	250	-40
Styrene butadiene rubber	60	200	-55
Butyl rubber	85	220	50

Fig. 66 Dependence of the heat deformation on the temperature for PE (1) and XLPE (2) [133]

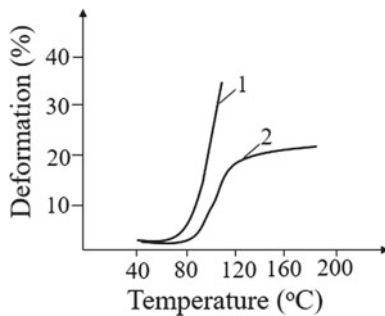


Fig. 67 Dependence of the tensile strength on the temperature for PE (1) and XLPE (2) samples [133]

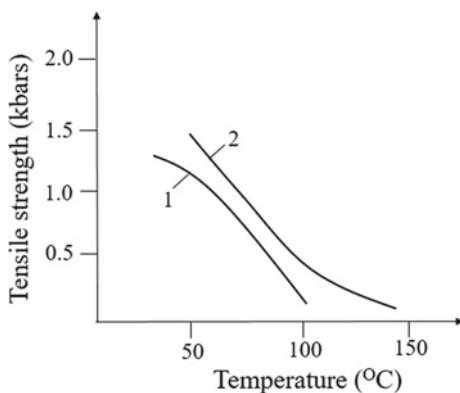
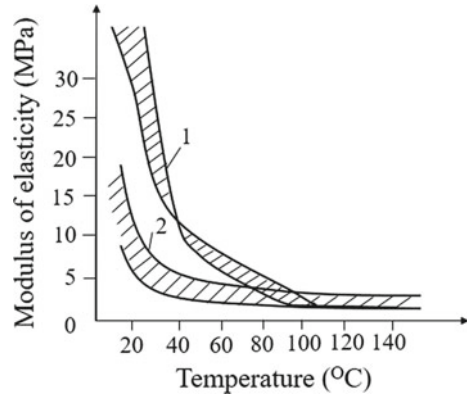


Table 21 Values of elongation at break of several polymers (%) [134]

Polymer	Minimum value	Maximum value
HDPE—High-density polyethylene	500	700
LDPE—Low-Density Polyethylene	200	600
LLDPE—Linear low-density polyethylene	300	900
XLPE—Cross-linked Polyethylene	100	550
PTFE—Polytetrafluoroethylene	200	400
PVC, Plasticized	100	400
PVC Rigid	25	80
PP (Polypropylene) homopolymer	150	600
PP (Polypropylene) copolymer	200	500
PA 6—Polyamide 6	200	300
FEP—Fluorinated ethylene propylene	250	300

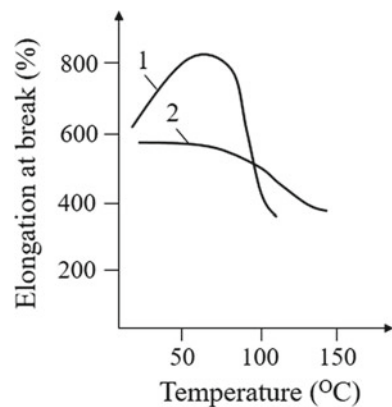
Fig. 68 Variation of modulus of elasticity in tension with temperature for XLPE (1) and EPR (2) (Reprinted, with permission, from [62])



6.2.7 Modulus of Elasticity

Cable insulation is stressed in tension (E_t) at temperatures below 40 °C during installation in trench or when pulling around corners and in ducts. Figure 68 displays the modulus of elasticity in tension as a function of temperature for XLPE and EPR. It was found that for temperatures below 90 °C, there are significant differences regarding the values of the modulus of elasticity in tension for XLPE and EPR. Thus, at 23 °C, E_t takes a value of 121 MPa for XLPE and values between 4.8 and 13.8 MPa for EPR [62]. For temperatures above 100 °C, these differences are insignificant (see Fig. 68). Similar variations were obtained in the case of modulus of elasticity in compression [62].

Fig. 69 Dependence of the elongation at break on temperature for PE (1) and XLPE (2) [133]



6.2.8 Tensile Elongation at Break

Elongation at break or tensile elongation at break is related to the ability of a plastic specimen to resist at changes of shape without cracking and represents the ratio between increased length and initial length after breakage of the tested specimen at a controlled temperature. For temperatures below 90 °C, the values of elongation at break for XLPE are lower than for PE (see Fig. 69) and higher than for EPR (see Table 21).

The toughness of a material is defined as the amount of energy that it can absorb before failure occurs, and it is related to its tensile strength and elongation. It is a function of the rate of strain. An estimation of the amount of energy absorbed during tension (extension or stretching) of a polymer sample is made by integrating the area under a stress–strain curve.

6.2.9 Tensile Strength and Toughness

Numerical or graphical integration of the areas under the XLPE and EPR curves presented in Fig. 70 (for a strain rate of 8 mm/sec starting with 25.4 mm long specimens) gives the toughness values of 143 J/cm³ for XLPE and 48 J/cm³ for EPR [62]. Results that EPR is soft and resilient at low stresses, but XLPE will absorb much more energy before it breaks.

To find out the behavior of insulators at low temperatures (for cryogenic cables), the tensile strength of EPR was measured in comparison with LDPE and XLPE, after that the samples were shrunk freely in liquid nitrogen [135]. As shown in Table 22, the tensile strength of EPR is equivalent to that of XLPE and is a little larger than that of LDPE. Then EPR had smaller shrinkage than XLPE and LDPE between room temperature and 77 K.

Fig. 70 Stress versus strain curves used for determination of toughness for XLPE (1) and EPR (2) (Reprinted, with permission, from [62])

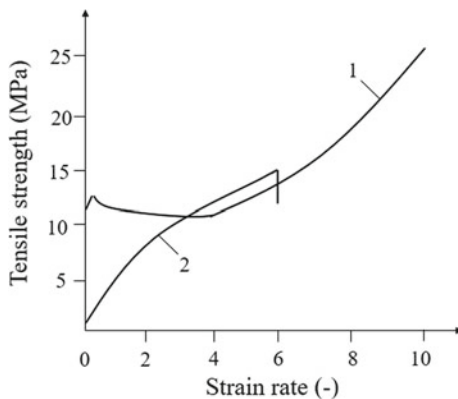


Table 22 Values of mechanical properties of samples shrunk freely at 77 K [135]

Property/ Material	Shrinkage (%)	Elongation (%)	Elastic modulus (GPa)	Tensile strength (MPa)
EPR	1.1	6.7	2.38	137
LDPE	1.6	5.6	2.28	119
XLPE	1.6	7.1	2.23	139

6.2.10 Compressibility

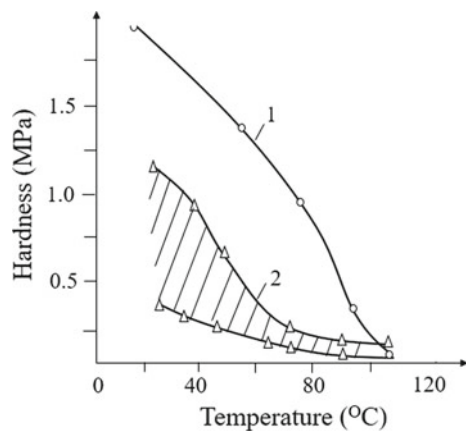
Compressibility (also known as the coefficient of compressibility or isothermal compressibility) is a measure of the relative volume change of a fluid or solid as a response to a pressure (or mean stress) change. It was stated earlier that all organic materials expand more than metals or minerals when heated. As shown in Fig. 62, XLPE expands from 12.5 to 15%, while EPR expands from 5 to 9% between the temperatures of 20 and 130 °C. Among 20 and 90 °C, the difference between materials is about 2% or less.

Therefore, if cables are not designed to accommodate this expansion that can destroy them because the force of thermal expansion is almost irresistible [62]. Therefore, the values of compressibility coefficient should be as low as possible.

6.2.11 Hardness

Hardness is a measure of the resistance to localized plastic deformation induced by either mechanical indentation or abrasion. This property relates directly to possible damage of a cable before or during installation. Figure 71 shows the relation between temperature and the force required to indent the surface of a thick section

Fig. 71 Variation of the hardness with the temperature for XLPE (1) and EPR (2) (Reprinted, with permission, from [62])



with a standard indenter [62]. At all important temperatures, the hardness of XLPE is about twice that of the hardest EPR and over ten times that of the softest EPR.

The study [131] showed that mechanical properties of EPR cable dielectrics are much more stable with temperature than TR-XLPE. EPR polymer is essentially amorphous so that EPR cable dielectrics do not suffer from the very large thermal expansion of TR-XLPE, as its crystallites melt between about 80 and 120 °C.

EPR cable dielectrics also have much more uniform stiffness as a function of temperature. Its stiffness varies only by a factor of 100 from -40 to 140 °C, while the stiffness of XLPE varies by a factor of 10,000 over the same temperature range. A combination of large thermal expansion and low stiffness (or yield stress) at elevated temperatures can cause problems with cable accessories, as discussed above. For these reasons, the upper temperature limit for operation of XLPE is often limited to 90 °C or 105 °C, and EPR cable dielectrics can operate safely until 140 °C.

6.3 Chemical Resistance

When solid organic materials are exposed to or immersed in organic liquids of lower molecular weight, they are usually swelling as they imbibe some of the lower molecular weight material. Thus, for cables immersed in oil at 23 °C, there is an

Table 23 Chemical resistance of some electro-insulating materials [43, 137–139]

Material	Chemical resistant to:
Polyisoprene	Acetone, acids, alkalies, alcohols
Butadiene	Glycerol, glycol, acids, alkalies, weathering
Styrene butadiene	Glycerol, glycol, acids, alcohols, salts, oxidation
Acrylonitrile butadiene	Glycerol, glycol, acids, ketones, alcohols, petroleum products, salts, heat or high temperature, vegetable oils, weathering
Polychloroprene	Glycerol, glycol, alcohols, petroleum products, salts, heat or high temperature, ultraviolet light, vegetable oils, weathering, ozone
Isobutylene-isoprene	Phenol, glycerol, glycol, alkalies, salts, ultraviolet light, vegetable oils, weathering, oxidation, ozone
Polyethylene	Acetic acid, glycol, ethanol, glycerin, mercury, methanol, acetone, formaldehyde 10–40%, oils, isobutanol, isopropanol, gasoline, phenol, vaseline
Polypropylene	Chlorhydric acid, caustic soda, sodium cyanide, aniline, alcohols, carbon dioxide, carbon monoxide, hydrogen sulfide
Polyvinyl chloride	Alcohols, chlorinated water, oils, diesel fuel, glycol, fatty acids, formaldehyde, gasoline, hydrocyanic acid, kerosene, mercuric chloride, phosphoric acid, sulfurous acid, water
Silicone rubber	Acetamide, aniline, clophene, salts, mineral oils, phenols, sulfuric acid, glycol
Epoxy resins	Acetylene, alcohols, amines, benzol, gasoline, hydrocyanic acid, kerosene, mercury, oils, propane

increase of the insulations diameter by 2.5% and of the masses by 7.6% in the case of XLPE and by 30% and, respectively, 151%, in the case of EPR [136]. As noted, the changes in weight and volume for EPR when immersed in oil are surprisingly great. The increase in temperature from 23 to 60 °C leads to a higher increase in diameters and masses of the insulations, as follows: The diameters increase by 12% and the masses by 13% for XLPE and 46.9%, respectively, by 232.9% for EPR. Similar tests with joint box compound (Bitumen) showed smaller changes: only 5.1% increase in weight for EPR and 3.6% for XLPE at 60 °C [136].

Tests performed on different electro-insulating materials under the action of chemical agents with which electrical equipment insulation can come in contact, showed that, in general, XLPE insulations have superior chemical resistance to those of tires. This means that the deterioration and aging process is much slower in XLPE than in other insulations. Some of the organic acids, bases, and solvents to which the materials used for electrical insulation have a good resistance are presented in Table 23.

6.4 *Microorganisms, Termite, and Rodent Resistance*

Cables insulation used especially in the field of irrigation are sometimes destroyed by microorganism, termites and, above all, by rodents (especially gophers).

Microorganisms (e.g., bacteria, mold, fungi) contribute to the degradation of insulating materials both by the action of the acids that they produce, and by the channels, they dig inside the bodies, subsequently penetrated by water. The action of microorganisms is more important in humid environments and at temperatures of 15–40 °C. Obviously, not all materials are attacked by bacteria or fungi and not with the same intensity. Thus, PVC has a very good resistance to the action of fungi, if plasticizers as aliphatic esters of phthalic acid, dimethyl- and dioctyl

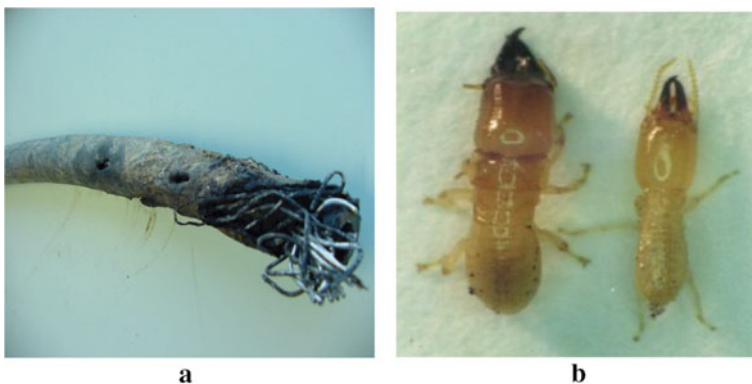


Fig. 72 Cable jacket (a) attacked by termites (b) (Reprinted, with permission, from author [13])

phthalates, etc., are used. However, its resistance decreases when using fatty acid derivatives. Natural and synthetic rubbers are attacked only if they come in direct contact with water, while mica, ceramics, phenolic, or melamine plastics with inorganic filling, etc., are not attacked by fungi. To avoid mold deposition, insulating materials have fungicidal substances (e.g., pentachlorophenolate and sodium trichlorophenolate, salicylic anhydride, phenyl mercury combinations, etc.) in their composition.

The termites, particularly, attack wood, synthetic fibers, polymer insulation, etc. [39] (see Fig. 72). In order to protect them from termites, the insulating materials are impregnated with pentachlorophenol, creosote, metal naphthalenes, zinc chloride, etc., which reduce the electrical and/or mechanical properties of cable insulations and jackets.

The teeth of a gopher grow about 18 cm per year and the chewing of hard objects is essential to keep the teeth trimmed and at a comfortable length. Unfortunately, neither PVC nor PE insulated conductors offer much resistance to the sharp teeth of rodents. In order to protect the insulations, all the recommendations require the protection of the wire with either a stainless-steel tape, a bronze tape, fine braided wire, or concrete. The armored cable could be either a PE or PVC insulated copper conductor with a steel covering and a PVC outer jacket. The product with PE insulation a slightly lower cost [39].

The selection of materials with respect to their resistance to chemical environments largely depends on the degree of exposure to these substances. In the case of occasional spills of hydrocarbon solvents, materials based on XLPE and EPR/EPDM would survive without significant loss of physical properties. However, if prolonged exposure is likely, the selection of materials based on chloroprene or chlorosulfonated polyethylene may be necessary [71].

6.5 Radiation Resistance

Under the action of solar radiation or other types of radiation (α , β and γ , fast or slow neutrons, electrons, etc.) in the structure of insulating materials (especially in the case of polymers) irreversible transformations occur, causing important variations (degradation) in their properties. The destructive action of the radiation becomes important only if their energy is comparable to the bonding energy w_l of the chemical elements that build the molecules of which the material subjected to the action of radiation is composed (see Table 24). This is achieved, not only in the

Table 24 Chemical bonding energy values

Bond	C–C	C=C	C–H	C–O	O–H	O–O	C=O	C–Cl
Bonding energy (kJ/mol)	350	610	410	360	470	150	750	340

case of high-energy radiation (used in nuclear technology), but even in the case of solar radiation. Indeed, if $w = hv = hc/\lambda$ represents the energy of the wavelength radiation λ , then for λ in the range 0.29–0.4 μm , radiations with energies values of $W = N_A w = 418\text{--}300$ kJ/mol (where $N_A = 6,022 \times 10^{23} \text{ mol}^{-1}$ is Avogadro's number) are obtained. Therefore, the energy of ultraviolet radiation, the value of which is in the range determined above, is sufficiently large to cause breaking of the chemical bonds as O–O, C–C, C–O, C–K, etc.

By fracturing the macromolecules, free radicals are formed and react with each other—giving rise to new products—or form bridges between the molecular chains that contribute to the cross-linking of the bodies and, therefore, to the modification of their mechanical and thermal properties. In addition, free ions and electrons, which modify their dielectric properties (reducing the resistivity and dielectric strength, increasing the electrical permittivity, forming space charges), etc., are produced. The modification of the materials properties subjected to the action of radiation depends, on both the nature and structure of the materials, as well as on the dose rate and the total dose of radiation absorbed (i.e., meaning the energy absorbed by 1 kg of material). For example, in the case of elongation at break by traction, a reduction of its value by 50% compared to the initial value is obtained by irradiation with a dose of 350 J/kg for XLPE and PE and only 1.5 J/kg for PTFE [13]. The tests performed at CERN on products prepared by PIRELLI GROUP [140] showed that, for the same value of the total irradiation dose, respectively, 100 Mrad, the values of the elongation at break by traction are reduced compared to the initial values of 3.2 times in the case of XLPE, of 3.4 either in the case of EPR and EPDM, 4.2 times in the case of PE, 9.7 times in the case of neoprene, and only 2.2 times in the case of PVC. In the same irradiation conditions, the tensile strength by traction decreases by 1.9 times in the case of XLPE, 1.5 times in the case of PE, 1.1 times in the case of EPR and remains unchanged in the case of PVC. It can be said that PVC insulation has the highest resistance to radiation.

The paper [141] presents a study on the behavior of the PCV cables insulation used in the nuclear power plants. Cables insulated with eleven different PVC compounds representing fire retardant, non-fire retardant with the rating temperatures 60, 75, and 90 °C were evaluated. The specimens were subjected to accelerated thermal, radiation, and sequential radiation and thermal exposure, simulating 15, 20, 30, and 40 years in-service environments in Ontario Power Generation Nuclear Plants. The radiation level was limited from 12 to 30 Mrad. A part of the samples was sequentially irradiated and thermally aged and subjected to an additional 5 Mrad accident radiation exposure, followed by a simulated loss of coolant accident (LOCA). Similarly, thermal only aged specimens with 2 Mrad of background radiation representing powerhouse environment were subjected to a main steam line break (MSLB) test. Although the present acceptance criterion used for installed cables is 50% absolute elongation at break [142, 143] after the stresses were applied, the elongation and insulation resistance were measured. It is generally assumed that this elongation value will provide sufficient margin to ensure that the insulation maintains its electrical properties during a design basis event.

The electrical behavior of PVC insulated cables during the steam test indicates that there was no correlation between the performance and the elongation value, specifically when cables were subjected to an irradiation environment >17 Mrad. On the other hand, in the case of fire retardant cross-linked polyethylene (FR-XLPE) and fire-retardant ethylene propylene rubber (FR-EPR) insulated cables, it was shown previously that those cables were working through the additional accident radiation and steam conditions with elongation values in the range of 5% [144–146]. The authors conclude that the elongation values were not a good indicator of electrical performance for radiation and thermal aged specimens.

7 Lifetime

Estimating the lifetime (L) of cables polymer insulation is of particular importance for their users. There are numerous models and methods for estimating L values, corresponding to electrical, thermal, mechanical, and environmental stresses, performed in laboratories based on accelerated, single- or multifactor tests [13, 22, 147]. In [147], the procedures for accelerated testing under thermo-electrical stresses are discussed and applied to EPR and XLPE used for HV cable insulation. It was concluded that EPR has a slightly larger temperature index, while XLPE displays a threshold that has not been detected for EPR. On the other hand, it shows that any comparison cannot be extended to the general category of materials to which insulation belongs, so that it cannot be said that XLPE is better than EPR.

The study [148] presents the lifetime curves of some insulated cables with XLPE and PVC subjected to permanent thermal stresses, using the weight loss as the diagnostic factor. As can be seen in Fig. 73, XLPE is more endurable than PVC. For example, at 100 °C XLPE lifetime is more than 10,000 h, while PVC lifetime is around 1,000 h.

Fig. 73 Thermal lifetime curves of XLPE (1) and PVC (2) based on weight loss (Redrawn and adapted figure from reference [148])

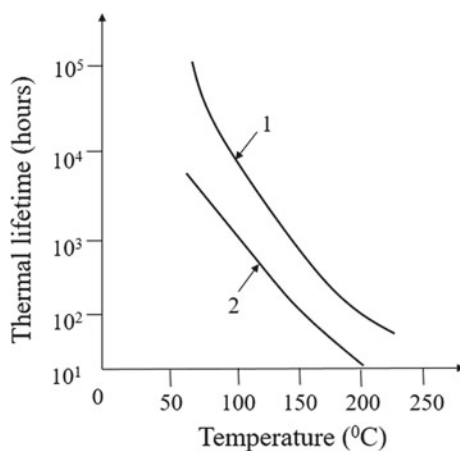


Fig. 74 Failure rate of 20 kV XLPE (■) and EPR (□) cables [26]

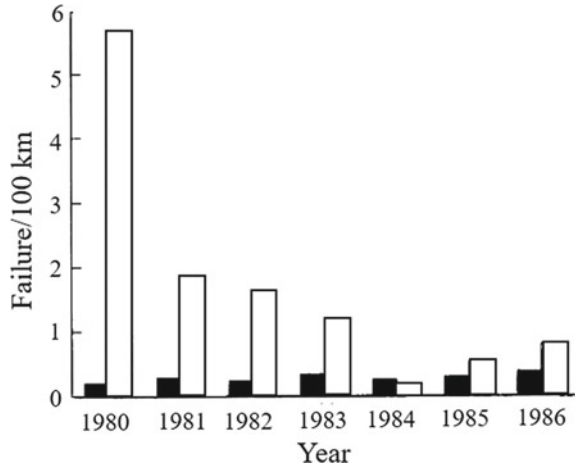


Figure 74 shows a failure rate data for 20 kV cables from 1980 to 1986 [26]. It was found that XLPE insulation for medium-voltage cables are superior to EPR, in terms of cable performance reliability. Moreover, as the insulating compounds used in medium-voltage cables are generally the same or very similar to the ones used in high voltage cables, it turns out that the same conclusion can be drawn for transmission cables.

Table 25 Comparison of common insulating materials

Material	Advantages	Disadvantages
PVC	Cheap; Durable; Widely available; Reduced risk of flammability, and fire propagation	Highest dielectric losses; Melts at high temperatures; Contains halogens; Not suitable for MV/HV cables
PE	Lowest dielectric losses; High initial dielectric strength; Reduced weight; Easier to repair faults	Highly sensitive to water treeing; Material breaks down at high temperatures
XLPE	Low dielectric losses; Improved material properties at high temperatures; Does not melt but thermal expansion occurs; Reduced weight; Easier to repair faults	Medium sensitivity to water treeing (although some XLPE polymers are water tree-resistant)
EPR	Increased flexibility; Reduced thermal expansion; Reduced weight; Low sensitivity to water treeing; Easier to repair faults	Medium-High dielectric losses; Requires inorganic filler/additive
Paper/Oil	Low-Medium dielectric losses; Not harmed by DC testing; High dielectric strength; Known history of reliability; Long lifetime	High weight; High cost; Requires pumps for insulating fluid; Difficult to repair; Degrades with moisture

XLPE is suitable for voltage ranges from low to extra high, surpassing other insulation materials such as PVC, ethylene propylene rubber (EPR), and silicone rubbers. Cross-linking PE also enhances the chemical and oil resistance at elevated temperatures and makes it suitable for use as a low smoke zero halogen material.

The mechanical properties of XLPE are superior to many other insulations, offering higher tensile strength, elongation, and impact resistances. The addition of carbon black can be used for further enhancement of hot deformation and cut-through resistance. The XLPE insulation will not melt or drip, even at temperatures of soldering irons, and it has increased flow resistance and improved aging characteristics.

Improved water tree resistance is another benefit of XLPE insulation for LV and MV cables over PE insulations. Water treeing is a defect, which is the result of imperfections in the insulation where fracture lines occur and grow in the direction of the electric field, increasing with electrical stress. A comparison of the advantages and disadvantages of some materials used as electrical insulation of the power cables is presented in Table 25.

The most readily available insulations for low-voltage (600 V) and medium-voltage (5–35 kV) cables installed in petroleum and chemical plants are polyvinyl chloride (PVC), polyethylene (PE), cross-linked polyethylene (XLPE), tree-retardant cross-linked polyethylene (TR-XLPE), and ethylene propylene rubber (EP, EPR, or EPDM). Chlorosulfonated polyethylene (CSPE), chlorinated polyethylene (CPE), and polyamide (nylon) are sometimes used for the second layer in dual-layer insulations. The temperature rating of these materials is usually 75 °C for thermoplastic materials and 90 °C for thermoset ones. For installations in areas with high ambient temperatures, cables with special high-temperature insulations are used. These cables carry temperature ratings ranging from 125 to 450 °C and beyond. High-temperature insulations include specially formulated EPR, cross-linked polyolefin, silicone rubber, various fluoropolymers, ceramic tapes, aramid fiber, and glass-reinforced mica tape. High-temperature cables are frequently constructed with a combination of one or more of the above materials. Common fluoropolymer insulations include fluorinated ethylene propylene (FEP), polytetrafluoroethylene (PTFE), and ethylene chlorotrifluoroethylene (ECTFE).

8 Conclusions

Cross-linked polyethylene (XLPE) has replaced, decades ago, oil-paper insulated systems as primary solution for medium and high voltage AC cables, due to its numerous advantages (very good dielectric properties, higher operating temperatures, etc.). They can be produced with high throughput and well-controlled extrusion technology. XLPE has become the global preferred insulation for power cables, both for distribution and transmission system applications. This insulation system provides cost efficiency in operation and acquisitions, installation and operation as well as lower environmental and maintenance requirements, reduced

risk of fire during earthquakes, when compared to older impregnated paper system. Currently, conventional XLPE is at the limit of its capabilities due to the intrinsic limits of purity that can be obtained with the most commonly adopted cross-linking chemistries, and thermal performance of the materials concerning their relatively low melting points. Nonetheless, XLPE technologies are widely adopted and are expected to remain a key cable insulation system into the future.

The very good general properties of XLPE and EPR recommend these materials for use as insulations of AC and DC medium, high and very high voltage power cables. Each of these insulation materials is used preferentially in different parts of the world: in France LDPE, in Italy EPR, and in most of Europe, Japan, and the USA, XLPE. The reason for this difference is that no one who extruded dielectric insulation material has emerged as conclusively superior to the others in all aspects for every application, including manufacturing, cost, and reliability. In general, these insulation systems have important advantages such as no operation and maintenance requirements, high reliability, higher normal operating, and short-circuit temperature ratings, reduced time required for repair, small dielectric losses, etc.

Materials used for semiconducting extruded conductor and insulation shields are semiconducting PE, XLPE, and EPR compounds. PE compounds are used with PE and XLPE insulation, XLPE compounds with XLPE insulation, and EPR compounds with EPR insulation. Cable jackets are typically extruded PE and on rare occasions polyvinyl chloride (PVC). XLPE and EPR, a copolymer of ethylene and propylene, offer good electrical characteristics, ease to process, at acceptable cost, and therefore have been popular extruded dielectric materials. When properly formulated and compounded, EPR is in some ways superior to XLPE, but it is generally more expensive.

The worldwide tendency to use HVDC transmission lines makes the demand for better insulation materials to increase greater and urgent. Many manufactures have developed XLPE materials that are more adapted to DC power cables insulation, such as super-clean cross-linkable polyethylene and XLPE-based nanocomposites. XLPE has higher dielectric losses than PE, but has better aging characteristics and resistance to water treeing. On the other hand, filled XLPE (with titanium dioxide) has a lower water resistance than XLPE. It can be said that, generally, XLPE is preferred where a material with excellent dielectric properties is required, while EPR/EPDM is preferred where there is a need for a more flexible cable.

The electrical properties of XLPE (e.g., volume resistivity, dielectric constant, and loss factor) are better or equal to those of thermoplastic polyethylene (PE). Under high temperatures, XLPE presents a breakdown voltage higher than PE and is practically equal at low temperatures. Physical properties are in many (but not all) cases more temperature sensitive than electrical properties, and XLPE is often (but not always) more temperature sensitive than EPR. As the electrical conductivity of XLPE is highly dependent on the presence of polar molecules (assisting in charge transportation), one way to reduce the conductivity is to decrease the concentration of potential charge carriers or polar substances, respectively, to create a material as clean as possible.

Syndiotactic polypropylene (sPP) has excellent insulating properties, but it is actually prohibitively expensive. On the other hand, PP has the disadvantages of poor low-temperature impact performance and low thermal conductivity, as well as the problem of space charge accumulation and aging of the polymer in the DC field. Therefore, PP needs to be modified in order to meet the electrical, thermal, and mechanical properties of the cable insulation material under the complex working conditions of DC high voltage. It should be emphasized that PP has shown great potential as recyclable HVDC cable insulation material.

The half of the failures of utility cable systems is due to the splice or termination failures. A greater potential for splicing and termination problems exists for XLPE/TR-XLPE cables than for those insulated with EPR/EPDM. During the manufacture of cables, the insulation is extruded on the conductor under high mechanical stresses and at elevated temperatures. As the conductor and insulation have different axial coefficients of thermal expansion, residual stresses can be ‘frozen in’ when the cable is quenched or cooled after extrusion. Stresses care are low in the case of EPR/EPDM than in XLPE/TR-XLPE. This can result in an appreciable amount of ‘shrink-back’ away from a splice or termination component interface, creating voids. Therefore, corona discharges may be produced and can eventually result in failure.

In general, unfilled insulation formulations of high-molecular-weight PE (HMWPE) and XLPE provide the highest level of dielectric strength. This does not mean, however, that any insulation will provide a stable dielectric strength over the lifetime of a cable, especially in wet operating environments. Filled or chemically altered formulations such as ethylene propylene rubber (EPR) and trees retardant cross-linked polyethylene (TR-XLPE) maintain their dielectric strength better in wet locations involving medium-voltage cable designs. Where higher voltage strength must be achieved because of the electrical system demands (overvoltages, switching surges, excessive ground-fault clearing time, etc.), increased insulation thicknesses (up to 133% or 173%) should be considered.

Acknowledgements Ilona Plesa’s contributions were accomplished within the K-Project PolyTherm at the Polymer Competence Center Leoben GmbH (PCCL, Austria) within the framework of the COMET-program of the Federal Ministry for Transport, Innovation and Technology and the Federal Ministry for Digital and Economic Affairs. Funding is provided by the Austrian Government and the State Government of Styria.

References

1. Notingher PV (2002) Insulation systems. PRINTECH, Bucharest
2. Notingher PV, Stancu C, Plesa I (2020) Failure mechanisms in XLPE cables. In: Thomas S (ed) Crosslinkable polyethylene: manufacture, properties, recycling, and applications. Springer (in press)
3. ***Wikipedia, the free encyclopedia. Power Cable, https://en.wikipedia.org/wiki/Power_cable. Accessed on 2 Feb 2020

4. Bartnikas R (2000) Characteristics of cable materials (chapter 2). In: Bartnikas R, Srivastava KD (ed) Power and communication cables. Theory and applications. IEEE Press, New York, pp 1–75. ISBN: 0071353852, 9780071353854
5. Couderc D, Bui-Van Q, Vallee A, Hata R, Murakami K, Mitani M (1996) Development and testing of an 800 kV PPPL-insulated oil-filled cable and its accessories. In: Proceedings of CIGRE, Paris, 1996. Paper 21/22-04
6. Chen G, Hao M, Xu Z, Vaughan A, Cao J, Wang H (2015) Review of high voltage direct current cables. *CSEE J Power Energy Syst* 1(2):9–21. <https://doi.org/10.17775/CSEEJPES.2015.00015>
7. ***EC21—Global B2B marketplace, extra-high voltage oil-filled cable 110 kV–500 kV. https://yxc194900.en.ec21.com/Extra_high_Voltage_Oil_filled-1854970_2545207.html. Accessed on 2 Feb 2020
8. Curci V, Nishioka T, Grimstad J (2018) Replacement of pipe type cables with cross-linked polyethylene (XLPE) cables by utilizing the existing steel pipe. EPRI Technical Report, pp 1–6. <https://doi.org/10.1109/tdc.2018.8440298>
9. ***HES KABLO. High voltage cables, <http://www.hes.com.tr/en/urunler-26-36-power-cables-high-voltage-cables.html>. Accessed on 16 Mar 2020
10. ***HENAN JIAPU. TR-XLPE Insulated URD cable. <http://www.xlpecables.net/URD-Cable/TR-XLPE-URD-Cable.html>. Accessed on 16 Mar 2020
11. ***CME wire and cable, EPR insulated, CPE Jacketed. <http://www.cmewire.com/catalog/sec15-mvs/mvs-07-mv105-epr-cpe-ts.pdf>. Accessed on 8 Feb 2020
12. Ohki Y (2013) Development of XLPE-insulated cable for high-voltage dc submarine transmission line (2) [News from Jpn]. *IEEE Electr Insul Mag* 29(5):85–87. <https://doi.org/10.1109/MEI.2013.6585863>
13. Notingher PV (2005) Materials for electrotechnics, vol 1 and 2. Politehnica Press, Bucharest, Romania, pp 350–403. ISBN: 973-8449-81-2/973-8449-81-0
14. Bartnikas R (1967) Dielectric loss in insulating liquids. *IEEE Trans Electr Insul EI-12* (1):35–54. <https://doi.org/10.1109/tei.1967.298847>
15. Bartnikas R (1994) Permittivity and loss of insulating liquids (chapter 1), In: Bartnikas R (ed) Engineering dielectrics: volume III electrical insulating liquids. ASTM International, West Conshohocken, PA, pp 3–146. <https://doi.org/10.1520/mono10049m>
16. Bartnikas R (1974) Electrical conduction in medium viscosity oil-paper films—part I. *IEEE Trans Electr Insul EI-9*(2):57–63. <https://doi.org/10.1109/tei.1974.299311>
17. Bartnikas R (1974). Electrical conduction in medium viscosity oil-paper films—part II. *IEEE Trans Electr Insul EI-9*(3):85–91. <https://doi.org/10.1109/tei.1974.299297>
18. Bartnikas R (1971) Dielectric losses in solid-liquid insulating systems—part II. *IEEE Trans Electr Insul EI-6*(1):14–21. <https://doi.org/10.1109/tei.1971.299129>
19. Bartnikas R (1970) Dielectric losses in solid-liquid insulating systems—part I. *IEEE Trans Electr Insul EI-6*(4):113–121. <https://doi.org/10.1109/tei.1970.299119>
20. Vincent G (1994) Molecular structure and composition of liquid insulating materials (chapter 5). In: Bartnikas R (ed) Engineering dielectrics: volume III electrical insulating liquids. ASTM International, West Conshohocken, PA, pp 380–436. <https://doi.org/10.1520/mono10053m>
21. Zheng Z, Jin Z, Chen L, Chen M, Liu J, Yu H, Meng Q, Xie P, Xu R (2011) A comparative study of the ageing phenomena in kraft paper and pressboard used in 500 kV class transformer. In: Annual report conference on electrical insulation and dielectric phenomena, pp 620–623. <https://doi.org/10.1109/ceidp.2011.6232733>
22. Setnescu R, Badicu LV, Dumitran LM, Notingher PV, Setnescu T (2014) Thermal lifetime of cellulose insulation material evaluated by an activation energy based method. *Cellulose* 21(1):823–833. <https://doi.org/10.1007/s10570-013-0087-0>
23. Emsley AM, Stevens GC (1994) Review of chemical indicators of degradation of cellulosic electrical paper insulation in oil-filled transformers. *IEEE Proc Sci Measur Technol* 141(5):324–334. <https://doi.org/10.1049/ip-smt:19949957>

24. ***Wikipedia, the free encyclopedia. Cellulose. <https://en.wikipedia.org/wiki/Cellulose> <http://www.xlpecables.net/URD-Cable/TR-XLPE-URD-Cable.html>. Accessed on 16 Mar 2020
25. Moses GL (1972) Insulation engineering fundamentals. In: *Insulation*, vol 17, no 7. Lake Publishing Company
26. Chan JC, Havtley MD, Hiivala LJ (1993) Performance characteristics of XLPE versus EPR as insulation for high voltage cables. *IEEE Electr Insul Mag* 9(3):8–12. <https://doi.org/10.1109/57.216782>
27. Arhart RJ (1993) The chemistry of ethylene propylene insulation—part I. *IEEE Electr Insul Mag* 9(5):31–34. <https://doi.org/10.1109/57.234676>
28. Arhart RJ (1993) The chemistry of ethylene propylene insulation—part II. *IEEE Electr Insul Mag* 9(6):11–14. <https://doi.org/10.1109/57.245979>
29. Tanaka J, Volter K (1983) Composition and structure of dielectrics solids (chapter 6). In: Bartnikas R, Eichhorn RM (ed) *Engineering dielectrics*, vol II A, electrical properties of solid insulating materials: molecular structure and electrical behaviour. ASTM International, West Conshohocken, Philadelphia, pp 521–618. <https://doi.org/10.1520/stp37841s>
30. Barlow A (1991) The chemistry of polyethylene insulation. *IEEE Electr Insul Mag* 7(1):8–19. <https://doi.org/10.1109/57.64966>
31. *Directory Encyclopedia Issue* (1972) *Insulation/Circuits*. Lake Publishing Co, Libertyville, IL, SUA
32. Hayami T, Yamada Y (1972) Effect of liquid absorption on the treeing resistance of polyethylene. In: *Annual report—conference on electrical insulation and dielectric phenomena*. Buck Hill Falls, PA, USA, pp 239–246. <https://doi.org/10.1109/ceidp.1972.7734171>
33. Katz C, Berstein B (1973) Electrochemical treeing at contaminants in polyethylene and cross-linked polyethylene insulation. In: *Annual report—conference electrical insulation and dielectric phenomena*. Varennes, Quebec, Canada, pp 307–316. <https://doi.org/10.1109/eidp.1973.7683924>
34. Braun JM (1980) Comparison of water treeing rates in steam and nitrogen treated polyethylenes. *IEEE Trans Electr Insul EI-15*(2):120–123. <https://doi.org/10.1109/tei.1980.298249>
35. Murata Y, Sakamaki M, Abe K, Inoue Y, Mashio S, Kashiyaama S, Matsunaga O, Igi T, Watanabe M, Asai S, Katakai S (2013) Development of high voltage DC-XLPE cable system. *SEI Techn Rev* 76:55–62
36. Eichorn RM, Schadlich H, Boone W (1991) Longer life cables by use of tree retardant insulation and super clean shields. In: *Third international conference on insulated power cables (JICABLE)*, Paris, pp 145–149
37. Steennis EF, van de Laur AMFJ (1989) Characterization test and classification procedure for water tree aged medium voltage cables. *Electra* 125:89–101
38. Wang S, Chen P, Li H, Li J, Chen Z (2017) Improved DC performance of crosslinked polyethylene insulation depending on a higher purity. *IEEE Trans Dielectr Electr Insul* 24(3):1809–1817. <https://doi.org/10.1109/TDEI.2017.006165>
39. Wald D, Campus A (2004) Medium voltage cable insulation system performance evolution and field experience. In: *Proceedings of the 4th international workshop—materials for electrotechnics*. Printech, Bucharest, Romania, 26–28 May 2004, pp 1–7
40. ***Rajasthan Electric Industries. Why are PVC insulated wires needed by electrical industries? <http://www.rajasthanelectric.com/blog/why-are-pvc-insulated-wires-needed-by-electrical-industries/>. Accessed on 17 Feb 2020
41. Maddah HA (2016) Polypropylene as a promising plastic: a review. *Am J Polym Sci* 6(1):1–11. <https://doi.org/10.5923/j.ajps.20160601.01>
42. Du D, Hou Z, Li J (2018) A review of polypropylene and polypropylene/inorganic nanocomposites for HVDC cable insulation. In: Shariatinasab R (ed) *New trends in high voltage engineering*. IntechOpen. <https://doi.org/10.5772/intechopen.80039>

43. ***The Engineering ToolBox. Chemical resistance of polypropylene—PP—to acids, bases, organic substances and solvents. https://www.engineeringtoolbox.com/polypropylene-pp-chemical-resistance-d_435.html. Accessed on 17 Feb 2020
44. Chung TCM (2012) Functionalization of polypropylene with high dielectric properties: applications in electric energy storage. *Green Sustain Chem* 2(2):29–37. <https://doi.org/10.4236/gsc.2012.22006>
45. Kim WJ, Kim SH, Kim HJ, Cho JW, Lee JS, Lee HG (2013) The fundamental characteristics of PPLP as insulating material for HTS DC cable. *IEEE Trans Appl Supercond* 23(3):5401704. <https://doi.org/10.1109/TASC.2013.2244158>
46. Kwon IS, Hwang JS, Koo JH, Na JY, Lee BW (2016) Comparison of the electrical conductivity of polypropylene laminated paper (PPLP) and kraft in LN₂ according to the number of layers. *IEEE Trans Appl Supercond* 26(4):1–5. <https://doi.org/10.1109/TASC.2016.2550182>
47. Green CD, Vaughan AS, Stevens GC, Pye A, Sutton SJ, Geussens T, Fairhurst MJ (2015) Thermoplastic cable insulation comprising a blend of isotactic polypropylene and a propylene-ethylene copolymer. *IEEE Trans Dielectr Electr Insul* 22(2):639–648. <https://doi.org/10.1109/TDEL.2015.7076758>
48. ***Wikipedia, the free encyclopedia. Polytetrafluoroethylene. <https://en.wikipedia.org/wiki/Polytetrafluoroethylene>. Accessed on 18 Feb 2020
49. Dhanumalayan E, Joshi GM (2018) Performance properties and applications of polytetrafluoroethylene (PTFE)—a review. *Adv Compos Hybrid Mater* 1:247–268. <https://doi.org/10.1007/s42114-018-0023-8>
50. ***Shobha Electricals. PTFE insulated high voltage cables. <https://www.shobhaelectricals.com/ptfe-high-voltage-cables.php>. Accessed on 18 Feb 2020
51. Gorur RS, Jewell W, Dyer M, Saint R, Dalal S, Luitel M (2006) A novel approach for prioritizing maintenance of underground cables—final project report. PSERC Publ 06–40:1–62
52. Bartnikas R (1972) Silicone-polycarbonate cable insulations. In: *Proceedings supplement—IEEE underground transmission conference, Pittsburgh*, pp 312–316
53. Eich ED (1996) Laminated synthetic insulation for extra high voltage cable. In: *Proceedings of CIGRE, part. II, Report 203, Paris*, pp 1–9
54. McMahon EJ, Pundersen JO (1970) Dissipation factor of composite polymer and oil insulating structures on extended exposure to simultaneous thermal and voltage stresses. In: *Annual report—conference on electrical insulation and dielectric phenomena, Pocono Manor, PA, USA*, pp 94–99. <https://doi.org/10.1109/ceidp.1970.7725111>
55. Yamamoto T, Isshiki S, Kakayama S (1972) Synthetic paper for extra high voltage cable. *Trans Power Appar Syst PAS-91(6)*:2415–2426. <https://doi.org/10.1109/tpas.1972.293399>
56. Hata R, Hirose M, Nagai T (1983) High-pressure dielectric strength tests on PPP (PPLP) insulation. EPRI Report EL-3131, Palo Alto
57. Jefferiers MS, Mathes KN (1970) Insulation system for cryogenic cable. *IEEE Trans Power Appar Syst PAS-89(8)*:2006–2014. <https://doi.org/10.1109/tpas.1970.292785>
58. Bartnikas R (2000) Cables: a chronological perspective (chapter 1). In: Bartnikas R, Srivastava KD (ed) *Power and communication cables. Theory and applications*. IEEE PRESS, New York. ISBN: 0071353852, 9780071353854
59. Srivastava KD (2000) Cryogenic and compressed gas insulated power cables (chapter 12). In: Bartnikas R, Srivastava KD (ed) *Power and communication cables. Theory and applications*. IEEE PRESS, New York. ISBN: 0071353852, 9780071353854
60. de Tourreil CH, St-Onge H (1978) Evaluation of epoxy resin formulation for SF₆ cable spacer materials. In: *IEEE International Symposium on Electrical Insulation, IEEE Conference Record 78CH287-2-EI, Philadelphia, USA*, pp 167–171. <https://doi.org/10.1109/eic.1978.7463619>
61. Wang R-M, Zheng S-R, Zheng Y (2011) *Polymer matrix composites and technology*. Elsevier, Woodhead Publishing. ISBN: 9780857092212

62. Eichhorn RM (1981) A critical comparison of XLPE and EPR for use as insulation on underground power cables. *IEEE Trans Electr Insul EI-16*(6), pp 469–482. <https://doi.org/10.1109/tei.1981.298377>
63. Taranu LV, Notingher PV, Stancu C (2018) The influence of electric field and temperature on the electrical conductivity of polyethylene for power cable insulations. *UPB Sci Bull 80* (4):45–56. ISSN 1223-7027
64. Xu Z, Choo W, Chen G (2007) DC electric field distribution in planar dielectric in the presence of space charge. In: *IEEE international conference on solid dielectrics*, Winchester, UK, pp 514–517. <https://doi.org/10.1109/icisd.2007.4290864>
65. Hestad OL, Mauseth F, Kyte RH (2012) Electrical conductivity of medium voltage XLPE insulated cables. In: *IEEE international symposium on electrical insulation*, San Juan, PR, USA, pp 376–380. <https://doi.org/10.1109/elinsl.2012.6251493>
66. Jiang G, Kuang J, Boggs S (2000) Evaluation of high field conduction models of polymeric dielectrics. In: *Annual report conference on electrical insulation and dielectric phenomena* (Cat. No.00CH37132), Victoria, Canada, vol 1, pp 187–190. <https://doi.org/10.1109/ceidp.2000.885258>
67. Vu TN, Teyssebre G, Vissouvanadin B, Roy S, Laurent C (2015) Correlating conductivity and space charge measurements in multi-dielectrics under various electrical and thermal stresses. *IEEE Trans Dielectr Electr Insul 22*(1):117–127. <https://doi.org/10.1109/TDEI.2014.004507>
68. Taranu LV, Notingher PV, Stancu C (2018) Dependence of electrical conductivity of ethylene-propylene rubber on electric field and temperature. *Rev Roum Sci Tehn Electr Et Energ 63*(3):243–248. ISSN 0035-4066
69. Zhang CC, Li YF, Hu MY, Ma FL, Zhao H, Han BZ (2018) Conductivity properties of XLPE insulation used for HVDC cable after accelerated thermal ageing. In: *12th IEEE international conference on the properties and applications of dielectric materials*, Xi'an, China, pp 500–503. <https://doi.org/10.1109/icpadm.2018.8401037>
70. Diego JA, Belana J, Orrit J, Cañadas JC, Mudarra M, Frutos F, Acedo M (2011) Annealing effect on the conductivity of XLPE insulation in power cable. *IEEE Trans Dielectr Electr Insul 18*(5):1554–1561. <https://doi.org/10.1109/TDEI.2011.6032824>
71. ***IEEE Std 1242-1999. IEEE guide for specifying and selecting power, control and special-purpose cable for petroleum and chemical plants, 26 June 1999
72. Stancu C, Notingher PV (2016) Reduction of the space charge in the composite insulations of the high-voltage DC cables junctions. Project UPB-UEFISCDI PN-II-RU-TE-2014-4-0280, Report stage II
73. Simoni L, Pattini G (1975) A new research into the voltage endurance of solid dielectrics. *IEEE Trans Electr Insul EI-10*(1), pp 17–27. <https://doi.org/10.1109/tei.1975.297852>
74. ***ASTM D149-09. Standard test method for dielectric breakdown voltage and dielectric strength of solid electrical insulating materials at commercial power frequencies. ASTM International, West Conshohocken, PA. <https://doi.org/10.1520/d0149-09r13>
75. ***IEC Publication 243 (1990). Methods of test for electric strength of solid insulating materials, Geneva
76. Sloman LM (1976) Comparing XLPE and EPR for cable insulation. *Electrical Times*, pp 13–18
77. Ohki Y, Ebinuma Y, Katakai S (1998) Space charge formation in water-treed insulation. *IEEE Trans Dielectr Electr Insul 5*(5):707–712. <https://doi.org/10.1109/94.729693>
78. Montanari GC, Seri P, Morshuis P, Stevens G, Vaughan A (2018) Next generation polymeric high voltage direct current cables—a quantum leap needed? *IEEE Electr Insul Mag 34*(2):24–31. <https://doi.org/10.1109/MEI.2018.8300441>
79. Montanari GC (2011) Bringing an insulation to failure: the role of space charge. *IEEE Trans Dielectr Electr Insul 18*(2):339–364. <https://doi.org/10.1109/TDEI.2011.5739438>
80. Hanley TL, Burford RP, Fleming RJ, Barber KW (2003) A general review of polymeric insulation for use in HVDC cables. *IEEE Electr Insul Mag 19*(1):13–24. <https://doi.org/10.1109/MEI.2003.1178104>

81. Dao NL, Lewin PL, Hosier IL, Swingler SG (2010) A comparison between LDPE and HDPE cable insulation properties following lightning impulse ageing. In: International conference on solid dielectrics, Potsdam, Germany, pp 1–4. <https://doi.org/10.1109/icstd.2010.5567944>
82. Montanari GC, Laurent C, Teyssedre G, Campus A, Nilsson U (2005) From LDPE to XLPE: part I: space charge, conduction and life. *IEEE Trans Dielectr Electr Insul* 12(3):438–446. <https://doi.org/10.1109/TDEI.2005.1453448>
83. Teyssedre G, Laurent C, Montanari GC, Campus A, Nilsson U (2005) From LDPE to XLPE: investigating the change of electrical properties. Part II Lumin *IEEE Trans Dielectr Electr Insul* 12(3):447–454. <https://doi.org/10.1109/TDEI.2005.1453449>
84. Ma DL, Hugener TA, Siegel RW, Christerson A, Mårtensson E, Önnby C, Schadler LS (2005) Influence of nanoparticle surface modification on the electrical behaviour of polyethylene nanocomposites. *Nanotechnology* 16(6):724–731. <https://doi.org/10.1088/0957-4484/16/6/016>
85. Meziani M, Mekhaldi A, Teguvar M, De Recherche L (2015) Effect of magnitude of space charges on the electric field distribution in XLPE insulation in presence of water trees. *Jicable*, Paris, pp 2–6
86. Stancu C, Notingher PV, Ciuprina F, Notingher P Jr, Agnel S, Castellon J, Toureille A (2009) Computation of the electric field in cable insulation in the presence of water trees and space charge. *IEEE Trans Ind Appl* 45(1):30–43. <https://doi.org/10.1109/tia.2008.2009659>
87. Stancu C, Notingher PV, Notingher P Jr, Plopeanu M (2010) Computation of electric field corresponding to space charge in water-treed power cable insulation. *Prz Elektrotechn (Electr Rev)* 86(5):114–118
88. Stancu C, Notingher PV, Notingher P Jr (2013) Influence of space charge related to water trees on the breakdown voltage of power cable insulation. *J Electrostat* 71(2):145–154. <https://doi.org/10.1016/j.elstat.2012.12.041>
89. Notingher P, Toureille A, Santana J, Martinotto L, Albertini M (2001) Study of space charge accumulation in polyolefins submitted to ac stress. *IEEE Trans Dielectr Electr Insul* 8(6):972–984. <https://doi.org/10.1109/94.971454>
90. Holé S, Bruzek C-É, Lallouet N (2017) PPLP and kraft paper under high voltage in liquid nitrogen. In: Conference proceedings of ISEIM, Toyohashi, Japan, 107–109. <https://doi.org/10.23919/iseim.2017.8088700>
91. Carstensen P, Gustafsson A, Farkas A, Ericsson A, Boström J, Gustafsson B, Nilsson U, Campus F (1999) An electric dc-cable with an insulation system. Asea Brown Boveri AB, International Patent WO9933069
92. Carstensen P (1999) A method for manufacturing a cable. Asea Brown Boveri AB, International Patent WO9940589
93. Zhou Y, Hu J, Dang B, He J (2017) Effect of different nanoparticles on tuning electrical properties of polypropylene nanocomposites. *IEEE Trans Dielectr Electr Insul* 24(3):1380–1389. <https://doi.org/10.1109/TDEI.2017.006183>
94. Wang SJ, Zha JW, Wu YH, Ren L, Dang ZM, Wu J (2015) Preparation, microstructure and properties of polyethylene/alumina nanocomposites for HVDC insulation. *IEEE Trans Dielectr Electr Insul* 22(6):3350–3356. <https://doi.org/10.1109/TDEI.2015.004903>
95. Ju S, Zhang H, Chen MJ, Zhang C, Chen X, Zhang Z (2014) Improved electrical insulating properties of LDPE based nanocomposite: effect of surface modification of magnesia nanoparticles. *Compos Part A Appl Sci Manuf* 66:183–192. <https://doi.org/10.1016/j.compositesa.2014.07.003>
96. Grzybowski S, Trnka P, Fulper JC (2007) Aging of high voltage cables by switching impulse. In: IEEE electric ship technologies symposium, Arlington, VA, pp 165–168. <https://doi.org/10.1109/ests.2007.372080>
97. Dao NL, Lewin PL, Swingler SG (2009) Lightning impulse ageing of HV cable insulation. In: Proceedings of the 16th international symposium on high voltage engineering, Innes House, Johannesburg, pp 1–4. ISBN 978-0-620-44584-9

98. Dao NL (2011) Impulse ageing of polymeric materials, Ph D Thesis. School of Electronics and Computer Science, University of Southampton, Southampton, July 2011
99. Komatsu K, Liu H, Shimada M, Mizuno Y (2019) Assessment of surface degradation of silicone rubber caused by partial discharge. *Energies MDPI Open Access J* 12(14):1–13. <https://doi.org/10.3390/en12142756>
100. Gamez-Garcia M, Bartnikas R, Wertheimer MR (1987) Synthesis reactions involving XLPE subjected to partial discharges. *IEEE Trans Electr Insul EI-22(2)*:199–205. <https://doi.org/10.1109/tei.1987.298882>
101. Wolter KD, Tanaka J, Johnson JF (1982) A study of the gaseous degradation products of corona-exposed polyethylene. *IEEE Trans Elect Insul EI-17(3)*:248–252. <https://doi.org/10.1109/tei.1982.298463>
102. Morshuis PHF (2005) Degradation of solid dielectrics due to internal partial discharge: some thoughts on progress made and where to go now. *IEEE Trans Dielectr Electr Insul* 12(6), pp 1275–1275. <https://doi.org/10.1109/TDEI.2005.1561811>
103. McMahon EJ (1968) The chemistry of corona degradation of organic insulating materials in high voltage fields under mechanical strain. *IEEE Trans Elect Insul EI-3(1)*:3–10. <https://doi.org/10.1109/tei.1968.299047>
104. Gamez-Garcia M, Bartnikas R, Wertheimer MR (1984) Circular degradation patterns on XLPE surfaced electrodes. In: *IEEE international symposium on electrical insulation*, IEEE Conf. Rec. No. 84CH 1964-6-El, Montreal Quebec, Canada, pp 356–359. <https://doi.org/10.1109/eic.1984.7465216>
105. Nikolajevic SV (1999) The behaviour of water in XLPE and EPR cables and its influence on the electric characteristics of insulation. *IEEE Trans Power Delivery* 14(1):39–45. <https://doi.org/10.1109/61.736677>
106. Bin Makmud MZ, Sayuti A, Arief YZ, Wahit MU (2011). Insulating performance of LLDPE/natural rubber blends by studying partial discharge characteristics and tensile properties. In: *International conference on electrical engineering and informatics*, Bandung, Indonesia, Paper E 10-5, pp 1–4. <https://doi.org/10.1109/iceei.2011.6021551>
107. Dissado LA (2002) Understanding electrical trees in solid: from experiment to theory. *IEEE Trans Dielectr Electr Insul* 9(4):483–497. <https://doi.org/10.1109/TDEI.2002.1024425>
108. Rouha N, Beroual A (2013) Physico-chemical diagnosis of EPDM electrical aging by tree phenomenon. *IEEE Trans Dielectr Electr Insul* 20(5):1577–1583. <https://doi.org/10.1109/TDEI.2013.6633686>
109. Johansson AB (2015) Characterising resistance to electrical treeing in new XLPE-based materials for high-voltage cables, PhD thesis. Chalmers University of Technology, Gothenburg, Sweden
110. Shimizu N, Laurent C (1998) Electrical tree initiation. *IEEE Trans Dielectr Electr Insul* 5(5):651–659. <https://doi.org/10.1109/94.729688>
111. Bamji S (1999) Electrical trees, physical mechanisms and experimental techniques. In: Webster JG (ed) *Wiley encyclopedia of electrical and electronics engineering*, vol 6. Wiley & Sons, USA, pp 264–275
112. Dissado LA, Fothergill JC (1992) *Electrical degradation and breakdown in polymers*. P. Peregrinus, London. <https://doi.org/10.1049/pbed009e>
113. Hozumi N, Ishida M, Okamoto T, Fukugawa H (1990) The influence of morphology on electrical tree initiation in polyethylene under AC and impulse voltages. *IEEE Trans Electr Insul* 25(4):707–714. <https://doi.org/10.1109/14.57094>
114. Tanaka T (1992) Charge transfer and tree initiation in polyethylene subjected to AC voltage stress. *IEEE Trans Electr Insul* 27(3):424–431. <https://doi.org/10.1109/14.142702>
115. Minoda A, Mizuno Y, Nagao M, Kosaki M (1995) Dc short-circuit treeing phenomenon in epr at cryogenic temperature. In: *Proceedings of 5th international conference on conduction and breakdown in solid dielectrics*. Leicester, UK, pp 621–625. <https://doi.org/10.1109/icstd.1995.523061>

116. Zhu L, Du B, Li H, Hou K (2019) Effect of polycyclic compounds fillers on electrical treeing characteristics in XLPE with DC-impulse voltage. *Energies* 12(14):2767. <https://doi.org/10.3390/en12142767>
117. Boggs S, Xu J (2001) Water treeing—filled versus unfilled cable insulation. *IEEE Electr Insul Mag* 17(1):23–29. <https://doi.org/10.1109/57.901616>
118. Bernstein BS, Srinivas N, Hogan JD, Katz C (1975) Electrochemical treeing in ethylene-propylene rubber compounds. *J Elastom Plast* 7(4):456–469. <https://doi.org/10.1177/009524437500700409>
119. Caronia PJ, Mendelsohn A, Gross LH, Kjellqvist JB (2006) Global trends and motivation toward the adoption of TR-XLPE cable. *IEEE/PES In: Transmission and. AVO NZ Conference*, pp 1–4
120. Campus A (2003) 20 years of experience with copolymer power cable insulation. *Jicable 03, Versailles, France*, pp 350–356
121. Du BX (2001) Discharge energy and dc tracking resistance of organic insulating materials. *IEEE Trans Dielectr Electr Insul* 8(6):897–901. <https://doi.org/10.1109/94.971443>
122. ***IEC Publication 587 (1984) Test methods for evaluating resistance to tracking and erosion of electrical insulating materials used under severe ambient conditions, second edn, Geneva, Switzerland
123. ***IEC Publications 112 (1979) Method for determining the comparative and the proof tracking indices of solid insulating materials under moist conditions, 3rd edn
124. Yoshimura N, Kumagai S, Du BX (1997) Research in Japan on the tracking phenomenon of electrical insulating materials. *IEEE Electr Insul Mag* 13(5):8–19. <https://doi.org/10.1109/57.620513>
125. Van Krevelen DW (1972) *Properties of polymers*. Elsevier, New York. <https://doi.org/10.1002/pi.4980040509>
126. ***The Engineering ToolBox. Thermoplastics—physical properties—https://www.engineeringtoolbox.com/physical-properties-thermoplastics-d_808.html. Accessed on 25 Feb 2020
127. Andritsch T, Vaughan A, Stevens GC (2017) Novel insulation materials for high voltage cable systems. *IEEE Electr Insul Mag* 33(4):27–33. <https://doi.org/10.1109/MEI.2017.7956630>
128. Brown M (1983) Performance of ethylene-propylene rubber insulation in medium and high voltage power cable. *IEEE Trans Power Appar Syst PAS-102(2):373–381*. <https://doi.org/10.1109/tpas.1983.317684>
129. Sheldon RP, Lane K (1965) Thermal conductivities of polymers II-polyethylene. *Polymer* 6(4):205–212. [https://doi.org/10.1016/0032-3861\(65\)90042-X](https://doi.org/10.1016/0032-3861(65)90042-X)
130. Morgan VT (1991) The thermal conductivity of crosslinked polyethylene insulation in aerial bundled cables. *IEEE Trans Electr Insul* 26(6):1153–1158. <https://doi.org/10.1109/14.108153>
131. Qi X, Boggs S (2006) Thermal and mechanical properties of EPR and XLPE Cable compounds. *IEEE Electr Insul Mag* 22(3):19–24. <https://doi.org/10.1109/MEI.2006.1639026>
132. Davidson DL (1979) Thermal stability of wire and polymers cable vulcanizable polyethylenes. In: *SPE RETEC, processing wire and cable*, Chicago, USA, 20 June 1979
133. ***Nexans—Comparison among insulation materials. https://www.nexans.com.br/SouthAmerica/2008/Comparing_us_5.pdf. Accessed on 25 Feb 2020
134. ***Omnexus. The material selection platform—Elongation at break values of several plastics. <https://omnexus.specialchem.com/polymer-properties/properties/elongation-at-break#values>. Accessed on 25 Feb 2020
135. Mizuno Y, Iizuka M, Mitsuyama Y, Nagao M, Kosaki M, Shimizu N, Morii K (1992) Performance of extruded ethylene-propylene rubber insulated cryogenic power cable. *Conference Record of the 1992 In: IEEE International Symposium on Electrical Insulation, Baltimore, USA*, pp 479–482. <https://doi.org/10.1109/ELINSL.1992.246954>

136. Paterson AB (1973) Practical advantages of crosslinked polyethylene for power cable. *Elect Rev* 23:280–286
137. ***The Engineering ToolBox (2001) Chemical resistance of rubbers and elastomers. https://www.engineeringtoolbox.com/chemical-resistance-rubbers-elastomers-d_1425.html. Accessed on 26 Feb 2020
138. ***The Engineering ToolBox (2006) Chemical resistance of rubbers and elastomers. https://www.engineeringtoolbox.com/peh-chemical-resistance-d_329.html. Accessed on 26 Feb 2020
139. ***The Engineering ToolBox (2018) Chemical resistance of rubbers and elastomers. https://www.engineeringtoolbox.com/PVC-polyvinyl-chloride-chemical-resistance-d_2147.html. Accessed on 26 Feb 2020
140. Schonbacher H, Stolarz-Izycka A (1979) Compilation of radiation damage test data, part I: cable insulating materials, RD—398/3000. CERN, Geneva. <https://doi.org/10.5170/cern-1979-008>
141. Anandakumaran K, Barreca S, Seidl W, Castaldo PV (2001) Nuclear qualification of PVC insulated cables. *IEEE Trans Dielectr Electr Insul* 8(5):818–825. <https://doi.org/10.1109/94.959709>
142. Stonkus DJ (1988) Physical degradation assessment of generator station cables. In: *Proceedings: EPRI power plant condition monitoring workshop*, San Francisco, USA, 16–18 Feb 1988
143. Michel W (1995) Prognosis on the aging of cables. In: *MEA specialists meeting on effectiveness of methods for detection and monitoring of age related degradation in nuclear power plants*, Bariloche, Argentina, 17–19 Oct 1995
144. Jacobus MJ (1992) Aging, condition monitoring, and loss-of-coolant accident tests of class 1 E electrical cables: crosslinked polyolefin cables. NUREG/CR-5772, SAND91-1766/1, vol 1
145. Jacobus MJ (1992) Aging, condition monitoring, and loss-of-coolant accident tests of class 1 E electrical cables: ethylene propylene rubber cables. NUREG/CR-5772, SAND91-1766/2, vol 2
146. Anandakumaran K, Seidl W, Castaldo PV (1999) Condition assessment of cable insulation systems in operating nuclear power plants. *IEEE Trans Dielectr Electr Insul* 6(3):376–384. <https://doi.org/10.1109/94.775626>
147. Mazzanti G, Montanari GC, Simoni L (1997) Insulation characterization in multistress conditions by accelerated life tests: an application to XLPE and EPR for high voltage cables. *IEEE Electr Insul Mag* 13(6):24–34. <https://doi.org/10.1109/57.637151>
148. Shwehdi MH, Morsy MA, Abugurain A (2003) Thermal aging tests on XLPE and PVC cable insulation materials of Saudi Arabia. In: *Annual report conference on electrical insulation and dielectric phenomena*, Albuquerque, New Mexico, USA, pp 176–180. <https://doi.org/10.1109/ceidp.2003.1254822>

Chapter 11

Theoretical Aspects of XLPE-Based Blends and Nanocomposites



Minu Elizabeth Thomas, Rajamani Vidya, Jince Thomas,
and Zakiah Ahmad

1 Introduction

The use of cross-linked polyethylene (XLPE or PEX) has been subjected to a development in a range of applications, such as in insulations in medium-voltage (MV) and high-voltage (HV) power cables [1], in pipes for domestic radiant heat systems and plumbing, in molded articles and in total hip anthropology [2]. However, these materials go through some defects that lead to the inefficiency of certain desired properties. This difficulty can somehow be decreased by the incorporation of nanofillers or blends. These new materials boost up the demand of XLPE in the global market. The knowledge of structure–property relation is very important for tuning the properties of new materials. Hence, computational studies are more relevant and become an essential tool for most experimental systematic investigations.

M. E. Thomas · R. Vidya

School of Chemical Sciences, Mahatma Gandhi University, Kottayam, Kerala, India
e-mail: minuputhen@gmail.com

R. Vidya

e-mail: vidyasree850@gmail.com

J. Thomas

Research and Post Graduate Department of Chemistry, St. Berchmans' College,
Changanassery, Kerala, India
e-mail: jincethomas25@gmail.com

J. Thomas

International and Inter University Center for Nanoscience and Nanotechnology,
Mahatma Gandhi University, Kottayam, Kerala, India

Z. Ahmad (✉)

Faculty of Civil Engineering, Universiti Teknologi Mara, Shah Alam, Selangor, Malaysia
e-mail: zakiah@uitm.edu.my

© Springer Nature Singapore Pte Ltd. 2021

J. Thomas et al. (eds.), *Crosslinkable Polyethylene Based Blends and Nanocomposites*, Materials Horizons: From Nature to Nanomaterials,
https://doi.org/10.1007/978-981-16-0486-7_11

2 Importance of Theoretical Studies in XLPE Nanocomposites and Blends

Molecular modeling [3] can be defined as the creation, calculation, interpretation and prediction of realistic molecular structures and assumption of physicochemical–biological properties by the aid of the computer. The attempt is completed to identify and recognize a molecular structure from its symbolic representations with a computer. Molecular modeling for a particular model gives exact results, can compare with experimental results and helps in its interpretations. These calculations can correlate the atomic/molecular level and extent to predict macroscopic properties. Molecular modeling acts as a blueprint for the experimental analysis and provides information that is not obtained through experimental details.

The progression in computer efficiency and computer graphics, user-friendliness of complicated algorithms, etc., makes the computational molecular modeling more comfortable to the scientific research society. The theoretical techniques like molecular mechanics, quantum mechanics, molecular dynamics and multi-scale simulations help to determine the physicochemical and structural properties involve in the molecular process.

3 Theories Behind Computational Molecular Modeling

The theoretical investigation of pristine XLPE is mostly dealing with quantum mechanical studies; hence, the quantum mechanical theories are explained in volume 1 of this series. The macromolecular structural studies are also analyzed by classical mechanics theories such as molecular mechanics (MM) and molecular dynamics (MD). A new field of computational studies, called ‘multi-scale stimulations,’ was being a trend in simulations nowadays. The interaction of nanoparticles must be studied using electronic structure theory which is more effective but the cost of time is more than the techniques using classical mechanics; hence, the importance of multi-scale simulations is drawn out. Thus, a clear idea of all those theories is important for a better understanding of such simulations. Here, it explains the theory behind molecular mechanics, molecular dynamics and multi-scale studies.

The computational molecular modeling is divided mainly into two: (exempting statistical mechanics) classical mechanics and quantum mechanics (QM). Classical mechanics works under Newton’s laws of motion [4] while quantum mechanics is under the Schrödinger wave equation [5].

3.1 *Classical Mechanics*

The simulations based on classical mechanics work under Newton's second law of motion,

$$F = ma$$

where 'F' is the total force, 'm' is the mass of the particle, and 'a' is acceleration; 'F' and 'a' are vector quantities. This classical mechanics molecular modeling is developed of a necessity to describe

- Molecular properties and structure as in real.
- Molecules with a high molecular mass.
- Valid for molecules such as organic, inorganic, metallo-organic, biomolecules.
- Studies in both vacuum and solvent environment.
- The minimum energy state, i.e., ground state analysis.
- Thermodynamic and kinetic properties prediction.

Thus, the classical mechanical technique is classified into two: molecular mechanics and molecular dynamics.

(a) Molecular mechanics

To study the behavior of large molecules like XLPE effectively, which is not possible by ab initio and semi-empirical methods, molecular mechanics [6] can be used. MM analysis uses classical-type models to predict the energy of a molecule as a function of its conformation. It predicts both ground and transition state geometries, and relative energy between its conformers. MM is based on certain principles in which the subatomic particles like nuclei and electrons are not considered. The atoms are considered as a spherical body with a certain net charge. The interactions between the spherical bodies are based on classical potentials and with pre-assigned values for a specific set of atoms. MM determines the energies and spatial distribution of the spherical bodies. These simplified assumptions and approximations enable to use MM for extensive applications to different systems.

Hence, MM is simply based on the mathematical model of a molecule with balls (represent atoms) and spring (represents bonds). Based on this model, we can say that energy changes with its geometry because of the alteration of bonds. MM model ignores electrons, so it cannot be used to study the electronic properties like charge distribution and electrophilic/nucleophilic behavior. The principle behind MM is to evaluate the energy of a molecule as a function of its resistance toward bond stretching, bond bending and atom crowding and to use this energy equation to find the bond lengths, angles and dihedrals corresponding to the minimum energy geometry. Since the energy expression and its parameters constitute a force field, thus, MM method is also known as force field methods. Force field is nothing but the set of mathematical expressions or set of parameters for the calculation of

potential energy of a system. The force field used in MM is specifically named as empirical force field [7].

The force field of spring deformation can be familiar with the capability of bonds to stretch, bend and twist and have some non-bonded interactions. The bond length (r) is associated with the stretching and bending with the bond angle (θ), the twist is associated with a change in dihedral angle (δ) and torsion angle (ϕ), and the non-bonded interaction is associated with *van der Waals* forces (ω). In some cases, long-range electrostatic interactions (q) are also added to the non-bonded interactions. The bond stretching and bond bending include stretch-bend and out/in-plane bends; torsion interactions are categories as bonded interactions because the atoms which are concerned must have a direct interaction to each other, i.e., they are bonded directly or bonded to a common atom. The *van der Waals* and electrostatic interactions are included in non-bonded interactions, in which atoms are not having any direct interactions but only have spatial interactions. The anatomy of MM is schematically represented in Fig. 1.

The interaction of the force fields is represented as

$$E_{\text{total}} = E_{\text{bonded}} + E_{\text{non-bonded}}$$

where $E_{\text{bonded}} = E_r + E_\theta + E_\phi$ and $E_{\text{non-bonded}} = E_\omega + E_q$, E_r is bond stretching energy, ' E_θ ' bond bending energy, ' E_ϕ ' energy for torsion interactions, ' E_ω ' is van der Waals interaction energy, and ' E_q ' is long-range electrostatic interaction energy.

The empirical force fields are represented or result in potential energy surfaces. These potential energy surfaces are the graphical representation of a parameter versus potential energy; this may be in different dimensions. The empirical potential energy function and the corresponding potential energy surfaces are represented in Fig. 2.

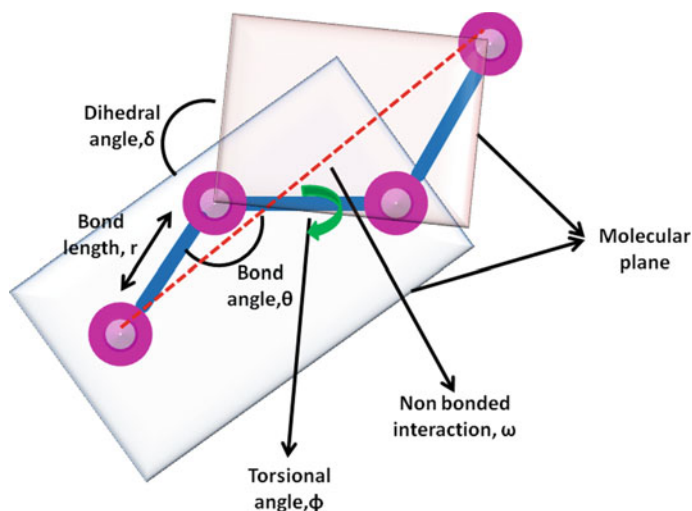


Fig. 1 Schematic representation of the anatomy of force field in molecular mechanics

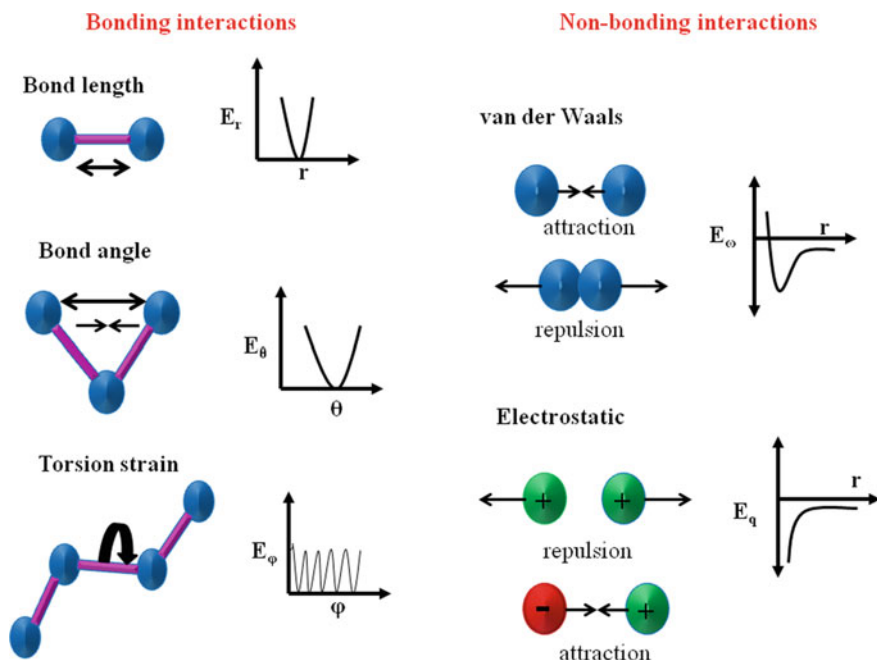


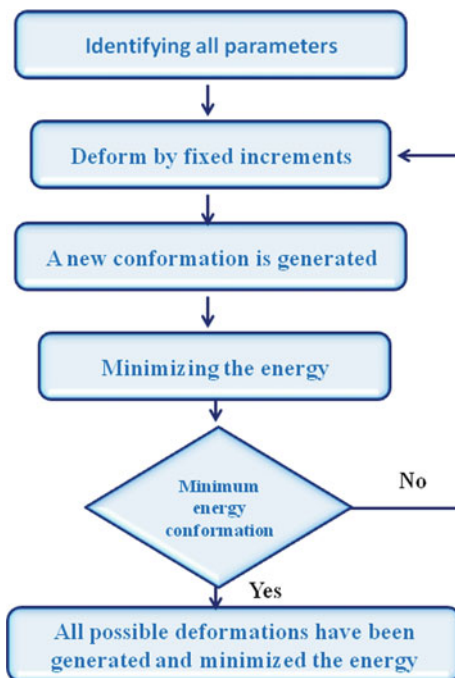
Fig. 2 Empirical potential energy function and corresponding potential energy surfaces

The history of the emergence of force field is in 1930 by D. H. Andrews [8], and he proposed an idea of extending the spectroscopic force field for doing MM. In 1940, F. H. Westheimer [9] determined the transition state calculations without computational techniques also. Conformational analysis of more than six-membered ring is done in 1961 by J. B. Hendrickson [10]. However, K. B. Wiberg published the program type 'MM' in 1965 to analyze the minimum energy of the system [11]. N. L. Allinger published the highly popular force field series of 'MM' in which MM1 was in 1976, and the next year MM2 was available [12]. In the following year, different research groups developed a large variety of force field to perform desired properties. Some important force fields are

- Assisted model building with energy refinement (AMBER) [13].
- DREINDING [14].
- MM series, MM2, MM3 [15].
- Chemistry at HARvard using molecular mechanics (CHARMM) [16].
- GROenigen molecular simulation (GROMOS) [17].
- Merck molecular force field (MMFF) [18].
- COMPASS [19].
- Optimized parameters for large-scale simulations (OPLS) [20].

Some software packages like TINKER [21], NAMD [22], etc., provide various MM force fields. Besides, some quantum mechanics software packages also

Fig. 3 General systematic flowchart representation of the working strategy of MM technique



provide various force fields which are able to perform computations for both MM and MD. For a force field, some specific steps or working pattern for the performance of the desired analysis. The general working steps of MM are schematically represented by a flowchart in Fig. 3.

Advantages of MM

- Less expensive than quantum mechanical techniques
- Easier to use on large systems.
- Easy to understand the output.

Limitations of MM

- Different atoms need different force field; hence, it is restricted by the parameters in the equation.
- MM is not applicable for analyzing electronic properties.
- Many chemical processes do not obey Newton's second law of motion hence is a limitation for many chemical reactions.
- Interaction potential is not obtained.

Due to limitations in the MM technique for obtaining a solution for real-world problems, it introduced a simulation with a motion called molecular dynamics.

(b) Molecular dynamics

In real life, atoms are always in constant motion. They will not go to a minimum energy state and be static. Hence, studies of molecular motions must be important for making the theoretical molecules in tune with reality. An advanced molecular mechanics with motion was developed; this theory is called molecular dynamics [23]. This technique also functions according to Newton's second law of motion, in which the energy can be calculated by MM or QM simulation. MM energies do not involve the electronic structure changes in bond breaking/making but in QM address it. QM energies are considered for changes in structure for chemical reactions. By the knowledge of the force and mass of the system, it is easy to solve the position of each atom concerning small time steps (approximately 10^{-15} s). Hence, Newton's second law of motion can be expressed according to the molecular dynamics process. If we considered all atoms, position coordinate as 'x' and 'E' is the potential energy of the system. Acceleration is derivative of velocity which is in turn the derivative of position over time. The force exerted on an atom is a result of the change in potential energy for a change in the position of the atom. Hence, Newton's second law of motion can be replaced by $F = -dE/dx$ and $a = d^2x/dt^2$, and then the equation is written as

$$-\frac{dE}{dx} = m \cdot \frac{d^2x}{dt^2}$$

The structural change over time is called a trajectory. Due to the lack of analytical techniques, the trajectory is not obtained directly from the above equation. Hence, the result is obtained by three steps. Firstly, acceleration is obtained from the forces and mass. The second step is that from this acceleration, velocity is obtained, and finally from this velocity, the position is calculated. MD has no accurate point of termination, and the order of time is limited only for some minor transformations are some pointed defects of MD. Figure 4 represents a general systematic flowchart representation of the working strategy of the MD technique.

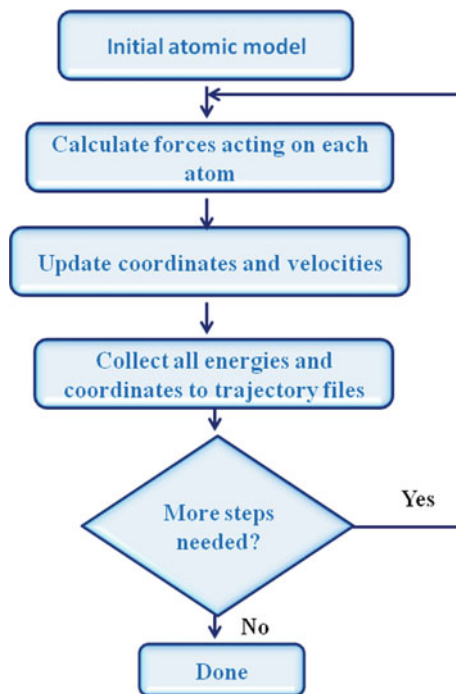
Advantages of MD

- Can apply for a large area of research.
- Able to simulate almost complex fluids, complex geometries, etc.
- Gives a comprehensive atomic/molecular level information.
- The only description of inter-atomic/molecular interaction is needed in the input model.

Limitations of MD

- Only analyzes a fixed number of atoms.
- Only conformational polarization is analyzed not electronic polarization.
- No bond creation or deletion is an account.
- Due to the quadratic form of potentials, the estimation obtained is far from equilibrium values.

Fig. 4 General systematic flowchart representation of the working strategy of the MD technique



Hence, the pitfall of both classical mechanical techniques MM and MD is

- Not dealt with electronic properties.
- Restricted to the explanation of equilibrium structure and its conformation.

To overcome the estimation of electronic properties introduced quantum mechanical simulations.

3.2 *Electronic Structure Simulations or Quantum Mechanical Theories*

The quantum mechanical (QM) simulations work under the Schrödinger wave equation

$$\hat{H}\psi = E\psi$$

where ' \hat{H} ' is the total Hamiltonian operator, ' Ψ ' is the total wave function, and ' E ' is the total energy. The model of QM is that the nuclei are fixed on the space with the electrons are surrounded all over the system with a continuous electronic density, i.e., QM provides the information about the nuclear position and electronic

distribution. Hence, the limitation of classical mechanics is removed. These studies are mainly based on the arrangements and interaction of nuclei and electrons in the system and the chemical reaction can explain accurately. This theory is free from parameters but works under certain assumptions such as Born-Oppenheimer approximation and variation principle. According to the mode of operation and analysis, QM simulations are mainly divided into three: ab initio, semi-empirical and density-functional theory (DFT), all those theories are well explained in volume 1 of this series. The electrical and water treeing in XLPE can well explain using these QM simulations. They also suggest better fillers for the reduction of DC breakages.

Advantages of QM

- Accurate.
- Deals with electronic structures and almost all chemical reactions.

Limitations of QM

- Restricted to a hundred atoms.
- No molecular/atomic motion calculations.

3.3 Pros and Cons of Classical Mechanical Simulations and Quantum Mechanical Simulations

Both classical and quantum mechanical simulations have their own merits and demerits. They are described as follows in Table 1.

By the analysis of both classical and quantum mechanical pros and cons, the necessity of the introduction of a new method or methods is very urgent. This important thought results with multi-scale computational methodologies. Before

Table 1 Pros and cons of classical and quantum mechanical simulations

Classical mechanical simulations	Quantum mechanical simulations
<i>Pros</i>	
<ul style="list-style-type: none"> • Fast, less expensive and surprisingly useful • Can calculate more than ten thousand atoms 	<ul style="list-style-type: none"> • QM deals with electronic structures in the system • It is accurate • Can deal with reactions, i.e., bond breaking and making • Often used to parameterize force fields
<i>Cons</i>	
<ul style="list-style-type: none"> • Not integrates the electron distribution in a molecule • Not describes the bond making and breaking 	<ul style="list-style-type: none"> • Limited to hundred of atoms • Static models only no dealings with time

discussing the multi-scale methodologies, some other type of simulations in which the XLPE works are not yet reported.

3.4 Monte Carlo Simulations

The first computer simulations are done using Monte Carlo techniques (MCS) [24, 25]. It works under the principle of probability. In this simulation, an ensemble of arrangements is created by either randomly repositioned atom or atoms in the model or by removing an atom or atoms from the model. Like MD, MCS also updates the force field but a difference is that in MCS, the updating depends on potential energy, not by forces acting on the atoms. MCS is mainly used in disordered materials like polymers and liquids. However, XLPE polymer studies using this method are not yet reported.

3.5 Mesoscale

Mesoscale is the method that works on the model between 10 nm and 1000 nm. This method consists of five techniques [26]: coarse-grained molecular dynamics (CGMD), dissipative particle dynamics (DPD), lattice Boltzmann (LB), time-dependent Ginzburg–Landau method (TDGL), and dynamic density-functional theory (DDFT). Out of these techniques, CGMD is most popular. Force field available for these techniques is mainly MARTINI [27, 28] and force field developed by Shinoda [29, 30]. These techniques are mostly used in polymer model but XLPE is not yet analyzed.

Nanomaterials and polymers consist of more than thousands of atoms, and their interaction is interfacially depended. They need simulations with multiple length and time scale. Molecular modeling only predicts the properties of the system within the range of 10 nm with exempt electronic interactions. In QM, it considers the electronic interaction but limited to around a thousand atoms. In support of the polymer nanocomposites or blends, a method that offers fast but accurate results that apply to a long-range scale is needed.

3.6 Multi-scale Computational Studies

Multi-scale modeling in which a variety of models at a different level of resolution and complexity is used simultaneously accounts for a system. There are two key approaches to multi-scale simulations: hierarchical and hybrid methods. Hierarchical method starts with high-resolution models like QM and uses its results for modeling a model with a low resolution like MM. It employs a single method at

a time and develops a high-level model with minimal reference to experimental data. However, in the hybrid method, multiple level models in a single step and a high-resolution study are depicted where it is needed. Most commonly used multi-scale modeling for XLPE polymer is a hybrid method called quantum mechanical/molecular mechanical or molecular dynamics models (QM/MM or QM/MD).

QM/MM method

In the QM/MM hybrid method, the uninterested part is treated with MM method and interesting part with QM method [31, 32]. Figure 5 represents the schematic representation of the QM/MM simulation.

In this hybrid method, three interactions are carried out QM, MM and QM/MM simulations. QM and MM can be obtained directly but the interface boundary of QM and MM is obtained by two schemes: additive scheme [33] and subtractive scheme [34]. If we consider 'A' as QM region and 'B' as MM region, then the total energy of the subtractive scheme is

$$E_{\text{total}}^{\text{sub}} = E_{\text{MM(A+B)}} + E_{\text{QM(A)}} - E_{\text{MM(A)}}$$

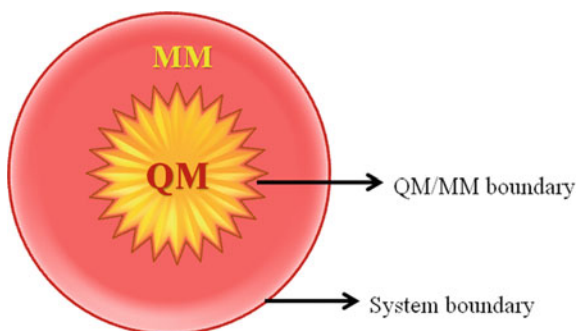
The total energy of the additive scheme is

$$E_{\text{total}}^{\text{add}} = E_{\text{QM(A)}} + E_{\text{MM(B)}} + E_{\text{QM/MM(A-B)}}$$

The $E_{\text{QM/MM(A-B)}}$ can be calculated by the electrostatic and bonded/non-bonded factors also included for obtaining accuracy. For electrostatic interactions, three models are available:

- **Mechanical embedding:** The electrostatic treatment of $E_{\text{QM/MM}}$ is estimated at MM level using QM calculation, mainly between the atomic point charges in that region. But polarization is not taken for an account [35].
- **Electrostatic embedding:** The QM region is estimated by QM in the presence of MM in which point charge is taken as the one-electron term for E_{QM} [16].

Fig. 5 Schematic representation of QM/MM simulation



- **Polarized embedding:** This method is the most popular one in which the back-polarization of MM region with QM is done using two methods, one-way or fully self-consistent scheme (SCF). Different schemes are implemented for the polarization of MM region; mainly, the induced dipole, charge-on-a-spring and the fluctuating charge [36].

Irrespective of the additive or subtractive method, non-bonded interactions are included in the QM/MM methodology. Non-bonded interaction (van der Waals) is done by Lennard–Jones potential but is difficult to obtaining for QM atoms, because during the reaction the parameters can change. Also, boundary treatments like link atoms, boundary atoms and localized orbital schemes are carried out [33, 37–40].

Hence, the steps for the QM/MM methodology [41] implementations are

1. The setting of the boundary between QM and MM region.
2. Selection of suitable QM method for calculation.
3. Selection of force field for the MM method.
4. Selection of suitable scheme for total QM/MM, i.e., additive/subtractive and setting of electrostatic QM/MM interactions and bonded/non-bonded interactions.
5. Optimization of QM/MM region.
6. Incorporate MD or statistical mechanics for accuracy.

QM/MM methods are excellent options for grasping the inimitable characteristics of polymer nanocomposites and blends in its chemical reaction and its bonding nature. This structure–property relationship will be key for the analysis and improvement of applications.

By selecting an appropriate theory for tailoring the desired properties of the material and task for the selection of force field or calculations for the studies. For the better performance of molecular modeling, appropriate force field or calculations are needed. The software mainly provides these force fields. In most of the software, a pre-built force field/calculation techniques are ensured. Most of the software is efficient for some specific studies. The selection of software is important for resultant properties and analysis that must be in tune with the real systems.

4 Software Used for Computational Calculations

Most of the computational techniques are done using many distinct software packages. These software packages were differed in efficiency, functionality, computerization, potency and effortlessness in operating. Here it gives some common software used for MM, MD and multi-scale simulations. Classifications are done between the software integrated and specific packages.

4.1 Integrated Software Packages

In integrated software packages, the software can perform various computational techniques. Commonly used are Alchemy, Chem3D, HyperChem, NWChem, SPARTAN, etc., and the details of the software were discussed in volume 1 of this series. Also, the force field of integrated software is listed in Table 2.

4.2 The Software Performs Only for Specific Functions

Other than the integrative software, some software is very specific in function. Some commonly used software for MM and MD simulations are listed below in Table 3.

Table 2 Some important integrated software packages

Software package	Mainly used for	Force field used
Alchemy	MM and semi-empirical	Tripes
Chem3D	MM, MD, extended Hückel molecular theory	MM2
HyperChem	ab initio, semi-empirical and MM	MM, OPLS, BIO and AMBER
NWChem	ab initio, MM, MD and QM/MM	AMBER95 and CHARMM
SPARTAN	ab initio, semi-empirical, DFT and MM	Merck molecular force field (MMFF) and SYBYL
Gaussian	ab initio, semi-empirical, DFT, MM, MD and QM/MM	Dreiding, UFF, AMBER

Table 3 Some important software with specific functions

Software package	Mainly used for	Force field used
TINKER	MM and MD	AMBER-95, CHARMM22, MM2(91), MM3(99), OPLS-AA, OPLS-UA and TINKER.
Macromodel	MM	Modified versions than the original in the literature of MM2, MM3, AMBER, OPLSA and unmodified AMBER94, MMFF
Molecular operating environment (MOE)	MM and MD	AMBER '89, AMBER '94, MMFF94 and PEF95SAC
PC Model	MM and MD	MMX, MM3, and MMFF94
CHARMM	MD	CHARMM, AMBER
GROMOS	MD	Gromos
NAMD	MD	CHARMM, AMBER, Gromos

5 Theoretical Studies in XLPE Nanocomposites and Blends

The importance of computational studies is increasing day to day due to the increase in the efficiency of the programs and computing time. The understanding of the structure and its geometry can give an intimation regarding the reason behind some desired properties and defects. In XLPE blends and composites or the pristine XLPE, the exploration in computational studies is mostly based on the power cable insulation application which is mainly due to the popularity of XLPE as power cable insulators.

5.1 Theoretical Studies in Pristine XLPE

The molecular simulation in pristine XLPE is mainly concentrated on the cross-linking process of PE to XLPE (both chemical and UV radiation) and suggesting some voltage stabilizers, antioxidants and cross-linkers for the future process for XLPE [26, 42–46]. All such studies are explained in volume one of this series.

5.2 Theoretical Studies in XLPE Blends

Different research groups do the computational studies of XLPE blends. However, all the calculations are mostly done by considering the most popular application of XLPE and cable insulation. These analysis factors are mainly focused on

- Molecular orbital analysis.
- Analysis to find the ability to trap electron.
- Interfacial interaction stability of the blend.

Li et al. studied the ability of electron trapping or space charge accumulation QM/MD calculation of XLPE/ethylene acrylic acid (EAA), XLPE/ethylene vinyl acetate (EVA) and XLPE/styrene-ethylene-butadiene-styrene (SEBS) [47]. The simulations are done in self-consistent-charge density-functional tight-binding method (SCCDFTB) was used to perform the electronic structure calculations. The DFT is performed in B3LYP/6-31G** and MD based on velocity Verlet algorithm. The whole simulations are done in the DFTB + program package. The degree of polymerization is taken to be low, and small additives are used to save the computational time. Using electron affinity (EA) and ionization potential (IP), voltage stability and the effect of additives on the electrical treeing are analyzed. These two factors are very important for enhancing the dielectric properties of insulating material. High EA may leads to breakdown due to trapping

electrons and delaying the formation of an electron avalanche. The IP and EA are also depending on the polymers chain length taken for analysis, which is not investigated here. By the investigation, all the blends with XLPE can trap the high-energy electron. The IP of all the other polymers except 2-EAA is less than PE could absorb high-energy electrons before the electrons reacted with polyethylene and enhance the electric field strength of tree initiation, which further resists the growth of the electric tree. It further prevents the direct bombardment of the electrified particles and avoids PE breakdown but by the cleavage of C–C and C–H bonds and finally leads to the formation of some new molecules and radicals that ultimately leads to the initial time of the electrical treeing. They suggest the modification of the polymer with the content of C_6H_6 , $-COOH$, $-OCOCH_3$ groups, which can increase the stability of XLPE. Finally, they stated that the DFTB method is more convenient and reliable for such systems.

Wang et al. studied in the dual layers to reveal the interfacial charge mechanisms of (XLPE)/ethylene-propylene-diene (EPDM) using the energy band structure [48]. Quantum mechanical calculations using B3LYP/6-31G + level of theory, the energy band structure of the interfacial region between the XLPE and EPDM layers are studied based on their calculated molecular orbital (MO) energy level structures. The inter-chain and the intra-chain interactions contribute to the formation of trapping sites at the interface because the occurrence of positive charge on EPDM and negative charges on XLPE sides leading to the formation of interface dipoles makes a potential barrier at the interface. Also, the blend makes the bending in the MO energy levels which leads to the vacuum shift of MO level, which is closely related to the charge transfer and the electron–hole barriers at the interfaces. The XLPE/EPDM interface is the main area for trapping the electron hence provides a shield for XLPE degradation.

The quantum chemical analysis of cross-linked polymers of LDPE/HDPE is studied by Chen et al. [49] analyzing the highest occupied molecular orbital lowest unoccupied molecular orbital (HOMO-LUMO) energy gap which is closely related to the indication of tree initiation voltage. They also analyzed the variation of these voltages by the addition of a voltage stabilizer m-aminobenzoic acid in which the trap depth decreases with the addition of the voltage stabilizer which leads to the reduction in the space charge accumulation.

There are only a hand full of analysis done for XLPE blends. However, these quantum chemical analyses are clear that it can give an idea about the reduction in the degradation of XLPE insulation material.

5.3 Theoretical Studies in XLPE/Nanocomposites

The computational studies of nanocomposites are most common, but a few studies are for XLPE/nanocomposites. Like blends, the computational calculations of the XLPE/composites are mainly dealing with the investigation for boosting the efficiency of XLPE as insulation power cables. Most of the XLPE/nanocomposites

cable computational studies are based on quantum mechanical studies and mainly depend on three factors

- **Space charge accumulation:** The charge carriers either produced from the system or injected from the electrode. The nanofillers in the system allow accumulating the electrons on their surface, and nanofillers are surrounded by negative charges. This will weaken the electric field of the cathode and suppress the electron injection hence reduces the space charge accumulation.
- **Mobility of polymer chain:** The interaction between the filler and the XLPE matrix at the interfacial region determines the mobility of the XLPE chain and stability of the system. The mobility can be controlled by the strong adsorption of the additives.
- **Chemical interactions:** Another factor is the chemical interactions like H-migration reactions, etc., if the chemical interaction between the filler and the XLPE matrix can destroy the bonds in XLPE that leads to the destabilization of XLPE matrix.

Song et al. [50] studied the role of functionalized graphene for preventing electrical treeing and degradation of XLPE matrix. The investigation is carried out via density-functional theory (DFT) calculations with Perdew–Burke–Ernzerhof (PBE) functional in Vienna Ab initio Simulation Package (VASP). The DFT-D2 approach was performed to calculate approximately the van der Waals interaction and energy calculations. Bader charge analysis provides work for the quantitative depiction of the charge distribution. They analyzed the nanofillers of pristine, doped and defect graphene, and they are graphene (G), graphene oxide (GO), doped graphene oxide, single valency graphene (SVG), doped single valency graphene (SVG) and doped single valency graphene oxide (SVGGO). The atoms like boron (B), nitrogen (N), silicon (Si) and phosphorus (P) are used for doping in graphene. Using the Bader charge analysis, all the nanofillers can effectively capture the electrons and resist the degradation of XLPE due to the attack of these electrons. The doped SVGGO, GO and N-doped SVG have a strong physical interaction with XLPE matrix, which restrict the mobility of the XLPE chain and hence restrict the H-migrations. This restriction in mobility leads to a weak chemical activity and prevent C–C and C–H bond cleavage. Hence, these are promising voltage stabilizer additives in power insulation cables. The adsorption ability to XLPE matrix of the nanofillers increases $G < GO < \text{doped GO} < \text{SVG} < \text{doped SVG}$, out of which N-doped SVG is the strongest interaction. By all these analyses, N-doped SVG is the best candidate for resisting the degradation of XLPE matrix in power cable insulation. N-doped SVG has strong ability to hinder the H-migration reaction with reaction energies (more than 1.15 eV), strongest adsorption capability to XLPE (−0.49 eV) and relatively high barriers (more than 1.63 eV) but SVG is the weakest candidate for this purpose.

Li et al. [47] predicted that black carbon (BC) and branched BC would possess the highest EA (1.40 eV for BC and 2.28 eV for branched BC) which suggest it as most promising filler for insulation in power cables. The high EA means higher

ability to trap electrons. Using MD calculation, branched BC exhibited the highest stability without bond cleavage (C–C or C–H), and Mulliken charge analysis shows the electron trapping is high in branched BC and well protects XLPE through trapping the electron. Hence, branched BC can be regarded as a potentially novel insulation material in high-voltage cables to reduce dielectric breakdown strength.

Zhang et al. do QM/MD calculation in SiO₂/XLPE nanocomposites. They conducted the computational calculations using self-consistent-charge density-functional tight-binding (SCC-DFTB) method in DFTB + program [51]. The highest EA identified in SiO₂ has been efficient for trapping the electron and prevents the C–C bond cleavage which further leads to the initiation of electrical treeing growth. Besides, Si and O atoms in the SiO₂ will interact with H of the polymer chain and reduce the mobility of the chain, which further restricts the chemical interactions.

Similarly, the role of α SiO₂-nanosized fillers used as a voltage stabilizer analyzed by Zheng et al. using the DFT method with PBE functional in VASP software package [52]. Analysis of different α -SiO₂ models like hydroxylated (H-SiO₂), reconstructed (R-SiO₂), doped SiO₂ (with B and N; B-SiO₂ and N-SiO₂) and oxygen vacancy surface structures. Two types of oxygen vacancy defect models are considered, one model by removing an oxygen atom from the top layer (E-SiO₂) and another is connecting two SiO₂ tetrahedrons on the lower layer (V-SiO₂). All the models restrict the polymer chain movement and strongly bind with physical interaction using van der Waals forces. Using Bader charge analysis reveals that all the models can effectively capture the electrons but incomplete hydroxylation in H-SiO₂, B-SiO₂ and E-SiO₂ undergoes chemical interaction with the XLPE matrix by H-migration and initiates the growth of electrical treeing but hydrated H-SiO₂, N-SiO₂ and V-SiO₂ are chemically stable. Besides hydrated H-SiO₂, N-SiO₂ and V-SiO₂, they have high adsorption energy too. Hence, completely hydrated H-SiO₂, N-SiO₂ and V-SiO₂ are a promising candidate as a voltage stabilizer in power cable insulation.

Like α -SiO₂ systems, Zhang et al. studied interaction of silicon carbide (SiC) systems with XLPE matrix for cable insulation [53]. They considered SiC systems like cubic (3C β -SiC), hexagonal (4H α -SiC) and rhombohedral (6H α -SiC), whose analysis is done using DFT calculation with PBE functional in VASP software package. Their studies mainly focus on the aging resistance of XLPE with help of SiC nanofillers and to understand its mechanism. Using Bader charge analysis, all the suggested models are capable of trapping the electrons and reduce the space charge accumulation. This suppression in the accumulation of space charges is due to the unsaturated electronic structure and magnetism of SiC, the Si or C-terminated surface. Also, these additives show a strong physical interaction with XLPE matrix, and this leads to a limit in the mobility of the polymer chain. The chemical interactions find that all models have high activation energy; hence, H-migration is reduced and protects XLPE matrix from aging.

An interesting study on XLPE composites are done by Li et al. [54] in which they analysed the effect of polyaromatic compounds (PAC) like 4,4'-difluorobenzophenone, 4,4'-dihydroxybenzophenone and 4,4'-bis(dimethylamino)benzyl

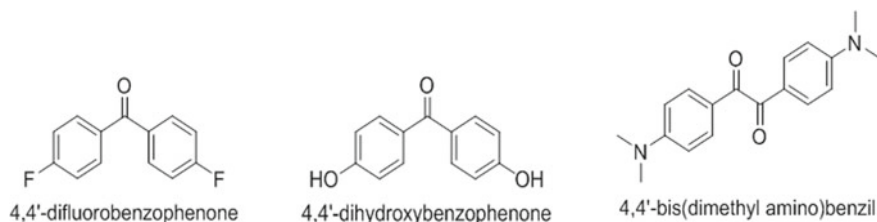


Fig. 6 Polyaromatic compound used in XLPE composites as voltage stabilizers

(Fig. 6) in the XLPE composites. The whole calculation is done in Gaussian 09 software using DFT-B3LYP/6–31G level of theory in which the 4,4'-bis(dimethylamino)benzil has high EA (1.8 eV) with the ability of deep traps of electrons which leads to the ability to suppress the space charge accumulation. Hence, it is a promising voltage stabilizer for power cable insulation.

To obtain a clear and an important information at atomic level of XLPE is very difficult through experimental investigations, in this point the importance of molecular chemistry. The above discussed computational studies of XLPE materials are of less sources due to the limited studies in this area. The results obtained from those studies can implement on experimental researches. For example, Zheng et al. predicted that the N-SiO₂-based filler can reduce the electrical treeing due to the chemical stability this can be practically incorporate to XLPE to the get a better reinforced material. All the quantum mechanical computational process of XLPE materials which are conducted by using DFT-hybrid-B3LYP level of theory gives a better agreement to the experimental results, even though self interaction errors (SIE) of DFT are reported. Hence, molecular modeling is a complementary tool for the XLPE experimental researches.

6 Conclusion and Outlook

The important application of XLPE nanocomposites or blends is the power cable insulation but space charge accumulation is the major problem facing in this field. This accumulation is the major factor for the early aging of the material. Computational studies are a promising tool for studies of structure–property relationship. This chapter discusses computational studies of XLPE nanocomposites and blends using the classical mechanical, quantum mechanical and its hybrid techniques in detail. Due to the popularity of XLPE materials as insulation material for the power cables, the major part of the computational studies is based on these applications. Modeling of new material investigation of new voltage stabilizers is included in those studies. Such studies based on the blends help to understand the role of the inserted polymer in the inhibition of the electrical treeing growth and illustrate the mechanism. For nanocomposites, computational studies offer a

promising ideology for designing and selecting the filler for power cable insulation. Exploration of XLPE nanocomposites or blends structure–property relationship studies using computation is very limited, and only a handful of such calculations are reported. The results obtained from hybrid QM/MM theory are in agreement with the experimental values. The combination of experimental and theoretical studies can make wonders in the research of XLPE nanocomposites and blends a promising material for various potential applications.

References

1. Thomas J, Joseph B, Jose JP et al (2019) Recent Advances in Cross-linked Polyethylene-based Nanocomposites for High Voltage Engineering Applications: A Critical Review. *Ind Eng Chem Res* 58:20863–20879
2. Hu CY, Yoon TR (2018) Recent updates for biomaterials used in total hip arthroplasty. *Biomater Res* 22:1–12. <https://doi.org/10.1186/s40824-018-0144-8>
3. Bachrach SM (2006) *Computational Organic Chemistry*. Wiley, Hoboken, NJ, USA
4. Morin D (2008) *Introduction to Classical Mechanics With Problems and Solutions*
5. Lowe JP, Peterson KA (2006) *Quantum chemistry*. Elsevier Academic Press
6. Lewars EG, Lewars EG (2011) *An Outline of What Computational Chemistry Is All About. Computational Chemistry*. Springer, Cham, pp 1–7
7. Altona C, Faber DH (2007) *Empirical force field calculations. Dynamic Chemistry*. Springer, Berlin, Heidelberg, pp 1–38
8. Kettering CF, Shutts LW, Andrews DH (1930) A representation of the dynamic properties of molecules by mechanical models. *Phys Rev* 36:531–543. <https://doi.org/10.1103/PhysRev.36.531>
9. Westheimer FH, Shookhoff MW (1940) The Electrostatic Influence of Substituents on Reactions Rates. I. *J Am Chem Soc* 62:269–275. <https://doi.org/10.1021/ja01859a009>
10. Hendrickson JB (1961) Molecular geometry. I. Machine computation of the common rings. *J American Chem Soc* 83(22):4537–4547
11. Wiberg KB (1965) A Scheme for Strain Energy Minimization. Application to the Cycloalkanes I
12. Allinger NL (1976) Calculation of Molecular Structure and Energy by Force-Field Methods. *Adv Phys Org Chem* 13:1–82. [https://doi.org/10.1016/S0065-3160\(08\)60212-9](https://doi.org/10.1016/S0065-3160(08)60212-9)
13. Wang J, Wolf RM, Caldwell JW et al (2004) Development and testing of a general Amber force field. *J Comput Chem* 25:1157–1174. <https://doi.org/10.1002/jcc.20035>
14. Mayo SL, Olafson BD, Iii WAG (1990) DREIDING: A Generic Force Field for Molecular Simulations. BioDesign, Inc
15. Allinger NL, Yuh YH, Lii J-H (1976) The Consistent Force Field. American Chemical Society
16. Field MJ, Bash PA, Karplus M (1990) A combined quantum mechanical and molecular mechanical potential for molecular dynamics simulations. *J Comput Chem* 11:700–733. <https://doi.org/10.1002/jcc.540110605>
17. Berendsen HJC, Van Der Spoel D, Van Drunen R (1995) GROMACS: A message-passing parallel molecular dynamics implementation PROGRAM SUMMARY Title of program: GROMACS version 1.0
18. Halgren TA (1996) Merck molecular force field. I. Basis, form, scope, parameterization, and performance of MMFF94. *J Comput Chem* 17:490–519. [https://doi.org/10.1002/\(SICI\)1096-987X\(199604\)17:5/6%3c490:AID-JCC1%3e3.0.CO;2-P](https://doi.org/10.1002/(SICI)1096-987X(199604)17:5/6%3c490:AID-JCC1%3e3.0.CO;2-P)

19. Sun H (1998) The COMPASS force field: Parameterization and validation for phosphazenes. *Comput Theor Polym Sci* 8:229–246. [https://doi.org/10.1016/S1089-3156\(98\)00042-7](https://doi.org/10.1016/S1089-3156(98)00042-7)
20. Damm W, Frontera A, Tirado-Rives J, Jorgensen WL (1997) OPLS all-atom force field for carbohydrates. *J Comput Chem* 18:1955–1970. [https://doi.org/10.1002/\(SICI\)1096-987X\(199712\)18:16%3c1955:AID-JCC1%3e3.0.CO;2-L](https://doi.org/10.1002/(SICI)1096-987X(199712)18:16%3c1955:AID-JCC1%3e3.0.CO;2-L)
21. Ponder J (2015) TINKER v6. 3, 2014
22. Phillips JC, Braun R, Wang W et al (2005) Scalable molecular dynamics with NAMD. *J Comput Chem* 26:1781–1802
23. Alder BJ, Wainwright TE (1959) Studies in molecular dynamics. I. General method. *J Chem Phys* 31:459–466. <https://doi.org/10.1063/1.1730376>
24. Fitzgerald G, DeJoannis J, Meunier M (2015) Multiscale modeling of nanomaterials: Recent developments and future prospects. Elsevier
25. Binder K, Heermann D, Roelofs L et al (1993) Monte Carlo Simulation in Statistical Physics. *Comput Phys* 7:156. <https://doi.org/10.1063/1.4823159>
26. Dong K, Liu X, Dong H et al (2017) Multiscale Studies on Ionic Liquids. *Chem Rev* 117:6636–6695. <https://doi.org/10.1021/acs.chemrev.6b00776>
27. Marrink SJ, Risselada HJ, Yefimov S et al (2007) The MARTINI force field: Coarse grained model for biomolecular simulations. *J Phys Chem B* 111:7812–7824. <https://doi.org/10.1021/jp071097f>
28. Monticelli L, Kandasamy SK, Periole X et al (2008) The MARTINI coarse-grained force field: Extension to proteins. *J Chem Theory Comput* 4:819–834. <https://doi.org/10.1021/ct700324x>
29. Shinoda W, DeVane R, Klein ML (2007) Multi-property fitting and parameterization of a coarse grained model for aqueous surfactants. *Mol Simul* 33:27–36. <https://doi.org/10.1080/08927020601054050>
30. Shinoda W, Devane R, Klein ML (2008) Coarse-grained molecular modeling of non-ionic surfactant self-assembly. *Soft Matter* 4:2454–2462. <https://doi.org/10.1039/b808701f>
31. Senn HM, Thiel W (2009) QM/MM methods for biomolecular systems. *Angew Chemie—Int Ed* 48:1198–1229
32. Warshel A, Levitt M (1976) Theoretical studies of enzymic reactions: Dielectric, electrostatic and steric stabilization of the carbonium ion in the reaction of lysozyme. *J Mol Biol* 103:227–249. [https://doi.org/10.1016/0022-2836\(76\)90311-9](https://doi.org/10.1016/0022-2836(76)90311-9)
33. Sherwood P, De Vries AH, Guest MF et al (2003) QUASI: A general purpose implementation of the QM/MM approach and its application to problems in catalysis. *J Mol Struct THEOCHEM* 632:1–28. [https://doi.org/10.1016/s0166-1280\(03\)00285-9](https://doi.org/10.1016/s0166-1280(03)00285-9)
34. Svensson M, Humbel S, Froese RDJ et al (1996) ONIOM: A multilayered integrated MO + MM method for geometry optimizations and single point energy predictions. A test for Diels–Alder reactions and Pt(P(t-Bu)₃)₂ + H₂ oxidative addition. *J Phys Chem* 100:19357–19363. <https://doi.org/10.1021/jp962071j>
35. Maseras F, Morokuma K (1995) IMOMM: A new integrated ab initio + molecular mechanics geometry optimization scheme of equilibrium structures and transition states. *J Comput Chem* 16:1170–1179. <https://doi.org/10.1002/jcc.540160911>
36. Dong K, Liu X, Dong H et al (2015) A new QM/MM method oriented to the study of ionic liquids. *J Comput Chem* 36:1893–1901. <https://doi.org/10.1002/jcc.24023>
37. Eichler U, Kölmel CM, Sauer J (1997) Combining ab initio techniques with analytical potential functions for structure predictions of large systems: Method and application to crystalline silica polymorphs. *J Comput Chem* 18:463–477. [https://doi.org/10.1002/\(SICI\)1096-987X\(199703\)18:4%3c463:AID-JCC2%3e3.0.CO;2-R](https://doi.org/10.1002/(SICI)1096-987X(199703)18:4%3c463:AID-JCC2%3e3.0.CO;2-R)
38. Sherwood P, De Vries AH, Collins SJ et al (1997) Computer simulation of zeolite structure and reactivity using embedded cluster methods. *Faraday Discuss* 106:79–92. <https://doi.org/10.1039/a701790a>
39. Théry V, Rinaldi D, Rivail J-L et al (1994) Quantum mechanical computations on very large molecular systems: The local self-consistent field method. *J Comput Chem* 15:269–282. <https://doi.org/10.1002/jcc.540150303>

40. Gao J, Amara P, Alhambra C, Field MJ (1998) A generalized hybrid orbital (GHO) method for the treatment of boundary atoms in combined QM/MM calculations. *J Phys Chem A* 102:4714–4721. <https://doi.org/10.1021/jp9809890>
41. Thiel W (2009) QM/MM Methodology: Fundamentals, Scope, and Limitations. *Multiscale Simul Methods Mol Sci* 42:203–214
42. Process C, Zhang H, Shang Y, et al (2018) Theoretical Study on the Grafting Reaction of Maleimide to Polyethylene in the UV Radiation. <https://doi.org/10.3390/polym10091044>
43. Uehara H, Iwata S, Sekii Y, et al (2018) Suppression of electrical tree initiation by antioxidant and ultraviolet absorber, using a density-functional study. *Annu Rep - Conf Electr Insul Dielectr Phenomena, CEIDP 2017:761–764*. <https://doi.org/10.1109/CEIDP.2017.8257509>
44. Zhang H, Shang Y, Zhao H et al (2017) Theoretical study on the reaction of maleic anhydride in the UV radiation cross-linking process of polyethylene. *Polymer (Guildf)*. <https://doi.org/10.1016/j.polymer.2017.11.045>
45. Wang Y, Zhang H, Zhao H, et al (2018) Theoretical study on the grafting reaction of maleimide and its derivatives to polyethylene in the UV radiation cross-linking process
46. Zhao H, Chen J, Zhang H (2017) Theoretical study on the reaction of triallyl isocyanurate in the UV radiation cross-linking of polyethylene. *RSC Adv* 7:37095–37104. <https://doi.org/10.1039/C7RA05535H>
47. Li C, Zhao H, Zhang H et al (2018) The role of inserted polymers in polymeric insulation materials: insights from QM/MD simulations. *J Mol Model* 24:1–11. <https://doi.org/10.1007/s00894-018-3618-7>
48. Wang W, Li S, Tanaka Y, Takada T (2019) Interfacial charge dynamics of cross-linked polyethylene/ethylene-propylene-diene dual dielectric polymer as revealed by energy band structure. *IEEE Trans Dielectr Electr Insul* 26:1755–1762. <https://doi.org/10.1109/TDEI.2019.008122>
49. Chen X, Yu L, Dai C et al (2019) Enhancement of insulating properties of polyethylene blends by delocalization type voltage stabilizers. *IEEE Trans Dielectr Electr Insul* 26:2041–2049. <https://doi.org/10.1109/TDEI.2019.008337>
50. Song S, Zhao H, Zheng X et al (2018) A density functional theory study of the role of functionalized graphene particles as effective additives in power cable insulation. *R Soc Open Sci* 5:170772. <https://doi.org/10.1098/rsos.170772>
51. Han B, Jiao M, Li C et al (2015) QM/MD simulations on the role of SiO₂ in polymeric insulation materials. *RSC Adv* 6:555–562. <https://doi.org/10.1039/c5ra19512h>
52. Zheng X, Liu Y, Wang Y (2018) Electrical tree inhibition by SiO₂/XLPE nanocomposites: insights from first-principles calculations. *J Mol Model* 24:1–10. <https://doi.org/10.1007/s00894-018-3742-4>
53. Zhang H, Liu Y, Du X et al (2019) Effect of SiC nano-size fillers on the aging resistance of XLPE insulation: A first-principles study. *J Mol Graph Model* 93:107438. <https://doi.org/10.1016/j.jmgm.2019.107438>
54. Li J, Han C, Du B, Takada T (2020) Deep trap sites suppressing space charge injection in polycyclic aromatic compounds doped XLPE composite. *IET Nanodielectrics* 3:10–13. <https://doi.org/10.1049/iet-nde.2019.0035>

Chapter 12

XLPE-Based Products Available in the Market and Their Applications



Detlef Wald and Harry Orton

1 Background

Prior to the adoption of polymer-based insulation products, the dominant cable insulation material used in power cables was an impregnated fluid Kraft paper composite insulation encased in a lead sheath. Although this cable design provided excellent in-service life, it is slowly being replaced by polymers for the following reasons:

- Environmental concerns with the lead sheaths used on fluid impregnated paper insulated cables,
- Reduced maintenance costs for polymer-insulated cables dielectric insulation,
- Loss of expertise required for installing fluid-impregnated paper-insulated cables,
- Reduced installation costs for polymeric-insulated cables,
- No fluid leaks to locate and repair,
- Weight reduction (no lead sheath required), allowing for the installation of longer cable lengths,
- Reduced risk of fire during earthquakes,
- Reduced dielectric losses [1].

From an historical perspective, the following timeline details the introduction of polymers as a power cable insulation material.

D. Wald
Eifelkabel, Rebenhugelweg 8, 5612 Villmergen, Switzerland
e-mail: d.wald@ieee.org

H. Orton (✉)
OCEI, Metropolitan PO, Box 38715, North Vancouver, BC V7M 3N1, Canada
e-mail: h.orton@ieee.org

- 1812 First power cables used to detonate mineral ores in Russia.
- 1880 DC cables insulated with jute in “Street Pipes”—Thomas Edison (USA).
- 1882 Thomas Edison used rubber-insulated cables on Pearl Street in New York.
- 1890 Ferranti developed the concentric construction for cables.
- 1900 Cables insulated with natural rubber.
- 1917 First screened cables.
- 1925 The first pressurized paper cables.
- 1925 Rubber-insulated cables could support voltages up to 7500 Volts.
- 1903 PVC first used in Germany.
- 1933 A natural rubber alternative was discovered in Germany by IG Farben.
- 1937 Polyethylene developed.
- 1942 First use of Polyethylene (PE) in cables.
- 1944 Butyl rubber was commercialized by Standard Oil.
- 1954 First DC power transmission cable—Gotland (Sweden) subsea connection.
- 1955 Ethylene propylene rubber (EPR) was developed.
- 1962 EPR insulated power cables commercially available.
- 1963 Invention of cross-linked polyethylene—XLPE.
- 1967 Use of HMWPE insulation on UG cables in the US (Unjacketed with tape shields).
- 1968 First use of XLPE cables for MV (mostly unjacketed, tape shields).
- 1972 Problems associated with water trees (MV) and contaminants (HV) first identified in unjacketed HMWPE and XLPE cables.
- 1972 Introduction of extruded semi-conductive screens.
- 1973 Superclean materials used for 84 kV Aland (Sweden–Finland) XLPE subsea cable.
- 1978 Widespread use of polymeric jackets in North America.
- 1982 Water Tree Retarding insulating materials introduced for MV in USA and Germany.
- 1988 First use of XLPE cables (without joints) at 500 kV within a pump storage scheme in Japan.
- 1989 Supersmooth conductor shields introduced for MV cable in North America.
- 1990 Widespread use of water tree retarding insulating materials in Belgium, Canada, Germany, Switzerland, and USA.
- 1993 and 1997 Long-term 400 kV qualification tests at CESI Italy for BEWAG Berlin (Germany) and Copenhagen (Denmark) projects.
- 1999 World’s first commercial DC cable using XLPE—Gotland (Sweden) 80 kV.

2000	First 500 kV long distance XLPE cable with joints installed in Tokyo (Japan).
2001	World's highest voltage ac XLPE cable – Dachaoshan Power Stn. (China); 525 kV.
2002	Murraylink (Australia) ± 150 kV HVDC 171 km
2018	First HVDC XLPE submarine at 400 kV HVDC—Nemo, Belgium to UK, 130 km.

A detailed overview of the early developments is provided by RM Black in “The History of Electric Wires and Cables” [2].

Today power cables use primarily solid-extruded insulation compounds of polyethylene in its cross-linked form. Thermoplastic polyethylene was first used, but quickly evolved into longer lasting cross-linked materials. In North America, high molecular weight polyethylene (HMWPE) was also used with poor results. For medium voltage cables, either cross-linked polyethylene (XLPE), ethylene propylene rubber (EPR), or polypropylene (PP) are used as insulation for medium voltage cables. For high and extra high voltage cables, mainly XLPE is used.

This chapter describes the commercially available XLPE compounds and the differences that exist in these compounds.

Most of the XLPE compounds that are used today are based on high pressure tubular reactor low density polyethylene (LDPE). This process maximizes the chance of producing clean compounds, one of the many requirements for power cable insulation compounds. On the other hand, EPR is produced in a different way and then compounded as cable insulation. EPR is mainly used for medium voltage cables and HV cables up to a maximum of 150 kV due to higher dielectric losses.

At the beginning of this century, polypropylene (PP) was introduced as an insulation compound for medium voltage cables and has recently seen equal market share with XLPE in several countries. With PP, the final formulation is produced during the cable production process. Further investigations are currently underway using other polymers such as polyolefin (POE) or polybutylene (PB-1) for medium voltage applications. PP is currently used up to 150 kV for AC cables and has passed Type and Prequalification (PQ) testing for 600 kV DC cables.

This chapter presents the differences between cable compounds and examines the specific features of individual XLPE compounds that are currently available on the market. In addition, details will be presented on the application of different polymers that are currently used for the semi-conductive layers as part of the cable insulation system.

After the discovery of water trees in the 1970s, more stringent requirements for the insulation were introduced, for example, cleanliness of the insulation must be at a certain level to avoid initiation of water trees. Furthermore, it should be highlighted that some of the properties of polyethylene may vary within commercially available materials. Also, some reflections on the inherent variability of a material that is produced in production campaigns of many thousands of tonnes will be discussed. This chapter will also go into more detail on commonly used cross-linked polyethylene (XLPE), which is the main material used for power cable

applications [3]. Moreover, it should be noted that cables insulated with EPR can have water trees, only the detection is more difficult than for XLPE-insulated cables.

The differences that exist will be described in commercially produced polyethylene, specifically high-pressure, low density polyethylene (LDPE), since this is most commonly used in power cable applications as the base resin. The basic “surprise” is that LDPE, even if it is called hydrocarbon, contains not just these two basic atoms, hydrogen and carbon. A basic knowledge of the production process reveals that oxygen might be added into the hydrocarbon chain. Indeed oxygen may have a significant influence on the electrical properties and in this case not just “oxidized particles” which are generated later during the production process. This oxygen might come from the chain transfer agent or the initiators that are used when producing LDPE in the reactor.

Insulations for cables, unlike almost all other polymer components are required to have a very long operational life (>50 years) and are installed in complex locations which make their replacement very problematic. Thus, as a consequence of the need for longevity, the different antioxidants used will also influence the overall properties of the cable insulation. They will additionally influence the decomposition of the peroxide that is used for cross-linking of polyethylene. The chemistry of the peroxide needs to be examined further.

2 Production of XLPE

XLPE is a compound where peroxide, antioxidant and maybe other additives are added to LDPE. To completely understand the different performances of XLPE it is important to understand the production process for LDPE and the variations that can occur between different manufacturing processes and producers.

2.1 Production of LDPE

First of all, normally only low density polyethylene (LDPE) is used for the insulation of power cables. In some rare cases, medium density polyethylene might be used, but most products are produced by a high pressure process. The catalytic low pressure process is not used to produce polyethylene that is the base material for XLPE. The structure of low density polyethylene is very simple, just an endless combination of C_2H_4 -groups, Fig. 1.

Already, this is not correct, as LDPE is in fact a branched polymer with long-chain and short-chain branching, plus the long chains might be the backbone of another chain (Fig. 2).

The first production of polyethylene by Pechmann only worked because the autoclave was leaking. Oxygen was unknowingly introduced into the process

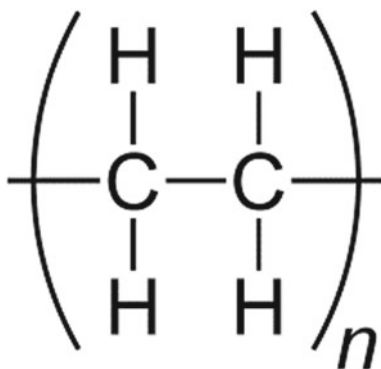


Fig. 1 Theoretical picture of LDPE

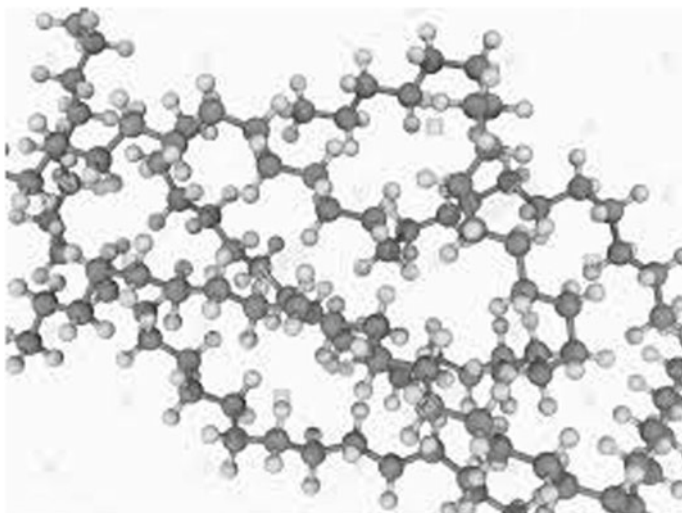


Fig. 2 Branched LDPE

during the production of LDPE where oxygen is needed in addition to carbon and hydrogen. Today, oxygen is introduced either directly or via peroxides. The type of peroxide might vary from producer to producer and with the product produced. This oxygen is incorporated with a low amount into the polyethylene chain. The amount of oxygen in the chain has an influence on the electrical properties such as loss factor and resistance. Simultaneously, a chain transfer agent is added into the reactor. This agent regulates the chain length of the polyethylene and is added into the chain of LDPE [4]. The reactor conditions are up to 2500 bar at 400 °C. LDPE can be produced in a tubular reactor or an autoclave reactor. The first reactor is the preferred method to produce LDPE for XLPE [5].

A low density polyethylene is characterized by the following parameters:

- Melt index at 2.16 kg, 190 °C
- Melt index at 21.6 kg, 190 °C
- Molecular weight distribution
- Melting point
- Short length branching
- Long length branching
- Terminal vinyl
- Vinyliden content.

These parameters are not exclusive.

2.1.1 Influence of the Chain Transfer Agent

In the polymerization reactor, organic peroxides dissociate homolytically to generate free radicals. Polymerization of ethylene proceeds by a chain reaction. Initiation is achieved by addition of a free radical to ethylene. Propagation proceeds by repeated additions of monomer. Termination may occur by combination (coupling) of radicals or disproportionation reactions. Chain transfer takes place primarily by abstraction of a proton from a monomer or solvent by a macro radical. A low molecular weight hydrocarbon, such as butane, may be used as chain transfer agent to lower molecular weight. Termination reactions illustrated how that the end groups in LDPE are most commonly a vinyl group or an ethyl group. In addition to the use of chain transfer agents, molecular weight may also be varied by adjusting pressure and temperature. Higher pressures lead to higher molecular weight. Branching tends to increase at higher temperatures. Reactivity ratios are important in determining reactor “feed” composition of ethylene and co-monomer required to produce a copolymer with the target co-monomer content. Because the relative proportion of co-monomer changes as polymerization proceeds, adjustment of co-monomer feed with time may be necessary [6].

During the polymerization of ethylene, different types of chain transfer agents (CTA) like alkanes, α -Olefinens, or ketones are used. Figures 3 and 4 show the influence of commercially used CTAs on the loss factor of cross-linked polyethylene with a common antioxidant (AO 1) for this process. The loss factor has been measured at a low stress level with a Schering Bridge using a low electrical field and a pressed plaque as the test specimen. On a tested cable, the loss factor can be significantly higher depending on an increased electrical field. The influence of antioxidants on the electrical properties will be explained.

Depending on the process and the producer, the amount of CTA could vary. Figure 3 shows the influence of the amount of CTA on the loss factor. As mentioned earlier, this influence could increase with a high electrical field. Certain types of CTA will create a polyethylene that is not suitable for cable applications.

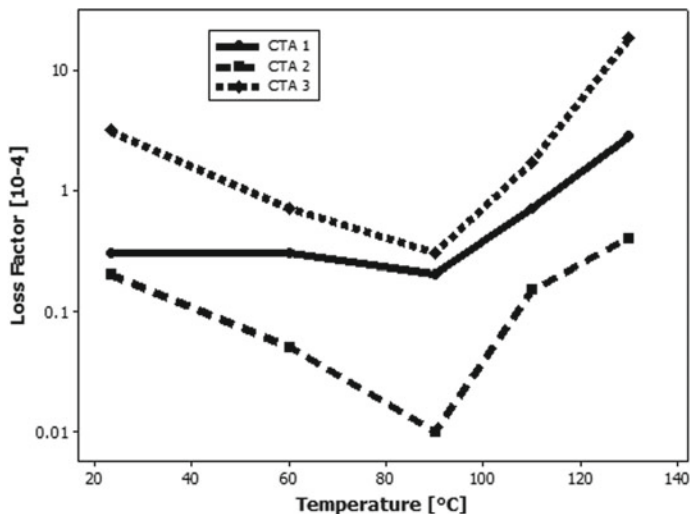


Fig. 3 Loss factor depending on the type of CTA used [1]

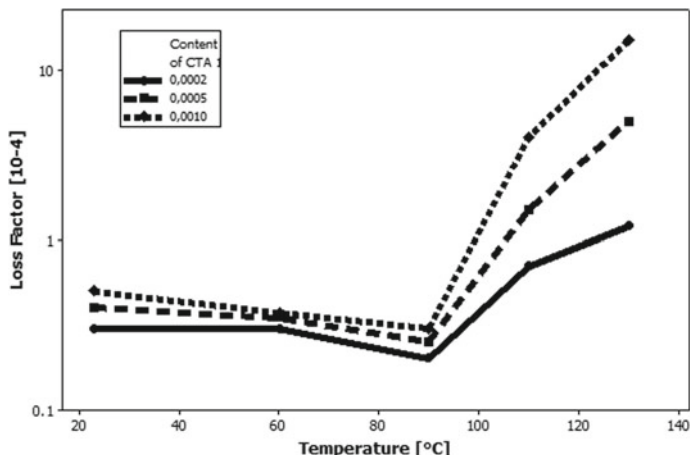


Fig. 4 Loss factor depending on the temperature and amount of chain transfer-agent CTA 2 [7]

In a recent study by Fothergill et al., the influence of the CTA on the electrical resistivity was demonstrated [7]. It was mentioned in this study that decomposition products of peroxide will increase the differences between these two polymers. Additionally, if the use of different types of peroxides is taken into the equation, only variation estimates can be achieved from this test.

During the last years, dienes have also been used as CTA [7, 8] to increase the reactivity of the polyethylene. The use of these dienes has much increased the

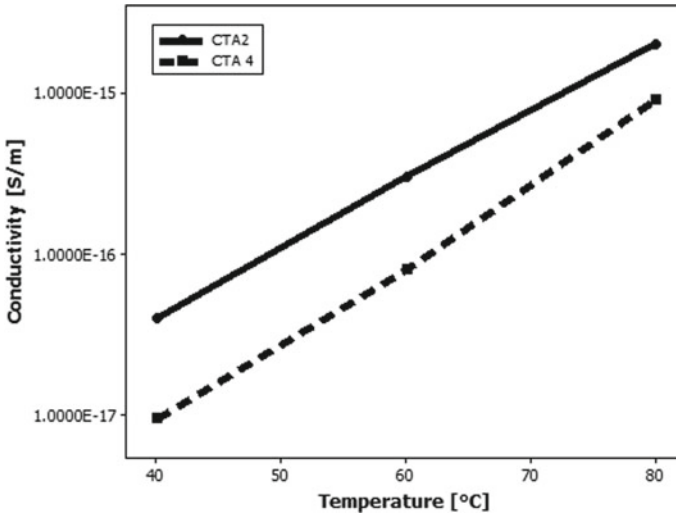


Fig. 5 Conductivity depending on the type of CTA [7]

reactivity of the polyethylene with peroxide. The total influence of the CTA on the properties of XLPE has not completely been studied and care should be taken if we transfer older knowledge to this cross-linking process since it is not a first order chemical reaction anymore. The dependence of conductivity on the type of CTA is shown in Fig. 5.

2.2 Cross-Linked Polyethylene

2.2.1 Cross-Linking Process

After this short introduction on polyethylene, it is now important to look more into the cross-linked polyethylene (XLPE) which is commonly used as an insulation material in the power cable industry. The different processes of cross-linking will not be discussed since this would go too far. Instead the focus will be on the peroxide cross-linking process since this is the predominant process in the industry. The chemical structure picture of cross-linked polyethylene normally given in the literature is very simplistic. However, recent studies by Smedberg et al. have shown that this picture is not correct and XLPE looks more like a spider web with different types of cross-linking points [10]. It was demonstrated in this research that besides chemical cross-linking, there are also physical cross-links that are nearly equally as strong and both influence the structure of the cross-linked polyethylene. A knowledge of the amorphous and crystalline structures will help to understand what is happening with these structures during the cross-linking process and manufacture of the cable.

2.2.2 Influence of Peroxide and Antioxidant

Polyethylene and especially cross-linked polyethylene are never used without peroxide and antioxidants. The choice of these additives will influence the morphology of the insulation. So far there have been limited studies done evaluating the influence of different peroxides. This is maybe due to the fact that dicumyl-peroxide is normally used as a cross-linking agent. However, several studies have been done evaluating the morphology using different antioxidants. The crystallization temperature (T_{cr}) of a pure LDPE was found to be 91.9 °C. This temperature can be influenced by additives like antioxidants. Several combinations of antioxidants were mixed with polyethylene such as:

- 1,1'-Thiobis-(2-methyl-4-hydroxy-5-tert-butyl-methylphenol) (AO1)
- Pentaerythritol-tetrakis-(3-3,5-di-tert-butyl-4-hydroxyphenyl)-propionate (AO2)
- Octadecyl-3-(3,5-di-tert-butyl-4-hydroxyphenyl)-propionate (AO3)
- 4,4-Thio-bis(2-tert-butyl-5-methyl-phenol) (AO4)
- Dioctadecyl 3,3'-thiopropionate (AO5)

There are other antioxidants on the market and in recent years, suppliers have come up with liquid antioxidants. The highest increase of T_{cr} was noted for the samples mixed with AO5 of 97 °C—a noteworthy increase in crystallization [8]. It should be noted that with a classical peroxide cross-linking process, AO1 is grafted to the polymer back-chain during the cross-linking process and therefore does not migrate and stays stable inside the cable during the material life time.

The Influence of Antioxidants

Several different mixtures of antioxidants are used in commercial XLPE formulations. The antioxidants are chosen both for their long-term protection (since cables are designed for a life-time of fifty plus years) and also for the interference or lack of interference in the cross-linking process. Several antioxidants are also used in combination. The influence of these antioxidants on the properties of XLPE have been evaluated in many studies with some highlighted here. Campus et al. demonstrated that a LDPE with methyl-ethyl-ketone (MEK) or Butanon-1 as chain transfer agent has large fully rounded spherulites which are present only in LDPE base resins without additives. Antioxidants like AO1 will influence these structures [9]. The advantage of this antioxidant is that it is grafted during the cross-linking process at the polyethylene backbone and therefore cannot be removed by solvents or other physical processes [10]. In a study by Fukunaga [11] the influence of different antioxidants on the crystallinity and conductivity of polyethylene was evaluated. The polyethylene used was produced in a tube reactor with propane as the CTA. This used AO5 together with a phenolic antioxidant AO2 and showed that the conductivity was dependent on the concentration and type of antioxidants.

The choice of a good antioxidant is very important since it not only influences the ageing behaviour of the cable but also the electrical properties in dry and wet conditions. The antioxidant should also stay within the cable over the total life time of 50 years (plus) and not exudate.

Campus, et al., confirmed [10] that the cross-linked segments of XLPE are situated in the amorphous phase and therefore do not modify the crystalline structure on the level of the elementary cells. They also confirmed that with (AO4), the crystallinity decreases from 48% to 45% for this particular LDPE [12]. The electrical properties like tree inception voltage were studied by Kjellqvist et al. [13]. He used as a base polymer a polyethylene that had been produced on a tubular reactor. More details about the polymer were not revealed in this study. However, he mixed several different antioxidants and combinations and their influence on the tree inception voltage compared to a virgin polymer. It is worthwhile to mention that this, as previously expressed, only one of the parameters for how to choose the additives.

The Influence of Peroxide and Cross-Linking Parameters

For low and medium voltage peroxide cross-linkable materials, silane cross-linking is utilized as well as radiation and UV cross-linking for low voltage materials. Dicumyl-peroxide is commonly used for insulation compounds, as this is a solid peroxide with a melting point of around 40 °C. It is melted and added via a so-called soaking process to the insulation compound (Figs. 6, 7, and 8).

Also in certain cases, liquid peroxide can be used at room temperature.

This peroxide has a melting point of 10 °C and can therefore be handled by pumps without prior melting. However, it also exudes faster and is therefore not

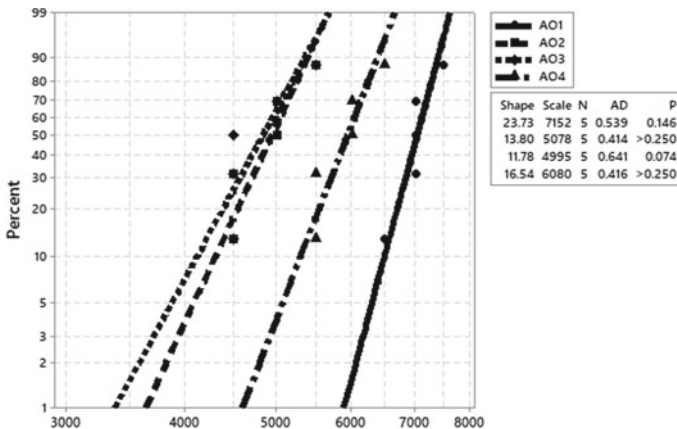


Fig. 6 Tree inception voltage depending on antioxidant type

Fig. 7 Structure of dicumyl-peroxide

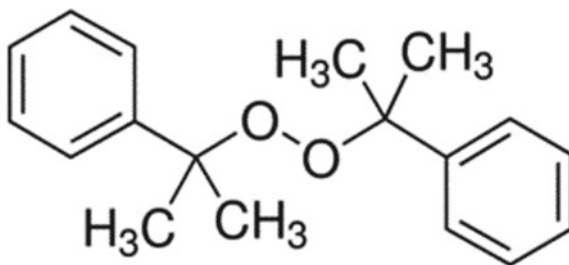
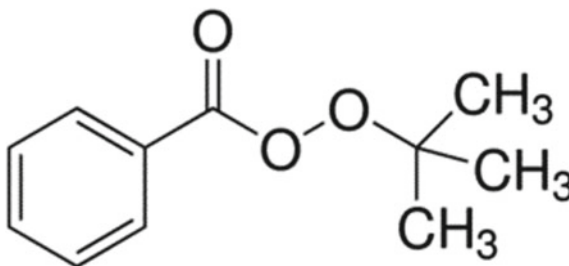


Fig. 8 Structure of tert Butyl-benzyl-peroxide



recommended for compounds that need to be stored or transported. Another peroxide is used for semi-conductive compounds; Bis(1-tert-butyl-dioxy-1-methylethyl) benzene. This peroxide exists in a meta and a para-form and is also solid at room temperature. It reacts slower than dicumyl-peroxide and is therefore preferred for these compounds to prevent scorch (Fig. 9).

The decomposition products of peroxide and the way they are created are described in several publications [14] and are mainly acetophenone (AP), α -methyl-styrene (MS), cumylalcohol (CA), methane and water. Methane should be removed from the cable for safety reasons [15]. However, the other cross-linking by-products will influence the electrical properties under AC and DC conditions. The creation of acetophenone and cumylalcohol is a competing reaction and,

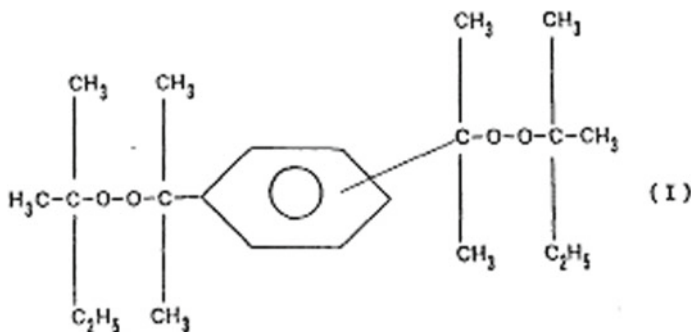


Fig. 9 Structure of 1,4-Bis(1-tert-butyl-dioxy-1-methylethyl) benzene

depending on the cross-linking temperature, one or the other is preferred. Cumylalcohol can further react to form α -methyl-styrene and water [12]. In this study, the amount of chemically created water is dependent on the curing time and temperature. It clearly demonstrates that today's thinking of faster and faster curing times might not be optimal for a good cable, but unfortunately economics are forcing the cable maker to go that way. This study was done on a polymer that was produced on a tubular reactor with CTA 1 and AO1. The amount of water created was calculated by the amount of α -methyl-styrene, since each time there is also a small amount of "other" water inside the polymer.

It is known that acetophenone increases the AC water tree inception voltage, decreases the insulation resistance and increases the space charge after a DC voltage application. In addition, it has recently been pointed out that the dielectric loss factor of PE increases considerably at high temperatures and in high electrical stress regions because of conductivity enhancement, in spite of PE being a non-polar polymer. This study was carried out on a polyethylene with a melt index of 3, produced in a tubular reactor. The authors soaked acetophenone into the polymer and also measured impurities of the added acetophenone. However, it is not clear if any acetophenone created inside the polymer would have had the same effect [14]. This leads to another subject on the influence of curing by-products, which were studied by Aida et al. [16]. This study was performed on an unknown polyethylene and discussed the influence of the by-products. It was demonstrated that during the time when these by-products evaporate, the electrical losses and the electrical resistivity will change. This only measured by-products created when using dicumyl-peroxide.

Hayami et al. evaluated the influence of these by-products on the leakage current under DC stress [17]. He recommended to remove all by-products to reduce the leakage current, but under practical conditions this will not be possible. One might reduce these products to an acceptable level determined by the manufacture and customer. It should be noted that in a real cable a semi-conductive layer will also be present, and in most of the commercial compounds supplied, at least for higher voltages, these compounds have a different peroxide as a cross-linking agent, Bis-(Tert-butyl-dioxyisopropyl) benzene. This peroxide is a bis-peroxide and has, besides methane, completely different reactive by-products to dicumyl-peroxide, which are also far more difficult to remove. These by-products present in lower amounts, will also migrate into the insulation during cross-linking and with further processing of the cable, influence the electrical parameters. In addition, the low molecular weight polar components of the semi-conductive compounds will migrate into the insulation changing the properties of the latter. This was confirmed by a study of Diego, et al. on a medium voltage cable with a strip-able screen [18]. The migration of low molecular weight from the outer and inner semi-conductive layers into the insulation is dependent firstly on the chemical structure of these layers and their molecular weight distribution. The temperature in the cross-linking tube and the time will influence the migration from the outer layer. Additionally, the type of cross-linking tube, whether Vertical Continuous Vulcanizing line (VCV), Catenary Continuous Vulcanizing line (CCV) or Mitsubishi, Dainichi Continuous

Vulcanizing line (MDCV or Long Land Die) has an influence on the stress introduced into the cable and this factor will also influence the electrical properties of a cable.

Choo et al. studied the space charge accumulation under temperature and electric field gradients on a commercial medium voltage cable [19]. Taking into account that the construction of these cables was relatively unknown and that interpreting results for a commercially produced DC cable application, and since the insulation and semi-conductive materials were specially selected for this application, it is recommended to use a non-polar screen with acetylene black for both the inner and outer semi-conductive screens. This was previously described in a patent from the former Alcatel Cable.

Generally, the compounder uses dicumyl-peroxide, which decomposes into several by-products (Table 1). The influence of these by-products themselves is evaluated under several conditions. The ratio of these by-products during the cable production nevertheless depends on the chemical composition of the XLPE itself, the production parameters and the degassing process. It should be noted that these are the by-products only for the peroxide used in the insulation. Generally, in Europe, different peroxides are used in the semi-conductive compounds.

In addition to the above by-products, additional decomposition products may be present from the other peroxides and antioxidants that have been used inside the compounds for power cable insulation.

Table 1 List of peroxide by-products

Chemical name	Percentage (typical), not all substances identified
Ethylbenzene	0.09
Styrene	0.14
Cumene	2.58
Phenol	0.13
α -methylstyrene	23.93
Methylacetophenones	0.52
C12 hydrocarbon	0.67
O-containing aromatic	0.04
C2-styrene	0.18
Acetophenone	45.3
Cumylalcohol	10.6
2-methoxy-2-phenylpropane	0.58
C5 benzyl derivative	0.18
C3 styrene	0.15
C6 benzyl derivative	0.38
Di-isopropenyl acetophenones	1.4
Diacetylbenzene	1.11

2.3 *Compounds for Medium Voltage Cables*

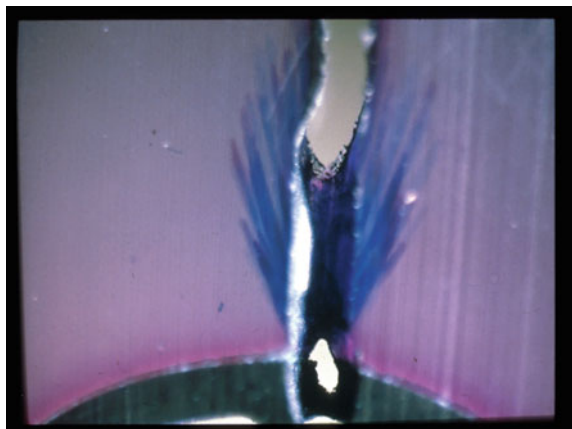
Resistance to water tree growth is very important for medium voltage cables since many of these cables are now produced without water barriers.

2.3.1 Water Treeing

During the early 1970s medium voltage cables were failing at a far too early stage. Intensive research discovered that tree-like dendritic structures were the reason for these failures. Since they were the result of water accumulation, these structures were called water trees. Water trees are small tree-like or dendritic growths that appear in the polymeric insulations of medium voltage power cables. They frequently look like bushes or trees and improved optical microscopy techniques concluded that every water tree is made up of chains of water filled voids, which are alignments of microcavities. Water trees grow during the service life of power cables from defects where the electric field is amplified. The longer the water tree, the more dangerous it becomes, because the insulation breakdown voltage decreases with the increase of the length of water trees. Or in other words, the dielectric strength in the immediate area of a water tree decreases. In Fig. 10, a dielectric failure occurred through a streamer water tree where the dielectric strength was reduced by the presence of the streamer water tree. The failure occurred during an AC withstand test on a full-size MV cable.

Another very important phenomenon in power cables affected by water trees is the conduction process. This is also of great interest for both users and manufacturers of cables because electrical conduction is one of the factors that reveals the level of degradation within the cable. Concerning polymer conductivity, the study of the mechanisms of thermo-electrical degradation of the polyethylene insulation is essential to develop improved assessment strategies.

Fig. 10 Electrical failure through a water tree during AC withstand testing on full-sized MV cable



The creation and growth of water trees can be traced to the following reasons:

1. Dirty compounds, physical and chemical contaminants.
2. Unclean handling of the compounds.
3. Voids or bubbles in the insulation.
4. Graphitised insulation screens.
5. Poor interface between screens and the insulation.
6. One plus two or two plus one extruder cross heads.
7. Steam curing and the resultant orange peel effect as well as an internal water halo.
8. No protection against water migration into the cable core.
9. Pure polyethylene has poor resistance to the growth of water trees.

It should be noted that a water tree alone will not lead to cable breakdown, but it reduces the dielectric strength of the insulation in the immediate area of the water tree. Eventually an electrical tree will initiate and thus a breakdown will occur (Fig. 11). An electrical tree is initiated at a water tree by over-voltages such as switching surges and/or lightning. Water trees in cable insulation can be present for many years without cable failure, but as soon as electrical tree forms, failure can be very quick by comparison. Also, of note, there is no partial discharge when water trees are present and growing, but partial discharge initiates as soon as an electrical tree appears.

Water tree structures are identified as vented trees, which start from the screens, and bow-tie trees which grow inside the insulation (Fig. 12). The reason for vented trees is normally an irregularity inside the screen or the interface of the insulation. For this reason, interfacial smoothness requirements are written into cable specifications along with chemical cleanliness of the screens to avoid ion migration into the insulation. Bow tie trees will grow from a void or contamination inside the insulation. But for water trees to grow, a certain concentration of water is required of 70 phr. Below this level, it will be a “dry” cable. There is always some ppm of water inside a cable, since water is created during the cross-linking process as described earlier.

Water trees in fact consist of an accumulation of water. If cable core wafers are left exposed to air, the water within the water tree will evaporate and the water tree structure will visibly disappear. To make a permanent record of a water tree, a staining method is widely used that often contains methylene blue die. Hence, the blue colour of most examples of water trees. It is very well documented for XLPE and most of their tree retardant variations, but for EPR or polypropylene, other staining agents need to be used, if not an erroneous assumption will be made that there are no water trees present.

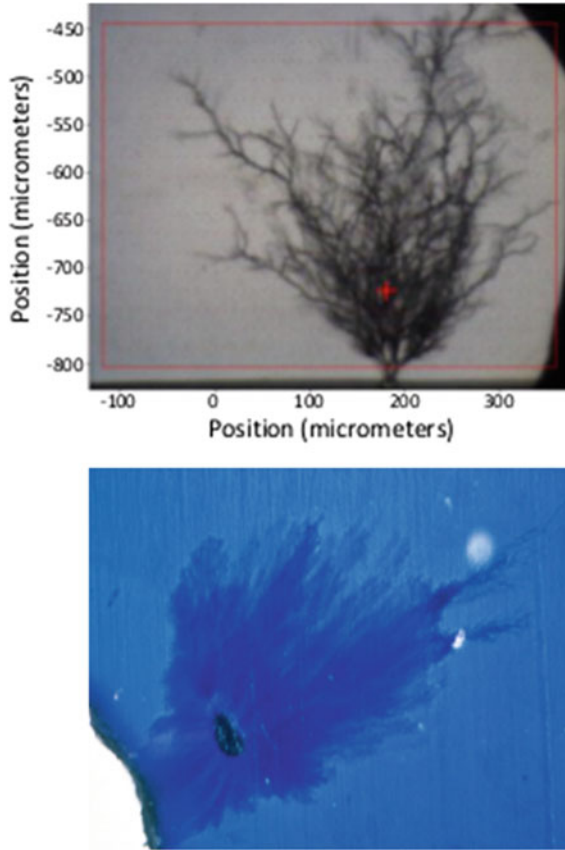


Fig. 11 Electrical tree (above) and an electrical tree initiated from water tree (below)

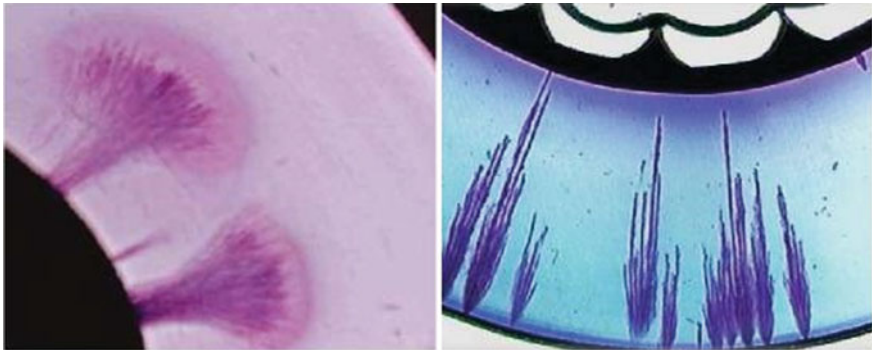


Fig. 12 Vented trees in XLPE [3]

Testing Compounds for the Resistance to Water Tree Growth

Since water trees in field aged cables can only be observed after several years in service, tests were developed to accelerate the growth of water trees. This test program should replicate as close as possible real cable life, but yet achieve this objective in a reasonable time. The most common tests last between one year and two years. There are several tests used in the industry to evaluate compounds, but only two tests on cables are recognized around the world to evaluate the cable performance in wet conditions. It should be emphasised that these tests accelerate the growth of water trees, but yet by changing one of the parameters will give different results. In IEEE Guide 1407, the different parameters are highlighted. The worldwide accepted tests are either according to CENELEC HD 605 protocol or according to ICEA S-97-682. Both tests will give different results. The CENELEC HD 605 protocol utilize two different frequencies, 500 Hz for 3000 h, and 50 Hz for two years.

Recently, CIGRE introduced an additional requirement for wet high voltage cables used in array systems [20]. In this program, the water, that is be used, should have a salt content of between 3.0 and 6.0% plus, the test-program should be carried out following specific requirements. There are also other local tests carried out that should be handled with care. Most of the tests just evaluate the insulation material with the influence of processing and the semi-conductive screens and therefore can only give a restrictive picture of cable performance. Additionally, if the test requirements are too remote from life-time requirements, the real performance of a cable may not be assessed. It has been shown in many tests that an Arrhenius approach, by doubling the frequency or increasing the temperature, or by adding salt content to the test water will only work up to a certain level. Above a certain accelerating factor threshold level the test will evaluate a different behaviour of the materials under a completely different set of conditions. It should be also noted that the staining effect is not as easy as it seems (Table 2).

2.3.2 Cleanliness

As already mentioned, early XLPE compounds were quite dirty, as at the time, there was no appreciation for the need of cleanliness, since water trees were not yet discovered, and contamination issues had not arisen. Moreover, recently, new processes have been used where other peroxides are used making the decomposition products different, so their influence needs to be investigated.

Additionally, tests have been performed using the same compound, once before the material handling was upgraded to a Class 1000 clean room and once again afterwards. Also, the influence of cleanliness on the long-term performance has been demonstrated.

In Fig. 13, a two-year wet ageing test was carried out with a current XLPE compound that does not fulfil the requirements in terms of cleanliness for medium voltage application. Three of the six cables failed during the test at 3 U₀ (Fig. 14).

Table 2 Conditions for water tree tests

Test protocol	CENELEC HD 605		ICEA S97-682	South African
Frequency	49–61 Hz	500 ±10 Hz	49–61 Hz	49–61 Hz
Preconditioning	wet		dry	wet
Temperature	55±5 °C		24 h. Cycle Regime ≥ 130±0.2 °C for ≥ 4 h ≤ 25±5 °C for ≥ 1 h.	
Time	500 h		14 cycles	
Testing conditions				
Voltage	3 U _o			2.5 U _o
Temperature	40 °C			23 °C
Time	3000 h	1 a, 2 a	180, 360 days	1 a, 2 a
Evaluation	Breakdown test with defined pass values		Breakdown test with defined pass values	Breakdown test with defined pass values
	Water tree count			

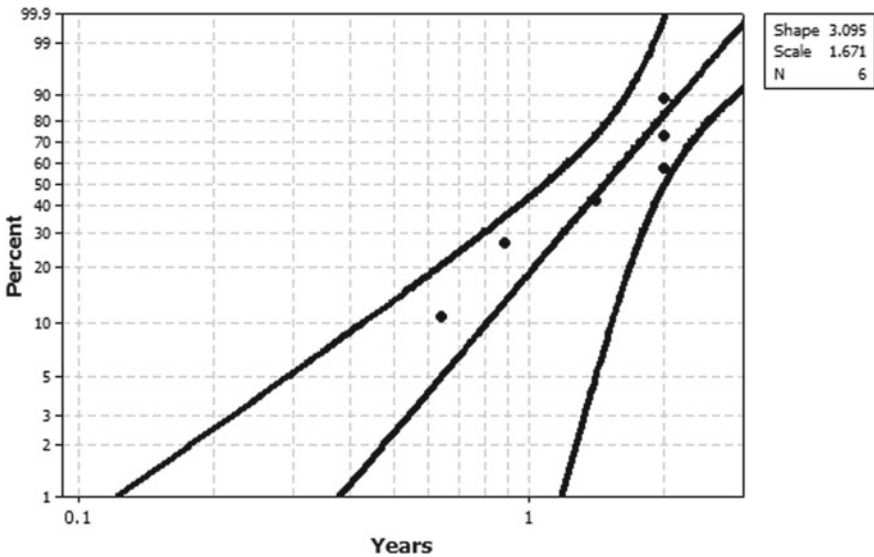


Fig. 13 Influence of cleanliness on the results of a two-year test according to CENELEC HD605

2.3.3 Material Handling

Furthermore, the handling of these compounds, for the program presented in Fig. 13, was done in a non-clean way. For medium voltage applications, it may not be necessary to use a clean room, but clean handling should be one of the

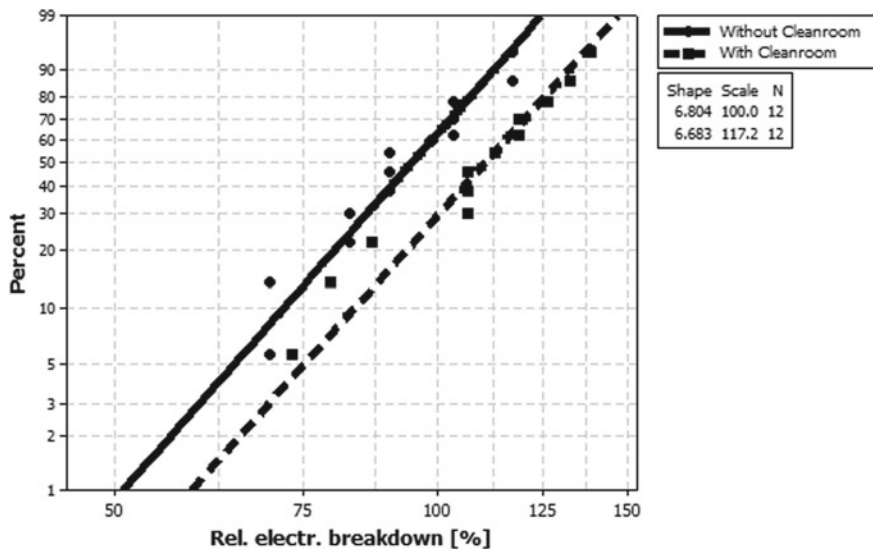


Fig. 14 Influence of cleanliness in material handling on the relative results of a two-year test according to HD605

recommendations that includes a closed feeding system to avoid the introduction of outside contaminations, like dust and insects, for example.

2.3.4 Influence of Extrusion

As mentioned earlier, historically, the first cables were produced either with separate extrusion heads or with a so-called 1 + 2 or 2 + 1 extrusion heads. Here, the inner semi-conductive screen was extruded through a separate head and only the two other layers were extruded with some distance in between. In the worst-case scenario, the hot inner screen was transported through plain air. In Fig. 12, the two-year results of two cables are compared; in one case, the cable was produced using a 2 + 1 extrusion head. First the conductor screen and the insulation screen were extruded together and then after roughly 50 cm distance the insulation screen was extruded. This resulted in a 50% drop in AC breakdown strength after a two-year ageing test program. The ageing process as outlined in the shape or β factor did not change. The reference cable was produced with a triple head, as it is the case for nearly all cables today and also required by most of the utilities (Fig. 15).

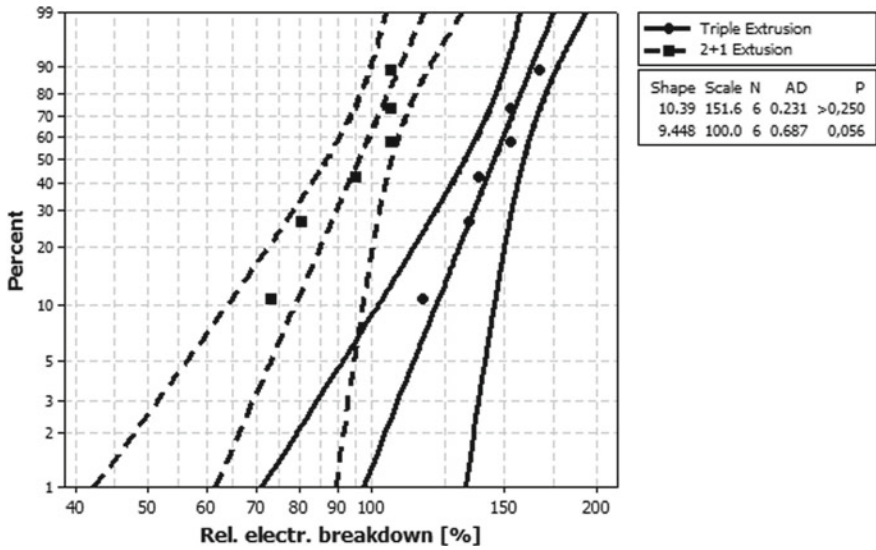


Fig. 15 Influence of triple extrusion

2.3.5 Water Tree Retardant Compounds

Cross-linked polyethylene proved to be unreliable for medium voltage power cable applications. So compound producers introduced special compounds that are marketed under the name of TRXLPE that is tree retardant XLPE. It should be noted that this name is not properly defined, and the requirements are not standardized. In fact, the IEEE ICC working group which had the task to define tree retardant cross-linked polyethylene (TRXLPE), could not come to a successful conclusion.

For these compounds two different approaches were taken:

1. Polymer-modified XLPE
2. Additive-modified XLPE

Both compounds have a slightly higher loss factor than XLPE without additives. But for medium voltage cables, this is not an issue since the electrical loss is below 1 mW/m at normal operation up to 130 °C.

For polymer-modified XLPE, the compound producer introduced a second polymer that needs to be compounded into the LDPE. The second polymer appears as small islands inside the LDPE base resin and acts as a retardant to water tree initiation and growth. The second polymer can be either a

1. polar compound
 - a. Ethyl-acrylate
 - b. Butyl-acrylate
2. or non-polar
 - a. LLDPE
 - b. SEBS
 - c. α -Polyolefines.

Both possibilities are commercially available and can be processed similarly to XLPE. The non-polar compounds have the advantage that they can also be used for higher voltages, since their loss factor is in the same low range as for XLPE and not dependent on electrical stress. In beginning, the 1990s trial versions, one of these compounds contained a 12 nm filler of fumed silica. Even if the laboratory test results like Ashcraft and mini-cable tests were promising, the end results on the final cable evaluation did not show any improvement over the commercially available compounds (Fig. 16).

Therefore, further production utilizing this product as well as another additive of a liquid silane compound was stopped. There were also other problems in the performance of these cables that are beyond the scope of this chapter.

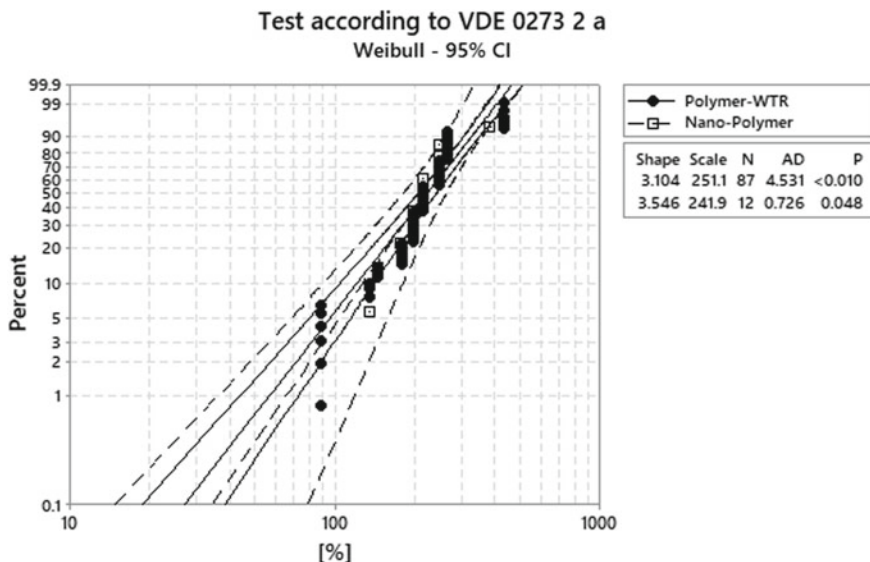


Fig. 16 VDE 0273 results of a fumed-silica filled polymer modified XLPE

2.3.6 Additive Modified XLPE

In this case, a special additive is added to the XLPE which retards the growth of water trees in the insulation. Here, special additives that will retard the growth of water trees inside the insulation are added during the production of the compound. The dispersion of these additives is very important, as a non-uniformly dispersed additive might act as a contamination or hot spot. These additives are relative neutral to the electrical strength of the compound, but will retard the growth of water trees in an efficient manner such that this is not a problem anymore. They also work very well with strippable insulation screens, since they are nonpolar (Fig. 17).

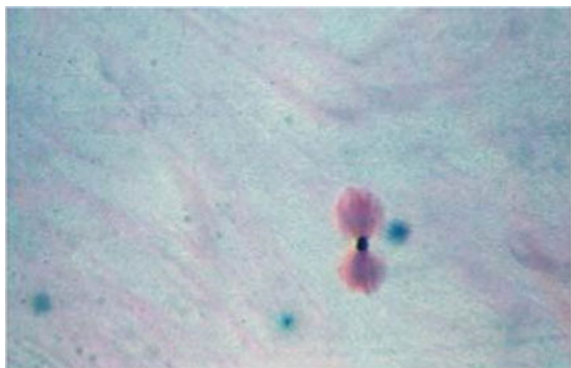
Today's cables using present day compounds with up-to-date production technology will give the utility a cable that last at least 50 plus years. Figure 18 shows the improvement in recorded failure rates between first- and second-generation insulation compounds (Fig. 18).

2.4 High Voltage and Extra High Voltage Compounds

Generally, these compounds are the same as medium voltage compounds and differ only in the requirements for cleanliness. Some special compounds are used for MDCV lines or cables with a small conductor. These compounds are called low sag as they have a lower melt index than the XLPE compounds commonly sold for this application. As mentioned above the TRXLPE compounds have a slightly higher dielectric loss factor and are therefore not considered. This is also the reason why EPR is limited to 150 kV. So for these compounds the main focus is cleanliness.

As shown in Fig. 19, water trees might be a problem for high voltage cables. However, these small vented trees observed after 40 years in service were not the reason for replacement of the cable. It was just that the conductor was too small to carry the future load. However, the use of water tree retardant additives, that are non-polar, and thus not negatively influencing the electrical loss factor, might provide an advantage for future development.

Fig. 17 Bowtie water tree (300 μm) in TR XLPE insulation after 17 years in service [3, p. 138]



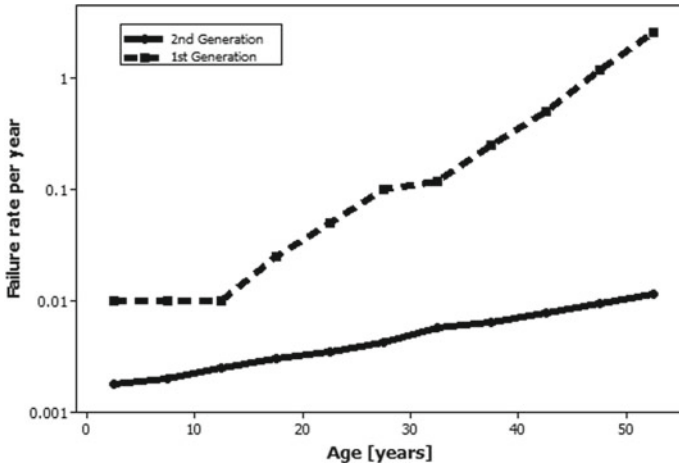
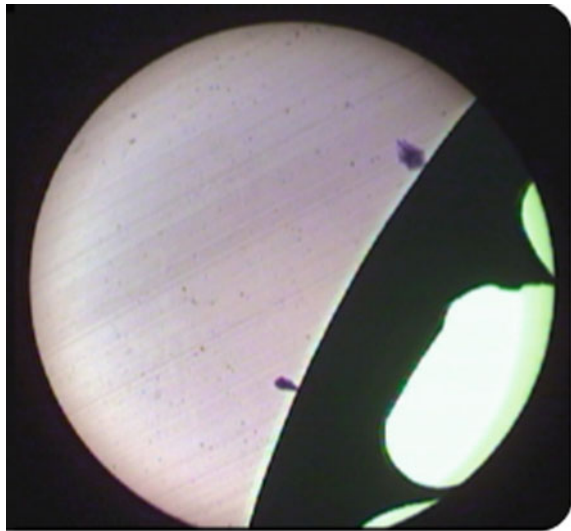


Fig. 18 Cable failures at a utility in Germany over the years [21]

Fig. 19 Water trees in a high voltage cable, 110 kV, 40 years in service



Already wet designed 66 kV array cables for offshore wind farms are the standard, while future work might extend to even higher voltages to reduce the weight of these cables which normally have outer lead sheaths as water barriers. Figures 20 and 21 show the loss factor on newly developed materials compared to older products that are already on the market.

The ease of processing a compound is a normal requirement for extruder operation as an over reactive compound will create pre-cross-linked particles, called scorch. These particles can reduce the electric breakdown strength and thus reduce

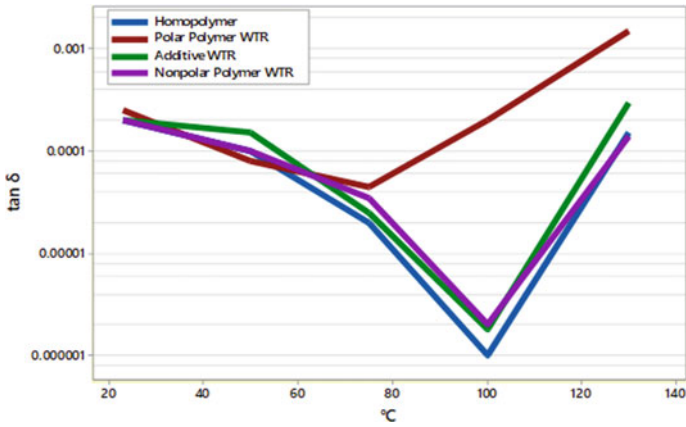


Fig. 20 Dielectric loss factor versus temperature on plaques

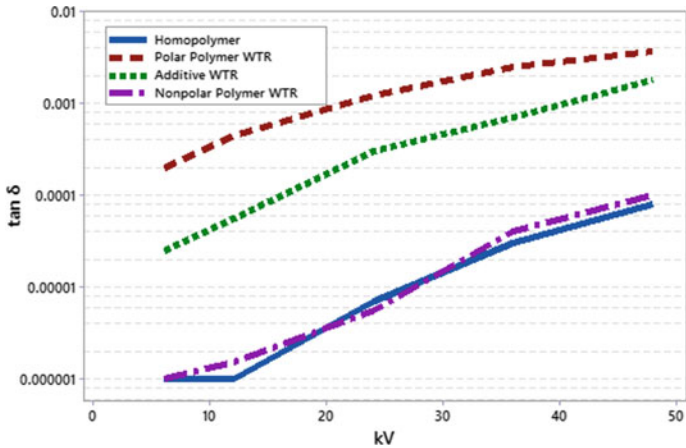


Fig. 21 Dielectric loss factor versus voltage at 100 °C on plaques

the performance of a cable. For cleanliness measurements different and diverse tests at the compounder are performed. Thus, it is difficult to compare cleanliness specifications without a background knowledge of each test. Also, the sample size plays a role since the compound supplier does not normally perform a 100% check of the compound supplied.

It is generally agreed that for high voltage cables (IEC 60840), particles bigger than 100 μm can create problems and for extra high voltage cables (IEC 62087), particles bigger than 70 μm can create problems. Also compound handling by the cable manufacturer, unloading, conveying etc., influences the contamination level inside the cable. Normally, all cable manufacturers use filters to reduce the amount of dust and hence contaminants inside the cable.

The choice of antioxidant for this application is also important since some of these have a polar characteristic or due to the influence of the pH-level of the compound can influence the creation of water during the cross-linking process. Both will negatively influence the dielectric loss factor.

Recently, compounds came on the market that reduce the degassing time; a process that needs to be carried out for XLPE cross-linked cable to remove the methane that is produced during the cross-linking process [22]. CIGRE has come up with recommendations on how to test for the amount of methane content in a cable [15]. Four laboratory methods were evaluated: gas chromatography (GC), gas pressure measurement, Raman spectroscopy, and conductivity method. The GC method proved to be the most popular as well as the most accurate.

2.5 *Compounds for DC Cables*

Extruded DC XLPE cables have been installed around the world since the 1990s. At first, the development of these cables was challenging, since at the beginning, space charges were created during a longer use of these cables which resulted in a pre-mature breakdown at very low levels. With understanding and the introduction of different convertor technology, extruded DC cables received a welcome boost. The first extruded DC cable was a ± 80 kV, 50 MW cable in Gotland, Sweden, which has been in operation since 1999. This cable was installed with voltage source convertors and was designed for a conductor temperature of 70 °C. The compounds used for these cables and for many more installations around the world was an unfilled, specially designed XLPE compound for DC application that included special semi-conductive screens. Today, cables up to ± 320 kV have been installed and are running without any major problems.

It should be noted that two other commercial extruded systems have been installed, one in Japan and one in Europe, where the conductor design temperature was 90 °C. The one in Japan, Honchu-Hokkaido link, is a ± 250 kV, 300 MW link and operates with line-commuting convertors without any problems. The link in Europe is currently the highest voltage with ± 400 kV DC, 1000 MW, currently installed (2019). The XLPE insulation compounds used for these cables have an inorganic filler to improve the volume resistivity of the insulation. There are projects in China and Germany at ± 525 kV DC. For these cable projects, new compounds, all unfilled XLPE, have been introduced, some cable makers have now approved HVDC cables for 90 °C conductor temperature.

2.6 *Compounding of XLPE*

The design of a compounding line has changed very little in the last sixty years. It has not changed for medium and high voltage compounds as well as for unfilled DC

LSHC

Linear Short Hyper Clean XLPE

AC/DC Line For MV-HV-EHV AC/DC Compounds

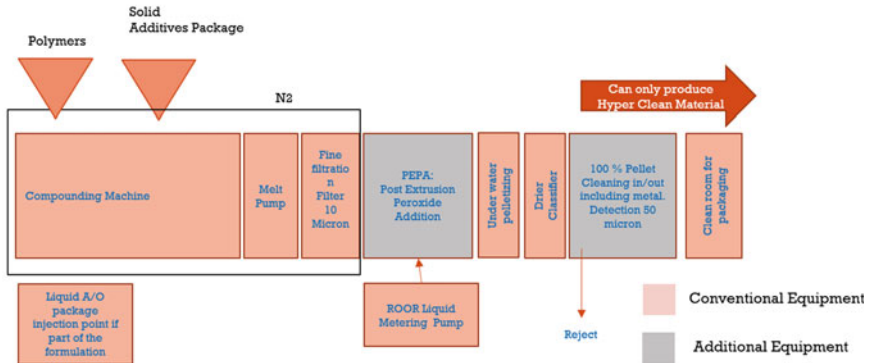


Fig. 22 XLPE compounding plant

compounds. For medium voltage compounds, the peroxide can be directly compounded into the insulation, but for high voltage and extra high voltage compounds due to cleanliness requirements, the peroxide is added by a physical absorption process, called “soaking”. An XLPE compounding plant is depicted in Fig. 22.

First a suitable LDPE resin at a higher temperature is mixed together with other polymers and the antioxidant or additives in a molten stage until completely homogenized. During this process the temperature profile is very important since the melt should not be too hot so as to degrade either the antioxidant or the polymer. Afterwards the melt is filtered according to the required melt filtration level making sure that the filter is not too tight as this may degenerate the polymer due to a high melt stress and thus create gels which can negatively influence the properties of the cable insulation. At this point, the polymer strands are cut into pellets and premixed with molten and filtered dicumyl-peroxide in a tumble mixer. This mixture is conveyed into a silo and kept for a certain time, some hours, at a certain temperature. During this time, the peroxide is absorbed into the granules and then after a defined cooling process packed for later transportation. During all of this handling, the properties of the product, especially the cleanliness has to be checked. The temperature during this process needs to be carefully monitored, since the compound has the tendency to exude. Polyethylene cannot tolerate a high amount of filler and can reject these fillers over time. This process is known to be an exudation process. Unfortunately, peroxides and antioxidants are also fillers for polyethylene and thus have the tendency to exude. The antioxidant at a temperature of around 50 °C and the peroxide at lower temperature below 5 °C. Therefore, it is important to keep the compound at a certain temperature. The exudation of peroxide in particular can create a so-called peroxide nest inside the conveying system and the

resultant accumulation of material or lumps will fall into the extruder. This in turn can create a slipping screw with cable core diameter variations and/or a higher amount of peroxide within the cable insulation and thus a weak spot within the cable, which can reduce both the withstand and impulse levels of the cable insulation.

Existing compounding plant designs originated at the beginning of the 1960s and since then, have been gradually optimized to produce consistent and reliable compounds, known worldwide as XLPE. XLPE applications span over a wide range of voltages from 5 to 600 kV and beyond. However, the concept remains the same, continuous compounding where different polymers are mixed along with additives such as antioxidants, scorch retarder, cross-linking enhancer, etc., followed by a batch peroxide soaking process with controlled heating, cooling and residence time sequences. Ideally, the soaking is conducted in an enclosed soaking tower (up to 50 m. high) where the chain of operations including polymer pre-weighing to packaging of the finished product is conducted. Both, the continuous and the batch processes are preferably harmonized to produce a regular output.

Here, polymers and additives, respectively, mean LDPE, copolymers, and combinations thereof. Additives mean antioxidant packages, plus optionally voltage stabilizers, cross-linking booster, scorch retarders, etc.

2.6.1 New Method to Produce XLPE

This new method is the same as for the conventional XLPE compounding line except that two types of equipment have been inserted, one after the filter and one, right before packaging (Fig. 23).

These two additional pieces of equipment, in light green colour, are first Post Extrusion Peroxide Addition (P.E.P.A) system and second, a large capacity pellet sorter. The pellet sorter removes contaminants above 60 μ .

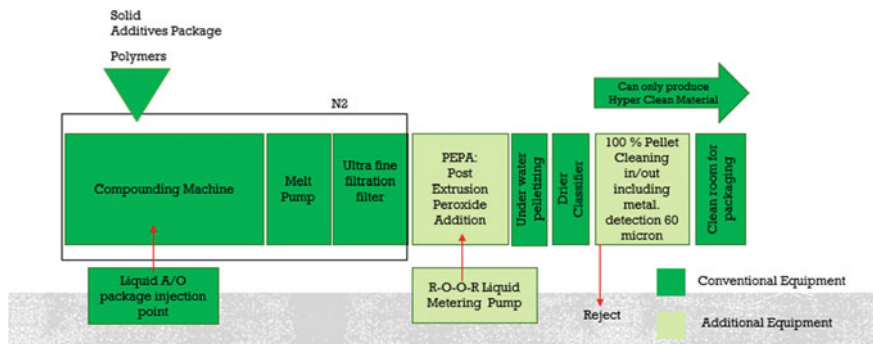


Fig. 23 New process to produce XLPE

PEPA is a cooler/mixer that takes the polymer's relatively high temperature (200 °C) necessary due to the fine filtration, down to 115–125 °C, well below the peroxide decomposition temperature. Reaching this relatively low temperature, the peroxide is then injected in filtrated liquid form.

2.6.2 Pros and Cons

Pros and cons are detailed in Table 3 below that is not an exhaustive list. Many more positive criteria can be found in favour of the LSHC (Linear Short Hyper Clean) process.

Table 3 Pros and Cons

	Conventional	LSHC XLPE
Innovation	60 years old proven technology	NEW
Peroxide dispersion/distribution Inside the pellets	Large, not optimal	Narrow, optimal
Low Temperature Peroxide Exudation (4 °C)	Yes	No
Does require expensive 50–30 m high soaking tower?	Yes	No
Polymer melt filtrated down to 10 μ absolute	Yes	Yes
Process Cleanliness Capability	Super	Hyper (Cleaner than super)
Metal Content	High probability	Very low probability
Process	Continuous/Batch	Only continuous
Manpower: number, qualification and cost	Compounding plant plus the soaking tower	Only Compounding
Functioning energy (power, water and air treatment, cleaning etc.)/ kWh/ kg of XLPE estimation	0.35	>0.2
Greenhouse Footprint Average (Equivalent CO ₂ /kWh) (g)	180–200	90–100
Lego Style Plant: Can easily be dismantled and transported from one location to another or requalify for different W&C compounds	No	Yes
Downtime and maintenance after each campaign	++++	++
CAPEX—Capital expenditure (including land, Infrastructure, Tower, everything inside)	100%	30–50% (*)
Plant erection time (Year)	2–3	1–1.5

The new process's main saving is contributing to carbon footprint reduction by the exclusion of the 50 m soaking tower infrastructure. Process engineers have compared kWh (energy) needed to produce one kilogram of final XLPE compound produced with the conventional process to that of the new one. Not surprisingly a reduction of some 40% has been demonstrated in favour of the new process. For example, it is 0.35 kWh/kg of XLPE for the old process versus less than 0.20 kWh/kg of XLPE with the new one.

(*) This is taking into consideration the huge tower infrastructure reduction including mirror polished, vessels, massive heating and cooling system, day bins, electrical valves, demineralized and deionized transportation water, air-compressor, air treatment, elevators, manpower, maintenance, etc.

2.7 *Production of Cable Cores*

As mentioned earlier, it is not only the compound and its chemical composition that influences the properties of a cable. It is also the production process, that is, how the cable core is produced has an influence on the properties of the cable. A VCV line is in principle a tower, where the cable is extruded down to the ground and cooled. Here, the handling of conductors and cables is of utmost importance. The stress added to the cable is high since the whole weight of the cable needs to be supported from the top.

For a CCV line, one needs to distinguish between lines used for medium voltage and high/extra high voltage cables. Medium voltage lines have a small angle and are designed for high speed processing. The conductor size is usually a maximum of 800 mm². For high voltage and extra voltage cables, the angle of the line is much steeper and very close to a VCV line. Here, the biggest problem is the small conductor and thick insulation layer, since the insulation has the tendency to droop, the so-called pear drop effect. This can be overcome by a special configuration of the line or by using so-called low-sag compounds.

In these lines, the material is cross linked with heated nitrogen gas at around 10 bar and then cooled down to a conductor temperature of around 80 °C, still under pressure of 10 bar either in water, for medium voltage cables or an inert gas like nitrogen. The latter is less efficient for cooling, but mostly required by utilities in their specification.

The third-line type, an MDCV line which is in principle a long die which forms the cable. Here, the cable is gently pushed through a die, which has the same diameter as the cable core and heated via an oil. The surface temperature is much lower than in the other processes. Also, here the core is under pressure to prevent foaming of the polyethylene due to the gases like methane that are created during the cross-linking process. One concern is that a large conductor might sag inside the insulation and not be centred.

All three processes have their advantages and disadvantages and are used to produce high quality cables up to 600 kV. A CCV line is the preferred line for medium voltage cables while a MDCV line is not used for this application due to the slow line speed.

References

1. Orton H (2019) The Indispensable Insulated Conductor, IEEE DEIS EIM Editorial, September/October 35(3). ISSN 0883-7554
2. Black R The History of Electric Wires and Cables, Peter Peregrinus Ltd. (ISBN 0863410014)
3. Orton H, Hartlein R (2006) Long-life XLPE Insulated Power Cables, Borealis and DOW
4. Smedberg A, Gustavsson B A cross-linking agent, EP 1944327A1
5. Smedberg A, et al (1997) Cross-linking reactions in an unsaturated low density polyethylene, Polymer 38(16), August
6. Malpass DB Introduction to Industrial Polyethylene: Properties, Catalysts, Processes, Chapter 2 Free Radical Polymerization of Ethylene
7. Fothergill JC et al (2011) The measurement of very low conductivity and dielectric loss in XLPE cables. IEEE Transactions on Dielectrics and Electrical Insulation 18(5), October
8. Cieloszyk GS (1976) Polyethylene Antioxidant Fundamentals, BP Chemicals Brochure
9. Campus A, Lafin B, Sterzynski T (1998) Structure—Morphology Modification of Cable Insulation Polymers. IEEE International Conference on Conduction and Breakdown in Solid Dielectrics, June 22–25, Västerås, Sweden
10. Campus A, et al (1998) Morphology of polyethylene for power cable insulation effects of antioxidant and cross-linking. IEEE International Conference on Conduction and Breakdowns in Solid Dielectrics, June 22–25, Västerås, Sweden
11. Fukunaga K, et al (1991) Measurement of space charge distribution in cable insulation using the pulsed electro-acoustic method. Third international conference on polymer insulated power cables, p 520
12. Campus A, Matey G (1983) The influence of cross-linking temperature on the properties of cross-linked low density polyethylene, PRI Conference on Polymers, May 18–19, Manchester, UK
13. Kjellqvist J, et al (2003) New XLPE Insulation Materials for HV and EHV Cables, Paper B2.2, JiCable
14. Nakatsuka T, et al (1994) The effect on dielectric loss of polyethylene caused by acetophenone and cumylalcohol, Conference Record of the 1994 International Symposium on Electrical Insulation, Pittsburgh, PA, USA, June 5–8
15. Basic principles to determine methane content in cross-linked solid extruded insulation of MV and HV cables, CIGRE TB501 WG D1.26, June 2012
16. Aida F, Tanimoto G, Aihara M, Hoshokawa E (1990) Influence of curing by-products on dielectric loss of XLPE insulation; CEIDP
17. Hayami T, et al (1981) Leakage Current Characteristic of XLPE. Conference on Electrical Insulation and Dielectric Phenomena, VI-7
18. Diego JA, et al (2011) Annealing Effect on the Conductivity of XLPE Insulation in Power Cable. IEEE Transactions on Dielectrics and Electrical 18(5):1554–1561, October
19. Choo W, et al (2009) Space Charge Accumulation under Effects of Temperature Gradient and Applied Voltage Reversal on Solid Dielectric DC Cable, ICPADM, Harbin, China, July 19–23
20. Recommendations for Additional Tests for Submarine Cables from 6 kV ($U_m=7.2$ kV) up to 60 kV ($U_m=72.5$ kV), CIGRE TB 722, April 2018

21. Stotzel M, et al (2001) Reliability calculation of MV-distribution networks with regards to ageing in XLPE-insulated cables, IEE Proceedings—Generation, Transmission and Distribution 148(6), November
22. Andrews T, et al (2006) The Role of Degassing in XLPE Power Cable Manufacture. IEEE Electrical Insulation Magazine 22(6), November/December

Chapter 13

Research Developments in XLPE Nanocomposites and Their Blends: Published Papers, Patents, and Production



Yinghui Han, Zhiwen Xue, Dongtao Liu, Feng Gao, Xiaosong Yang,
Wenchao Dong, Junxiu Zhou, Guodong Jiang, Junzhe Lin, Yifei Xia,
and Huanhuan Luo

List of abbreviation

XLPE	Cross-linked Polyethylene
PEX	Cross-linked Polyethylene
CAGR	Compound Annual Growth Rate
SiO ₂	Silicon Dioxide
SiC	Silicon Carbide
MgO	Magnesium Oxide
MMT	Montmorillonite
Al ₂ O ₃	Aluminum Oxide
PPy	Polypyrrole
TiO ₂	Titanium Dioxide
GO	Graphene Oxide
PE	Polyethylene
SEM	Scanning Electron Microscope
LDPE	Low-density Polyethylene
AC	Alternating Current

Y. Han (✉) · Z. Xue · X. Yang · W. Dong · J. Zhou · J. Lin · Y. Xia · H. Luo
Department of Mathematic and Physics, North China Electric Power University,
Baoding 071003, People's Republic of China
e-mail: yinghuihan@ncepu.edu.cn

D. Liu
College of Chemistry, Northeast Normal University, Changchun 130024,
People's Republic of China

F. Gao
Beijing Tsingsoft Innovation Technology CO. LTD, Beijing 100085,
People's Republic of China

G. Jiang
College of Materials Science and Engineering, Nanjing Tech University,
Nanjing 211816, People's Republic of China

DC	Direct Current
VI or VS	Vinylsilane
α	Scale parameter
β	Shape parameter
PD	Partial Discharge
PSMA	Polystearl Methacrylate
DCP	Dicumyl Peroxide
PEA	Pulsed Electroacoustic
HVDC	High-Voltage Direct Current
PHC	Half Cycle of Voltage
NHC	Negative Half Cycle of Voltage
OMMT1	Ommt Octadecyl Quaternary Ammonium Salt
OMMT2	Double Octadecyl Benzyl Quaternary Ammonium Salt
T_m	Melting Temperature
EVA	Ethylene Vinyl Acetate
MFI	Melt Flow Index
MDOS	Dimethyloctylsilane
DSC	Differential Scanning Calorimetry
FTIR	Fourier Transform Infrared Analysis
OIT	Oxidative Induction Time
fGO	Functionalized Graphene Oxide
PAC	Polycyclic Aromatic Compounds
QWs	Quantum Wells
DBD	Dielectric Barrier Discharge
CF ₄	Carbon Tetrafluoride
BRNN	Bidirectional Recurrent Neural Networks
2-D	Two-Dimensional
MMC	Maximum Margin Criterion
DIV	Discharge Inception Voltage
TGA	Thermogravimetric Analysis
wXLPE	Waste Cross-linked Polyethylene
MWCNTs	Multiwalled Carbon Nanotubes
PIF	Pressure-Induced Flow
CCD	Charge-Coupled Device
UHF	Ultra-High Frequency
LV	Low Voltage
MV	Medium Voltage
FEM	Finite Element Method
EPDM	Ethylene Propylene Diene Monomer
SEBS	Styrene-b-(ethylene-co-butylene)-b-styrene
TAIC	Triallyl Isocyanate
TAC	Triallyl Isocyanurate
DLTP	Dilauryl Thiodipropionate
PVC	Polyvinyl Chloride

ASTM	American Society for Testing Material
EEA	Eval Ethylenevinyl Alcohol
SCLC	Space Charge Limiting Current
EPR	Ethylene Propylene Rubber
VOCs	Volatile Organic Chemicals

1 Introduction

Polyethylene is one of the most important polymers and widely used in the world today. Due to its structural characteristics, polyethylene is often unable to withstand higher temperatures and lacks of mechanical strength, which limits its application in many fields. Cross-linking is an important method for the modification of polyethylene. Treated by cross-linking, polyethylene changes its structure from linear macromolecular to a three-dimensional network, and thus, a series of physical properties (e.g., wear and creep resistance, mechanical strength, transparency, flexibility, etc.) and chemical properties (e.g., long-term service, temperature, heat and chemical corrosion resistance, etc.) of polyethylene would be obviously improved. Such polyethylene which has cross-linked covalent bonds between connecting its polymer chains is known as cross-linked polyethylene (abbreviated as XLPE or PEX). XLPE has been around for quite some time. The first cross-linking methods emerged in the 1930s and practices have continued to evolve since other processes being developed throughout the years. The cross-linking process is extremely strict and sophisticated. During the cross-linking process, if the degree is too high, the products could become brittle and cause stress cracking. If too low, the physical properties could be very poor and unusable. But as long as the cross-linking process is properly controlled, XLPE raw material powder is formed and processed into sturdy, durable end products. It is usually formed into cylindrical shapes that can be used for pipe and tubing and is used predominantly in building services pipework/plumbing systems, insulation for high tension (high voltage) electrical cables, mining industry, etc. Cross-linked polyethylene-based plumbing products utilized in hot water supply system are required for their high creep resistance and cracking strength at high temperature. Probably the most common reason for using XLPE is to replace traditional galvanized steel, copper, and PVC piping due to rusting, cost, and circulation. Cross-linking can solve plumbing issues at competitive pricing and can sometimes be easier to install. In addition, XLPE has very high insulation resistance, a stable dielectric constant over all frequencies, and a low dielectric constant. So XLPE has gained substantial attention in the area of insulation in the electric industry, and these materials play a prodigious role in the arena of cable insulation in terms of

XLPE electrical properties, flexibility, thermal and moisture resistant. Increasing demands from plumbing products manufacturing, and wires and cable insulation sector are likely to boost the market growth. The global cross-linked polyethylene market value is estimated to reach USD 8.60 billion by 2025, which is expected to expand with a compound annual growth rate (CAGR) of 6% over the forecast period. And viewed in this way, cross-linked polyethylene will keep going in popularity from development to market.

In recent years, the technical emphasis of cross-linked polyethylene (XLPE) is the development of synthetic XLPE nanocomposites and blends because of their academic and practical importance. Various strategies for XLPE coupled with different nanofillers to enhance the corresponding performances according to application requirements. Polymer nanocomposites and blends based on XLPE are often used in extreme circumstances that can include high temperature differences, intense radiation, and strong electric fields. In the case of insulating systems for high-voltage applications, they are often applied to cables, generators, motors, cast resin dry-type transformers, etc. Such conditions demand high-quality insulating materials with superior electrical, thermal, and mechanical properties as well as resilience to other environmental stresses. A suitable secondary component is added to the polymer matrix, which either modifies the nanostructure or introduces new functional moieties that are located at the surface of the filler material. A flood of scientific papers and patents related to the preparation and application of XLPE nanocomposites and blends have been sprung up. Many XLPE nanocomposites, such as silicon dioxide (SiO_2), silicon carbide (SiC), magnesium oxide (MgO), montmorillonite (MMT), aluminum oxide (Al_2O_3), polypyrrole (PPy), titanium dioxide (TiO_2), graphene oxide (GO), and so on, are chosen as potential candidates for fighting against in the challenges in dielectric insulation for cables, like partial discharge, space charge accumulation, water trees, volume resistivity, and DC breakdown strength. Some studies on the structure-property relationship of composite materials used in power engineering exploited fundamental theories as well as numerical/analytical models and the influence of material design on electrical, mechanical, and thermal properties.

This chapter focuses on advances in XLPE nanocomposites and blends and reviews the recent developments in their compositions, properties, productions, and applications, including electric breakdown strength, thermal conductivity, temperature resistance, corona resistance, and specific energy storage in dielectrics. Some research on other properties is also covered, such as nonlinearity and radiation resistance. At the same time, the microstructures and morphological characteristics of XLPE nanocomposites and blends closely related to their properties are thoroughly analyzed, and the corresponding synthesis methods and physicochemical mechanisms are summarized. The market prospect of emerging products of XLPE nanocomposites and blends is also discussed. The goal of this chapter is to keep abreast of the latest developments of XLPE nanocomposites and blends, to understand the behaviors of XLPE nanocomposites under operating stresses, and to provide references for budding scientists in this field.

2 Published Papers on XLPE Nanocomposites and Blends

Cross-linked polyethylene (XLPE) and its nanocomposites and blends have been intensively studied because of their academic and practical importance. Published papers describe the latest regional and global research results and forefront developments in XLPE field.

2.1 Structure and Composition of XLPE Nanocomposites and Blends

2.1.1 Morphologies and Chain Alignment of XLPE Nanocomposites and Blends

Generally, polyethylene (PE) containing a repetition of CH_2 units has a linear structure and a rough-textured cross section (Fig. 1a). Cross-linked polyethylene contains little in the way of large-scale morphological features, and it appears smooth on both surface and cross section (Fig. 1b).

After being etched with carbon tetrachloride or trichlorotoluene, XLPE appears a clear three-dimensional network (Fig. 2a). By increasing the magnification by high-resolution scanning electron microscope (SEM), it can be clearly seen that XLPE has a nearly spherical structure, manifested as a porous morphology, with a large number of nodes on the particle surface and a certain number of micron-size gaps between nodes (Fig. 2b).

When combined with nanoparticles or blended with other functional polymers, XLPE will undergo great changes in its microscopic morphology and structure. For example, complexed with octylsilane-modified silica nanoparticles, XLPE achieved the hydrophobicity and high specific surface area (Fig. 3).

Different hypothetical models such as Lewis model, multicore model, multiregion model, dual-layer model have been proposed to explain the interfacial reactions (Fig. 4).

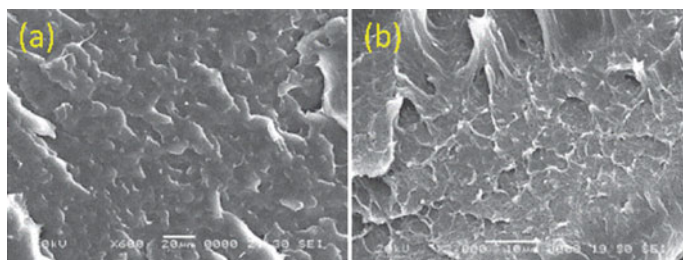


Fig. 1 SEM micrographs **a** cross section of PE, **b** cross section of XLPE. Reproduced with permission from Ref. [1]

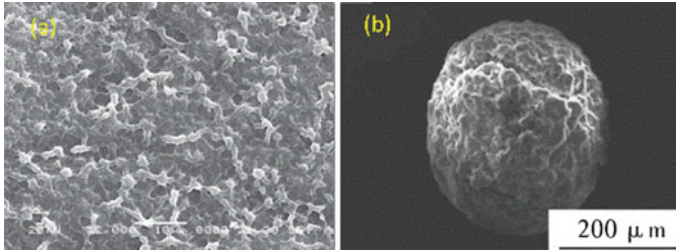


Fig. 2 SEM micrographs. **a** Cross section of typical XLPE after etched by carbon tetrachloride at a magnification of 10 μm . Reprinted with permission from Ref. [1]. **b** Apparent morphology of J0253-type XLPE at 200 μm magnification. Adapted with permission from Ref. [2]

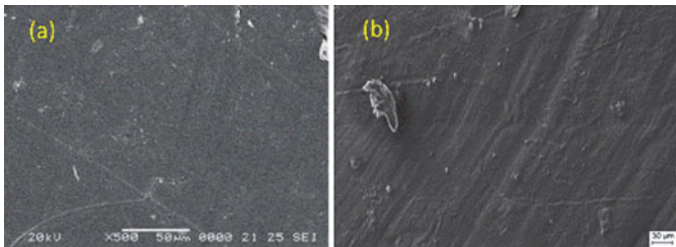


Fig. 3 Surface morphology images by SEM. **a** Surface morphology of XLPE without any composites, **b** XLPE complexed with octylsilane-modified nanosilica (2wt%), Ref. [3], Open access

The cross-link structure and cross-link density will have the impacts on the properties of XLPE, such as water tree growth, electrical tree growth, and electrical breakdown strength [4]. One reference low-density polyethylene (LDPE) was compared with a LDPE containing a higher number of vinyl groups, introduced via the copolymerization with a diene. Because of the chemical difference, the initially formed cross-link structure will be different from the materials. A range of various cross-link densities was considered for the two materials. It was found that along with a noticeable change in morphology after cross-linking, significant changes in particularly water tree growth, electrical tree growth, and electrical breakdown strength could be observed.

2.1.2 Nanocomposites, Cross-Linking Agents, and Blends

Consider the rapid growth of power grid, which depends on the stability and reliability of transmission cable. The performance of the main materials of cable determines the service life and applicable environment of the cable. According to different application scenarios and performance requirements, nanocomposites, cross-linking agents, and blends are commonly added into XLPE to enhance its

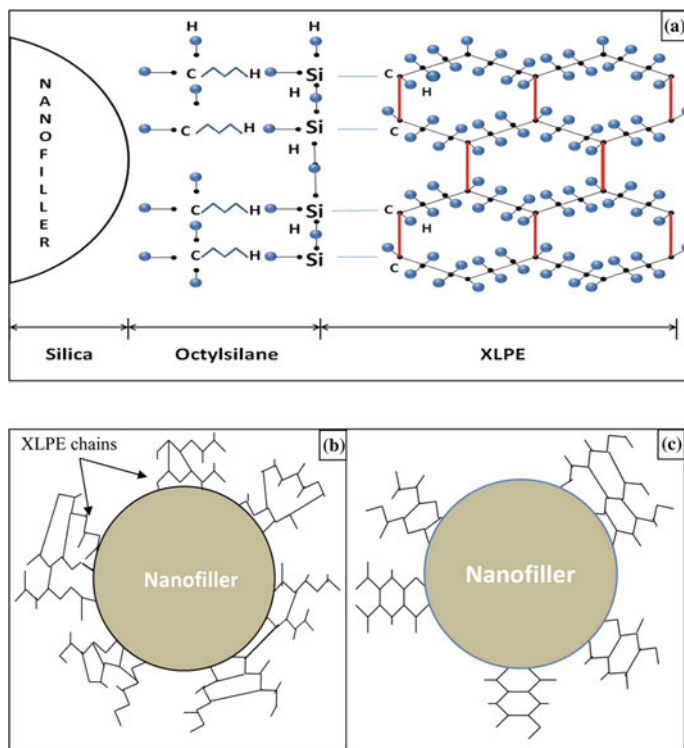


Fig. 4 a Chemical attachment of octylsilane-modified nanosilica into XLPE matrix, representation of polymer chain alignment with **b** unmodified; **c** octylsilane surface-modified nanosilica, Ref. [3], Open access

electrical, mechanical, and thermal properties, for adapting to higher working temperature and delaying the aging caused by oxidation under long working hours. For example, SiO_2 -based XLPE nanocomposites are perfect for medium-voltage AC and DC cables. SiC -based XLPE nanocomposites can be used for DC cable insulation. MgO -based XLPE nanocomposites show better DC properties compared with raw XLPE, and it can be used for DC cable applications. Alumina/silicate/nanoclay-based nanocomposites are efficient for low-voltage insulation. Incorporation of SiO_2 , Al_2O_3 , and TiO_2 nanoparticles in an XLPE matrix show enhanced thermal and chemical stability and higher mechanical performance than conventional insulation. Graphene-based nanocomposites in XLPE are used for improving durability of electrical insulators and devices. The following is the detailed research progress.

i XLPE/ SiO_2 -based Nanoparticles

SiO_2 fillers can restrict the movement of the polyethylene chain through van der Waals physical interaction. SiO_2 could effectively capture hot electrons to suppress

space charge accumulation in XLPE on the basis of the Bader charge analysis [5]. The interfacial area of SiO_2 fillers with different scale is obviously different. Nanoscale SiO_2 nanofillers have small size, large specific surface area, and quantum effect, moreover, as well as the larger interfacial region (interaction zone) which is pivotal in controlling properties of XLPE. So nanosilica is considered to be a good nanofiller for improving the electrical insulation performance of XLPE and resisting some electro-destructive behaviors, such as partial discharge, water tree, space charge, DC breakdown, and so on. In spite of that, the morphological studies of the XLPE/unmodified silica nanocomposite still show the presence of agglomeration. Some particular modified-surface SiO_2 , such as incompletely hydroxylated, B-doped, and oxygen vacancy defect on the top layer, could induce the H migration reaction and consequent electrical tree growth of the XLPE chain. In contrast, the SiO_2 nanocomposite that has N-doped or oxygen vacancy on the lower layer with completely hydroxylated surfaces, as well as the reconstructed surface, is predicted to be favorable additives because of their quite strong physical interaction and very weak chemical activity with XLPE [5]. In addition, the introduction of coupling agents like vinylsilane could help to reduce the agglomeration rate and size. The vinylsilane (abbreviated as VS or VI) coupling agent can enhance the interaction between XLPE and silica nanoparticles by imparting a hydrophobic nature. Inclusion of inorganic nanoparticles in the polymer matrix can introduce a huge extent of cavernous trap spots, which act as barriers to the injection of space charge from electrodes and also reduce the bulk local electrical field distortion. The results in tremendous dispersion of SiO_2 nanoparticles are due to the enhanced compatibility between the surface of the nanoparticle and the polymeric matrix.

The cable joint is a vital part of cable lines which cause defects and faults easily through partial discharge (PD) test internal discharge can be noticed. Sharad et al. [6] studied the PD characteristics of XLPE nanocomposites for unmodified, agglomerated, and octylsilane-modified silica nanofillers with nano 1, 2, 3, 4, 5, 10 wt% in the range of 0–27.5 kV. The SEM morphology studies revealed that neither the unmodified nanosilicon filler nor the commercial polydimethylsiloxane modified nanosilica (14 nm, 100 m²/g) could disperse uniformly. As shown in Fig. 5a, b, obvious agglomeration occurs in the specimens of 2 wt% and 3 wt% unmodified nanosilicon. Due to its lesser size (7–14nm), hydrophobicity and high specific surface area (150 m²/g), octylsilane is suitable as a surface modifier to form a

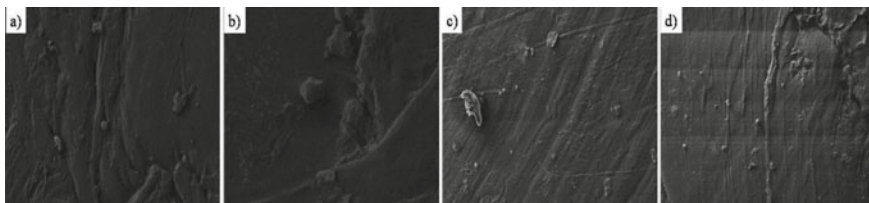


Fig. 5 SEM images of **a** XLPE/silica nano 2 wt% agglomerated nanocomposite; **b** XLPE/silica nano 3 wt% agglomerated nanocomposite; **c** XLPE/silica nano 2 wt% octylsilane-modified nanocomposites; **d** XLPE/silica nano 3 wt% octylsilane-modified nanocomposites, Ref. [6], Open access

stronger chemical adhesion at the interface of nanofiller and polymer matrix. Meanwhile, octylsilane can facilitate the separation of the nanoparticles from each other by acting as a compatibilizer between the nanoparticle surface and polymer matrix. As depicted in Fig. 5c, d, the octylsilane surface-modified nanocomposites show better homogeneous dispersion. No matter what kind of nanosilicon filler is introduced, it will have a promoting effect on reducing PD activity, but the optimal weight percentage of nanofiller is different when reaching the lowest PD activity. The unmodified and agglomerated nanocomposites show the lowest PD activity at nano 5 wt%. The surface modification of nanofiller helps to reduce the PD formation marginally due to improved nanofiller dispersion. Octylsilane surface-modified XLPE/silica nano 3 wt% exhibits the lowest PD activity [6].

A water tree is the most common degradation observed in polymer-based insulating materials especially in XLPE, which arises because of water and electrical stress. Nanosilica is often as a typical additive to impede the progression of water trees. The XLPE-functionalized silica nanocomposites were proved to inhibit the water tree growth [7]. Due to the high interface/volume ratio in nanocomposites, it is believed that scattering in the interfacial region inhibits tree growth [8]. When they were exposed to high voltage, the vinyl silane-treated silica nanocomposites show better water tree growth reduction for long times than neat XLPE. Neat XLPE shows a water tree growth more toward the ground plane with an angle close to 60° , while in nanocomposites the water trees had a wider fan-like morphology with an angle of about 180° . The reason behind the water tree growth reduction in XLPE/vinyl silane-treated silica nanocomposites is the scattering effect produced by the interfacial region between the nanosilica and XLPE matrix. In this case, vinyl silane creates an interfacial layer between nanosilica and the XLPE matrix. The interfacial region hinders the passage of charges and assists scattering sites to restore high energy and thus inhibits the progress of degradation.

The addition of nanocomposites that are more or less compatible with the matrix and with a polar or non-polar nature will impact the breakdown strength [9]. Under an extreme electric field, the inorganic nanoparticles are able to suppress the space charge carriers. Vinyl silane-modified XLPE/silica nanocomposites show a smaller amount space charge deposit. This is due to the presence of a large interface area. The surface modification results in the formation of deeper trap sites that can effectively capture homocharges from the electrodes forming an immobile space charge in the vicinity of electron. A silica/cross-linked polyethylene (XLPE) system has found a significant increase in breakdown strength in the nanoscale composites as well as two orders of magnitude increase in the voltage endurance compared to the unfilled XLPE. The electric field between the immobile space charge layer and electrode is reduced, and further, the continuous injection and movement of space charge from the electrode is hindered which leads to the improvement of the DC endurance property of the modified XLPE nanocomposites. The DC breakdown characterization of XLPE and SiO_2 nanocomposites can be calculated with two-parameter Weibull distributions as shown in Eq. (1) [10, 11].

$$P(E) = 1 - e^{-\left(\frac{E}{\alpha}\right)^\beta} \quad (1)$$

Here, E is breakdown strength of DC and $P(E)$ is cumulative probability of breakdown. α is the scale parameter and indicates the DC breakdown strength at the breakdown cumulative probability of 63.2% (also known as Weibull breakdown strength). β is shape parameter and represents the inverse of data scatter. Weibull probability parameters β and α were used to predict the breakdown voltage for solid dielectric materials. β (shape parameter) provides a measure of sensitivity of the insulation system with increasing voltage, and α (scale parameter) is the characteristic breakdown voltage. The lowest value of β is perfect for dielectric materials. Modified silica in the XLPE matrix has a high DC breakdown strength as compared to neat XLPE and XLPE-unmodified silica nanocomposites. High Weibull breakdown strength in XLPE/VI-SiO₂ is due to the excellent dispersion of silica nanoparticles in the XLPE matrix [12]. The addition of unmodified SiO₂ to the XLPE matrix has no change in scale parameter and breakdown voltage compared with neat XLPE; and the only changes occur in the presence of modified silica nanocomposites. The increasing trends of scale and shape parameter were found for the XLPE/VI-SiO₂ system. In addition, the temperature will affect the DC average breakdown strength [11, 12]. With increasing temperature, the DC average breakdown strength decreases due to the softening phenomena and formation of microholes. At 30 °C, XLPE and unmodified silica XLPE have the same average breakdown strength, while modified silica XLPE nanocomposites have high strength. The decrease in DC average breakdown strength of XLPE nanocomposites with increasing temperature is due to the formation of microholes. At glass transition temperature below 0 °C, polyethylene has the largest expansion coefficient than other common polymers [13]. When the temperature increases, the thermal expansion coefficient becomes much larger than that below the glass transition temperature [14]. In this case, XLPE insulation would produce microholes with radii of 1 μm and which are much larger than the radius of SiO₂ nanoparticles. The introduction of nanoparticles could fill the newly generated microholes.

The inorganic nanoparticles were introduced into the polymer matrix for quenching space charge effects. The silica nanocomposites can effectively suppress the space charge of XLPE. In view of the difficulty of homogeneous dispersion of the inorganic nanoparticles in high molecular weight polymers, the cross-linked polyethylene-filled compatible polymer matrix brushes support the homogeneous dispersion of spherical colloidal SiO₂ nanoparticles (10–15 nm diameters) in the XLPE matrix by grafting. This resulted in improved space charge reduction, enhanced DC breakdown strength, and constrained internal field distortion ($\leq 10.6\%$) over an extensive range of external DC fields from -30 to -100 kV/mm at room temperature. Morphological studies of unmodified SiO₂/XLPE nanocomposites showed that several microscale agglomerates were produced due to the core–core van der Waals interaction of the nanofillers, whereas polystyrene methacrylate (PSMA)-SiO₂/XLPE nanocomposites exhibited relatively homogeneous distribution morphology with small levels of agglomerations [15]. The space

charge distribution studies under -30 kV mm showed that after the polarization all samples showed a net positive charge with a reduction in the positive net charge on the anode. After being polarized for 30 min, the net positive charge is spread across the neat XLPE material. Approximately 7 C/m³ of positive transporters advanced and were stored in the bulk of the unmodified SiO₂/XLPE nanocomposites. In comparison, free-PSMA/XLPE composites displayed a minor number of positive carriers, and ~ 1 C/m³ of positive carriers were slowly stored near the cathode during polarization. In PSMA-SiO₂/XLPE nanocomposites, there is no detectable charge found after 60 min. In PSMASiO₂/XLPE, permeation of both positive and negative space charge was inhibited, and approximately no net charge seemed in the bulk. PSMA had a great role in the suppression of net charge, which means PSMA contains carbonyl groups which act as catching spots capable of suppressing the positive charge. The addition of SiO₂ powders to the polymer matrix improved the AC and DC breakdown voltage by 15% compared to raw polymers [15]. Hence, the incorporation of SiO₂ nanoparticles in an XLPE matrix reduces the water tree growth and space charge deposit and shows a higher breakdown strength. These improvements are mainly due to the better dispersion of SiO₂ in the XLPE matrix and are achieved by the surface modification of SiO₂ nanoparticles and the enhanced interaction of Si–O–Si bonds in the XLPE matrix. Insulation industries can adapt these methods to produce long-life cables [11].

ii XLPE/SiC Nanocomposites

SiC filler can be used for improving the aging resistance of XLPE. The Bader charge redistribution calculations between different types of silicon carbide and XLPE suggest that SiC fillers have the strong ability of capturing hot electrons to suppress the accumulation of space charges because of their unsaturated electronic structures and magnetism on the Si- or C-terminated surfaces. The interfacial behavior between SiC and XLPE was investigated based on the physical interaction and chemical reactivity. As shown in Fig. 6, the 3C, 4H, and 6H-type SiC with flat Si-terminated surfaces are proposed to be favorable additives by showing relatively strong physical interaction with XLPE to limit its movement, and high activation energy for the hydrogen migration reaction to protect the XLPE [16].

The dielectric properties, DC breakdown strength, and space charge distribution in XLPE/SiC nanocomposites were also improved. A representative study is to use 1, 3, and 5 wt% SiC nanoparticles as the mixing nanocomposite and dicumyl peroxide (DCP) as the cross-linking agent for forming XLPE/SiC [17]. According to the SEM images of XLPE and dispersion of SiC in XLPE from Fig. 7, it can be found that the SiC nanoparticles were dispersed well in the 1 wt% nanocomposite, but the 3 or 5 wt% nanocomposite showed noticeable agglomerations. Space charge accumulation can be suppressed effectively in nanocomposites by adding SiC nanoparticles. Thus, SiC nanocomposite with 1 wt% concentration shows the least amount of space charges.

Weibull probability plots were used for analyzing the DC breakdown strength of XLPE/SiC and the scale parameters and shape parameters were shown in Table 1

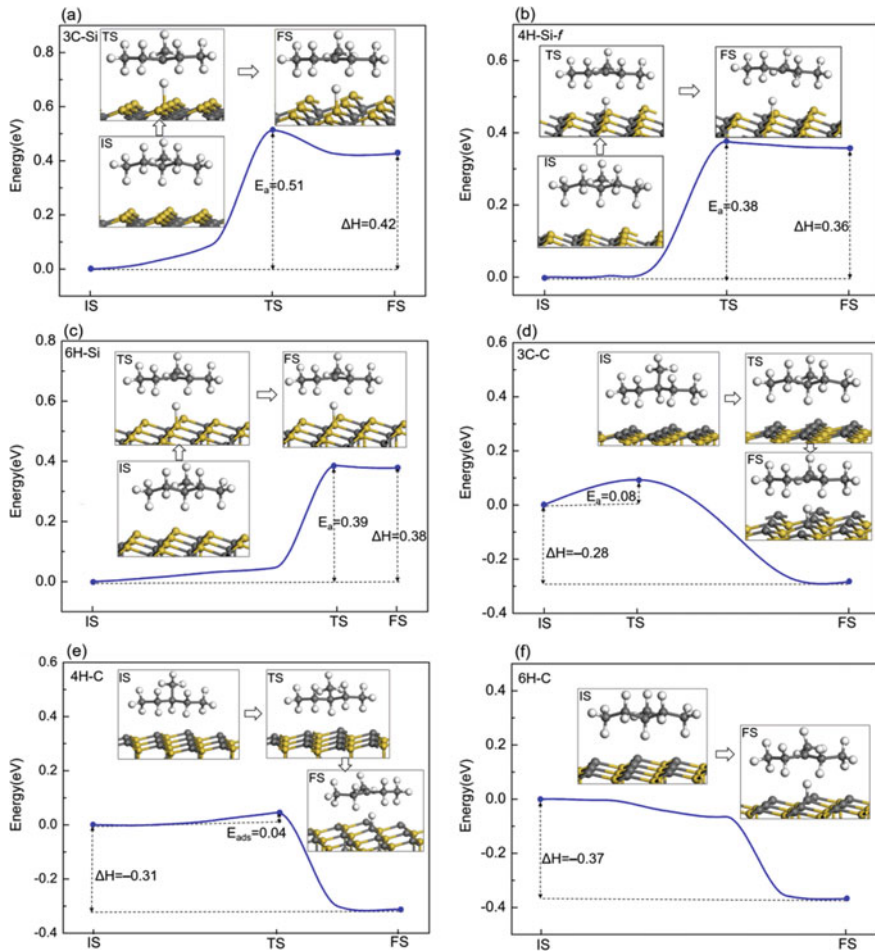


Fig. 6 Minimum energy paths for hydrogen migration reaction including the initial state (IS), transition state (TS) and final state (FS) of SiC incorporation into XLPE. Reprinted with permission from Ref. [16] Copyright 2019, Elsevier

[17]. It can be seen that shape parameter is sensitive to applied voltage because SiC nanoparticles decrease the randomness of the DC breakdown data.

1 wt% and 3 wt% XLPE/SiC nanocomposites showed higher-scale parameters compared with raw XLPE. However, in the 5 wt% XLPE/SiC nanocomposites, smaller-scale parameters predominate, and this causes the reduction in DC breakdown strength. This reduction is due to the poor distribution of nanoparticles in the composite, which was clearly observed in Fig. 8. Clearly, nanocomposites with a concentration of 1 wt% have the highest DC breakdown strength with a scale parameter of 331.99 kV/mm.

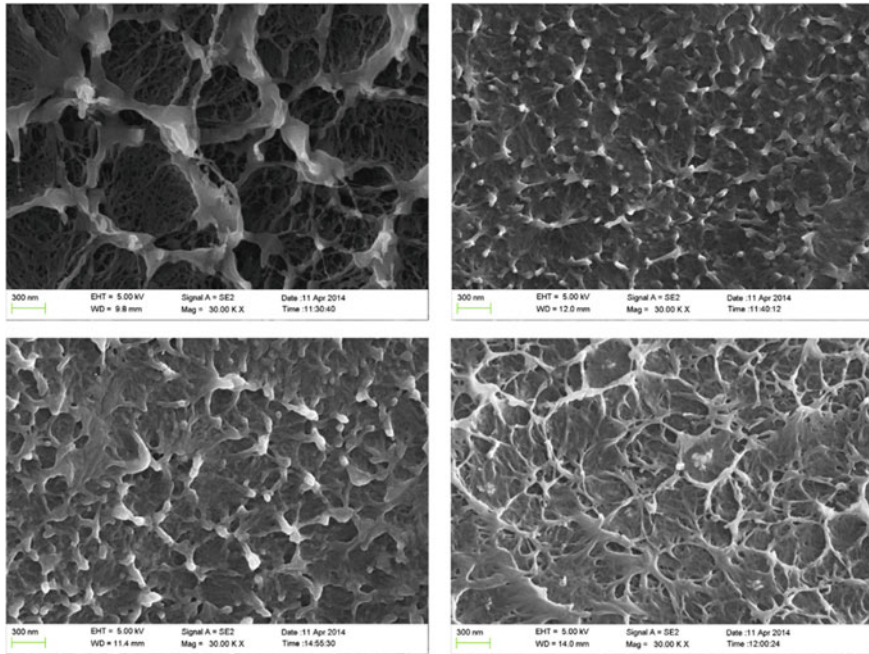


Fig. 7 SEM section images of XLPE/SiC. Reprinted with permission from Ref. [17] Copyright 2016, Elsevier

Table 1 Weibull parameters for XLPE/SiC nanocomposites. Rewritten with permission from Ref. [17] Copyright 2016, Elsevier

	XLPE	XLPE/1 wt% SiC	XLPE/3 wt% SiC	XLPE/5 wt% SiC
α	260.67	331.99	297.19	244.71
β	13.08	24.72	15.97	9.71

According to the multicore model proposed by Tanaka et al. [18], nanocomposites having lower concentrations of nanoparticles cannot overlap the Gouy–Chapman diffuse layers due to the large distance between nanoparticles. When the concentration is low, the distance between nanoparticles is large, which means that each nanoparticle can be seen as an independent individual. So it showed the better DC breakdown voltage and less space charges of 1 and 3 wt% samples than that of 5 wt% nanocomposites by a pulsed electroacoustic (PEA) method. Nanoparticles in the nanocomposite create deep traps near to the nanoparticle in the system, and each trap could attract a number of electrons and holes [16]. The electrical neutralization occurs when electrons and holes surround a single nanoparticle, which helps the prevention of charge accumulation in the 1 wt% XLPE/SiC nanocomposite. On the other hand, increasing the nanoparticle concentration results in nanoparticle

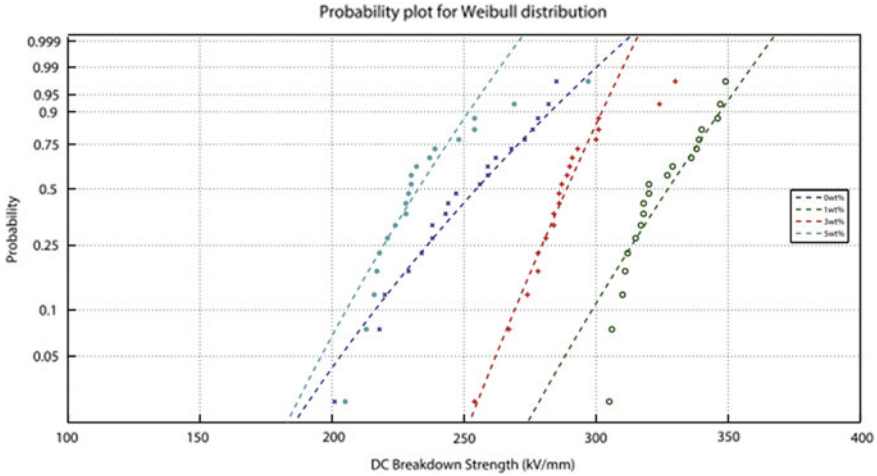


Fig. 8 Weibull probability plot for the DC breakdown strength of XLPE and XLPE/SiC nanocomposites. Reprinted with permission from Ref. [17] Copyright 2016, Elsevier

agglomeration which may affect the interfacial characteristics between the polymer and nanoparticle.

iii *XLPE/MgO Nanocomposites*

Magnesium oxide (MgO) is often used as the inorganic filler of XLPE to avoid water tree and space charge accumulation for high-voltage direct current (HVDC) cables. The particle size with the variation of Mg source, basic source, organic additives, surfactants and dispersants under hydrothermal or microwave treatment, and sonication will affect the performances of composites. Nagao et al. [19] studied the water tree retardant characteristic of MgO nanofiller addition to a cross-linked polyethylene (XLPE). They found that water tree retardation of XLPE at 313 K was improved with adding the MgO nanofiller at the content of more than 2 phr, while it was almost the same level at the nanofiller content of less than 2 phr. Above 2 phr, the distribution shifted to the side of shorter water length with increasing MgO nanofiller content, showing the improvement of water tree retardation by the adding MgO nanofiller. As the area of the interface between the nanofiller and matrix in nanocomposite is enormously large, it was considered that MgO nanofiller trapped water, and less aggregation of water at the tip of the water trees under the local high field suppressed the water tree propagation. As for the influence of temperature, the water tree at 333 K tends to grow faster and the retardation of water tree due to MgO addition became less effective than those at 313 K. Moreover, the growth rate of water tree became smaller with increasing MgO nanofillers, showing the water tree retardant property of MgO nanofiller addition. In addition, the space charge distributions of XLPE/MgO composites were affected by the particle size and the content of dispersed MgO in XLPE matrix. To prevent the breakdown under high

DC stress, the reduction of space charge of MgO/XLPE composite depends upon the smaller size of MgO particle and its content above 0.5 phr (per hundred part of resin, wt%) [20]. XLPE/MgO nanocomposites had a high range of volume resistivity due to the synergetic effect of nanosized MgO and minimum amount of cross-linking by products present in it [11]. A positive packet-like charge formed in front of the anode, then transferred to the cathode. The nanosized MgO particles play behind it for the disappearance of the packet-like charge [19]. Virgin XLPE showed higher homocharge accumulation than MgO/XLPE nanocomposites. In MgO/XLPE nanocomposites, a heterocharge was found to be near both electrodes due to the decomposition impurities from nanoparticles under high DC voltage. The homocharge present in XLPE causes high space charge distribution, and as a result, it generates an electrical tree [11]. In a recent study on the effect of MgO nanofillers on partial discharge (PD) and electrical tree growth in cross-linked polyethylene (XLPE), it showed that the PD intensity in positive half cycle of voltage (PHC) is larger than that in negative half cycle of voltage (NHC), and the PD magnitude in MgO/XLPE is lower than that in XLPE [21]. The tree length and morphology in MgO/XLPE are similar to those in XLPE. A finite element simulation based on the bipolar charge transport model was applied to investigate the effect of space charge on PD under AC voltage. The distribution of negative charges in NHC would be wider than that of positive charges in PHC, which would weaken the electric field in NHC and lead to the less PD in NHC. Moreover, the range of charge shield in MgO/XLPE may be larger and is equivalent to increasing the effective radius of curvature of needle tip, which would lead to smaller electric field and lower PD magnitude in MgO/XLPE. Nevertheless, MgO/XLPE does not show significant resistance to AC tree growth because the addition of MgO nanofillers reduces the crystallinity of material based on the differential scanning calorimetry (DSC) result.

iv *XLPE/Montmorillonite Nanocomposites*

Due to the organic quaternary ammonium salt with the lipophilicity of long chain, the cations of ammonium root can exchange with montmorillonite cations, which is commonly used for the intercalating agent of polymer/montmorillonite nanocomposites. Li et al. [22] used two organic intercalants, i.e., octadecyl quaternary ammonium salt (OMMT1) and double octadecyl benzyl quaternary ammonium salt (OMMT2), to treat montmorillonite and then obtained XLPE/OMMT composite. The increase of the melting point T_m of the matrix resin and the broadening of the melting temperature range ΔT_m are closely related to the intercalation efficiency of matrix resin molecules into OMMT. The double octadecyl benzyl quaternary ammonium salt also enlarged the interlayer spacing of montmorillonite, but contributed little to the intercalation of polymer in OMMT. OMMT1 has a larger impact on the melting point and the melting temperature range of the composites than OMMT2, that is, the intercalant 1 has a greater impact on the degree of crystallization and crystalline morphology of the composites than intercalant 2. Montmorillonite quickens the nucleation in XLPE/OMMT composite. But the enhanced interfacial interaction and the use of ethylene vinyl acetate (EVA) finally

reduce the overall crystallization speed rate, which means that the procedure of the crystallization becomes slow. The addition of nano-OMMT increases the relative dielectric constant of XLPE/OMMT composite. The dielectric properties of XLPE/OMMT composites were analyzed with the help of broadband dielectric spectroscopy within the frequency range from 10^{-2} to 10^6 . The composites with two kinds of OMMT particles are represented by single dielectric loss peak and double dielectric loss peaks in the high frequency range, respectively. With the rising of temperature, the width of the double peaks is broadened, interface interaction restricts the molecular chain segment motion, the distribution of relaxation time widens, so as to the low-frequency peaks are more diffused in low frequency band. The intercalant of octadecyl quaternary ammonium salt enables a good compatibility between OMMT1 and the matrix resin. The dielectric spectrum displays the single-component dielectric loss peak. The use of intercalant double octadecyl benzyl quaternary ammonium salt results in very few PE molecules intercalated into OMMT2. The long molecular chain introduced by the intercalant is distributed outside the layer. Dielectric constant and dielectric loss of nanocomposite associate with intercalating degree in broadband range, the higher the intercalating degree, the lower dielectric constant and dielectric loss. The dispersion of nanoparticles in matrix resin under the action of compatibilizer depends on how the compatibilizer matches with the organic intercalants.

v XLPE/Alumina-based Nanocomposites

By the addition of nanosized Al_2O_3 filler, both the DC breakdown strength and the volume resistivity of XLPE were increased. A little homogeneous space charge distributed in $\text{Al}_2\text{O}_3/\text{XLPE}$ nanocomposite material in the vicinity of electrode through the polarity reversal breakdown test by Park et al. [23], which indicated that the addition of Al_2O_3 nanofiller is effective for the improvement of DC electrical insulating properties of XLPE. The $\alpha\text{-Al}_2\text{O}_3$ nanosheets have also impact on the direct current voltage breakdown strength and space charge accumulation in cross-linked polyethylene/ $\alpha\text{-Al}_2\text{O}_3$ nanocomposites [24]. The XLPE/ $\alpha\text{-Al}_2\text{O}_3$ can be made by $\alpha\text{-Al}_2\text{O}_3$ nanosheets and a cross-linked polyethylene matrix through mechanical blending and hot press cross-linking. The introduction of $\alpha\text{-Al}_2\text{O}_3$ nanosheets brings a large number of deep traps, blocked the charge injection, and decreased the charge carrier mobility, thereby significantly reducing the conductivity, improving the direct current breakdown strength and suppressing the space charge accumulation in the cross-linked polyethylene matrix [24]. As shown in Fig. 9, the SEM micrographs of the cross section of XLPE/coated $\alpha\text{-Al}_2\text{O}_3$ nanocomposites and XLPE/uncoated $\alpha\text{-Al}_2\text{O}_3$ nanocomposites containing 2.0 wt% $\alpha\text{-Al}_2\text{O}_3$ indicated that the $\alpha\text{-Al}_2\text{O}_3$ nanosheets were dispersed evenly in the XLPE/coated $\alpha\text{-Al}_2\text{O}_3$ nanocomposites, while the $\alpha\text{-Al}_2\text{O}_3$ nanosheets aggregated in the XLPE/uncoated $\alpha\text{-Al}_2\text{O}_3$ nanocomposites. Moreover, the most of the $\alpha\text{-Al}_2\text{O}_3$ wafers were laid in the matrix along the thickness direction of the pressed specimen, which perhaps had a blocking effect on the transport of the injected charge along the thickness direction and improved the breakdown strength of cross-linked polyethylene.

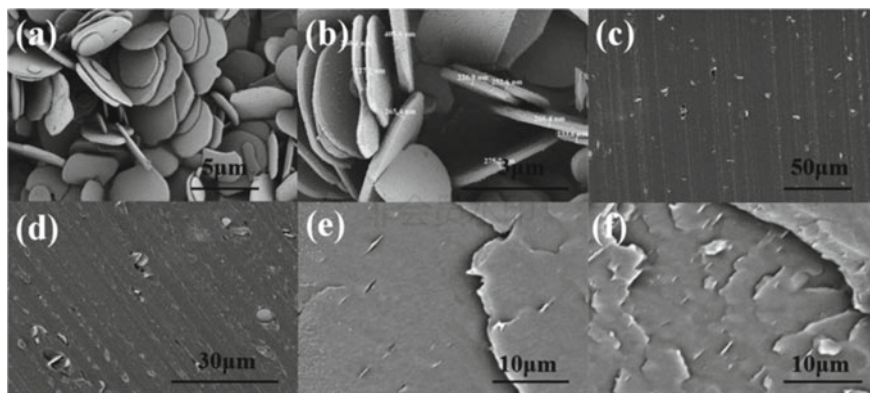


Fig. 9 SEM images of **a, b** uncoated α - Al_2O_3 nanosheets, **c, d** the cross section of cross-linked polyethylene (XLPE)/coated α - Al_2O_3 nanocomposites and XLPE/uncoated α - Al_2O_3 nanocomposites containing 2.0 wt% α - Al_2O_3 and **e, f** the cross sections of the nanocomposite specimens containing 1.0 and 2.0 wt% α - Al_2O_3 nanosheets after the liquid nitrogen quenching section, Ref. [24], Open access

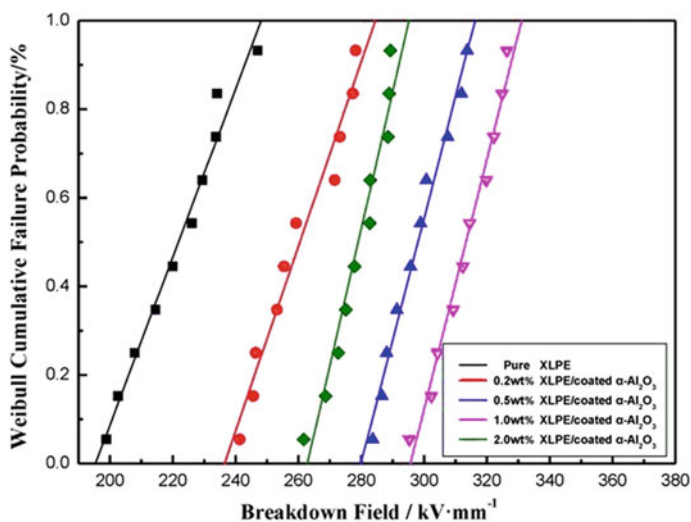


Fig. 10 Weibull plots comparing the direct current DC breakdown strength of pure XLPE and XLPE/ α - Al_2O_3 nanocomposites containing 0.2, 0.5, 1.0, and 2.0 wt% coated α - Al_2O_3 , Ref. [24], Open access

Besides, the surface modification of α - Al_2O_3 nanosheets effectively improved the direct current breakdown strength and reduced the conductivity of cross-linked polyethylene/ α - Al_2O_3 nanocomposites. Figure 10 shows a comparison of the DC breakdown strengths of pure XLPE and XLPE/ α - Al_2O_3 nanocomposites containing

0.2, 0.5, 1.0, and 2.0 wt% coated α -Al₂O₃. Clearly, the introduction of α -Al₂O₃ improved the DC breakdown field strength of the nanocomposites to various degrees. The DC breakdown field strength of pure XLPE was only about 220 kV/mm. In the XLPE/ α -Al₂O₃ nanocomposites, the DC breakdown field strength increased with increasing α -Al₂O₃ content; even an α -Al₂O₃ content as low as 0.2 wt% led to a significant increase (to 260 kV/mm). When the content of α -Al₂O₃ increased to 1.0 wt%, the DC breakdown field strength underwent a dramatic increase to 320 kV/mm. However, when the α -Al₂O₃ content continued to increase to 2.0 wt%, the DC breakdown field strength of the nanocomposite was reduced to 280 kV/mm (lower than for 0.5 and 1.0 wt%, but higher than for 0.2 wt%). The breakdown field strength (320 kV/mm) of the XLPE/coated α -Al₂O₃ nanocomposites (1.0 wt%) was higher than that (200 kV/mm) of the sandwich-structured Al₂O₃/LDPE nanocomposites, and lower than that (450 kV/mm) of the polyethylene/alumina nanocomposites.

Figure 11 showed the space charges of pure XLPE and the XLPE/ α -Al₂O₃ nanocomposites containing 0.2, 0.5, and 1.0 wt% of α -Al₂O₃ varied over time under the application of a DC voltage of 20 kV/mm. At the beginning of applied voltage, both electrons and holes are injected from the cathode and anode separately. After 120 s, the heterocharges and homocharges accumulated rapidly near the cathode in XLPE and reach a maximum, which was about 6 C/m³ in contrast to 3 C/m³ around the anode. The amount of space charge near the both electric poles increased with time and rapidly reached a maximum. At the same time, a small amount of space charge packets developed within the specimen, and the same was true for the XLPE/ α -Al₂O₃ nanocomposites. However, compared with pure XLPE, the space charge densities near the anode and cathode of XLPE/ α -Al₂O₃ nanocomposites were markedly reduced. This was particularly notable in the XLPE/ α -Al₂O₃ nanocomposites containing 0.2 wt% of α -Al₂O₃, in which the space charge density near the cathode was only about 3 C/m³, which was half that observed for pure XLPE.

Hamzah et al. compared alumina with two other nanofiller (zinc oxide and organoclay) embedded in cross-linked polyethylene (XLPE) at different filler loadings (0.5, 1.0, 1.5, and 2 wt%) [25]. Melt flow index (MFI) was investigated and the comparison results were presented in Fig. 12a. The addition of 0.5 wt% organoclay drastically decreased the MFI values, while no significant change in MFI values is observed for alumina and zinc oxide. The flammability of alumina, zinc oxide, and organoclay filled XLPE nanocomposites were investigated by horizontal burning test. Figure 12b shows that zinc oxide filled XLPE nanocomposites has lower burning rate compared to alumina and organoclay.

For better performances of cable materials, very high mechanical and thermal property elements are important [11]. Jose et al. [26] studied the mechanics and thermal properties of an alumina/clay nanoscale hybrid filler assembling in cross-linked polyethylene. XLPE/alumina/clay hybrid nanocomposites showed improved thermomechanical properties. In the hybrid system, aggregation formation of Al₂O₃ nanoparticles was reduced by the presence of nanoclay platelets. The introduction of clay nanoplatelets into the nanocomposites resulted in filling the gaps between the Al₂O₃ nanoparticles. These nanoparticles were connected jointly

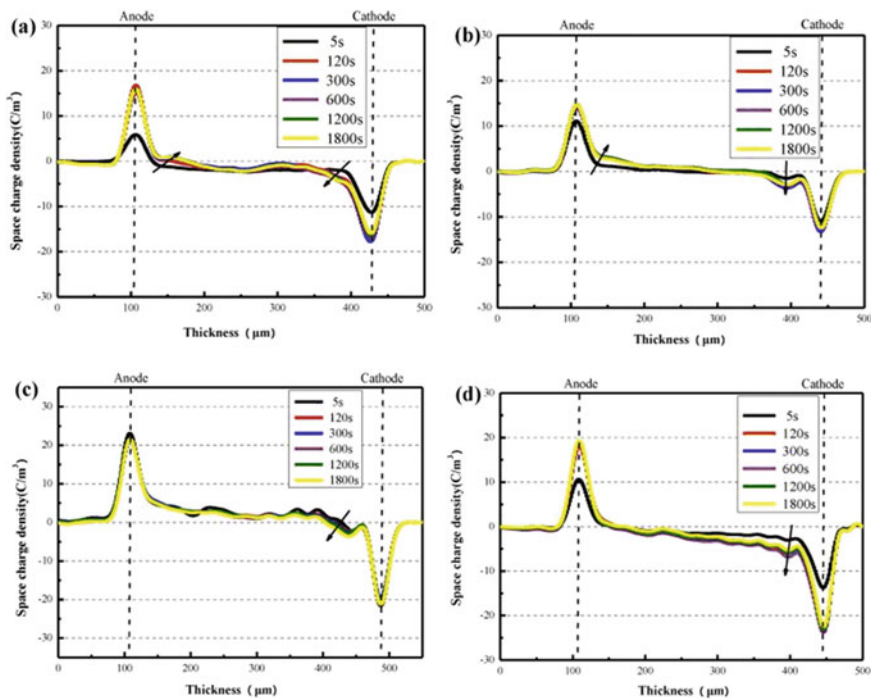


Fig. 11 a Space charge density of pure XLPE varied with the application time of DC voltage (20 kV/mm) b–d The space charge density of the XLPE/ α -Al₂O₃ nanocomposites containing 0.2, 0.5, 1.0 wt% α -Al₂O₃ varies with the application time of DC voltage (25 kV/mm), Ref. [24], Open access

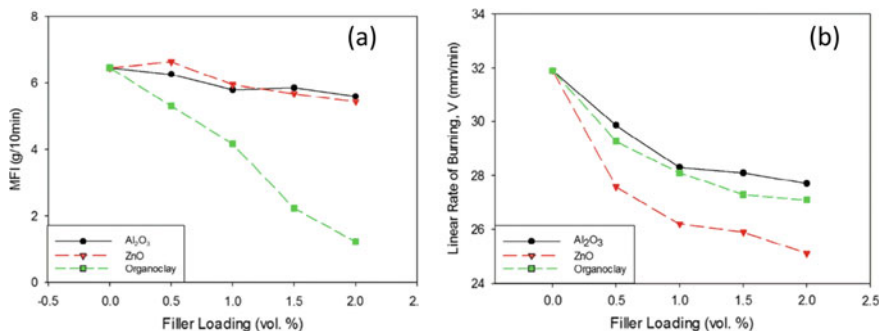


Fig. 12 a Effect of filler loading on melt flow index (MFI) and b effect of filler loading on linear burning rate of Al₂O₃, ZnO and organoclay filled XLPE nanocomposites. Redrawn and reprinted with permission from Ref. [25] Copyright 2019, Elsevier

through clay platelets, resulting in the creation of network morphology. In addition, Al_2O_3 can enhance the stress–strain behavior of neat XLPE over the entire range of strain. The hybrid nanocomposites (XLPE/ Al_2O_3 :clay = 1:1) exhibited the optimal yield strength and Young's modulus. The incorporation of clay particles reduces or eliminates the aggregation tendency of Al_2O_3 nanoparticles, and their variance in surface characteristic properties provides a well-dispersed morphology. The enhancement in Young's modulus could be attributed to the synergistic stabilization of alumina and clay that involves the formation of network morphology.

vi XLPE/PPy nanocomposites

The addition of a certain amount of polypyrrole (PPy) nanocomposites could suppress the space charge accumulation and improve effectively the direct current (DC) electrical characteristics of XLPE. Zhang et al. [27] prepared nanopolypyrrole (nano-PPy) and doped them in cross-linkable PE by melt blending and then obtained XLPE/PPy nanocomposites after cross-linking. They investigated DC conduction and breakdown strength of XLPE/PPy nanocomposites. The DC electrical characteristics measurement results were shown in Fig. 13. It can be seen that when different contents of nano-PPy were added to XLPE, the magnitude of the heterocharges adjacent to the cathode and anode was dramatically reduced, and the amount of space charges increased with time and rapidly reached a maximum. At the same time, a small amount of space charge packets developed within the specimen. As the short-circuit time prolonged, the space charges in the specimen did not decay, which perhaps could be attributed to the deeper trapping states provided by the nano-PPy, and the detrapping of the trapped space charges became difficult. The conductivity of the nano-PPy prepared in the experiment was 0.414 S/cm. It is noticeable that the introduction of nanopolypyrrole (nano-PPy) could reduce the DC electrical conduction current density of XLPE/PPy nanocomposites, improve the space charge distribution but not affect the cross-linking reaction and crystallinity of XLPE. While assuring excellent electrical conduction and space charge distribution characteristics, there was an optimum nano-PPy content to reduce the DC breakdown strength of XLPE/PPy nanocomposites insignificantly (Fig. 13).

vii XLPE/ TiO_2

When the TiO_2 nanoparticles and TiO_2 nanofibers were chosen as inorganic fillers to dope into cross-linked polyethylene (XLPE), their morphological, mechanical, thermal, and swelling properties will be enhanced. Jose et al. [28] prepared XLPE/ TiO_2 nanocomposites by melt mixing. They introduced silane surface modification agents on nanofillers, which promoted good dispersion of fillers into the polymeric matrix by overcoming the incompatibility between organic polymer and inorganic TiO_2 in hybrid nanocomposites. According to the results of tensile, thermogravimetric analysis and swelling studies, its performances showed an upward trend while further addition exhibited a downward trend, when the concentration reached 5 wt%, due to the improved interface and the combined effect of surface treatment and cross-linking mechanism. Once the threshold limit crossed, the particle–particle

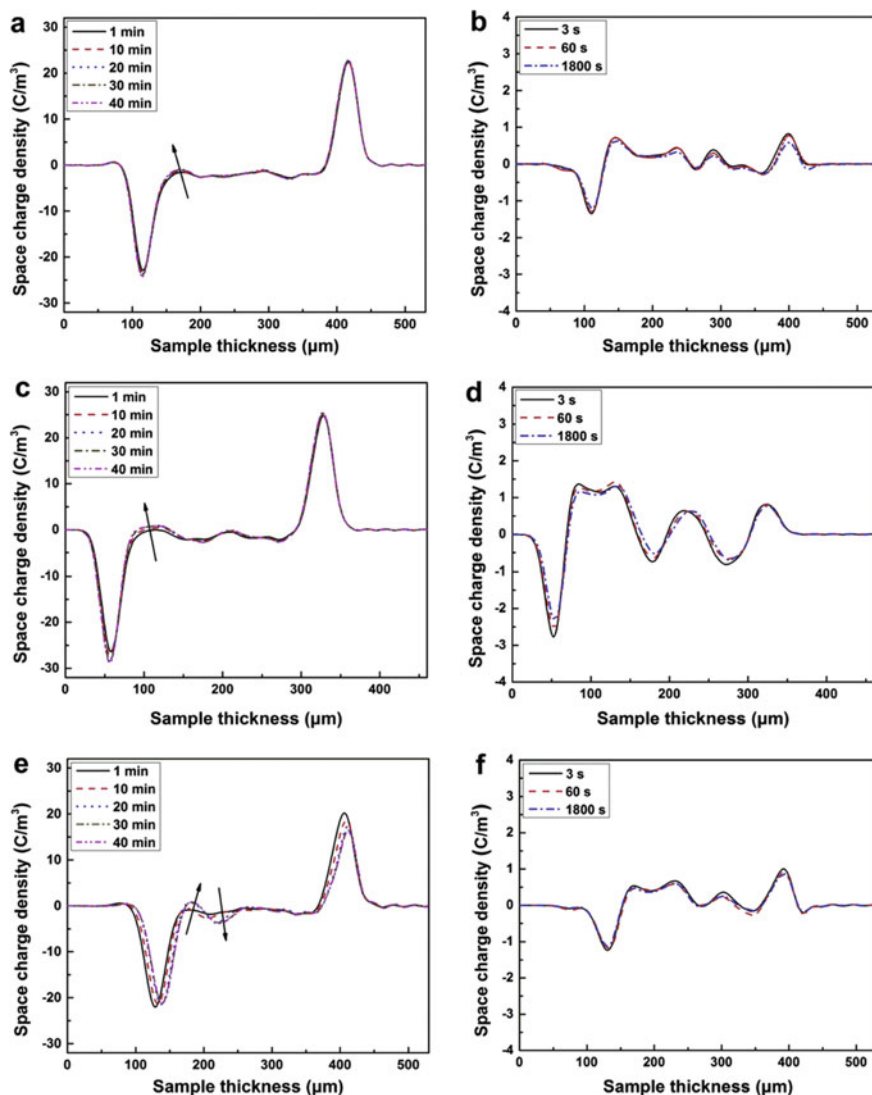


Fig. 13 Space charge distribution in the XLPE/PPy nanocomposites containing different nano-PPy contents during polarization or depolarization **a, b** corresponding to 0.2 phr, **c, d** to 0.5 phr, **e, f** to 1.0 phr; **a, c, e** corresponding to polarization, **b, d, f** to depolarization. Reprinted with permission from Ref. [27] Copyright 2018, Elsevier

interaction dominates over the particle–matrix interaction and the properties showed a decreasing trend. Some researchers proposed that hydroxyl groups on the UN-TiO₂ nanoparticles surface could easily react with each other to form a chemical bond, leading to the TiO₂ nanoparticles’ tendency to agglomerate [29]. Wang and his co-authors have conducted corresponding researches on the issue

with the space charge characteristics and dielectric properties in TiO_2/XLPE nanocomposites [29, 30]. They used dimethyloctylsilane (MDOS) as coupling agent to improve the compatibility between TiO_2 nanoparticles and XLPE matrix and reduce the agglomeration of TiO_2 nanoparticles. Figure 14 showed the SEM images of the four types of TiO_2/XLPE with different mass concentrations (1, 3, and 5 wt%). It can be seen that TiO_2 nanoparticle dispersion was uniform in UN- TiO_2/XLPE nanocomposite, but agglomeration phenomenon was serious, with particle radius of 400 ~ 600 nm. However, the agglomeration phenomenon in MDOS- TiO_2/XLPE was better than UN- TiO_2/XLPE nanocomposite, with particle radius of 25 ~ 200 nm. Therefore, the TiO_2 nanoparticle dispersion and compatibility in XLPE could be improved to a certain extent by MDOS coupling agent. The electric field distribution of pure XLPE and TiO_2/XLPE under DC stress of 30 kV/mm at 1800 s was shown in Fig. 15. The electric field distortion at the electrode was obvious in pure XLPE, because a large number of heterocharges accumulated at XLPE–electrode interface, and the maximum electric field near the anode was -36 kV/mm. The electric field distribution of TiO_2/XLPE nanocomposites was significantly improved, among which the electric field distortion of MDOS- TiO_2/XLPE nanocomposites was the weakest. In particular, the intensity of the internal electric field of MDOS- TiO_2/XLPE was basically the same as that of the external electric field. Generally, the mean volume density of space charge was used to quantitatively describe the space charge accumulation. Figure 16 shows the relationship between mean volume density of space charge in TiO_2/XLPE and polarization time. It can be found that the total charge accumulation volume was effectively suppressed both in UN- TiO_2/XLPE and in MDOS- TiO_2/XLPE

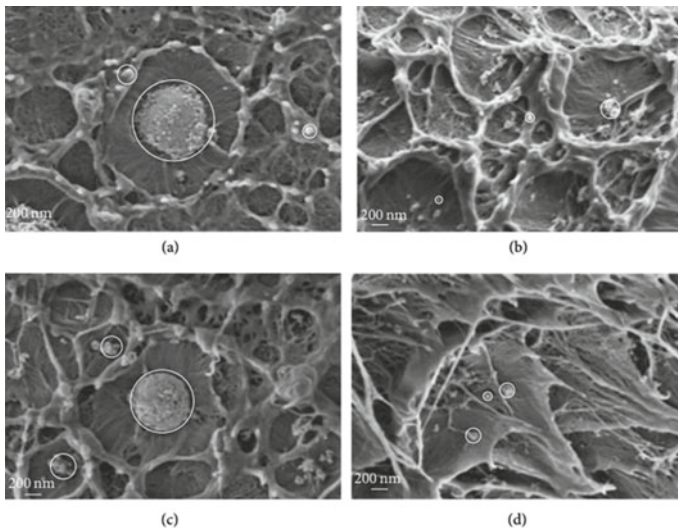


Fig. 14 SEM of TiO_2/XLPE . **a** UN- TiO_2/XLPE (1 wt%), **b** MDOS- TiO_2/XLPE (1 wt%), **c** UN- TiO_2/XLPE (5 wt%), and **d** MDOS- TiO_2/XLPE (5 wt%), Ref. [29], Open Access

Fig. 15 Electric field distribution of pure XLPE and TiO₂/XLPE under DC stress of -30 kV/mm at 1800 s, Ref. [29], Open Access

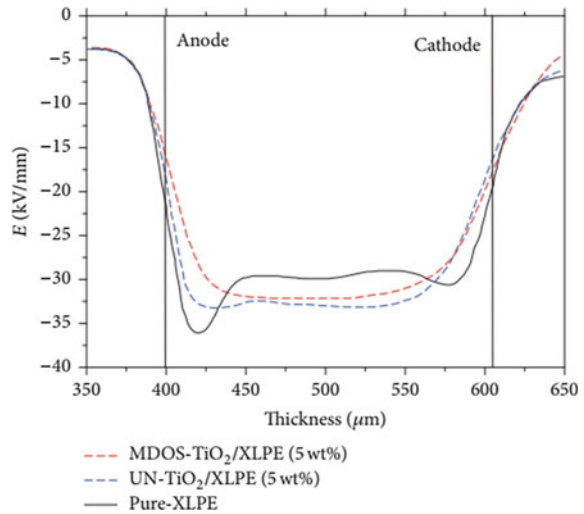
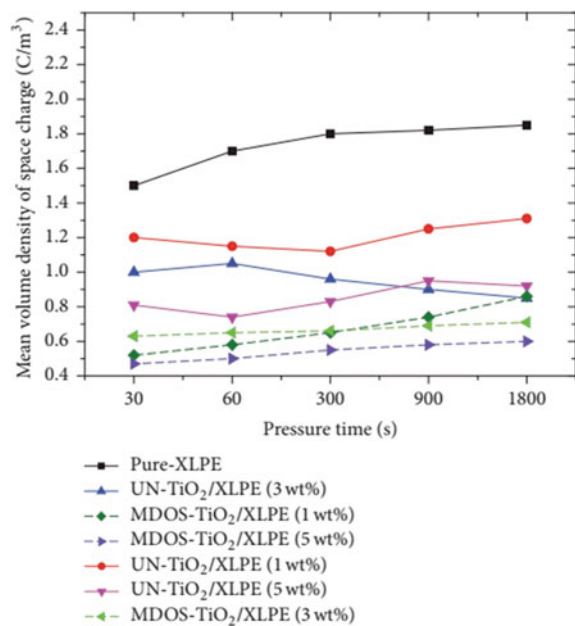


Fig. 16 Mean volume density of space charge in TiO₂/XLPE, Ref. [29], Open Access



nanocomposite. By contrast, MDOS-TiO₂/XLPE is better at suppressing charges than UN-TiO₂/XLPE. In addition, the TiO₂/XLPE nanocomposites had higher volume resistivity, lower permittivity, and dielectric dissipation, which increased with the filling concentrations and decreased with the measured frequency. This is because those TiO₂ nanoparticles bring deep traps, which can shorten the effective distance of “solitary waves” migration and greatly reduce carrier mobility. Such

low carrier mobility improves the recombination process and weakens the ionization of impurities, leading to the disappearance of heterocharge in TiO_2/XLPE . The interface reverse electric field not only suppresses the charge injecting from the electrodes, but also strengthens the electric field in the middle of matrix [30].

viii *XLPE/GO*

Given that graphene oxide (GO) can improve the thermal stability and the fire safety properties of non-polar polymers, it is often used as the nanoadditive or blends to boost the electrical performance of XLPE. Toselli et al. [31] prepared a kind of cross-linked polyethylene (XLPE) coated with hybrid organic–inorganic thin films obtained via sol–gel reactions and containing small amounts (from 0.2 to 0.8 wt%) of graphene oxide (GO). The thermo-oxidation of XLPE substrate was assessed by isothermal differential scanning calorimetry (DSC) and Fourier transform infrared (FTIR) analysis to determine the oxidative induction time (DSC-OIT) and the oxidation index, respectively. The results showed that the presence of GO significantly increases the thermo-oxidative resistance of the coated XLPE. The effect of GO is attributable to an improved barrier against oxygen diffusion, which in turn results in a lower damage of XLPE with significant improvement of mechanical properties (durability) over long aging times. Figure 17 showed the strength and strain at fracture versus aging time of XLPE/GO. For the uncoated samples, after a first slight increase in the values of tensile strength, a strong and progressive reduction in both tensile strength and strain at fracture can be observed as aging proceeds. The coated specimens undergo a similar increase in tensile strength at relatively short aging times, whereas they show a significantly different behavior for the strain at fracture even at relatively short aging times. However, the most relevant effects of the coating are shown at long aging times. In particular, from 500 to 1500 h of aging, the strain at fracture shows an almost steady value and the tensile strength slightly increases. The comparison of the mechanical properties of uncoated and coated XLPE after long aging times is impressive; coated samples still have properties similar to pristine XLPE after 1500 h of aging, while uncoated samples are so brittle that their properties cannot be measured at aging times over 800 h [31].

Recently, Han et al. prepared a kind of XLPE/GO nanocomposites by mechanical blending [32]. The functionalized graphene oxide (fGO) quantum wells (QWs) with quantum confinement effects were produced by chemically grafting the polycyclic aromatic compounds (PAC) onto the surface of GO QWs. They investigated the DC conductivity, the space charge behaviors, the charge transport characteristics, and breakdown properties of cross-linked polyethylene (XLPE)/graphene oxide (GO) nanocomposites. The GO QWs showed a synergistic effect with PAC on the modification of insulating properties in XLPEs. The grafted PAC on the surface of GO QWs still retains its original function of attenuating the energy of charge carriers, while the interlayer distances of fGO QWs increase after functionalization. So the XLPE/fGO nanocomposites own a much lower conductivity, fewer space charge accumulation, and higher breakdown strength than those of the other XLPEs.

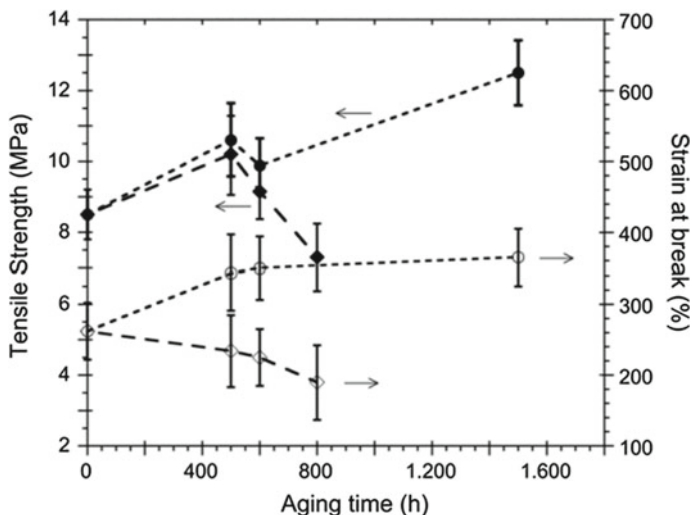


Fig. 17 Tensile strength (full symbols) and strain at fracture (empty symbols) of uncovered XLPE (diamonds) and covered XL-SiO₂-GO_{0.5} (circles) as a function of aging time. Reprinted with permission from Ref. [31] Copyright 2014, Elsevier

2.2 Properties of XLPE Nanocomposites and Blends

XLPE nanocomposites and blends have the preternatural interface structures and unique functions, and they are largely changed in electrical, thermal, mechanical, and chemical properties. The following is an overview of the latest progress in XLPE nano composites and blends according to different properties.

2.2.1 Electrical Properties

i. Dielectric Properties

Dielectric property, one of the most essential XLPE properties, has been a popular topic as its charming highlights increasingly emerge. In this section, the recent research progress of XLPE dielectric properties is reviewed. As is well known, cross-linked polyethylene (XLPE) is often manufactured as pipe, film, and foam products and used as electric insulation material. To improve the dielectric properties of XLPE film, a study applied carbon tetrafluoride (CF₄) dielectric barrier discharge (DBD) as a surface modification method [33]. The surface of XLPE film was modified at the low pressure of 1 kPa with different treatment time (15, 30, 60, 120, 240, and 480 s). After the surface modification, the water contact angle, trap depth, and breakdown voltage increase first and then decrease with treatment time extending. Meanwhile, the dielectric loss has an opposite trend, which represents

better dielectric properties. The reason is that fluorine can reduce the surface energy, which can significantly influence the water contact angle. Better hydrophobicity can restrain the accumulation of outside pollution on the surface. Moreover, fluorine has strong electronegativity, so amorphous crystalline and impurities interface trap depth become deeper and the dielectric loss becomes lower. Therefore, appropriate DBD treatment conditions can apparently improve XLPE dielectric properties. Lately, another study investigates the performance of nano-reinforced cross-linked polyethylene for high-voltage insulation applications with particular focus on dielectric characteristics, treeing behavior, and mechanical properties [34]. The nanocomposites with varying content of nanoclay were prepared by melt mixing of polyethylene, cross-linking agent, and nanoclay. X-ray diffraction and atomic force microscopy studies showed that layered silicates were uniformly dispersed with exfoliation in XLPE matrix up to 5 wt% nanoclay content with formation of intercalated structures with slight agglomeration at higher nanofiller content. The dielectric loss, relative permittivity, and dielectric strength of the nanocomposites increased with increasing nanoclay content, which was attributed to the inherent properties of XLPE and nanoclay, nanofiller dispersion and interfacial polarization. Incorporation of nanoclay in XLPE altered the electric field stress distribution in the material and consequently retarded water tree growth. Additionally, mechanical properties (e.g., tensile strength and modulus) of the nanocomposite were also enhanced. The changes in the properties were correlated to the morphology of the nanocomposites, as well as polymer filler interactions.

ii. *Space Charge Behaviors*

Cross-linked polyethylene is widely used as an insulating material in high-voltage cables. However, space charge accumulation under the DC field is one of the most challenging problems in the further development of XLPE insulated cable. The space charges can distort the distribution of the electrical field strength in the XLPE applied in the insulation materials, which can shorten the service life of the insulation materials. Therefore, the space charge characteristics of XLPE under the strong direct current (DC) electric field have been the focus of scholars and engineers all over the world. Due to the potential electrical degradation aging process triggered by the accumulated space charges, the IEEE standard 1732 was established for measuring space charge in HVDC extruded cables as the qualification tests. Space charge originates from either charge injection at the electrodes or ionization of impurities presenting inside the bulk. The accumulation of space charge in XLPE under DC stress can be simulated by a modified bipolar charge transport model [35]. The space charge behavior and electric field distribution were shown in Fig. 18. Both the calculated charge dynamics and field variation are consistent with the experiment results. Compared with the experimental observations, the simulation results can also reveal appropriate features of heterocharge formation.

The cross-linking degrees will affect the space charge characteristics of XLPE. Rogti et al. studied the space charge behavior in dielectric material and the

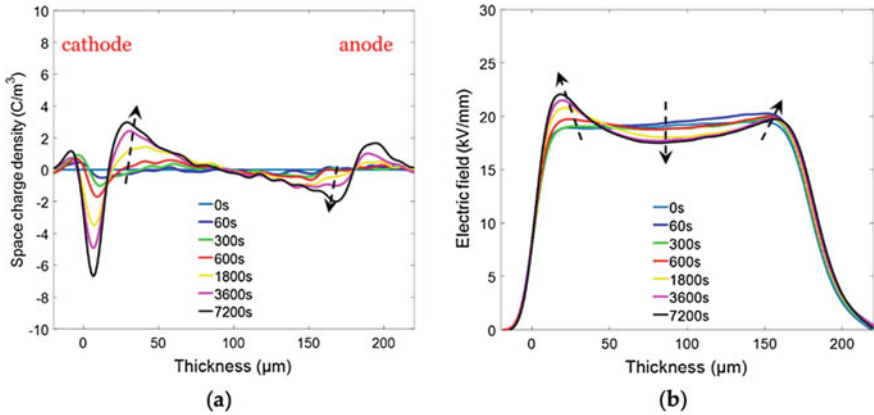


Fig. 18 **a** Space charge behavior in XLPE samples at 20 kV/mm field (capacitive charge removed). **b** Electric field distribution across the XLPE film, Ref. [35], open access

capacitive charge in an electrode–dielectric interface at room temperature under an applied electric field [36]. They found that a negative charge injection takes place at the dielectric interface and the charge can be affected by the electric field and the temperature. Kato et al. investigated space charge behavior and conduction current in polyethylene under DC stress [37]. One of the reasons for the different breakdown property in cross-linked polyethylene (XLPE) from that in low-density polyethylene (LDPE) may be based on the existence of cross-linking by-products in XLPE. Furthermore, a thermal history in cross-linking process for XLPE may also cause of the difference. The existence of the cross-linking by-products increases the conduction current in XLPE under DC stress. It is also said that an anneal treatment in air atmosphere may affect to the electrical properties under DC stress. The increasing dissipation power in XLPE is the cause of the breakdown in it under DC stress. Wang et al. measured the space charge distribution by the pulsed electroacoustic method (PEA) with dicumyl peroxide (DCP) as the cross-linking agent and low-density polyethylene (LDPE) as the base material [38]. The results show that the cross-linking effect significantly increases the threshold electrical field strength of XLPE, and as the content of cross-linking agent increases, the threshold electrical field strength increases at first and then decreases, and the threshold electrical field strength reaches the maximum value when the content of the cross-linking agent is 1.0 or 2.1%. The cross-linking effect introduces negative charge traps into the LDPE and increases the densities of the deeper charge traps. The presence of cross-linking by-products suppresses space charge formation. The addition of nanofillers, such as SiO₂, to XLPE enhances the formation of negative space charge near the cathode [39, 40]. In order to avoid agglomeration of nanoparticles and overcome the phenomenon of uneven distribution in XLPE, voltage stabilizer were often applied, which can reduce the energy of high energy electrons that injected into the materials from electrodes under high temperature (thermal-assisted

emission) and high electric field, prevent the energy from these electrons being transferred to the polyethylene chains and ensure that the polymer matrix is not damaged. Compatibility is an important consideration when selecting high-pressure stabilizers [41]. In addition, insulation thickness is also an influential factor in space charge accumulation [42]. There is a thickness dependence between space charge accumulation and insulation thickness, due to the effects of charge injection, extraction, trapping, recombination, mobility, and diffusion.

As the previous section described, nanofiller addition, such as SiO₂, SiC, TiO₂, MgO, GO, and so on, particularly surface-modified nanofiller due to its better dispersion significantly can suppress the space charge accumulation and conductivity. Nevertheless, the choice of suitable nanocomposites with higher nanofiller permittivity and a series of practical problems related to actual industry has still remained a challenge.

iii. *Partial discharge (PD) characteristics*

Cross-linked polyethylene (XLPE)-insulated power cable has a wide application in transmission and distribution networks, and flexible DC transmission areas. Meanwhile, cross-linked polyethylene (XLPE) power cables can be subjected to alternating voltage with superimposed impulse transients. Such impulse transients may initiate partial discharges (PD) in insulation defects even below AC inception voltage, so PD is usually considered as an important factor to evaluate the condition of electrical insulation. An initiated PD may persist under AC, which will cause insulation degradation. Partial discharge (PD) measurement is considered as an effective tool to detect premature degradation and even identify insulation defects for power cable. To measure discharges, very low frequency (VLF—0.1 Hz or lower) excitation has emerged as an attractive alternative to the conventional power frequency (PF—50/60 Hz) testing as it significantly reduces the required reactive power from the test supply. As the discharge process mainly resulted from the enhanced electric stress, it is necessary to understand how the electric field distributes on the XLPE dielectric surface when it is exposed to a high-voltage AC excitation. Recently, the distribution of surface electric field before, during, and after a PD event at VLF and PF test voltage was investigated by Morsalin et al. [43]. Finite element analysis (FEA)-based numerical simulation shows that the space charge dynamics cause the differences in the field distribution. In addition, the high-frequency PD detection technique can be used to locate the position of discharge. Hao et al. [44] used a high-frequency PD detection technology to study a suspected PD signal in the inside of T-joint and intermediate joints nearby during a 110 kV XLPE cable PD test. A trace of discharge was found at the air gap of the metal ring and the epoxy sleeve in the front of the T-joint stress cone.

PD characters often varied with different aging phases, leading to the fluctuation of PD fingerprint parameters. Song et al. [45] made an investigation about PD aging tests at DC voltage for four kinds of insulation defects, i.e., inner semiconductive layer breakage, internal air cavity defect, insulation surface scratch defect, and outer semiconductive layer creepage. Without taking the time-sequence feature of PD

data into consideration, the recognition rate was only 72.93% in the usage of fingerprint parameters. For the aim to improve recognition effect, a model based on bidirectional recurrent neural networks (BRNN) algorithm was proposed. With the dataset acquired by four insulation defects testing, the recognition rate of the BRNN model is 93.71%. The BRNN-based recognition model serves to eliminate the influence of insulation aging on the PD fingerprint of XLPE cable, and to improve the identification efficiency to a certain extent. A feature extraction method for gray intensity image of partial discharge (PD) is applied to recognize the insulating defects in high-voltage cross-linked polyethylene power cable joint [46]. The method is based on a two-directional and two-dimensional (2-D) maximum margin criterion (MMC). A 2D orthogonal projection of gray intensity image of PD was performed in horizontal and vertical directions. Projected image data were taken as discriminant vector of different gray intensity images to solve the high dimensional and small sample size of PD gray intensity image. The nearest neighbor classifier was used to classify the PD gray intensity image to recognize different insulating defects in the joint. The recognition results of four typical insulating defects in the laboratory indicated that the extraction speed of the gray intensity image feature and recognition rate of insulating defects are superior compared with the common principal component analysis and Fisher discriminant analysis with MMC.

In XLPE cable systems, partial discharges primarily occur along dielectric interfaces or splices and cable terminations. PD may also occur within the cable insulation itself around mechanically degraded spots or impurities. Some XLPE nanocomposites and blends have lower PD formation, higher discharge inception voltage (DIV) as well as breakdown voltage as compared with virgin samples. The differential scanning calorimetry (DSC), thermogravimetric analysis (TGA), Fourier transform infrared (FTIR), and contact angle measurement study conducted suggest that the addition of nanofillers or nanocomposites, such as nanosilica and so on, leads to the change in the melting point, thermal degradation temperature, heat of fusion, bonding structure, and the contact angle of the polymer, respectively.

2.2.2 Thermal Properties

XLPE processes thermal properties which permit a continuous maximum conductor temperature of 90 °C and a maximum short-circuit temperature of 250 °C.

Carbon nanotube-reinforced cross-linked high-density polyethylene nanocomposites were synthesized for geothermal applications requiring higher polymer thermal conductivity and a comprehensive thermal decomposition study in 2014 [47]. The prepared nanocomposites were investigated by laser flash analysis and temperature modulated DSC revealing a great enhancement on the specific heat capacity along with a further enhancement on the thermal diffusivity, resulting in some cases in an overall thermal conductivity increase of more than 200%. For the thermal decomposition or recycling process of the produced nanocomposites, a thorough examination of the decomposition process and its kinetics was performed by using thermogravimetry and analytical pyrolysis-gas chromatography–mass

spectroscopy. The conducted decomposition kinetics using isoconversional and model-fitting methods were in agreement with the proposed decomposition mechanisms. From the complementary use of analytical pyrolysis and thermal analysis techniques study, it was revealed that the presence of carbon nanotubes hinders the diffusion of the primary scission products of PEX and enhances its thermal stability.

In order to investigate the progress of waste cross-linked polyethylene (wXLPE) thermomechanical degradation, Formela et al. [48] used a simultaneous thermogravimetric/differential scanning calorimetry analyzer coupled with Fourier transform infrared spectroscopy, swelling measurements, tensile tests, and scanning electron microscopy to analyze it. Volatile organic compounds generated during wXLPE degradation were determined using static headspace and gas chromatography–mass spectrometry. It was observed that duration of thermomechanical processing of wXLPE has significant impact on content of low molecular degradation products, chemical structure, swelling, thermal, and morphological properties of degraded wXLPE, while its impact on physico-mechanical properties was negligible. This indicates complex structural and chemical changes in wXLPE during its thermomechanical degradation, which is related to two opposite factors: (i) decross-linking efficiency during thermomechanical processing of wXLPE and (ii) partial plasticization of polyethylene matrix by volatile degradation products.

2.2.3 Mechanical Properties

The mechanical properties of the XLPE are superior to many other insulations, offering greater tensile strength, elongation, and impact resistances. The addition of some nanocomposites such as carbon black can be used to further enhance hot deformation and cut through resistance. The XLPE insulation will not melt or drip, even at the temperatures of soldering irons, and it has increased flow resistance and improved aging characteristics.

Recently, the significantly improved mechanical performance of cross-linked high-density polyethylene reinforced with multiwalled carbon nanotubes (MWCNTs) is examined by Roumeli [49]. The scanning and transmission electron microscopy and micro-Raman spectroscopy revealed a major turning point of the elastic and deformation behavior of these composites as a consequence of filler content. This experimentally detected behavioral turning point inspired the use of various micromechanical models for the prediction of the composites' elastic behavior. A modern three-phase approach accounting for the matrix, aggregated, and finely dispersed filler states adequately describes the experimental data below the turning point, while for higher concentrations, a standard two-phase model is selected to describe the nanocomposites' elastic behavior. Based on the combination of microscopic observations and micro-Raman analysis, it is suggested that the observed and modeled change in the mechanical behavior occurs as a consequence of two competitive mechanisms governing the incorporation of MWCNTs in

XLPE: a tendency to enhance its mechanical properties by successful load transfer and a drive to form bundles, reducing this positive effect.

Another research reported a high-performance high-density polyethylene with significantly enhanced mechanical strength by means of pressure-induced flow (PIF) and low-temperature cross-linking treatment [50]. The tensile and flexural strengths increased from 23.5 and 36.2 MPa, up to 74.8 and 78.6 MPa, respectively. This was achieved by the elongated and flattened “brick-and-mud” like crystal structure of HDPE occurred during PIF, and an adequate cross-linking network that was formed in the amorphous region beneath the melting point. Furthermore, high strength foams of this material could also be produced under supercritical CO₂ batch foaming in solid state.

Lately, the cross-linked polyethylene scrap from electrical wire and cables was micronized and separated in average particle sizes of 100, 500, and 900 μm, after which sheets of XLPE concentrates in high-density polyethylene HDPE were produced, using a calendaring process [51, 52]. The sheets were ground and incorporated into HDPE by means of a twin-screw co-rotating extruder and subsequently injection molded into test specimens. A 2 by 2 factorial design with center point was used, where XLPE contents varied between 1 and 9 wt% and average particle size between 100 and 900 μm were assessed as to the effect of XLPE content and particle size on HDPE mechanical properties. Increase in XLPE content significantly increased only impact strength and decreased tensile and flexural strength, and flexural modulus. The effect on tensile modulus and strain at break was not significant for the adopted 95% confidence interval. The increase in XLPE average particle size affected positively only impact strength of the material and decreased strain at break and flexural modulus. The effect on tensile and flexural strength and on tensile modulus was not significant for the adopted 95% confidence interval. The interaction between the two variables decreased impact strength and increased tensile modulus and was not significant for the other properties.

2.2.4 Aging Properties

i. *Electrical Trees*

Electrical tree is an important factor in the threat of the safety of cross-linked polyethylene insulation, eventually leading to the electrical failure of cables. Electrical tree structure is one of the most important influencing factors for electrical treeing characteristics in polymers [52]. In 2005, Sarathi et al. made a research on electrical treeing phenomena in XLPE cable samples using acoustic techniques [53]. Electrical trees were generated experimentally in the actual 33 kV underground XLPE cable insulation material under the AC voltages. A tree-like structure and a bush type of tree structure can form from the point of defect site under the AC voltages. Acoustic emission technique was adopted to identify the point of inception, propagation, and termination of electrical trees. A variation in the dominant

frequency content of the acoustic signal was observed as and when the tree propagates in the insulation structure. The characteristic variation in the magnitude of the acoustic emission signal with time, indicates that tree propagation as an intermittent growth process. The energy content of the acoustic signal characterizes that the energy released due to partial discharges, at every step growth of the tree structure is not the same. The partial power measurement provides an indication to the growth process of electrical trees and to the near point of failure of polymer insulation material due to electrical treeing. In 2011, the characteristics of electrical tree growth in XLPE samples have been investigated by Bao et al. [52] XLPE samples are obtained from a commercial XLPE power cable, in which electrical trees have been grown from pin to plane in the frequency range of 4000–10,000 Hz, voltage range of 4–10 kV, and the distances between electrodes of 1 and 2 mm. Images of trees and their growing processes were taken by a charge-coupled device (CCD) camera. The fractal dimensions of electric trees were obtained by using a simple box-counting technique. The tree growth rate and fractal dimension were bigger when the frequency or voltage was higher, or the distance between electrodes was smaller. Contrary to their expectation, the required voltage of the similar electrical trees decreased only 1 or 2 kV when the distance between electrodes changed from 1 to 2 mm. In order to evaluate the difficulties of electrical tree propagation in different conditions, a simple energy threshold analysis method has been proposed. The threshold energy, which presents the minimum energy that a charge carrier in the well at the top of the tree should have to make the tree grow, has been computed considering the length of electrical tree, the fractal dimension, and the growth time. The computed results indicate that when one of the three parameters of voltage, frequency, and local electric field increases, the trends of energy threshold can be split into three regions. At the same year, they went on to study the structure characteristics of electrical treeing in cross-linked polyethylene (XLPE) insulation under high-frequency voltages [54]. The tree structure characteristics include structure distribution characteristics and structure conversion characteristics. The influences of voltage, frequency, and pin-plane spacing on tree structure characteristics were analyzed based on the experimental results. It can be concluded that tree structures regularly change with the local electric field and frequency. The electric field in a very small zone near the needle tip is an important influencing factor for the formation of bush-like trees, and the lowest frequencies for the observed pure-vine-like trees increased with voltage. For double-structure trees, the local electric field at the transition location of the two structures remained almost unchanged with voltage and pin-plane spacing, but obviously increased with frequency. In order to investigate the relations of the growth rate and fractal dimension with tree structure characteristics, a new parameter, the energy threshold W_t , has been introduced and calculated for different tree structures. The shape of electrical trees formed in XLPE cable insulation at low temperature under AC and harmonic voltages are generally fibrillar type. When Mittal et al. analyzed the cable insulation failure, they observed that the voltage wave shape and peak factor exhibit high influence on the life of cable insulation due to electrical treeing [55]. Harmonics with higher THD and the failure rate of cable insulation due to

treeing are the same. The presence of 4th and 5th harmonics in supply voltage could cause early failure of cable insulation. Ultra-high-frequency (UHF) signal radiated during tree growth process under harmonic voltages lies in the range 0.5–1.5 GHz. Phase-resolved partial discharge (PRPD) analysis using spectrum analyzer has revealed that under 50 Hz, discharges occur near zero crossing and in the presence of harmonics, it occurs when the rate of voltage rise is high. The discharge occurs at its peak under low-frequency AC voltage of 1 Hz.

Effective strategies to prevent the electrical tree growth and extend the lifetime of cross-linked polyethylene (XLPE) insulation are of crucial importance for the development of power cable industry. Since polycyclic compounds have the potential to suppress electrical treeing growth, Zhu et al. [56] made an investigation that three types of polycyclic compounds, 2-hydroxy-2-phenylacetophenone, 4-phenylbenzophenone, and 4,4'-difluorobenzophenone, are added into XLPE, denoted by A, B, and C. Electrical treeing characteristics are researched with DC-impulse voltage at 30, 60, and 90 °C, and the trap distribution and carrier mobility are characterized. It has been found that although three types of polycyclic compounds can all suppress the electrical tree propagation at different voltages and temperatures, the suppression effect of these polycyclic compounds with the same DC-impulse polarity is worse than with the opposite polarity. As the temperature increases, the suppression effect becomes weak. The energy level and deep trap density are the largest in XLPE-A composite, leading to a decrease in the charge transportation and resulting in the suppression of electrical treeing growth, which might have great application prospects in high-voltage direct current (HVDC) cables.

ii. *Water Treeing*

Water treeing is a defect which is the result of imperfections in the insulation where fracture lines occur and grow in the direction of the electric field, increasing with electrical stress. It is a predominant mechanism of premature failure of underground XLPE distribution cables. Improved water tree resistance is a benefit of XLPE insulation for low-voltage (LV) cables and medium-voltage (MV) cables over PE insulations. Recent studies show that insulation degradation is due to injection of hydrophilic ionic species into the insulation and its rupture under the action of electromechanical and electrochemical processes operating at the microscopic level in the presence of strong field enhancement. Therefore, the ionic contamination in semicon screens as well as in the matrix of insulation play dominant role. In order to understand the role of contaminants in the semiconducting screens of medium-voltage XLPE insulated cables in electric power utilities, Qureshi et al. [57] studied the effect of two purposely selected ionic aqueous species on the treeing parameters evolved in these cables as a result of accelerated stress aging in the presence or absence of outer semiconducting screens. Results show that ionic impurities present in semicon screens that belong to transitional metallic group do catalyze the treeing process. If the semiconducting screens were produced and extruded over insulation using extra clean carbon then these would

act as a barrier toward the degradation of cable's insulation. If some suitable ion trapping materials are blended in the base matrix of semiconducting screens, the water tree growth in polymeric insulation can be effectively retarded.

Water trees are localized degraded zones that can be found in the polymeric insulation of service-aged underground cables and observed as microchannels or chains of microcavities in the bulk of a solid dielectric material. Since water trees have microscale local structures, some phenomena related to them can be understood and analyzed in detail only when using numerical analysis methods such as finite element method (FEM). For the artificial accelerated growth of water trees, water electrodes in needle form or with conical structure are often utilized, and then some unexpected initiation positions and shapes of water trees have frequently been observed. Kim et al. [58] made an investigation of the influence of the geometrical configuration of water electrodes on water tree initiation and its shape, on the basis of numerical experiment results using the FEM and accelerated water treeing test data.

The power cable insulation is in permanence subjected to thermal aging during its operating service. Thermal aging may influence not only the electrical, physicochemical and other properties of the XLPE cable insulation, but also the initiation and propagation of water tree inside it. In 2007, Kim et al. [59] made a research on the influence of thermal degradation to the water treeing behavior of XLPE cable insulation and it shows that thermal oxidation is the most influential to the initiation and growth of water treeing from the surface of XLPE cable insulation among all the probable factors caused during thermal aging. In 2010, Ma et al. [60] investigated the effects of an ethylene propylene diene monomer (EPDM) and poly[styrene-*b*-(ethylene-co-butylene)-*b*-styrene] (SEBS) on the water tree resistance in cross-linked polyethylene (XLPE). The XLPE/EPDM and XLPE/SEBS blend samples were prepared by melting compounding and subsequent compression molding. It was found that SEBS could greatly increase the water tree resistance of XLPE and the resistance performance was improved with SEBS content within 15 phr, whereas EPDM did not show any improvement in the water tree resistance of XLPE. The frequency-dependent behaviors of the water treeing phenomena and the effects of EVA on the water tree resistance of XLPE/EPDM and XLPE/SEBS blends were also investigated. The water treeing phenomena of the blends were interpreted from the viewpoints of electromechanical and electrochemical mechanisms. In 2011, Qureshi et al. [61] subjected technical grade cross-linked polyethylene (XLPE) cable's insulations to heat cycling in the presence of electric stress and aqueous ionic solutions composed of NaCl, Cu(NO₃)₂ and CuSO₄. The results show a large water tree propensity index due to the sulfates. To evaluate contribution of cationic and anionic parts of salt compositions, trees were grown in solutions containing a fixed sulfate anion but different cations with valences of +1(Na⁺, K⁺), +2(Cu²⁺) and +3(Fe³⁺). The results of tree lengths show that cations play an important role in the growth of water trees. Different models which suggest that the water tree generation is based on the ionic nature of chemical species are examined in the light of present results and it is suggested that the physical and electrochemical nature of cations play an important role in the

reactions that cause degradation of the polymer in the presence of the applied electric field. In 2016, Chen et al. [62] investigated the effect of cross-linking degree on accelerated water tree aging in cross-linked polyethylene (XLPE). The peroxide cross-linking process was adopted to make XLPE specimens with different degrees of cross-linking by controlling the doping content of dicumyl peroxide (DCP) in low-density polyethylene (LDPE). The water blade electrode method was applied to accelerate water tree aging of LDPE and XLPE specimens (hereafter referred to as the specimens), and their morphologies were observed using an optical microscope. The variation of crystalline morphology and anti-cracking performance of the amorphous region in the specimens were analyzed by differential scanning calorimetry (DSC), scanning electron microscopy (SEM), and an electronic universal testing machine. Based on the experimental results, it was found that XLPE has great anti-water treeing performance compared to LDPE. In addition, the higher the cross-linking degree, the better the anti-water treeing performance. Although crystal growth is inhibited due to the cross-linking reaction, the density of tie molecular chains greatly increases in the amorphous region and exhibits significantly tighter lamellar stacking, which is the reason that water tree growth is restrained with increasing cross-linking degree.

3 Patents on XLPE Nanocomposites and Blends

Polyethylene (PE) is one of the most widely used plastics, which has excellent chemical stability (almost insoluble in any solvent at room temperature), low temperature toughness, easy to process and shape, low price, and good dielectric properties, and is widely used in industrial production and daily life in many fields. Ordinary polyethylene is a polymer composed of two elements C and H, and its molecular formula is $\text{CH}_2\text{-CH}_2\text{-}$. The molecular chain is of a linear structure. Its biggest disadvantage is its poor heat resistance and creep resistance, which limits its application in many fields. Especially in the aspect of PE pipe, its temperature and pressure resistance, environmental stress cracking resistance, weather resistance, oil resistance, and creep resistance are difficult to meet its requirements as a cold and hot water conveying pipeline for construction. Therefore, the heat resistance and creep resistance of PE can be greatly improved by changing the linear structure of PE into the three-dimensional network structure of cross-linked PE by physical or chemical means, resistance to environmental stress cracking and its wear resistance, resistance, fatigue resistance, mechanical properties, and transparency are significantly improved. Moreover, cross-linked polyethylene (XLPE) obtained by the cross-linking reaction of polyethylene (PE) can greatly enhance the mechanical properties and other properties of PE, which makes XLPE widely applied in the field of electric power engineering. With the diversification of XLPE market demand, the new patents related to XLPE nanocomposites and blends preparation methods, characterization technologies and production equipment keep emerging. The following are some typical patents authorized in recent years.

3.1 Invention on the Preparation and Synthesis of XLPE Nanocomposites and Blends

The cross-linking is the use of chemical cross-linking agents or high-energy rays to cross-link the polymer from a linear structure to a network structure. The choice of cross-linking agent should depend on the polymer variety, processing technology, and product performance. The cross-linking methods of polyethylene include irradiation cross-linking, peroxide cross-linking, silane cross-linking, and azo cross-linking.

3.1.1 Irradiation Cross-Linking

Polyethylene, such as coated PE sheathed on wire, film, thin wall pipe, and other products, is converted into cross-linked polyethylene products by using a gamma rays, or high-energy rays irradiation on cross-linking (polyethylene molecules to produce free radicals, formation of C–C cross-linking chain). Cross-linking degree is affected by the radiation dose and temperature, and the junction increases with the increase of radiation dose. Therefore, cross-linked polyethylene products with a certain degree of cross-linking can be obtained by controlling the radiation condition.

CN210025961U [63] developed a new device for feeding additives used in the production of irradiated cross-linking polyethylene foam, including the main body of additive feeding machine, a conveyor belt installed inside the main body of additive feeding machine, an additive storage tank, a sealing cover under the conveyor belt, the support frame installed in the middle of the lower part of the sealing cover, and a fastening nut above the support frame at the connection with the sealing cover. CN108264646A [64] disclosed a method for preparing cross-linked polyethylene film. Under normal pressure, the cross-linking was conducted by infrared irradiation. The cross-linking temperature was 100 ~ 170 °C. Over 80% of the infrared wavelengths used by infrared irradiation were concentrated in the range of 3 ~ 16 μm. The production of cross-linked polyethylene film can achieve high cross-linking degree and overcome the problem of sticky roller.

3.1.2 Peroxide Cross-Linking

Peroxide cross-linking generally uses organic peroxide as a cross-linking agent, which decomposes under the action of heat and releases active free radicals. These free radicals abstract hydrogen from the polymer carbon chain and generate active sites, resulting in the production of carbon–carbon cross-linking, forming a network structure. Peroxide crosslinking is often applied for providing materials with well heat stability due to high bonding strength of C-C bond. The technology requires a high-pressure extrusion device with reliable plasticizing effect, stable extrusion

pressure and low energy consumption. The shaping process performs “hot” cross-linking at elevated temperatures. The benefit of peroxide cross-linking is that the crosslinking process is done when polyethylene is in the amorphous state (above the melting point of the crystal).

Lyu et al. [65] prepared a chemical cross-linked polyethylene composition by adding 0.01 ~ 5% of assistant cross-linker by weight of polyethylene into the formula of peroxide cross-linked polyethylene, in which the assistant cross-linker are allyl organic compounds. This assistant cross-linker can effectively reduce the amount of organic peroxides, maintain the cross-linking density of pipe products, and effectively increase the oxidation induction time of pipe, thus improving the service life of pipe. This method can be widely used in the preparation of chemical cross-linking and has a good application prospect. Denis [66] invented an installation for manufacturing cross-linkable polyethylene compounds which comprises a melting machine, a melt pump, and a filtration unit. The installation allows to produce cross-linkable polyethylene compounds that may be further used for manufacturing insulating parts of medium, high, and extra-high-voltage power cables. Chen et al. [67] invented a cross-linked polyethylene composition that comprises 100 parts by weight of polyethylene, 0.05–5 parts by weight of a cross-linking agent, and 0.03–3 parts by weight of a cross-linking aid. Polyethylene is a copolymer, a homopolymer, or a mixture of both. The cross-linking agent is an organic peroxide having a half-life longer than 3 min at 190 °C and a multicomponent heterocyclic alkane consisting of 3–6 carbon atoms and 3–6 oxygen atoms and a derivative of both. The cross-linking aid is an organic substance containing a maleimide group, a (methyl) acrylate group and an allyl group and a polymer having a vinyl content higher than 50%. Preferably, the cross-linking aid is triallyl isocyanate (TAIC), triallyl isocyanurate (TAC), or a mixture of both. The cross-linked polyethylene composition has a cross-linking efficiency index >1000 Nm/g and a δ torque value >15 Nm at 220 °C, a high safe processing temperature and long cross-linking delay, and therefore it is particularly suitable for rotationally molded products. Stephen Cree et al. [68] invented a method to reduce peroxide migration in cross-linked ethylene-based polymer compositions. The cross-linked polyethylene composition prepared by this method has a high curing rate without any significant reduction in scorch resistance, heat aging and electrical performance, and are particularly useful as insulation sheaths for medium and high-voltage power cables. Chen et al. [69] disclosed a cross-linked polyethylene blend composition and its preparation method. The cross-linked polyethylene compositions include: 100 parts by weight polyethylene resins, 0.5 ~ 12 parts by weight unsaturated carboxylic acids, anhydride and polyolefin grafted with its ester derivatives, 0.2 ~ 6 part by weight peroxide cross-linking agents and 0.01 ~ 10 part by weight auxiliaries. This cross-linked polyethylene composition has excellent adhesion to various metals (e.g., aluminum, copper, steel, etc.) and other polar materials after cross-linking. And they also disclosed another cross-linkable polyethylene composition [70]. The composition comprises polyethylene, wherein the mass fraction of trichlorobenzene dissolving deposition of 90 °C of the composition is 49–83%; the composition is heated for 10–20 min at the temperature of 180–200 °C and subjected to

cross-linking, the content of gel of the obtained product is smaller than 20% in weight. By means of the cross-linkable polyethylene composition, the cross-linked polyethylene which is high in rigidity and capable of remarkably improving the impacting performance is obtained and can be applied in polymer welding.

3.1.3 Silane Cross-Linking

Silane cross-linking is a technology that uses a double-stranded vinyl silane to react with a molten polymer under the action of initiator to form a silane grafted polymer, which hydrolyzes in water in the presence of a silane alcohol condensation catalyst to form a network of oxane chain cross-linking structure. Silane cross-linking technology greatly promotes the production and application of cross-linked polyethylene due to its simple equipment, easy control of process, low investment, high cross-linking degree, and good quality of finished products. In addition to polyethylene, silane, cross-linking also need catalysts, initiators, antioxidants, etc.

Duan et al. [71] disclose a new silane cross-linked polyethylene composition and its preparation method. The two-step silane cross-linked technology is used to prepare the polyethylene composition, which can be used in the production of cross-linked polyethylene pipes, cross-linked polyethylene aluminum–plastic composite pipes, etc. By selecting the distribution of cross-linking agents, the increase of a compound inhibitor to prevent graft material premature cross-linking solved the problem of the storage time which is short in the existing technology, the adoption of HDPE solved the problem of low strength of materials, and the selection of the appropriate carrier resin solved problems of the silane and other liquid fertilizer loss. Therefore, a new type of silane cross-linked polyethylene composite was prepared. The aluminum–plastic composite pipe and cross-linked polyethylene pipe have good processing adaptability and product performance. Wang et al. [72] disclosed a cross-linked polyethylene composite material which inhibits the internal space charge and its preparation and application. The composite material is composed of low-density polyethylene and SiC nanoparticles with the assistance of cross-linking agent. The content of SiC nanoparticles was 1 ~ 5 wt %. The polymer matrix was low-density polyethylene, with a density distribution of 0.910 ~ 0.925 mg/cm³, a melting index of 2.1 ~ 2.2 g/10 min, and a melting point of 105 ~ 112 °C. The inner space charge density of this XLPE/SiC composite medium is smaller than that of the cross-linked polyethylene without adding nanoparticles, indicating that SiC nanoparticles can effectively improve the spatial charge distribution inside the cross-linked polyethylene and weaken the distortion of the electric field. Zhen [73] invented a silane cross-linked polyethylene special material which comprises common linear polyethylene resin, high-flow rate linear resin, a silane coupling agent, a catalyst, an initiating agent, a copper-resistant agent, an emulsus rheological agent, an antioxidant, and a lubricating agent, wherein the mass ratio of the common linear polyethylene resin, the high-flow rate linear resin, the silane coupling agent, the catalyst, the initiating agent, the copper-resistant agent, the emulsus rheological agent, the antioxidant, and the

lubricating agent is 80: (10.0 ~ 12.5): (1.5 ~ 2.0): (1.0 ~ 1.25): (0.5 ~ 1.25): (0.5 ~ 0.75): (0.5 ~ 1.0): (0.75 ~ 1.5): (0.75 ~ 1.6): (1.25 ~ 1.5). The product has excellent stability, mainly used in the water supply pipe industry, wire and cable industry, and autoparts industry. After being stored under the condition of certain temperature (25 °C and more than 25 °C), it also can be naturally cross-linked, which is superior to the two-step cross-linked insulating material in effect and has the advantages of simple process and convenience for operation.

Zhao et al. [74] invented a silane cross-linked polyethylene wire and cable insulation material preparation method. Silane cross-linked polyethylene insulating material for wires and cables is prepared from the following components: LLDPE-7042, LDPE, silane coupling agent, cross-linking agent DCP, antioxidant 300 and catalyst masterbatch; the catalyst masterbatch consists of the following components: LLDPE-7042, LLDPE-8320, PP, antioxidant 1010, antioxidant dilauryl thiodipropionate (DLTP), antioxidant 1024, organotin, and fluororubber masterbatch. As the main substitute to current polyvinyl chloride (PVC) materials, this material is mainly used for the insulation layer of cables whose insulation performance is better than PVC which will emit toxic and harmful gases when the wires are aged and caught on fire, while silane insulation material is non-toxic and harmless. Xia et al. [75] also disclosed a preparation method of one-step silane naturally cross-linked polyethylene aerial insulating material. The raw materials are composed by weight of components as follows: 85 ~ 95 parts of linear low-density polyethylene, 60 ~ 70 parts of high-density polyethylene, polypropylene 2 ~ 6 parts, 1 ~ 3 parts of the silane cross-linking agent, organic fertilizer 0.5 ~ 2 parts, rheological agent 1 ~ 2 parts, 1 ~ 3 parts of the composite antioxidant, catalyst 0.3 ~ 1 parts, copper resistance agent 1 ~ 3 parts, and processing agent 0.2 ~ 0.5 parts. This kind of insulating material can reduce silane cross-linking time effectively, which can reduce energy consumption, reduce cost, and improve production efficiency effectively.

3.1.4 Azo Cross-Linking

Azo cross-linking technology is to mix azo compounds into PE, and then extruding it below decomposition temperature of azo compounds. The extruded product is subjected to a high temperature salt bath. The azo compounds break down to form free radicals, which trigger polyethylene cross-linking.

3.2 *Inventions Related to XLPE Characterization*

WO2017112642A1 [76] invented a partially cross-linked multimodal polyethylene composition having the first molecular weight ethylene-based polymer component and a second molecular weight ethylene-based polymer component, wherein the partially cross-linked multimodal polyethylene composition comprises a density

from 0.930 to 0.943 g/cc measured according to ASTM D792, a melt index (I_2) from 0.01 g/10 min to 5 g/10 min, when measured according to ASTM D1238 at 190 °C and a 2.16 kg load, a molecular weight distribution (MWD) from 5 to 10, wherein MWD is defined as M_w/M_n with M_w being a weight average molecular weight and M_n being a number average molecular weight, and a complex viscosity ratio from 250 to 450, wherein the complex viscosity ratio is defined as the complex viscosity at a shear rate of 0.01 rad/s divided by the complex viscosity at a shear rate of at a shear rate of 100 rad/s. Zhu et al. [77] disclosed a multifunctional cross-linked polyethylene (XLPE) insulating performance tester. The multifunctional XLPE insulating performance tester is technically characterized by comprising a shell, and a high-voltage bin and a test circuit which are arranged in the shell, wherein a control panel is arranged on the shell; an insulating cover is arranged on the high-voltage bin; a fixed frame is arranged in the high-voltage bin; an insulating oil cup is arranged on the fixed frame; a high-voltage electrode and a ground electrode are oppositely arranged in the insulating oil cup; a temperature control device which is used for controlling oil temperature is arranged below the insulating oil cup; and the test circuit comprises a high-voltage power supply, a voltage meter, a timer, an over-current protection device, and a digital temperature meter. The multifunctional XLPE insulating performance tester can be configured to test a XLPE sample by regulating voltage between the two electrodes and adjusting the oil temperature of the insulating oil cup. It has voltage regulation and display functions, temperature regulation and display functions, time setting and display functions, and an over-current protection function. By using this method, the stability of an XLPE insulating test environment is guaranteed, and the insulating performance of the polyethylene at different operating temperatures and compressive strengths is truly and effectively reflected.

In 2015, Zheng et al. [78] proposed an assessment method of insulation aging of XLPE cables and their accessories. First, samples are positioned in thermal aging oven and subjected to aging test under four temperature spots. And then, the reserved elongation at break of the samples taken at different times are evaluated through tensile tests and color coded. According to Arrhenius theory, the residual life of aging cable is estimated. The advantages of this assessment method are that sampling is accurate but not blind and the process is simplified but not complicated, thus saving the test time and cost. Liu et al. [79] disclosed a judging method on XLPE cable insulation aging condition. First, the partial discharge of the first cable sample is used to determine whether the aging occurs. If not, the isothermal relaxation current of the second cable sample is calculated to obtain the aging factor, and the activation energy of the cross-linked polyethylene of the third cable sample is calculated, then, the aging factor and activation energy of cross-linked polyethylene are used as the general standard to obtain whether the cable under test has aging state and the severity of aging state. According to the invention, the isothermal relaxation current method and the activation energy method are adopted to comprehensively judge the aging condition of the cable insulation, so that it overcomes the defect that a large judgment error occurs when judging the aging condition of the XLPE insulation cable through a single index, and provides more

accurate evaluation of the aging condition of the XLPE cable insulation by combining two indexes of electrical quantity (aging factor) and non-electrical quantity (activation energy), and the judgment method is simpler.

In 2016, Li et al. [80] disclosed an anti-leakage ring for measuring polarization current of cross-linked polyethylene cable and an anti-leakage method. For the measured cross-linked polyethylene cable, the metal shielding layer and the outer semiconductor layer at both ends of the stripped cable are taken as reserved edge surfaces of the cable, and the metal copper strip with a width of 15 mm and a thickness of 2 mm is selected, and the length of the metal copper strip is selected according to the diameter of the cable core and the thickness of the insulating layer. The diameter and insulation thickness are assumed to be d mm and D mm, respectively. The length of the metal copper bar is $[\pi \times (D + d \times 2) + 30]$ mm if the allowance of 30 mm is considered. A hole with a diameter of 5 mm is drilled at a position 5 mm from the edges of the two ends of the metal copper bar, and then the metal copper bar is bent until the holes at the two ends are aligned to form a copper ring, namely an anti-leakage ring. The leakage current along the surface flows directly back to the power supply side without passing through the current measurement module, and the influence of leakage current along the surface on polarization is avoided. The current measurement module measures polarization current without including leakage current along the surface.

In 2017, Xu et al. [81] disclosed a kind of apparatus and method for detection and evaluation of cable partial discharge (PD), including tested cable and the detector of DC partial discharge for obtaining local discharge signal; the both ends of tested cable are connected with high direct voltage output device and current output device; temperature-detecting device is laid with tested cable. A comprehensive analysis of the virtual cable with current output device under no-load, offline, and load condition is carried out to measure the partial discharge at room temperature and to evaluate the insulation of the cable. Along with the XLPE market application domain broadening, the performance requirements become diversifying. In recent years, patents related to XLPE preparation technologies, characterization methods, and production equipment have been constantly emerging to meet the increasing market demand.

3.3 Inventions About XLPE Fabrication Equipment

For cross-linked polyethylene, its preparation equipment is also important. In the whole manufacturing process, the equipment at each step needs to control its accuracy and operation mode. In recent years, there are many research in the field of equipment.

CN210233955U [82] developed a coaxial two-way reactive extruder for preparation of cross-linked polyethylene, including tub and guide roller, and several support bars fixed on both sides of the tub wall along the relative vertical transporting direction. The support bar is juxtaposed with a relative on the lateral wall of

the vertical feed direction equipped with several hooked claws. Through the hooked claws, the limit space was formed between the sidewalls of the support bar. The two ends of the guide roller are installed in two relative limit spaces by means of a rotating shaft. The invention is used to solve the problems in the traditional techniques such as time-consuming and force consumption when adjusting the height of the guide roller in the cooling tank, inconvenience of extruded material bending on subsequent cutting, and contamination of the working environment due to leakage of liquid in the cooling tank. CN209552434U [83] provided a radiation cross-linked polyethylene molding device, which is used for the formation of radiation cross-linked polyethylene foam so that the radiation cross-linked polyethylene foam can have a strong anti-slip property after it passes through the furnace mouth after double roll and double-sided pressing. The device includes the first heating tube group, the second heating tube group, the grain forming machine, and the corona treater. The first heating tube group and the second heating tube group are used for heating the radiation cross-linked polyethylene foam. The grain forming machine is used for extruding the heated radiation cross-linked polyethylene foam to form the grain. The corona treater is used for corona treatment of the radiation cross-linked polyethylene foam transmitted by the grain forming mechanism. The device has the advantages of simple structure, convenient use, and strong anti-slip ability of the formed radiation cross-linked polyethylene. CN202607928U [84] disclosed an electron-beam irradiation cross-linking polyethylene foam production line, which mainly consists of an automatic feeding device, a vertical foaming chamber unit, an electron-beam dome facility, an electron accelerator set, foam cooling and winding units. Two parallel symmetrical amplifiers are cleverly designed on both sides of the vertical foaming chamber unit, which promotes line speed and manufacturing capacity. CN103223704A [85] exposed a chemical cross-linking polyethylene foam equipment, including feeding device, horizontal foaming device, continuous roller and pressure device, and cooling and winding device. The horizontal foaming furnace with three heating zone involves the three circulation heating units including the foaming furnace body, the casing gas combustion machine, the heat transfer system, and the hot air circulation fan. The opening end of the combustion barrel is connected with the spitfire nozzle of the gas burner. There are several output holes on the side wall of the combustion barrel. The advantage is that it can avoid the flame into the impeller to make it deform and damage, and improve the service life of the hot air circulation fan.

3.4 Application and Utilities

Because of its excellent properties, cross-linked polyethylene is used as a high-voltage, high-cycle, heat-resistant insulating material, and wire and cable cladding for rockets, missiles, motors, transformers, etc., and is also intended in manufacture of heat-shrinkable tubes, heat-shrinkable films, various heat-resistant tubes, foam plastics, corrosion-resistant chemical equipment linings, components

and containers, manufacture fire-retardant building materials, etc. At present, the largest area of use is mainly in wire and cable, pipe and foam plastic, and so on. The consumption of cables is about 2/3 of the total market in the world in 2015, followed by the tubes with a share of 21%.

3.4.1 Cable

The heat resistance of the insulated cable of cross-linked polyethylene is higher than that of PVC, so it can be used at 90 °C for a long time, and the heat resistance temperature can reach 250 °C at the time of the short circuit. It has the advantages of high insulation resistance, small dielectric loss angle tangent, and little influence of temperature, good wear resistance and resistance to environmental stress cracking. Carbon dioxide and water are produced when cross-linked polyethylene cables are burned, while PVC cables produce hydrogen chloride during the combustion process. In addition, the density of cross-linked polyethylene is about 40% less than that of PVC, which can significantly reduce the quality of areal wires.

CN101602870A [86] invented a soft cross-linked polyethylene insulating material, which comprises the following components in parts by weight: 100 parts of low-density polyethylene, 35 ~ 50 parts of polyisobutylene, 20 ~ 35 parts of polyethylene vinyl acetate, 1.7 ~ 2.5 parts of cross-linking agent, and 0.2 ~ 0.5 parts of antioxidant. The softness of the soft cross-linked polyethylene insulating material of this invention is equivalent to that of the soft polyvinyl chloride insulating material for cables, and the main electrical parameters, such as ρ_v value, ϵ value, and $\tan \delta$ value, can reach $\geq 1 * 10^{16} \Omega\cdot\text{cm}$, ≤ 2.4 and ≤ 0.0008 , respectively. The power loss caused by the transmission medium of the cable made of this material is at least one order of magnitude lower than that of the ethylene-propylene rubber insulated cable, which is the same order of magnitude as that of the 20kV cross-linked polyethylene medium-voltage cross-linked insulating material made of a single low-density polyethylene. Jin et al. [87] invented a water-tree-retardant cross-linkable polyethylene cable compound material. This cable material compound comprises following components: polyethylene, polyolefin containing polar groups, an antioxidant, water-tree-retardant additives, an ethylenevinyl alcohol (EEA)-modified polymer, an organic peroxide cross-linking agent, and nanometer inorganic additives. The water-tree-retardant cross-linkable polyethylene cable material compound is produced and processed by using water-tree-retardant additive masterbatches and nanometer inorganic additive masterbatches. This compound has the advantages that the water-tree-retardant performance and the durability of an insulating layer are greatly improved. Sohn et al. [88] disclosed a fire-resistant cable for high voltage. According to the fire-resistant cable for high voltage of the present invention, both fire-resistant performance and electrical features are satisfied. It is possible to prevent creation of curvatures and gaps, which are formed due to a small radius of curvature for winding a mica tape which forms a fire-resistant layer, and partial discharge generated by the curvatures and gaps can be suppressed. Since the fire-resistant layer is

formed at a position having optimum electric field strength considering insulation thickness, withstand voltage, partial discharge and the like, convenience in installing the cable and electrical features of the cable can be improved. CN203746440U [89] invented a novel composite structured aluminum alloy cable which comprises a PVC sheath, a fiberglass composite thin layer, a sparsely wrapped neutral wire layer, and an XLPE cross-linked polyethylene layer. Two aluminum conductor cores are arranged in the XLPE cross-linked polyethylene layer. A basalt fiber flame-retardant layer and a metallic sheath layer are arranged between the sparsely wrapped neutral wire layer and the XLPE cross-linked polyethylene layer. The cable provided by the utility model has excellent conductivity and excellent flame retardation and can reach FT1 combustion standard in UL and accords with ROHS. As creep resistance and compactness of the cable are raised by 300%, loosening problem caused by creep is avoided. By a special processing technology, an 8176 aluminum alloy cable has higher yield strength than a pure aluminum cable, ductility is raised by 30%, springback value is small, and there is no memory effect. He et al. [90] disclosed a polyethylene cable material, its components are as below: linear low-density polyethylene 20–80 parts, low-density polyethylene 20–80 parts, catalyst nitrobenzoic acid 1–5 parts, antioxidant 300 1–3 parts, silane cross-linking agent vinyl trimethoxy-silane 0.4–2 parts, and initiator diisopropyl peroxide 0.01–0.04 parts. The catalyst masterbatch are obtained by extruding the mixture of linear low-density polyethylene (LDPE), LDPE, antioxidant, and catalyst through a single screw extruder. Then linear LDPE, LDPE, and catalyst masterbatch were placed together in an airtight mixer. Silane cross-linking agent and DCP initiator were vaporized and permeated into polyethylene after vacuum drying under heating conditions. Control the speed and time of the closed mixer, discharge, vacuum packaging, so as to get one-step silane cross-linked polyethylene cable material. Zhou et al. [91] invented a novel flame-retardant XLPE insulated cable. The preparation raw materials of the novel flame retardant XLPE insulated cable comprise: XLPE 60 ~ 100 parts by mass and 3 ~ 4 parts by mass of catalyst; 5–30 parts by mass of flame retardant. The flame retardant comprises one or more of the following reagents: 10 ~ 30 parts of self-made modified hydrotalcite, 1 ~ 4 parts of antioxidant, 0.6 ~ 1.5 parts of plasticizer, and 5 ~ 11 parts of nanoactive agent. The novel flame retardant XLPE insulated wire and cable has better mechanical property, flame retardant property, and heat resistance. Jia et al. [92] invented an XLPE (cross-linked polyethylene) cable insulating material that comprises, by weight, 80 ~ 100 parts of low-density polyethylene, 0.5 ~ 2 parts of ferrite nanoparticles, 10 ~ 20 parts of carbon black, 0.1 ~ 3 parts of antioxidants, 1 ~ 3 parts of stabilizers, and 10 ~ 20 parts of solvents. This preparation method of the ferrite nanoparticles includes the steps: preparing mixed solution of Ni^{2+} and Fe^{3+} , adding a molecular sieve, stirring for 12 ~ 36 h at the normal temperature, filtering, washing, drying, rising temperature to range from 800 to 1100 °C in a muffle furnace, and roasting for 1 ~ 6 h; placing a roasted product into hydrofluoric acid solution, stirring for 2 ~ 3 h, and filtering, washing and drying a solid sample to obtain a nickel ferrite nanotube. The mole ratio of the Ni^{2+} and Fe^{3+} is (1 ~ 3):1. The cable insulation material can effectively restrain the accumulation

of space charge in the insulation material and increase the threshold of electric field injected by space charge, and it also reduces the increasing effect of the electrical conductivity of the insulating material caused by space charge limiting current (SCLC). Wang et al. [93] provided a nanocomposite cross-linked polyethylene insulation material with high DC breakdown field strength and its preparation method. The insulation material used here was prepared by mass from the following components: low-density polyethylene 100 parts, boron nitride nanoparticles 0.1 ~ 3 parts, cross-linking agent 1 ~ 2.5 parts, and antioxidant 0.1 ~ 0.5 parts. This kind of insulation material can be used in DC cables. Compared with the cross-linked polyethylene without boron nitride particles, the DC breakdown field strength is significantly increased, and the DC breakdown field strength at 20, 70, and 90 °C is improved by 27.5, 14.2, and 26.5%, respectively, which has a higher DC breakdown field strength. Xia [94] disclosed a cross-linked polyethylene track cable insulation material and its preparation method. One of the cross-linked polyethylene track cable insulation materials is made up by weight of 40 ~ 50 parts of low-density polyethylene, 20 ~ 40 parts of high-density polyethylene, 20 ~ 30 parts of polyvinyl chloride, 8 ~ 10 parts of tin oxide, 0.5 ~ 1.5 parts of silane cross-linking agent, 1 ~ 2 parts of stabilizer, 1 ~ 3 parts of compound antioxidant, 3 ~ 5 parts of plasticizer, and 4 ~ 6 parts of microcrystalline wax. This method of producing insulating material can effectively reduce silane cross-linking time, reduce energy consumption, reduce cost, and effectively improve production efficiency for cable plant, and its performance is stable.

3.4.2 Pipes and Foamed Plastics

The pipe produced with cross-linked polyethylene generally has the advantages of high creep strength, lightweight, corrosion resistance, and good heat resistance. Cross-linked polyethylene foam material not only has good mechanical properties, but also has very good chemical, physical, shock absorption, and noise reduction properties. It has been widely used in packaging, automobile, and construction engineering. CN110404748A [95] invented a method of preparing vehicle tank loading dangerous chemicals with cross-linked polyethylene lining. It is characterized by smooth transition of edges and corners in the tank after welding and machining. With the aid of appropriate physical/chemical methods, the inner surface of the tank is subjected to oil and rust removal treatment. A plastic rolling device is installed on the outside of the tank. Holes punched in the heating window of the process. In the early stage of heating, ensure that all the materials melt before the cross-linking reaction, and uniformly adhere to the surface of the tank. In the later stage of heating, when reaching the required temperature for the cross-linking reaction of the materials and the duration of heat preservation, it is guaranteed that the related reaction is uniformly and fully completed. After visual inspection of the inner surface of the tank with plastic lining without defect, it is tested for conductivity. This method can obviously shorten the processing cycle, greatly reduce the tank body weight, and improve the environmental stress resistance of

anticorrosive materials. CN110239123A [96] provides a method for the preparation of large-diameter high-density cross-linked polyethylene wall tube with hot-winding structure. The preparation method comprises the following steps: mixing the raw materials including high-density polyethylene and vinyl siloxane, adding them into the extruder, and winding the resulting strip material to form the inner cylinder; the ribbed tube material is wrapped around the joint of adjacent flat strip material, and the ribbed tube material is bonded to the inner tube composite at the same time; after molding, demolding and cooling, winding pipe is obtained. In the invention, by controlling the extrusion temperature and the cross-linking degree of the belt material, the welding property between the rib tube and the inner tube is guaranteed and the overall strength of the wound tube is maintained. Welding of ribbed tube and winding of inner tube are carried out synchronously to form a solid welding and grafting layer between ribbed tube and inner tube, so as to ensure product strength.

4 Related Productions of XLPE Nanocomposites and Blends

Polyethylene is a low-cost commodity plastic that can be reused and remolded due to its thermoplastic nature. Cross-linking of polyethylene helps to produce a polymer that exhibits high molecular weight, which enhances the abrasion resistance, thermal resistance, impact strength, and environmental stress cracking resistance of polyethylene without affecting its tensile strength and density. Moreover, after cross-linking, the end product is transformed from thermoplastic to thermosetting plastic having high mechanical strength.

4.1 Advantage of XLPE Produces

Cross-linking is an important technique to improve PE performances. XLPE obtained by the cross-linking modification of PE could significantly improve the mechanical properties, environmental stress cracking resistance, chemical corrosion resistance, creep resistance, electrical properties, etc. Cross-linking enables to increase the heat-resistance temperature from 70 to 95 °C or higher, which greatly widens the application range of PE, such as used in pipe, film, cable material, and foam products. Compared with general polyolefin, cross-linked polyethylene has improved performance in extension, oil resistance, cold resistance, and crack resistance, etc., and can be used in more severe environments. So XLPE is suitable for voltage ranges from low-to-extra high voltage, surpassing other insulation materials. The cross-linking of the polyethylene also enhances the chemical and oil resistance at elevated temperatures, making it suitable for use as a low-smoke

zero-halogen material. Specifically, the advantages of cross-linked polyethylene pipe compared with metal pipe, silicone rubber, and other plastic pipe, such as PVC, ethylene propylene rubber (EPR), and so on, are as follows:

- (1) Wide working temperature range. It can be used for a long time at $-75 \sim 95$ °C, with a service life of up to 50 years;
- (2) Excellent chemical corrosion and environmental stress cracking resistance. It can be used to transport a variety of chemicals and fluids that have accelerated the stress cracking of existing pipes even at high temperatures;
- (3) Superior resistance to weather, moisture and rust, which is incomparable to the metal pipe;
- (4) Effective scaling prevention, due to low surface tension;
- (5) No mildew, mold and bacteria;
- (6) Smooth interior and small fluid resistance. In the same pipe dimension, the conveying capacity is larger than that of steel pipe, and lower noise;
- (7) Good insulation and heat preservation. Its thermal conductivity is much lower than that of metal pipes, and it has less heat loss when used in the heating system;
- (8) Pliable, flexible and shatterproof. It can be bent without breaking;
- (9) Lightweight and steerable, making it easier to install and more cost effective than other options.

4.2 Market Synopsis

The growth of the global cross-linked polyethylene market is primarily driven by its high demand in piping systems, water service lines, and heating and cooling systems. This polymer is rapidly replacing copper, zinc, and other materials in pipes and tubes owing to its high flexibility, low cost, high corrosion resistance, and ability to withstand a wide temperature range. Although, a shift toward the use of polypropylene pipes over XLPE pipes is observed due to the chance of leakage and release of organic carbon and VOCs, which is likely to pose a major challenge to the market players, the market prospect of XLPE is still confirmed well by all trades. In Europe and American market, cross-linked polyethylene pipe has long been widely used for forty years, and this pipe has been a dominant position in the plastic pipe market. In China, the galvanized steel is no longer in use for potable water pipes and air conditioning heating system, but is replaced by cross-linked polyethylene or other plastic pipe. At the current stage of China, the use of plastic pipe has reached more than 50% of the total pipe, and thereinto, polyethylene, polypropylene, and polyvinyl chloride pipes occupy the dominant position, that of cross-linked polyethylene pipe in particular would have huge development capacity in china market because of its excellent performance and low prices. In addition, the widespread usage of XLPE in wires and cables is another important factor propelling the growth of the global cross-linked polyethylene market. Furthermore, the

growing demand of XLPE foam in the medical packaging applications to protect surgical instruments, implants, and other surgical devices from damage is predictable to create immense opportunities for the producers of XLPE.

4.3 Typical Produces

4.3.1 Industrial Cables

i Construction of XLPE Cable

Different types of power cables used for electricity transmission and distribution are shown in Fig. 19. There are strict requirements in the design of XLPE insulated wire-armored cables for voltages up to 3.3 kV. The construction of XLPE cable is basically similar to that of PVC cables, except for the difference in insulant. Because of the increased toughness of XLPE, the thicknesses of insulation are slightly reduced compared with PVC. A typical armored construction of XLPE cable which has been supplied in substantial quantities was shown in Fig. 20. The polymeric forms of cable insulation are more susceptible to electrical discharge than impregnated paper and at the higher voltages, where the electrical stresses are high enough to promote discharge, so it is important to minimize gaseous spaces within the insulation or at its inner and outer surfaces of the insulation. XLPE cables for 6.6 kV and above have semiconducting screens over the conductor and over each insulated core. The conductor screen is a thin layer extruded in the same operation as the insulation and cross-linked with it so that the two components are closely bonded. The screen over the core may be a similar extruded layer or a layer of semiconducting paint with a semiconducting tape applied over it.

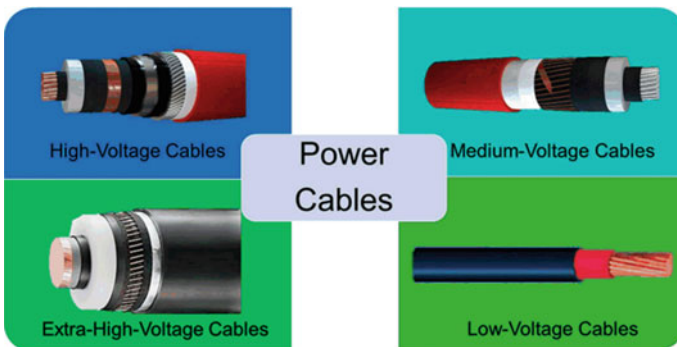


Fig. 19 Different types of power cables, Ref. [97], open access

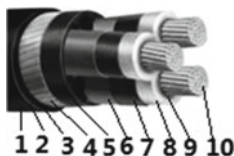


Fig. 20 XLPE cable construction 1. Extruded PVC over sheath 2. Galvanized steel wire amour, 3. Extruded PVC sheath, 4. Binder, 5. PVC filler, 6. Copper tape screen, 7. Semiconducting tape screen, 8. XLPE insulation, 9. Semiconductor XLPE screen, and 10. Circular stranded conductor

ii *XLPE/PVC Control and Power Cable*

This cable can be classified into three types: XLPE/PVC unshielded control cable, XLPE/PVC unshielded low-voltage power cable, and XLPE/PVC shielded low-voltage power cable. The first two cables have the similar properties, so we combined both of them to discuss.

(1) XLPE/PVC Unshielded Control Cable and Low-Voltage Power Cable

Both XLPE/PVC unshielded control cable and XLPE/PVC unshielded low-voltage power cable have excellent electrical properties, wear resistance, and chemical corrosion resistance, greatly improving the safety of the cable. They are rated to work at 90 °C in dry or wet conditions and they are often applied to all cables with a jacket thickness of 60 mils or less. The two kinds of cables can be used in different environments due to their good sun and climate durability. They have passed the ICEA and CSA cold bend test at -25 °C. They also have advantages in mechanical strength, such as meets the crush and impact requirements of type MC.

(2) XLPE/PVC Shielded Low-Voltage Power Cable

Compared with XLPE/PVC unshielded control cable and XLPE/PVC unshielded low-voltage power cable, XLPE/PVC shielded low-voltage power cable has dual shielded characteristics and can provide the maximum shielded range required for VFD application. So, it can use in AC motors controlled by pulse width modulated inverters, in VFD applications rated up to 2000 V. These motor drive systems require cables that are designed to prevent radio frequency interference (RFI), otherwise, can lead to malfunction.

iii *RW90/XLPE Unshielded Cable*

XLPE/ARCTIC-FLEX unshielded cable is a typical cable for insulation. It can work stably under rated working conditions of wet or dry temperature of 90 °C. As its components also contain XLPE, it is applied to all cables with jacket thickness of 60 mils or less and able to meet CSA cold impact test at -40 °C and ICEA and CSA cold bend test at -65 °C. Compared with the ABA, it can withstand lower temperatures.

iv XLPE/XL-CPE Unshielded Power Cable

This cable has excellent physical, thermal, and electrical properties and excellent moisture resistance, so it can work stably in the moisture environment. In addition, it has excellent flame resistance and oil-resistant jacket, which makes this cable highly safe. It can also be used in some extreme environments due to its outstanding resistance to crush, compression cuts, and heat deformation. In terms of the low-temperature bending characteristics, it is subjected to a slightly higher temperature than RW90/XLPE unshielded cable.

4.3.2 Pipes

PE-X pipe can be divided into peroxide cross-linked polyethylene (PE-Xa) pipe, cross-linked polyethylene (PE-Xb) pipe and radiation cross-linked polyethylene (PE-Xc) pipe. PE-Xa pipe is produced by mixing PE and peroxide cross-linking agent into batch impact extruder. Under high temperature and high pressure, chemical bonds are formed between the long molecular chains of PE to realize chemical cross-linking. PE-Xb pipe is made by grafting PE and vinyl silane (such as vinyl trimethoxysilane and vinyl triethyl chlorosilane) in an extruder to produce cross-linking PE pipe with silane, and then in the presence of polycondensation catalyst, it is hydrolyzed and cross-linked to prepare PE-Xb pipe connected by a –Si–O–Si– bond. To produce the PE-Xc pipeline, common pipe material extruder was first put into irradiation plant under a certain dose of radiation, where part of the molecular structure of PE main chain or side chain was ray cut the number of free radicals. These free radicals in combination with each other clinch a deal the chain, the molecular structure of PE by linear macromolecular structure into a mesh. PE-X pipe has been used in industry for more than 40 years. At present, PE-X occupies an absolute dominant position in the floor heating pipeline market. The actual use of domestic water and heating water has proved that PE-X pipe has unmatched safety performance and cost performance. PE-X tubes have been widely used in the fields of cold and hot water supply, floor heating, municipal water supply, melting of ice and snow, indoor skating rink, refrigerator, etc. PE-X pipe is three times better than the general PE pipe wear resistance, so it is used for ore transport. In recent years, PE-X tubes have been used in gas field because of their excellent resistance to slow crack propagation and excellent long-term performance.

The cross-linked polyethylene pipe (Fig. 21a) has advantages such as non-toxic, tasteless, health, corrosion resistance, no pollution, water quality creep resistant, aging resistant, and wide range of applicable temperature (20 ~ 90 °C). It has a high cross-linking degree, solid and tough quality, high resistance to internal pressure, high thermal conductivity, and therefore, it is very suitable for laying of floor heating materials, etc. The inner wall of pipe is smooth, the resistance of fluid flow is small, and the surface tension is low, which makes it difficult for water to infiltrate the inner wall of cross-linked polyethylene pipe and effectively prevent scaling. The metal parts in the heating system have some oxygen corrosion during

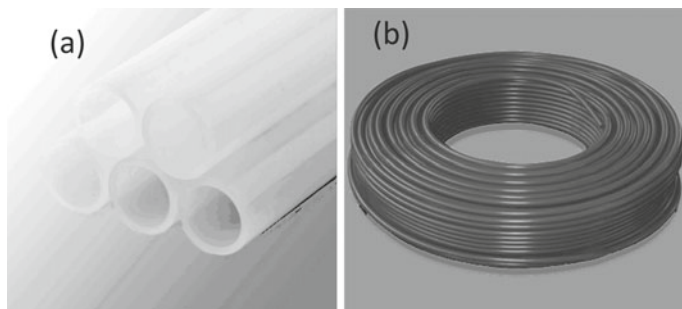


Fig. 21 **a** Cross-linked polyethylene (PE—Xb) pipe, **b** oxygen-resistant heat-resistant polyethylene (PE-RT/EVOH) pipe

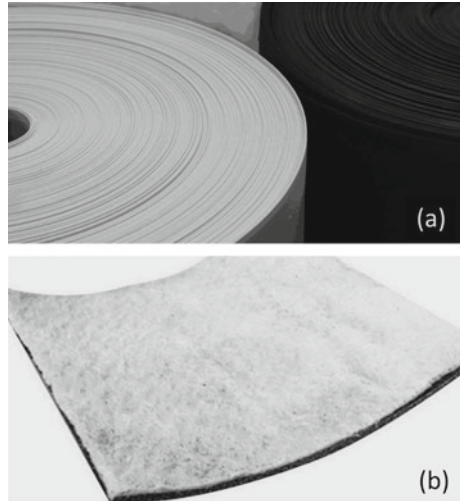
operation, which has a certain impact on the safety and economy of the heating system operation, and the oxygen permeation of plastic pipe is one of the main causes of oxygen corrosion. Ordinary PP-R, PE-X, PE-RT, PB and other plastic pipes have the property of oxygen permeability, which increases with the increase of temperature. In order to achieve the purpose of blocking oxygen, such as this oxygen-resistant heat-resistant polyethylene (PE-RT/EVOH) pipe (Fig. 21b), the surface of the pipe is squeezed with a layer of gas barrier material—ethylene—ethylene alcohol copolymer (EVOH), while the EVOH and PE-RT pipe are bonded together with an adhesive.

The potential for the nanocomposite to help in sustaining the pipeline infrastructure was also viewed as a strong point. The endurance of current pipe wrap products will be increased by the incorporation of nanoparticles.

4.3.3 Foam Plastic and Mat

The radiation cross-linking polyethylene foam plastics (Fig. 22a) can be widely used in packaging materials, insulation materials and automobile industry, and many other fields for its advantage of good thermal stability (the highest temperature of 130 °C), high temperature stability, high toughness, tensile strength and impact strength, fit and smooth surface, and excellent microwave adaptability. A kind of cross-linked polyethylene pad composite nanosilicon dioxide thermal insulation felt (Fig. 22b) can be made from cross-linked polyethylene pad and nanosilicon dioxide thermal insulation felt by infrared light wave technology bonded together, with vibration and sound insulation, thermal insulation composite pad. Cross-linked polyethylene cushion composite nanosilicon dioxide thermal insulation blanket is mainly used in residential building floor thermal insulation engineering building floor, in the application, with thermal insulation, noise reduction, moisture-proof antibacterial, health and environmental protection, can increase the use of housing space, reduce the cost, good formability, and simple construction process.

Fig. 22 a Radiation cross-linking polyethylene foam plastics, **b** cross-linked polyethylene mat with composite nanosilica thermal insulation felt



5 Conclusions

This chapter has dedicated to overview the recent development of cross-linked polyethylene (XLPE) nanocomposites and blends. In this chapter, the composites and the corresponding properties of XLPE nanocomposites and blends have been analyzed in depth on the basis of the publications. Additionally, a comprehensive summary on the practical technology about preparation, characterization, and equipment of XLPE nanocomposites and blends were presented according to the authorized patents. Finally, it covers the XLPE market size and emerging products. Along with the discussion on the challenges and opportunities, this chapter is targeting to forecast the research trend, to estimate the growth potential, and to provide the reference for researchers.

Acknowledgements This work was supported by Hebei Key Laboratory of Distributed Energy Storage and Micro-Grid and the foundation of the National Key R&D Plan (No. 2017YFC0210202-1). The authors thank the editorial team, especially Dr. Jince Thomas and Mr. Vishnu Muthuswamy, for their professionalism, carefulness and patience.

References

1. Chang Y, Jiang J, Bing S (2010) The microstructure of cross-linked polyethylene observed by scanning electron microscopy. *China Rubber/Plastics Technol Equip* 36:33–36
2. Wang J, Zhang L, Li K (2018) Structures and properties of crosslinked polyethylene composite materials. *Petrochem Technol Appl* 36:22–24
3. Sharad PA, Kumar KS (2017) Application of surface-modified XLPE nanocomposites for electrical insulation—partial discharge and morphological study. *Nanocomposites* 3:30–41

4. Nilsson S, Hjertberg T, Smedberg A, Sonerud B (2011) Influence of morphology effects on electrical properties in XLPE. *J Appl Polym Sci* 121:3483–3494
5. Zheng X, Liu Y, Wang Y (2018) Electrical tree inhibition by SiO₂/XLPE nanocomposites: insights from first-principles calculations. *J Mol Model* 24:200
6. Sharad PA, Kumar KS (2017) Application of surface modified XLPE nanocomposites for electrical insulation of high voltage cables-partial discharge study. *Energy Procedia* 117:260–267
7. Boggs S, Xu J (2001) Water treeing- filled versus unfilled cable insulation. *IEEE Electr Insul Mag* 17(1):23–29
8. Hui L, Smith R, Nelson JK, Schadler LS (2009) Electrochemical treeing in XLPE/silica nanocomposites. In: 2009 IEEE conference on electrical insulation and dielectric phenomena, CEIDP'09, Virginia Beach, VA, pp 511–514
9. Roy M, Nelson JK, MacCrone RK, Schadler LS (2007) Candidate mechanisms controlling the electrical characteristics of silica/XLPE nanodielectrics. *J Mater Sci* 42:3789–3799
10. Jevtic M, Andreev AM (1996) The method of testing of XLPE cable insulation resistance to partial discharges and electrical treeing. *Bull Mater Sci* 19(5):823–829
11. Thomas J, Joseph B, Jose JP, Maria HJ, Main P, Rahman AA, Francis B, Ahmad Z, Thomas S (2019) Recent advances in cross-linked polyethylene-based nanocomposites for high voltage engineering applications: a critical review. *Ind Eng Chem Res* 58:20863–20879
12. Zhang L, Zhou Y, Cui X, Sha Y, Le T, Ye Q, Tian J (2014) Effect of nanoparticle surface modification on breakdown and space charge behavior of XLPE/SiO₂ nanocomposites. *IEEE Trans Dielectr Electr Insul* 21(4):1554–1564
13. Crine JP (2005) Influence of electro-mechanical stresses on electrical properties of dielectric polymers. *IEEE Trans Dielectr Electr Insul* 12(4):791–800
14. Crine JP (2005) On the interpretation of some electrical aging and relaxation phenomena in solid dielectrics. *IEEE Trans Dielectr Electr Insul* 12:1089–1107
15. Zhang L, Khani MM, Krentz TM, Huang Y, Zhou Y, Benicewicz BC, Nelson JK, Schadler L (2017) Suppression of space charge in crosslinked polyethylene filled with poly(stearyl-methacrylate)-grafted SiO₂ nanoparticles. *Appl Phys Lett* 110:132903
16. Zhang H, Liu Y, Du X, Wang X, Zheng X, Li Z (2019) Effect of SiC nano-size fillers on the aging resistance of XLPE insulation: a first-principles study. *J Mol Graph Model* 93:107438
17. Wang Y, Wang C, Xiao K (2016) Investigation of the electrical properties of XLPE/SiC nanocomposites. *Polym Test* 50:145–151
18. Tanaka T, Kozako M, Fuse N, Ohki Y (2005) Proposal of a multi-core model for polymer nanocomposite dielectrics. *IEEE Trans Dielectr Electr Insul* 4:669–681
19. Nagao M, Watanabe S, Murakami Y, Murata Y, Sekiguchi Y, Goshowaki M (2008) Water tree retardation of MgO/LDPE and MgO/XLPE nanocomposites. In: Proceeding of 2008 international symposium on electrical insulating materials, ISEIM 2008, September 7–11, Yokkaichi, Mie, Japan, pp 483–486
20. Kim DS, Lee DH, Kim YJ, Nam JH, Ha ST, Lee SH (2013) Investigation of space charge distribution of MgO/XLPE composites depending on particle size of MgO as inorganic filler. *Appl Mech Mater* 481:108–116
21. Zhu X, Wu J, Yang Y, Yin Y (2020) Characteristic of partial discharge and AC electrical tree in XLPE and MgO/XLPE nanocomposites. *IEEE Trans Dielectr Electr Insul* 27(2):450–458
22. Li X, Xu M, Zhang K, Xie D, Cao X (2014) Influence of organic intercalants on the morphology and dielectric properties of XLPE/montmorillonite nanocomposite dielectrics. *IEEE Trans Dielectr Electr Insul* 21(4):1705–1717
23. Park Y, Kwon J, Sim J, Hwang J, Seo C, Kim J (2014) DC conduction and breakdown characteristics of Al₂O₃/cross-linked polyethylene nanocomposites for high voltage direct current transmission cable insulation. *Jpn J Appl Phys* 53:08NL05
24. Guo X, Xing Z, Zhao S, Cui Y, Li G, Wei Y (2020) Investigation of the space charge and dc breakdown behavior of XLPE/ α -Al₂O₃ nanocomposites. *Materials (Basel)* 13:1–14

25. Hamzah MS, Mariatti M, Ismail H (2019) Melt flow index and flammability of alumina, zinc oxide and organoclay nanoparticles filled cross-linked polyethylene nanocomposites. *Materials Today: Proceeding* 17:798–802
26. Jose JP, Thomas S (2014) Alumina-clay nanoscale hybrid filler assembling in cross-linked polyethylene based nanocomposites: mechanics and thermal properties. *Phys Chem Chem Phys* 16:14730
27. Zhang C, Zhang H, Li C, Duan S, Jiang Y, Yang J (2018) Crosslinked polyethylene/polypyrrole nanocomposites with improved direct current electrical characteristics. *Polym Test* 71:223–230
28. Jose JP, Mhetar V, Culligan S, Thomas S (2013) Cross linked polyethylene/TiO₂ nanocomposites: morphology, polymer/filler interaction, mechanics and thermal properties. *Sci Adv Mater* 5(4):385–397
29. Wang Y, Xiao K, Wang C, Yang L, Wang F (2016) Effect of nanoparticle surface modification and filling concentration on space charge characteristics in TiO₂/XLPE nanocomposites. *J Nanomater* 2840410
30. Wang Y, Xiao K, Wang C, Yang L, Wang (2016) Study on dielectric properties of TiO₂/XLPE nanocomposites. In: 2016 IEEE international conference on high voltage engineering and application (ICHVE), Sept 19–22, Chengdu, China
31. Toselli M, Sacconi A, Pilati F (2014) Thermo-oxidative resistance of crosslinked polyethylene (XLPE) coated by hybrid coatings containing graphene oxide. *Surf Coat Technol* 258:503–508
32. Han C, Du B, Li J, Li Z, Tanaka T (2020) Investigation of charge transport and breakdown properties in XLPE/GO nanocomposites part 1: the role of functionalized GO quantum wells. *IEEE Trans Dielectr Electr Insul* 27(4):1204–1212
33. Zhao A, Chen X, Chen S, Yao C, Zhao X, Deng J (2019) Surface modification of XLPE films by CF₄ DBD for dielectric properties. *AIP Adv* 9:15102
34. Balachandran M (2019) XLPE—layered silicate nanocomposites for high voltage insulation applications: dielectric characteristics, treeing behaviour and mechanical properties. *IET Sci Meas Technol* 13(6):1019–1025
35. Zhan Y, Chen G, Hao M, Pu L, Zhao X, Wang S (2020) Space charge measurement and modelling in cross-linked polyethylene. *Energies* 13. <https://doi.org/10.3390/en13081906>
36. Rogti F (2013) Space charge behavior and its modified electric field in the cross-linked polyethylene under applied voltage DC and different temperatures. *J Electrostat* 71:1046–1054
37. Kato T, Onozawa R, Miyake H, Tanaka Y, Takada T (2017) Properties of space charge distributions and conduction current in XLPE and LDPE under DC high electric field. *Electr Eng Japan* 198:19–26
38. Wang S, Zhou Q, Liao R, Xing L (2019) The impact of cross-linking effect on the space charge characteristics of cross-Linked polyethylene with different degrees of cross-linking under strong direct current electric field. *Polymers* 11(7):1149
39. Arai Y, Kanegae E, Tanaka T, Ohki Y, Sutton (2011) Space charge behavior of XLPE/Silica nanocomposites under high electric field. In: Proceeding of 2011 international conference on electrical insulating materials, ISEIM 2011, Sep 6–11, Kyoto, Japan, pp 362–365
40. Piah M (2018) Space charge and conductivity measurement of XLPE nanocomposites for HVDC insulation-permittivity as a nanofiller selection parameter. *IET Sci Meas Technol* 12(7):1058–1065
41. Du B, Han C, Li Z, Li J (2019) Improved DC conductivity and space charge characteristic of XLPE for HVDC cable application: effect of voltage stabilizers. *IEEE Access* 7:66576–66583
42. Lv Z, Wang X, Wu K, Chen X, Cheng Y (2013) Dependence of charge accumulation on sample thickness in nano-SiO₂ doped LDPE. *IEEE Trans Dielectr Electr Insul* 20(1):337–345
43. Morsalin S, Phung T (2020) Electrical field distribution on the cross-linked polyethylene insulation surface under partial discharge testing. *Poly Test* 82:106311

44. Hao Z, Yubing D, Bin W, Hui L, Ying L, Xiaoli H (2017) Case analysis on partial discharge signal of XLPE cable T-joint by using high-frequency pulse current method. *Energy Procedia* 141:545–550
45. Song W, Tang J, Pan C, Meng G, Zhang M (2020) Improvement of insulation defect identification for DC XLPE cable by considering PD aging. *Int J Electr Power Energy Syst* 114:105409
46. Wei G, Tang J, Zhang X, Lin J (2014) Gray intensity image feature extraction of partial discharge in high-voltage cross-linked polyethylene power cable joint. *Int Trans Electr Energy Syst* 24:215–226
47. Roumeli E, Markoulis A, Kyratsi T, Bikiaris D, Chrissafis K (2014) Carbon nanotube-reinforced crosslinked polyethylene pipes for geothermal applications: from synthesis to decomposition using analytical pyrolysis-GC/MS and thermogravimetric analysis. *Polym Degrad Stab* 100:42–53
48. Formela K, Wołosiak M, Klein M, Wang S (2016) Characterization of volatile compounds, structural, thermal and physico-mechanical properties of cross-linked polyethylene foams degraded thermo-mechanically at variable times. *Poly Degrad Stab* 134:383–393
49. Roumeli E, Pavlidou E, Bikiaris D, Chrissafis K (2014) Microscopic observation and micromechanical modeling to predict the enhanced mechanical properties of multi-walled carbon nanotubes reinforced crosslinked high density polyethylene. *Carbon* 67:475–487
50. Kuang T, Chen F, Fu D, Chang L, Peng X, Lee L (2016) Enhanced strength and foamability of high-density polyethylene prepared by pressure-induced flow and low-temperature crosslinking. *RSC Adv* 6:34422–34427
51. Freitas R, Bonse B (2019) Cross-linked polyethylene (XLPE) as filler in high-density polyethylene: effect of content and particle size. *AIP Conf Proc* 2055:20009
52. Bao M, Yin X, He J (2011) Analysis of electrical tree propagation in XLPE power cable insulation. *Phys B Condens Matter* 406:1556–1560
53. Sarathi R, Raju PG (2005) Study of electrical treeing phenomena in XLPE cable samples using acoustic techniques. *Electr Power Syst Res* 73:159–168
54. Bao M, Yin X, He J (2011) Structure characteristics of electrical treeing in XLPE insulation under high frequencies. *Phys B Condens Matter* 406:2885–2890
55. Mittal L, Sarathi R, Sethupathi K (2015) Electrical treeing in XLPE cable insulation at cryogenic temperature under harmonic AC voltages. *Cryogenics (Guildf)* 71:62–67
56. Zhu L, Du B, Li H, Hou K (2019) Effect of polycyclic compounds fillers on electrical treeing characteristics in XLPE with DC-impulse voltage. *Energies* 12:1–15
57. Qureshi M, Ahaideb A, Arainy A, Malik N (2005) Role of semiconducting screens on water treeing in medium voltage XLPE cables. *J King Saud Univ Eng Sci* 17:227–242
58. Kim C, Jang J, Huang X, Jiang P, Kim H (2007) Finite element analysis of electric field distribution in water treed XLPE cable insulation (1): the influence of geometrical configuration of water electrode for accelerated water treeing test. *Polym Test* 26:482–488
59. Kim C, Jin Z, Huang X, Jiang P, Ke Q (2007) Investigation on water treeing behaviors of thermally aged XLPE cable insulation. *Polym Degrad Stab* 92:537–544
60. Ma Z, Huang X, Jiang P (2010) A comparative study of effects of SEBS and EPDM on the water tree resistance of cross-linked polyethylene. *Polym Degrad Stab* 95:1943–1949
61. Qureshi M, Malik N, Arainy A (2011) Impact of cations toward the water tree propensity in crosslinked polyethylene insulation. *J King Saud Univ Eng Sci* 23:43–48
62. Chen J, Zhao H, Xu Z, Zhang C, Yang J, Zheng C (2016) Accelerated water tree aging of crosslinked polyethylene with different degrees of crosslinking. *Polym Test* 56:83–90
63. Chen Z, Fang R (2020) An additive feeding device for producing irradiation crosslinked polyethylene foam. *China Patent CN210025961U*, Feb 2020
64. Ren D, Chen X, Liang B (2018) A preparation method of crosslinked polyethylene film. *China Patent CN108264646A*, Jul 2018
65. Lyu M, Zhang S, Zhang W (2011) A chemical crosslinked polyethylene composition and its preparation method. *China Patent CN102140193A*, Aug 2011

66. Denis L (2019) Installation and method for manufacturing cross-linkable polyethylene compounds. US Patent 20190070752A1, Mar 2019
67. Chen X, Liang W, Niu Y (2013) Crosslinked polyethylene composition. PCT (World) Patent WO2013185302A1, Dec 2013
68. Stephen Cree H (2013) Process for reducing peroxide migration in crosslinkable ethylene-based polymer compositions. US Patent 9758638B2, Sep 2017
69. Chen X, Liang W, Lai S (2018) A crosslinkable polyethylene blending composition. China Patent CN103865142A, Dec 2018
70. Chen X, Liang W, Lai S (2017) Crosslinkable polyethylene composition, crosslinkable polyethylene, preparation method, product and application. China Patent CN106366430A, Feb 2017
71. Duan J, Wang X, Li J (2006) Silane crosslinked HDPE composition and its preparation method. China Patent CN1511873A, Aug 2006
72. Wang Y, Wang C, Chen W (2017) Crosslinked polyethylene composite with internal space charge suppression and its preparation and application. China Patent CN104927175A, Apr 2017
73. Zhen G (2013) Silane crosslinked polyethylene special material. China Patent CN103289167A, Sep 2013
74. Zhao Y, Li S, Yu L (2016) Silane crosslinked polyethylene insulation material for wire and cable and its preparation method. China Patent CN106117738A, Sep 2016
75. Xia J, Wu W (2018) Natural-crosslinked aerial insulating material of polyethylene of one-step method silanes and preparation method thereof. China Patent CN107556600A, Jan 2018
76. Patricia F, Miguel A, Molano N (2017) Partially-crosslinked polyethylene formulations and methods of making same. PCT (World) Patent WO2017112642A1, Jun 2017
77. Zhu X, Meng Z, Zhou F (2014) Multifunctional cross-linked polyethylene insulation tester. China Patent CN102495341B, Feb 2014
78. Zheng M, Chen L, Lu Y (2015) The decision method of XLPE material heat ageing sample time. China Patent CN103487331B, Nov 2015
79. Liu G, Jin S (2017) A judgment method of XLPE cable insulation aging. China Patent CN104749503A, Aug 2017
80. Li H, Rao J, Lin F (2016) Leakage-proof ring and method of XLPE (crosslinked Polyethylene) cable polarization current measurement. China Patent CN105353280A, Feb 2016
81. Xu Y, Kang Q, Chen H (2017) A device and method for detecting and evaluating partial discharge of XLPE cable. China Patent CN104714155B, Dec 2017
82. Wang X, Wang G, Wang R (2020) A kind of coaxial bi-directional reactive extruder for the preparation of cross-linked polyethylene. China Patent CN210233955U, Apr 2020
83. Sun L, Wang J (2019) A radiation crosslinking polyethylene forming device. China Patent CN209552434U, Oct 2019
84. Zhao J, He C (2012) Electron irradiation crosslinked polyethylene foaming equipment. China Patent CN202607928U, Dec 2012
85. Zhang L, Zhao J, He C (2015) A chemical crosslinked polyethylene foaming equipment. China Patent CN103223704A, Oct 2015
86. Zhang L, Pan F, Jiang C (2011) A kind of soft crosslinked polyethylene insulating material. China Patent CN101602870A, Oct 2011
87. Jin H, Xiao Y, Deng X (2013) A water resistant crosslinkable polyethylene cable compound and its preparation method. China Patent CN102911417A, Feb 2013
88. Sohn S, Yang H, Jeong S (2014) Fire resistant cable for medium or high voltage. PCT (World) Patent WO2014081096A1, May 2014
89. Gu M, Zhang S (2014) Novel composite structured aluminium alloy cable. China Patent CN203746440U, Jul 2014
90. He M, Liu Y, Luo Z (2015) One step silane natural crosslinked polyethylene cable material and its preparation method. China Patent CN104497409A, Apr 2015

91. Zhou X, Yin G (2015) New flame retardant XLPE insulated wire and cable and its preparation method. China Patent CN105017661A, Nov 2015
92. Jia Z, Zhang W, Song W (2019) XLPE (cross-linked polyethylene) cable insulating material. China Patent CN106366419A, Feb 2019
93. Wang S, Chen Z, Chen P (2019) Nanocomposite crosslinked polyethylene insulation material with high DC breakdown field strength and its preparation method. China Patent CN106633303A, Oct 2019
94. Xia J (2018) A crosslinked polyethylene insulating material for track cable and its preparation method. China Patent CN108794851A, Nov 2018
95. Xu J, Wei (2019) A preparation method of vehicle tank lined with XLPE. China Patent CN110404748A, Nov 2019
96. Jiang J, Wei W, Liu S (2019) Preparation and application of large diameter high density cross linked polyethylene hot wound structure wall pipe. China Patent CN110239123A, Sep 2019
97. Plea I, Notingher PV, Stancu C, Wiesbrock F, Schlogl S (2019) Polyethylene nanocomposites for power cable insulations. *Polymers* 11(24):11010024

Chapter 14

Risks and Limitations Associated with XLPE Nanocomposites and Blends



Navid Mostofi Sarkari , Mohsen Mohseni ,
and Morteza Ebrahimi 

1 Introduction

Introducing nanoparticles in the XLPE matrix has been confirmed to materialize superior properties from numerous points of view. Besides, blending PE with other components such as ethylene-vinyl acetate (EVA), ethylene propylene diene monomer (EPDM), or polypropylene (PP) for fabricating XLPE can be desirable due to the advantageous properties brought by these components to the blend. However, all the advantages cannot gather at one side simultaneously; therefore, XLPE nanocomposites and blends also encounter different problems and issues originating from their components and structures. These problems result in risks and limitations in the application of XLPE materials. Therefore, progressively ongoing studies are struggling to address the concerns associated with these materials. Categorizing these limitations and risks in specific and independent groups is not straightforward due to complications and contributions of several factors in them. However, in this chapter, an attempt is made to classify the respective limitations and risks based on the components (nanoparticles, crosslinking agent, matrix, and whole mixture as the nanocomposite). Such a classification can help to define the specific challenges, review the offered solutions for each of them, and understand what is about to happen within that particular area. Prior to starting to discuss the limitations and risks caused by the components, a brief definition is brought from the essential electrical issues that XLPE

N. Mostofi Sarkari · M. Mohseni (✉) · M. Ebrahimi
Department of Polymer Engineering and Color Technology, Amirkabir University
of Technology (Tehran Polytechnic), 15875-4413 Tehran, Iran
e-mail: mmohseni@aut.ac.ir

N. Mostofi Sarkari
e-mail: navid.mostofi@aut.ac.ir

M. Ebrahimi
e-mail: ebrahimi@aut.ac.ir

nanocomposites may encounter during their adoption as insulations (which per se can also be considered as electrical risks and operational limitations of XLPE nanocomposites). These concerns are repetitively seen throughout the chapter in case studies. Hence, definitions of these issues are discussed at first, in order to perceive their importance in the upcoming sections. Moreover, the most related case studies that are specifically about these electrical characteristics in XLPE nanocomposites are briefly included in the next section. However, in-depth and comprehensive discussions for controlling these issues are brought later.

2 Electrical Issues Observed in XLPE Nanocomposites

2.1 Partial Discharge (PD) Formation

According to IEC 60270, PD is a localized electrical discharge that only partially bridges the insulation between conductors, and which may or may not occur adjacent to a conductor. Homogeneous distribution of electric field can hardly be attained under a high-voltage environment. Thus, someplace will exist where the local electric field strength is greater than the breakdown strength of air domains (30 kV/mm), such as the terminal of high-voltage generator winding and cable insulation, hence, as a consequence, PD will happen. PDs occur inside cavities, cracks, and/or gaseous inclusions inside solid insulations and at conductor-dielectric material interfaces in solid and liquid insulations. PD accelerates the degradation of polymer chains and acts as a predecessor to significant faults and problems. PDs with longer lengths deteriorate the insulation characteristics due to factors such as erosions of cavity walls by charge carriers, increment of the local temperature, atomic excitation-generated and charge carrier recombination-generated radiation, intensification of the chemical degradation reactions, and initiation of new chemical reactions [1, 2]. Previous researches have approved improvements in partial discharge resistance of nanocomposites in contrast to polymer matrices without nanofiller owing to the emerged interfacial area by the nanoparticles [3]. In a comprehensive investigation by Tanaka et al. [4], various dielectric properties of XLPE/SiO₂ (fumed silica) nanocomposites have been examined. The obtained results in terms of PDs demonstrated that the addition of nanoparticle could be effective in enhancing the resistance to discharge. Therefore, nano-filled XLPE exhibited dramatically improved endurance to PDs than non-filled XLPE. Moreover, the surface treatment of nanoparticles with a coupling agent seemed to add more advantages, and the best performance of resistance to PD was shown by the XLPE filled with surface-treated nanoparticles. Hence, it can be stated that XLPE nanocomposites can be superior in terms of resistance to PD when compared with unfilled XLPE, although they, more or less, encounter PDs, which is regarded as an operational risk and limitation in their long-term voltage endurance.

2.2 *Space Charge Accumulation*

Space charge occurs in a dielectric material when the rate of charge accumulation is different from the rate of charge removal upon the application of an electric field. Space charge arises owing to moving or trapped charges, which can be discussed in terms of electrons, holes, and ions, depending on the mechanism of charge transfer [5]. A range of phenomena can cause space charge formation; however, the most fundamental ones are the combination of current density and spatially inhomogeneous resistivity, ionization of species within the dielectric to form heterocharge, charge injection from a stress enhancement (although such space charge will often be too localized to be detected), and polarization in structures such as water trees [6]. Temperature and applied field are important extrinsic parameters for space charge development. Injection, recombination, and transport are the three determining conditions for space charge development, which exhibit high temperature and field dependence [7]. Space charge accumulation is a crucial concern in electrical insulations. The severe accumulation of space charge inside the XLPE has been a critical problem to be solved in the application of HVDC cable insulations, which can result in distorting local electric field, accelerating insulating aging, and reducing the service life of the cable [8]. Introducing nanoparticles in the XLPE matrix can positively affect to reduce the space charge accumulation. Actions such as surface modification of nanoparticles can bring about further improvements in space charge accumulation (will be discussed later). Wang et al. [9] have explored the electrical properties of XLPE/SiC nanocomposites with 1, 3, and 5 wt% concentrations of SiC. Their results indicated that the space charge accumulation could be suppressed effectively in nanocomposites by the introduction of SiC nanoparticles. The interface between the nanoparticles and the polymer matrix dominates the electrical properties of nanocomposites, and it can effectively suppress space charge accumulation in nanocomposites. However, the optimization of the nanofiller concentration is necessary for obtaining the best suppression of space charge accumulation. As reported by Wang et al. [9], the nanocomposite with the concentration of 1 wt% exhibited the highest effectiveness. When the concentration of the nanoparticle is low, the distances between the nanoparticles are large, which means that each nanoparticle can be regarded as an independent individual. Therefore, low-concentration nanocomposites, such as 1 wt%, have lesser amounts of space charges. Increasing the concentration of nanoparticles might persuade nanoparticles to agglomerate. This can influence the interface characteristics between the nanoparticles and the polymer matrix, leading to the accumulation of more space charges in high-concentration loaded nanocomposites. Xiang et al. [10] have explored improving the space charge characteristic of XLPE for HVDC cable by adding various amounts of BN nanoparticles. Since the electrical features of XLPE often depend on temperature, space charge injection characteristics of XLPE nanocomposites have been assessed under different temperatures. The outcomes of this study have revealed that the temperature and the introduction of nano-BN both had significant effects on the space charge properties of XLPE/BN nanocomposites.

2.3 *Electrical Treeing*

An electrical tree is a network of very narrow channels that propagate relatively quickly in a manner resembling a tree structure through the insulation resulting in failure and breakdown. Electrical trees can initiate from eroded surfaces in a void, water trees, and also stress increments without voids. The latter case includes two phases of electrical treeing. In the first phase, an initiation phase takes place in which, charge motion of each half cycle of the applied voltage gradually degrades the polymer, leading to the formation of a small void. The second phase consists of a growth phase induced by the extension of the initial void to form a tree-like network of branches due to PD within the branches. Presence of impurities or contaminants can be other reasons for electrical treeing [11, 12]. Different factors can influence the extent of electrical treeing in the XLPE insulations and predicting the exact individual effect of these factors (or in combination with other factors) is complicated. As reported by Chen et al. [13], temperature and voltage level have pronounced effects on the process of electrical tree formation in XLPE cable insulation materials. The level of voltage could impact the type of formed trees. Also, the time for tree initiation and tree growth time could be altered by temperature and voltage level. Bao et al. [14] have concluded that the structures of formed trees in the XLPE insulations are regularly changed with the alterations of voltage, local electric field, and frequency. For instance, bush-like trees appeared only under higher voltages, and vine-like trees were more likely to appear under higher frequencies. Qi et al. [15] have explored the influence of different defects in the XLPE insulations on the trigger and growth of electrical trees. Existence of defects in the insulation layer of XLPE cable is the leading cause of electrical tree formation. Based on their findings, the raised air gap and metal foreign matter on the semiconductor layer were the most important factors inducing electrical trees. Furthermore, spur curvature, the micro-pore pressure, and the initial energy of generating electric tree were the main parameters that had positive impacts on the increment of the initial voltage of the electrical tree, and thus, hindering the formation of tree. They have also proposed several treatment strategies for increasing the initial voltage of the electrical tree and decreasing the degradation of the actual XLPE cable, such as applying changes in the extrusion procedure of cable insulating layer and semiconductor layer, enhancing the heat treatment process of insulation, and modifying materials and using inert gas to fill micro-pores.

Nanoparticles have shown outstanding performance in the mitigation of electrical treeing in the XLPE nanocomposites when compared to unfilled XLPE or microparticle-filled XLPE. For instance, Paramane and Kumar [12] have considered the role of micro and nanofillers in electrical tree initiation and propagation in XLPE composites. For this purpose, they have compared electrical treeing characteristics in unfilled XLPE and XLPE nano- and microcomposites with various wt % concentrations of micro- and nano-sized silica. Their findings indicated that the initiation and propagation of electrical trees were dramatically restricted by the addition of the nanosilica, and the nanosilica-embedded XLPE composites

exhibited noticeable growth in duration of electrical tree initiation and breakdown times compared to the microcomposites and unfilled XLPE. However, an optimum concentration of nanoparticle was found for the lowest tree growth and the highest durations for tree initiation and breakdown times. Li et al. [16] have examined the effects of SiO₂ nanoparticles on the AC and DC electrical treeing resistance of XLPE. The findings in this study indicated that doping 1 wt% of SiO₂ nanoparticle in the XLPE matrix could introduce a plethora of deep traps, which was able to inhibit the injection and migration of charge, and thus significantly impede the initiation and growth of DC grounded electrical tree in the resultant SiO₂/XLPE nanocomposite. Moreover, the resistance to DC of this nanocomposite was seemed to be better than a commercial XLPE for ± 500 kV DC cable, which was used as a reference sample in the study. Furthermore, the tree under AC power frequency grew faster in comparison with the DC grounded tree. Under the power frequency AC voltage, the SiO₂/XLPE nanocomposite including 1 wt% of nanoparticle could hinder the initiation and growth of electrical tree at the early stage of tree initiation; however, when the tree growth exceeded a specific level at a high voltage, the growth rate of electrical tree became greater than that of unmodified XLPE (which was used as another reference in this study).

2.4 Water Treeing

Water treeing is a special form of degradation in XLPE insulations that happens in humid environments under DC voltage. Under electric field, water molecules in the cables are drawn in the imperfect parts due to polarization migration, then gradually accumulate to generate saturation, and finally form liquid water. Therefore, water trees consist of large numbers of voids filled with water inside them. Under the effect of electromechanical forces, electrochemistry, and microdischarge, water trees start to propagate gradually. A high electric field is formed on the edge of water trees and promotes the propagation of trees. Then, water trees develop to electrical trees and finally lead to the insulation breakdown. Generally, it is believed that the generation and development of water trees in insulation material is the result of long-term interactions by a non-uniform electric field and infiltrated water [17, 18]. The same as electrical treeing, various factors can be decisive on the extent of water tree formation or growth in the XLPE insulations. Chen et al. [19] have examined the influence of different degrees of peroxide crosslinking on the accelerated water tree aging of XLPE. Their findings demonstrated that crosslinking LDPE could drastically enhance the anti-water-treeing performance of LDPE, and the higher degree of crosslinking led to a better anti-water-treeing performance. Furthermore, in spite of the hindrance in crystal growth induced by crosslinking, the lamellar arrangement became extremely compacted due to the conduction of crossbonds. This caused the compression of the amorphous region among lamellae, which contributed to the difficulty of water molecules to creep. Moreover, the density of tie molecule chains between two crystalline layers was found to be

increased with the crosslinking degree, so that the generation and propagation of cracks due to Maxwell stress imposed by water molecules among lamellae was blocked. Identical deduction has been reported by Sun et al. [18] in a study investigating the water tree resistance of XLPE initiated by ultraviolet (UV) irradiation technique (UV irradiation-crosslinked XLPE). Their obtained experimental results suggested that the crosslinking reactions could effectively delay water tree growth, which was principally attributed to the large number of interconnecting molecular chains generated by activating the crosslinking bonds in the region of the amorphous phase under UV irradiation. The growth of water trees might cause damages in the amorphous zones as well as the crystalline domains in XLPE. It has been reported by Tao et al. [20] that the propagation of water tree resulted in declined crystallinity and reduced density of XLPE in water tree containing areas and subsequent destruction of the crystalline structure.

Nanocomposites have mostly illustrated promoted water tree resistance properties when nanoparticles are embedded in the XLPE matrix. However, it should be noted that the optimization of the nanocomposites' concentration is mandatory for attaining the most favorable properties. Nagao et al. [21] have studied the influences of adding different concentrations of magnesium oxide (MgO) nanofiller to LDPE and XLPE on the water tree retardant characteristic. Besides, they have assessed the effects of temperature on the water treeing properties. According to their findings, at 313 K, water tree retardation of both LDPE and XLPE was boosted through introducing the nano-MgO with the content of more than 2 phr, while it was at almost the same level with the nanofiller content of less than 2 phr. The lower water tree growth with increased nano-MgO content suggested the beneficial water tree retardant effect of this nanoparticle. Furthermore, the water tree retardation of MgO/XLPE nanocomposites seemed to be superior to that of MgO/LDPE at the nanofiller content of less than 2 phr, where MgO nanofiller showed no sensible impact on the water tree retardant property. However, with the introduction of nanofiller in 5 phr concentration, water tree resistance of both MgO/LDPE and MgO/XLPE nanocomposites demonstrated substantial improvements, and their resultant water tree retardation properties reached the same level. In terms of the influence of temperature on the water treeing, they observed at 333 K that the growth rate of water trees tended to be faster, and the retardation performance of MgO nanoparticles in the formation of water trees became less effective than that at 313 K. Qingyue et al. [22] have examined the influence of melt blending treated lamellar organic nanomontmorillonite (OMMT), modified spherical nano-silicon dioxide (SiO₂), and ethylene-vinyl acetate copolymer (EVA) with XLPE on the water tree resistance characteristics of resultant blend and nanocomposites. Their findings indicated that the three doped components were beneficial in advancing the water tree resistance. The lamellar OMMT prevented the propagation of water tree via conducting interfacial interaction with the matrix to bind the movement of the molecular chain and also through its lamellar barrier effect. Spherical SiO₂ nanoparticles homogenized the grain size and increased the constraint of water penetration in the amorphous region. EVA enhanced the interaction between XLPE and water, reducing the possibility of moisture condensation in the amorphous

region and consequently restrained the growth of water tree. According to their results, dopants with different structures noticeably modified the crystal morphology of XLPE, homogenized the crystal size, and optimized the crystal structure, which made the diffusion path of water molecules more tortuous; hence, the diffusion of water was slowed down. Moreover, the morphologies of water trees were different based on the doped component and nanoparticle. With respect to the morphological observations of water trees, the water trees of pure XLPE grew uniformly in divergent form, while the growth of the water tree of XLPE/OMMT nanocomposite was non-uniform diverging from the tip defect with more branches. Also, in the XLPE/SiO₂ nanocomposite, the water tree was relatively uniform with few branches and smooth edge.

3 Concerns Associated with Nanoparticles in XLPE Nanocomposites and Proposed Solutions

3.1 Cases Related to the Dispersion Quality of Nanoparticles in the XLPE Matrix

Effectiveness of nanoparticles in improving the electrical properties of XLPE nanocomposites has been widely studied in the literature and confirmed in most of the cases. However, one of the most critical factors that influence the function of XLPE nanocomposites as cable insulator materials, is the dispersion quality of nanocomposites in the matrix. Inadequate and non-uniform distribution and dispersion of nanoparticles in XLPE due to the polymer/filler incompatibility can lead to the appearance of severe problems in the insulation during its service, such as the formation of water tree, electrical tree, partial discharge, accumulation of space charge, and high-voltage arc. Each of these phenomena can eventuate in other unfavorable electrical and functional consequences that significantly affect the performance of insulations. Improving the dispersion quality of nanoparticles requires rigorous care due to the high tendency of nanoparticles to decrease their surface area through accumulation. This accumulation of the nanoparticles can be in the form of aggregation or agglomeration. Both cases result in sophistication in the dispersion process and homogenous distribution of primary particles in the matrix. Enhanced electrical properties of insulating materials containing nanoscale filler particles (nanocomposites) are attributed to an interfacial area that is formed between the polymer matrix of the base material and the filler particles [23]. Different models have been developed for describing the effect of nano-sized fillers on the dielectric properties of nanocomposites. These models can be named as electrical double layer model [24], intensity model [25, 26], multi-core model [27], interphase volume model [28], polymer chain alignment model [29], and the recently introduced particle interphase model [30]. Detailed information concerning these models is out the scope of current chapter and can be found in the mentioned

references. However, an identical fact exists regarding all of the suggested models. They are all based on the assumption that introducing nano-sized filler particles in the polymer matrix causes a remarkably grown interfacial area between the filler particles and the matrix polymer. It can be said that “It’s all interface”, referring to the large volume fraction of interfacial polymer compared to the volume fraction of filler in nanocomposites [31]. The models mentioned above assume that a layer is formed at the interface between filler particle and polymer. Since the layer is considered to possess a certain thickness and thus forms a specific part of the nanocomposite, it is called interphase [32]. The interphase region between the nanoparticles and the polymer can be divided into particle interphase and polymer interphase [30]. The properties in the interphase can be different from the properties of the polymer and the filler particles when considered individually. Thus, the interphase may drastically influence the properties of the nanocomposite. The reason for the determinative role of the interphase in nanocomposites is originated from the high surface to volume ratio, which leads to taking a remarkable percentage of the whole composite material [23, 32]. At modest particle loadings, the interfacial volumes may begin to overlap, leading to effective percolation of the interfacial areas and dramatic effects on the properties of the nanocomposites [33]. Percolation threshold or threshold content in the nanocomposites, generally refers to the minimum amount of external filler to be added in polymer matrix (in terms of percentage volume fraction) after which there will be a sudden transition in measured values [34].

The premier characteristics of XLPE nanocomposites over its microcomposites have been confirmed in several case studies. For instance, superior electrical characteristics (partial discharge) of XLPE/silica nanocomposites over XLPE/silica microcomposites have been shown by Paramane and Kannaiah [35]. The definition of partial discharge was mentioned earlier. Partial discharges are, in general, a consequence of local electrical stress concentrations in the insulation or on the surface of the insulation. Generally, such discharges appear as pulses having a duration of much less than 1 μ s. Partial discharge formation is caused due to existing internal voids, defects, and cracks in the electrical insulation. Most of the failures of electrical insulation are caused due to partial discharge, which paralyzes the electrical insulation [35]. The reasons that have been counted for enhanced partial discharge characteristics of XLPE nanocomposites over microcomposites [35] are less interparticle distance and grown interface area between nanofillers and polymer matrix. Moreover, lamellar thickness, crystallinity, and glass transition temperature (T_g) of XLPE nanocomposites are introduced as other significant parameters that hinder the formation of partial discharge to a larger extent. Grown lamellar thickness, crystallinity, and T_g cause a reduction in the chain mobility, which increases the amount of tightly bound XLPE chains resulting in resistance against the formation of partial discharge. Furthermore, it has been noted that the possibility of partial discharge propagation in case of agglomerated nanocomposites is due to concentration of nanoparticles at the several locations. This situation allows the partial discharge to reach to the ground electrode. Accordingly, it can be deduced that dispersion quality of fillers in the polymer matrix is crucial. In

microparticle/polymer composites, surface modification is widely used as an effective technique to improve filler dispersion. With the development of nanocomposites, the surface modification for nanoparticles has attracted more and more attention [36]. During the recent years, different electrical concerns associated with the XLPE nanocomposites have been investigated extensively in a correlation with the type of nanoparticles and extent of their dispersion in the XLPE nanocomposites. In the undertaken investigations, different nanoparticles and modification methods have been proposed and utilized for the surface modification in an attempt to overcome their unfavorable aggregation problem and enhance the electrical properties of the nanocomposites.

3.1.1 Organofunctional Silanes: Outstanding Surface Modifiers for Improving Dispersion and Interfacial Interactions of Nanoparticles in XLPE Nanocomposites

The effect of nanoparticles on reducing the electrical conductivity values and space charge accumulation is stronger if their surfaces are covered or treated by, for example, chemical modification [2]. Organofunctional silanes (also called as organosilanes) are extensively used promising chemicals utilized for the surface treatment of nanoparticles in the nanocomposites. In these conditions, organosilanes act as coupling agents. Basically, silane coupling agents have a general chemical structure of four substituents attached to a single silicon atom. The coupling feature of organosilanes is correlated with a stable link between the organofunctional group (Y) and hydrolyzable groups (X) in compounds of the structure X_3SiRY [37]. XLPE-based blends and nanocomposites are majorly composed of inherently non-polar polyethylene backbone. Therefore, they are inert in terms of their chemical nature. This leads to non-wetting or very poor wetting behavior (depending on the other components in XLPE blends and nanocomposites) when they are exposed to polar substances [38]. The organofunctional groups are chosen for reactivity or compatibility with the organic polymer, while the hydrolyzable groups act as intermediates in the formation of silanol groups for bonding to mineral surfaces [37, 39]. Thus, it can be concluded that organosilanes couple organic polymers with inorganic filler particles. In fact, the interface between the filler and polymer is improved through the surface modification, and this positively affects not only the nanoparticle dispersion but also the stability and specific surface area, resulting in enhanced electrical strength [40].

In a study by Huang et al. [41], which has investigated the surface treatment of dispersed silica nanoparticles in LLDPE by octyl-trimethoxysilane, it has been noted that agglomerates of nanoparticles were visible in both composites containing surface-treated and un-surface-treated silicas. However, the agglomerates of un-surface-treated silica were clearly larger, indicating the effectiveness of octyl-trimethoxysilane treatment in improving the dispersion of silica nanoparticles in LLDPE. Such an enhanced dispersion behavior has been explained by the combination of the chemical nature of the matrix primarily, as well as the surface

chemistry characteristics of the inorganic particles. The improved dispersion of the surfaced-treated nanoparticles should be firstly ascribed to the substitution of hydroxyl groups and the removal of molecularly absorbed water on the surface of the nanoparticles, which not only decreases the surface free energy of nanoparticles but also prevents the formation of hydrogen bonds between the nanoparticles during the preparation of the composite samples. It is well known that the silanol groups at the surface of the silica nanoparticles tend to form hydrogen bonds, which can result in a strong tendency toward agglomeration in the polymer matrix, especially in non-polar polymers. Another reason for obtaining good dispersion of silica nanoparticles is that the employed silane molecules in this work had a long alkyl chain, which had good compatibility with LLDPE, and this enhanced the adhesion between the silica and LLDPE. Several studies also have investigated the same treatment methods in polyethylene nanocomposites to achieve superior electrical properties. Liu et al. [42] have utilized three different alkyl-terminated silane coupling agents for surface treatment of Al_2O_3 nanoparticles in LDPE/ Al_2O_3 nanocomposites. The difference between the organosilanes was attributed to the length of terminal alkyl groups (number of C), and these organosilanes were methyltrimethoxysilane (C1), n-octyltriethoxysilane (C8), and n-octadecyltrimethoxysilane (C18). They have reported reduced DC conductivity in all of the prepared nanocomposite samples (containing unmodified and silane-modified nanoparticles) when compared to pristine LDPE, and large agglomerates of nano- Al_2O_3 were found to increase the conductivity of the nanocomposites. The modified nanocomposite with n-octyltriethoxysilane showed significantly shorter nearest neighbor particle distances both in the short and the long range, implying the superiority of this type of silane agent in promoting good dispersion of the nanocomposites, which is followed by n-octadecyltrimethoxysilane and methyltrimethoxysilane coupling agents. Moreover, their findings suggested that the coated layer by n-octyltriethoxysilane was the more permeable and receptive to charged and dipolar species than the methyltrimethoxysilane and n-octadecyltrimethoxysilane modified layers. In addition to acceptable dispersion, adequate interaction between the nanoparticles and polymer matrix is necessary for obtaining favorable characteristics in the final nanocomposite materials. The inadequate interfacial adhesion between the nanoparticles and the polymer matrix might cause early de-bonding of the nanoparticles leading to cavitation in the nanocomposite under mechanical strain/stress [43, 44]. Wang and Li [45] have analyzed the effect of organosilane surface modification of nanoparticles in LDPE/ TiO_2 nanocomposites with 3-glycidoxypropyl-trimethoxy-silane. According to their results, this treatment yielded a more uniform dispersion of nanoparticles in the LDPE matrix and led to improved dielectric breakdown performance.

Identical case studies are found in the literature discussing surface modification of nanoparticles in XLPE nanocomposites to assess consequent electrical properties. Herein, the most relevant case studies with respect to the state of nanoparticles in the XLPE matrix and the assessed specific electrical properties are reviewed for obtaining better insight regarding the effect of nanoparticles' dispersion on the electrical properties.

Ashish Sharad and Kumar [46] have investigated partial discharge characteristics of XLPE/silica nanocomposites in unmodified, agglomerated, and octylsilane-modified states of the silica nanofillers. Based on their findings, octylsilane-modified XLPE/silica nanocomposites proved their efficacy over unmodified and agglomerated nanocomposites in terms of partial discharge properties. The resultant partial discharge activities could be summarized as surface-modified case < agglomerated < unmodified < Virgin XLPE, when considered comparatively. Furthermore, the nanocomposites containing surface-modified nanoparticles exhibited low optimal content of nanofiller toward partial discharge characteristics in comparison with the unmodified and agglomerated nanocomposites. Hence, the surface-modified XLPE/silica nanocomposites could be considered as an economically viable variant over the unmodified and agglomerated nanocomposites. In this study, the superior performance of octylsilane-modified nanocomposites has been explained by the modified polymer chain alignment model, which suggested that the octylsilane-modified nanofillers had better alignment with XLPE polymer chains resulting in enhanced performance of octylsilane-modified XLPE nanocomposites. Moreover, they have reported increased water contact angle value after nanofiller addition in all nanocomposite samples leading to changing the hydrophilic nature of the surface to a hydrophobic state. In the case of octylsilane-modified nanocomposites, such an observation has been ascribed to the replacement of the silanol group of unmodified nanosilica by the octyl groups of octylsilane-modified nanosilica.

As described earlier, filler particles must have compatibility and sufficient interaction with the polymer matrix. However, this cannot be reached most of the time due to the difference in their surface energies. Therefore, it can be concluded that the surface wettability acts as a decisive factor in obtaining desired dispersibility and compatibility. Contact angle measurement is a suitable technique to attain information regarding surface energy. In nanocomposites, alteration of contact angle on the surface versus filler loading gives insight into the hydrophilic or hydrophobic behavior of the nanoparticles in correlation with the polymer matrix [47]. Jose et al. [48] have investigated wetting properties and surface energy characteristics of XLPE nanocomposites containing Al_2O_3 , SiO_2 , TiO_2 , and clay nanofillers, from which the spherical nanofillers (Al_2O_3 , SiO_2 , TiO_2) were surface-treated with trimethoxyoctylsilane. Based on their outcomes, XLPE/ Al_2O_3 nanocomposites indicated growth in contact angle values with the increase in nanofiller concentration for both the water and dimethyl sulfoxide test liquids. Theoretical predictions of contact angle and the experimental results demonstrated an identical trend of progression in contact angle with filler introduction. While comparing spherical nanofillers and clay, 3D spherical nanofiller reinforced systems had higher contact angle and better hydrophobicity. Among different spherical nanofillers, TiO_2 and Al_2O_3 caused higher contact angle values. Comparing interfacial energy, interaction parameter, and other wetting properties revealed that the XLPE/ Al_2O_3 nanocomposite was the best candidate having higher non-wetting behavior. Thus, they were successful in fabricating non-wettable XLPE

nanocomposite surfaces from a wettable surface of XLPE through addition of surface-treated inorganic nanofillers in the XLPE matrix.

Zhang et al. [49] have studied the effect of surface modification of SiO₂ nanoparticles on DC breakdown and space charge behavior in XLPE/SiO₂ nanocomposites. They have utilized titanate and vinylsilane coupling agents for modifying the surface properties of SiO₂ nanoparticles. As they have reported, the utilized modifiers aided in decreasing the agglomeration (some of which had diameters over 1 μm) significantly. Also, the space charge measurements during DC endurance test revealed that the introduction of unmodified SiO₂ nanoparticles could not suppress the injection and movement of space charge until their surfaces were modified, which seemed to contribute to the formation of more and deeper trap sites considering the better dispersion of SiO₂ nanoparticles within XLPE. Furthermore, the surface modification of nanoparticles could effectively improve DC breakdown strength under various temperatures.

Zhang et al. [50] have examined the effect of surface modification of SiO₂ nanoparticles on charge transport characteristics in XLPE/SiO₂ nanocomposites. For the purpose of modification, they have employed 3-(methacryloyloxy)propyl-trimethoxysilane and titanate coupling agents. According to their results, the effect of both coupling agents in decreasing the agglomeration was significant as a consequence of inducing surface hydrophobicity on the nanoparticles and boosting their compatibility with the XLPE matrix. Examining the impact of nanoparticles' surface modification on the charge transport properties led to several conclusions on different properties. The DC conductivity decreased more in the nanocomposites containing surface-modified nano-SiO₂, and it increased much more slowly than that in unfilled and filled with unmodified SiO₂ nanocomposites when temperature was raised. Also, dispersing surface-modified SiO₂ nanoparticles increased the relative permittivity and tan delta. The nanocomposite including unmodified SiO₂ had higher relative permittivity than the unfilled XLPE matrix. In contrast, its tan delta was slightly lower than unfilled XLPE in the low frequency regions and higher in the high-frequency regions. Moreover, the presence of SiO₂ nanoparticles in the XLPE matrix increased the trap density and produced more trap energy levels, while surface modification of the nanoparticles could further increase the corresponding trap depth and the trap density. In the case of XLPE nanocomposites containing modified SiO₂ nanoparticles, trapped homocharges formed an independent electric field and mitigated the effective electric field. This resulted in a declined charge injection and raised charge injection barrier height. Accordingly, the formation of space charge in the material bulk was suppressed.

Wang et al. [8] have evaluated the effect of TiO₂ nanoparticle surface modification and filling concentration on space charge characteristics in TiO₂/XLPE nanocomposites. The surface modification has been done by dimethyloctylsilane (MDOS) coupling agent. Their outcomes have confirmed the efficiency of dimethyloctylsilane in enhancing the dispersion of nano-TiO₂ in the XLPE matrix and reducing their agglomeration. The nanocomposite containing MDOS-modified TiO₂ had the highest volume resistivity, followed by the nanocomposite including unmodified TiO₂ nanoparticles and then pure XLPE (unfilled). This trend has been

explained by the presence of a large number of deep traps in TiO₂/XLPE nanocomposites, which causes reduced carrier mobility and enhanced volume resistivity. Moreover, the surface-modified nanoparticles led to the existence of more traps than their unmodified state, resulting in more carriers to be captured and attaining the largest volume resistivity. Furthermore, it has been reported that TiO₂ nanoparticles had a significant influence on space charge accumulation behavior that led to noticeably improved electric field distribution in TiO₂/XLPE nanocomposite under DC electric field. Based on the reported outcomes in this study, on the one hand, a large number of interface regions generated lots of deep traps, which could shorten the effective distance of migration of space charge packets (named “solitary waves”) and considerably decreased carrier mobility. On the other hand, low carrier mobility enhanced the neutralization process and weakened the impurity ionization, leading to the disappearance of heterocharge in TiO₂/XLPE nanocomposites. The interface reverse electric field not only suppressed the charge injected from the electrodes, but also strengthened the electric field in the middle of the matrix, so that the accumulated space charge could be transferred out of the material timely. The homocharge injection was more evident in the nanocomposite containing MDOS-modified TiO₂, and homocharge injection volume reduced with the increase of filling concentration. The other findings of this study indicated that the MDOS-modified TiO₂/XLPE nanocomposite had deeper traps than the unmodified TiO₂/XLPE nanocomposite, which resulted in more homocharges to be injected in the MDOS-modified TiO₂/XLPE nanocomposite. The established reverse electric field by homocharge was known to be the main reason for the homocharge decrease with increasing filling concentration.

Donghe et al. [51] have investigated the influence of 3-aminopropyltriethoxysilane, γ -(2,3-epoxypropoxy)propyltrimethoxysilane, and triethoxyvinylsilane surface modifiers on SiO₂ nanoparticles in XLPE/SiO₂ nanocomposites. The intended properties to be studied after embedding the modified nanoparticles were the structural morphology and dielectric property of the resultant XLPE/SiO₂ nanocomposites. According to the reported findings, the surface-modified nano-SiO₂ particles were dispersed substantially uniformly in the XLPE matrix after preparation by melt blending process. Therefore, it was proved that the modified nano-SiO₂ particles achieved nanoscale dispersion in the XLPE matrix. Moreover, the microstructure analysis demonstrated that the introduction of different modified SiO₂ nanoparticles in the XLPE matrix changed parameters such as melting enthalpy, melting point, melting range, crystallization peak temperature, and the crystallization temperature range of the nanocomposites containing the three modified nanoparticles when compared with pure XLPE. The alterations of these parameters indicated that the addition of modified nano-SiO₂ particles increased the crystal size and broadened the size distribution of polyethylene. Assessing the dielectric properties has shown that the conductivity of nanocomposites was relatively low, and the rate of change decreased with the temperature increment, which manifested the binding of interfacial forces on the molecular motion and the influence of the addition of nano-SiO₂ on the structural morphology of the nanocomposites. Also, it has been deduced that embedding SiO₂

nanoparticles could drastically improve the breakdown strength of nanocomposites. The main reasons for the breakdown strength of nanocomposites were attributed to the interface region characteristics that were induced by different organosilane-modified SiO₂ nanoparticles.

3.1.2 Other Proposed Strategies for Improving the Dispersion Quality and Dielectric Properties in XLPE Nanocomposites

In addition to silane coupling agents, other materials and methods have been employed to enhance the dispersion and packing of nanoparticles in the XLPE nanocomposites, and improve the host-guest compatibility between the matrix and nanofillers, and subsequently promote dielectric properties. Since these methods are mostly based on case studies, they are being reviewed in a case-specific manner.

Surface-Initiated Polymerization on the Nanoparticles

Zhang et al. [52] have adopted surface-initiated reversible addition-fragmentation transfer (RAFT) polymerization to synthesize poly(stearl methacrylate) (PSMA) brushes on the surface of SiO₂ nanoparticles, and prepared SiO₂/XLPE nanocomposites with relatively uniform nanoparticle distribution of small agglomerates (smaller than 100 nm). Through this method, they achieved enhanced space charge suppression, improved DC breakdown strength, and restricted internal field distortion over a wide range of external DC fields. The relatively uniform nanoparticle dispersion state contributed to an increase in interfacial volume and a significant increase in deep trapping sites. The efficient charge trapping ensured that most charges were trapped near the injecting electrode, and the field distortion was considerably alleviated. Free-PSMA chains also provided some trapping sites for positive carriers.

Modification of XLPE with an Agent Possessing Polar Functionalities and High Boiling Point

Zhang et al. [53] have prepared XLPE modified with 2-(4-benzoyl-3-hydroxyphenoxy) ethyl acrylate (BHEA) compound via melt blending (XLPE/BHEA composite). BHEA is a type of compound with many kinds of polar functional groups and a high boiling point, and the researches have benefited from these advantages in the mixtures. A high boiling point minimizes air bubble formation, which is considered as a defect in the insulation and can adversely affect its performance. The existence of functionalities such as carbonyl and conjugated double bonds create deep traps that capture electric charge carriers in polymer materials [54]. According to findings by Zhang et al. [53], in the optimized sample of XLPE/BHEA composites, BHEA could effectively suppress space charge

accumulation, reduce DC conduction, and improve DC breakdown strength of XLPE at a higher temperature. Polar functional groups of BHEA (including carbonyl, hydroxyl, ether, and ester group) resulted in deeper traps in XLPE/BHEA composites, which could raise the potential charge injection barrier and reduce the charge carrier number and mobility to suppress space charge accumulation and reduce the conduction current density. Also, they have found that BHEA did not interfere with the crosslinking process and instead improved it slightly. Moreover, BHEA slightly affected the mechanical properties and crystallization of XLPE.

Introducing Polypyrrole (PPy) Nanoparticles in XLPE (XLPE/PPy Nanocomposites)

Zhang et al. [55] have prepared XLPE/polypyrrole (XLPE/PPy) nanocomposites by introducing various contents of nano-PPy in XLPE. They have synthesized nano-PPy with a bowl-like structure possessing a diameter of about 100 nm. The bowl-like structure of PPy increased its specific surface area and, consequently, increased the interface between nano-PPy and XLPE matrix. After obtaining XLPE/PPy nanocomposites, they have examined the effect of PPy conductive nano-polymer on the crystalline structure, crosslinking degree, space charge behavior, DC electrical conduction, and breakdown of the nanocomposites. Resultant findings indicated that the introduction of nano-PPy in XLPE did not change the crystalline structure of XLPE, and the nano-PPy was mainly dispersed within the amorphous regions of XLPE. Moreover, gel content investigations of the XLPE/PPy nanocomposites revealed that the crosslinking degree slightly changed after embedding the nano-PPy due to combination of the effects of nano-PPy as a scavenger of radicals and a physical crosslinking point. From the electrical point of view, introducing conductive nano-PPy in XLPE could produce deep traps to capture space charge carriers and suppress space charge accumulation in the XLPE/PPy nanocomposites. In the case of a lower electric field, the deep traps could capture and scatter the charge carriers in the transport process, and then reduce the conduction current density of the nanocomposites. However, when a higher electric field was applied, the number of free electrons increased due to the dissociation of the polaron and the field electron emission effect of nano-PPy, which would reduce the DC breakdown strength of XLPE/PPy nanocomposites. With increasing the nano-PPy content, the nano-PPy started to agglomerate, and the DC electrical characteristics decreased slightly.

Embedding NanoScale Hybrid Fillers in XLPE (Ternary Hybrid Nanocomposite)

Jose and Thomas have introduced XLPE- Al_2O_3 -clay ternary hybrid nanocomposites and performed comprehensive analyses on their mechanical and thermal properties [56] and transport characteristics [57]. In both studies, XLPE- Al_2O_3 -

clay hybrid ternary composites of Al_2O_3 and clay in 1:1 and 2:1 compositions, binary composites of XLPE- Al_2O_3 , and XLPE-clay composites have been prepared through melt mixing (Al_2O_3 nanoparticles were initially silane-modified). According to the results of mechanics, superior properties of ternary hybrid composites were confirmed, and the trend of variation in terms of tensile strength and Young's modulus between the prepared samples was (Al_2O_3 :clay = 1:1) > (Al_2O_3 :clay = 2:1) > XLPE- Al_2O_3 binary system > XLPE-clay binary system. The dispersion status of nanofillers in the polymer provided evidence for the mechanics' results, which illustrated network formation in the ternary hybrid system. The mentioned effective network only occurred in Al_2O_3 :clay = 1:1 nanocomposites. Whereas, the aggregation of Al_2O_3 was predominant in Al_2O_3 :clay = 2:1 sample over the network hybrid effect. The decreased aggregation of Al_2O_3 owing to the creation of network morphology has been explained by the presence of nanoclay platelets. In fact, introduced clay nanoplatelets into the nanocomposites caused filling the gaps between the Al_2O_3 nanoparticles. Accordingly, these nanoparticles were connected jointly through clay platelets, resulting in the creation of network morphology. The positive hybrid effect, which was recognizable from the theoretical and experimental values of Young's modulus and tensile strength in Al_2O_3 :clay = 1:1 sample, evidenced that there would be a factor of synergism in addition to the arithmetic average of the properties of the two fillers. This synergism is associated with the operation of filler networks in the hybrid system due to the networking associated with self-assembly.

In [57], transport properties of hybrid nanoparticle-based XLPE- Al_2O_3 -clay binary and ternary nanocomposites have been investigated with special significance to the self-assembling hybrid filler effect and its impact on polymer chain dynamics, and accordingly its influence on the transport mechanism. The comparative variation trend of solvent uptake was (Al_2O_3 :clay = 1:1) < (Al_2O_3 :clay = 2:1) < binary nanocomposites. In ternary hybrid composites, effective filler-filler networks could trap the polymer chains resulting in highly reduced polymer segmental mobility. Furthermore, in the ternary systems, filler networks were strong, and the polymer-filler interaction was superior to binary systems owing to the synergism of Al_2O_3 and clay nanofillers. The investigations on the mechanism of transport in hybrid nanocomposites revealed that the time taken by polymer segments to respond to swelling stress and rearrange them to accommodate the solvent molecules was very high. Obtained transport coefficient values and the swelling parameter confirmed the premiere solvent resistance properties of the nanocomposites, especially of the ternary system of Al_2O_3 :clay = 1:1, in which the microstructure-assisted diffusion mechanism controlled the solvent penetration process.

3.1.3 Risks Attributed to Presence of Surface Moisture on Nanoparticles

Interactions with water constitute a ubiquitous feature of the environmental exposure of materials. As such, if nanodielectrics are ever to be exploited in anything

other than niche applications, a key factor will be to understand the mechanisms by which they interact with water and also the consequences of this for bulk properties [58]. One might think that the improved dispersion can guarantee enhanced dielectric properties. However, this is not always the case, and circumstances exist whereby enhanced dispersion leads to inferior dielectric behavior. Problems can occur in well-dispersed nanocomposites when the nanoparticles are spaced sufficiently closely that percolation effects dominate. An example of such conditions can be the impact of adsorbed moisture on the surface of nanoparticles, which influences drastically on a range of electrical parameters [59]. Many of the nanoparticles that are embedded in XLPE nanocomposites possess hygroscopic nature. This property of nanoparticles causes absorption of moisture from the surrounding environment and the presence of water on their surface, which per se leads to accumulation of nanoparticles and formation of agglomerates. Thus, separating the nanoparticles and achieving their uniform dispersion will be a considerable challenge. Existence of a water layer (water shell) on the nanoparticles can result in further effects on their behaviors in the nanocomposites, giving rise to alterations in dielectric properties independent of dispersion issues [33, 60].

Most studies regarding the effects of water on the electrical performance of nanocomposites consider that the water shells can percolate at a larger particle content and finally lead to a poor insulating material with a large amount of heterocharge formation and decreased breakdown strength [61]. However, this is not a universally conducted case, and counterexamples are seen in the literature. Therefore, determining the exact effect of moisture on the dielectric behavior of nanocomposites seems sophisticated and requires further inspections. For instance, Fabiani et al. [62] have investigated the effect of water absorption in organically modified nanoclays embedded in ethylene-vinyl-acetate (EVA) matrix on electrical properties of nanocomposites with respect to the contribution of aspect ratio of the nanoparticles. Based on their conclusions, filler with a higher aspect ratio exhibited a more effective role in impacting the electrical properties of the final nanocomposite. In fact, the formation of a thin water shell around the filler particles with a low aspect ratio does not modify the dielectric properties of the composite significantly. This is due to the much smaller size of shell thickness when compared to the average distance among the particles. Therefore, the formation of percolative paths on a large scale is very unlikely. Meanwhile, in the case of fillers with high aspect ratio, percolative paths are formed when a critical amount of water is adsorbed and accumulated around the particles, resulting in increased conductivity and loss factor of the specimens. Furthermore, the accumulated space charge under DC increases and dielectric strength is drastically decayed.

Several studies are available in the literature examining the effects of water on the electrical characteristics of PE-based nanocomposites. Nilsson et al. [63] have evaluated the influence of water uptake on the electrical DC conductivity of insulating LDPE/MgO nanocomposites. As they have reported, the DC conductivity of LDPE can be reduced 100 times by adding 1–3 wt% of well-dispersed metal-oxide nanoparticles (MgO, ZnO, Al₂O₃), although the fundamental physics attributed to this phenomenon remain unclear. One of the several possible

explanations is stated to be that the nanoparticles attract electrical charges, polar molecules (H_2O and crosslinking by-products), and ions (H^+ , OH^- , salts, and ionic species originating from the crosslinking by-products) on their surfaces, thus, these species become trapped, leading to cleaning and purification of the surrounding polymer matrix. This hypothetic explanation has been strengthened by conductivity measurements on pristine LDPE and octyl(triethoxy)silane-modified MgO/LDPE nanocomposites with 3 wt% of fillers at 0 and 50% of relative humidity, showing a 100-fold increase in conductivity at elevated humidity for the nanocomposites, compared to a twofold increase for the pure LDPE. As a conclusion in this study, the long-term insulation efficiency of an insulating polymer nanocomposite is optimal if the material is carefully initially dried and also surrounded by an impenetrable moisture barrier before use since the performance of insulation deteriorates with time in the insufficient diffusion barrier condition. Pourrahimi et al. [64] have introduced a method for synthesizing highly insulating nanocomposites based on LDPE and moisture-resistant MgO nanoparticles. The surface regions of the MgO nanoparticles can undergo a conversion to the hydroxide phase in a humid environment. Hence, they have proposed a facile method to obtain MgO nanoparticles with a large surface area and remarkable inertness to humidity. The employed key step for attaining moisture-resistant MgO has been introduced to be applying a silane coating on the nanoparticles as an intermediate step after a low-temperature thermal decomposition of $\text{Mg}(\text{OH})_2$ prior to a high-temperature heat treatment. In such a method, the specific surface area of nanoparticles was successfully preserved after the high-temperature heat treatment. The moisture-resistant MgO nanoparticles retained their phase/structure even after extended exposure to a humid medium. Furthermore, the moisture-resistant MgO nanoparticles showed their improved dispersion and interfacial adhesion in the LDPE matrix with smaller nano-sized particle clusters than conventionally prepared MgO. Moreover, the inclusion of 1 wt% moisture-resistant MgO nanoparticles has been reported to be sufficient to decrease the conductivity of polyethylene 30 times, and the decline of conductivity has been discussed in terms of defect concentration on the surface of the moisture-resistant MgO nanoparticles at the polymer/nanoparticle interface.

Lau et al. [65] have studied the effect of two different silicone nanoparticles (oxide- (SiO_2) and nitride- (Si_3N_4) based) on the water absorption and dielectric breakdown properties of LDPE. Based on their findings, the type of embedded nanoparticle was decisive in the water absorption behavior of nanocomposite, and LDPE/ Si_3N_4 attracted much less water than LDPE/ SiO_2 nanocomposites. The different water absorption behaviors subsequently influenced the breakdown strength of the resultant nanocomposites, where LDPE filled with SiO_2 nanoparticles indicated lower breakdown strength than LDPE filled with Si_3N_4 nanoparticles. According to their conclusions, the observed variations in the water absorption and breakdown strength of the nanocomposites were attributed to the interfacial mechanisms of the nanocomposites, in particular, in relation to the surface chemistry natures of SiO_2 and Si_3N_4 nanoparticles. Yang et al. [66] have explored the influence of moisture absorption on the DC conduction and space charge

characteristic of MgO/LDPE nanocomposite. In their test condition (exposing LDPE and MgO/LDPE to 40% relative humidity) for 9 days, absorbed water contents in LDPE and MgO/LDPE nanocomposite were recorded to be roughly 2.3% and 3.6%, respectively. These amounts implied that the damp nanocomposites still could maintain the ability to suppress space charge and even keep the conducting current from increasing below 20 kV/mm. This could be due to the fact that the trap or scatter centers created by the nanoparticle/polymer matrix interface were powerful enough to inhibit mobility and space charge accumulation generated by water dissociated ions and hydrated ions. Damp MgO/LDPE nanocomposite had poor space charge suppression ability at high electric fields of about 40 kV/mm, which was indicative of the negative influence of moisture absorption on the dielectric properties. The weakly bound water molecules may be converted to free ones, increasing the ion generation by means of a high electrical field to enhance the charge accumulation. Absorbed water molecules could be considered to be divided into three forms, free water molecules which were assumed into the polymer matrix, weakly bound water molecules which may be gathered around nanoparticles, and tightly bonded water molecules, bound by hydrogen bonds. The analysis showed that the tightly bonded water molecules could not be removed from the nanocomposite after the drying process at 80 °C in vacuum conditions.

Wang et al. [67] have examined the impact of moisture absorption on electrical properties and charge dynamics of PE silica-based nanocomposites. In this study, Zhuravlev model has been adopted to identify the effects of OH groups and absorbed moisture on the nanosilica surface. According to Zhuravlev model [68], the adsorbed moisture can be divided into two regions: (i) multilayer moisture, which can be removed at 25 °C in vacuum, and (ii) monolayer moisture, which requires a temperature of 190 °C in vacuum for its elimination. Based on their results, the loading ratio of nanosilica and the humidity of the environment determine the amount and rate of absorbed moisture. Furthermore, the main contribution to the deterioration in the electrical properties of nanocomposites comes from the large amount of moisture absorbed in the multilayer form. However, the impact of multilayer moisture can be easily eliminated without the destruction of material. According to the findings by Wang et al. [67], moisture absorption by the nanocomposites caused the fall of DC breakdown strength and improvement of charge dynamics. Also, the loading ratio of nanosilica was the most significant factor in decreasing DC breakdown strength, followed by the amount of moisture absorbed. Besides, employing trimethoxy(propyl)silane surface treatment agent to reduce the amount of surface OH groups was not totally successful in substituting surface OH groups with propyl groups of silane agent, and the remaining OH functionalities still were capable of absorbing moisture. From the reviewed case studies above, it can be inferred that several factors, including the type of nanoparticles, surface treatment of nanoparticles, physical specifications of the nanoparticles, humidity of the environment, electrical operation condition, and loading ratio of nanoparticle are a number of determinative factors in the extent of water uptake and absorption, which can subsequently influence the dielectric behavior of the nanocomposites.

In the case of XLPE nanocomposites' exposure to humid environments, moisture is also likely to dominate their dielectric behavior [2]. Much limited number of publications are available concerning the effects of humidity on the electrical aspects of XLPE nanocomposites when compared to the number of publications considering uncrosslinked PE-based nanocomposites. Hui et al. [69] have investigated dielectric behavior of XLPE/silica nanocomposites in humid environments. With respect to their findings, the introduction of unfunctionalized or partially functionalized silica particles could increase the amount of absorbed moisture. Formation of water shells likely occurred surrounding the silica particle/aggregates and led to their percolation when the interparticle/aggregate distance was decreased due to a larger particle loading and a given particle mixing state. Such a phenomenon resulted in decreased dielectric performance, such as reduced breakdown strength, increased loss, and a large amount of heterocharge formation. Taken together in this study, it has been hypothesized that the creation of a concentric shell surrounding the particle with a high concentration of water (water shell), and the change in the interparticle/cluster distances are two major factors governing the dielectric behavior in the wet XLPE/silica nanocomposites. In another study by Hui et al. [70] concerning the influence of moisture on the electrical performance of XLPE/silica nanocomposites, obtained results have shown that an optimum particulate loading could exist for the nanoparticle, in which nanocomposites were able to maintain the original properties to a large extent in the presence of moisture, even in acutely humid conditions.

4 Possible Risks Attributed to the Adverse Effect of Nanoparticles in the Microstructure and Crystalline Domains of XLPE Matrix

XLPE is composed of PE chains, and PE chains are able to orient and form crystalline structures. Therefore, XLPE can also contain crystalline domains, although crosslinking reduces the degree of crystallinity by hindering mobility, orientation, and crystallization of chains leading to disordered patterns that cannot be aligned in the crystalline lamella and crystal lattice [71, 72]. Nevertheless, crystalline regions exist in their structure along with amorphous zones, and the resultant crosslinked polymer is semicrystalline. The interfaces between the crystalline and amorphous domains in the structure of semicrystalline PE are associated with the existence of charge trapping sites, which are likely to impact the charge accumulation. Embedding nanofillers in the matrix results in a sophisticated charge transport mechanism owing to the insertion of numerous interfaces and addition of interactions between the polymer and nanofillers [73]. This state is related to dielectric properties of the XLPE nanocomposite, whereas the introduction of nanoparticles can influence the microstructure of the polymeric matrix as well. Embedding nanoparticles in the polymeric matrix may result in effects on the

characteristics of the nanocomposite, such as on its morphology or thermal transitions, through the interaction of the nanoparticles with the matrix or through changes in processing parameters during compounding [33]. Nanoparticles can alter the crystallinity of the polymeric matrix in two ways, reducing the crystallinity or improving it. In the first effect, particles disturb the packing of polymer chains and, thus, alleviate some of the decreases in chain mobility that accompanies crystallization. Inevitably, this increases the free volume, and crystallinity reduces. In the second effect, the nanofillers act as nucleating agents, improving the crystallinity and decreasing the free volume. The net influence of nanoparticles on the crystallinity will depend on the crystallization characteristics of the matrix and its interaction with nucleation agents [74]. In low nanofiller loading values, nanoparticles can act as nucleating agents and result in increased crystallinity of the nanocomposites. However, when the loading of nanoparticles exceeds specific values, it can lead to decayed crystalline structure most likely due to the agglomeration of nanoparticles [75]. Furthermore, the effects of nanoparticles' surfaces on the polymer properties propagate to noticeably large distances. The long-ranged interactions between nanoparticles can correspond roughly in size to the radius of gyration of the bound chains [76]. These discussions reveal the reason why, in many of the mentioned studies in the previous sections of this chapter, the microstructure of the nanocomposites was also assessed through appropriate methods along with the dielectric properties.

As mentioned, predicting the exact effect of nanoparticles on the crystalline behavior is not possible due to the structural complications, and the reported results in the literature show different outcomes. In some publications, the presence of nanoparticles has demonstrated negative effects on the crystalline structure and morphology of the nanocomposite. For example, in the previously discussed study by Donghe et al. [51], crystallization ability was decreased due to the introduction of surface-modified SiO₂ nanoparticles in XLPE/SiO₂ nanocomposites. On the other hand, in several studies, neutral or not significant effects of nanoparticle on the crystallinity and crystallization behavior of nanocomposites have been reported. According to the investigation by Pourrahimi et al. [77], no significant changes in crystallinity or melting peak temperature were observed when different ZnO nanoparticles (the differences were in their sizes, treatment strategies, and coatings) were added to LDPE. As they have reported, this indicated that the nanoparticles had no significant effect on the microstructure of the polymer matrix, suggesting that the observed particle-induced improvement in electrical insulation was related to the nanoparticle/polymer interface and not to any changes in the matrix. Identical findings have also been reported for LDPE/surface-modified Al₂O₃ nanocomposites [42, 43].

Introduction of nanoparticles has also shown enhanced crystalline morphology in the nanocomposite. For instance, Jose et al. [78] have examined the non-isothermal crystallization kinetics, crystal morphology, and the parameters contributing to the crystallization mechanism in the XLPE nanocomposites filled with different wt% concentrations of trimethoxyoctylsilane surface-treated ZnO. They have attempted to determine the crystallization characteristics of the

crosslinked system (XLPE) in the presence of nanomaterials. According to their reports, the addition of nano-ZnO could accelerate the overall crystallization process, and the fine dispersion quality of the nanoparticles could improve the microstructure and accelerate the crystallization kinetics of XLPE matrix. Moreover, the activation energy values of all the nanocomposites were lower than neat XLPE, which have been attributed to the reduction in the energy barrier for crystallization. Furthermore, their conclusions based on non-isothermal crystallization kinetic parameters and the theoretical estimation of the nucleation activity certified the nucleating capability of ZnO nanomaterials in the crosslinked continuous phase of XLPE.

5 Risks Associated with the Peroxide Crosslinking Agent and Suggested Solutions

Generally, in most of the medium voltage and high-voltage XLPE insulations, crosslinking is carried out through the peroxide method. In the structure of peroxide molecule, each $-O-O-$ link can give rise to a maximum of one chemical crosslink in the network structure (generally one per peroxide molecule). Every decomposed peroxide molecule, whether it conducts a crosslink or not, produces at least two by-product materials. These by-products are contained within the structure. If they are not constrained by high external pressure (most usually hot nitrogen), the by-products form bubbles in the molten insulation, thereby leading to partial discharges and electrical failures. After completion of the crosslinking process, an approximately constant level of by-products will remain throughout the thickness of insulation as expected from the uniform distribution of peroxide at extrusion. This distribution will change with time after crosslinking as these by-products will diffuse out of the cable, depleting the exposed layers first then the inner layers. It can be stated that all cables that are crosslinked through peroxides will retain some of the decomposition by-products within their structure [79]. As insulation for HVDC cables, XLPE has an inherent disadvantage since the crosslinking by-products can cause significant space charge accumulation and substantially decreased electrical lifetime of cable insulation. Degassing process can reduce the by-products, but this process is not only time- and cost-consuming but also cannot completely remove the by-products because of the large thickness of insulation in HVDC cables [80]. Xu et al. [81] have inspected the space charge behavior of XLPE samples produced from LDPE with different concentrations of dicumyl peroxide (DCP). The obtained results showed that the space charges closely depended on the concentration of introduced DCP and the trap distributions. Furthermore, altering the amount of DCP could have simultaneous effects on the degree of crosslinking and space charge behavior. In addition to adverse dielectric effects, introducing peroxide as the crosslinking agent during the manufacturing process of XLPE causes hazardous environmental pollution problems [82].

Therefore, some other crosslinking methods are proposed in the literature. The following sections review suggested alternative crosslinking plans to peroxide crosslinking.

5.1 Polyhedral Oligomeric Silsesquioxane (POSS); a Crosslinker with Superior Characteristics (XLPE/ POSS Nanocomposites)

Wu et al. [83] have proposed the introduction of nanostructured hybrid octavinyl polyhedral oligomeric silsesquioxane (OVPOSS) agent as a crosslinker for crosslinking LDPE and producing XLPE/OVPOSS nanocomposite. As has been stated in this study, OVPOSS crosslinker could drastically reduce the amount of inserted peroxide agent and thus prevented the chain scission, scorch, and production of small pores as that of seen in the conventional peroxide crosslinking strategy. According to morphology analysis and elemental mapping results, OVPOSS aggregates were dispersed homogeneously in the LDPE matrix after melt blending and crosslinking, with the content of 0.2–2 wt% and the size ranging from tens of nanometers to several micrometers. They have rationally contented a crosslinking mechanism in which the radicals from peroxide decomposition preferentially react with the vinyl groups of OVPOSS and then are grafted to LDPE chains to form a three-dimensional network. Results indicated that the crosslinking speed increased with peroxide content, whereas the crosslinking degree increased with OVPOSS content. Therefore, an optimal combination of OVPOSS and peroxide was required for attaining better crosslinking. The crosslinking led to increase in storage modulus and decrease in the thickness of the lamellar crystal of PE due to the restricted chain mobility and folding to form crystal domain. The noticeable effect of OVPOSS has been confirmed by observing the same rheological behaviors between two samples, one containing 0.5 wt% OVPOSS and 0.2 phr peroxide, and the other with 2 phr peroxide prepared by the conventional peroxide crosslinking.

Morici et al. [84] have prepared PE/POSS organic-inorganic hybrids by one-step reactive melt mixing. The utilized POSS nanoparticles in their study were a mono-functionalized nanofiller, allyl-heptaisobutyl-substituted polyhedral oligomeric silsesquioxane (1POSS), and a multi-functionalized octavinyl polyhedral oligomeric silsesquioxane (8POSS). The numbers mentioned before POSS in the parentheses indicate the number of reactive groups in their structure. 0.1 wt% (to the total weight) of dicumyl peroxide has also been used in the preparation of samples as an initiator for the reaction between PE matrix and POSS molecules. Occurrence of chemical reactions between functionalized nanofillers and macromolecular chains during the processing step resulted in enhanced dispersion of nanofillers in the polymeric matrices and fabrication of crosslinked materials in a one-step process. Their findings indicated that the presence of multi-reactive groups in 8POSS molecules led to successful POSS grafting/crosslinking in the polymeric

backbone. Besides, the double bonds of POSS functional groups were triggered by radicals coming from the peroxide decomposition or the degradation reactions occurring during preparation. The latter source was inferred from the retained mass of the PE/8POSS sample, which was fabricated in the absence of a peroxide initiator. Thus, these radicals could originate from the degradation reactions or impurities, and they could initiate the reactions of vinyl groups, allowing the grafting of 8POSS onto PE chain and crosslinking. The type of the functional groups in POSS (mono- or multi-reactive) along with radical content in the systems was known to be determinative factors in the formation of a polymeric network. Therefore, the presence of peroxide agent (DCP) influenced the grafting/crosslinking reactions. Although DCP mainly interacted with the PE matrix leading to its crosslinking and entrapping POSS molecules, it could directly react with the POSS molecules. DCP enhanced the degradation phenomena during the processing of PE matrix, and the resultant macroradicals could activate the double bonds in POSS functional groups. In particular, the presence of multi-reactive groups in 8POSS molecules caused successful POSS grafting/crosslinking on the PE backbone and formation of covalent bonds between the nanofillers and matrix during the process improved POSS dispersion within the polyolefin matrix and led to a network structure formation. Performing an annealing step on the investigated samples improved the POSS dispersion degree, increasing grafting degree, but also promoted the aggregation of the not-linked molecules, promoting POSS mobility, and favoring POSS–POSS interaction in the polymeric matrix.

In another study by Morici et al. [85], they have grafted POSS on PE and maleic anhydride-grafted PE by one-step reactive melt mixing. The utilized types of POSS nanostructures were [3-(2-Aminoethyl)amino]propyl-Heptaisobutyl POSS (named as NPOSS) and allyl-heptaisobutyl substituted POSS (named as IPOSS). Here, DCP has also been used as a radical initiator. As they have stated, the grafting of POSS molecules plays a fundamental role in determining the dispersion degree in the resulting polymeric hybrids. However, Van der Waals interactions between POSS molecules and polymer segments may not be sufficient to avoid POSS agglomeration. An efficient grafting leads to the formulation of homogeneous POSS polymer-based hybrids. In this study, they have analyzed two different grafting approaches based on the amino–maleic reaction (amino on POSS and maleic of the maleic anhydride-grafted PE) and double bonds triggered in the presence of DCP. Findings demonstrated the point that different amounts of grafted POSS affected the properties of the nanocomposite differently. In the case of not efficient grafting, the yielded hybrid contained some POSS agglomerates and crystallites. Furthermore, interactions between grafted IPOSS were found to be negligible, and the dominating interactions between the physically dispersed nanoparticles did not considerably affect the viscoelastic response of PE matrix and the mechanical properties in the solid state. On the other hand, grafting NPOSS molecules in maleic anhydride-grafted PE was proved to be efficient because of the high efficiency of the amine–anhydride reaction in the molten state. The grafting helped the POSS dispersion in the polymeric matrix; moreover, a solid-like behavior was recorded

for the hybrid melt mainly due to the formation of a network within the matrix, which per se affected the mechanical performance.

The mentioned studies considering the fabrication of XLPE/POSS nanocomposites were mainly discussing the structural, mechanical, morphological, and rheological properties, and they have not focused on dielectric properties. However, it is clear that introducing POSS nanoparticles in the mentioned nanocomposites may influence the dielectric behavior. Thus, it seems beneficial to seek these properties to evaluate the efficiency of XLPE/POSS nanocomposites as cable insulations.

Huang et al. [86] have fabricated LDPE/octavinyl polyhedral oligomeric silsesquioxane (LDPE/POSS) nanocomposites by solution compounding. Conducting crosslinks by using POSS moieties has not been considered in this study (unlike [83–85]). The findings on the dielectric properties [86] revealed that the frequency dependence of the dielectric parameters of LDPE/POSS composites showed unusual behaviors when compared with conventional polymer/filler systems at a very low voltage (4 V/mm). The dielectric constant and dielectric loss in the composites with low POSS concentration were found to be lower than those of the neat LDPE. When the applied voltage was high (1000 V/mm), however, the measured dielectric constant and loss of all the composites by a Schering bridge showed marginally higher values than those of the neat LDPE. The AC breakdown strength of the neat LDPE and LDPE/POSS composites has been analyzed according to Weibull statistic distribution method. Although the characteristics dielectric breakdown of LDPE/POSS composites has decreased gradually with POSS concentration, the breakdown strength of the LDPE/POSS composites at lower cumulative failure probability showed higher values than those of the neat LDPE which showed the lowest dielectric strength in the minimum cumulative failure probability. Based on their findings, they have concluded that LDPE/POSS composites have potential engineering application since the real dielectric strength of products such as wire and cables is determined by the weakest part of their insulation.

Bhutta et al. [87] have examined the effect of different concentrations of POSS on space charge behavior and trap levels of XLPE/POSS nanocomposites. In their study, they have incorporated octaisobutyl polyhedral oligomeric silsesquioxane (OibPOSS) in XLPE in order to prepare the intended nanocomposites by melt mixing. Based on the reported findings, the formed interface between the XLPE matrix and OibPOSS nanofillers was important in space charge accumulation and mitigation. The outcomes from pulsed electroacoustic and trap level revealed that a large number of heterocharges appeared at the interface between XLPE and electrode. However, heterocharges and total space charge were both suppressed in XLPE/OibPOSS nanocomposites. Moreover, the total accumulated charge in XLPE/OibPOSS was less than that of XLPE and reduced with the increase of filler concentration. Also, the density of deep traps was higher in virgin XLPE than XLPE/OibPOSS nanocomposites. Furthermore, the shallow trap density was found to be greater with a higher concentration of filler. Trap energy levels are produced mainly due to the non-uniform arrangement of atoms in the polymer chain, and the

density of such regions reduces from surface to the internal regions. Shallow traps formed in XLPE/OibPOSS nanocomposites further help in the process of charge migration. Moreover, these shallow traps reduce charge mobility in the bulk. This is the reason for less arriving of charges at opposite electrodes and less space charge accumulation to create heterocharges. Also, low charge mobility increased the neutralization process among heterocharges. This has been introduced as the reason for the disappearance of heterocharges in XLPE/OibPOSS nanocomposite samples. The homocharges continue to accumulate on the surface of samples and hence increase the field in the center of matrix, leading to accumulated space charges to move out by volume conductivity of the bulk matrix in time. Therefore, space charge was suppressed in XLPE/OibPOSS nanocomposite (containing 1 and 3 wt% concentration of OibPOSS).

5.2 Click Chemistry Type Reactions Between Two Polyethylene Copolymers: A By-product-Free Curing Approach to Produce XLPE as an Alternative Approach to Peroxide Crosslinking

Mauri et al. [88] have introduced a novel curing approach for XLPE that can be a viable alternative to peroxide crosslinking. This method is based on click chemistry reactions between two PE copolymers and has the valuable advantage of additive-free curing procedure without the production of any by-products. In this method, the crosslinking was explored in a copolymer blend consisting of statistical ethylene-glycidyl methacrylate copolymer, p(E-*stat*-GMA), and a statistical ethylene-acrylic acid copolymer, p(E-*stat*-AA). This thermoplastic copolymer blend was able to offer a broad processing window up to 140 °C, where the compounding and shaping processes could be carried out without the occurrence of curing reactions. Once the temperature was raised above 150 °C, epoxy and acrylic acid functional groups rapidly reacted without by-product production to fabricate an infusible network. The striking point about the crosslinked copolymer blend was that it exhibited a very low DC electrical conductivity value, which was on par with values measured for both ultra-clean LDPE as well as a commercial XLPE grade. Therefore, the suggested curing strategy enabled the possibility to replace peroxide crosslinking with click chemistry type reactions. Mauri et al. have done comprehensive investigations on the alternative curing approaches based on click chemistry type reactions involving a statistical ethylene-glycidyl methacrylate copolymer in three other studies [89–91].

6 Limitations Associated with Recyclability of XLPE

Nowadays, XLPE is extensively employed as insulation materials in most of the extruded high-voltage cables. It has excellent dielectric and thermo-mechanical properties and low dielectric loss, which, to a great extent, makes it an ideal material for cable insulation applications. More importantly, XLPE has a considerably improved thermo-mechanical performance at high temperatures because of the crosslinked macromolecular networks. However, the crosslinking process also results in thermosetting materials, making the XLPE difficult to be recycled after being retired at the end of its service lifetime [92–94]. Several routes have been introduced for employing thermoplastic materials instead of XLPE as insulations, while the designed materials have shown similar or superior properties to XLPE. Hosier et al. [95] have prepared PE and PP blends crystallized under non-isothermal conditions and compared their properties with a XLPE reference material. Specific blends contained a gelation agent that could form a network structure inside the material. When the resultant blends were compared to XLPE, the blends offered higher melting points, reduced electrical conductivity, increased electrical breakdown strength, improved space charge performance, and enhanced thermo-mechanical stability. Additional improvements in space charge behavior were also observed in systems containing the gelation agent. Accordingly, these blends suggested the ability to provide recyclable insulation materials capable of operating at much higher temperatures than XLPE, combined with enhanced dielectric properties. Other studies have also suggested potential thermoplastic alternatives for XLPE that are recyclable, such as isotactic polypropylene, propylene-ethylene copolymers [96], and isotactic polypropylene/ethylene-octene polyolefin/SiO₂ nanocomposites [92]. Nevertheless, due to extensive usage of XLPE insulations in the past, at the current time, and in future, seeking for solutions to overcome the recyclability limitation of XLPE seems vital. Due to recycling difficulties, most waste XLPE is burned as a fuel or land-filled [97]. However, several approaches have been suggested in the literature for recycling XLPE. What follows is the suggested strategies over the recent years for recycling and reusing XLPE.

6.1 Chemically Recycling of XLPE Using Sub- and Supercritical Fluids

One of the most investigated approaches for chemical recycling of XLPE is based on utilizing sub- and supercritical fluids [98]. In the following paragraphs, several case studies are briefly covered in this regard that have been accomplished during the recent two decades.

Goto et al. [99] have studied thermoplasticization of silane-crosslinked polyethylene (Si-XLPE) insulations of wires and cables. They have performed the recycling of Si-XLPE by using a chemical reaction in supercritical alcohol. Based

on their obtained results, only the crosslinking element was decomposed by supercritical alcohol. Therefore, it seemed to be the ideal reaction for material recycling, since the recycled PE could be used as a raw PE, and mechanical and electrical properties of recycled PE were good enough to be used as insulation. For evaluating this expectation, they tested mechanical and electrical properties, ability of crosslinking reaction, mechanical properties after aging, processability, and thermal deformation of the recycled material. All results indicated that the recycled PE could be used as the insulation of wire and cable.

Ashihara et al. [100] have introduced a method for recycling Si-XLPE by using supercritical alcohol through a continuous process inside an extruder. Thus, this method had the advantage of ability for industrialization. The obtained production rate of the recycled product was 20 kg/h, and the gel fraction of the recycled PE was 0%, being able to have similar properties to virgin PE. This indicated that the siloxane bonds were selectively decomposed through this recycling process. The recycled PE material has been used for making insulations of 600 V XLPE cable, and the properties of the resultant material were in accordance with the Japanese Industrial Standards of 600 V XLPE insulated cable. The findings of this study confirmed that this technology could be applicable to cable recycling. Furthermore, based on calculations, CO₂ emission could be reduced by this technology in comparison with virgin PE; hence, it could provide a method for preventing global warming.

Other identical studies have also been carried out by Goto et al. [101, 102]. In [101], they have utilized supercritical alcohol and a twin-screw extruder for continuous recycling of Si-XLPE. According to the results, the mechanical properties of the recycled PE satisfied the requirements for its usage as a wire and cable insulation material. In [102], they have employed single screw extruder for continuous recycling of Si-XLPE using supercritical alcohol. Single screw extruder is less expensive and simpler than a twin-screw extruder, and enables a significant reduction in the initial cost for the equipment. Their findings revealed that the productivity of the single screw extruder system was sufficient for application in commercial plants. Baek et al. [103, 104] have performed comprehensive studies on the kinetics of Si-XLPE decrosslinking reactions with sub- and supercritical fluids in a continuous extrusion process.

The earlier mentioned case studies in this section were based on silane-crosslinked PE (Si-XLPE); however, peroxide method is the foremost approach that is used for manufacturing the insulations of high and medium voltage cables. Therefore, the following case studies are relied on the recycling of peroxide crosslinked XLPE materials with sub- and supercritical fluids.

Lee et al. [105] have evaluated the effect of methanol, ethanol, 2-propanol, n-hexane, acetone, and isopropyl ether solvents on the decrosslinking of peroxide crosslinked (XLPE) under sub- and supercritical conditions. They found that the effect of different solvents on the chemical structure of the decrosslinked XLPE was marginal. They found that the decrosslinking rate was an order of magnitude higher in supercritical acetone and supercritical isopropyl ether compared to those in other solvents. The gel content of the decrosslinked PE decreased from 60 to 0.8–2.5% at

380 °C within 5 min in all of the tested solvents. When water, ethanol, and 2-propanol were used, the M_w of the decrosslinked PE decreased from 349,000 to 200,000–227,000 g/mol, and much lower M_w values of 70,000–90,000 g/mol were observed when acetone and diisopropyl ether were used. The decrosslinked PE treated in the different solvents demonstrated very similar chemical structures to raw PE, although the conditions of decrosslinking reaction required to be optimized in order to minimize the decrease in molecular weight, which is vital for efficient recycling.

Baek et al. [106] have successfully decrosslinked peroxide crosslinked PE through reaction in supercritical methanol and in a continuous multiscale single screw extrusion process. They have reported decreased gel content with the increase in the reaction temperature and methanol content. According to their results, although XLPE exposed to supercritical methanol for less than 2 min of retention time in the continuous supercritical extruder, it was decrosslinked entirely above 390 °C at the methanol feeding rate of 7 mL/min. Based on their conclusions, the decrosslinking efficiency of the continuous supercritical extruder was expected to be improved through the optimization of extruder design to accept more methanol feeding rates and provide longer retention time.

6.2 Other Suggested Methods for Recycling, Reprocessing, and Reusing Waste XLPE

Several investigations have introduced other strategies than using sub- and supercritical fluids for recycling XLPE wastes or employing them in other applications. The following section includes the specific reported methods and applications in the literature, along with a brief definition for each of them.

6.2.1 Blending Waste XLPE with Thermoplastics

Qudaih et al. [107] have added 5–15% of waste Si-XLPE in virgin LDPE, and prepared Si-XLPE-LDPE compounds. The result of this compounding was increased Young's modulus, yield stress, and stress at break in comparison with virgin LDPE. Lindqvist et al. [108] have blended recycled XLPE cable from production waste and end-of-life cables with virgin PP in order to assess the ability of these mixtures to be employed in new injection molded products. In the blending step, they have blended recycled XLPE from manufacturing waste and from a mixture of manufacturing waste and end-of-life cables with PP by compounding and injection molding. According to their findings, the mechanical properties of the blends have shown similar values, and the origin of the recycled XLPE has not been considered to have any significant influence. However, the thermal behavior and mechanical properties after aging demonstrated a significant difference between the

blends. The blend containing end-of-life cable indicated severe degradation due to the existence of higher content of metal impurities in it when compared to the plastic from manufacturing waste. Addition of a metal deactivator to the blend containing end-of-life cable showed that the thermal behavior and mechanical properties were retained for a long time. Navratil et al. [109] have investigated the possibility of using recycled electron beam irradiation-crosslinked HDPE after the end of its lifetime as a filler into virgin LDPE with different concentrations. They also have studied the effects on the processability and mechanical properties of the blend. Their results indicated that the processability, as well as mechanical behavior, highly depends on the amount of the filler. The most important finding that has been mentioned in their study is that the recycled irradiated HDPE can be utilized as the filler into the virgin LDPE, thus, preventing the generation of other plastic wastes. Manas et al. [110] have studied the possibility of using radiation-crosslinked HDPE (HDPE_x) as a filler in the original HDPE matrix. According to their findings, affecting the mechanical behavior of the composite was possible by altering the concentration of filler. Furthermore, the mechanical properties of the produced composite (that were recorded at room temperature) were generally comparable or better than the same properties of the original thermoplastic. This created very good assumptions for the effective and economically-acceptable processing of radiation-crosslinked HDPE waste.

6.2.2 Incorporating XLPE Waste in Concrete

Zéhil and Assaad [111] have evaluated the feasibility of incorporating XLPE cable waste materials into concrete mixtures. Their findings indicated that the XLPE inclusions influenced the concrete workability and air content marginally. Also, the density difference between aggregates and XLPE shreds led to declined unit weight. Moreover, XLPE inclusions resulted in superior concrete performance in terms of water permeability. However, some shortcomings were appeared by increasing XLPE content and particle size, such as adverse effects on concrete strengths and shrinkage, although these shortcomings could be mitigated by decreasing the water-to-cement ratio.

6.2.3 Energy Recovery from XLPE Waste Using Pyrolysis and CO₂-Assisted Gasification

Singh et al. [112] have investigated pyrolysis and gasification of XLPE waste to understand the capability and potential of pyrolysis and CO₂ gasification in converting this waste to syngas. They have used CO₂ as a gasifying agent to help support CO₂ utilization and lower the carbon footprint. According to the outcome of their investigation, the produced syngas had a sample mass-specific heating value of 47 MJ/kg. Thus, the possibility of clean energy production using syngas as fuel suggested the attractive potential of using gasification for the disposal of XLPE

wastes. It also revealed that CO₂-assisted gasification process was efficient in maintaining the product quality while utilizing waste XLPE and CO₂. Their proposed strategy provided a sustainable disposal solution of XLPE and CO₂.

6.2.4 Selectively Decrosslinking by Solid-State Shear Mechanochemical (S³M) Technology

Sun et al. [113] have studied recycling Si-XLPE by S³M technology. Through this strategy, waste Si-XLPE could be recycled effectively, and a thermoplastic material was attained. Their findings showed that the crosslinks (crosslinking bonds of Si-XLPE) were destroyed effectively rather than the decomposition of the backbone chains. Taken all results together, they have introduced the S³M technology as a cost-effective, reliable, and environmentally friendly method for recycling Si-XLPE at ambient temperature without any additional materials or chemicals.

6.2.5 Recycling Through Compression Molding

Santos and Jayaraman [114] have performed a study on the recycling of crosslinked HDPE through compression molding. Their findings revealed that despite the crosslinking, the recycled crosslinked HDPE could be remelted with a higher viscosity than the virgin crosslinked HDPE. Consolidation studies indicated that both the recycled crosslinked HDPE and the virgin crosslinked HDPE could be compression molded to a density of 0.952 g.cm⁻³. However, higher consolidation stress was required for the recycled crosslinked HDPE to realize the same density. The recycled crosslinked HDPE that was compression molded at 1.6 MPa and 230 °C had properties similar to those of the virgin crosslinked HDPE molded at 0.32 MPa.

6.2.6 Annealing Retired XLPE Insulations

Xie et al. [115] have investigated the annealing effects on the improvement of thermal and electrical properties in three retired 110 kV AC XLPE cables. The retired cables had encountered degradation; however, the annealing treatment on the XLPE insulation remained effective. The optimal values of the melting point, crystallinity, melting range, lamellar thickness, electrical conductivity, and dielectric breakdown strength were observed when the samples were annealed at 95 °C. Longer temperature holding hour was further enhanced the thermal and electrical properties when the samples were annealed at this optimum point. Another study has also been done by Xie et al. [116] exploring rejuvenation of retired 110 kV AC XLPE power cables by heat treatment.

6.2.7 In Situ Formation of a PE–PP-Type Copolymer Through Reactive Compounding

Ouyang et al. [117] have introduced a promising approach to enable designing recyclable thermoplastic cable insulation material through the formation of PE–PP-type copolymer. In this approach, ternary blends of an ethylene-glycidyl methacrylate copolymer, a maleic anhydride-grafted polypropylene, and up to 70 wt% low-density polyethylene (LDPE) were compounded at 170 °C. The reaction between epoxy and carboxyl groups caused formation of covalent bonds, resulting in production of a PE–PP-type copolymer that showed good compatibility with LDPE. The blends consisting of the PE–PP-type copolymer and LDPE displayed thermoset-like properties between the melting temperatures of PE and PP. The authors have argued that the melt creep of the almost molten material was arrested through a continuous network held together by PP crystallites. Reprocessing of the ternary blend at 170 °C could be carried out without compromising the excellent melt creep resistance and dielectric properties, confirming that the explored formulation was recyclable. Furthermore, a very low DC electrical conductivity value was measured for the ternary blend, which was on a par with values attained for LDPE and XLPE.

7 Limitations Associated with Surface Characteristics of XLPE Blends and Nanocomposites and Offered Occasional Solutions

7.1 Surface Modification of XLPE for Overcoming Surface Bonding Challenges

As defined earlier, XLPE-based blends and nanocomposites are chemically inert and hydrophobic to a great extent due to the dominant presence of PE backbone in their structure, which leads to problems in the dispersion of nanoparticles possessing polar and hydrophilic surfaces in them. This lack of adequate dispersion has been investigated in a wide body of literature, and details of proposed solutions were described in the previous sections. However, another problem is raised by this hydrophobic nature of XLPE that has not been addressed sufficiently in the literature. Surface bonding problems are consequences of the XLPE nature that results in poor printability and interlayer adhesion problems in the XLPE insulations. Marking or printing the production data (such as manufacturer, technical data, and production date) on the cables is mandatory in most of the cases for enabling the possibility of tracking the reasons for issues during the service life. Inkjet printing is a method that is extensively used for printing on the cable insulations. The adhesion quality of deposited ink drops on the polar insulations, such as polyvinylchloride (PVC), is sufficient. Whereas, this method encounters severe bonding problems on

untreated PE and XLPE insulations, leading to instant delamination of printed information. Standard test methods such as IEC 60227-2 [118] can readily confirm this state. Typical methods such as flame treatment or engraving the characters on just extruded insulations can be short-term effective or harmful solutions. However, in the aggressive service condition of insulations (direct sun exposure, abrasion by dust, etc.), they cannot be viable and long-lasting. In addition to the surface printability challenge in the XLPE insulations that exists in the topmost XLPE layers, interlayer adhesion in the cables with multilayer insulations may also be a challenge. In other words, medium and high-voltage cables consist of insulations with more than one layer. These layers can be semiconductive (containing carbon black, graphene, carbon nanotube, etc.), insulation, jacketing, etc., and satisfactory bonding between these layers is vital for attaining sustainable production line and durable final product. Mostofi Sarkari et al. [119] have utilized plasma surface modification for improving surface hydrophilicity of a medium voltage XLPE insulation material. In this study, they have adopted gliding arc plasma system, which is technically compatible with cable production lines. In this approach, the modification could be done continuously, with relatively high speed, and in the atmospheric pressure with high efficiency. The obtained results indicated that this method was a promising method for improving surface hydrophilicity by introducing polar chemical functionalities on the surface and plasma etching/ablation effect. The main advantage of plasma-based surface modification methods is the very small effectiveness depth of the treatment. In other words, the treatment depth does not exceed nanometric scale, which is enough for altering the surface properties, but it does not affect the bulk and dielectric characteristics negatively. In another study by Mostofi Sarkari et al. [120], plasma treatment has been adopted along with (3-aminopropyl)trimethoxysilane (APTMS) coupling agent to be grafted on the XLPE surface as an anchoring layer for the further layers. Since XLPE surface is hydrophobic and does not have enough active sites for conducting bonds with the deposited aminosilane coupling layer, plasma functionalization effect has been used to enable the strong interaction between the XLPE surface and grafted (3-aminopropyl)trimethoxysilane self-assembled layer. The outcomes of the study proved plasma grafting to be a feasible tool for attaching a modifier layer on the XLPE surface with a nanometric thickness. Furthermore, Mostofi Sarkari et al. [121] have adopted 3-glycidyloxypropyltrimethoxysilane (GLYMO) coupling molecules for modifying the surface properties of XLPE through plasma grafting approaches. Their findings suggested that the plasma-assisted grafting strategies (post-irradiation grafting and syn-irradiation grafting) provide suitable and appropriate conditions for grafting GLYMO molecules with a more uniform distribution on the surface and fabricating an anchoring layer on the surface of XLPE, capable of further reactions with an active functionality to other materials to attach to them.

7.2 *Surface Modification of XLPE for Improving Dielectric Properties and Hydrophobicity*

As discussed in the previous paragraph, the lack of surface hydrophilicity on the XLPE surface can be problematic in some cases, and improving surface wettability of XLPE is inevitable. On the other hand, surface hydrophilicity can cause electrical concerns on the XLPE surface. Zhao et al. [122] have carried out a study considering surface modification of XLPE films by CF_4 dielectric barrier discharge plasma for improving dielectric properties. According to their reported findings, appropriate treatment time could enhance hydrophobicity, dielectric properties, and breakdown voltage of XLPE films. These evidenced improvements in insulation properties. The key reason for the mentioned enhancements was attributed to fluorine, and change of functional groups on the surface. Presence of fluorine and its functional groups led to grown hydrophobicity and declined surface energy, which enabled the insulation to restrain the accumulation of outside pollution on the surface, leading to improved insulation properties. Furthermore, fluorine and its groups possess relatively strong electronegativity, which produced more deep traps to capture more free electrons. These electrons in traps reduce the external electric field, which restrains the carrier injection, and the dielectric loss becomes lower.

8 Risks Associated with Thermal and Radiation Aging of XLPE

Electrical aging of XLPE insulation materials involves partial discharge, electrical treeing, and water treeing [123]. These issues were discussed in previous sections. However, other types of aging can also happen during the service life of XLPE insulation due to the environmental factors, such as temperature alterations and irradiations caused by the sun rays. Presence of these factors, along with the available electric field, can cause severe harmful effects on the insulation in the prolonged durations. For instance, high thermal action and its long duration could facilitate the formation of short chains, micro-cracks, voids, and other impurities, giving negative influences to the dielectric strength of XLPE materials [124]. Hence, thermal and radiation aging phenomena are the risks that can threaten the performance of XLPE insulations. These aging phenomena might also be affected by the electric field and lead to combined aging effects with electrical aging. These aging aspects of XLPE nanocomposites and blends have been assessed in several studies, and a review of the relevant case studies is brought here.

8.1 Thermal or Thermal-Oxidation Aging

The thermal aging refers to a condition that under thermal stress and over a period of time, the polymer structure undergoes cracking reaction, consequently, the performance of insulation decays, and the failure of insulation takes place. The thermal aging can also be interpreted as chemical deterioration since the chemical structure of polymer alters under thermal stress [17]. Herein, several case studies investigating the thermal or thermal-oxidation of XLPE are reviewed.

Ouyang et al. [125] have investigated the influence of thermo-oxidative aging on the space charge distribution of a 110 kV XLPE cable insulation. Their findings indicated that the XLPE insulation showed moderate alterations in microstructure and space charge distribution until the moment when the oxidation induction time dropped to zero. When the aging temperature was lower than the melting point, the thermo-oxidative aging mainly affected amorphous regions of XLPE, since the structures of crystalline domains were much denser, which made oxygen diffusion proceed more difficult. When XLPE samples were aged at the temperature above the melting point, the aging impacted the melted spherulites, and led to obvious effect on lamellae, resulting in a significant decrease in crystallinity and the destruction of spherulites. Carbonyl groups (as the main oxidation products of thermo-oxidative aging) and interfaces of crystal/amorphous introduced shallow and deep traps on the surface of XLPE. Thermo-oxidative aging at 160 °C caused a significant reduction of deep traps due to the decline of crystallinity and destruction of spherulites.

He et al. [126] have carried out a study on mechanical and dielectric properties of a 10-kV XLPE cable under accelerated electrical-thermal aging. The outcomes of the study revealed that the mechanical strength and gel content of XLPE vary significantly under different aging temperatures. This finding was originated from the crystallization characteristics of the material. When the temperature was higher than the glass transition temperature, the crystalline region wholly melted. Whereas, at the aging temperature lower than the glass transition temperature, the crystalline region did not melt or only slightly melted. Furthermore, the breakdown voltage exhibited a slightly decreasing trend with aging time. Moreover, the dielectric constant decreased with aging time in high-frequency areas, while the dielectric loss factor increased with aging time at low frequencies. This relationship exists, since as the cable encounters aging, some of the crosslinking by-products and antioxidants escape, while the rest bind to PE molecule end groups, which are attached to the macromolecular chains. This results in a reduction of micromolecular polar substances and an increase in macromolecular polar substances. Thus, these two parameters could be used to characterize the degree of aging in a cable.

8.2 Radiation Aging

8.2.1 Exposure of XLPE to UV Radiation

Hedir et al. [127] have evaluated the UV radiation aging impacts on the physico-chemical properties of XLPE insulations. The attained results in this investigation revealed that the DC volume resistivity is weakly affected by UV radiation. However, a slight increase was observed after 200 h of UV exposure, which might be associated with the higher degree of crosslinking of UV exposed specimens, since crosslinking decreases ionic and molecular mobility. Their surface chemistry evaluation results indicated that UV radiations reduced the cohesive forces between the chains and induced growth in crosslinking rate and chain mobility. In addition to crosslinking, exposure of XLPE to UV could induce oxidation. The oxidation was confirmed by chains cleavage and an increase of carbonyl and double bond index. Crystallinity assessments illustrated that a slight increase in crystallinity happened possibly due to the development of a secondary crystallization. Thermogravimetric analysis confirmed that UV irradiation did not significantly modify the thermal degradation behavior of XLPE. UV irradiation-induced degradation on the surface of XLPE was highlighted by the morphology micrographs and also through visually perceivable hue alteration. Such a variation on the surface could originate from photo-oxidation on it, which led to the creation of an oxidized layer on the polymer surface.

8.2.2 Exposure of XLPE to Gamma Radiation at Elevated Temperatures

Instrumentation cables employed in nuclear power plants may be exposed to gamma irradiation and/or elevated temperature during their service life. Long-term operation of nuclear power plants presents the necessity to understand the alterations in cable insulation materials, such as commonly used XLPE, that may affect cable performance. Accordingly, Shao et al. [128] have conducted a study on the dielectric response of XLPE cable insulation material to the simultaneous radiation and thermal aging. As has been found out in this study, dielectric loss tangent was observed to increase as a function of dose, dose rate, and exposure time for XLPE samples. Dielectric loss tangent did not, however, show sensitivity to thermal aging for the range of temperatures that were considered in their study. Dielectric breakdown strength initially increased as the material oxidized, then decreased for more extreme aging, due to chain scission. They have concluded that dielectric loss tangent can be a promising indicator of XLPE aging due to gamma radiation exposure.

9 Concluding Remarks and Requirements for the Future Works

Introducing nanoparticles in XLPE can improve its operational properties (such as mechanical, thermal, and electrical features). However, optimizing their usage condition in the nanocomposite is mandatory for attaining favorable promoted characteristics. The concluding remarks of this chapter are as follow:

- Nanoparticles are promising materials for mitigating electrical challenges such as partial discharge formation, space charge accumulation, electrical treeing, and water treeing. However, adjusting the properties of nanoparticles (e.g., concentration, dispersion quality, surface treatment, etc.) is vital for obtaining the most improved characteristics. In the case of uncontrolled filling of XLPE matrix with nanoparticles, not only can they not improve the characteristics of nanocomposite, but also they can lead to adverse effects on its properties.
- Adequate dispersion quality of nanoparticles is crucial for attaining enhanced characteristics. If the uniform distribution of nanoparticles would not be achieved, adverse properties will emerge as a consequence of nanoparticles' accumulation (in the form of aggregates or agglomerates).
- Employing silane coupling agents or organofunctional silanes for surface modification of embedded nanoparticles in XLPE nanocomposites is a versatile and effective method to enhance the homogenous dispersion of nanoparticles in the XLPE matrix. Even though organosilanes have proven to be successful nominates for this purpose, optimization of the treatment process, in terms of selecting the appropriate type of silane agent, hydrolyzation and condensation condition, concentration of nanoparticles, etc., are critical for acquiring the ultimate possible dispersion quality.
- In addition to surface modification of conventional nanoparticles with silane coupling agents, other methods also have been suggested for improving the dispersion quality and dielectric properties in XLPE nanocomposites. A number of these methods can be named as surface-initiated polymerization on the nanoparticles, modification of XLPE with agents possessing polar functionalities and high boiling point, introducing polypyrrole (PPy) nanoparticles in XLPE, and embedding nanoscale hybrid fillers in XLPE.
- Presence of moisture on the surface of nanoparticles can result in negative effects on the dielectric properties of obtained XLPE nanocomposites. Several factors can be decisive in the extent of water uptake and absorption. These factors can be counted as type of nanoparticles, surface treatment of the nanoparticles, physical specifications of the nanoparticles, and humidity of the environment, electrical operation condition, and loading ratio of the nanoparticle. Controlling these parameters is crucial in processing XLPE since they can consequently influence the dielectric behavior of the nanocomposites.
- Introduction of nanoparticles in the XLPE matrix can cause adverse, inert, or positive effects on the crystal morphology and microstructure of the matrix.

Therefore, assessing the microstructure after embedding nanoparticles in the XLPE matrix is required for obviating negative effects.

- Peroxide, as the crosslinking agent in the medium and high-voltage XLPE insulations, can result in undesirable effects by the formation of by-products and microvoids during the curing process. These products import impurities in the insulation that can be the origin of future failures and breakdowns in the insulations. Although there have been controlling methods for avoiding such problems during the shaping and crosslinking process, large thickness of insulations prevents complete evacuation of by-products. New alternative strategies have been introduced for overcoming the risks induced by peroxide agents, such as utilizing polyhedral oligomeric silsesquioxane (POSS) and click chemistry type reactions between two PE copolymers.
- The thermoset nature of XLPE hinders it from being recycled after finishing its service life and being retired. Researches on this topic have led to several chemical and physical approaches. Recycling XLPE using sub- and supercritical fluids and energy recovery from XLPE waste using pyrolysis and CO₂-assisted gasification are examples of chemical procedures. The physical methods that have been offered for reprocessing and reusing XLPE can be named as blending waste XLPE with thermoplastics, incorporating XLPE waste in concrete, recycling through compression molding, etc.
- Surface characteristic of XLPE can cause different problems leading to production process limitations. One of these problems can be the lack of surface bonding to other polymeric matrices, which can be addressed by plasma-assisted treatment methods. The other problem can emerge in the conditions that the surface does not have sufficient dielectric properties. For such cases, a plasma-based treatment method can also be a solution.
- XLPE insulations may encounter various environmental threatening factors during their service life. Examples can be high temperature and irradiation rays emitted from the sun. Therefore, considering and addressing the thermal, thermal-oxidative, and radiation aging of these materials are obligatory for avoiding operational failures.

For the future of this material, several aspects seem crucial to be carefully considered and addressed via feasible and industrially oriented solutions:

- Introducing new processing methods for superior and more efficient dispersion of nanoparticles in the XLPE matrix.
- Researching on production methods that can result in more controlled manufacturing processes that can prevent the negative environmental effects on the nanoparticles and adverse impact on the microstructure of XLPE matrix.
- Developing new environment-friendly XLPE grades with ease of recyclability for using them in future insulations.
- Attempt on discovering suitable substituents for peroxide crosslinking agents, in order to prevent the emission of volatile by-products causing defects in the insulation

- Researching on more viable and efficient methods for recycling and reprocessing retired XLPE materials that have been used since a couple of decades ago till the current time.
- Investigating surface-related issues of XLPE materials to address the respective limitations in an industrially oriented manner.

References

1. Zhong S-L, Dang Z-M, Zhou W-Y, Cai H-W (2018) Past and future on nanodielectrics. *IET Nanodielectrics* 1:41–47. <https://doi.org/10.1049/iet-nde.2018.0004>
2. Pleșa I, Noțingher P, Stancu C et al (2018) Polyethylene nanocomposites for power cable insulations. *Polymers (Basel)* 11:24. <https://doi.org/10.3390/polym11010024>
3. Izzati WA, Arief YZ, Adzis Z, Shafanizam M (2014) Partial Discharge Characteristics of Polymer Nanocomposite Materials in Electrical Insulation: A Review of Sample Preparation Techniques, Analysis Methods, Potential Applications, and Future Trends. *Sci World J* 2014:1–14. <https://doi.org/10.1155/2014/735070>
4. Tanaka T, Bulinski A, Castellon J et al (2011) Dielectric properties of XLPE/SiO₂ nanocomposites based on CIGRE WG D1.24 cooperative test results. *IEEE Trans Dielectr Electr Insul* 18:1482–1517. <https://doi.org/10.1109/TDEI.2011.6032819>
5. Lau K, Vaughan A, Chen G et al (2014) On the space charge and DC breakdown behavior of polyethylene/silica nanocomposites. *IEEE Trans Dielectr Electr Insul* 21:340–351. <https://doi.org/10.1109/TDEI.2013.004043>
6. Boggs S (2004) A rational consideration of space charge. *IEEE Electr Insul Mag* 20:22–27. <https://doi.org/10.1109/MEI.2004.1318836>
7. Zimmerling IM, Tsekmes IA, Morshuis PHF et al (2015) Space charge analysis of modified and unmodified XLPE model-cables under different electric fields and temperatures. In: 2015 IEEE conference on electrical insulation and dielectric phenomena (CEIDP). IEEE, pp 134–137. <https://doi.org/10.1109/CEIDP.2015.7352121>
8. Wang Y, Xiao K, Wang C et al (2016) Effect of nanoparticle surface modification and filling concentration on space charge characteristics in TiO₂/XLPE nanocomposites. *J Nanomater* 2016:1–10. <https://doi.org/10.1155/2016/2840410>
9. Wang Y, Wang C, Xiao K (2016) Investigation of the electrical properties of XLPE/SiC nanocomposites. *Polym Test* 50:145–151. <https://doi.org/10.1016/j.polymertesting.2016.01.007>
10. Xiang J, Wang S, Chen P, Li J (2018) Space charge characteristics in XLPE/BN nanocomposites at different temperatures. *Proc IEEE Int Conf Prop Appl Dielectr Mater* 2018–May:952–955. <https://doi.org/10.1109/icpadm.2018.8401195>
11. Densley J (2001) Ageing mechanisms and diagnostics for power cables—an overview. *IEEE Electr Insul Mag* 17:14–22. <https://doi.org/10.1109/57.901613>
12. Paramane A, Kumar KS (2018) Role of micro and nanofillers in electrical tree initiation and propagation in cross-linked polyethylene composites. *Trans Electr Electron Mater* 19:254–260. <https://doi.org/10.1007/s42341-018-0040-x>
13. Chen X, Xu Y, Cao X, Gubanski SM (2015) Electrical treeing behavior at high temperature in XLPE cable insulation samples. *IEEE Trans Dielectr Electr Insul* 22:2841–2851. <https://doi.org/10.1109/TDEI.2015.004784>
14. Bao M, Yin X, He J (2011) Structure characteristics of electrical treeing in XLPE insulation under high frequencies. *Phys B Condens Matter* 406:2885–2890. <https://doi.org/10.1016/j.physb.2011.04.055>

15. Qi F, Wan D, OuYang X et al (2019) Influence of different XLPE cable defects on the initiation of electric trees. *J Electr Eng Technol* 14:2625–2632. <https://doi.org/10.1007/s42835-019-00296-6>
16. Li C, Yang J, Zhang C et al (2019) The effects of nano-SiO₂ on the electrical treeing resistance of XLPE. In: 2019 2nd international conference on electrical materials and power equipment (ICEMPE). IEEE, pp 313–316. <https://doi.org/10.1109/ICEMPE.2019.8727248>
17. Zhang C, Li C, Zhao H, Han B (2015) A review on the aging performance of direct current cross-linked polyethylene insulation materials. In: 2015 IEEE 11th international conference on the properties and applications of dielectric material. IEEE, pp 700–703. <https://doi.org/10.1109/ICPADM.2015.7295368>
18. Sun K, Chen J, Zhao H et al (2019) Dynamic thermomechanical analysis on water tree resistance of crosslinked polyethylene. *Materials (Basel)* 12:746. <https://doi.org/10.3390/ma12050746>
19. Chen J, Zhao H, Xu Z et al (2016) Accelerated water tree aging of crosslinked polyethylene with different degrees of crosslinking. *Polym Test* 56:83–90. <https://doi.org/10.1016/j.polymertesting.2016.09.014>
20. Tao X, Li H, Rao J et al (2018) Trap characteristic and potential trap model of water trees in XLPE. *annu rep—conf electr insul dielectr phenomena. CEIDP* 2018–Octob:378–381. <https://doi.org/10.1109/ceidp.2018.8544867>
21. Nagao M, Watanabe S, Murakami Y et al (2008) Water tree retardation of MgO/LDPE and MgO/XLPE nanocomposites. In: 2008 International symposium on electrical insulating material (ISEIM 2008). IEEE, pp 483–486. <https://doi.org/10.1109/ISEIM.2008.4664592>
22. Qingyue Y, Xiufeng L, Peng Z et al (2019) Properties of water tree growing in XLPE and composites. In: 2019 2nd International conference electrical material power equipment. IEEE, pp 409–412. <https://doi.org/10.1109/ICEMPE.2019.8727376>
23. Seiler J, Kindersberger J (2014) Insight into the interphase in polymer nanocomposites. *IEEE Trans Dielectr Electr Insul* 21:537–547. <https://doi.org/10.1109/TDEI.2013.004388>
24. Lewis TJ (1994) Nanometric dielectrics. *IEEE Trans Dielectr Electr Insul* 1:812–825. <https://doi.org/10.1109/94.326653>
25. Lewis TJ (2004) Interfaces are the dominant feature of dielectrics at the nanometric level. *IEEE Trans Dielectr Electr Insul* 11:739–753. <https://doi.org/10.1109/TDEI.2004.1349779>
26. Lewis TJ (2005) Interfaces: nanometric dielectrics. *J Phys D Appl Phys* 38:202–212. <https://doi.org/10.1088/0022-3727/38/2/004>
27. Tanaka T, Kozako M, Fuse N, Ohki Y (2005) Proposal of a multi-core model for polymer nanocomposite dielectrics. *IEEE Trans Dielectr Electr Insul* 12:669–681. <https://doi.org/10.1109/TDEI.2005.1511092>
28. Raetzke S, Kindersberger J (2006) The Effect of Interphase Structures in Nanodielectrics. *IEEE Trans Fundam Mater* 126:1044–1049. <https://doi.org/10.1541/ieejfms.126.1044>
29. Andritsch T, Kochetov R, Morshuis PHF, Smit JJ (2011) Proposal of the polymer chain alignment model. In: 2011 Annual report conference electrical insulation and dielectric phenomena. IEEE, pp 624–627. <https://doi.org/10.1109/CEIDP.2011.6232734>
30. Alhabill FN, Ayooob R, Andritsch T, Vaughan AS (2018) Introducing particle interphase model for describing the electrical behaviour of nanodielectrics. *Mater Des* 158:62–73. <https://doi.org/10.1016/j.matdes.2018.08.018>
31. Schadler LS, Brinson LC, Sawyer WG (2007) Polymer nanocomposites: a small part of the story. *JOM* 59:53–60. <https://doi.org/10.1007/s11837-007-0040-5>
32. Raetzke S, Kindersberger J (2010) Role of interphase on the resistance to high-voltage arcing, on tracking and erosion of silicone/SiO₂ nanocomposites. *IEEE Trans Dielectr Electr Insul* 17:607–614. <https://doi.org/10.1109/TDEI.2010.5448118>
33. Calebrese C, Hui L, Schadler L, Nelson J (2011) A review on the importance of nanocomposite processing to enhance electrical insulation. *IEEE Trans Dielectr Electr Insul* 18:938–945. <https://doi.org/10.1109/TDEI.2011.5976079>
34. Paramane AS, Kumar KS (2016) A review on nanocomposite based electrical insulations. *Trans Electr Electron Mater* 17:239–251. <https://doi.org/10.4313/TEEM.2016.17.5.239>

35. Paramane AS, Kannaiah SK (2016) Superiority of partial discharge characteristics of cross-linked polyethylene nanocomposites over microcomposites for electrical insulation application. *Micro Nano Lett* 11:844–847. <https://doi.org/10.1049/mnl.2016.0496>
36. Niu Y, Wang H (2019) Dielectric nanomaterials for power energy storage: surface modification and characterization. *ACS Appl Nano Mater* 2:627–642. <https://doi.org/10.1021/acsanm.8b01846>
37. Plueddemann EP (1991) Chemistry of silane coupling agents. Silane coupling agents. Springer, US, Boston, MA, pp 31–54. https://doi.org/10.1007/978-1-4899-2070-6_2
38. Mostofi Sarkari N, Mohseni M, Ebrahimi M (2019) Investigating the crosslinking effects on surface characteristics of vinyltrimethoxysilane-grafted moisture-cured low-density polyethylene/ethylene vinyl acetate blend. *J Appl Polym Sci* 136:47147. <https://doi.org/10.1002/app.47147>
39. Pape PG (2017) Adhesion promoters: silane coupling agents. In: *Applied plastic engineering handbook*, 2nd edn. Elsevier, pp 555–572. <https://doi.org/10.1016/B978-0-323-39040-8.00026-2>
40. Thomas S, Jose JP (2017) Cross-linked polyethylene nanocomposites for dielectric applications. *Adv Compos Mater Prop Appl*. <https://doi.org/10.1515/9783110574432-012>
41. Huang X, Liu F, Jiang P (2010) Effect of nanoparticle surface treatment on morphology, electrical and water treeing behavior of LLDPE composites. *IEEE Trans Dielectr Electr Insul* 17:1697–1704. <https://doi.org/10.1109/TDEI.2010.5658219>
42. Liu D, Hoang AT, Pourrahimi AM et al (2017) Influence of nanoparticle surface coating on electrical conductivity of LDPE/Al₂O₃ nanocomposites for HVDC cable insulations. *IEEE Trans Dielectr Electr Insul* 24:1396–1404. <https://doi.org/10.1109/TDEI.2017.006310>
43. Liu D, Pourrahimi AM, Olsson RT et al (2015) Influence of nanoparticle surface treatment on particle dispersion and interfacial adhesion in low-density polyethylene/aluminium oxide nanocomposites. *Eur Polym J* 66:67–77. <https://doi.org/10.1016/j.eurpolymj.2015.01.046>
44. Liu D, Pallon LKH, Pourrahimi AM et al (2017) Cavitation in strained polyethylene/aluminium oxide nanocomposites. *Eur Polym J* 87:255–265. <https://doi.org/10.1016/j.eurpolymj.2016.12.021>
45. Wang W, Li S (2019) Improvement of dielectric breakdown performance by surface modification in polyethylene/TiO₂ nanocomposites. *Materials (Basel)* 12:3346. <https://doi.org/10.3390/ma12203346>
46. Ashish Sharad P, Kumar KS (2017) Application of surface-modified XLPE nanocomposites for electrical insulation partial discharge and morphological study. *Nanocomposites* 3:30–41. <https://doi.org/10.1080/20550324.2017.1325987>
47. Palakattukunnel ST, Thomas S, Sreekumar PA, Bandyopadhyay S (2011) Poly (ethylene-co-vinyl acetate)/calcium phosphate nanocomposites: contact angle, diffusion and gas permeability studies. *J Polym Res* 18:1277–1285. <https://doi.org/10.1007/s10965-010-9530-1>
48. Jose JP, Abraham J, Maria HJ et al (2016) Contact angle studies in XLPE hybrid nanocomposites with inorganic nanofillers. *Macromol Symp* 366:66–78. <https://doi.org/10.1002/masy.201650048>
49. Zhang L, Zhou Y, Cui X et al (2014) Effect of nanoparticle surface modification on breakdown and space charge behavior of XLPE/SiO₂ nanocomposites. *IEEE Trans Dielectr Electr Insul* 21:1554–1564. <https://doi.org/10.1109/TDEI.2014.004361>
50. Zhang L, Zhou Y, Huang M et al (2014) Effect of nanoparticle surface modification on charge transport characteristics in XLPE/SiO₂ nanocomposites. *IEEE Trans Dielectr Electr Insul* 21:424–433. <https://doi.org/10.1109/TDEI.2013.004145>
51. Donghe D, Xiufeng L, Jin S et al (2017) The influence of surface modifier on structural morphology and dielectric property of XLPE/SiO₂ Nanocomposites. In: *2017 1st International conference electrical material power equipment*. IEEE, pp 432–435. <https://doi.org/10.1109/ICEMPE.2017.7982120>

52. Zhang L, Khani MM, Krentz TM et al (2017) Suppression of space charge in crosslinked polyethylene filled with poly(stearyl methacrylate)-grafted SiO₂ nanoparticles. *Appl Phys Lett*. <https://doi.org/10.1063/14979107>
53. Zhang C, Chang J, Zhang H et al (2019) Improved direct current electrical properties of crosslinked polyethylene modified with the polar group compound. *Polymers (Basel)* 11:1624. <https://doi.org/10.3390/polym11101624>
54. Teyssedre G, Laurent C (2005) Charge transport modeling in insulating polymers: from molecular to macroscopic scale. *IEEE Trans Dielectr Electr Insul* 12:857–875. <https://doi.org/10.1109/TDEI.2005.1522182>
55. Zhang C, Zhang H, Li C et al (2018) Crosslinked polyethylene/polypyrrole nanocomposites with improved direct current electrical characteristics. *Polym Test* 71:223–230. <https://doi.org/10.1016/j.polymertesting.2018.09.020>
56. Jose JP, Thomas S (2014) Alumina–clay nanoscale hybrid filler assembling in cross-linked polyethylene based nanocomposites: mechanics and thermal properties. *Phys Chem Chem Phys* 16:14730–14740. <https://doi.org/10.1039/C4CP01532K>
57. Jose JP, Thomas S (2014) XLPE based Al₂O₃–clay binary and ternary hybrid nanocomposites: self-assembly of nanoscale hybrid fillers, polymer chain confinement and transport characteristics. *Phys Chem Chem Phys* 16:20190–20201. <https://doi.org/10.1039/C4CP03403A>
58. Hosier IL, Praeger M, Vaughan AS, Swingler SG (2017) The effects of water on the dielectric properties of aluminum-based nanocomposites. *IEEE Trans Nanotechnol* 16:667–676. <https://doi.org/10.1109/TNANO.2017.2703982>
59. Hosier IL, Praeger M, Vaughan AS, Swingler SG (2017) The effects of water on the dielectric properties of silicon-based nanocomposites. *IEEE Trans Nanotechnol* 16:169–179. <https://doi.org/10.1109/TNANO.2016.2642819>
60. Zou C, Fothergill J, Rowe S (2008) The effect of water absorption on the dielectric properties of epoxy nanocomposites. *IEEE Trans Dielectr Electr Insul* 15:106–117. <https://doi.org/10.1109/T-DEI.2008.4446741>
61. Pourrahimi AM, Olsson RT, Hedenqvist MS (2018) The role of interfaces in polyethylene/metal-oxide nanocomposites for ultrahigh-voltage insulating materials. *Adv Mater* 30:1703624. <https://doi.org/10.1002/adma.201703624>
62. Fabiani D, Montanari G, Testa L (2010) Effect of aspect ratio and water contamination on the electric properties of nanostructured insulating materials. *IEEE Trans Dielectr Electr Insul* 17:221–230. <https://doi.org/10.1109/TDEI.2010.5412021>
63. Nilsson F, Karlsson M, Pallon L et al (2017) Influence of water uptake on the electrical DC-conductivity of insulating LDPE/MgO nanocomposites. *Compos Sci Technol* 152:11–19. <https://doi.org/10.1016/j.compscitech.2017.09.009>
64. Pourrahimi AM, Pallon LKH, Liu D et al (2016) Polyethylene nanocomposites for the next generation of ultralow-transmission-loss HVDC cables: insulation containing moisture-resistant MgO nanoparticles. *ACS Appl Mater Interfaces* 8:14824–14835. <https://doi.org/10.1021/acsami.6b04188>
65. Lau KY, Zafrullah SNRM, Ismail IZ, Ching KY (2018) Effects of water on breakdown characteristics of polyethylene composites. *J Electrostat* 96:119–127. <https://doi.org/10.1016/j.elstat.2018.10.011>
66. Yang J, Wang X, Zhao H et al (2014) Influence of moisture absorption on the DC conduction and space charge property of MgO/LDPE nanocomposite. *IEEE Trans Dielectr Electr Insul* 21:1957–1964. <https://doi.org/10.1109/TDEI.2014.004334>
67. Wang Y, Qiang D, Alhabill FNF et al (2018) Influence of moisture absorption on electrical properties and charge dynamics of polyethylene silica-based nanocomposites. *J Phys D Appl Phys* 51:425302. <https://doi.org/10.1088/1361-6463/aadb7b>
68. Zhuravlev LT (2000) The surface chemistry of amorphous silica. Zhuravlev model. *Colloids Surf A Physicochem Eng Asp* 173:1–38. [https://doi.org/10.1016/S0927-7757\(00\)00556-2](https://doi.org/10.1016/S0927-7757(00)00556-2)

69. Hui L, Schadler LS, Nelson JK (2013) The influence of moisture on the electrical properties of crosslinked polyethylene/silica nanocomposites. *IEEE Trans Dielectr Electr Insul* 20:641–653. <https://doi.org/10.1109/TDEI.2013.6508768>
70. Hui L, Nelson JK, Schadler LS (2010) The influence of moisture on the electrical performance of XLPE/silica nanocomposites. In: 2010 10th IEEE International conference on solid dielectrical IEEE, pp 1–4. <https://doi.org/10.1109/ICSD.2010.5568040>
71. Nilsson S, Hjertberg T, Smedberg A (2010) Structural effects on thermal properties and morphology in XLPE. *Eur Polym J* 46:1759–1769. <https://doi.org/10.1016/j.eurpolymj.2010.05.003>
72. Zhang X, Yang H, Song Y, Zheng Q (2012) Influence of crosslinking on physical properties of low density polyethylene. *Chinese J Polym Sci* 30:837–844. <https://doi.org/10.1007/s10118-012-1194-3>
73. Pleša I, Nožingher P, Schlögl S et al (2016) Properties of polymer composites used in high-voltage applications. *Polymers (Basel)* 8:173. <https://doi.org/10.3390/polym8050173>
74. Choudalakis G, Gotsis AD (2012) Free volume and mass transport in polymer nanocomposites. *Curr Opin Colloid Interf Sci* 17:132–140. <https://doi.org/10.1016/j.cocis.2012.01.004>
75. Wang W, Min D, Li S (2016) Understanding the conduction and breakdown properties of polyethylene nanodielectrics: effect of deep traps. *IEEE Trans Dielectr Electr Insul* 23:564–572. <https://doi.org/10.1109/TDEI.2015.004823>
76. Jouault N, Moll JF, Meng D et al (2013) Bound polymer layer in nanocomposites. *ACS Macro Lett* 2:371–374. <https://doi.org/10.1021/mz300646a>
77. Pourrahimi AM, Hoang TA, Liu D et al (2016) Highly efficient interfaces in nanocomposites based on polyethylene and ZnO nano/hierarchical particles: a novel approach toward ultralow electrical conductivity insulations. *Adv Mater* 28:8651–8657. <https://doi.org/10.1002/adma.201603291>
78. Jose JP, Chazeau L, Cavaillé J-Y et al (2014) Nucleation and nonisothermal crystallization kinetics in cross-linked polyethylene/zinc oxide nanocomposites. *RSC Adv* 4:31643–31651. <https://doi.org/10.1039/C4RA03731F>
79. Andrews T, Hampton RN, Smedberg A et al (2006) The role of degassing in XLPE power cable manufacture. *IEEE Electr Insul Mag* 22:5–16. <https://doi.org/10.1109/MEI.2006.253416>
80. Gao Y, Huang X, Min D et al (2019) Recyclable dielectric polymer nanocomposites with voltage stabilizer interface: toward new generation of high voltage direct current cable insulation. *ACS Sustain Chem Eng* 7:513–525. <https://doi.org/10.1021/acssuschemeng.8b04070>
81. Xu Z, Zhou F, Zhimin Y et al (2016) Effect of dicumyl peroxide on space charge accumulation characteristics of cross-linked polyethylene. In: 2016 IEEE International conference dielectric. IEEE, pp 196–199. <https://doi.org/10.1109/ICD.2016.7547578>
82. Meng P, Zhou Y, Yuan C et al (2019) Comparisons of different polypropylene copolymers as potential recyclable HVDC cable insulation materials. *IEEE Trans Dielectr Electr Insul* 26:674–680. <https://doi.org/10.1109/TDEI.2019.8726011>
83. Wu J, Wu ZL, Yang H, Zheng Q (2014) Crosslinking of low density polyethylene with octavinyl polyhedral oligomeric silsesquioxane as the crosslinker. *RSC Adv* 4:44030–44038. <https://doi.org/10.1039/C4RA04886E>
84. Morici E, Di Bartolo A, Arrigo R, Dintcheva NT (2016) Double bond-functionalized POSS: dispersion and crosslinking in polyethylene-based hybrid obtained by reactive processing. *Polym Bull* 73:3385–3400. <https://doi.org/10.1007/s00289-016-1662-y>
85. Morici E, Di Bartolo A, Arrigo R, Dintcheva NT (2018) POSS grafting on polyethylene and maleic anhydride-grafted polyethylene by one-step reactive melt mixing. *Adv Polym Technol* 37:349–357. <https://doi.org/10.1002/adv.21673>
86. Huang X, Xie L, Jiang P et al (2009) Morphology studies and ac electrical property of low density polyethylene/octavinyl polyhedral oligomeric silsesquioxane composite dielectrics. *Eur Polym J* 45:2172–2183. <https://doi.org/10.1016/j.eurpolymj.2009.05.019>

87. Bhutta MS, Yang L, Ma Z et al (2018) Influence of polyhedral oligomeric silsesquioxane (POSS) on space charge behavior and trap levels of XLPE/POSS nanocomposite. In: 2018 IEEE 2nd International conference dielectric. IEEE, pp 1–4. <https://doi.org/10.1109/ICD.2018.8514731>
88. Mauri M, Peterson A, Senol A et al (2018) Byproduct-free curing of a highly insulating polyethylene copolymer blend: an alternative to peroxide crosslinking. *J Mater Chem C* 6:11292–11302. <https://doi.org/10.1039/C8TC04494E>
89. Mauri M, Hofmann AI, Gómez-Heincke D et al (2020) Click chemistry-type crosslinking of a low-conductivity polyethylene copolymer ternary blend for power cable insulation. *Polym Int* 69:404–412. <https://doi.org/10.1002/pi.5966>
90. Mauri M, Svenningsson L, Hjertberg T et al (2018) Orange is the new white: rapid curing of an ethylene-glycidyl methacrylate copolymer with a Ti-bisphenolate type catalyst. *Polym Chem* 9:1710–1718. <https://doi.org/10.1039/C7PY01840A>
91. Mauri M, Tran N, Prieto O et al (2017) Crosslinking of an ethylene-glycidyl methacrylate copolymer with amine click chemistry. *Polymer (Guildf)* 111:27–35. <https://doi.org/10.1016/j.polymer.2017.01.010>
92. Diao J, Huang X, Jia Q et al (2017) Thermoplastic isotactic polypropylene/ethylene-octene polyolefin copolymer nanocomposite for recyclable HVDC cable insulation. *IEEE Trans Dielectr Electr Insul* 24:1416–1429. <https://doi.org/10.1109/TDEI.2017.006208>
93. Li L, Zhong L, Zhang K et al (2018) Temperature dependence of mechanical, electrical properties and crystal structure of polyethylene blends for cable insulation. *Materials (Basel)* 11:1922. <https://doi.org/10.3390/ma11101922>
94. Mostofi Sarkari N, Mohseni M, Ebrahimi M (2021) Examining impact of vapor-induced crosslinking duration on dynamic mechanical and static mechanical characteristics of silane-water crosslinked polyethylene compound. *Polym Test* 93:106933. <https://doi.org/10.1016/j.polymertesting.2020.106933>
95. Hosier IL, Vaughan AS, Pye A, Stevens GC (2019) High performance polymer blend systems for HVDC applications. *IEEE Trans Dielectr Electr Insul* 26:1197–1203. <https://doi.org/10.1109/TDEI.2019.007954>
96. Huang X, Fan Y, Zhang J, Jiang P (2017) Polypropylene based thermoplastic polymers for potential recyclable HVDC cable insulation applications. *IEEE Trans Dielectr Electr Insul* 24:1446–1456. <https://doi.org/10.1109/TDEI.2017.006230>
97. Okajima I, Sako T (2014) Energy conversion of biomass and recycling of waste plastics using supercritical fluid, subcritical fluid and high-pressure superheated steam. In: *Supercritical fluid technology for energy environmental application*. Elsevier, pp 249–267. <https://doi.org/10.1016/B978-0-444-62696-7.00013-7>
98. Goto M (2009) Chemical recycling of plastics using sub- and supercritical fluids. *J Supercrit Fluids* 47:500–507. <https://doi.org/10.1016/j.supflu.2008.10.011>
99. Goto T, Yamazaki T, Sugeta T et al (2003) Recycling of silane cross-linked polyethylene for insulation of cables by supercritical alcohol. *Proc IEEE Int Conf Prop Appl Dielectr Mater* 3:1218–1221. <https://doi.org/10.1109/icpadm.2003.1218644>
100. Ashihara S, Goto T, Yamazaki T et al (2008) Recycling of insulation of 600 V XLPE cable using supercritical alcohol. In: *2008 International Symposium on electric insulating materials (ISEIM 2008)*. IEEE, pp 522–525. <https://doi.org/10.1109/ISEIM.2008.4664473>
101. Goto T, Ashihara S, Yamazaki T et al (2011) Continuous process for recycling silane cross-linked polyethylene using supercritical alcohol and extruders. *Ind Eng Chem Res* 50:5661–5666. <https://doi.org/10.1021/ie101772x>
102. Goto T, Ashihara S, Kato M et al (2012) Use of single-screw extruder for continuous silane cross-linked polyethylene recycling process using supercritical alcohol. *Ind Eng Chem Res* 51:6967–6971. <https://doi.org/10.1021/ie202303y>
103. Baek BK, La YH, Lee AS et al (2016) Decrosslinking reaction kinetics of silane-crosslinked polyethylene in sub- and supercritical fluids. *Polym Degrad Stab* 130:103–108. <https://doi.org/10.1016/j.polymdegradstab.2016.05.025>

104. Baek BK, La YH, Na WJ et al (2016) A kinetic study on the supercritical decrosslinking reaction of silane-crosslinked polyethylene in a continuous process. *Polym Degrad Stab* 126:75–80. <https://doi.org/10.1016/j.polymdegradstab.2016.01.019>
105. Lee H, Jeong JH, Hong G et al (2013) Effect of solvents on de-cross-linking of cross-linked polyethylene under subcritical and supercritical conditions. *Ind Eng Chem Res* 52:6633–6638. <https://doi.org/10.1021/ie4006194>
106. Baek BK, Shin JW, Jung JY et al (2015) Continuous supercritical decrosslinking extrusion process for recycling of crosslinked polyethylene waste. *J Appl Polym Sci* 132. <https://doi.org/10.1002/app.41442>
107. Qudaih R, Janajreh I, Vukusic SE (2011) Recycling of cross-linked polyethylene cable waste via particulate infusion. In: Seliger G, Khraisheh MMK, Jawahir IS (eds) *Advance Sustainable Manufacture*. Springer, Berlin Heidelberg, Berlin, Heidelberg, pp 233–239. https://doi.org/10.1007/978-3-642-20183-7_34
108. Lindqvist K, Andersson M, Boss A, Oxfall H (2019) Thermal and mechanical properties of blends containing PP and recycled XLPE cable waste. *J Polym Environ* 27:386–394. <https://doi.org/10.1007/s10924-018-1357-6>
109. Navratil J, Manas M, Mizera A et al (2015) Recycling of irradiated high-density polyethylene. *Radiat Phys Chem* 106:68–72. <https://doi.org/10.1016/j.radphyschem.2014.06.025>
110. Manas D, Manas M, Mizera A et al (2018) The high density polyethylene composite with recycled radiation cross-linked filler of rHDPE. *Polymers (Basel)* 10:1361. <https://doi.org/10.3390/polym10121361>
111. Zéhil G-P, Assaad JJ (2019) Feasibility of concrete mixtures containing cross-linked polyethylene waste materials. *Constr Build Mater* 226:1–10. <https://doi.org/10.1016/j.conbuildmat.2019.07.285>
112. Singh P, Déparrois N, Burra KG et al (2019) Energy recovery from cross-linked polyethylene wastes using pyrolysis and CO₂ assisted gasification. *Appl Energy* 254:113722. <https://doi.org/10.1016/j.apenergy.2019.113722>
113. Sun F, Bai S, Wang Q (2019) Structures and properties of waste silicone cross-linked polyethylene de-cross-linked selectively by solid-state shear mechanochemical technology. *J Vinyl Addit Technol* 25:149–158. <https://doi.org/10.1002/vnl.21636>
114. Santos JN, Jayaraman R (2019) Recycling of crosslinked high-density polyethylene through compression molding. *J Appl Polym Sci* 136:48145. <https://doi.org/10.1002/app.48145>
115. Xie Y, Zhao Y, Liu G et al (2019) Annealing effects on XLPE insulation of retired high-voltage cable. *IEEE Access* 7:104344–104353. <https://doi.org/10.1109/ACCESS.2019.2927882>
116. Xie Y, Liu G, Zhao Y et al (2019) Rejuvenation of retired power cables by heat treatment. *IEEE Trans Dielectr Electr Insul* 26:668–670. <https://doi.org/10.1109/TDEL.2018.007783>
117. Ouyang Y, Mauri M, Pourrahimi AM et al (2020) Recyclable polyethylene insulation via reactive compounding with a maleic anhydride-grafted polypropylene. *ACS Appl Polym Mater* 2:2389–2396. <https://doi.org/10.1021/acscapm.0c00320>
118. IEC 60227-2 Polyvinyl chloride insulated cables of rated voltages up to and including 450/750 V—test methods
119. Mostofi Sarkari N, Darvish F, Mohseni M et al (2019) Surface characterization of an organosilane-grafted moisture-crosslinked polyethylene compound treated by air atmospheric pressure non-equilibrium gliding arc plasma. *Appl Surf Sci* 490:436–450. <https://doi.org/10.1016/j.apsusc.2019.06.007>
120. Mostofi Sarkari N, Doğan Ö, Bat E et al (2019) Assessing effects of (3-aminopropyl) trimethoxysilane self-assembled layers on surface characteristics of organosilane-grafted moisture-crosslinked polyethylene substrate: a comparative study between chemical vapor deposition and plasma-facilitated in situ. *Appl Surf Sci* 497:143751. <https://doi.org/10.1016/j.apsusc.2019.143751>

121. Mostofi Sarkari N, Doğan Ö, Bat E et al (2020) Tethering vapor-phase deposited GLYMO coupling molecules to silane-crosslinked polyethylene surface via plasma grafting approaches. *Appl Surf Sci* 513:145846. <https://doi.org/10.1016/j.apsusc.2020.145846>
122. Zhao AX, Chen X, Le Chen S et al (2019) Surface modification of XLPE films by CF₄ DBD for dielectric properties. *AIP Adv.* <https://doi.org/10.1063/1.5078489>
123. Thomas J, Joseph B, Jose JP et al (2019) Recent advances in cross-linked polyethylene-based nanocomposites for high voltage engineering applications: a critical review. *Ind Eng Chem Res* 58:20863–20879. <https://doi.org/10.1021/acs.iecr.9b02172>
124. Kim C, Jiang P, Liu F et al (2019) Investigation on dielectric breakdown behavior of thermally aged cross-linked polyethylene cable insulation. *Polym Test* 80:106045. <https://doi.org/10.1016/j.polymertesting.2019.106045>
125. Ouyang B, Li H, Zhang X et al (2017) The role of micro-structure changes on space charge distribution of XLPE during thermo-oxidative ageing. *IEEE Trans Dielectr Electr Insul* 24:3849–3859. <https://doi.org/10.1109/TDEI.2017.006523>
126. He D, Gu J, Wang W et al (2017) Research on mechanical and dielectric properties of XLPE cable under accelerated electrical-thermal aging. *Polym Adv Technol* 28:1020–1029. <https://doi.org/10.1002/pat.3901>
127. Hedir A, Moudoud M, Lamrous O et al (2019) Ultraviolet radiation aging impact on physicochemical properties of crosslinked polyethylene cable insulation. *J Appl Polym Sci* 48575:48575. <https://doi.org/10.1002/app.48575>
128. Shao Z, Byler MI, Liu S et al (2018) Dielectric response of cross-linked polyethylene (XLPE) cable insulation material to radiation and thermal aging. In: 2018 IEEE 2nd international conference dielectric, pp 1–4. <https://doi.org/10.1109/icd.2018.8514664>